



Architecture  
and the  
Built environment

#11  
2017



## Thermal Comfort in Sun Spaces

To what extent can energy collectors and seasonal energy storages provide thermal comfort in sun spaces?

Christian Wiegel



# Thermal Comfort in Sun Spaces

**To what extent can energy collectors and seasonal energy storages provide thermal comfort in sun spaces?**

Christian Wiegel

*Delft University of Technology, Faculty of Architecture and the Built Environment,  
Department of Architecture and Technology - Architectural Engineering*

**Design:** Sirene Ontwerpers, Rotterdam

ISBN 978-94-92516-81-7

ISSN 2212-3202

© 2017 Christian Wiegel

All rights reserved. No part of the material protected by this copyright notice may be reproduced or utilized in any form or by any means, electronic or mechanical, including photocopying, recording or by any information storage and retrieval system, without written permission from the author.

Unless otherwise specified, all the photographs in this thesis were taken by the author. For the use of illustrations effort has been made to ask permission for the legal owners as far as possible. We apologize for those cases in which we did not succeed. These legal owners are kindly requested to contact the publisher.

# Thermal Comfort in Sun Spaces

**To what extent can energy collectors and seasonal energy storages provide thermal comfort in sun spaces?**

Proefschrift

ter verkrijging van de graad van doctor  
aan de Technische Universiteit Delft,  
op gezag van de Rector Magnificus Prof. ir. K.Ch.A.M. Luyben,  
voorzitter van het College voor Promoties,  
in het openbaar te verdedigen op donderdag 12 oktober 2017 om 10:00 uur

door CHRISTIAN WIEGEL

Diplom-Ingenieur (FH) Architektur, MSA - Münster School of Architecture,  
Master of Engineering - IFDC, Hochschule Ost-Westfalen-Lippe,  
geboren te Bocholt, Duitsland

## **Dit proefschrift is goedgekeurd door de promoter and copromoter**

---

Prof. Dr.-Ing. Ulrich Knaack  
Prof. Dipl.-Ing. Thomas Auer  
Dr.-Ing. Tillman Klein

## **Samenstelling promotiecommissie bestaat uit**

---

Rector Magnificus, Prof. ir. K.Ch.A.M. Luyben voorzitter  
Prof. Dr.-Ing. Ulrich Knaack, promotor  
Dr.-Ing. Tillmann Klein, daily supervisor  
Prof. Dipl.-Ing. Thomas Auer, copromotor

## **Onafhankelijke leden**

---

Prof. Dr.-Ing. Ulrich Knaack, Technische Universiteit Delft, promotor  
Dr.-Ing. Tillman Klein, Technische Universiteit Delft, daily supervisor  
Prof. Dipl.- Ing. Thomas Auer, Technische Universiteit München, copromoter  
Prof. ir. Peter G. Luscuere, Technische Universiteit Delft  
Prof. Dr.- Ing. Uta Pottgiesser, Universiteit Antwerpen  
Prof. Dipl.- Ing. Matthias Rudolph, Staatliche Akademie der Bildenden Künste Stuttgart  
Dipl.-Wirt.-Ing. Stefan Holtgreife, Solarlux GmbH

---

This research was funded by Solarlux GmbH, Melle, Germany.

**“Hawkes (1982) found that energy efficiency improved when people were given control of their environment.”**

*Philomena Bluysen, 2009*

**“Die Bauindustrie spielt eine Schlüsselrolle für die Umsetzung einer nachhaltigen Entwicklung in unserer Gesellschaft.”**

*Mach, Grobbauer, Streicher und Müller, 2015*

**“It could have also be shown that the functionalization of facades is not only a trend, but environmentally reasonable.”**

*Mach, Grobbauer, Streicher und Müller, 2015*



# Acknowledgements

I am grateful for  
Prof. Dr.-Ing. Ulrich Knaack and Dr.-Ing. Tillmann Klein  
for their enthusiasm, guidance, and criticisms.

My earnest thank for both covering and pushing me.

My gratitude also to  
Prof. Dipl.-Ing. Thomas Auer and Dr.-Ing. Thaleia Konstantinou  
for precious support and inspring communication.

Herbert und Stefan Holtgreife  
for ignition, thrust and patience.

Claudia, Henrike, Vincent and Elisabeth  
my intimate thank for your love, patience and encouragement.

Norbert Rieger, Jens Krenitz, Uwe Wechsel,  
Klaus Fischer, Toni Grossmann, Mario Fliehe, Matthias Fark,  
Ingo Möller, Werner Helmich, Gaby Gregory and Tanja Hoyja,  
Sascha Kühn, Bianca Flottesch und Thomas Grässler  
for their enthusiasm and indispensable support in Osnabrück.

Inge Meulenberg-Ammerlaan, Barbara van Vliet-van der Haas,  
Sandra de Koning, Hilma Bleeker, Sjoerd Zwart and Maaike Beliën  
for their essential help in Delft.

You spent a lot what lasts beyond the project itself.



# Contents (concise)

1	Introduction	1
2	Literature survey and empirical evaluation of thermal comfort in sun spaces	21
3	Literature survey of façade integrated renewable energy collector technology	167
4	Literature survey of seasonal electro-chemical and sorption energy storage technology	271
5	Description & evaluation of BIPV combined with electro-chemical storage for sunspace heating	333
6	Description and evaluation of the product development "HEATBEAM®"	359
7	Parametrization and algorithms for comfort and annual energy yield modelling in Chapter 08	393
8	Comfort and yield analysis of dynamic modelling of passive and active sun space facades	425
9	Conclusion	463



# Contents

Abbreviations [XXI](#)  
Summary [XXV](#)  
Samenvatting [XXVII](#)

[1](#) Introduction [1](#)  
.....

[1.1](#) Situation and Conflict [1](#)  
.....

[1.2](#) Problem stating [2](#)  
.....

[1.3](#) Solution [3](#)  
.....

[1.4](#) Relevance [4](#)  
.....

[1.5](#) Scope: Thermal comfort, façade integrated collectors and seasonal energy storage [6](#)  
.....

[1.6](#) Research Question – Knowledge Gap [7](#)  
.....

[1.7](#) Purpose Statement [9](#)  
.....

[1.8](#) Result and Deliverables [9](#)  
.....

[1.9](#) Research Structure [10](#)  
.....

[1.10](#) Preparation, Limits and Quality of Evaluation [14](#)  
.....

[1.11](#) Thesis Outline [17](#)  
.....

[2](#) Literature survey and empirical evaluation of thermal comfort in sun spaces [21](#)  
.....

[2.1](#) The archetype sun space - a constructional differentiation [21](#)  
.....

2.2	Description of the Solarlux experimental test-set up : sun space	26
2.2.1	Intention of empirical assessment	26
2.2.2	Meteorological background	26
2.2.3	Physical description	27
2.2.4	Sensor equipment and data logging	32
2.2.5	Control and Monitoring and signal definition	35
2.2.6	Solar thermal tube collectors attached to sun space façade	36
2.3	Thermal comfort - an interior space quality	37
2.4	Milestones and divers approaches in research of thermal comfort	39
2.4.1	The heat balance model	40
2.4.2	The Adaptive Comfort model	47
2.4.3	Methodology : applicable procedures for sun spaces depending on season	51
2.5	Contemporary research on indoor thermal comfort	53
2.6	Research on thermal behaviour, thermal comfort and energy on sun spaces	56
2.6.1	Optimisation potential of standards and digital models for sun spaces calculations	57
2.6.2	Thermal comfort related to design and strategy	63
2.6.3	Energetic benefits related to facades qualities and sun space design	64
2.6.4	Detected constructional parts on sun space energetic management	73
2.6.5	Inertia as a control tool for heating energy saving and thermal comfort	77
2.6.6	Summary	81
2.7	Thermal and energetic analysis of an experimental test sun space	84
2.7.1	Determination of comfort category according standards	84
2.7.1.1	Evaluation prerequisites : comfort categories and threshold values	85
2.7.1.2	Winter / Summer according Bewertungssystem Nachhaltiges Bauen (BNB)	86
2.7.1.3	Major sun space occupational period (5 to 10 PM)	86
2.7.2	Method of empirical data processing, synchronization and fault distinction	86
2.7.3	Active heating : floor heating schedule	87
2.7.4	Empirical analysis of major thermal comfort aspects	88
2.7.5	Empirical monthly analysis of resultant temperature in set-point interval	90
2.7.5.1	Special days, overheating, cooling by natural ventilation	95
2.7.5.2	Monthly cumulative frequencies of resultant temperature	97
2.7.5.3	Monthly analysis of resultant temperature by mean of running external temperature interval	103

2.7.5.4	Monthly analysis of comfort chart	114
2.7.5.5	Description and determination of sun space specific inertia	120
2.7.5.6	Monthly analysis of dry bulb temperature related to external temperature and irradiation as indication of inertia	127
2.8	Analysis of minor detailed sun space specific local thermal discomfort	131
2.8.1	Monthly analysis of dry bulb striation / air temperature gradient	132
2.8.1.1	Monthly analysis cold or warm floor	136
2.8.1.2	Monthly analysis radiation asymmetries	141
2.8.1.3	Summary of local discomfort	151
2.9	Predicted Mean Vote in long term perspective according EN ISO 15251	152
2.9.1	Explanation of method DIN EN ISO 15251, Appendix F or G	152
2.9.2	Winter month evaluation according DIN EN ISO 15251, App. F : method A	153
2.9.3	Summer month evaluation according DIN EN ISO 15251, App. F : method B	155
2.9.3.1	Cumulative frequencies of hours with exceeding of category III	156
2.10	Analysis of effective utilized end energy to auxiliary energy ratio	158
2.10.1	Renewable Energy generated by sun space facades	159
2.10.2	Net power consumption as auxiliary energy	161
2.10.3	Ratio-autarky ratio	162
2.10.4	Summary	162
2.11	Summary	163
3	Literature survey of façade integrated renewable energy collector technology	167
3.1	Integral facades – from added component to multi-functional layer	167
3.2	Specific Effectiveness and Performance of façade embedded collector typologies	168
3.2.1	Performance criteria of envelope embedded collectors	168
3.2.2	In relation to internal load profile, envelope properties and location	185
3.2.3	Summary	187

3.3	Systematic planning of yield in context of façade typology and location	188
<hr/>		
3.3.1	Optimizing Periphery – Optimizing System	194
3.3.1.1	Thermal losses by distribution piping and string components	197
3.3.1.2	Exergy increase related to operation pressure and modified distribution medium	198
3.3.1.3	Circulation pump pulsing determines auxiliary energy efficiency, thermal comfort and yield	199
3.3.2	The f-chart	200
3.3.3	Summary	201
3.4	Concurrent embedded collector technology : status quo	202
<hr/>		
3.4.1	Summary	212
3.5	Thinking about polymers	212
<hr/>		
3.5.1	Polymer cover sheets and polymer absorbers	216
3.5.1.1	Key performance criteria for polymer cover sheets and absorbers	217
3.5.1.2	Summary of state-of-the-art polymer performance	222
3.5.2	Nano-technologies for crucial collector components	223
3.5.2.1	Transparent conductive oxides	223
3.5.2.2	Thickness insensitive spectrally selective paints	225
3.5.2.3	Nano-tubes and fibres for enhanced strength	226
3.5.2.4	Co-polymers retard destruction by ultra-violet radiation	226
3.5.2.5	Transparent low <sub>e</sub> -coatings substitute opaque backside insulation	227
3.5.2.6	Self-regulating absorbers by spectrally-shutting coatings	229
3.5.3	Enhanced integral collector developments	230
3.5.4	Summary	243
3.6	Inspection of negative impact on interior thermal comfort	243
<hr/>		
3.6.1	Impact of solar thermal collectors	244
3.6.1.1	Behavior of combined collector-storage systems	254
3.6.1.2	Investigations on effects of hybrid-systems	255
3.6.2	Technical solutions for radiation barriers	258
3.6.3	Impact of photovoltaic collectors	261
3.6.4	Summary	266
3.7	Summary	266
<hr/>		

4	Literature survey of seasonal electro-chemical and sorption energy storage technology	271
4.1	Energy storing : logical consequence whilst a chronological offer-demand mismatch	271
4.1.1	Storing a question of energy conservation	271
4.2	Key performance criteria of energy storages	273
4.2.1	Volumetric density	274
4.2.2	Gravimetric density	274
4.2.3	Charge efficiency	274
4.2.4	Discharge / Power supply density	276
4.2.5	Monthly losses related to environmental conditions	277
4.2.6	Charge cycles – life span	278
4.2.7	Availability of crucial key materials	278
4.2.8	Safety and environmental impact	279
4.3	Electro-chemical storages	280
4.3.1	Current research on electro-chemical storages: improvement of details	280
4.3.1.1	DC or AC systems : tumble of a dogma	282
4.3.1.2	DC/AC converter : despite tri-phase - a nonessential efficiency choke	283
4.3.2	Accumulator types : space heating - a question of discharge-power	284
4.3.3	Cell type specific performance tendencies : key skills of accumulators	286
4.3.4	Most eligible secondary cell block typologies for sun space seasonal power storages	290
4.4	Thermo-chemical sorption storages	290
4.4.1	Storage principal of desorption	291
4.4.2	Competitive storage performances	293
4.4.3	Differentiated consideration of energy and exergy efficiency	297
4.4.4	Beneficial side effect : evaporative cooling	300
4.4.5	Research projects and practical experiences	300
4.5	Storage materials for sorption storages	303

4.5.1	Material groups	303
4.5.1.1	Designing material towards specific application : solar thermal heat source	306
4.5.1.2	Composite materials	307
4.5.1.3	Salt Hydrates	310
4.5.2	Storage densities and operation temperatures	312
4.5.3	Conductivity and reaction kinetics	313
4.6	Reactor design and prerequisite for process control	314
4.6.1	Opened & Closed systems	314
4.6.1.1	Advantages & Disadvantages	316
4.6.2	Mechanical reaction systems	318
4.6.3	Heat exchanger geometry	320
4.7	Specific process characteristics and detected aspects for further research	323
4.7.1	Required energy source and temperature for desorption	324
4.7.2	Potential temperature and released energy by adsorption	325
4.8	Summary thermo-chemical storages	328
4.9	Summary	329
5	Description&evaluation of BIPV combined with electro-chemical storage for sunspac heating	333
5.1	Power-to-heat: sun space envelope integrated photovoltaic for space heating	333
5.2	The System – components and constraints	335
5.2.1	Glass-to-glass photovoltaic: envelope integrated power generator	335
5.2.2	Circuitry and charge controller extent	337
5.2.3	Lead-acid accumulator: more than monthly storage, the sole power supplier	338
5.2.4	Heating system: ohmic resistant mats as radiant panel heating	340
5.2.4.1	Source related measurement of radiative heating: additional sensors	341
5.2.5	Additional provided functions and consumers	342
5.2.5.1	Source related measurement of radiative heating: additional sensors	342

5.2.6	Additional provided functions and consumers	343
5.2.6.1	Cooling system: AC split cooling (optional)	344
5.2.7	Control parameters	344
5.3	Performance evaluations	344
.....		
5.3.1	Monthly evaluation of power yield: PV performance	345
5.3.2	Monthly energy consumption, load profiles and battery charge status	347
5.3.3	Battery charge performance	349
5.3.4	Limits of heating power: effect	352
5.3.5	Limits of cooling power: effect	354
5.4	Summary	355
.....		
6	Description and evaluation of the product development "HEATBEAM®"	359
.....		
6.1	HEATBEAM - A collector becomes constructional component of a sun space rafter	359
.....		
6.1.1	Requirements for an efficient operation in order to verify Hypothesis II	362
6.1.2	Decisive performance features based on literature review	363
6.1.3	Constraints regarding façade integration and distribution and assembly	365
6.1.3.1	Constraints regarding impact on thermal comfort	366
6.2	Concept/construction of a rafter integrated solar thermal collector HEATBEAM©	367
.....		
6.2.1	Physical and technical description HEATBEAM I	367
6.2.1.1	Casing	368
6.2.1.2	Cover sheet	370
6.2.1.3	Sealings	370
6.2.1.4	Condenser penetration	371
6.2.1.5	External Linear Heat exchanger	372
6.2.1.6	Unconventional piping and connection	373
6.2.2	Physical and technical description HEATBEAM II – beneficial integral design	373

6.3	Description of the experimental test set-up: HEATBEAM	376
6.3.1	Sensing + Monitoring	377
6.3.2	Variants of investigation	378
6.3.3	Meteorological background	379
6.3.4	Monitoring and Control rules	380
6.4	Results (descriptive knowledge)	380
6.4.1	Vacuum duration and collector performance	380
6.4.2	Monthly yields	381
6.4.3	Maximum feeding temperature – collector performance	384
6.4.4	Potential sorption storage charging performance vs. potential local discomfort	386
6.5	Summary	390
7	Parametrization and algorithms for comfort and annual energy yield modelling in Chapter 08	393
7.1	Dynamic Thermal Simulation Software	393
7.2	Software Limits – Additional Post processing	394
7.2.1	Methodology	394
7.3	Weather – climate regions according DWD	395
7.4	Residential home	396
7.4.1	Calendar	396
7.4.2	Building physics – Residential home	398
7.4.3	Sun Protection	400
7.4.4	Zone Conditioning	400
7.4.4.1	Thermostats	402

7.5	Sun Space	403
.....		
7.5.1	Building physics – sun space	403
7.5.1.1	Aperture opening rules	404
7.5.2	Sun Protection	406
7.5.2.1	Schedule of sun protection (substitute element schedules)	406
7.5.3	Zone Conditioning	407
7.5.3.1	Thermostats	408
7.6	Sun space floor heating	408
.....		
7.6.1	Zone Conditioning	409
7.6.2	Inter-zonal Air Movements (IZAMS)	409
7.7	Collector systems	410
.....		
7.7.1	Sun space roof glazing embedded photovoltaic modules	410
7.7.2	Sun space rafter integrated evacuated solar thermal tube collector	412
7.8	Seasonal energy storage systems	413
.....		
7.8.1	Electro-chemical storage	414
7.8.1.1	DC/AC converter	415
7.8.1.2	Applied pv module-converter-battery algorithms	416
7.8.2	Thermo-chemical storage	417
7.8.2.1	Charging and discharging strategy of sensible and thermo-chemical storage	418
7.8.2.2	The solar thermal collector cycle	419
7.8.2.3	The physical storage systems	419
7.8.2.4	Physical description of the thermo-chemical sorption storage	420
7.8.2.5	Periphery equipment : pumps, heat exchanger, flow heater and free cooler	421
7.8.2.6	The Adsorption process	421
7.8.2.7	The Desorption process	422
7.8.2.8	Applied Sorption storage algorithms	422
8	Comfort and yield analysis of dynamic modelling of passive and active sun space facades	425
.....		
8.1	Evaluation of effectiveness of façade embedded collectors combined with seasonal storages	425
.....		

8.2	Evaluation of dynamic simulation of operative temperature exclusively by passive solar gains	427
8.2.1	Bandwidths of cumulative frequencies of hours with focused operative temperature	435
8.2.2	Cumulative frequencies of hours with focused operative temperature	436
8.3	Operative temperature feasible with embedded PV collectors combined with electro-chemical storage and floor heating	436
8.3.1	Internal surface temperature by façade embedded PV collector	442
8.3.2	Influence on thermal comfort by façade embedded PV collector	443
8.3.3	Auxiliary energy consumption	444
8.3.4	Surplus energy of PV collector – contribution to residential building	444
8.4	Operative temperatures by passive solar gains and façade embedded solar thermal collectors combined with sorption storage and floor heating	447
8.4.1	Internal surface temperature by façade embedded solar thermal collector	455
8.4.1.1	Influence on thermal comfort by façade embedded solar thermal collector	455
8.4.2	Evaluation of energy management	455
8.4.2.1	Surplus energy related to required auxiliary energy	456
8.4.2.2	10% energy substitution by surplus energy - Verification of Hypothesis Vst	457
8.5	Effect comparison of the two different collector and storage combinations	459
8.6	Summary	460
9	Conclusion	463
	References	471
Appendix A	Chapter 01	482
Appendix B	Chapter 02	484
Appendix C	Chapter 03	505
Appendix D	Chapter 04	511
Appendix E	Chapter 08	514
	Curriculum Vitae	523
	Imagery credits	525

# Abbreviations

$\alpha$	Greek alpha: absorption factor
a-Si	amorphous Silicon
AC	alternating current
AC/DC	alternating current
$\alpha/\epsilon$	absorption / emission ratio
AIPOs	alumina-phosphates
AM	Air Mass
AM	ante meridiem
Append.	Appendix
AR	anti-reflective
ASHRAE	American Society of Heating, Refrigerating and Air Conditioning Engineers
AZO	alumina-doped tin oxide
BIPV	Building integrated photovoltaic
Cat.	Category
CE/BCE	Current era/ Before current era
cm	centimeter
©	Copyrights
CMC	carboxy methyl cellulose
CO <sub>2</sub>	carbon dioxide
CPC	Solar compound parabolic collector
CR	climate region
$\Delta T$	temperature difference
°	degree (geom.)
°C	degree Celcius
DC	direct current
dgu	double glazing unit
$\Delta$	difference
DIN EN ISO	Deutsches Institut für Normung, European Norm, International Standard Organisation
DN-KF	nominal diameter, small flange
DoD	Depth of Discharge
DWD	Deutscher Wetterdienst
$\epsilon$	Greek epsilon: emission factor
e.g.	for example

>>>

$\eta_0$	Greek eta: conversion factor
$\eta_{60}$	Greek eta: conversion factor related
e.V.	registered society, eingetragener Verein
et al.	et alterae
Fc-value	shading factor of sun protection device
Fig.	Figure
g	gram
g-value	total energy transmission factor for multiple glazings 0-1 [-]
GJ/m <sup>3</sup>	giga Joule per cubic meter
GmbH	private limited company, Gesellschaft mit begrenzter Haftung
>	greater than
HFK	Hocheffizienz-Flachkollektor
H't value	averaged area weighted transmission factor of total envelope building elements [W/m <sup>2</sup> K]
I-beam	double T steel beam
IEA	International Energy Agency
II	Roman numeral two
ITO	tin-doped indium oxides
K	Kelvin
Kcal/h	kilo calories per hour
kJ/kg	kilo Joule per kilo gram
KNX	building management and control bus standard
kWh	kilo Watt hour
kWh/kg	kilo Watt hours per kilo gram
kWh/m <sup>3</sup>	kilo Watt hours per cubic meter
$\lambda$	Lambda
LT	light transmission factor
L	liter
m	meter
mm	millimeter
m <sup>2</sup>	square meter
mbar	millibar
mbar/d	millibar per day
min.	minute
MOF's	metal-organic matrix materials
MPPT	Multi Power Point Tracking
OSB	oriented strand board
%	per cent
PCM	Phase Change Material

>>>

PD	percentage of dissatisfied
PhD	the doctorate
PID	Potential induced cell degradation
PIK	Potsdam – Institut für Klimafolgenforschung, e.V.
PM	post meridiem
PMV	Predicted Mean Vote
PPD	Predicted Percentage of Dissatisfied
pv	photovoltaic
PVB	polyvinyl-butyl
Tab.	table
3D	three dimensional
SAPOs	silicon-alumina-phosphates
SBS	Sick Building Syndrome
SEI	solid electrolyte interphase
SiC	silica carbon
Tab.	Table
TAS	Thermal Analysis Software, E.D.S.L, U.K.
TCO	transparent conductive oxides
TES	thermal energy storage
TGA	thermogravimetric analyses
TiNOx	Titanate-Sodium-Oxide
TISS	thickness insensitive spectrally selective
TRNSYS®	Transient System Simulation Tool®
TRY	Test Reference Year, Deutscher Wetterdienst
U <sub>g</sub> -value	U-value glazing, transmission value [W/m <sup>2</sup> K]
UV	ultra-violet
V	Volt
V	volume [m <sup>3</sup> ]
V2A	stainless steel
VRLA	valve-regulated lead-acid
W	Watt
Wh/kg	Watt hour per kilo gram
WHO	World Health Organisation
W/m <sup>2</sup>	Watt per square meter
W/m <sup>2</sup> K	Watt per square meter per Kelvin



# Summary

Preparation for fossil fuel substitution in the building sector persists as an essential subject in architectural engineering. Since the building sector still remains as one of the three major global end energy consumer – climate change is closely related to construction and design.

We have developed the archetype sun space to what it is today : a simple but effective predominant naturally ventilated sun trap and as well as living space enlargement. With the invention of industrial glass orangery's more and more changed from frost protecting envelopes to living spaces from which we meantime expect thermal comfort in high quality.

But what level of thermal comfort provide sun spaces? And to what extend may sun spaces manage autarkic operation profiting from passive solar gains and, beyond that, surplus energy generation for energy neutral conditioning of aligned spaces? We deliver detailed information for this detected gap of knowledge.

We know about limited thermal comfort in sun spaces winter times.

This reasons the inspection of manifold collector technologies, which enable to be embedded in facades and specifically in sun space envelopes. Nonetheless, effective façade integrated collectors are ineffective in seasons with poor irradiation. Hence, the mismatch of offer and demand we have experienced with renewable energies ignites thinking about appropriate seasonal energy storages, which enlarges the research scope of this work. This PhD thesis project investigates on both, a yearly empirical test set up analysis and a virtual simulation of different oriented and located sun spaces abroad Germany. Both empirical and theoretical evaluation result in a holistic research focusing on a preferred occupation time in terms of cumulative frequencies of operational temperature and decided local discomfort, of potential autarkic sun space operation and prospective surplus exergy for alternative heating of aligned buildings. The results are mapped geographically for Germany.

Fossil fuel substitution, as far as this thesis elaborated, is closely related to quality of thermal comfort, sun space orientation and energetic standard of the aligned building. Unexpectedly, spaces, which define envelopes incorporating collectors in combination with storage technologies both profit and suffer to some extend in respect to thermal comfort.

Essentially, we can conclude, that the more area-wise efficient and the more integral the collector technology is incorporated into façade design, the more distinct significance of thermal comfort quality and fossil fuel substitution is.

Eventually, this dissertation determines the potential of a new generation of sun spaces in the context of energy transition.

# Samenvatting

Een belangrijk doel in de bouwtechnologie is om vervanging te vinden voor het gebruik van fossiele brandstoffen in de bouw. Wereldwijd is de bouw nog steeds één van de drie grootste energieslupers – en klimaatverandering is daarmee sterk verbonden met bouwkundig ontwerp en constructie.

De typische standaard serre is ontwikkeld tot wat deze heden ten dage is: een uitbreiding van de bestaande woonruimte gecombineerd met een eenvoudige, maar effectieve zonzanger. Met de uitvinding en verbetering van modern industrieel glas veranderde de oorspronkelijke oranjerieën steeds meer van vorstbescherming (voor planten) naar een leefruimte waar we hoge comfort- en kwaliteitseisen aan stellen.

Wat voor thermisch comfortniveau verschaffen deze zonkamers? En in welke mate kunnen zelfstandig te regelen serres profiteren van passieve zonne-energie en gelijk het overschot aan opgevangen energie afgeven aan naburige ruimten om deze te klimatiseren? Dit project geeft een precies en gedetailleerd antwoord op dit gebrek aan kennis.

Wat we weten is dat serres een zeer beperkt thermisch comfort in de winter kennen.

Dit geeft aanleiding voor de analyse van veel verschillende collector-technieken, die speciaal in serre-gevels kunnen worden opgenomen. Evengoed blijven in de gevel geïntegreerde collectoren niet erg effectief in seizoenen met weinig zon. Bij hernieuwbare energie sluiten vraag en aanbod vaak niet erg op elkaar aan. Dit zet ons aan het denken over passende seizoensopslag van energie. En dit vergroot de reikwijdte van dit onderzoek.

Het promotieonderzoek gaat over beide; een analyse op basis van een metingen in een proefopstelling gedurende de jaarcyclus en een virtuele simulatie van verschillend gesitueerde en georiënteerde serres op verschillende plekken door heel Duitsland. De evaluatie van deze, zowel empirische als de theoretische data leidt tot een alomvattend onderzoek dat zich richt op de meest gunstige gebruikstijden (van een serre) in termen van cumulatieve schommelingen in gevoelstemperatuur, vastgesteld plaatselijk discomfort, potentieel autarkisch serre-gebruik en anticiperend overhevelen van energie naar aangrenzende gebouwen. De resultaten worden geografisch voor Duitsland in kaart gebracht.

Vervanging van fossiele brandstoffen is, binnen het kader van dit proefschrift, sterk verbonden met het niveau van het thermisch comfort, serre-oriëntatie en het energielabel van het aangrenzende gebouw. Het thermisch comfort in ruimten blijkt onverwacht zowel te profiteren als te lijden van de combinatie van collectors en opslagtechniek in de gevel. Maar uiteindelijk kunnen we vaststellen dat hoe efficiënter het oppervlak wordt benut en hoe beter de collectortechniek in het gevelontwerp wordt geïntegreerd, des te onafhankelijker worden thermische comfort en het gebruik van fossiele energie van elkaar.

Deze dissertatie brengt het potentieel in kaart van een nieuwe generatie serres in het kader van de energietransitie.





# 1 Introduction

---

## § 1.1 Situation and Conflict

---

Although buildings are currently thermally insulated at a maximum level in order to minimize heating energy losses, scientific observations of the last twenty years reveal that beside transport, industry and crafts, buildings in Germany account for an averaged final energy proportion of 30% [1]. This fact is closely related to a building stock whose building physical energetic standard is comparable to the standard of the 1970s. Moreover, investigations show a disproportion of 82% (including 16% for tap water) [2] of the entire final energy consumption regarding building heating, while only 15% covers consumed power. Essentially, residential heating occupies 19,8% of the total end energy demand. Despite the fact that the overall primary energy consumption of Germany has decreased over the last ten years (2004 to 2014) [2], the primary energy demand for the housing sector has increased. The European Energy Agency (IEA) [3] observes a persistent growth of the world population and a strongly related growth of energy consumption and carbon dioxide emissions. The IEA calculated an averaged growth of energy consumption of +1.1% per year. This insistent ascent in demand results in a 37% higher energy consumption in 2040 compared to today. In parallel, this increase congruently results in a rise of carbon dioxide emission of +20% until 2040. The aim of a limited temperature increase of maximum 2°C of the world air temperature is extraordinary difficult to obtain from the IEA's point of view.

In 2009, the Potsdam-Institut für Klimafolgenforschung [4] (PIK) established a concept on how to define and to determine anthropogenic irrevocable impacts on the environment. PIK defines nine planetary limits, which determine resistance and stability of the planetary ecological system. A PIK report from 2015 elaborated that four of nine limits have already been exceeded, namely: climate change, biodiversity, land use and biogeochemical circular flows. Fossil fuels like mineral oil and natural gas together fulfil more than 70 percent of the worldwide primary energy demand [2]. Actually, fossil fuels still play and will play the dominant part in alternating operation modes including renewable energy. Thus, apparently building heating explicitly determines climate change.

Since humans in our modern societies stay indoors for 80% of day time, thermal comfort is a major living space quality.

Maslow (1970), as psychologist, describes humans' needs, aspirations and pursuit of happiness with a five-levelled pyramid. Basic needs placed at the bottom levels of the pyramid comprise physical shelter from external extreme climate impacts and thermal comfort. Thermal comfort was firstly physically determined by Fanger's (1970) energy exchange model.

This model describes sufficient thermal comfort by either comparably low or no losses of heating energy of a human to the ambient environment, or considerably less or no transpiration effort for body cooling in order to adapt to ambient space conditions. Generally, the metabolic effort of a human in order to adapt depends on clothing and activity. If there is no active space heating or cooling, it is only building physical conditions of a space that regulate thermal comfort. These conditions are mainly determined by space enclosing surfaces, i.e. a building's outer shells.

Thus, we can see that beside fundamental physical shelter, interior space quality is basically determined by the effort of a person to adapt to internal climate conditions.

---

## § 1.2 Problem stating

---

"Façades" is a technical term for the outer shell of buildings. Façades form a particular point of focus with present-day technical architectural and engineering research. Ultimately, it is façades which actually transfer thermal energy out of a building. The transfer of heating or cooling energy losses requires active compensation in terms of space conditioning. This forces humans to adapt in metabolic terms. Thus, it is façades which define energy consumption and thermal comfort as well. The worldwide final energy demand rises continually. In this context, renewable energy has established to substitute only 2.5% [2] of the entire worldwide energy demand within the last five decades. Thermal comfort is the main objective in the residential sector and main driver for final energy consumption.

These facts reason thinking about façade technologies and space systems which effectively save energy. However, as explained next, sun spaces as simple façade technology and space system offer a high potential for alternative energy supply as well

as additional contribution for residential buildings. Nonetheless, we still face the lack of knowledge about feasible thermal comfort in sun spaces including the consideration of possible overheating, about a feasible ratio of autarky and feasible ratio of contribution of fossil fuel free heating energy for adjacent residential buildings. Although sun spaces have been popular for many decades and are widely spread, the above described potential is still underestimated and misjudged.

---

## § 1.3 Solution

---

Besides research on thermal insulation technology, research has lately concentrated on technically equipped or “integral” façades. Technically equipped façades gain additional environmental energy. In particular, Knaack [5] puts emphasis on research of integral façades. Thus, he entitles this emerging field of energy and building science ‘performance oriented envelopes’ or ‘multi-functional building envelopes’, which constitutes an innovative branch in modern architecture.

Multifunctional building envelopes manage diversified operations in order to regulate energy fluxes efficiently between spaces and environment and to also provide fundamental functions like natural ventilation or shading. For example, Vollen and Winn, (2014) [6], Rudolph, (2013) [7] or Klein, (2009) [8], concentrate research and development on multifunctional façades. However, spaces can either profit from simple envelopes, which utilizes irradiation for space heating, or from building skins which are partly equipped with collector technologies (Durst, (2013) [9], Gosztanyi, Rennhofer, Zauner, Windholz, (2013) [10]). The latter provide alternative renewable energy for additional space conditioning.

Simple envelopes are typical for sun spaces. Since sun spaces archetypically benefit from an incomparably high ratio of transparency, sun spaces uncompromisingly utilize irradiation for space heating. The benefit of fossil free space heating with regards to sun spaces increases as compared to alternative heating of adjacent living spaces. Thus, as they represent simple space enclosures, sun spaces provide beside the risk of overheating enormous potential for fossil fuel substitution. Since sun spaces adjoin to living spaces and are either planned or later attached, they represent a common and simple construction type. And as they are part of what we consider residential architecture, they either are or can be easily installed many hundred thousand times in Germany. Therefore, sun spaces offer a simple solution with multiplication effect in the framework of an effective energy transition.

## § 1.4 Relevance

Humans qualify spaces unconsciously in relation to the energy they metabolically consume for thermal adaptation. If thermal adaptation requires incomparable high effort or is ineffective, additional external energy is necessary for space heating or space cooling. Thus, thermal comfort in spaces is always a question of external energy. This thesis elaborates descriptive knowledge about thermal comfort and energy contribution of sun spaces and provides a planning tool as the final result that covers all climate regions in Germany.

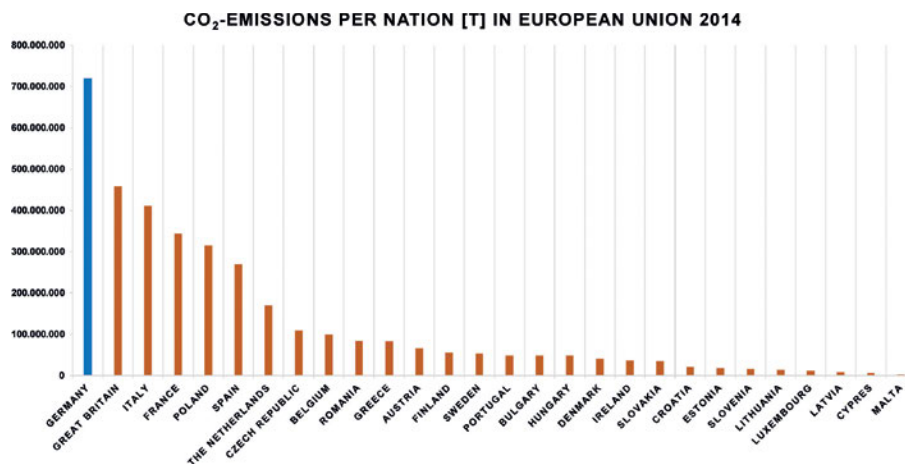


FIGURE 1.1 CO<sub>2</sub> emissions per nation (t) in the European Union in 2014

The German parliament created the “Aktionsprogramm Klimaschutz” [2] on 03.12.2014. This program aims at a CO<sub>2</sub> reduction of 40% until 2020 (Fig.1.1), a reduction of greenhouse gases of 40% until 2030 related to the reference values in 1990. Renewable energy as a portion of all primary energy sources within Europe needs to rise significantly from 15% to at least 27% until 2030. The World Health Organisation (WHO), founded in 1948, defines health as “A state of complete physical, mental, spiritual (added in 1999) and social well-being and not merely the absence of disease or infirmity.” [11](Fig. 1.2). In this context façades meet several present-day macro-economic, social and ecological concerns. Beside the most important benefit of saving natural resources, façades that generate energy contribute to higher macro-economic energy efficiency of the existing public power and heat supply net in general. In parallel, health (Fig. 1.3) and saving natural resources are directly linked to façades.

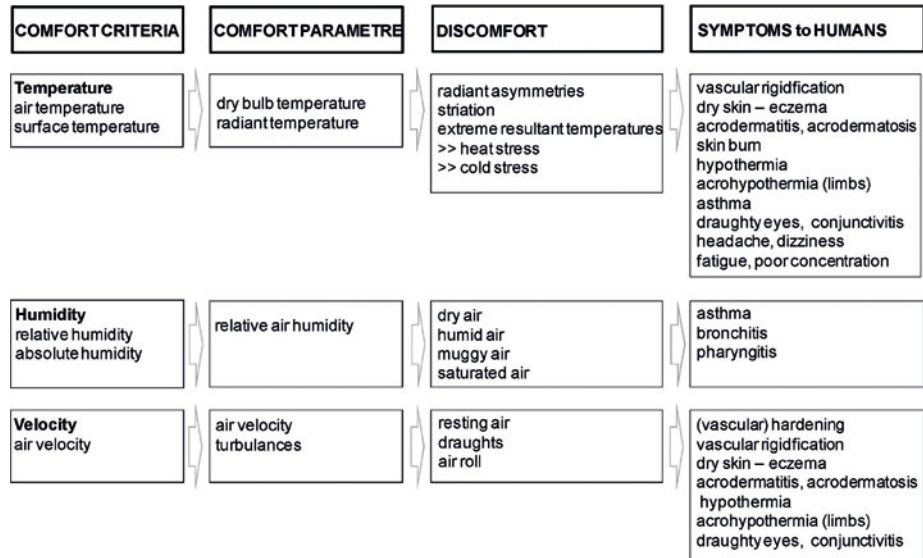


FIGURE 1.2 Exemplifying discomfort related symptoms

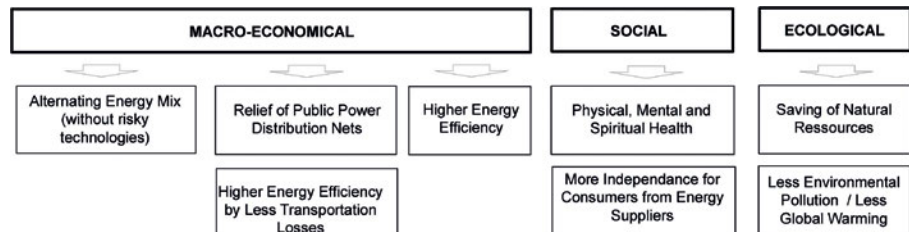


FIGURE 1.3 Relevance and benefits of research in energy generating façades

If we aspire toward energy savings in residential houses or more efficient energy utilization, research in sun spaces is vital and relevant.

---

## § 1.5 Scope: Thermal comfort, façade integrated collectors and seasonal energy storage

---

Vitruvius and Palladio apprehended a balance of light and heat in summer and winter as being essential for our well-being. Environmental qualities are closely linked to architecture and indoor aesthetics. Vitruvius (80 BCE) already wrote about daylight, colours and interior design in the first and seventh of his ten books. Sixteen centuries later, the architect and engineer Palladio defined in *Quattro Libri* rules and recommendations of light suffused space design [12]. A central aspect of his urban mansion and palace design was a courtyard, as can be seen in Palazzo Porte, Breganze, Vincenza (Fig. 1.4). Following these ideals, Alvar Aalto [13] designed light flooded transitional spaces, since he was convinced that sufficient daylight, especially in the northern parts of Europe is essential for health. The sun space at Maison Artek (Fig. 04b) symbolizes his thinking of daylight and health inherence. Sun spaces are transitional spaces implemented in or adjacent to buildings. The outer shells of sun spaces consist of glass-aluminium constructions and are characterized by disproportionately high shares of transparent parts such as glazing.

Typically, sun spaces manage to gain extraordinarily high amounts of solar irradiation. The greenhouse effect causes heating in sun spaces. Hence, generally speaking, sun spaces are the most eligible building construction principle to provide thermal comfort by renewable energy by themselves. Auer [14] shows with the Manitoba Hydro headquarter a keen profanatory building complex that works exclusively with multi-storey sun spaces for year-round heating. Many recent examples of buildings, e.g. the headquarter of the Rijkswaterstaat in Utrecht, the Netherlands, exemplify different scales of well operating sun space applications. This thesis concentrates on 15 to 35 m<sup>2</sup> sized sun spaces that are adjoined to single family homes. Although sun spaces passively provide final energy for heating explicitly by solar gains, they require additional heating energy in winter. As a crucial drawback, passive solar gains and environmental energy in general vary in terms of power and intensity related to geographical location, orientation, daytime and season. Paradoxically, from the perspective of sun spaces this drawback despite generous openings for natural ventilation (fold-works, see Chapter 03) also results in potential overheating during sunny periods. Thermal comfort in sun spaces suffers from deviation by overheating. Whether generous openings for natural ventilation generally manage to compensate deviations is not clear. As a consequence, irradiation especially in winter is proportionally lower in contrast to the extraordinary high heating demand. Thus, the characteristic time shift between offer and demand raises the question for additional collectors that collect environmental energy while being implemented in sun space façades.

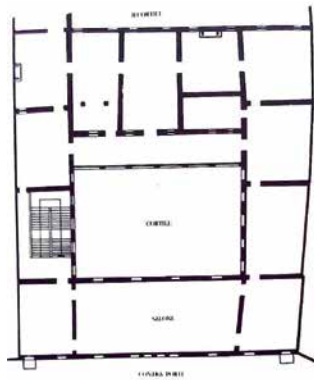


FIGURE 1.4 a.) Floor plan palazzo Porte, Breganze, Vincenca, b.) Sun space of Maison Artek

Moreover, an effective utilization and a considerable proportion of renewable energy of the entire final energy is faced with the problem of temporal fluctuations and, thus, implies the necessity of seasonal thermal loss-free energy storage technology (Hausladen, (2009) [15]; Henning, (2013) [16]; Hohmeyer, (2013) [17]). Therefore, this thesis focusses on an expanded concept of a collector equipped sun space envelope in combination with a loss-free seasonal storage, offering several benefits of energy supply and management. This expanded concept enlarges the utilization ratio of fossil-free energy and contribution for both sun space and single family home.

## § 1.6 Research Question – Knowledge Gap

To what extent sun spaces are able to provide sufficient thermal comfort exclusively by passive solar gains has not yet been identified holistically for Germany. Moreover, missing detailed descriptive knowledge about potential local discomfort constitutes a knowledge gap that has not been investigated by other authors so far.

Research on thermal comfort has been extended within the last years to cover psychological, social and cognitive disciplines. The reason herefor is research, that increases physical perception of thermal comfort to a combined and interacting socio and psychological cognitive impression (Bluyssen, (2009) [18], Heller, (2002), [19]. Since sun spaces profit from nearly 100 per cent transparency, an enhanced perception of the environment opens the stage for enforced psychological and cognitive influence of thermal perception. However, this field of research has been elaborated but is excluded in this thesis.

This research investigates the question what impact renewable energy has, whether this energy is provided by sun spaces as simply passive solar gains or converted by façade integrated collector technology. The relation between thermal comfort in sun spaces and fossil fuel substitution potential has not yet been scientifically investigated. In this field of architecture and building construction, only fragmented laymen knowledge exists based on personal experiences. Furthermore, it has not been evaluated yet how thermal comfort can be improved by façade integrated renewable energy collector technology. The problem of time fluctuations related to renewable energy has been explained above. Hence, it is furthermore of interest to determine the influence of a loss-free seasonal renewable energy storage on thermal comfort in sun spaces. Such an investigation logically leads to the question whether sun spaces could operate autarkic.

In summary, this thesis project focuses on the research question:

*To what extent can energy collectors and seasonal energy storages provide thermal comfort in sun spaces?*

supported by three objectives (see Figure 05):

- *thermal comfort in sun spaces provided by passive solar gains*
- *thermal comfort in sun spaces provided by façade integrated renewable energy collectors*
- *thermal comfort in sun spaces provided by loss-free seasonal energy storages*

Figure 1.5 schematically illustrates the main research question concerning permutable thermal comfort in sun spaces and the three previously determined major complementary objectives, which will be proven as solutions in this research project. These three major objectives describe the fundamental level of investigation and additionally relate to further but minor sub-questions of this thesis.

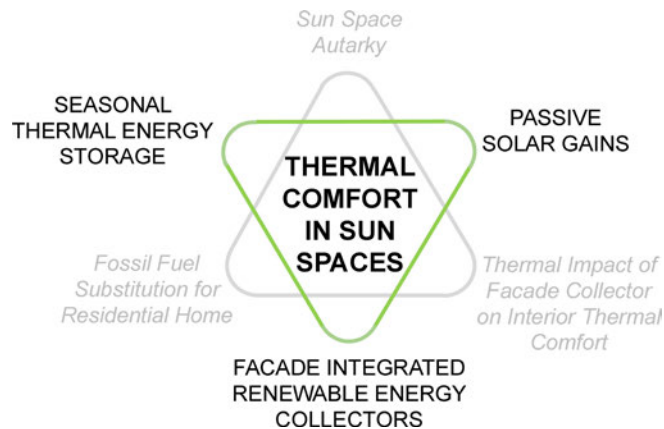


FIGURE 1.5 Triangle of research objectives

## § 1.7 Purpose Statement

With this thesis the author intends to contribute scientific and descriptive knowledge about how sun spaces react building physically on solar gains in terms of permutable thermal comfort related to size, orientation and to the climate region specific meteo-logical impacts of Germany. In this context, sun space size, direction and climate region influence maximum frequencies of annual hours with satisfying thermal comfort.

## § 1.8 Result and Deliverables

The result of this project is descriptive knowledge about cumulative frequencies of hours with satisfying operational temperature mapped for 15 different climate regions in Germany and sufficient sun space orientations. Further, surplus heating energy is going to be investigated, accounting for an increase of annual hours with satisfying thermal comfort. To gain this surplus energy, the thesis inspects additional sun space façade integrated renewal heating energy and power collectors combined with loss

-free seasonal thermal and power storage technology. Besides a product development, the main result of this project is a map with theoretical statistical information about permutable thermal comfort in different climate regions of Germany related to the three above mentioned objectives. As an additional result, this project will provide essential empirical design knowledge about a prototype of a solar thermal collector by which sun space rafters can be equipped integrally. In consequence, this investigation identifies relationships between building physical constraints of sun spaces which causes non-sufficient thermal comfort and performance oriented façades combined with renewable energy storage technology.

By reason of the two chosen objectives building skin integrated renewable energy collector and seasonal loss-free thermal energy storage, this thesis incorporates two subordinate aims. The subordinate aims related to these two objectives are, firstly, to investigate whether sun spaces are to be maintained autarkic and, secondly, whether they can contribute surplus heating energy to adjacent family homes in order to substitute fossil fuels.

Thus, to answer the main and the subordinate research questions, extended research is obligatory.

---

## § 1.9 Research Structure

---

An essential ingredient of this research thesis is empirical investigation on thermal comfort. That is the reason for the erection and empirical measurement of an experimental test sun space. The 25 m<sup>2</sup> sized sun space was designed by Stefan Holtgreife and constructed with SL80© sun space profiles and nobiles© roof profiles by Solarlux GmbH, Osnabrück (Fig. 1.6).

The sun space was situated solitarily without any adjoining living space on the head-quarter site of Solarlux GmbH in Bissendorf, Osnabrück, and equipped with sensors in 2012 (Fig. 1.7). Further detailed information on the sun space is given in Chapter 02. In order to structure this research, different steps have been defined. These steps contribute to the main and subordinate aims.



FIGURE 1.6 Experimental sun space, Solarlux GmbH, Bissendorf

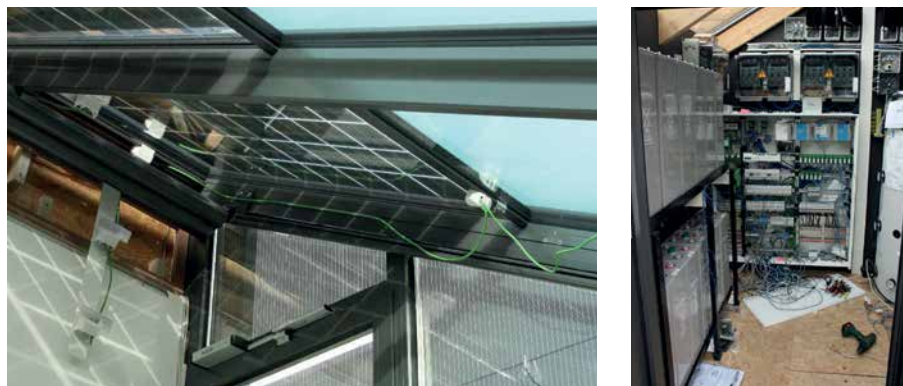


FIGURE 1.7 Diverse interior sensors for real time monitoring, b.) Back space for control and energy storage

Figure 1.8 illustrates the different steps (A to F and 1 to 5) and thereby logical interdependencies between thermal comfort, sun space autarky, fossil fuel substitution and building skin integrated collector technology and seasonal loss-free thermal storage technology. Furthermore, the different steps describe the necessity of different thesis chapters and their logical correlations. Finally, the scheme also explains the research mode; correspondingly, which chapters include literature review, which empirical test set-up evaluations and which the product development. In order to prove scientifically both the research question and sub-questions five hypotheses have been established.

The hypotheses have been formulated with considerable effort to detail. This effort is substantial in order to operationalize and qualify them to be workable. As a result, the hypotheses are extensive and contain numerous technical terms.

CHAPTER	MAJOR RESEARCH AIM	SUBORDINATE RESEARCH AIMS	OBJECTIVES	STEP	RESEARCH MODI
CHAPTER 01				INTRODUCTION	
CHAPTER 02	<b>THERMAL COMFORT in sun spaces</b>		Passive solar gains, Building physical constraints	STEP A	Literature Review + empirical evaluation : Test Set-Up
CHAPTER 03			Building skin integrated renewable energy collectors	STEP B	Literature Review
CHAPTER 04			Loss free seasonal energy storage technology	STEP C	Literature Review
CHAPTER 05			Efficiency of in situ combined system	STEP D	empirical evaluation : Test Set-Up
CHAPTER 06			Product Development	STEP E	empirical evaluation : Test Set-Up
CHAPTER 07			Preparation for Simulation	STEP F	Literature Review
CHAPTER 08				1.) SUN SPACE AUTARKY 2.) FAMILY HOME FOSSIL FUEL SUBSTITUTION	
CHAPTER 09				CONCLUSION	Outlook

FIGURE 1.8 Content and logical order of investigation

5 Hypotheses :

I

.....

*Cumulated frequencies of hours of resultant temperature > 20°C in order to determine indoor thermal comfort in SL80 Solarlux sun spaces according to DIN EN 15251-A regarding south directed 25m<sup>2</sup> dimensioned sun spaces in 15 different climate regions in Germany, provided by renewable heating energy by solar gains exclusively, are less than 1060 hours per annum during autumn to spring time (Oct.-April).*

II

.....

*Cumulated frequencies of hours of resultant temperature > 20°C in order to determine indoor thermal comfort in SL80 Solarlux sun spaces according to DIN EN 15251-A regarding south directed 25m<sup>2</sup> dimensioned sun spaces in climate region -1-, -4-, -5- and -13-, representing four major cities in Germany, provided by renewable heating energy by solar gains and additionally by façade integrated technologies are closer to but not quite 1060 hours per annum during autumn to spring time (Oct.-April).*

### III

---

*Cumulated frequencies of annually 1060 hours of resultant temperature >20°C is realizable regarding indoor thermal comfort in SL80 Solarlux sun spaces according to DIN EN 15251-A regarding south directed 25m<sup>2</sup> dimensioned sun spaces in climate region -1-, -4-, -5- and -13-, representing four major cities in Germany, provided by renewable heating energy by solar gains and additionally by façade integrated technologies in combination with seasonal thermal storage technologies in order to generate renewable energies.*

### IV

---

*The sum of solar gains and additional renewable energies, which are generated by façade integrated collector technologies and seasonally stored with sorption storage technologies in climate region -1-, -4-, -5- and -13-, representing four major cities in Germany, provide at least 20°C resultant temperature based on heating energy autarkic operation from 5 to 10 PM in 25m<sup>2</sup> dimensioned south directed SL80 sun spaces during autumn to spring time (Oct.-April).*

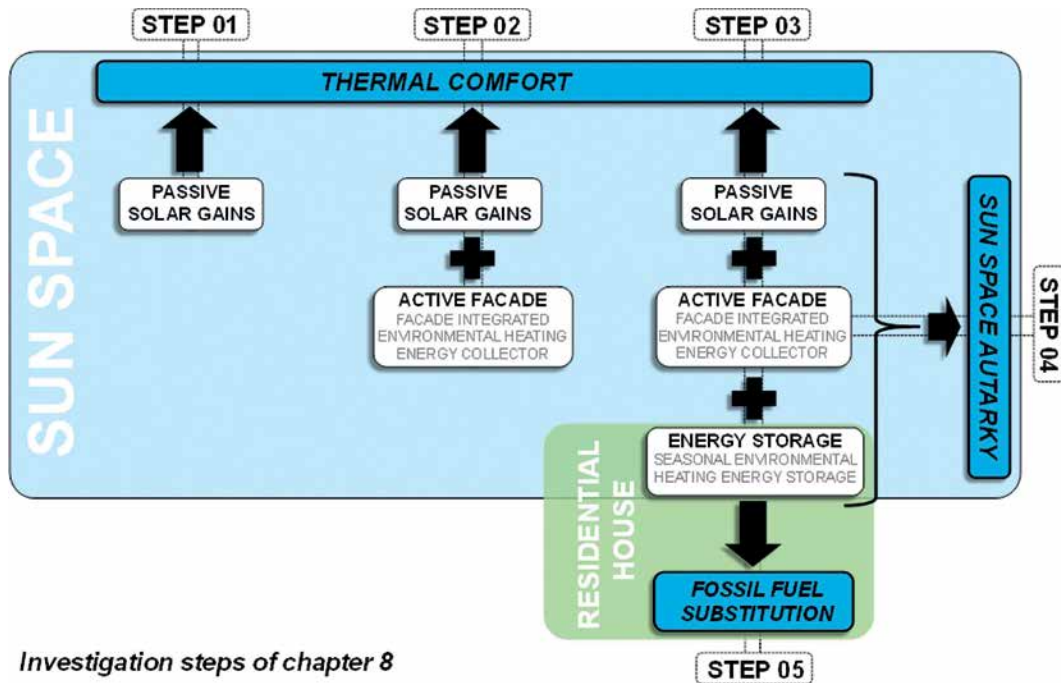
### V

---

*10 per cent of the effective heating energy demand of sun space adjacent residential houses can be substituted by a surplus of solar gains and additional renewable energy that is generated by sun space façade integrated collector technologies and seasonally stored by sorption storage technologies of 25m<sup>2</sup> dimensioned and south directed SL80 sun spaces.*

In particular, chapter 8 aims at a holistic investigational computational simulation research of permutable sufficient thermal comfort in sun spaces. Transferred into a geographical map of the German federal territory, the data is a result of chapter 8. In this context, this chapter combines all previously elaborated knowledge and incorporates it in dynamic thermal simulation models.

Figure 1.8 demonstrates the cascaded model strategy to evaluate the effect of different technology approaches. Accordingly, Figure 1.9 defines 5 different steps in the simulation chapter. Each step of investigation includes the previous but is extended by a sub-question, analogous to an objective of research.



*Investigation steps of chapter 8*

FIGURE 1.9 Steps of investigation in chapter 8

Steps 01 to 03, in particular, address thermal comfort in sun spaces with various model architecture, step 04 focusses on sun space autarkic maintenance regarding sufficient thermal comfort, and step 05 raises attention for surplus heating energy for possible fossil fuel substitution in adjacent residential houses. Since the subordinate aims of step 04 and 05 "Sun space autarky" and "Fossil fuel substitution" imply perfect thermal comfort in sun spaces, they are optional. Hence, they dependent on steps 01 to 03 and coevally on independent variables such as sun space size, orientation, climate region and energetic standard of residential houses.

## § 1.10 Preparation, Limits and Quality of Evaluation

Sun spaces are considered to be naturally ventilated spaces with minor fraction of active heating. For design and research investigations thermal comfort is defined as a statistical term of cumulative frequencies of hours with identified interior resultant

temperatures and relative humidity of ambient air. These cumulative frequencies have to be valued in relation to lower and upper limits of generated floating daily means of external temperature according to DIN EN ISO 15251:2007, Appendix A, A2., category II [20]. For further long-term evaluation of indoor thermal comfort qualities, cumulative frequencies are valued according to method A and B in Appendix H of EN ISO 7730:2005 [21]. In this context, method A helps to evaluate long-term assessment of the winter months, and method B likewise for the summer months.

In this framework, potential local discomfort in particular was inspected for the empirical data set of the experimental test sun space according to EN ISO 7730:2005, section 6 (6.3 – 6.5) with reference to Tab A.1-A.4 in Appendix A. Further information is given in chapter 02. Consequently, sufficient thermal comfort in sun spaces according to regulations is defined in this thesis by a negative hypothesis (cumulated frequencies of hours [...] are less than 1.060 [...]). This basic hypothesis and exaggerated variants have been formulated to execute five different steps of investigation in this project. The hypothesis has to be refuted by experiments and dynamic computer simulations as well.

As a consequence, the triangle of key objectives convinced the author to use well established complex dynamic computational simulation methods and regulations. The purpose of the models is to balance energy flows between sun space and house hourly for an entire annual period. The models allow to simulate a huge number of physical relationships simultaneously and dynamically.

The simulation environment was built with TAS – Thermal Analysis Software, EDSL, U.K., for dynamic space modelling. The model environment additionally allowed to simulate daily yield and resulting space adjoined surface temperature. Hence, modelling enabled to analyse potential negative thermal impact of the façade integrated collectors. The modelling environment was limited to the fact, that daily yields cannot be daily balanced in order to investigate heating effect and thermal comfort improvement. The models also lacked electrochemical and loss-free sorption storages. Thus, the author decided to evaluate the effect of additional collectors and combined seasonal storages separately by post-processing. For that reason, reference thermal comfort and solar yield of collectors were numerically dynamically calculated separately.

Then, the hourly values of thermal comfort and hourly yields were transferred to Microsoft Office EXCEL. Yields were cumulated day-wise and managed in virtual power or heat storages in order to provide and control additional energy for heating. Provided energy was applied for several single days in question and the heating power of the floor heating in TAS was sized for a period from 5 to 10 PM with one preconditioning hour ahead of time.

The days in question with additional floor heating were then simulated once again and the results reviewed in EXCEL. Chapter 7 provides more information on the procedure.

In order to clearly explicate the extent of the models they have previously been reconfigured and calibrated both by results of a three year lasting experimental test set-up and an experimentally proven product development (see chapters 02 and 06). The recalibration allows to simulate possible enlargement of annual heating energy earnings if hypothesis I cannot be refuted. The main quality of the models is the ability to analyse and to synchronize various actions or operations by iteration. Hereby, the models ignore insignificant influences (abstraction) and simplify complex contexts. In addition, physical limits related to independent variables (weather, sun space size, orientation) will be determined, and possible key improvements for physical design can be derived from simulation results. The models are true and reliable to the extent that they operate according to norms and normed algorithms. This attribute makes models comparable and reputable. Results related to the models are no 'precision landings', but they are more than simply trends. Simulation models represent climate regions rather than actual locations exclusively within Germany.

Thus, deductions from climate regions to specific localities and deductions from residential sun spaces to catering spaces or high-rise building sun spaces are not valid. Especially weather data sets (Test Reference Years, TRY, Normales Jahr) do not allow provision for daily meteorological extrema related to global warming. As a summary, the models do not take into account extreme individual behaviour, controlling and adaption of people, extremely populated spatial occupation or physical, technical malfunction. Essentially, these incidents result in an optimized annual performance to what attention should be paid.

This thesis evidences originality and relevance because it holistically evaluates thermal comfort in sun spaces; also regarding envelope embedded collectors. In particular, it investigates local discomfort by empirical evaluation. The thesis investigates the proportions of renewable energy to permute this, feasible autarkic sun space operation and feasible fossil fuel substitution for residential houses. These four reasons make this PhD project original.

## § 1.11 Thesis Outline

The second chapter distinguishes relevant criteria from literature and standards to determine interior thermal comfort in sun spaces. The experimental test set-up in Bissendorf is explained in detail to emphasize and evaluate specifics of construction-building physical behaviour of sun spaces. As a conclusion, sun space unique drawbacks and relationships are determined and compared to information in literature to improve thermal comfort in sun spaces.

Chapter 3 exemplifies by literature review state-of-the-art technologies of envelope integrated collectors for renewable energies. The chapter focuses on photoelectrical and solar thermal technologies. It concludes with recommendations for sun space related technologies and executions.

Chapter 4 demonstrates in more detail the necessity of seasonal loss-free thermal energy storage technology in order to compensate time shift problems related to renewable energy.

The chapter provides explanations of different thermal storage technologies and describes thermo-chemical sorption storages in detail. However, thermo-chemical sorption storages are still on a prototype level; nonetheless, the chapter concludes with detailed information as prerequisite for the dynamic modelling in chapter 8.

Chapter 5 contains a technical description and performance evaluation of the experimental test set-up of a solitary sun space. This was equipped with sun space roof glazing photovoltaic integrated collectors combined with an electro-chemical storage.

Chapter 6 is dedicated to the product development of an envelope integrated collector and gives a technical design description. While this chapter technically entitles all derived decisive performance features, it exemplifies and completes the picture of the selected and promoted technical triple-system (sun space + envelope integrated collector + thermal seasonal storage).

Chapter 7 prepares boundary input data and definitions as parametrization for the holistic dynamic thermal computational simulation study in chapter 8. The preparation is executed along standards and regulations. Moreover, this chapter critically emphasizes the limitations of the models and consequently of the results that can be produced.

After simulation is processed, chapter 8 shows theoretical results and verifies all hitherto determined hypotheses and key questions concerning thermal comfort.

Besides investigation on the system efficiency, impacts on thermal comfort by the envelope integrated technologies will be inspected as well. Moreover, autarky and surplus energy are calculated and evaluated.

Finally, chapter 9 concludes the results in respect to the research questions, the hypotheses and the key questions (Fig.08). Additionally, the methodology and the models are critically inspected and potential for further investigation is determined. The chapter concludes with defining an outlook.





## 2 Literature survey and empirical evaluation of thermal comfort in sun spaces

### § 2.1 The archetype sun space - a constructional differentiation

#### *What are sun spaces?*

Sun spaces and winter gardens (synonym) as they are called colloquially characterizes with light weight constructions of a several decades lasting construction quality (Fig.2.1). Although sun spaces slightly differ from orangeries, green houses, glass houses and glass atriums in terms of construction, they separate significantly in terms of usage. In the past orangeries and nowadays more common greenhouses have contented flowers and plants. Orangeries typically have been very close to manorial buildings and have been intended specially within a representative design context (Fig. 2.2). Green houses on the opposite are enclosed spaces normally separated from greater estates. Normally orangeries and greenhouses prevent flowers and plants during winter time from freezing.



FIGURE 2.1 a.) Rosenberg Residence, Tucson, Arthur Brown, 1946, b.) Ulf residential house, Solarlux

Green houses as well as orangeries as enclosed spaces do not need to be heated mechanically either to promote growing of agriculture or to meet the particular usage. Green houses provide growing and freezing protection only by natural solar irradiation via enormous areas of transparent glazing. The glazing does not actually need to keep heat isolation properties. Glass houses are very close to orangeries, green houses and winter gardens in terms of construction principle. Attached to mostly residential buildings glass houses offer additional living space. Glass houses are by definition equipped with single glazing (Fig.2.3) which comprehends no heat isolation properties. Depending on this construction related properties the availability of glass houses in comparison to sun spaces is straight addicted to external climate. In consequence glass houses do only provide appropriate living qualities when weather is close to interior comfort conditions.



FIGURE 2.2 orangerie a.) palais de verres, b.) of county parliament Mecklenburg-Vorpommern, c.) The Eden project, Rainforest Biome, Cornwall, England

The amount of hours glass houses are appropriate living room extensions are less in comparison to sun spaces. In terms of construction glass houses are simpler sun spaces. Glass atriums base on similar construction principles as the beforehand mentioned typologies [22]. Differences to sun spaces, orangeries and greenhouses can be detected in sort of usage, indoor comfort quality and construction dimensions. Glass atriums normally are used as entrance or exposition areas mainly in non-residential buildings. Significantly for glass atriums through this is short term occupancy and more or less transitional traffic. Typical for glass atriums also is a multi-story elevation. The multi-storey elevation constitutes side walls not necessarily being filigree glass-metal constructions but also being solid. That makes glass atriums attractive as a design component within a non-residential building to enhance sight relations and to express corporate identity for especially passing persons. While long term occupancy is not typical for glass atriums the need for high level indoor comfort is low. As long as extreme comfort conditions are excludable only a minimum conditioning of glass atriums is the standard. By summarizing, glass atriums define as a highly transparent glass-metal constructions but also solid surrounded glass-metal roof closed spaces. Related to the extraordinary space height glass atriums not seldom suffer from draught and elongated time of reverberation. Opposed to that, these aerodynamic and often acoustic phenomena exclude living space conditions.



FIGURE 2.3 a.) solitary glas house (Glashaus), b.) orangerie to café of county parliament Mecklenburg Vorpommern

### *What is especially the use of sun spaces?*

Sun spaces differ in terms of usage from other typologies of glass-metal constructions or living spaces. Sun spaces exaggerate living area. Living sun spaces as conditioned spaces provide comfortable indoor temperatures and allow adjusting temperature, relative humidity and ambient air quality via different façade openings. Winter gardens especially allow a very close contact to nature and environment due to their unique construction principle. In comparison to glass houses, which by definition are not heated, sun spaces are heated and preserve comfort over the entire winter time. This special feature concerning indoor comfort make occupants free to decide if the sun spaces is physically separated from main living spaces or not.

The physical separation in matter of functional or thermal separation normally is executed by a separation wall, respectively a door. The separation also can be realized by a fold work wall. If a fold work wall is established, separation is easily to achieve on demand. Fold-work separations enable (Fig. 2.4) occupants to create individual crossover living areas.

Hereby, occupants are instantly able to adopt to external climate change and to adopt thermal comfort to living space demands. As light weight and optimally suffused with light rooms sun spaces define transitional spaces in residential houses.



FIGURE 2.4 transitional space between cooking and garden, fold-works allow various ventilation openings

### *What are the benefits of sun spaces?*

Sun spaces in general offer several benefits for occupants related to the construction principle.

Beside the additional living area benefit sun spaces light adjacent interiors by natural light as well. Through thermal insulating bearing profiles and glazing the possible occupation time all over the year with appropriate indoor thermal comfort enlarges (Fig.2.5) especially in the intermediate period. In comparison to glass houses sun spaces need less additional energy to be heated.

Related to the insulation qualities of the construction parts solar irradiation is kept for longer time within the space preserving the space from cooling. In consequence, occupants benefit from less end energy consumption normally provided by fossil fuels.

Normally, sun spaces are equipped with several openings as tilt windows, sliding roof windows, fold-works or doors. All these different opening facilities enable occupants to regulate heat, relative humidity and air quality in terms of pollutants easily on demand, either by hand or automatically. Beyond that, opening facilities which are incorporated in winter gardens constructions also partly help to improve indoor quality in solid closed residential spaces.

Especially typologies as winter gardens and atria as transient spaces positively affect a buildings energy performance and stimulate occupants senses [18] in a versatile way as well.



FIGURE 2.5 living space enlargement and physical transitional shelter

### *What is the conflict with sun spaces?*

The filigree glass-metal construction of sun spaces also provides drawbacks. Related to in principle huge transparent envelope areas the immediate impact of external climate condition to interior is high. Sun spaces in principle are configured to gain solar irradiation in winter time, both to ensure appropriate indoor thermal qualities, and if not sufficient, save domestic end heating energy as well. Solar gains can be maximized in sun spaces with heat saving and low emission coated glazings. Consequently, in summer time solar irradiation cause overheating due to the neglected solar protection qualities of the glazing.

Hence, in comparison to solid enclosed living spaces with a minor partition of transparent façade areas, the area specific heating demand is higher. Typical for sun space constructions is a comparably low thermal storage mass of the envelope building elements. Thermal mass is only provided by massive floor building elements and if existing by a massive separation wall. Additionally, beyond winter time sun spaces tend to overheat if solar irradiation is over-averaged or solar shading placed inwards. Overheating is possible in dependency to location within a wide annual range including March and October. Normally, sun spaces are not actively cooled. Natural ventilation by openings as tilt or sliding windows or fold-works not necessarily effects sufficient cooling of overheated sun spaces. Chapter 03 gives further information.

It has to be mentioned, that thermal comfort in sun spaces during irradiation intensive periods - spring or summer - cannot be more comfortable than external climate conditions. Changes in thermal comfort are more often and immediately recognizable in sun spaces than in massive living spaces.

## § 2.2 Description of the Solarlux experimental test-set up : sun space

In the following section an experimental test set up is described, which intendedly erected by Solarlux GmbH in order to examine and evaluate internal thermal comfort. Dimensions, building physical quality, ventilation openings and computer aided controls as well are explained in detail.

### § 2.2.1 Intention of empirical assessment

The test sun spaces was erected in order to measure outdoor and indoor climatic parameter. Primary aim was to evaluate, how and in respect of retardant a sun space in building physical terms react on external climatic conditions and impacts. Hence, beside dry bulb temperature and surface temperature, also relative humidity, irradiation and external temperature as well were recorded and analysed from various perspectives and established technical rules.

### § 2.2.2 Meteorological background

The experimental test set up was built in Bissendorf. Bissendorf, district of Osnabrück, belongs to the county of Niedersachsen and thus is located in the northern western parts of Germany. Bissendorf coordinates with  $52^{\circ} 31' 16''$  North and  $9^{\circ} 44' 26''$  East with 99 m above sea level.

Basic meteorological data are listed in Figure 2.6.

MONTH/ CLIMA	Mean T <sub>ex</sub> [°C]	Mean Global Radiation [W/m <sup>2</sup> ]	Mean Radiant Temperature [°C]	Mean Dry Bulb Temperature [°C]	Mean Resultant Temperature [°C]	Mean Internal Relative Humidity [%]
January	2,2	10	5,1	5,5	5,3	77
February	3,5	36	7,6	8,4	8,0	71
March	7,6	71	15,1	15,9	15,3	52
April	10,3	99	20,0	20,4	20,2	44
May	13,3	112	22,6	22,9	22,7	39
June	17,7	114	27,2	27,8	27,5	43
July	19,5	120	28,7	28,7	28,7	42
August	21,5	117	28,3	28,5	28,4	48
September	15,1	69	21,4	21,7	21,6	53
October	11,9	34	16,5	16,8	16,6	61
November	7,8	23	11,9	12,5	12,2	71
December	8,3	12	10,6	11,2	10,9	75

FIGURE 2.6 Cmean month-wise values of local climate Bissendorf, (test sun space site)

### § 2.2.3 Physical description

The experimental test set-up sun space in Bissendorf as already introduced in 1 is placed on the former headquarter site of Solarlux GmbH. Since it is located on a lawn close to the distribution center, the sun space is erected solitary without any link to any other building. The sun space has overall dimensions of 6,0 by 6,0 m. While the ground area is squared, one equal-sided quadrant of the total ground area is separated for a building service room. Thus, although the main orientation is south, related to all-sided glazing and to the technique space in the north-east quadrant, the sun space consists of a south and a west flank. Both flanks are area-wise equal and form one single room. In account of the spacially separated quadrant, the test sun space additionally benefits from a shortened but glazed east and north façade. Both flanks are enclosed by each a totally glazed roof, that is declined for 30° (Fig. 2.7).

Two opaque separation walls separate the test space from the room for techniques. The technical service room can be entered by a double-glazed alumina framed door with all sided rubber gasket that separate from the test space as well as from the environment

also by a double-glazed alumina framed door. The intermediate door is thermally executed to eliminate both transmission and ventilation losses from one space to another in order to avoid influences on empirical measurement.



FIGURE 2.7 Erection phase, roofing and sensor distribution

### Intermediate walls

---

Furthermore, the separation walls are built by prefabricated timber frame shoring which partitions are filled with 260 mm thermal insulating mineral wool. The walls are planked with oriented strand boards (2x 12mm OSB), with battens for installation and both-sided planked with 2x12 mm gypsum plaster boards. They are finished with a white mineral paint. The walls overtop the roof weathering for 0,8 m and perform two perpendicular attics. The separation walls are founded on the construction floor. The floor construction is made by a frame of wood truss, that is performed to a stiffened plate by joist hangers and OSB boards. Jointings are sealed with wind proved sealing tapes in order to interrupt ventilation losses.

*U-value : 0,09 W/m<sup>2</sup>K*

### Floor and foundation

---

Continuatively, the floor is also thermally isolated in divisions by 280 mm mineral wool. The floor contains 28 mm expanded polystyrene sound protection, a wetting proved foil, a locking plate with floor heating tubing, 48 mm floating floor screed and 10 mm natural floor tile. The flooring is wet-sealed to the sun space vertical façade element, as well as all façade elements are wind-proved sealed by tape to the floor construction.

Thus, ventilation losses via element joints can be obviated. Intermediate walls are intersected and sealed for tubing of the floor heating and power and data wires as well.

The entire wood truss floor construction is carried by a steel I-beam construction that is founded on gridded isolated foundations. The floor is approximately 0,35m above the ground.

*U-value : 0,15 W/m<sup>2</sup>K*

### The vertical facades

---

Vertical facades of the sun space test room are oriented east, south, west and north. The facades are built by alumina profile frames which incorporate either glazings, glazed doors, glazed sliding-shift doors or glazed fold-works. By a length of 6,0m, 3,0 m respectively, the façade frames are subdivided by a grid of 1,0m. Each an element is approximately 1,0 m wide and 2,0 m high. Consequently, since the eaves measure 0,2 m, the upper point of the eaves and junction level of the lower part of the roof is 2,20 above floor, in respect 2,55 m above the ground. The east façade contains a door and an automatic ventilation flap, while the upper trapezoidal part incorporates a tilt window. The south façade includes a door and a three-part fold-work. On the west side, the vertical façade solely incorporates a four-part fold-work, whereas on the north a sliding-shift door is integrated. All fold-works opens towards outside.

*U-value : 1,27 W/m<sup>2</sup>K*

### Roof construction

---

Since the test sun space is a space resulting from a south and a west flank, the sun space is closed by a south and a west roof. Both roof constructions follow the axis of the correspond-*ding* vertical facades.

The roofs start with lower connection joints at +2,20 m above the floor, respectively, +2,55m above the ground and finish at attics in +3,60 m (fig. 17) . Thus, the roofs declination each is 30°. Both roof parts are connected by an arris beam. Each a roof is regularly subdivided asymmetrically by a horizontal crossbar. In the area of the ridge beam two additional divisions are formed by crossbars. Openings in the roofs exclusively in the west roof, what incorporates a AC-current run sliding window in the second last partition. This sliding window provides opened halfway an aerodynamic opening area of 0,29 m<sup>2</sup> (0,45 m<sup>2</sup> x 0,65). Next to the sliding window, the west roof

additionally runs an automatic AC-current roof drum vent Elsner WFL. That drum vent allows a 10 time air change rate per hour on maximum step 10.

*U-value : 1,93 W/m<sup>2</sup>K*

### Natural ventilation

---

Natural ventilation as explained above is possible by divers facilities. The most effective natural ventilation is achievable via fold-works, by reason of the comparable high aerodynamic opening area. The South four-part fold-work allows an aerodynamic opening of approximately 4,88 m<sup>2</sup> (7,5m<sup>2</sup>\*0,65), the west three-part foldwork (Fig.2.8) of approximately 3,57 m<sup>2</sup> (5,50 m<sup>2</sup>\*0,65) respectively. The east and south doors each provide an ventilation area of 1,26 m<sup>2</sup> (1,95 m<sup>2</sup>\*0,65), opposed to that the sliding-shift door on the north side opens with 1,70 m<sup>2</sup> (2,60 m<sup>2</sup>\*0,65). The bottom hung window in the east provides 0,067 m<sup>2</sup> (0,22 m<sup>2</sup>\*0,3) aerodynamic opening area with maximum tilt angel <25°C.



FIGURE 2.8 Rafter construction, openings and sensor distribution

### Sun protection

---

The test sun space benefits from active sun protection. Sun protection is provided by canvas blinds. Since the test sun space roof areas implement collector technology, it was not sensible to arrange the sun protection outwards, nonetheless it is placed inside consequently. The south and the west roofs are protected exclusively the triangular-shaped ridge areas by interior bright and white canvas roller blinds, that are activated automatically by the automatic sun space controls Elsner WS1000. Reason for the

drive by the sun space controls opposed to the central computational controlling system is an elaborated combined sun tracking and sun intensity algorithm of the sun space controls. The  $f_c$ -value of the roller canvas is 0,30 what result in combination with the  $g$ -value of the double-safety glazing of 0,67 in 0,17.

*g<sub>total</sub> : 0,17*

The sun space controls were programmed to activate the roller canvas blind south :

- *with an irradiation exceeding 20.000 Lux,*
- *between an azimuth of 60 to 270°,*
- *a sun height angle between 30 to 90°,*

and initially, when dry bulb temperature *exceeds 22,5°C*. Similarly, the west roller canvas blind is activated :

- *with an irradiation exceeding 20.000 Lux,*
- *between an azimuth of 160 to 300°,*
- *a sun height angle between 9 to 85°,*

and initially, when dry bulb temperature *exceeds 22,5°C*.

### Building physical qualities

---

Figure 2.9 illustrates transmission specified by separate building elements as well as the overall transmission losses accounting for a temperature difference of 30 Kelvin. More detailed building physical information is listed in [APPENDIX A.1](#).

FACADE	BUILDING ELEMENT SPECIFIC TRANSMISSION LOSSES PER K TEMPERATURE DIFFERENCE [W/K]	EXTERNAL/ AMBIENT TEMPERATURE (°C)	TEMPERATURE-DIFFERENCE [K]	ABSOLUTE TRANSMISSION LOSSES OF BUILDING ELEMENT [W]	TOTAL HEAT LOSSES OF SPACE (HEATING LOAD) [KW]
ROOF SOUTH	37,25	-10 / 20	30,0	1117,5	<b>4.286</b>
ROOF WEST	36,86	-10 / 20	30,0	1105,8	
FACADE SOUTH	18,55	-10 / 20	30,0	556,5	
FACADE WEST	18,55	-10 / 20	30,0	556,4	
FACADE ATTIC EAST	5,17	-10 / 20	30,0	155,1	
FACADE EAST	10,12	-10 / 20	30,0	303,7	
FACADE ATTIC NORTH	4,14	-10 / 20	30,0	124,1	
FACADE NORTH	8,18	-10 / 20	30,0	245,5	
FLOOR	3,90	-10 / 20	30,0	117,1	
INTERMEDIATE WALL	2,30	18 / 20	2,0	4,6	

FIGURE 2.9 overall transmission losses of primary building elements – experimental test set-up

## § 2.2.4 Sensor equipment and data logging

The experimental test sun space was equipped with manifold climatic sensors. Sensors were installed outside and inside the experimental set-up in order to measure external climatic impact on the interior space climate. Following, the most important sensor functions and its locations are explained to give an overview of the set-up. Subsequently, sensor types and related standard errors and deviation are exemplified.

### Measure Parameter

Focus of this thesis is an empirical and theoretical evaluation of space interior temperature, mainly operative temperature, relative humidity and surface temperatures.

These interior values are related to external temperature, irradiation, illumination and relative humidity. Beside this main parameters secondary parameters were measured in order to validate the main values and to give more insight in sun space behavior.

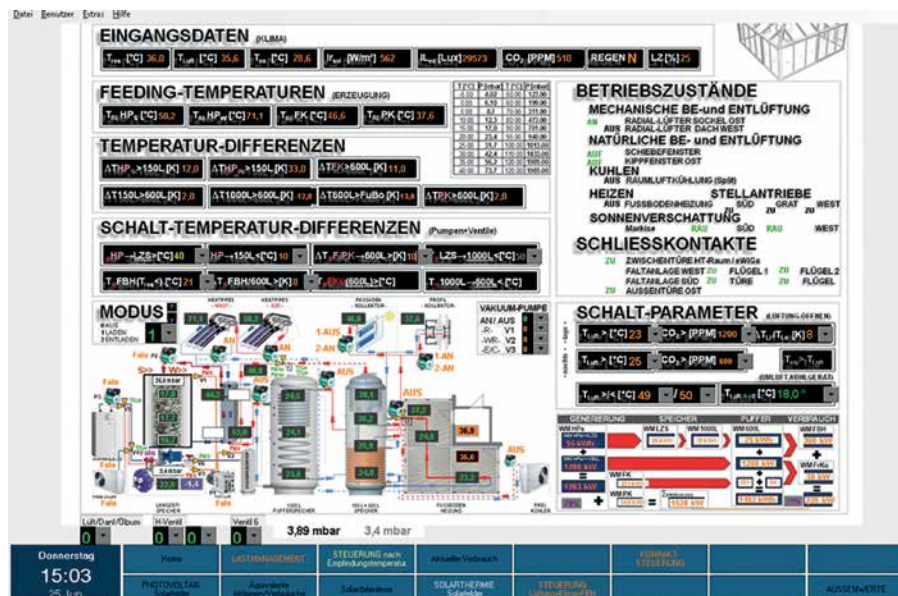


FIGURE 2.10 designed KNX-Eisbaer-control page Steuerung 2.0 for experimental sun space

For example irradiation and illumination were logged inside the space in order to identify day light quality and effecting solar gains in the space after passing double-glazing and internal sun protection. Further, specific building elements like space adjoined surface of rafter or cross beams and ridge profiles have been equipped with temperature sensors in order to detect data for local discomfort evaluations. Moreover, wind direction and wind velocity were measured to gather crucial information for a wind generator installation that is appropriately designed for the specific location sun space roof in Bissendorf. Finally, explicitly temperature sensors were installed in building technical systems like floor heating, roof collector or heat exchanger in order to generate second-wise or by change prevailing information of action (Fig. 2.10).

	No.:	FUNCTION, VALUE	SENSOR-TYPE	MEASURE INACCURACY	VALUE MESSAGING FREQUENCY	LOCATION		
external	01	dry bulb temperature [°C], <i>external</i>	Elsner TH65-AP	- 10°C to +65° "+- 0,5°"	minute-wise	attic north		
	02				minute-wise	attic east		
	03	relative humidity [%], <i>external</i>	Elsner TH65-AP	10 to 90%rF "+- 4,5%rF"	minute-wise	attic north		
	04				minute-wise	attic east		
	05	irradiation [W/m²,global], <i>external</i>	Pyranometer, Elsner KNX PY	> 150 W/m² "+- 15%" of value	minute-wise	attic south, 4,55 m a.g.		
	06	illumination [Lux], <i>external</i>	weather station	0 to 10 klx "+- 20%"; 10 to 150 klx "+- 15%"	minute-wise	attic south, 4,55 m a.g.		
	07	sun azimuth [°], <i>external</i>	Elsner Suntracer KNX-GPS light		minute-wise			
	08	sun height [°], <i>external</i>			minute-wise			
	09	precipitation [Y / N], <i>external</i>			minute-wise			
	10	wind velocity [m/s], <i>external</i>			minute-wise			
	11	wind direction [°], <i>external</i>	rb-messtechnik	signal : 360° >0 to 10V	by-change	attic south, 4,55 m a.g.		
internal	12	dry bulb temperature [°C], <i>internal</i>	Elsner T-100 + KNX T-UN-100/130	at 25°C; "+- 2,5°" in - 30°C to +70°	by-change	pendulum south, 1,10 m a.f.		
	13				by-change	pendulum south, 1,70 m a.f.		
	14				by-change	pendulum west, 1,10 m a.f.		
	15				by-change	pendulum west, 1,70 m a.f.		
	16	surface temperature [°C], <i>internal</i>	Elsner T-100 + KNX T-UN-100/130	at 25°C; "+- 2,5°" in - 30°C to +70°	by-change	facade east, 0,15 m a.f.		
	17				by-change	facade east, 1,70 m a.f.		
	18				by-change	facade east, 2,45 m a.f.		
	19				by-change	facade south, 0,15 m a.f.		
	20				by-change	facade south, 1,70 m a.f.		
	21				by-change	roof south, 2,45 m a.f.		
	22				by-change	facade west, 0,15 m a.f.		
	23				by-change	facade west, 1,70 m a.f.		
	24				by-change	roof west, 2,45 m a.f.		
	25				by-change	facade north, 0,15 m a.f.		
	26				by-change	facade north, 1,70 m a.f.		
	27				by-change	facade north, 2,45 m a.f.		
	28				by-change	floor screed south, center		
	29				by-change	floor screed west, center		
	30		minute-wise	arris beam, 2,45 m a.f.				
	31	surface temperature [°C], <i>internal</i>	Elsner KNX AQS/TH-B-UP	at 25° "+- 0,4°"	by-change	intermediate wall north, 0,15 m a.f.		
	32				by-change	intermediate wal north, 1,70 m a.f.		
	33		Elsner KNX TH-AP	at 25° "+- 0,9°"	by-change	intermediate wall east, 0,15 m a.f.		
	34				by-change	intermediate wal east, 1,70 m a.f.		
	35		Elsner KNX TH-AP	at 25° "+- 0,9°"	minute-wise	ridge profile south, 3,60 m a.f.		
	36				minute-wise	ridge profile west, 3,60 m a.f.		
	37				minute-wise	cross beam profile south, 3,00 m a.f.		
	38				minute-wise	ridge south above internal roller blind		
	39	relative humidity [%], <i>internal</i>	Elsner KNX TH-AP	20 to 80%rF "+- 3,0%rF"	minute-wise	eave south, left, 2,10 m a.f.		
	40				minute-wise	eave south, right, 2,10 m a.f.		
	41		Elsner KNX AQS/TH-B-UP	+ 5% rF	minute-wise	eave west, left, 2,10 m a.f.		
	42				minute-wise	eave west, right, 2,10 m a.f.		
	43				minute-wise	intermediate wall north, 0,15 m a.f.		
	44				minute-wise	intermediate wal north, 1,70 m a.f.		
	45				minute-wise	intermediate wall east, 0,15 m a.f.		
	46				minute-wise	intermediate wal east, 1,70 m a.f.		
	47	illumination [Lux], <i>internal</i>			Siemens AP 255/12 Helligkeitsregler	0 to 2000 lx at 30% reflection	minute-wise	pendulum south, 1,10 m a.f.
	48						minute-wise	pendulum west, 1,10 m a.f.
	49	irradiation [W/m²], <i>internal</i>	Pyranometer, Elsner KNX PY	> 150 W/m² "+- 15%" of value	minute-wise	ridge south above internal roller blind		
	50				minute-wise	ridge south beneath internal roller blind		
	51				minute-wise	ridge west above internal roller blind		
	52				minute-wise	ridge west beneath internal roller blind		
	53	carbon dioxide [PPM], <i>internal</i>	Elsner KNX AQS/TH-B-UP	"+- 50 PPM"	by-change	intermediate wall north, 0,15 m a.f.		
	54				by-change	intermediate wal north, 1,70 m a.f.		
	55				by-change	intermediate wall east, 0,15 m a.f.		
	56				by-change	intermediate wal east, 1,70 m a.f.		
	57	make contact element (openings)	Jung reed-contact sensor, FUS4410WW	max. 40V, 1-pole, 0,5 A	by-change	tilt-window east, 2,70 m a.f.		
	58				by-change	door east, 2,10 m a.f.		
	59				by-change	threepart fold-work south, 2,10 m a.f.		
	60				by-change	door south, 2,10 m a.f.		
	61				by-change	fourpart fold-work west, 2,10 m a.f.		
	62				by-change	roof sliding window west, 3,40 m a.f.		
	63				by-change	intermediate door towards technique room		
					by-change	technique room external door		

FIGURE 2.11 Technical survey of applied sensors and digital measurement components

Figure 2.11 tables all integrated sensors and recorded climate parameters.

## § 2.2.5 Control and Monitoring and signal definition

---

The entire test set up system was controlled by two different control systems. The first system was an automatic sun space control unit with touch screen placed on the north wall in 1,70 m height above the floor. This control is called WS1000 Color by Elsner Elektronik GmbH. WS 1000 is an KNX-Bus-based control system exclusively designed to process KNX-Bus-based sensor data and to control 12 different actuators. The exclusively task of the WS1000 Color unit was to control the south and west interior sun protection roller canvas blinds, because of a elaborated algorithm considering space coordinates, sun height and sun azimuth according to date and day time.

The second controls was designed with a content based plug&play KNX-Bus-based software called Eisbär®, the busbaer® from Alexander Maier GmbH. The software run the version 1.8.00 – architect (2013) and actually 42 pages were programmed and partly run simultaneously during the project. A personal desktop computer run the software, while being linked to the closed internal KNX-Bus-network by Elsner Power Supply KNX PS640-IP network module, what splits and decodes 20 Volt signals of the decentralized sensor group modules into Eisbär® processing code. Summarized, the Eisbär software allowed to trigger sensor signals once a minute either minute-wise or simply by defined change and reverse to activate determined channels of multiple actuators by which certain devices were set on or off. By software, firstly sensor data was converted or set in specific numerical relation (coefficients) like operational temperature or percentage of gained energy in relation to annual demand data was secondly processed in logics with Boolean operators for further limit-based sub-controls of devices like floor heating or collector pumps or gear control of motorized windows.

Thirdly, status response signals of the actuator channels as well as for example temperature, humidity or carbon dioxide sensors were logged minute-wise and group-wise in a software chronological data base for later access. Moreover, all openings in the envelope and in intermediate walls towards the technical service room as well were equipped by read-sensors. These read-sensors by current signals also allowed to supervise and retrace opened devices time-wise in order to detect minutes, hours and days of disrupted test conditions (figure 11).

## § 2.2.6 Solar thermal tube collectors attached to sun space façade

With subject to the product development HEATBEAM I© and an empirical evaluation of façade integrated collectors, evacuated tube collectors were mounted on the roof rafters of the test sun space. As solely attached tube collectors they are a primary step of rafter integrated renewable energy collectors. This section explains dimension, amount and power of the collectors and their integration into the heating system.

Evacuated tube collectors, respectively heatpipes (also see Chapter 06), were chosen, since they offer opportunity to arrange axis-wise on or in rafters. Hence, spaced occupants profit from an axis-wise arrangement since the arrangement has no impact on optical and perusal quality. Thus, with evacuated tube collectors, a collector typology is applied, which on the one hand provide high area-wise efficiency (60-70%), high feeding temperature ( $>120^{\circ}\text{C}$ ) with subject to seasonal sorption storage technology and does not minimize perusal in any way.



FIGURE 2.12 a.) tube circuits, b.) rafter attached evacuated tube couples, c.) sensible 750 l tank

Figure 2.12 shows a schematic arrangement of the tubes. The south oriented rafters were equipped by tubes of 0,8, 1,5 and 2,0 m length, as well as the hip rafter and the west roof rafters. Each a rafter was equipped with couples of tubes, which were distanced to the rafter by 80 mm. Heat exchanger were couple-wise arranged above the lower and upper circle. Hence a south circuit and a west circuit, including the hip rafter, were established. Since the maximum power of the 56 mm tubes related to length ranges between 28 to 76 W, the south circuit provided a maximum power  $p_{\text{peak}}$  of 1.250 W, while the west circuit provided a power of  $p_{\text{peak}}$  : 1.196 W. In total, the entire plant provided maximum 2.446 Watt.

The solar thermal tubes were characterized by the following technical parameters :

$$\eta_0 = 0,75$$

$$\eta_{40} = 25 \text{ to } 68 \text{ kWh/a with STG } 1.000 \text{ W/m}^2 \text{ and } \Delta T = 40 \text{ K}$$

$$a_1 = 1,12 \text{ W/m}^2\text{K}$$

$$a_2 = 0,004 \text{ W/m}^2\text{K}^2$$

$$d = 56 \text{ mm}$$

Solar thermal heat was transported to service room (4. Quadrant) and fed a 150L volume within a 600 L tank. The tank was thermally insulated by 50 mm poly-urethane foam with  $\lambda = 0,040 \text{ W/m}^2\text{K}$ . The transport fluid was equipped by 30% with a freezing agent, hence the heat capacity was determined with  $3,65 \text{ kJ/kg}$ . Each of the two circuit pumps run on low-flow with hourly volumes of  $0,180$  to  $0,250 \text{ m}^3$  per hours and started at a temperature difference of  $>8\text{K}$ . Every 5 minutes, the pumps started for 15 seconds to flush the T-100 temperature sensor with the hottest medium provided by the collectors. Thus, the  $2.500 \text{ W}$  solar thermal plant charged a  $750$  volume. The volume itself supplied two floor heating circuits with heat.

---

## § 2.3 Thermal comfort - an interior space quality

---

*"We spend more than 80 per cent of our daily lives indoors" [18]*

By evolution humans attend to be in balance with their body and the immediate environment. This environment can be nature in general or enclosed spaces, which shelter from extreme climatic conditions in nature. Humans have the need to be sheltered against extreme climatic conditions. Extreme climatic conditions evoke stress on human bodies in order to regulate, either to adapt to external dominant climatic conditions or to keep preferred status of well-being. This stress forces human to react on climatic deficits and to spend metabolic energy on adaption.

Well-being in general is a status for human beings when firstly the necessity and secondly the amount of energy required to comprehend metabolic deficits is comparably low. Maslow (Fig. 2.13) defined the pyramid of human's seven basic needs.

Indoor environment is the sum of various interior physical status which define human well-being. Major criteria that can be physically determined are thermal comfort, indoor air quality, visual and lighting quality and acoustical [23] quality as well. Thermal environment is defined by ASHRAE Standard 55 (2010) [24]: “The characteristics of the environment that affect a person’s heat loss.”

- *Thermal comfort*
- *Indoor air quality*
- *Visual lighting quality*
- *Acoustical quality*

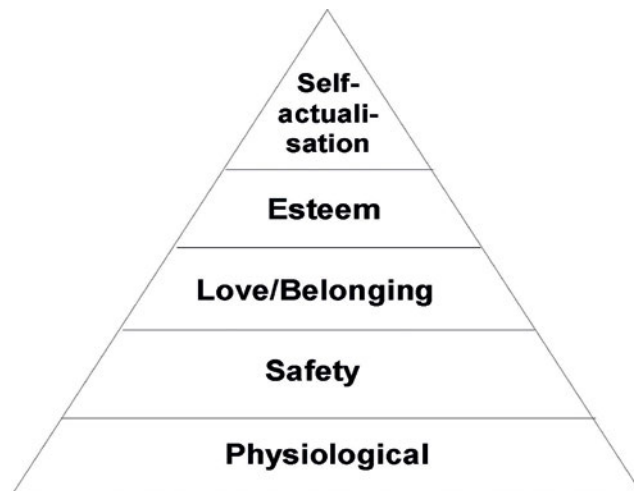


FIGURE 2.13 Maslow’s hierarchic pyramid of needs

According to ASHRAE standards [24] thermal comfort is “[...] that condition of mind that expresses satisfaction with the thermal environment and is assessed by subjective evaluation. “Most disorders or even diseases are linked to environmental air and thermal comfort and less acoustical and lighting specifics. As a major cause for comfort complaints and a decrease of productivity thermal discomfort have been determined in literature. Individual’s productivity has been related to air quality by the Lawrence Berkeley National Laboratory in means of 13 per cent higher with better air quality [14].

Direct access to daylight enhances productivity between 15 to 50%. These actions are controlled by two parts of the brain named anterior and posterior hypothalamus (Bluyssen, 2009).

---

## § 2.4 Milestones and divers approaches in research of thermal comfort

---

### SICK BUILDING

---

At the beginning of the 1980 years it became obvious by extended epidemiological studies in focussing of office buildings that insufficient internal conditions are called sick-building-syndrome (SBS). Spengler et al. (2001), Burge et al. (1987), Skov et al. (1987), Preller et al.(1990) report about that. In the 1990ties it was realized that complaints, disorders and diseases are not solely caused by one single parameter, but by a mingle of parameters what makes detection and prevention more complex.

It became of interest to know what inter-relations between different parameters provoke SBS. Research has to be aware of specific application and thus of synergistic effects. It was found that mechanically ventilated buildings have more symptomized workers than naturally ventilated ones. Even women are more sensible to these affects than men.

These problems occur the most in public sector buildings than comparably in private sector buildings. It was revealed that the higher the social status, the salary and the encouragement of employees the greater the acceptance of indoor environment status and on the contrary then little are the symptoms. In literature two different approaches have been estimated within the last forty years to estimate quality of thermal comfort [23]. The older one is a mathematical method regarding the energy balance of humans in interaction with their indoor environment (Fanger).

This method bases on calculations of energy losses or wins of humans in relation to their actual activity, their kind of clothing and its correlated ratio of thermal insulation and the actual space air temperature and space defining surface temperatures. The before described method is also known as 'heat balance method'. This model is going to be explained in more detail first.

## § 2.4.1 The heat balance model

---

### Environment and Equilibrium

---

The heat balance method bases on the perception of humans maintaining their bodies in thermal balance. Balance is accomplished with heat losses and heat production gained in equilibrium. The human body keeps different temperatures in different body parts to ensure diversified vegetative (metabolic) actions. The mean body temperature is about 37°C, the mean skin temperature is closely to 34°C. Literature defines the physiological zero point – the temperature between 28 and 33°C at what for humans no temperature sensation is possible. A temperature of 37°C [14] is important to keep all vital functions on going. If body temperature falls below 33°C humans suffer from moderate hypothermia, if it falls below 25°C humans suffer from death risk. On the other hand a body temperature above 41°C means very high fever what results in circulatory failures. Circulatory failures themselves can end up in death above a body temperature of 42.6°C. In this context the human body does have heat storage capacities.

In case the temperature difference between the mean body temperature and the space environment is to large the human instinctively react to compensate the difference and to regain the body mean temperature. For this control mechanism human rely on multiple temperature receptors in different parts of the skin and mucous membranes. These are the only parts of human body to detect temperature. Partition of cold and warm temperature receptors differ significantly from ten per square centimetre for cold and only one per square centimetre for heat.

### Metabolism

---

In concern is taken the mean body temperature, the temperature of vital organs and the skin.

If the body temperature starts to increase because of significant heat losses towards the environment the organism begins to exploit before collected nutrients. Nutrients are converted by combustion into heat energy which rises the body mean temperature. About 100 kilocalories per hour (kcal/h) provide 120W body heat [14].

Nutrients combustion in humans causes exhausts in terms of carbon dioxide (CO<sub>2</sub>), which are removed from the organism via blood vessel distribution to the lungs (4.4%)

of entire air change volume) and emitted to the environment. This humane corporal regulation method is called metabolism. Metabolic conversion of nutrients is an unconscious action of the automatic vegetal nervous system. The metabolic rate of a comfortable feeling human is equal to averaged heat loss of  $58.15 \text{ W/m}^2$  skin. This is equal to  $100 \text{ W}$  by a body surface of  $1.7 \text{ m}^2$ .

Before further detailed information the author gives substantial definitions on crucial parameters :

### Ambient air and clothing – two decisive parameters on proper metabolism

---

Basic point of human energy losses is radiation. Radiation means that objects radiate energy if other objects in the close surrounding remain significant lower surface temperatures than the object in question. Hence, if surface temperatures enclosing a space reveal low temperatures, humans tend to radiate. Energy from humans is attracted via electromagnetic waves by low temperature surfaces.

However, objects radiating energy via electromagnetic waves effect molecules of the ambient air on the way to low temperature objects. Air molecules can be effected by human radiation and can be stimulated to move faster [25]. Consequently, human being's electromagnetic radiation induces ambient air molecules to move in a different way or frequency. In any case of ambient air with significant low temperature humans tend to lose energy via convection. Nevertheless, moderate surface temperatures in relation to mean body temperature, clothing rate and activity draw more decisive effect on thermal comfort and energy savings as well as moderate ambient air temperature.

Logically, the only active control humans have is clothing and activity. With clothing and activity ( $5 \text{ W}$  while sleeping,  $400 \text{ W}$  while running) humans can compensate heat discrepancies partly. Nonetheless, also adaption of clothing is physically limited and grades of activity considering infant, elderly or disabled human beings as well. Air normally is a low heat conductor. Heat losses to a cubic volume of ambient air are 3.200 times lower than to comparably a volume of water. In order to conclude, humans inevitably loose energy to the environment by radiation and convection.

In particular, radiation bases physically spoken on emission of electromagnetic waves.

Humans exchange air to emit incorporated pollutants and exhausts and to regain oxygen. As a major-vegetative mechanism breathing is essential for human metabolism and survival. During breathing also humidity [14] within the exchange air volume is emitted to the ambient environment (in relaxed state :  $19 \text{ W}$  exhale,  $3 \text{ W}$

sensible heat, 22 g of water). Humans also lose humidity via the skin. Skin concerned humidity losses are caused by perspiration or easily vaporization. The human body contents about two to four million respiratory glands. Essentially, loss ratios of humidity via breathing and skin vaporization have been investigated to be 99% to 1% (Transsolar, 2009).

### Reactive actions as counterpart of metabolism

---

Mechanisms of unconscious heat loss, which humans can not actively influence are based on the above mentioned radiation, convection and evaporation, account of the apportionment of approximately 33%. Opposed to that humans assess diverse mechanism to compensate heat losses. Also these diverse mechanisms are controlled vegetative.

*This reactive actions are reactions of heat losses :*

- *shivering*
- *blood vessel constriction*
- *vascular constriction*
- *blood flow acceleration*

*in case of heat gains : perspiration*

- *blood vessel extension*
- *vascular relaxation*

Summarized, thermal comfort mainly is predominated by mechanisms like radiation, convection and evaporation in physical terms what humans are not able to control actively, consciously respectively. Heat losses via conduction, as explained before, can consciously be avoided. Thus, thermal comfort engineering has to concentrate on the beforehand mentioned three mechanisms.

Furthermore, engineering in this has to be aware of diverse groups of individuals are not enabled to compensate and improve their immediate thermal situation by all possible mechanisms. In some cases architects and engineers have especially to plan for these groups of individuals with obvious lacks of autonomy in activity.

In this context, Fanger introduced basic tools for comfort engineering. These models include a model to predict the predicted mean vote (*PMV: predicted mean vote*) of space specific thermal comfort of a large group of space occupants and a model for *predicting the percentage of dissatisfied space occupants (PPD)*. The models were developed huge diversified evaluations and occupant investigation Fanger did in front.

## FIRST APPROACH

---

Fanger describes the heat balance model by formula :

Heat production = heat dissipation

$$\begin{aligned} M - W - q_d - q_w - q_{re} - q_l &= q_t & (01) \\ &= q_c + q_r \text{ [W]} \end{aligned}$$

where :

$M$  = metabolic rate of human body [W]

$W$  = external mechanical power [W]

$q_r$  = heat transfer via conduction through clothing [W]

$q_c$  = heat transfer via convection from a clothed body [W]

$q_r$  = heat transfer via radiation from a clothed body [W]

$q_d$  = heat loss by water vapour diffusion through skin [W]

$q_{sw}$  = heat loss by sweat evaporation [W]

$q_{re}$  = heat loss by latent respiration [W]

$q_l$  = heat loss by dry respiration [W]

Normally humans are clothed in civilized societies. Clothing in thermodynamic matters functions as thermal isolation. Thus, all heat that leave a body via radiation and evaporation across the skin firstly need to be conducted through clothing. As we already

highlighted before, heat losses of humans by radiation are significantly high and can be described as :

$$Q_r = A_{\text{eff}} \epsilon \sigma (T_m^4 - T_{\text{mrt}}^4) \text{ [W]} \quad (02)$$

where :

$A_{\text{eff}}$  = the effective body surface area = f x surface area of body (f depends upon position and on type of clothing) [m<sup>2</sup>]

$T_m$  = mean temperature of body surface (clothed and unclothed areas) [°C]

$T_{\text{mrt}}$  = mean radiant temperature [°C]

Parallel, heat transfer via conduction through clothing can be expressed by :

$$q_t = A(T_s - T_{\text{clo}})/0.155 I_{\text{clo}} \text{ [W]} \quad (03)$$

where :

$T_s$  = temperature of skin [°C]

$T_{\text{clo}}$  = temperature of clothing [°C]

$I_{\text{clo}}$  = thermal resistance from the skin to the outer surface of the clothed body (clo)

In this context is to be explained the specific conductance value of clothing:

$$h_c = 2.38 (T_m - T_a)0.25 \quad \text{for } 2.38 (T_m - T_a)0.25 > 12.1\sqrt{v} \quad (04)$$

$$\text{and } 12.1\sqrt{v} \quad \text{for } 2.38 (T_m - T_a)0.25 \leq 12.1\sqrt{v} \quad (05)$$

(with v = air velocity in cm/s)

Finally, heat emission of a human (man) via convection can be calculated by :

$$q_c = A h_c (T_m - T_a) \text{ [W]} \quad (06)$$

where :

$A_c$  = mean body surface area in standing position in  $m^2$  (for a man this is  $1.8m^2$  and for a woman  $1.65m^2$ ; for a sitting person, 75 per cent is taken);

$T_m$  = mean temperature of body surface (clothed and unclothed areas) [ $^{\circ}C$ ];

$T_a$  = air temperature in the space [ $^{\circ}C$ ]

#### Definition of Predicted Mean Vote (PMV) :

---

“An index that predicts the thermal sensation of a person for a certain combination of environmental parameters and a known clothing resistance and metabolism. The thermal resistance of clothing is expressed in clo. One clo is defined as the thermal insulation required to keep a sitting person comfortable, with a temperature of  $21^{\circ}C$  (SIO, 2005). The PMV index predicts the mean value of the thermal sensation votes of a large group of people on a seven-point scale (+3 : hot; +2 : warm; +1 : slightly warm; 0 : neutral; -1 : slightly cool; -2 : cool; -3 : cold).

The PMV is deducted for stationary conditions, but can also be applied for small fluctuations of more than one variable if the mean of these variables during one hour earlier is applied. PMV values should only be used for values between -2 and +2, and only if the six main parameters lie in the following ranges.[18] ”:

$M$  = metabolism :  $46-232 W/m^2$

$I_d$  = thermal resistance of clothing :  $0-0.310 mC/W$ ;

$T_a$  = air temperature :  $10^{\circ}$  to  $30^{\circ}C$ ;

$T_r$  = mean radiant temperature:  $10^{\circ}C-40^{\circ}C$ ;

$V_a$  = air velocity:  $0$  to  $1 m/s$

$P_a$  = partial water vapour pressure :  $0$  to  $2700 Pa$

The PMV index helps to identify and to readjust operative temperature in ranges when thermal comfort is appropriate.

### Definition Predicted Percentage of Dissatisfied (PPD):

---

The predicted percentage of dissatisfied (PPD) is an calculated index which basing on PMV outcomes defines how many people will still stay uncomfortable although the greater figure of occupants are feeling well.

$$PPD = 100 - 95 * \exp(-0.03353 * PMV^4 - 0.2179 * PMV^2) \quad [\%] \quad (07)$$

The following definitions give better understanding of the before mentioned terms:

### Definition of mean radiant temperature (tr) :

---

“The uniform surface temperature of an imaginary black enclosure in which an occupant would exchange the same amount of radiant heat as in the actual non-uniform space.[18]”

### Definition of thermal sensation :

---

“A conscious feeling commonly graded using the categories cold, cool, slightly cool, neutral, slightly warm, warm, and hot; it requires subjective evaluation.[24]”

### Definition Operative (resultant) temperature (top) :

---

“The uniform temperature of a black environment in which a person exchanges the same amount of heat via radiation and convection as in a real non-uniform environment. In most cases, if the difference between the mean radiant temperature and the air temperature is small (<4°C), the operative temperature is calculated as the mean of air temperature and the mean radiant temperature.[18]”

Beside determinations of thermal comfort by solely heat balance calculations and subsequently PMV and PPD calculations, thermal comfort can be defined by in particular local thermal discomfort inspections. Local thermal discomfort has been identified in terms of vertical sensible ambient air (dry bulb) temperature differences, what physically appears as striation, in terms of sensible radiant temperature differences of facing and space enclosing building surfaces (radiant asymmetries) and floors, that are perceived as too cold or too warm.

Definitions below further exemplify:

#### Definition of vertical temperature difference (striation) :

---

“A large vertical temperature difference between head and ankles: between **0.1 m** and **1.1 m above the floor.**”

#### Definition of radiant asymmetry :

---

“Caused by warm ceiling (vertical direction) or a cold window or another cold vertical surface area (horizontal direction) [Blyussen].” Or “The difference between the plane radiant temperature of two opposite sides of a small plane element.[24]”

### § 2.4.2 The Adaptive Comfort model

---

#### THE SECOND APPROACH

---

The second major further development in thermal comfort research has been developed in the seventies and eighties of the former century. This development concentrates on an exaggerated derivation of the heat exchange method. Similar to the heat balance model does this approach focus on heat balances of humans in relation to their environment, but is exaggerated by cognition of humans tolerating a more wide indoor temperature range in especially naturally ventilated spaces. Thus, this approach bases essentially on the opportunity to self-control openings for natural ventilation. Humphrey and Nicol 1998 explained “This approach is based on the biological insight that the human being is a comfort-seeking animal who will, given the opportunity, interact with the environment in ways that secure comfort.”

In this discussion it is inevitable to remark that the PMV model is perfect for mechanically ventilated buildings like office buildings. On the contrary, PMV calculations are solely partly correct for naturally ventilated buildings. According the approach, occupants of naturally ventilated zones tolerate a spread range of operative temperature, that is closer to the external environmental thermal situation and its dynamic changes (Fig. 2.14). Along this, also climate change is a long lasting slightly perceptible adaptation to the current situation and midterm future. Figure 2.14 schematically illustrates the different scientific approaches and related standards.

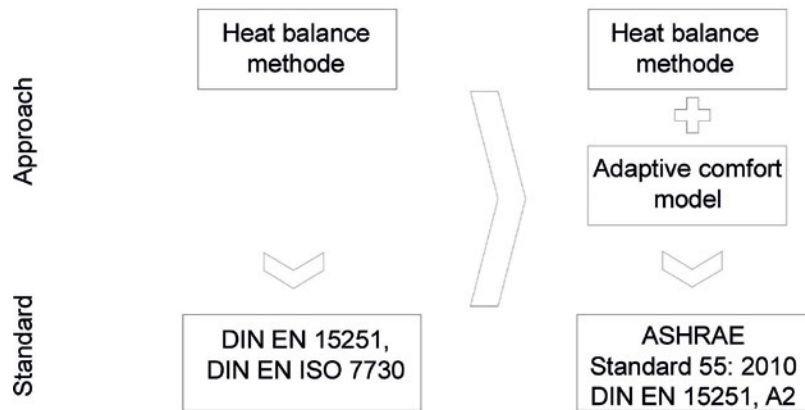


FIGURE 2.14 Distinction between the major different approaches to determine indoor thermal comfort

Since space occupants of naturally ventilated spaces are principally willing to largely adapt to climate circumstances, the approach is called the ‘adaptive comfort model’. Research focuses on human’s reaction to adapt to extreme climatic differences. Individuals are seen as independent participants of an dynamic environment who not at all simply react on stimuli but try to change the environment or their range of parameters (activity, clothing, controls, etc.) in order to proactively to improve thermal situation.

Substantially, this attitude towards the environment implies a human intelligence (Humphreys, 1978) like decision making skills and an experience feeding cognition of climate and weather conditions of the past and the near future as well. Both have influence on our physical and psychological perception of thermal situations and control adaption to it according our preferred thermal status as Bluysen explains (2009). The ASHRAE standard firstly bases on the heat exchange model and was later on reworked to include the adaptive comfort algorithm.

In this context, Humphrey initiated two central but slightly different key parameter : the comfort temperature  $T_{com}$ , also known as neutral operative temperature and plotting a bandwidth by upper and lower limits, and the optimum operational temperature  $T_{o,op}$ .

Humphreys initiated :

$$T_{com} = a \cdot T_{out} + b \text{ [}^\circ\text{C]} \quad (08)$$

where :

$T_{com}$  = comfort temperature (neutral operative) [ $^\circ\text{C}$ ];

$T_{o,op}$  = optimum operational temperature [ $^\circ\text{C}$ ];

$T_{out}$  = outside temperature index [ $^\circ\text{C}$ ];

a, b = constants

The optimum operational temperature for naturally ventilated zones in relation to the external dry bulb temperature is defined :

$$T_{o,op} = 0.31 T_{a,out} + 17.8 \text{ [}^\circ\text{C]} \quad (09)$$

Application of the  $\pm 0.5$  and  $\pm 0.85$  PMV criteria to a specific buildings thermal sensation a 90%- and 80%- range of acceptable operative temperature reveals for each of an investigated building and its unique location.

Necessary premises for a 'adaptive comfort model' application are :

- *a naturally ventilated building / space*
- *occupants essentially regulate comfort via openable windows*
- *spaces may have a heating system (if applied, model is not useful)*
- *spaces can have a mechanical cooling system, but it needs to be out of run*
- *spaces can have a mechanical ventilation system, but it needs to be out of run, ventilation primarily by windows*
- *activity of occupants need to be closely to sedentary action with a metabolic rate of 1 to 1.3 met.*
- *occupants need to be free to adopt autonomously clothing towards activity, in – and outdoor temperatures.*
- *outdoor temperatures shall be in a range between +10 and +33°C. If outdoor temperatures exceed +33°C, predictions according to PMV limit bands are no longer reasonable*

COUNTRY	ADAPTIVE CONTROL ALGORITHM	
	for external temperature $\leq 10^{\circ}\text{C}$ ( $T_{a,out}$ )	for external temperature $\geq 10^{\circ}\text{C}$ ( $T_{a,out}$ )
SWEDEN	$0,051 * T_{a,out} + 22,83$ [ $^{\circ}\text{C}$ ]	$0,051 * T_{a,out} + 22,83$ [ $^{\circ}\text{C}$ ]
GREAT BRITAIN	$0,104 * T_{a,out} + 22,58$ [ $^{\circ}\text{C}$ ]	$0,168 * T_{a,out} + 21,63$ [ $^{\circ}\text{C}$ ]
The NETHERLANDS		$0,31 * T_{a,out} + 17,8$ [ $^{\circ}\text{C}$ ]
FRANCE	$0,049 * T_{a,out} + 22,58$ [ $^{\circ}\text{C}$ ]	$0,206 * T_{a,out} + 21,42$ [ $^{\circ}\text{C}$ ]
GREECE	-	$0,205 * T_{a,out} + 21,69$ [ $^{\circ}\text{C}$ ]
PORTUGAL	$0,381 * T_{a,out} + 18,12$ [ $^{\circ}\text{C}$ ]	$0,381 * T_{a,out} + 18,12$ [ $^{\circ}\text{C}$ ]
ALL	$22,88^{\circ}\text{C}$	$0,302 * T_{a,out} + 19,39$ [ $^{\circ}\text{C}$ ]

FIGURE 2.15 Adaptive control algorithms for diverse European countries according McCartney & Nicol (2002)

STANDARD	DESCRIPTION of COMFORT TEMPERATURE CALCULATION and range for 10-20% acceptability for mechanically cooled and naturally ventilated (adaptive comfort) spaces
PMV / PPD ISO 7730	$T_{comf}$ is $22^{\circ}\text{C}$ in winter and $24^{\circ}\text{C}$ in summer. Summer days are defined by a daily maximum temperature of $25^{\circ}\text{C}$ . A total of 90% and 80% of people satisfied are calculated using PPD model, but come at approximately $T_{comf} \pm 2,5$ and $3,5^{\circ}\text{C}$ , respectively.
ASHRAE 55	Derived from a global comfort database, $T_{comf}$ is $22^{\circ}\text{C}$ in winter and $17,8^{\circ}\text{C} + 0,31 * T_m$ in summer, where $T_m$ is the <i>monthly average of the daily average</i> outdoor dry bulb temperatures. A total of 90% and 80% of people satisfied are assumed to fall at $T_{comf} \pm 2,5$ and $3,5^{\circ}\text{C}$ , respectively.
EN 15251	Derived from a European comfort database, $T_{comf}$ is $18,8^{\circ}\text{C} + 0,33 * T_{a,out7}$ in summer, where $T_{a,out7}$ is the <i>exponentially weighted running mean</i> of the daily outdoor temperature, approximated using <i>the previous week's temperatures</i> as : $T_{a,out7} = (t_1 + 0,8 * T_{-2} + 0,6 * T_{-3} + 0,5 * T_{-4} + 0,4 * T_{-5} + 0,3 * T_{-6} + 0,2 * T_{-7}) / 3,8$ , where $T_{-n}$ is the average outdoor temperature $n$ days before the day in question. A total of 90% and 80% of people satisfied are assumed to fall at $T_{comf} \pm 2,0$ and $3,0^{\circ}\text{C}$ , respectively.
NPR - CR 1752	Dutch code of practice. $T_{comf}$ is $17,8^{\circ}\text{C} + 0,31 * T_{a,out3}$ for type "beta" buildings in cooling mode, where $T_{a,out3}$ is calculated from <i>the average of the maximum and minimum outdoor temperature of the day under study and the three preceding days</i> as : $T_{a,out3} = (T_0 + 0,8 * T_{-2} + 0,4 * T_{-3} + 0,2 * T_{-4}) / 2,4$ , where $T_{-n}$ is the average outdoor temperature $n$ days before the day in question. A total of 90% and 80% of people are assumed to be not uncomfortable hot at $T_{comf} \pm 2,5$ and $3,5^{\circ}\text{C}$ , respectively (there is a separate calculation for the lower bounds of comfort)

FIGURE 2.16 Differentiated and detailed calculation methods of lower and upper comfort temperature bandwidths accd. Borgeson & Brager (2011)

Beside the optimal comfort temperature  $T_{o,op}$  as part of the ASHRAE 55 developed by deDear and Brager at the end of the nineteen nineties and with revision in 2002 [26], McCartney and Nicol [27] conducted 2002 thermal comfort algorithms for different inspected European countries in order to determine climate related comfort bandwidths.

Figure 2.15 shows a tabular survey. In relation to the operation mode, different standards provide calculation methods for upper and lower 90 to 80% acceptability comfort bandwidths. For standards focusing on adaptive comfort, the mean daily temperature, mean daily temperature of the previous week or the mean of daily minima and maxima of external temperature are basis for actual day calculation. Borgeson and Brager [28] surveyed the methods in 2011 (Fig. 2.16).

Upon this fundamental descriptive knowledge in science a proper choice of applicable methods for sun space is essential. The next section rates by table the eligibility of applicable standards.

### § 2.4.3 Methodology : applicable procedures for sun spaces depending on season

---

Especially for sun spaces as extremely glazed and local climate impacted spaces indoor thermal comfort is a complex issue. Since, sun spaces tend to react amplitude-modulated [29] on external local climate impact despite optimum thermal insulation and sun protection and since maximum transparency may suggest a reduced perception of shelter thermal comfort calculation on heat balance model basis could become unilateral. However, sun spaces seldom are mechanically ventilated or actively cooled. For that reasons PMV and PPD calculation can turn into nonsense.

METHOD / PROCEDURE		APPLICABLE		LIMITATIONS
VARIANT		WINTER	SUMMER	
<b>A</b>	<b>PMV / PPD</b>	<u>NO</u>	<u>NO</u>	only for mechanically ventilated spaces : errors and deviations are heavy
<b>B</b>	<b>ADAPTIVE COMFORT MODEL</b>	<u>NO</u>	<u>YES</u> , <small>restricted</small>	for adaptive control via windows in summer, but: +10°C < Tex < 33°C test sun space : -12°C to +36°C
<b>C</b>	# CUMULATIVE FREQUENCIES OF OPERATIVE TEMPERATURES # TEMPERATURE BANDS OF RUNNING MEAN OF EXTERNAL TEMPERATURE (DIN EN 15252, A2) # LOCAL THERMAL DISCOMFORT (DIN EN ISO 7730, 6.3-6.5)	<u>YES</u>	<u>YES</u>	all fit, no restraints

FIGURE 2.17 Survey of calculations procedure for thermal comfort in sun spaces

Moreover, since sun spaces per definitionem incorporate considerable area of openings for natural ventilation, a thermal comfort calculation according the adaptive approach may be sufficient in summer under certain conditions (maximum and minimum external temperatures within the limitations), but strongly restricted in winter by reason of extreme low external temperature which drastically limits window opening.

Thus thermal comfort calculations for sun spaces firstly are limited to evaluations of cumulative frequencies of hours with sufficient operative temperature and secondly to evaluations of the operational temperature related to the running mean of external temperature and generated upper and lower comfort band limits, and thirdly to comfort charts relating relative humidity and detailed analysis of local discomfort.

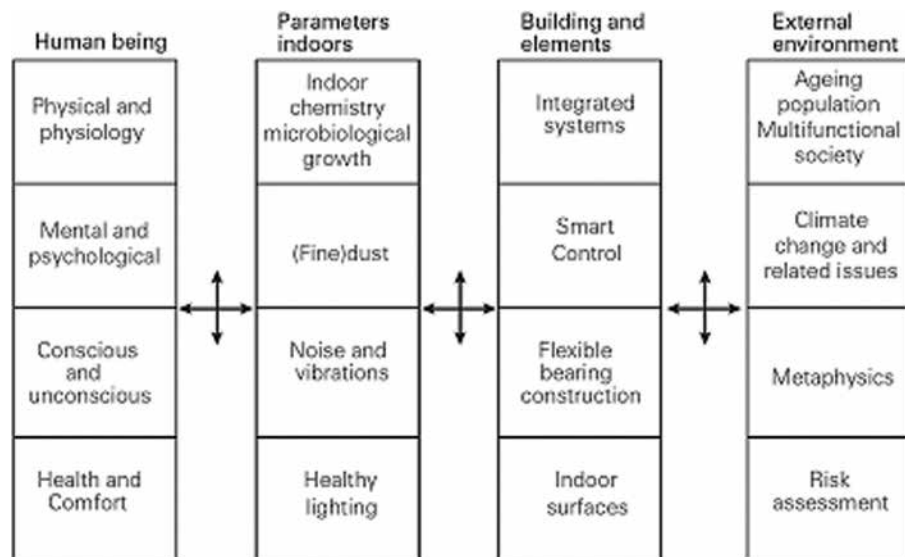
Figure 2.17 gives a tabular survey of procedures available and procedures actually applicable for sun spaces.

## § 2.5 Contemporary research on indoor thermal comfort

Thermal comfort is part of the scientific field environmental quality. Environmental quality includes beside thermal comfort many different aspects like acoustics, visual comfort and indoor air quality focusing on indoor air pollutions and disruption by odours. Even these before mentioned aspects despite of different weighting, are interdependently connected and influence each other.

However, thermal comfort as a simple and naturally physical space quality has by science been evaluated to unanticipatedly basing on additional psychological and social dimensions. Thus, thermal comfort engineering is not limited to actual heat or cold stress.

In fact, beside proper thermal conditions, which theoretically might satisfy the very majority of space occupants, the number of dissatisfied can raise according to influences that are beyond simple physical perception. In this context of contradictory influences (Fig. 2.18) environmental design and engineering has been developed as profession during the last century.



Source: Bluyssen (2008)

FIGURE 2.18 Interactions at different levels (complexity of indoor environment parameter matrix)

Thus, focussing and optimizing one inevitably means influencing other. Hence, environmental design on simply physical level is even a complex duty.

## Summary

---

A strong relation between architecture and health was already identified by historical master builder like Vitruv and Palladio many centuries ago. For example, as well as Palladio Aalto concentrated in the last century on design that promotes daylight provision and experimented with transitional spaces. Nevertheless, sick-building syndrome was a fundamental design and health related problem many designers and engineers had to face in the Nineteen-seventies and Nineteen-eighties. While Blyussen and Auer demonstrate a close relation between thermal space conditions and human health, Fanger was the first who evaluated a complex thermal comfort model that considers human specific metabolism, clothing and convective laws in order to optimize mechanical ventilation, active heating and cooling space design.

He bases the model on manifold statistics and climate chamber experiments.

However, practice revealed that this heat balance model fails in naturally ventilated spaces with considerable active control of the occupants on indoor climate. Moreover, the model was limited to stationary but for not dynamic and continuous evaluations. As a consequence the adaptive comfort approach established and was further developed and refined for diverse European localities. But, also the adaptive comfort algorithms encounter critique for being too simplified and simple dependant to external temperature.

Basically, engineering concentrates on simply those two different approaches the last three decades, although many differentiated approaches considering social, psychological, genological, physical and cognitive level of human perception and qualification of thermal comfort. But, nevertheless, all mentioned and certainly legitimated deliberations remain as side effects and diversification with no essential influence on the two basic and oppositional methods. While the classical heat balance method was extended by Fanger himself to a more deliberated and adaptable model including expectations values, and while the classical model was improved and made more workable by introducing the adaptive clothing insulation value, some researchers spend time on making the adaptive more even more simpler, and thus rather vague.

Interestingly, opposed to Fanger clear-cut metabolism concentrating model, several scientists have pushed cognition and psychological influences on the effective thermal perception in the foreground.

That might not be relevant for classical massive and solid build space with a predominant proportion of opaque façade elements, but sun spaces per definitionem and based on the specific archetype related light and transparent building skin qualities, bear potential and justification for a fundamentally different perception of indoor thermal comfort, related to the immediate and radical perception of the local climatic conditions.

Thus, in this context, the relation of daylight and physical shelter as Vitruv and Palladio once determined for historical massive buildings experiences nowadays once again attention, but on a completely different level of perception. While cognition in terms of memory of thermal perception of archetypes like churches can rule our all thermal space sensation, a similar influence on thermal sensation in sun space can overrule a simple receptor signal based or rigid metabolism and gender neutral understanding of thermal space perception.

Chun and Tamura [30] exemplified that thermal space perception is partly dominated by the actual metabolism of course, but nonetheless, further partly a result of our average space perception of either deep memory or memory of the late space perception. That makes stationary non-dynamic evaluations of thermal comfort exclusively based on metabolism and concurrent activity disputable. Moreover, the scientific cognition of PMV/PPD error sensitivity related to changing clothing insulation factor and permanently resulting skin temperature changes and thus the logical necessity for immediate adaption limits the strength of heat balance model to simply punctiform assessment in strongly controlled thermal environments.

For that reasons, thermal comfort evaluations for highly transparent and mostly naturally ventilated transitional spaces becomes complex and distances from exclusively metabolism determined calculation methods.

On the other hand complicates the achievement of optimal thermal comfort in spaces where different façade functions contradict like natural effective ventilation and effective external sun protection. When interrelations become complex also control becomes complex and less effective. The more architects and engineers have to focus either on multifunctional but non-contradictive façade designs or on smart and effective integral façade designs.

## § 2.6 Research on thermal behaviour, thermal comfort and energy on sun spaces

Research on sun spaces as a result of literature review was already established in the 1970ties [31,32,33]. While sun spaces still based on thermally non-decoupled alumina profiles, steel profiles or simply squared wooden timber that stuck to frames in order to incorporate single glazing, the vicinity towards green houses and winter gardens was high. Compared to housing and residential spaces especially sun spaces remained to be single glazed far to the nineteen nineties [34]. Thus, awareness to enhance sun space façade qualities in energetic manner came within the last thirty years, whereas first double heat protection glazing established in the end of the nineteen seventies. Furthermore, in this line, literature review revealed that single glazing is still common in southern countries with over averaged high daily mean temperatures and exclusively sunny days.

Interestingly, literature puts an intensive focus on proper calculation and simulation algorithms representing in particular proper radiation transmittance and internal reflection of infrared radiation that are crucial for mainly glazed and thus highly transparent spaces, than on thermal insulation properties of the glazing itself. Within research on sun spaces different objectives established over the decades. Objectives mainly were driven by constructional concern (Lumbis, 1988) [35], followed by energetic issues and thermal comfort optimization, which strongly relate to operational strategies and finally optimization of calculation procedures and algorithms for numeric simulations.

Also derivatives of sun spaces and greenhouses respectively, have been investigated. Those studies focused on passive solar collectors. They, for example incorporated rock beds and heat storages (Chen and Liu, 2004) [36] or were minimized to actually box-windows, which exclude any living space quality (Sanchez-Ostiz, Monge-Barrio, Domingo-Irigoyen, Gonzalez-Martinez) [37], but in order to enlarge solar gain utilization.

This section of chapter 02 focusses on diverse perspectives of research on building physical and constructional investigations.

Interestingly, that beside research on sun spaces per definitionem concentrates on a single room, tentatively on a room couple, namely living space and sun space, investigators have tended to focus on simply one single subject. Subjects in this context were comparisons of single glazing or double glazing, inertia and thermal mass, the influence of separation elements or simply location. Compared to this thesis, more focus have been set on the potential of heating energy saving, than on interior thermal comfort.

Moreover, within literature research and review beside this thesis no contribution was found which elaborated descriptive knowledge on local thermal discomfort as for instance radiation asymmetries.

### § 2.6.1 Optimisation potential of standards and digital models for sun spaces calculations

---

Calculations on energy and comfort in sunspaces have been executed within the last forty years (Glässel 1979 [31], Achad and Gicquel 1982 [38], Parson 1983 [33], Mottard, Fissore 2007 [39], Passerini 2012 [40]). Starting with monthly balancing calculation algorithms and stationary examination (Method 5000, DIN ISO 13790 [41]), the critique and call for dynamic and detailed simulations models emerged, when engineers comprehended that the unique potential of sun spaces, namely solar gains, were not considered depletively. Thus, there were detected diverse starting points to correct and to refine calculation algorithms. This section will roughly highlight the points of improvement and report about the development in science of physical numerical calculation on sun spaces of the last decades.

Since for simulations of sunspaces as solar systems existed solely various assumptions but many limitations, Parsons (1983) [33] developed on a TRNSYS model a routine, which more correct models the envelope transmission of radiation beams and vectors, splitting into internal reflection and thermal storing by capacitive mass as well as heat losses to the environment and the adjacent zone. Space glazing and thermal mass were detected to be crucial points of improvement, since fraction indices as is well known, define gains and losses.

However, previous algorithms did not differentiate between entering and relinquishing radiation. Further he claims that monthly mean input parameter and reference to degree days result simply in rough information for configuration, but according to him, estimations never tell about precise hourly balancing and about internal physical processes. His criticism points at the so far developed solar saving fraction (SSF) and solar load ratio (SLR), which based on monthly mean values and degree days and does not consider solar gains at all. Moreover, he detected ambiguous values varying with the element thickness of the sunspace / living space separation element. Parsons major contribution to science is a TRNSYS model development, which includes refined radiation algorithms, a nodal network of the space itself and based on hourly weather data files. By this he provides a modular and flexible calculation tool to predict inter-zonal balanced energy flows, indoor conditions and auxiliary energy demand more precisely.

Notwithstanding, Mottard and Fissore (2007) [39] state more than twenty years later that simulation algorithms have demonstrably improved, but still encounter considerable deviations in values compared to empirical data when assessing extraordinary high transparent spaces.

To them, algorithms still do not model solar radiation distribution and reflection inside sun space, for example, well. The researcher in reference to Wall (1997) [42] determine internal longwave-radiation and reflection as a substantial issue in order to predict or reproduce thermal processes in sun spaces accurately. Multiple reflection of direct radiation results in diffuse re-directioning. They concentrate on the glazing properties view factor method, which from their perspective does not model reflection and absorption considering furniture or other internal storage capacities sufficiently. Essential for Mottard and Fissore is the splitting of radiation into absorbed fraction by sun space envelope glazing itself and into remaining longwave-radiation after several reflections, what is originally considered by the  $G_{jk}$  Gebhart coefficient.

The authors emphasize that simulation models simplify indoor air to a homogeneous volume without any stratification or different gravity refer to Laouadi, Atif and Galasiu 2003 [43] and Voetzel et al. (2001) who developed a model of subdivide air volumes in order to reproduce stratification, air movement by turbulences and hot spots. In consequence, this leads to a consideration of precise internal convective coefficients representing vertical cold air flow accompanied with high glazed facades.

With empirical measurements in this context they validated and thus confirmed the importance of air stratifications modelling in particular in sun spaces on bright sunny days. Finally, they focused on proper algorithms for modeling intermediate walls or separation elements like fold-works.

Since absorption properties, thermal mass, convection coefficients and conductance rule itself the thermal behavior, a proper modeling defines energy remaining in the system what promotes heat return or energy leaving the system, hence heating adjacent rooms.

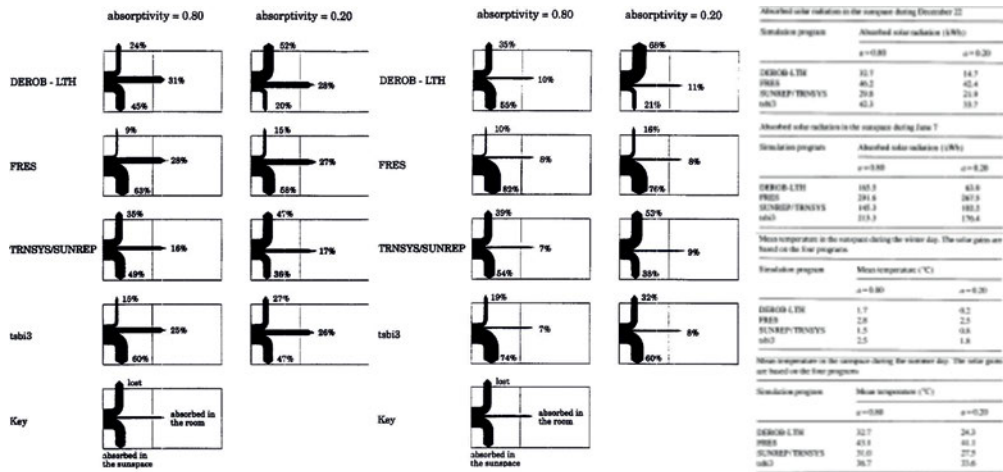


FIGURE 2.19 Wall 1997, a.) different calculated energy flux distribution, b.) solar absorption and mean indoor temperature for a representative winter and summer day for four different calculation algorithms

Especially Wall [42] calls attention for the simplified solar radiation transmission and internal reflection algorithms, which are substantially for a prediction of internal energy flux. He disclaims the consequences on internal temperature, surface temperature as well as cumulative heating and cooling load. In latest consequence also thermal comfort evaluations are affected by incorrect calculation of independent variables.

According to Wall temperature and cooling by the most of inspected calculations algorithms were overestimated, consequently heating load underestimated. Figure 2.19a and 2.19b visualize by table resulting proportions of energy fluxes, proportions of absorbed solar radiation as well as resulting indoor temperature. Obviously, solar distribution on a summer day differs considerably higher from calculation method to method. While dynamic simulation models are already established and were reviewed, parallel common stationary calculation methods have encountered critique and improvement as well. In this context, Rabenstein [34] exemplifies the limits of the DIN 4108-6 [46] in terms of the disregarded potential of preheating of a living space by solar gains of an in quasi-static calculation algorithms of DIN EN 832 [44], DIN EN ISO 13790 [45] and particular unheated sun space by driven natural air exchange. Further, beside the thermal mass of sun spaces is limited, he demonstrates that solar gains and heat return is inevitably related to sun space thermal mass.

Thereby he illustrates the necessity of algorithms, which also considers and consequently balance heat gains of sun spaces. The crucial point, according to him, is not

simply a significance of the reduction of transmission losses from the living space to the sun space, but beyond that also heat transport by ventilation vice versa. Thus, alternative heat gains and ventilation heat losses, that are based on specific thermal mass and specific cooling constants, call for severely attention. Since utilization factors are related to zonal set points the utilization calculation of unheated sun spaces with above listed standards is difficult to reproduce.

Since thermal comfort is a question of thermal balance equation and thus of energy conservation, Oliveti, De Simone and Ruffolo (2008) [47] concentrate less on radiation distribution but more on absorption, geometry, orientation and optical properties of high transparent buildings. Inferentially, they introduced the effective absorption coefficient for sun spaces. Prove and refinement was executed by 34.560 dynamic simulations cases and statistical evaluation of correlations. Interestingly, according to them, absorption of entered radiation is strongly related to the ratio of transparency. Opposed to common sense, not all entered radiation is fully absorbed. For that reason they postulate a definite geometrical compilation of the space in question. A definite compilation of surfaces allows a detailed calculation of reflections, absorptions in the context of energy conservation.

Similar to Rabenstein [34], Oliveti, Arcuri, Bruno and De Simone (2011) [48] criticize incorrect and simplified routines in DIN EN ISO 13790. Whereas EN ISO 13790 assumes entered radiation as entirely absorbed, they demonstrate by statistics that this mostly is true for little glazed, only partly transparent spaces, but not for predominant glazed spaces and least of all for sunspaces. Since, according to them, radiation first transmits glazing, and for that in consequence partly get absorbed by the cavity of double-glazing, fractioned radiation affects the space by direct convective radiation of the glazing and by indirect convective-radiative fractions caused by reflections of internal surfaces and the glazing, the DIN EN ISO 13790 code needs to be revised.

Their deliverable for the science world is the development of a calculation method for solar heat gains through glazed surfaces, that can be used in simplified calculation procedures.

The following equation calculates solar heat gains:

$$Q_{sol} = \sum F_{sh,r} \cdot k \cdot F_{sh,gl,k} \cdot (1 - FF_{,k}) \cdot A_{w,k} \cdot I_{sol,k} \cdot F_{w,k} \cdot k \cdot [\tau_{b,n} \cdot \alpha_{cav} + q_i + \tau_{b,n} \cdot (1 - \alpha_{cav}) \cdot q_e], k \cdot \Delta t \quad (10)$$

where:

$F_{sh,k}$  = reduction factor for external shading

$F_{sh,gl}$  = reduction factor for mobile internal shading

$A_{w,k}$  = frame area

$I_{sol,k}$  = average solar irradiance

$F_{w,k}$  = average correction factor

$\alpha_{b,n}$  = beam solar transmission factor for normal incidents

$q_i$  = secondary internal radiative-convective heat transfer

$q_e$  = secondary external radiative-convective heat transfer

$\Delta t$  = time step

$1-\alpha_{cav}$  = fraction of internal surface reflections

Finally, the calculation code for double glazing is more correct than for single glazing. In detail Oliveti, Arcuri, Bruno and De Simone detect a reduction of the effective absorption factor by rising glazing fraction in spaces with smooth and light surface from 0,93 to 0,44 for clear single glazing, a reduction from 0,94 to 0,52 for clear double-glazing and from 0,95 to 0,56 for clear triple-glazing. Hence, calculations with variable glazing to floor area proportions of 0,033 to 0,60 were applicable, which correlation error was less than 1%.

Whereas Oliveti, Arcuri, Bruno and De Simone concentrate on the façade, the filtering element towards environment, Asdrubali, Contana and Messineo (2012) [49] act on the focus of Mottard and Fissore [39] and elaborate influence factor of the separation wall as filtering element between sun space and adjacent zone. By validating Method 5000 and the algorithm of DIN EN ISO 13790 with dynamic TRNSYS simulations and empirical data (Fig. 2.20), they determine the contribution ratio of the sun space, namely by transmission losses through the separation wall or element, to adjacent space heating.

Furthermore, they likewise to Wall [42] identify a tendency of Method 5000 and DIN EN ISO 13790 to overestimate the contribution of the passive solar system for adjacent zones. Similar to Asdrubali, Contana and Messineo (2012), Oliveira Pnao, Camelo and Goncalves (2012) [50] evaluated on congruency of Method 5000 and

DIN EN ISO 13790 with simulation results. The authors state failures of ISO 13790 in terms of slightly to low loss-to-gain ratio in mid-season months when utilizable solar gains are higher than heating load and vice versa too high loss-to-gain ratio in cold months, when losses are demonstrably high. They address the correct calculation of indirect gains and they established a renewed solar load ratio formula, that both can be integrated into ISO 13790 in order to recalibrate.

By sensitivity analysis the scientists conclude, that indirect gains from sun spaces can be added to the heat source term, heat gains respectively, and analogously, can be subtracted from the heat transfer term, namely heat losses, of ISO 13790. This integration is verified without any influence on the utilization factor.

Figure 3. Influence of the sunspace evaluated according to the three methodologies during the heating period (global heat transfer coefficient of the partition wall 9.89 W/K).

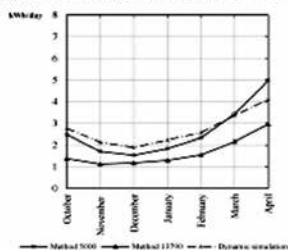


Figure 3. Influence of the sunspace evaluated according to the three methodologies during the heating period (global heat transfer coefficient of the partition wall 9.89 W/K).

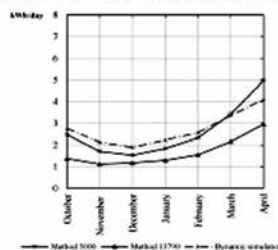


FIGURE 2.20 Comparison of effect of different calculation methods

Passerini (2012) [40] was motivated to enhance the DIN EN ISO 13790 code more from perspective of correct exploitable solar gains collection than from thermal comfort the since he argues the code is practically applied by many engineering and architectural offices, which cannot afford time consuming dynamic modelling.

Thus, he especially inspects by numerical simulation and two experimental test set ups the surface envelope to volume ratio, called compactness ratio  $C_{f,s} = S_{\text{south}} / V$ , in relation to direct south orientation. Beside measured extraordinary exclusively high glazing surface temperature of above 70°C (South Tyrol), similar to Babae, Fayaz and Sarshar [51] (2015), he detects a strong relation between roof glazing inclination and heating demand.

He is convinced that a decrease in compactness can be regulated dependently to the degree of south direction and likewise Rempel, Rempel, Gates and Shaw claim that floor mass is substantial for inertia. Within this frame a three-dimensional calculation model is necessary first to calculate and predict internal iterative radiation reflections

and ultimately absorption and second resulting differing surface temperatures and consequently air stratification. Following, the potential of adjacent space heating, either via natural ventilation or at least transmission is strongly related to air stratification. And yet, correction factors are elaborated which concern solar transmission of windows, shading factors, indirect gain, heat dispersion of solar gain through the ground and air ventilation, he explicitly states, that they are not universally valid, thus only partly applicable in the code.

For that reason he calls attention for numerous and diversified dynamic fluid simulations of representative situations including climate, geometries and operation modes in order to increase correlation to the real world. According to him, further scientific work concerns inevitable modeling, despite it is not applicable by the code itself. Additionally, Passerini criticizes, that the ISO 13790 code solely considers one single ventilation rate, what definitely contrasts to reality. In congruency to previous authors, he expels bioclimatic behavior of for example sun space to be strictly related to local climate conditions.

## § 2.6.2 Thermal comfort related to design and strategy

---

Lumbis (1988) [35] argues, that beside low external temperature the ambient air temperature of a sun space can be sufficient. Thus, acceptable interior dry bulb temperature is more a question of local irradiation than of external temperature, respectively low temperature difference. In addition to that, Lumbis (1988) points out, that cooling loads typical for Canada raised to maximum with west instead of east oriented sunspaces.

If sufficient natural ventilation is part of the design as well as freedom of orientation and low thermal mass, in general a west oriented sun space has potential to provide acceptable dry bulb temperatures for the majority of months a year.

Van den Dobbelen (2012) [22] points out, that energy efficiency and thermal comfort in sun spaces are controversial. To him, either extraordinary energy efficiency exacerbates indoor thermal comfort, or high quality of thermal comfort considerably effects energy efficiency.

### § 2.6.3 Energetic benefits related to facades qualities and sun space design

---

Rabenstein (2005) inspects different modi of conditioning, designs and façade glazing qualities in order to maximize days with appropriate ambient temperature and heating energy saving for sun spaces in Germany. Beside existing numeric simulation tools and appropriate models, he calculates maintenance costs for unheated and heated sun spaces and residential heating energy savings with calculations algorithms established in DIN EN 832 [44]. In this context he differentiates between existing buildings with poor energetic insulation standard and modern low-energy houses.

He first confirms higher energy saving potential for unheated sun spaces, but emphasizes potential energy saving also for heated sun spaces. He justifies this with less transmission losses of adjacent zones towards environment by the buffer mechanism, with location specific climate and the energetic standard of the residential house itself. One result is the shortening of heating period in the beginning and at the end for each a month of a low-energy house combined with an unheated sun space.

This is compared to a heated sun space still demonstrably valid with increased extrinsic shading and standard double-glazing instead of heat-protection glazing. But what is more, that according to his calculations, the absolute energy saving potential of sun spaces is higher in combination with old houses of poor energetic standard than with modern houses of premium thermal insulation quality.

Moreover, Rabenstein reasons low savings in modern houses with comparably low insulation standard of sun space envelopes compared to modern houses, what results in increased thermal losses across the sun space envelope instead of a proper insulated wall.

Thus, sun spaces normally cool faster in evening time than enhanced insulated housings, what eliminates in terms of time the preheating potential of sun spaces for low-energy-houses (Fig.2.21). Rabenstein accounts for a time-shift problem of offer and demand. He also calls attention for decreased solar gains, which low energy houses by principle rely on, but however, inevitably encounters as sun space adjacent zone. Since global radiation is additionally filtered by sun space glazing, adjacent zones consequently profit less.

Süd-Wintergarten	$q_h$ in kWh/(m <sup>2</sup> a)	$t_{HP}$ in Monaten/a
<b>Niedrigenergiehaus</b>		
ohne Wintergarten	60,5	8,3
mit unbeheiztem Wintergarten	54,4	8,6
mit Lüftung aus dem unbeheizten Wintergarten	36,3	8,2
mit beheiztem Wintergarten	68,7	6,5
<b>Bestandsgebäude</b>		
ohne Wintergarten	138,0	9,6
mit unbeheiztem Wintergarten	115,1	9,8
mit Lüftung aus dem unbeheizten Wintergarten	92,8	9,5
mit beheiztem Wintergarten	128,3	7,6

FIGURE 2.21 Annual heat use per net floor area and duration of heating period for a south orientated conservatory

Beyond that, the author explains that with a sun space thermally decoupled by a thermally insulated separation element (fold-work, door, wall) either the annual number of hours of acceptable occupation can be elongated or the air volume can be used for preheating of an adjacent space. In respect to sun space design, he figures out, that sun spaces with single glazing and adjacent living spaces energetically benefit from a limited space depth of the sun space. Concluding, either width or height are design parameters to enlarge, nonetheless, a high space depth accounts to be counterproductive.

This rule overcomes, if the glazing turns into double glazing, hence the lower the  $U_g$ -value [W/m<sup>2</sup>K] the lower the heating energy consumption regardless of sun space depth. Related to Rabenstein, a rising sun space depth correlated with high quality heat protection glazing, even triple glazing, enlarges correspondingly solar gain absorbing floor area. This is, as he claims, beneficial in the context of low-energy houses. In order to conclude, Rabenstein summarizes decisive factors that are relevant for calculations of the energy saving potential:

- 1) *Energetic quality of residential house*
- 2) *Geometry and thermal quality of sun space*
- 3) *Constructive coupling with the residential house*
- 4) *Utilization form / modi of sun space (heated/unheated)*
- 5) *Absorption ability and thermal storage capacity of sun space*
- 6) *Orientation*
- 7) *Sun protection quality*
- 8) *Configuration of intermediate element*
- 9) *Geometric configuration and control of natural ventilation*

While Rabenstein elaborates by calculation heating energy saving potential for sun space-single family homes, Ignjatovic, Popovic and Kavran [52] (2015) lately calculates by simulation energetic benefits of sun space-apartment flats.

Against the background of Serbian climate conditions they inspected a multi-family high-rise housing in Belgrade with 98m<sup>2</sup> flat net-area and additional 16m<sup>2</sup> south facing sun space. Each sun space was incorporated block-wise into a south facing chimney façade with cantilevering floor slabs as story-wise partition.

Their simulation model considered a compact flat building which solid façade consisted of hollow-block brickwork, 120 mm thermal insulation and a second plaster covered masonry shell exceeding Serbian contemporary energetic standards while corresponding to German standards of 2009 to 2012. Further the sun space façade was an alumina construction with less than 50% of ventilation openings which incorporated glazing with shading coefficient changing between 0,20 to 0,85.

Whereas apartment heating was modelled with gas boiler and radiator, flat cooling was modelled according to Serbian tradition and experiences with split cooling units. The authors evaluate considerably low heating and cooling savings of 2 and 3% in respect of the total building. Nonetheless, unit-wise they calculated heating and cooling energy consumption savings of 11%, and 18% respectively for the zone directly adjacent to sun spaces. That does not correspond either to Lumbis [35], who evaluate 30 to 60% of cooling load reduction of sun spaces located in Canada by applying an effective external

blind as sun protection nor to Gorgolewski, Grindley and Probert [69] (who in 1996 numerically evaluated approximately 25% for a first level and 30 to 40% heating energy reduction for a 10th level apartment refurbished with sunspaces). Interestingly, Ignjatovic, Popovic and Kavran reveal a predominant high reduction in cooling demand with ambitious shading coefficients of 0,20 to 0,35, what results in higher heating loads.

On the contrary, optimal balanced reduction in heating and cooling consumption is achieved with moderate, hence higher shading coefficients of 0,85. While the ratio of ventilation openings remains constant with 30%, changes in shading coefficient from 0,20 to 0,5 results in changes of proportions of cooling and heating load reduction, but not considerably in total reduction. Moreover, likewise [53] they evaluate opening proportions of 30% to 50% to be sufficient, whereas more than 50% result in no significant improvement of cooling reduction. Concluding, a shading coefficient of 0,5 (g-value : 0,4) and 30% ventilation opening area provides optimal energy reduction.

Similarly, Babaee, Fayaz and Sarshar [51] (2015) inspects sun spaces attached to flat apartments in Iran, which especially in Tabriz serves cold winters with  $-25^{\circ}$  but moderate summers. The scope of their simulation study bases mainly on changes in sun space glazing quality representing single, glazing, double glazing and low-coated glazings, in changing tilt angles of roof ( $30^{\circ}$ ;  $45^{\circ}$ ;  $60^{\circ}$ ;  $75^{\circ}$  and  $90^{\circ}$ ) and aside glazing ( $30^{\circ}$ ;  $45^{\circ}$  and  $90^{\circ}$ ) and in transparent or opaque side walls. Despite the research climate is Iranian with more than 2.800 annual hours of sun shine, but frost period between end October to beginning of April with 30 days of frost in January, sun spaces are considered to be heated in winter. Thus, living room and sun space were modelled as thermally separated by a wall including windows and a door. Beside a comparably long heating period, the building modelled was of poorer energetic quality than German standard. Simulations carries out, that a sun space with an opaque east and west side wall provides the highest heating energy reduction of about 30% annually and about 25% in particular in January, what inevitably results in overheating in summer [53]. A tilt angle of  $45^{\circ}$  is evaluated to be the most effective in order to maximize solar gains and save heating energy. In this line, a low<sub>e</sub>-coated glazing results in 40% of heating energy savings compared to a single glazing.

However, low<sub>e</sub>-glazing solely improves heating consumption for 10% compared to double-glazing. Moreover, sun space temperature was remained on the coldest day in January to  $16,28^{\circ}\text{C}$  exclusively with lowe-glazing, whereas the (Fig. 2.22) maximum sun space temperature with single glazing was  $10,7^{\circ}\text{C}$ . Then again, the opaquely flanked sun space version results in 2,8 Kelvin higher hourly mean ambient temperature of the living room compared to the worst simulation variant. Finally, as an overall finding, similarly to Rabenstein the researcher calculates a heating period shortening of the adjacent living room from eight to nearly six month.

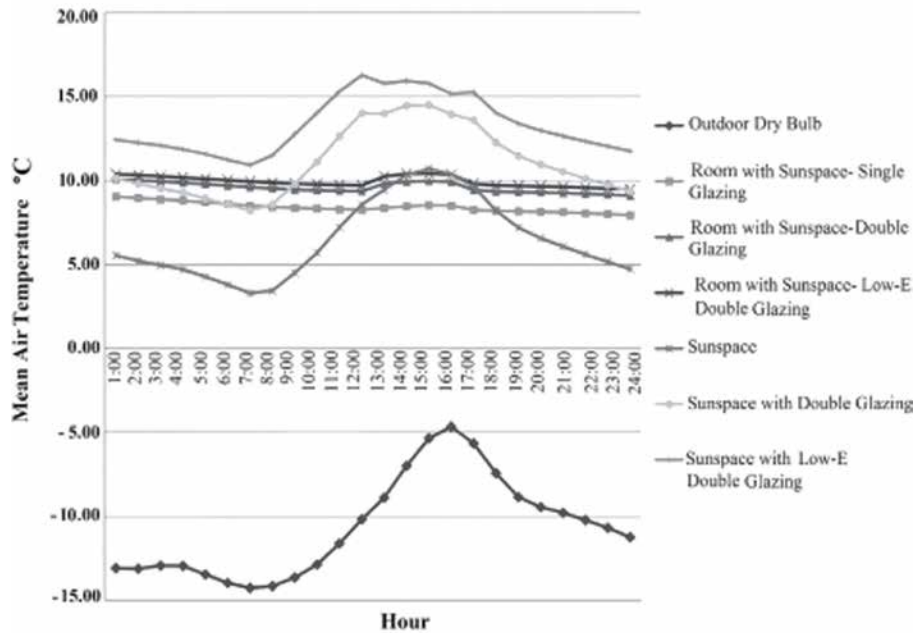


FIGURE 2.22 Room and sun space temperatures with different glazing materials on January 22th

Furthermore, they identify a relation between sun space depth and heating reduction. Hence, the lower the sun space depth disregarding the width is, the lower the heating losses are. Reasons for that relation, according to the researcher, are less transmission losses by sun space roof area and higher internal solar gains in adjacent zones by less shadowing by sun space elements.

Babae, Fayaz and Sarshi similar to Rempel, Rempel, Gates and Shaw [54] determine a sun space glass area to sun space floor area ratio, in this context of 2.21 to be most efficient in respect of heating energy consumption. Additionally, they recommend a south-south-east orientation, despite any definition of preferred utilization period or expected hat return interval. Summarizing, all actions result in 46% of heating energy saving compared to an apartment in Tabriz without sun space. In terms of orientation Monge-Barrio and Sanchez-Ostiz [53] reveals by simulation a clear-cut relation between south-south-west, south-west and west direction of sun spaces in Spain and a raise in cooling demand of 40 to 100% compared to south direction.

Table 3. Energy needs with attached-sunspace relatively to reference case; negative percentage indicates relative reduction, positive percentage indicates relative increase

Configurations (Fig. 1)	a)	b)	c)	d)
Cities	Winter/Summer/Annual	Winter/Summer/Annual	Winter/Summer/Annual	Winter/Summer/Annual
Faro	-93/-10/-16	-57/-16/-19	-35/-13/-15	-100/-15/-23
Lisboa	-72/-10/-30	-60/-12/-24	-46/-10/-21	-90/-10/-38
Évora	-70/1/-30	-40/-8/-20	-27/-7/-16	-66/-9/-34
Coimbra	-70/5/-35	-43/-9/-24	-32/-7/-20	-68/-9/-40
Porto	-70/28/-53	-45/-3/-35	-32/-1/-26	-66/-4/-55
Bragança	-48/10/-38	-33/-5/-26	-24/-5/-20	-46/-6/-38

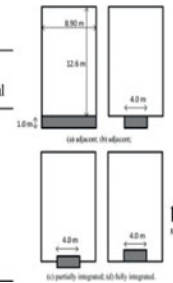


FIGURE 2.23 Energy needs with attached sun spaces relatively to reference case negative percentage indicates relative reduction, positive percentage indicates relative increase

The table of results above (Fig. 2.23) shows, that related to the sun space configuration a to d (attached, semi-integrated, fully-integrated) reduction and enhancements could have been calculated. Interestingly, configuration 8,9 m wide and configuration fully integrated achieved comparably high savings. In particular, configuration **a** and **d** call special attention in respect of city Faro, since savings are 93% and 100% respectively for heating demand, while total annual savings of 16, and 23% respectively, are below average. However, total energy demand reduction of 40 to 55% are calculated, despite the authors allude common difficulties to model users occupation and ventilation behavior.

While Babae, Fayaz and Sarshar [51] (2015) set focus on inclination of sun space roof glazing in the context of Iran and Aelenei, Leal and Aeleni [55] investigated sun space variants that are also fully or semi-integrated, thus three-side flanked, into the common flat living spaces, Taleghani, Tenpierik and van den Dobbelsteen (2013) [56] inspected heating energy demand and thermal comfort of terraced houses in the Netherlands, that either include open courtyards or closed courtyards, atriums respectively.

The researcher in particular consider for numeric simulations weather files, that consider climate change and predicted climatic conditions of a horizon of 2050. Although, they look ahead into far future, and although they model with courtyard and atrium glazing with  $U_g$ -value of 1,96 and 2,55 W/m<sup>2</sup>K, they find out, that as traceable, atriums generally save heating energy in winter, but causes more hours of discomfort in summer. Moreover, they develop the simulations models towards optimum closed or opened roof variants in order to adopt to monthly climate. Essentially, in the Netherlands, an atrium shall be opened between May and August, while a courtyard shall be covered between November and April in order to minimize heating energy consumption and overheating in summer. Interestingly, for September and October the authors detect no worth mentioning difference in demand and comfort quality in respect of an atrium and courtyard.

That goes along with a 4,8 to 8,5% reduction of cooling energy demand in British atria houses if cooling set points are widened, respectively raises for 3K, as a study of Pitts and Saleh [57] elaborate in 2007.

Likewise Monge-Barrio and Sanchez-Ostiz (2015) [53] accredit definite cooling and heating energy savings as well as lowered averaged indoor temperature, lower temperature swings and daily amplitudes and less radiant asymmetries for house with attached sun spaces in six Spanish cities (Sevilla, Valencia, Madrid, Barcelona, Santander and Pamplona) of different climate zones.

However, according to them, a Netherland terraced dwelling profits in future by an openable and adjustable atrium roof in terms of at least halving the hours of summer discomfort, and even reducing them to one-third compared to a contemporary serial house without living space appendix.

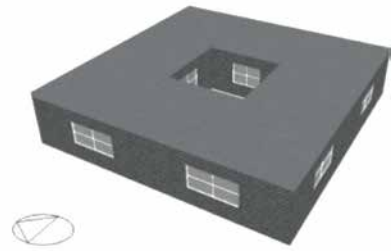
Parallel to this Taleghani, Tenpierik and van den Dobbelsteen (2012) also investigated for qualitative scope different courtyard-, atrium- and sunspace houses (Fig. 2.24) exposed to different climate represented by cities like Rotterdam (temperate climate), Cairo (hot arid climate) and Barcelona. Previously, Aldawoud and Clark [58] inspect changes and effects in energy demand for modelled geometrically equal one-levelled courtyard and multileveled atrium houses in cold, temperate, hot-arid and hot-dry climates. Aldawoud and Clark identify a clear-cut relation between increasing number of stories and energy efficiency for the atrium houses. Among Taleghani, Tenpierik and van den Dobbelsteen, beside the dimensions of the inner courtyards or sun spaces as well as the building height and maximum sun height fundamentally influence the compensation of heating losses and tendency for overheating, they evaluated heating and cooling energy demand and thermal comfort.

Interestingly for Rotterdam, as representative for moderate mid-European climate, a courtyard solution encounters higher transmission losses than solar gains could comprehend.

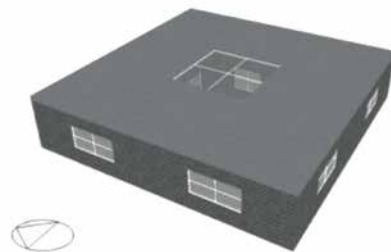
The Normal Building



The Courtyard Building



The Atrium Building



The Sunspace Building

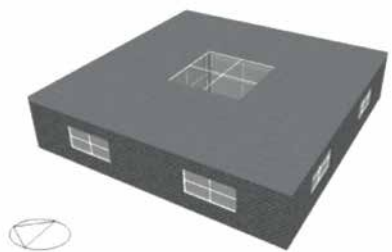


FIGURE 2.24 Different rendered typologies of atrium, courtyard and sun space

A roof covered courtyard, an atrium respectively, profits from less transmission losses than the courtyard and is equal to the reference and from 25% higher solar gains than the reference but from 22% less than the courtyard. Finally, a sun space equals the atrium with slightly higher heat losses as the reference and the atrium, but with considerable higher solar gains, which compensate the losses. Opposed to that, provides a courtyard solution in Cairo best prerequisites for an optimal cooling load and solar gain ratio.

While solar gains are the highest in courtyards, the energy demand for cooling reveals to be comparably low, however considerably higher than the reference.

While atrium and sunspace significantly tend to overheat and cooling is essential objective for north African location the only benefit of courtyards are additional solar gains, whereas the reference model stays the most economic one. On the contrary, for Barcelona heat losses demonstrably increases with investigation variants different to the reference. Although solar gains increases with atrium and sunspace solutions and in particular with courtyards, also heating losses raises which compensate the gains. Nonetheless, the most crucial insight is, that cooling loads become a problem when deviating from the reference.

On the other way round, thermal comfort in living spaces can be improved in particular locations and related to specific solution despite heating demand raises. Thus, whereas a courtyard solution with considerable heat losses during winter is no appropriate solution for Rotterdam, especially an atrium provides the most comfort hours and thus additional 150 hours of comfort compared to the reference model. For Cairo, actually no transitional space solution provides better comfort or more comfort hours, but a significant and higher tendency for overheating. Thus, in the context of Cairo, the courtyard next to the reference is the most comfortable and economic solution. Although heating losses of an atrium in Barcelona is only slightly higher than the reference, the mean indoor air temperature [ $^{\circ}\text{C}$ ] is the highest.

As a conclusion of Taleghani, Tenpierik and van den Dobbelsteen, the reference model shows advantages in terms of energy demand, since compared to the solutions the demand remained the lowest at all. This study highlights benefits of transitional spaces in respect of indoor thermal comfort, especially sunspaces and atriums in moderate mid-European climates (Rotterdam) and in particular atriums in warmer climates like Spain (Barcelona). Opposed to that, no transitional space provides benefits for hot arid climate (Cairo). Interestingly, most energy sufficient (reference) solution do not generally provide most comfort. Thus, this detected disproportion turns into a plea for transitional space in general.

Among this Mihalakakou (2002) [36] with Ferrante (1999) [59] investigates the temperature difference of the external temperature and the calculated indoor temperature of a 30m<sup>2</sup> south directed TRNSYS sunspace model attached to a solitary residential building in Milano, Dublin, Athens and Florence on a representative day in January 1996. Although the researcher focused on one single day in mid-winter, the simulation figures out 4 Kelvin higher indoor than outdoor temperature for Milano, a difference of 5 K for Dublin, 3 Kelvin for Athens and 2 Kelvin for Florence at 3 PM. Essentially, all simulated indoor temperatures are higher than the corresponding external temperatures. Analogously for 4th of July in summer, the calculated indoor temperature in the sunspace in Milano varies between 14,8 and 35,6 $^{\circ}\text{C}$ , whereas the indoor temperature in the building ranges from 14,2 to 32,6 $^{\circ}$  without sunspace

and several degrees higher up to 36,2 $^{\circ}$  with attached sunspace. For Dublin simulation results figured out interior temperature in the building changing from 10,3 to 18,0 $^{\circ}\text{C}$  as solitary building and in case of an attached sunspace from 11,1 to 19,6 $^{\circ}\text{C}$ . Likewise for Athens and Florence the indoor living space temperature spreads from 21.1 to 37,0 $^{\circ}\text{C}$  without sunspace and from 23,6 to 38,1 $^{\circ}\text{C}$  with sun space. In case of Florence the temperature ranged from 13,6 to 29,9 $^{\circ}\text{C}$  and 14,1 to 31,9 $^{\circ}\text{C}$  analogously.

However, as well described above by Taleghani, Tenpierik and van den Dobbelseen (2013) [56], sun spaces in southern longitudes like Italy, Spain, Greece and Northern Africa caused higher internal temperature in the building. In spite of this, Mihalakakou [67] identified a 5 to 6 Kelvin lower internal temperature in the residential building during summer in Milan and Athens respectively, when the sunspace south and west façade was shaded.

Similarly, although Monge-Barrio and Sanchez-Ostiz [53] constitute a proportional relation of both raising overheating and cooling loads with rising change in orientation from south to west for sun spaces in Spain, they advance the view of general benefits of shaded sun spaces for the adjacent living spaces in terms of lower daily temperature amplitudes, lowered averaged internal temperature and less radiant asymmetries verified for six Spanish cities.

#### § 2.6.4 Detected constructional parts on sun space energetic management

---

Rempel, Rempel, Gates and Shaw (2016) [54] investigate on a slab of a small sun space and verify that it is not eligible to heat the ground in order to store. Moreover the floor heats up and store. Thus it is more reasonable to thermally insulate and drainage the floor against the soil area-wise. This is reasonable in order to avoid heat losses in winter and by conduction with wet soil and to minimize risk of mould and water in construction.

The author (Rabenstein [34]) detects in the context of intermediate elements between living space and sun space a strong relation between the fraction of glazing within the element and heating energy demand. In case of low-energy houses it is essential to minimize glazing proportion, even if glazing profit from extreme low transmission value, high thermal quality respectively. Thus, low-energy houses loss demonstrably more heating energy via glazing towards the sun space than to environment via highly thermally insulated external walls. Moreover, by extreme glazing proportions, the sun space encounters less solid absorption area of comparably high thermal mass.

That consequently, on one the hand reduces the daily amount of potential heat return and on the other hand, regarding the living space energy management, increases losses due to the lower buffer potential of the sun space. Although, the living room principally benefits from solar gains through the intermediate element glazing, however according to filtering by the sun space envelope the amount is less and does not comprehend losses.

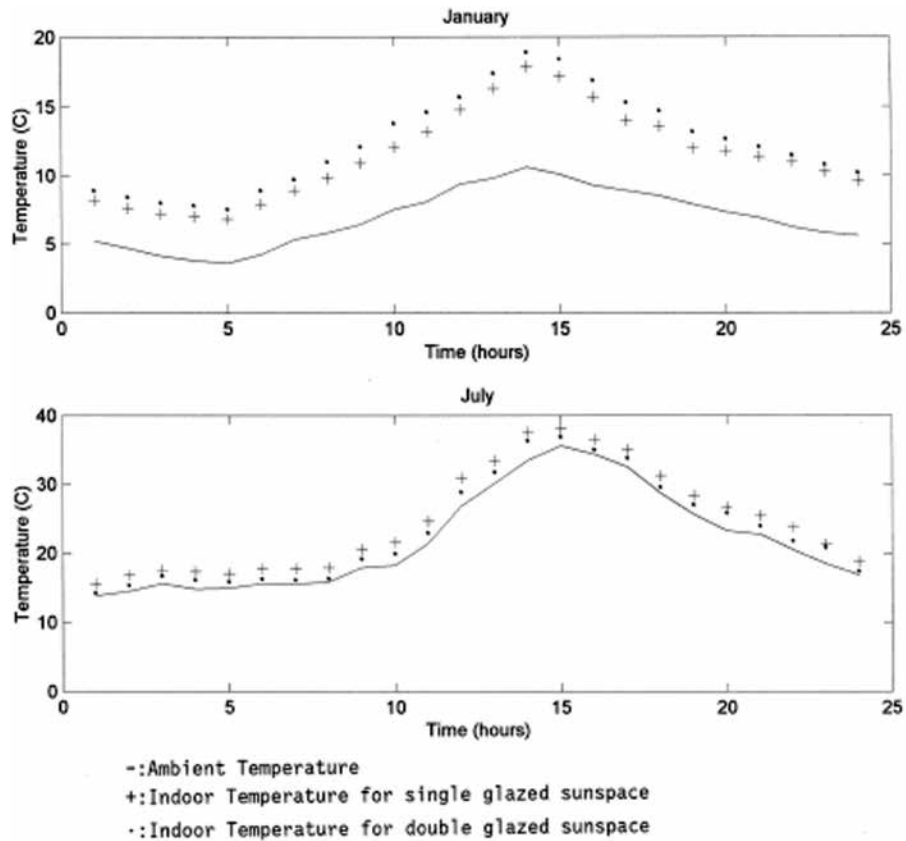


FIGURE 2.25 Fluctuation of ambient temperature related to glazing quality

Beside that findings does the building physical configuration of the intermediate element play an decisive role for the energy management of a sun space-living room system. As explained above, is minimizing transmission losses from the living space to the sun space crucial in respect to a substantial heating energy demand of low-energy houses.

As consequence, the intermediate element as wall or door or fold-work needs to be perfectly thermally insulated. According Rabenstein, nonetheless, in regard to an effective sun space energy management basing on a sufficient buffer and passive collector effect, the absorption abilities of this element calls for attention. As Rempel, Rempel, Gates and Shaw illustrate by a decided south façade / thermal mass area - ratio, a south facing and thus irradiation affected area of an intermediate element is crucial in terms of thermal absorption mass.

Thus, these interdependencies stipulate an intermediate element configuration, that on the one hand qualifies by comparably high thermal mass, that is open to absorb solar gains, and on the other hand, is thermally insulated inside towards the living room in order to minimize transmission losses.

Interestingly, Mihalakakou and Ferrante 2000 [59] detected higher indoor temperature in January with double-glazing applied (Fig.2.25), and higher indoor temperature in July with single glazing applied.

Babaei, Fayaz and Sarshar (2015) evaluated, that for Iranian cold winter conditions a flat apartment benefits mostly from an attached sun space with three flanking opaque walls, namely east and west wall and the intermediate wall. They, likewise Rabenstein, determined the sun space temperature to raise with applying an opaque masonry wall instead of an glazed partition element. Opposed to common sun space – adjacent zone configurations validates Tan [60] (1997) a sun space-air duct system, which heats north oriented spaces, for instant sun spaces with solar gains of south oriented sun spaces (see Fig. 2.26a). The projection is not heating the immediately adjacent space, but to raise temperature in a distant sun averted space. While the southern envelope of a single family home principally is built as a double skin façade, what incorporated double-glazing, it heats up.

By axial air ducts of less than 150 mm diameter a distance of 10 m is resolved simply by passive natural ventilation. No mechanical drive is necessary, solely temperature difference provokes the air exchange.

In this context, Holford and Hurt (2003) [61] (Fig.2.26b) investigated on design parameters of natural ventilation in atrium in order to initiate ventilation under inappropriate conditions. Similar to him they focus on solar gains as initiating force. Though the researcher also detect relations between atrium dimensions, thermal enclosure surface qualities, atrium height and, what reveals to be crucial, small but effective opening area of supply air. Thus, they developed by physical models and theoretical calculations prediction algorithms of thermal stratification as well as air internal air flow rates.

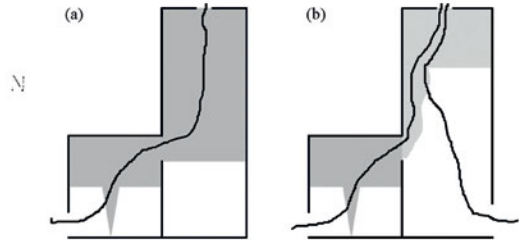
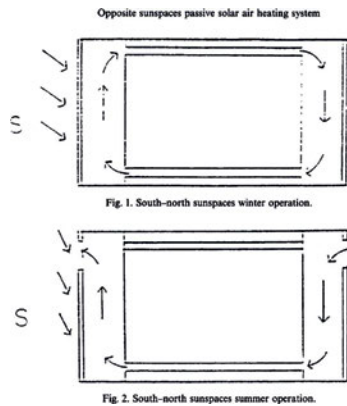


Fig. 1. An enclosure with (a) an unventilated atrium, and (b) a ventilated atrium. The arrows indicate the flowpaths through the enclosure. The shading represents the warm air in the upper regions of the room and atrium. The lighter shading in the upper atrium in (b) is representative of the cooler layer which forms due to the direct ventilation.

FIGURE 2.26 a.) principle of opposed sun spaces by Tan,1998, and buoyancy effect by Holford, Hunt, 2003

By this concept, according Tan, 70% of heating energy is saved for this global radiation averted space in respect to certain temperature set points. Beside Tan states that energy saving strongly depends on climatic conditions, for Ankara winter 1993-94 is achieved 100% in October, 70% in November, 58% in December, 72% in January and 69% in February, 81% in March and 100% in April. On the contrary, beside 35°C external temperature overheating in sun spaces is limited since the ambient temperature never exceeded 26°. This system shows comparable efficiency with a case study of east-west orientation, whilst 13 m space distant was overborn.

Typical for the sun space design is a depth of not more than 1.5 m. Against the background of Ankara climate conditions, sun spaces turns facades that loose energy, into façade, that generate energy.

Despite common sense in science, Aelenei, Leal and Aelenei [55] in 2014 evaluate for six Spanish cities an interior sun protection, although of high reflection quality, as sufficient and recommendable for still acceptable indoor temperature in south directed sun spaces. Effective internal blinds have additionally been proven by Wang, Pichatwatana, Roaf, Zhao, Zhu and Li (2013) [62] for large multi-story atriums in tropical climate, as well as Abdullah and Wang (2011) [63] did. They differentiate between high level blinds, which are close to roof glazing and low level blinds with a distance of 3 to 5 m below roof glazing. Since the authors inspected dry bulb temperature, surface temperature, operational temperature and air velocity in a natural ventilated office building, they conclude, that low level blinds provide more acceptable operational temperature and parallel sufficient illumination by internal reflections. To them, lower blinds, of significant distance, reduce solar gains for 50% opposed to that higher blinds solely for 10%.

Along the lines Abdullah and Wang also recommend considerable voids between transparent roof, windows respectively and internal sun shading. A distance of at least 1 m helps to keep inevitable overheating close to the roof space in order to prevent lower occupational spaces. Although, they inspect a three-story office building in the tropics they derive and recommended applying the findings to levelled space volumes to whom exalted or elevated sun spaces definitely belong.

According to their investigations, they substantiate Holford and Hunts conclusions of the positive effect of narrowed roof spaces aside clerestory windows, similar to sun space gable incorporated tilt-windows, on the effectiveness of natural ventilation. Furthermore, the authors emphasize the positive effect of low longwave re-emitting internal blinds to prevent surfaces from heating up.

## § 2.6.5 Inertia as a control tool for heating energy saving and thermal comfort

---

Thermal mass and resulting inertia have been inspected recently by Rempel, Rempel, Gates and Shaw (2016) and Sanchez-Ostiz, Monge-Barrio, Domingo-Irigoyen and Gonzalez-Martinez (2014) [37]. Typical for Northwest Pacific climates according to the researcher are mild winters, but, nonetheless long cold springs. Consequently, heating period extends from mid-September to mid-June, what justifies investigations on heating energy saving by sun space thermal mass. According to their hypothesis and opposed to Lumbis (1988) [35], who advocates south direction and maximum thermal insulation for maximum saving, is glazing and orientation for planning overrated.

But, however, thermal mass is a key parameter for substantial sun space design and matches actually the occupants specific space utilization. From perspective of the researcher, the occupants specific space utilization either justifies maximum heating energy saving for sun space and adjacent space by preheating or proper ambient temperature in forthcoming morning hours, in night time or in the evening. Especially in the evening, they identify the time between 5 to 10 PM as preferred period of occupation. Hence, main research subject is the influence of thermal mass on remaining indoor temperature in Northwest Pacific climates. Consequently, the researcher investigate on diverse thermal mass of intermediate and enclosing walls and of the floor as well.

First, they established a floor and wall thermal mass area ratio related to the area of south facing and correspondingly solar gaining façade area.

This ratio varies between one to three times. Secondly, they essentially varies floor thermal mass by screed thickness between 1,5 to 15cm.

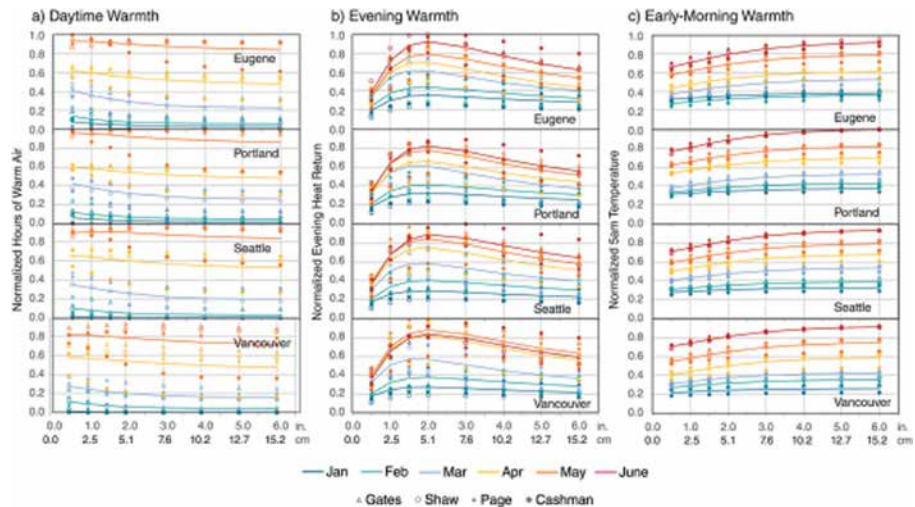


FIGURE 2.27 Heat return measurement in relation to floor thermal mass

Numerical simulations recovers that conventional high thermal floor mass by screed and concrete of > 15cm, beside it is eligible for preventing overheating in summer and minimizing diurnal temperature swings as well, prevents heat to return before the next morning (4 to 6AM). Further, the thermal effect of thermal floor mass of > 15 cm is limited.

Thus, the researcher recommend a maximum thermal mass of 15 cm. If heat return for space heating or night cooling is intended, the authors identify maximum 5,0 cm to be the most appropriate (Fig. 2.27) thermal mass dimension.

Moreover, this dimension supports the highest ambient and floor temperatures between the desired occupation time between 6 to 9 PM for Northern Pacific climates with wintertime exaggerated to April and even mid-June. Furthermore in details, with less mass the heat return is increased by 50% in the evening, namely 6 to 12PM period, compared to conventional thermal mass dimensions. In case, the sun space is used diurnal or is intended to preheat effectively adjacent space by natural warm air exchange, thermal floor mass were identified to be sufficient of less than 2,5 cm.

While Rabenstein [24] as well as Monge-Barrio and Sanchez-Ostiz [53] advocate intermediate walls of high thermal mass, the above mentioned researcher neglect the importance of this part in context of thermal mass.

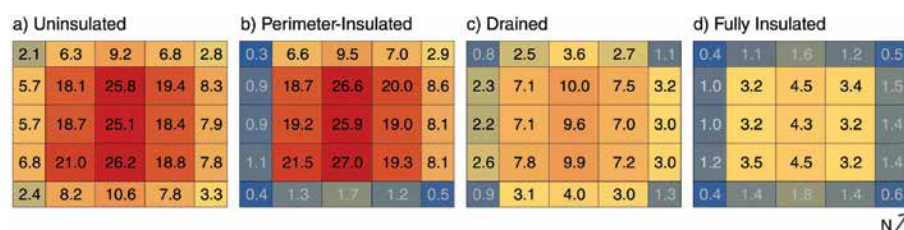


FIGURE 2.28 Transmission loss rates of sun space floor slab related to building physical quality and water treatment

Summarizing, Rempel, Rempel, Gates and Shaw detect that the design of thermal mass substantially depends on the kind of usage, specific preferred occupational daytime and specific energetic intend of the sun space. Further, in respect to any kind of usage the floor slab need to be thermally insulated area-wise more than perimeter-wise against wetly (Fig. 2.28) soil in order to minimize transmission losses that causes ambient temperature to descend. Besides, they identify conventional thermal mass rules to be overestimated, solely smart thermal mass is eligible to provide preheating and energy saving on adjacent spaces by natural interzonal ventilation. Nevertheless, proper thermal mass still contradicts heat return potential by design and less temperature swings whilst the day.

In a more theoretical and abstract way, Oliveti, Arcuri, De Simone and Bruno [48] in 2011 develop the “effective absorption coefficient”  $\alpha_e$ , which expresses the monthly determined collection capacity of a specific sun space to absorb heat from radiation entering the space. That characteristic was subdivided into  $\alpha_f$  and  $\alpha_w$  what represent the effective absorbed energy by floor and walls, respectively, and is substantially depending on the mean monthly radiation transmission  $\alpha_e$  through transparent fractions of the sun space envelope.

This factor expresses the ability of sun space massive elements to partly absorb energy by solar gains. This parameters were conducted and validated by numerical simulation and experimental verification and considered with the Fresnel formalism directional aspects of beam radiation and temperature field of opaque walls and floors.

In this context, the researcher detect sun space walls in general to be more capacitive than floors. Further, Oliveti, Arcuri, De Simone and Bruno investigated similar to

Rempel, Rempel, Gates and Shaw the heating energy emitted by opaque building elements in terms of heat return. Therefore, they set the energy emitted and transported simply by convection in relation to the energy absorbed, and hence, developed a mean monthly utilization factor of the solar energy  $\eta_{\text{eff},u}$ . A further distinction sets the energy re-emitted and transported mechanically in relation to the energy absorbed  $\eta_{\text{eff},u,v}$ .

They developed this characteristic further by considering the energy, that could be used for heating adjacent living space zone of  $>+20^{\circ}\text{C}$  ambient air temperature, and thus, the effect remaining emitted energy is describes as the mean monthly utilization factor of the adjacent spaces obtained by the ventilation flow  $\eta_{\text{eff},u,v}$ .

Due to their simulations, the authors seek the indoor air temperature in a  $18\text{m}^2$  and double-glazed sun space in Cosenza in January to be higher than external temperature as soon as the external temperature outrun  $+4^{\circ}\text{C}$ . Regarding an  $af$ ;  $\alpha_w$ -value of 0,2, the opaque surface temperature is 2,6 K [64] higher at night than the air temperature. Consequently, nocturnal energy contributions by thermal mass to the sun space were observed to be higher than diurnal ones. Surface temperatures of transparent surface arranged between the air and solid surface temperatures night times, but, nonetheless exceeded air temperature in diurnal perspective. Thus, interestingly, they find out in respect to January observations, that roughly spoken opaque surfaces heated the sun spaces and transparent surfaces cooled the sun space.

In order to figure out different utilization factors and thereby optimum sun space thermal design, they vary between a moderate  $af$ ;  $\alpha_w$ -value of 0,2 and an enhanced of 0,5 effective absorption factor and between an unshaded and unventilated and an shaded and ventilated model for Cosenza. The month-wise investigation shows, that the utilization factor was the highest in winter month with 0,15 to 0,18 and lowers towards the mid of year. Mean ambient air temperature raises in mid-year month to  $32,7$  to  $37,3^{\circ}\text{C}$ . If the higher effective absorption factor is applied, utilization factor raised to 0,2 to 0,24 in winter and to 0,19 to 0,20 in summer, whereas ambient air temperature by mean increases by 3K in winter in up to  $42,8^{\circ}\text{C}$  in mid-summer months.

In order to conclude, a rise in effective absorption leads to a rise in utilization factor and ambient air temperature. On the contrary causes shading and ventilation to the  $af$ ;  $\alpha_w=0,2$  version no significant lowering in the utilization factor, but causes slightly lower ambient air temperature in winter month and considerable lowering of 5 to 10 Kelvin in summer time.

Likewise the shaded and ventilated  $af$ ;  $\alpha_w=0,5$  version profits from 18% higher utilization factors in winter, whereas utilization lowered slightly in summer. Parallel, the

ambient air in winter remains comparably high, while it lowers significantly in summer for 15 Kelvin to maximum 28,1°C (42,8°C with  $\alpha_f$ ;  $\alpha_w=0,2$ ).

Oliveti, Arcuri, De Simone and Bruno observes, that the sun space air temperature is mostly close to the mean radiant temperature. An investigation of the monthly mean operational temperature showed, that with change from  $\alpha_f$ ;  $\alpha_w = 0,2$  to  $0,5$  the operational temperature from March to October inclusively raised for by mean 5 Kelvin in unshaded and unventilated sun spaces for all three inspected Italian cities Cosenza, Rome and Milan. Opposed to that, shading and ventilation results in lower operational temperature in month from February to October. Especially in summer a difference of 7 to 10 K is evident.

What is more, with shading and ventilation of the  $\alpha_f$ ;  $\alpha_w = 0,5$  version the differences of operational temperature assess with 1,5 to 3 Kelvin in winter month, but with 12 to 15 Kelvin in summer. A comparison of the low effective absorption unshaded and unventilated version with the high effective absorption and shaded and ventilated version beside Milan show, that on the one hand in winter month the shaded heavier variant shows 3 to 5 Kelvin higher indoor operative temperature, however on the other hand in summer month 7 to 10 Kelvin lower temperature.

Concluding, this study shows balanced mean monthly operative temperature within a tight bandwidth of 10 to 12 Kelvin without considerable amplitudes the entire year in combination of high effective absorption and internal shading and ventilation.

## § 2.6.6 Summary

---

Literature research on sun spaces elaborated four major investigational focal points, that have called scientists for attention the last four decades. The four sub-jects include theoretical refined model algorithms for proper energy and comfort calculations, design rules that optimize energetic and thermal behavior, constructional enhancements and detailed descriptive knowledge about thermal mass and inertia.

Summarizing literature review points out, that researcher and practitioner have investigated on dry bulb and operational temperature, on building physical optimization of building elements, on calculation models and operational strategies as well, but, however, very few on detailed local discomfort analysis regarding striation, radiation asymmetries, outrunning surface temperature and little on building physical comprehension by renewable energy. Unanimous opinion of the science body put em-

phasis on the significant influence of the local climate conditions on effective indoor thermal comfort quality and energy management.

Among the field of calculation and simulation methods, many researcher state that calculation algorithms in the past allowed either only stationary and momentary evaluations, which lack of preciseness and neglected to comprehensive annual analysis. While calculations codes based on monthly mean external temperature values and generated quasi-steady-state analysis, dynamic weather data based hourly simulations significantly more precise investigate on internal energy management and thermal comfort qualities. Modern codes firstly improved by including and balancing internal gains, secondly by calculating demonstrably differentiated absorption, reflection and transmission of irradiation and space internal absorption and reflection as well as relinquishing long wave radiation. Moreover, scientists evaluated the lack of concurrent existing codes of being applicable, beside moderate transparent ribbon facades types, for one hundred per cent transparent spaces.

Further, others enhanced existing codes in order to change from a nodal notion of a space to a net notion of especially high and multi-levelled spaces. That development gives room for a specified ambient air and volume analysis, which in particular considers stratification and thermal lift. As a consequence of previous established codes, cooling loads have been overestimated, while heating loads diametrically have been underestimated. As a result, the effective absorption coefficient was developed and established as a ratio expression of monthly weighted potential of storing capacity of entering irradiation and effective utilization factor.

On the other hand diverse researcher determined a clear-cut relation between the transparent envelope area to floor area and balanced energy consumption. A factor of 2,21 was introduced to be sufficient. Beside glazing to floor ratio, also space depth influences considerably energy consumption. Thus, scientists recommend rather wide than deep sun space dimensions in order to optimize heating by passive solar gains. As a conclusion, an increase in depth can solely be comprehended by a descend in glazing U-value, what actually is finite.

The body of researcher comes along, that sun spaces in general help to shorten the heating period of adjoined living spaces or even entire living units. While for Iranian climate recently heating energy saving potential between 40 to 45% was evaluated, in 1997 an opposite sun space concept was calculated to provide 70% of heating energy saving for Greek climates.

Several studies point out, that high absolute energy saving potential grows the older and worse insulated the adjacent building is.

Opposed to that modern and thus highly thermally insulated residential buildings are eligible for high relative energy saving potential since the absolute energy consumption level is extremely low anyway. Most interesting information is the insight of divers researcher, that opaque and thermally insulated flank sides of sun spaces or an three-sided embedding of the sun space in an energetically high quality living space are demonstrably beneficial for reduced heating energy consumption. That goes along with a recommended inclination of the roof of 45°.

Nonetheless, researcher evaluated that energy sufficiency and high quality thermal comfort are controversial. Hence, either extraordinary energy efficiency exacerbates indoor thermal comfort, or high quality of thermal comfort considerably effects energy efficiency.

In terms of construction researcher identified beside the necessity of effective sun protection the importance of intermediate elements between sun space and adjacent room. Either build as opaque wall with small door opening or as window or fold-works, energy saving and management calls for a physical separation. Among this scientists revealed that the separation element should profit from high absorption ability and thermal mass in order to utilize internal solar gains, but is asked to provide only little transmission in order to minimize losses from the living space towards the sun space. Although a sun space in general offers thermal buffer qualities and adjacent spaces generally benefit from passive solar gains, intermediate elements especially implemented in modern building are recommended to minimize transparent glazed parts in favor of thermally highly insulated layers which equal thermal quality of low energy house external walls. The risk of glazed intermediate walls to transmit heating energy towards the sun space is bigger than external walls to transmit to environment.

Researcher unanimously recommend restrained opening areas for natural ventilation. Simulation studies and practice evident that natural ventilation in terms of space cooling is most efficient with opening areas less than 30% of the entire sun space envelope. Accordingly, shading coefficients were evaluated to be energetically most sufficient in order to promote a balanced heating and cooling energy consumption in the range between 40 to 60%.

Thinking about inertia is inevitably linked to considerations of actual space use and occupation patterns. Inertia can be engineered with designed thermal mass. In this context thermal floor made of common floor screed or concrete density can vary in terms of thickness between 2,5 and 15 cm.

Either thermal mass provides preheating of adjacent living zones or thermal buffer effect immediately, or thermal mass provides heat return in evening hours during

preferred occupational time from 5 to 10 PM. If thermal mass is enforced, heat return can be displaced to night and supports effective nocturnal free cooling or even preheating for consecutive morning hours.

Thus, beside local climate a specific defined utilization factor represents the amount of energy absorbed and the amount of energy emitted and transported by convection and by this accentuates significance of inertia.

Rather scientists identified a strong relation between floor and wall thermal mass area ratio related to the area of south facing and correspondingly solar gaining façade area. This knowledge helps to engineer thermal comfort and heating energy demand if detailed local climate data and dynamic simulation methods are applicable.

All in all, the studies put emphasis on substantial thermal benefits sun spaces provide in general. Hence, this archetype is promoted to shave peak indoor temperatures of adjacent zones as well as reducing amplitudes and fluctuations of even this.

---

## § 2.7 Thermal and energetic analysis of an experimental test sun space

---

Empirical investigations on sun spaces or on any other architectural archetype or specifically focussed types of zone require determination of prerequisites and background conditions. Standards define categories of thermal comfort qualities. Reference for thermal comfort either can be set point temperatures of resulting (operative) temperature, or temperature differences between external and internal temperature. Additionally accounts in terms of heat balance model the calculated predicted mean vote (PMV) of space occupants in relation to activity, metabolic rate, clothing insulation factor and ambient air velocity and percentages of predicted dissatisfied (PPD).

### § 2.7.1 Determination of comfort category according standards

---

For that reason, we once prerequisite define reference values on which both experimental (Chapter 02) and theoretical measurement (Chapter 08) values refer to. Substantially, research on sun spaces considers research on potentially and mainly

naturally ventilated spaces. Yet, natural ventilation is limited in winter months related to extremely low external temperature, opposed to that intermediately periods and summer allow occupants to control thermal conditions by ventilation. Especially, investigation on summer months calls for explicit application of adaptive comfort algorithms since external and internal climate conditions often changes on which occupants rapidly have to adapt to in terms of activity, clothing and ventilation.

Since sun spaces mostly provide living space elongations, recreation and leisure are main space utilization forms. Relaxed and sedentary activity of occupants is typical for this space typology. Space occupants normally belong to no specific group of sanitary restricted persons like old man, neonates or extraordinary debilitated persons (DIN 15251, Tab.1, Cat. I,[20]).

### § 2.7.1.1 Evaluation prerequisites : comfort categories and threshold values

---

For that reason it is sensible to determine sun spaces in the context of DIN 15251-2007 to residential buildings, and thus according table A3 to category II with indoor set points for winter of 20°C to 25°C and 23°C to 26°C for summer for not mechanically ventilated spaces. In this context metabolic rate  $M$  is limited to 1,2 met, what equals typical relaxed and sedentary activity level of  $\approx 58$  W according to EN ISO 7730 [21], Append. B, Tab. B.1.

Further, clothing factor is determined about 1,0 clo in winter and 0,5 clo for summer months. Accordingly, the clothing isolation factor  $I_{cl}$  regulated in EN ISO 7730:2005, Tab. C.1, is limited to 0,110 W/m<sup>2</sup>K for winter and to 0,08 W/m<sup>2</sup>K during summer time. Since thermal sensation beside radiation (skin temperature, clothing insulation) is ruled by convection for more than 30%, air velocity is a parameter, that is not to be neglected. Since no mechanical ventilation but exclusively naturally induced air movement, air velocity is considered to be constantly  $< 0,1$  m/s related to EN ISO 7730:2005, Append. A, table A.2. Against the background of evaluations of PMV and PPD DIN EN ISO 7730 limits PMV interval according thermal comfort quality category II to -0,5 to +0,5, while PPD is limited to  $< 10\%$  (Append. A, Tab. A1).

In this context, acceptable calculated percentages of dissatisfied (PD) occupants for evaluated local discomfort are restricted to  $< 5\%$  for vertical air temperature striation analysis,  $< 10\%$  for cool or warm floor temperature analysis and  $< 5\%$  for radiation asymmetry analysis. Thermal comfort evaluations on sun spaces in this thesis either empirical or theoretical consider this appointed before mentioned framework of categories and threshold values.

### § 2.7.1.2 Winter / Summer according Bewertungssystem Nachhaltiges Bauen (BNB)

---

The Bundesministerium für Verkehr, Bau und Stadtentwicklung (Federal Ministry for Traffic, Build Environment and Urban Development) defines the winter and summer period in the context of thermal comfort and dynamic thermal building simulation in BNB characteristics. Hence, the period, when buildings require to be heated, respectively winter, lasts from 1st of November to 31th of April [65]. Accordingly summer is defined from 1st of May to 31th of October. This thesis refers in terms of methodology to the by BNB defined summer and winter periods.

### § 2.7.1.3 Major sun space occupational period (5 to 10 PM)

---

Evaluations of indoor thermal comfort in sun spaces especially require considerations of daily hours to investigate and time intervals of special interest. Consequently, since sun spaces are living spaces mainly for recreation purpose, sun spaces are mainly utilized in the early evening and late afternoon hours. Thus analysis of even this period of time is characteristic and essential. Similar to Rempel, Rempel, Gates and Shaw [54] (2016; see Chapter 2, section 3.5), who identified sun spaces in the time period of 5 to 10 PM to be most frequently occupied, the author of this thesis decided to determine the five hours from 17 to 22 o'clock to be of special interest.

In terms of passive solar gains this late period of day calls for special attention.

Consequently, inertia is a subject closely related to local climate conditions, sun space preheating and potential for peak shaving of maximum peak temperatures.

## § 2.7.2 Method of empirical data processing, synchronization and fault distinction

---

Evaluation of empirical test set up data (see figure 2.11) requires different intermediate steps of data conversion. Figure 2.29 illustrates the different steps of differentiated data quality in chronological order. Starting with minute-wise single value logging of all selected KNX data points, the first action is group-wise storing in the Eisbaer software database. After finishing experimental measurements, the single values can be searched by time interval of interest.

Single minute values from the database can be selected and copied to Excel for further information handling. Before any closer evaluation, the copied values have to be proven on minutes, hours and days of system fallout, no measurements data points and time periods of accidental opened openings. Consequently, either affected data is to be eliminated or times to be excluded from further investigation.

After prove of quality check, single minute-wise data can be transformed into hourly values, that are common in science for thermal comfort evaluations. Generating the mean of minute values considers all climatic changes during an hours that effects indoor thermal comfort. Transformation was sufficient with generation of pivot tables, since this automatic procedure reliably generates means of selected minute values even when neither 60 values represent a specific hour nor consecutive phases of several minutes are applicable.

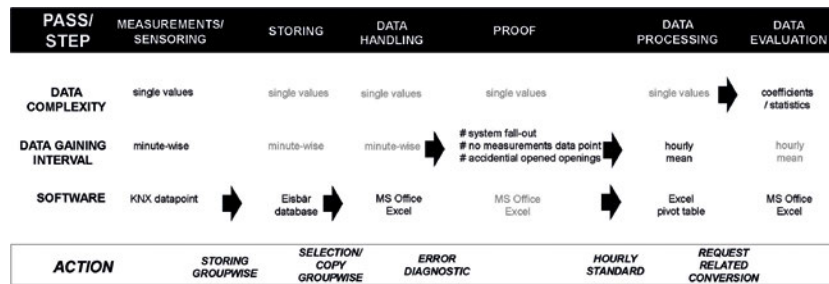


FIGURE 2.29 Process scheme of empirical data generation and prove of quality

After the generation of hourly values, further transformation of data allows the allocation of value sets of interest in order to generate coefficients or calculation to other key parameters.

### § 2.7.3 Active heating : floor heating schedule

Monthly schedules were generated as a workable result of the process of data quality prove. Figure 71 illustrates a representative schedule covering October to December 2015. The schedules contain all 24 hours a day and remark by color, if the data is complete and of quality without any undesired influence of opened apertures. Colors additionally inform about action of floor heating or ohmic heating. Additional

schedules are in Appendix A1 for the period of October 2013 to March 2016. In the context of the quality evaluation and prove routine of the empirical data explained in 4.2 monthly schedules of reliable data days and heating schedule was (Fig. 2.30) plotted.

These schedules helped (for more see [APPENDIX B.1](#)) to visualize days of qualified hours with reliable data as well as the days of conditioning actions. Days of recorded system fall out, missing hours or unintended opened envelope openings are lighted out. Hours with activated floor heating are lighted red.

## § 2.7.4 Empirical analysis of major thermal comfort aspects

---

The empirical data from the test set up sun space was evaluated from different perspectives of thermal comfort quality. Especially the resultant temperature was plotted against different independent variables like external temperature, humidity or thermal mass in order to inspect comfort quality. The following sections exemplify major thermal comfort aspects in detail.



## § 2.7.5 Empirical monthly analysis of resultant temperature in set-point interval

Heating set point in winter period has been set to 20°C resulting temperature for a prerequisite thermal space design based on an indoor thermal quality according Category II of DIN EN 15251 (residential buildings, and activity level of 1 to 1,2 met, clothing factor 0,7 to 1,0), Tab. A3.

The following comfort evaluation bases on a typical set in function of the resulting indoor temperature and the external dry bulb temperature. Commonly cloud diagrams illustrate trends of distribution. Although, the test sun space is considered to be non-mechanically ventilated, for a resulting temperature analysis the upper temperature level of 26°C, normally for mechanically ventilated spaces, was applied. This limit was put into consideration to determine cumulative frequencies of hours above a standardized limit value. Starting with January, several month are represented as cloud diagrams in [Appendix B.2](#). The most informative cloud diagrams are explained and analysed in this section.

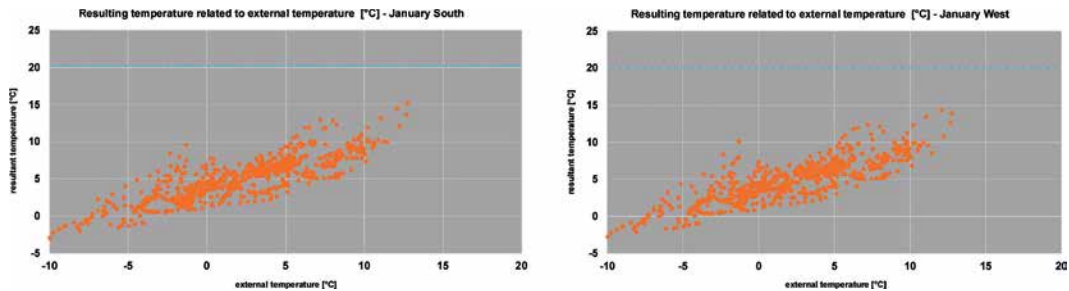


FIGURE 2.31 Cloud diagrams of operative temperature distribution related to external temperature for January – South/West

Hours with operative temperature related to the external dry bulb temperature in January were plotted for the south and west space flanks separately in the Figure 2.31. In January, 20°C operative temperature was not reached at any time either in the south and the west flank. Maximum resulting temperature was about 15°C, whereas the body of temperature was between 0 and 10°C. The plots show, that freezing limit was exceeded for a couple of hours. The minimum temperature was about -4°C. The plots interestingly additionally illustrate, that even though the external temperature was below zero °C, the sun space profited for many hours from operative temperatures between zero to five or even ten degree Celsius.

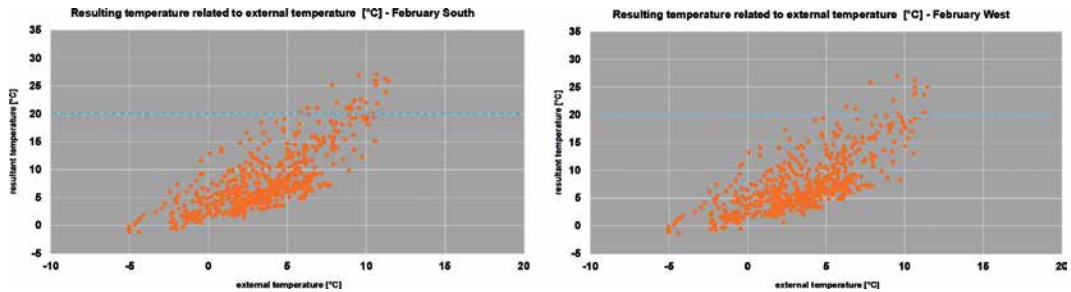


FIGURE 2.32 Cloud diagrams of operative temperature distribution related to external temperature for February – South/West

In Figure 2.32 are plotted the operative temperature towards the external temperature for February. In February for a couple of hours the resulting temperature exceeded 20°C set point limit. The gross of operative temperature is distributed between zero to ten degree Celsius. Figure 2.32 imposingly shows that even in February the resulting temperature in the sun space can be 5 to 10 and even 18 Kelvin higher than the external temperature actually is. Between -5 and +5°C external temperature the correlation to operative temperature is demonstrably strong. But, however, above +5°C the field of correlated resulting temperature is widespread and less homogeneous. Even in February maximum resulting temperature of 28°C is identifiable. The south and west flank behave similar to each other.

The resulting temperature in March exceeds for approximately 30% of the 775 surveyed hours 20°C. Maximum temperature of 38°C is possible in March. Despite overheating is no serious aspect in March, operative temperature above 26°C results actually with external temperature of +4°C and higher. Considering April, approximately half the 408 observed hours represent resultant temperatures above the set point value for winter of 20°C. Despite of external temperature below zero degree Celsius, indoor temperature always remains above +9,5°C. Typical for the last winter month April is a tendency of a considerable amount of hours above 26°C.

These operative temperature level includes maximum temperature of 30 and 35°C, even correlated to external temperature of less than 15°C and 20°C. The graphs for March and April demonstrate, that south and west flank thermally behave equal.

The operative temperature in May also does not lower 10°C and rarely exceeds 35°C. (Fig.2.33). The correlation field appears to be more tight compared to March and April without many outliers. From this we can derive, that for May thermal behaviour appears to be well stable and balanced. The body of resultant temperature is related

to the comfort interval 20 to 26°C. Obviously, against the background of internal sun protection and no active natural ventilation, nearly one third of 720 analysed hours represents operative temperature above 26°C. This observation makes aware of the beginning tendency of overheating.

In June, July, and August an operative temperature of at least 15°C is always attained. However, in June more than the half of 552 hours belong to the temperature interval 26 to 50°C. Significant for June is the observation of the highest scored operative temperature of 50°C considering the entire summer period. Thus, maximum resulting temperature raised for 15 K compared to April. In terms of correlation homogeneity June shows the most outliers and thus an inhomogeneous reaction of the resulting temperature on the external temperature and irradiation.

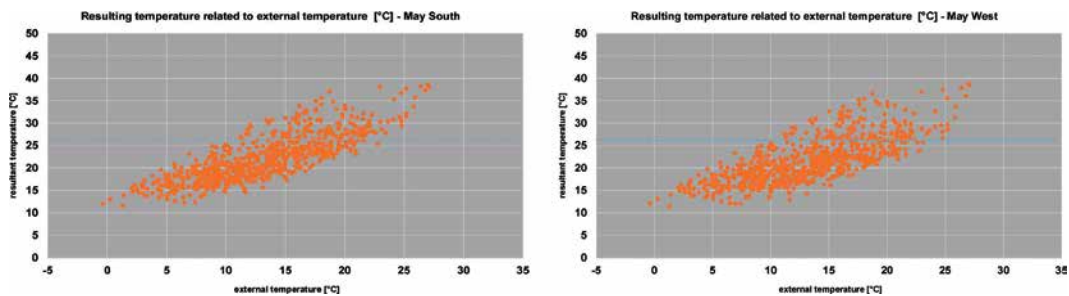


FIGURE 2.33 Cloud diagrams of operative temperature distribution related to external temperature for May – South/West

Focussing on July, more than two third of all recorded 432 hours recovered resultant temperature higher than 26°C. Maximum temperature is 44°C. In August two third of 648 observed hours were accompanied with operational temperature far above 26°C. Maximum operational temperature of 46°C was specific for August and equals July. Since outliers minimized in July and August, the clouds shows more homogeneous correlation between external climate impact and resulting operative temperature.

For some hours, the operational temperature in August above 26°C is equal or even lower than the external. This indicates an effective night cooling process. South and west flank behave similar to each other. Nonetheless, overheating is a dominant aspect typical for June, July and August.

The gross of hours in September covers resultant temperature between 15 and 25°C. Approximately one of five of the 696 surveyed hours actually exceed 26°C, what drastically limits the tendency to overheat. Maximum temperature is about 34°C. September represents a well-balanced thermal comfort for a sporadically heated and natural ventilated not cooled space.

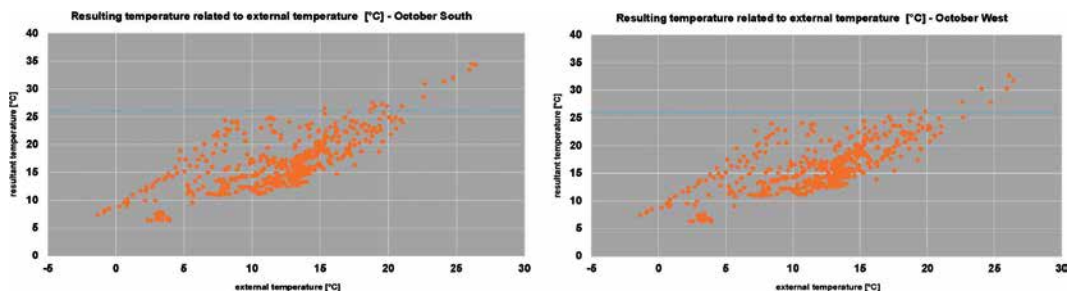


FIGURE 2.34 Cloud diagrams of operative temperature distribution related to external temperature for October – South/West

October is the last month belonging per definition to the summer period. Figure 2.34 shows two cloud diagrams, which demonstrably show a significant general decrease in operational temperature. Firstly, the upper limit relevant for summer of 26°C is exceeded simply for a couple of hours. The body of hours is plotted in the band between 10 to 20°C. This distribution calls for attention, because the test sun space tended to represent more colder than warmer resultant temperature compared to the six previously discussed months. The lowest temperature is about +6°C. This is even resulting with correlated external temperature of +4 or -2°C. The cloud shape expresses representation of indoor operational temperature of 10 or 20°C both at 5 and 17°C. This wide reactive correlation intervals indicates, that the test sun space in October does not profit from such irradiation and daily sun shine periods that are typical for June or August.

The cloud diagrams (Fig.2.35) for November undoubtedly illustrate, that the temperature minimum set point of 20°C operational temperature is rarely accomplished. Only a dozen of hours satisfy comfort requirement exclusively by passive solar gains and additional renewable energy fed floor heating. The cloud shape is very inhomogeneous, what indicates many diametric changes in external conditions. Beside maximum temperature of 28°C, the minimum temperature lowers towards +4°C. Although, both sun space

flanks thermally behave similar, the south flank profits from a few more hours with slightly higher operational temperature.

Considering December, for both flanks cannot be identified any hours with resultant temperature of or above 20°C. While the body of resultant temperature ranges between +6 and +14°C, maximum temperature solely reached 19°C, respectively 18°C for the west flank. Since there are outliers of straightforward number and the cloud shapes appear straight and homogeneously, we can implicate for December a clear-cut linear relationship between external and resulting temperature.

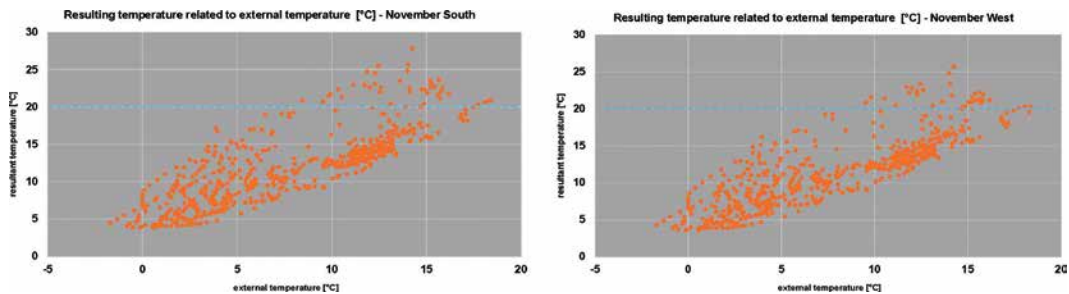


FIGURE 2.35 Cloud diagrams of operative temperature distribution related to external temperature for November – South/West

## Summary

In order to summarize the findings of the before analysed cloud diagrams, there is clear information about the frequency of satisfying the lower thermal comfort limit, respectively the 20°C set point. Essentially, in all twelve analysed month providing operational temperature exclusively by solar gains and additional floor heating was difficult. Since only in June, July and August operational temperature mostly exceed 20°C and in the rest of summer month almost two third of monthly hours represent temperature above the set point, the minimum thermal comfort requirements are passively fulfilled solely in midsummer periods. September and May as intermediate months, showed balanced proportions of hours above and slightly below 20°C.

In October the gross of hours covers the interval between +5 to 15°C. By contrast, all midwinter months like November, December, January and partly February display resultant temperatures far below the lower limit. Hence, thermal comfort is roughly not provided. However, although February belongs to winter, it is obvious, that a significant

high number of hours represent operational temperature above 20°C. March and April behave similar, what highlights a possible wide spread in operational temperature typical for spring month including +5° to 40°C.

Opposed to that, linearity in thermal indoor-outdoor relation raised in winter months like December, January and February. Nevertheless, cloud diagrams in Figure 2.33 impressively illustrate, that the test sun space tended to exceed the upper comfort limit of 26°C and thus tended to overheat. Overheating dramatically raised in May to August. In order to be more precise, while overheating raised, the number of outliers also raised. This notice foster the finding of decreasing linearity in correlation between outdoor and indoor temperature with external temperature above 25°C.

More of interest is the surveillance of considerable hours in which the operational temperature is despite of over-average high external temperature of 30°C or 35°C explicitly lower than the external. This difference can amount about 5 to 10K. This observation is typical for July, August and September. Although previous observations developed an insight in a positive non-linearity of external-internal temperature relation, this discovery provides a disproportional completely diametrical negative understanding. Finally, we can conclude, that in contrast to massive and predominant opaque building archetypes with incomparably higher thermal mass like brick enclosed living spaces this sun space partly extremely unpredictably reacted on external conditions.

A detailed analysis of resultant temperature in terms of absolute and relative assessment is elaborated in 4.5.3 of this chapter. Further, this section contains a decided analysis of the floor heating effect on operational temperature on monthly basis.

### § 2.7.5.1 Special days, overheating, cooling by natural ventilation

---

High internal temperature caused by high irradiation can turn into overheating of sun spaces. Overheating can be compensated, eliminated respectively, by especially natural ventilation. Natural ventilation in sun spaces is practicable with opening of vertical fold-works, doors or roof integrated sliding windows. The following graph in Figure 2.36 and further six graphs provided in [Appendix B.3](#) plots sensed indoor dry bulb temperature with entirely closed sun space envelope (overheating) and following with opening of especially large area fold-works (south : 2,2x3m = approx. 6m<sup>2</sup>, west: 2,2x4m = approx. 8m<sup>2</sup>). The recorded progress of dry bulb temperature indicates for different moments in the year the effectiveness of natural ventilation.

Figure 2.36 shows an indoor dry bulb temperature of 25,3°C at 13:45 on 27th of March 2014. Following on the opening of fold-works dry bulb temperature immediately descends towards a level of 20 to 20,5°C.

Within a time span of 135 minutes dry bulb temperature never narrows external temperature on March 27th, nonetheless a shift of 5 Kelvin always remained. Figure 92.2 illustrates the progress of dry bulb temperature of approximately a month later on 23.4.2014. When openings were opened at 14:24 o'clock dry bulb temperature increased from 33,8°C within 35 minutes onto a level of 31°C.

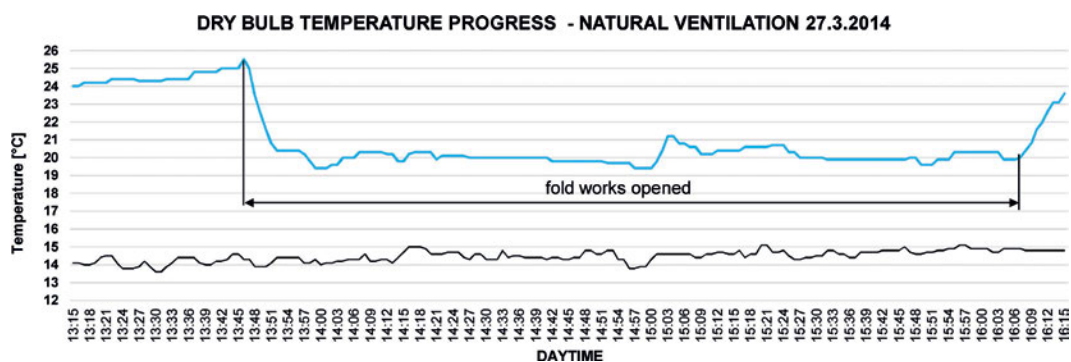


FIGURE 2.36 Dry bulb temperature progress – natural ventilation 27.3.2014

Natural ventilation was marginally effective for 3 Kelvin although external temperature changed on a level between 21,2 to 23,7°C. However, 90 minutes of opened fold-works resulted in an effective dry bulb temperature of 29,8°C.

Figure 2.37 plots the temperature progress of dry bulb and external temperature recorded on July 30th in 2014. Although external temperature continues to decrease from up 12:48 o'clock significantly for 10 Kelvin, and once again starting from 13:22 o'clock, internal dry bulb temperature starts to increase at 13:19 o'clock while fold-works remained opened. Similar, this progress indicated especially in a midsummer month the compensating power of thermal mass.

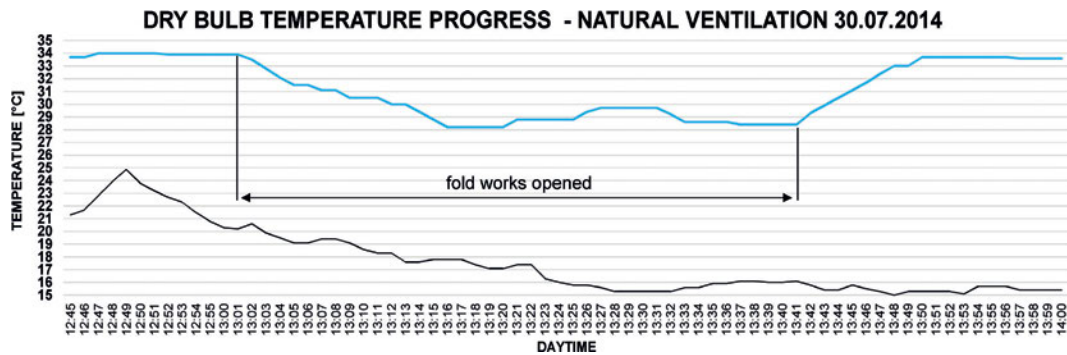


FIGURE 2.37 Dry bulb temperature progress – natural ventilation 30.7.2014

### Summary

Cooling efficiency of natural ventilation in an internally shaded sunspace was inspected. Observations and analysis of effective dry bulb temperature show, that natural ventilation is not effective in order to approximately accomplish external temperature level in the test sun space. Overheating cannot be compensated diurnally. Dry bulb temperature remains a demonstrable off-set to external temperature of six to ten Kelvin (*also see Appendix B.3*). This is valid for inspected spring and midsummer months. Although fold-works are opened dry bulb temperature was observed to raise in July. As reason for that was identified heat return from thermal mass.

### § 2.7.5.2 Monthly cumulative frequencies of resultant temperature

Resultant temperature is visualized and analysed and in the tables below. The results are coded absolutely and relatively, while there was made a distinction between 24 hours a day and a 5 to 10 PM period. Further, it is of interest, if and when floor heating, which was fed by façade integrated renewable energy collectors, was effective.

The tables made a differentiation between the south and west flank. Figure 2.38 illustrates month-wise absolute numbers of hours, when the resulting temperature in the test sun space was 0 or higher than 20°C. In January was no single hour recovered with an operational temperature of at least 20°C. In February twenty three hours fulfilled the lower thermal comfort requirement in the south flank, of which fourteen belonged to the time interval 5 to 10 PM. That is equal to 4% of the entire surveyed hours of

624 hours in total for February. In the west flank the numbers are similar, but slightly lower. Moreover, solely two hours in addition have been provided by the floor heating in February outside the preferred occupational time. In March the number of hours with desired operational indoor temperature was six times higher in the south flank than for February, namely 135 hours.

By contrast, despite less than the half, exactly 51, were detected between 5 to 10 PM, in 41% of the preferred occupational time the thermal comfort was satisfying. Nonetheless, floor heating was involved for less than 3 hours in total, what is equal to 1% during evening. Results for the west flank were slightly lower.

### Analysis of monthly Resultant Temperature $T_{res}$ (absolute) with additional floor heating

MONTH	ANALYZED DAYS	ANALYZED HOURS	South Flank				West Flank			
			Tres >20°C	Tres >20°C (5to10PM)	Tres 20°C per FLOOR HEATING	Tres 20°C per FLOOR HEATING (5to10PM)	Tres >20°C	Tres >20°C (5to10PM)	Tres 20°C per FLOOR HEATING	Tres 20°C per FLOOR HEATING (5to10PM)
January 2015	29 von 31	696	0	0	0	0	0	0	0	0
February 2015	26 von 28	624	23	14	2	0	13	9	1	0
March 2015	25 von 31	775	135	51	3	1	119	51	2	1
April 2015/14	17 von 30	408	179	70	24	6	166	69	20	6
May 2015	30 von 31	720	448	146	31	4	420	146	29	4
June 2015/14	23 von 30	552	452	116	14	0	438	115	8	0
July 2015/14	18 von 31	432	406	91	15	0	399	91	13	0
August 2015	27 von 31	648	600	136	29	1	584	135	21	1
September 2015	29 von 30	696	384	140	29	6	368	140	21	6
October 2015/14	21 von 31	504	109	40	12	6	95	46	10	6
November	25 von 30	600	43	7	0	0	33	6	0	0
December	30 von 31	720	0	0	0	0	0	0	0	0

FIGURE 2.38 Cumulative frequencies of resultant temperatures absolute

April shows a considerable different analysis, since 179 of 408 observed hours fulfilled thermal requirements, what is equal to 44%. Actually, 88% of hours between 5 to 10 PM recovered satisfying resultant temperature, namely 70 hours, of which in 6 of in total 24 exactly provided heat by floor heating. Seven per cent of all hours between 5 to 10 PM were supported by floor heating. Analogously, the west flank showed slightly lower values. The proportion of satisfying resultant temperature demonstrably improved in May, since 448 of 720 hours supplied ambient conditions >20°C. This is equal to 62% of all surveyed hours in May. In addition, 146 hours satisfied in the preferred evening period, what equals 97%. With 31, respectively 4 hours of action, floor heating contribution with 4 to 3% was menial.

Similar to May, numbers of hours with operational temperature above 20°C had a major fraction on hours in total, and in fact, accomplished 100% in the evening time. Despite comparably high monthly yields related to high irradiation, the fraction of contribution by floor heating decreases in respect to rich passive gains and, thus, less demand. Four hundred and six of in total 432 analyses hours provided satisfactory resultant temperature in July.

Relatively spoken, 94%, respectively 100% in the evening time, of hours could have been detected exceeding the lower thermal limit of comfort. Interestingly, in case of the west flank the numbers differ for the first time for more than 10%.

<b>Analysis of monthly Resultant Temperature <math>T_{res}</math> (relative) with additional floor heating</b>									
MONTH	ANALYZED HOURS	South Flank				West Flank			
		Tres >20°C	Tres >20°C (5to10PM)	Tres 20°C per FLOOR HEATING	Tres 20°C per FLOOR HEATING (5to10PM)	Tres >20°C	Tres >20°C (5to10PM)	Tres 20°C per FLOOR HEATING	Tres 20°C per FLOOR HEATING (5to10PM)
January 2015	696	0%	0%	0%	0%	0%	0%	0%	0%
February 2015	624	4%	11%	0%	0%	2%	7%	0%	0%
March 2015	775	17%	41%	0%	1%	15%	41%	0%	1%
April 2015/14	408	44%	82%	6%	7%	41%	81%	5%	7%
May 2015	720	62%	97%	4%	3%	58%	97%	4%	3%
June 2015/14	552	82%	100%	3%	0%	79%	99%	1%	0%
July 2015/14	432	94%	100%	3%	0%	92%	100%	3%	0%
August 2015	648	93%	100%	4%	1%	90%	99%	3%	1%
September 2015	696	55%	97%	4%	4%	51%	97%	3%	4%
October 2015/14	504	22%	38%	2%	6%	19%	44%	2%	6%
November	600	7%	6%	0%	0%	6%	5%	0%	0%
December	720	0%	0%	0%	0%	0%	0%	0%	0%

FIGURE 2.39 Cumulative frequencies of resultant temperatures relative

Although the number of days analysed in August differ from 18 to 27, the absolute and relative figures equal those of July. Interestingly, while the absolute number of hours on total day basis for the west flank differ significantly from those for the south flank, the number of hours with satisfactory thermal minimum requirements does not differ to that for the south flank.

Since both flanks generated 136, respectively 135 hours with Tres >20°C between 5 to 10 PM, the non-existent difference compared to total day surveillance indicates that sun space orientation, sun path and sun height in respect to reflection of irradiation

and, in consequence, utilizable solar gains is decisive for satisfactory ambient temperature based on solar gains.

For September the analysis constitutes 55% of all 696 hours to provide operational temperature above 20°C. While in total 384 hours can be detected within the month, especially 384 hours could have been identified within the 5 to 10 PM period.

This is 97% of all hours in this preferred occupation time. Floor heating supported with in total 29 additional hours of what 4 hours belonged to the evening time interval. Related to observed hours, floor heating contribution in the evening was less than 4%.

<b>Analysis of monthly Resultant Temperature T<sub>res</sub> (relative) without floor heating</b>				
<b>MONTH</b>	<b>ANALYZED HOURS</b>	<b>South Flank</b>		
		<b>T<sub>res</sub> &gt;20°C exclusively passive solar gains</b>	<b>T<sub>res</sub> &gt;20°C with Floor Heating</b>	
January 2015	696	0	0%	0%
February 2015	624	21	3%	4%
March 2015	775	132	17%	17%
April 2015/14	408	155	38%	44%
May 2015	720	417	58%	62%
June 2015/14	552	438	79%	82%
July 2015/14	432	391	91%	94%
August 2015	648	571	88%	93%
September 2015	696	355	51%	55%
October 2015/14	504	97	19%	22%
November	600	43	7%	7%
December	720	0	0%	0%

FIGURE 2.40 Cumulative frequencies of resultant temperatures relative without floor heating

Number of hours with satisfactory temperature in the west flank is equal to the south flank, also the absolute number of floor heating contribution between 5 to 10 PM. However, floor heating distribution in total in the west flank differs to the counterpart south flank, what indicates a lack of passive solar gains, respectively charging of the west flank thermal mass in the early phases of day in this month.

Figure 2.40 illustrates 109 hours in total of operational temperature  $>20^{\circ}\text{C}$  for October. Relatively spoken, 22% of the total day time is satisfactory.

While indoor thermal comfort between 5 to 10 PM is enjoyable for 97% of the hours in September, this figure lowers to 38%, namely 40 hours, in October. Total floor heating contribution lowers from 4 to 2%, whereas it increases for the evening period from 4 to 6% compared to September. The figures for the evening period slightly improves for the west flank compared to the south flank.

For November could have been detected 43 hours of operational temperature  $>20^{\circ}\text{C}$  in the south flank, respectively 33 for the west flank.

That is equal to 7% of entirely 600 observed hours for November. Simply seven hours account for  $20^{\circ}\text{C}$  between 5 to 10 PM. However, floor heating contributes nothing effectively to thermal comfort in November. The table figures terminatorily out, that in December a resulting temperature of  $20^{\circ}\text{C}$  or higher is not accomplished. Likewise, floor heating provides any contribution. This notice is true for both sun space flanks. Figure 2.40 shows cumulative frequencies of hours with operational temperature above  $20^{\circ}\text{C}$  lower comfort limit for the south flank that would have been generated if floor heating did not contribute any heating energy.

The right column repeats for comparison relative figure from figure 48. This tabular survey demonstrates the effect of the floor heating system as it was dimensioned in the test sun space, in particular and fed by façade integrated façade collectors.

Accordingly, the relative difference between column 4 and 5 expresses the proportion of effective operational satisfying temperature provided by floor heating. The differences range between zero to 5%. In midwinter months like January, November and December cannot be determined any difference, thus no contribution at all. For all other winter months (February, March, April) the difference is marginal, at most 1%. On the contrary, during summer months, floor heating is able to contribute up to 5% (August).

Although knowing, that several months are not entirely represented (all days), especially in May and additional August and September are months with highest number of hours of contribution (29 to 34 hours). Floor heating is able to contribute in April, May, September and October up to 6 hours maximum in the 5 to 10 PM period.

## Summary

---

In order to give a summary, within the winter month the maximum relative amount of hours satisfying lower thermal requirements could have been evaluated to be 20%, one of five hours. In April and September, belonging per definition first to winter and second to summer, nearly 50% of all hours recover operational temperatures above 20°C.

By contrast, during summer months at least two thirds or even 100% accomplish thermal minimum requirements. Interesting fact to point out is, that the cumulative frequencies of hours between 5 to 10 PM during preferred occupational time for each month are all higher than the corresponding frequencies of the counterpart day periods.

For example, the cumulative frequency in April with 82% excelled the counterpart period with solely 44% tremendously, likewise September with 97% to 55%. In consequence does this mean, that the time period 5 to 10 PM as preferred occupational time is the most appropriate time to enjoy thermal comfort in a sun space exclusively by solar gains. Interestingly, the south flank outmatched the west flank in all months, except October.

According to evaluated empirical data,

*Hypothesis I*, stating that 1.060 hours a year of satisfying thermal comfort is manageable exclusively by solar gains

*is to be rejected.*

The second Hypothesis, *Hypothesis II*, stating that 1.060 hours a year of satisfying thermal comfort is manageable by solar gains and additional façade integrated renewable energy collectors

*is also to be rejected.*

In this context, inefficiency of floor heating, floor heating control or considerable thermal losses of the sensible water tank as reasons for the rejection can be excluded. Reason for that conclusion by the author bases on the evaluated fundamental distance towards 100% fulfilment that has been detected as to be too essential to give room for that secondary reasons.

### § 2.7.5.3 Monthly analysis of resultant temperature by mean of running external temperature interval

---

Indoor thermal comfort evaluations based on the “Predicted Mean Vote (PMV)” and “Predicted Percentage of Dissatisfied (PPD)” according EN ISO 7730 are detailed and concise. Since occupation specific and space utilization specific metabolic rate, clothing area and clothing thermal resistances, mean radiant temperature of surfaces, dry bulb

temperature and water vapour pressure are parameters of calculation, the evaluation of thermal comfort strongly considers human activity, space specific thermal conditions, human adaption in clothing and activity to the environment and season.

That makes stationary hourly and limited day-wise analysis effective. But, nonetheless, the PMV and PPD procedure is by research (Yang and Yan, 2014 [23]) only applicable to mechanically ventilated and actively heated and cooled spaces. Firstly, mechanical conditioning narrows thermal lower and upper comfort limits naturally to 20 to 26°C, secondly sun spaces normally are naturally ventilated and thirdly these limits are too strict for sun spaces and users who are able to adapt by opening over-average wide façade openings. These reasons make the PMV and PPD procedure not suitable for sun space thermal comfort evaluations.

By contrast, DIN EN 15251 suggests an alternative procedure, that prerequisites space natural ventilation and considers occupants to be free and competent to both regulate and adapt to thermal conditions but founds evaluation on PMV method. In consequence, this procedure widens the thermal comfort limits and especially tolerates higher indoor temperature in summer, namely exceedance of 26°C. In order to express indoor thermal quality at least roughly on PMV basis it determines metabolic rate to 1,0, respectively 1,3 met, what is equal to balanced and sedentary activity, and space typology to office or even either residential usage.

Finally, this procedure allows against the background of the before mentioned boundary conditions PMV evaluations considering category I, II and III according DIN EN 15251, section 5, Tab.1 and EN ISO 7730 appendix A.1, Tab.A.1.

Thus, an evaluation by graphical relation allows rough thermal comfort determination with 90% (PMV : -0,5 to + 0,5; subtle cooler , subtle warmer ), respectively 80% (PMV : -0,7 to + 0,7; slightly cooler, slightly warmer) predicted mean vote of space occupants. These limits are equal to <10 , respectively < 15% of predicted percent of dissatisfied (PPD).

This procedure is described in DIN EN 15251:2007 in Appendix A, A.2, S.27-28, and refers to section 3, 3.11, external temperature–running mean. The mechanism of analysis bases on a relation of the running daily mean of external temperature, considering 4 days beforehand, and the actual hourly operational temperature. The procedure is limited to external temperature between +10°C and 30°C for upper and +15°C and 30°C for lower limits in summer. For winter months the same limit calculations are valid with different limits. Although DIN EN 15251 restricts appliance in winter month exclusively to non-heated spaces, the authors decided to apply the rules for the floor heated test sun space in winter.

The reason is the evident short number of hours (see Sec.2.7.5.2) in which the floor heating actually was active and contributed renewable heating energy. Moreover, the national standard Energieeinsparverordnung (EnEV) [66] clearly differentiates between heated and non-heated buildings, respectively spaces. Consequently, as long as a space with dry bulb temperature above 19°C is actively heated for less than 4 months a year, it is considered to be “non-heated”.

In order to determine day-wise the individual upper operational temperature limit in summer ( $10^{\circ}\text{C} < \theta_i < 30^{\circ}\text{C}$ ), respectively winter ( $< 10^{\circ}\text{C}$ ), formula :

*category II*

$$\theta_{i \max, o} = 0,33 * \theta_{rm} + 18,8 + 3 \quad (11)$$

*category III*

$$\theta_{i \max, o} = 0,33 * \theta_{rm} + 18,8 + 4 \quad (12)$$

has to be applied, for the lower limit in summer ( $15^{\circ}\text{C} < \theta_i < 30^{\circ}\text{C}$ ), respectively winter ( $< 15^{\circ}\text{C}$ ), formula

*category II*

$$\theta_{i \max, u} = 0,33 * \theta_{rm} + 18,8 - 3 \quad (13)$$

*category III*

$$\theta_{i \max, u} = 0,33 * \theta_{rm} + 18,8 - 4 \quad (14)$$

has to be applied.

As a reference the optimal operational temperature  $T_{res,op}$  can be calculated as previously described in 2.1.2. The optimum operational temperature also depends on the hourly external temperature and is plotted against the running daily mean. Distances between  $T_{res}$  and  $T_{res,op}$  explain the deviation from satisfactory or still acceptable thermal comfort.

$$T_{res,op} = 0,31 * T_{ex} + 17,8 [^{\circ}C] \quad (15)$$

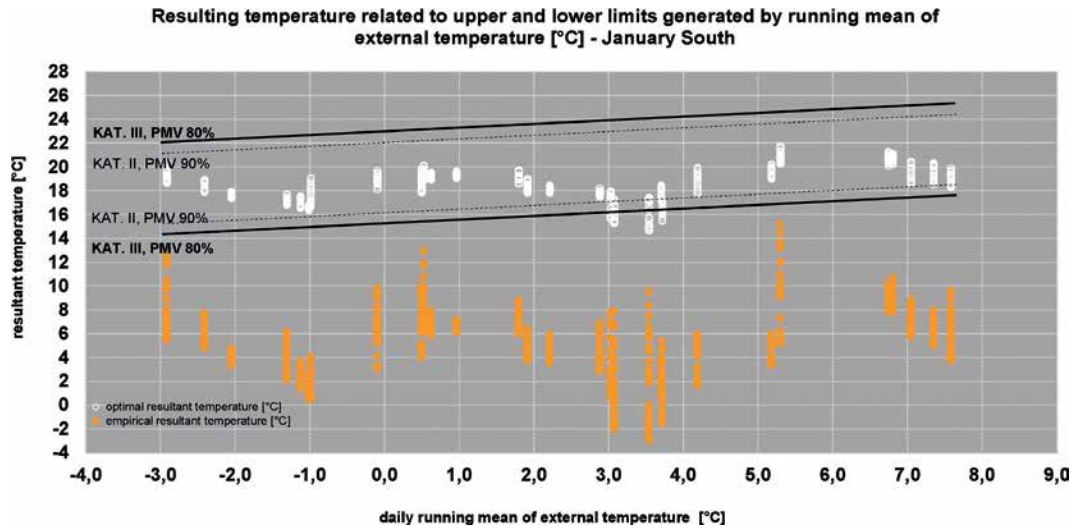


FIGURE 2.41 Operative temperature related to PMV upper / lower limits of running mean of external temperature – January

Figure 2.41 describes operational indoor temperature investigated in January. In January the running mean external temperature is evaluated to range from approximately  $-3^{\circ}C$  to  $+7,7^{\circ}C$ . In relation to this temperature interval the resultant indoor temperature spreads from  $-3^{\circ}C$  to nearly  $+15,5^{\circ}C$ . Interestingly, the lowest operational temperature occurred not as being expected correlating to the lowest mean temperature, but with  $+3$  to  $3,5^{\circ}C$ . Similarly, one of the highest indoor temperature correlates to the minimum of running mean external temperature of about  $-3^{\circ}C$ . The lower adaptive comfort range correlates to the low external temperature starts with category III with approximately  $+14^{\circ}C$  and ends with nearly  $+18^{\circ}C$ . Although the lower limits starts on a low level, not simply a single hour is identified to provide satisfying operational temperature of cat. III.

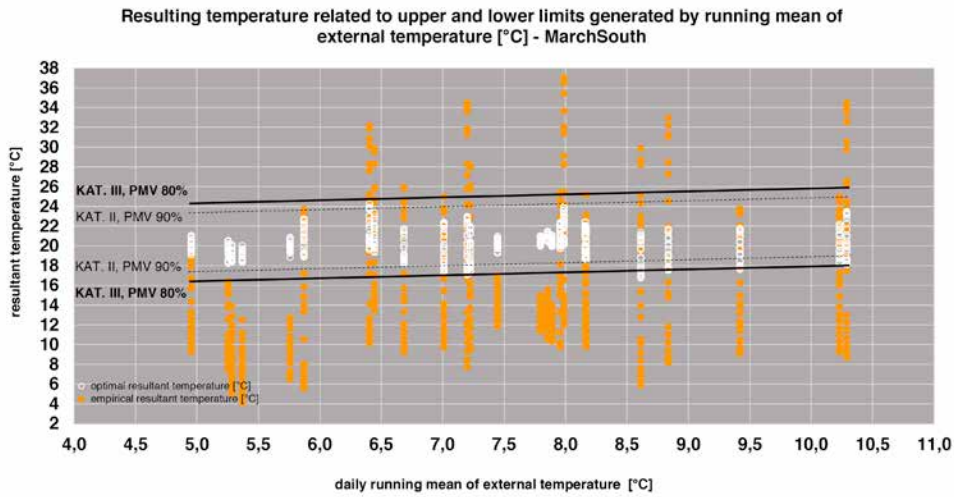


FIGURE 2.42 Operative temperature related to PMV upper / lower limits of running mean of external temperature – March

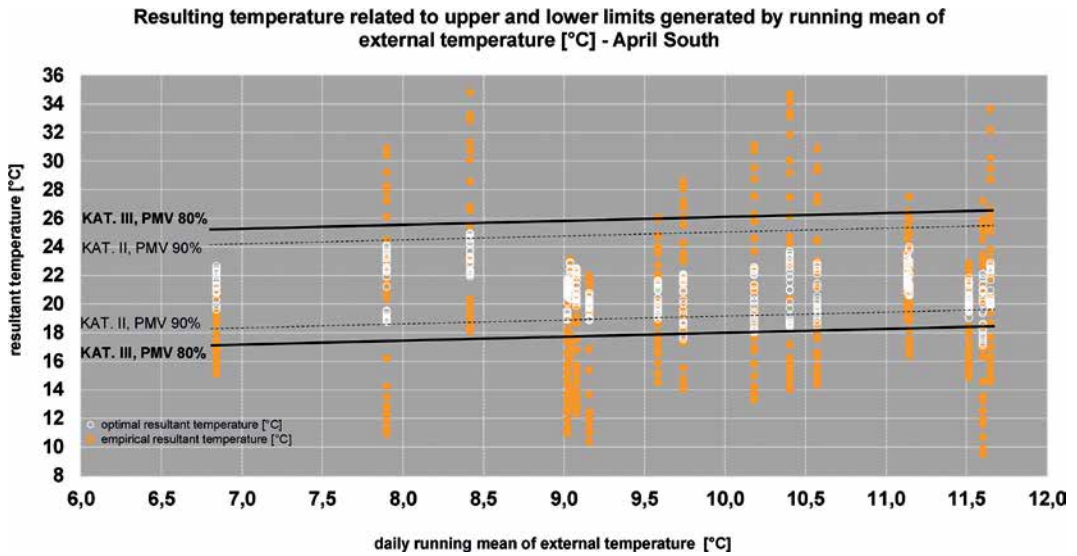


FIGURE 2.43 Operative temperature related to PMV upper / lower limits of running mean of external temperature – April

The graphically determined predicted mean vote for January is higher than 80%, respectively worse than slightly cold and tends to be cold. More than 15% of occupants will claim thermal comfort as being dissatisfying.

Analysis of February illustrates a proportional trend of rising external and rising operative temperature. However, although the lower limit in category III and respectively II start with 15°C and 16°C about 70% of all hours of operative temperature valued below the limit. Less than 20% of all resultant temperature is within the category II interval. Consequently, occupants will vote with slightly cool, whereas more than 70% of all hours will have been perceived as cold and too cold. In Figure 2.42 is plotted the external against the operational temperature correlation for March.

It becomes obvious, that highest operational temperature is correlated around +8,0°C, disproportional to the maximum external temperature of about +10,2°C. For March the lower comfort limits starts with 16,2°C and the upper limit in category III ends with 26°C. Amazingly for March is, that the body of hours of operational temperature (about 60%) was below the lower limit of cat. III and that a considerable amount of hour account with operational temperature above the upper limit of cat. III. Thus, we can summarize for March, that it tended to be cold, but that operational hours considerably improved compared to February and January. Moreover, we can state, that March is the first winter month with a tendency to sporadically overheat. Space occupants would by trend rather adapt to operational temperature exceeding the upper limit of cat. III, than adapt to cold thermal conditions. Finally, the sum of hours within the thermal adaptive limits were still too low.

In Figure 2.43 the running mean of external temperature for April spread from nearly +6,7°C to +11,7°C, while the operational temperature differed between +9°C to +35°C. According to higher external temperature also the upper and lower limits were generated higher compared to the previous months. Nearly one third of all hours correlates to the external temperature comply the limits of at least category III. While the gross of hours tends to be too cold, a growing fraction of approximately 20% exceeded upper limits and provokes overheating with maximum resultant temperature of up to 34 to 37°C. Since the distribution towards “warm” and “too warm”, as well as “cold” and “too cold” is intense and demonstrably high, the optimum operational temperature field is underrepresented.

For May are calculated running mean external temperature between 9,5°C and 15,8°C. Correlated operational temperature dilates from +11°C to + 39°C. Accordingly, lower limit starts with 19°C and upper limit, what interests more for a summer month, starts with 27°C and ends with 28°C. Within this adaptive 6K range located nearly half the hours of May. In consequence, occupants had to adapt to colder opera-

tional conditions maximum 8K lower than the limits or adapt to a warmer environment that at maximum differs for 12K. Furthermore, exciting to observe, that the highest derivations of operational temperature from optimal operational temperature is detected in a range of running mean of external temperature between 11,7 and 12,7°C, despite as expected, at maximum of 16°C. Essentially, May is the first month to find with a well-balanced distribution of all operational temperatures.

In June dilatations of operational temperature below the lower limits are restricted, thus do not fall into account. For occupants adaption towards slightly cool or cold environmental conditions were not the major problem in June. Moreover, it demonstratively nearly half of the hours of June operational temperature within the comfort limits of PMV 90 and 80%, a mostly satisfying thermal comfort.

Occupants of the test sun space had to adapt to extremely high operational temperatures (see [Appendix B.4](#)) even at daily mean external temperatures of solely 14°C to 15,5°C. This observation demonstrates the enormous potential of the test sun spaces configuration (internal sun shading, no executed natural ventilation, local climate) to overheat even at moderate mean external temperatures.

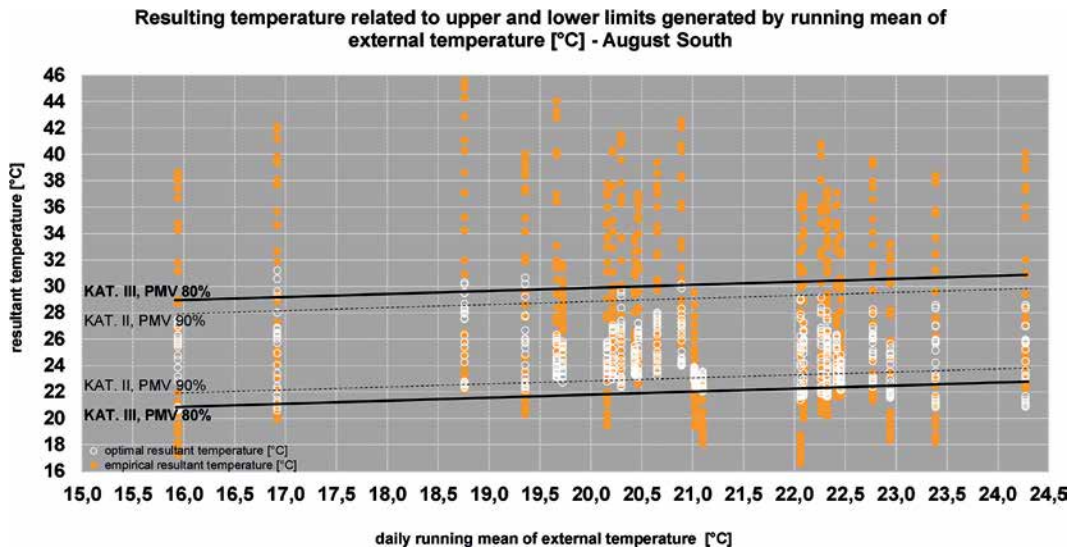


FIGURE 2.44 Operative temperature related to PMV upper / lower limits of running mean of external temperature – August

Although the external temperature interval in July starts with 16,7° and ends with 22,7°C and maximum operational temperature stops at 43°C, boundary conditions are similar to the of June. Half of hours are within the comfort limits, thus half of hours at latest satisfied 80% of occupants, and half of hours significantly exceed the upper limits. Differently compared to June is a cold perception of the test sun space related to averaged high mean external temperature field of 21,4 to 22,7°C. In August, which is illustrated in Figure 2.44, running means of external temperature spreads from nearly 16°C to 24,3°C. Correlated operational temperature includes 16°C to 46°C at maximum. Specific for August, the comfort band is plotted with lowest limit at 21°C and highest limit at 31°C.

Essentially for August is a main body of hours with operational temperature within the comfort band. However, significant number of hours exceed upper limits and represented resulting temperature between 32 and 40°C.

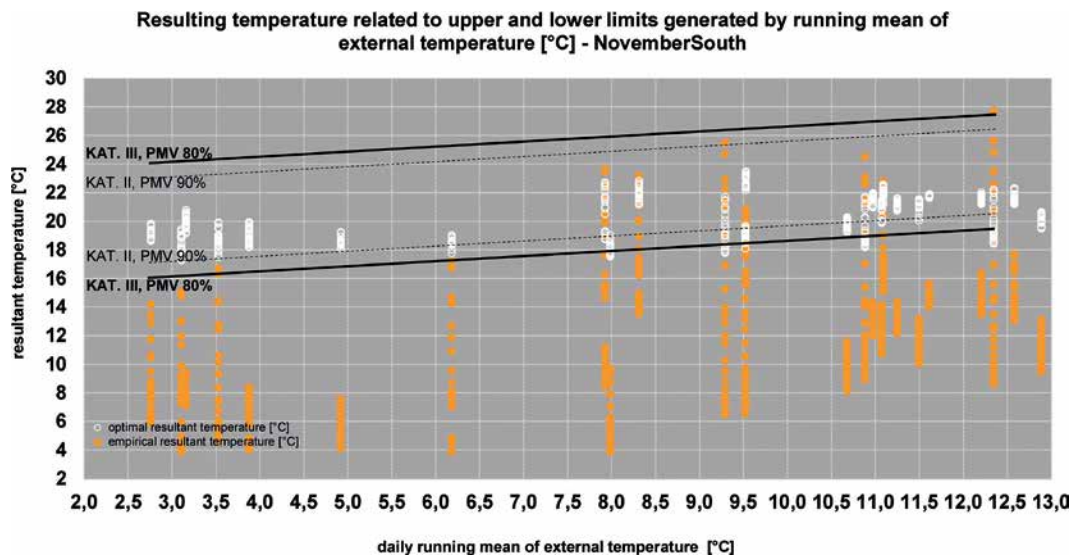


FIGURE 2.45 Operative temperature related to PMV upper / lower limits of running mean of external temperature – November

A maximum temperature of 46°C is related to nearly 19°C running mean external temperature. Thus, the maximum temperature level is similar to July, but differs demonstrably from June. On the contrast, the main body of overheating operating temperature is related to a warmer mean external temperature band defined from

roughly 19 to 24°C, whereas in July, June and May it started lower at 13°C and ended with 19°C external temperature. This correlation is significant for August and, since August being in the second half of summer and the entire year, thus indicates also a strong relation to daily maximum sun height and sun path. September's comfort band equals the one of August and nearly 50% of operational temperature in September is within the comfort band. Approximately 40% is slightly below and reaches 12°C.

Significant for hours of operational temperature are high frequencies in the band of 14,2 to 16,7°C and in the second band between 18,7 to 20,5°C. Nonetheless, high operational temperatures that could be perceived as warm or too warm are mostly related to the external temperature band 14,2°C to 15,7°C. However, September displays straight a homogeneous band of operational temperature abroad the entire mean external temperature interval. Moreover, astonishing related to the comfort band, occupants will suffer from too warm operational temperature in lower sections and from too cold within higher external temperature interval sections.

According to external temperature, for October the comfort limit band starts nearly above 18°C and ends with 27°C. In October the major fraction of operational temperature is outside the comfort band of 90 to 80% predicted mean vote. The body within the band is located between 20 to 24°C, but correlated to an external mean temperature of at least 12,7°C and higher.

Thus, essentially, beside particular dispersed hours of operational temperature without the comfort temperature band, the gross of hours is located to neutral, subtle cold, slightly cooler and cold area related to an mean external temperature of > 12,5°C. Finally, surveyed hours in October mainly tended to undercool than to overheat.

Figure 2.45 describes relations between external and resultant temperature for hours surveyed in November. Whereas the running mean of external temperature varied from 2,7 to 12,7°C, resultant temperature was calculated ranging from nearly 4°C to 28,0°C. Accordingly, the comfort band spanned from 16°C to 26°C in maximum. The body of hours, approximately 60%, is located outside the comfort band in lower temperature fields. Hours within the comfort mostly tended to be warmer than optimum operational temperature. Thus, according to each the minimum and maximum temperature correlated to external temperature, the graph indicates a rough linear positive trend between rising external and rising internal temperature.

Significant for December ([Appendix B.4](#)) is a running mean outside temperature from 4,3 to 10,9°C. The operative temperature interval includes 4,5 to 19,0°C. Consequently, the comfort band spread from 16,2 to maximum 26,2°C, respectively 80% PMV (20%PPD). Solely two hours fulfil the lower 80% PMV limit, when 80%

of occupants would accept operational temperature with slightly cool perception. Likewise to January, in December no thermal comfort at all was accomplished by solely passive solar gains and additional floor heating.

### Statistical evaluation

A closer view on absolute and relative statistical elaboration gives a clear-cut insight in thermal quality in terms of frequency. The values in figure 2.46 demonstrate, how often the broader limits according category III (EN ISO 7730, A.1) with slightly cool and slightly warm perception of at least 80% satisfied occupants have been actually exceeded by calculated operational temperatures. Consequently, the difference to 100% expresses the relative frequency of surveyed appropriate thermal comfort each a month. The table in Figure 2.46 distinguishes between the south and west flank of the test set up sun space. Further it differentiates between entire day analysis and 5 to 10 PM evaluation. A 5 to 10 PM analysis follows an entire day analysis.

CATEGORY III EXCEEDED, accord. EN ISO 7730 A.1, Tab.A.1,								
MONTH	SOUTH		SOUTH 5 to 10PM		WEST		West 5 to 10PM	
	absolute [h]	[%]	absolute [h]	[%]	absolute [h]	[%]	absolute [h]	[%]
January (696 h)	696	100%	145	100%	696	100%	145	100%
February (624 h)	580	93%	112	86%	585	93%	112	86%
March (600 h)	483	81%	80	64%	484	81%	79	63%
April (408 h)	242	59%	34	40%	242	59%	34	40%
May (720 h)	370	51%	74	49%	363	50%	68	45%
June (552 h)	306	55%	69	60%	303	55%	69	60%
July (432 h)	231	53%	66	73%	224	52%	66	73%
August (648 h)	371	57%	121	90%	362	56%	121	90%
September (696 h)	384	55%	36	25%	388	56%	37	26%
October (504 h)	375	74%	57	54%	389	77%	59	56%
November (600h)	521	87%	96	77%	529	88%	96	77%
December (720 h)	718	100%	150	100%	720	100%	150	100%

FIGURE 2.46 Frequencies of hours with operational temperatures [°C] exceeding the upper and lower cat. III comfort limit

In January and December, midwinter month, the comfort band is exceeded for 100% of all surveyed hours. Following, in February and November 93% and 87% (88% west) of all 580 and 521 hours exceed the cat. III limits.

Thus, appropriate comfort is achievable for not more than 7%, respectively 13% of the observed time. For March and October are evaluated a limit exceedance of 81% and 74% respectively. Reversed, a satisfying thermal comfort with simply 10 to 20% percent of dissatisfied is accomplishable in these month for nearly 20 to 25 per cent of observed hours (483/600 [80%] and 375/504 [74%]). By contrast, in April and September, almost half of the surveyed hours exceeds the comfort limits (April: 59%; September: 55%). Hence, a satisfying thermal comfort is given with 41 to 45% surety. Although the mean running external temperature raises to maximum in be-tween January to December, the number of surveyed hours in May and August with operational temperature, which exceeded the outer limits of the comfort bands remained high with 51% and 57%. Consequently, the number of hours with resulting temperature within the comfort band with respect to no active natural ventilation and internal sun shading were about 43 to 49% at max. So, within summer month, a maximum frequency of roughly 40 to 50% of appropriate and mainly acceptable thermal comfort is applicable. The relation did not change for June and July. In June 55% and in July 53% of hours were outside the comfort band.

Expressed reversed, also maximum 45 to 47% of all surveyed hours provide an appropriate and at least acceptable thermal comfort. Outliers, which represent too warm temperature, respectively overheating, are predominant and prevented a prevalent more than the half fraction of hours with enjoyable thermal comfort.

Interestingly, the west flank compared to the south flank behaves equal, but however slightly changes can be detected in frequency of exceedance. For the first eight months of the year, exceedance was equal or was even slightly lower for one or two per cent points. On the contrary, exceedance slightly raised for the month September to De-cember for one to three per cent points compared to the south flank. Thus, it can be concluded, that thermal comfort in the west flank of test sun space was in the late summer and autumn month more difficult to provide than in the south flank.

More concise information that is more related to occupation gives an analysis of frequency of comfort exceedance during 5 to 10 PM each a day.

Thus, the table in Figure 2.46 is enlarged by 5 to 10PM evaluation. This evaluation generally shows, that the frequency of exceedance between 5 to 10 PM is for most month less than the entire day analysis reveals.

Although, in January and December 100% of hours correlate to operational temperatures that exceed the comfort band, the before mentioned trend becomes obvious with the differences in February and November. In February, simply 86% of hours ex-

ceed the comfort band between 5 to 10 PM, whereas focussed on entire days the quote is 93%. November is similar, when evaluation recovers comfort exceedance between 5 to 10 PM for 77% of all hours in the contrast to 96% for an entire day surveillance. The differences of entire day and 5 to 10 PM analysis widens the more a month is closer to midyear. In March the difference is 17%, in October 20%. Thus, in March argumentum e contrario in 36% of all hours between 5 to 10 PM operational temperature is observed to be within the comfort band exclusively by solar gains and additional floor heating. Likewise, in October the quote is 46% of at least 80% satisfying thermal comfort during occupation in evenings.

This ratio raises to maximum in September and April, when exceedance is identified for 25%, and 40% for April respectively. Essentially, thermal comfort is observed to be within the comfort band for 75% of all hours within September and for 60% of all hours within April. In the end, maximum more than the half to three of four hours between 5 to 10 PM provide enjoyable thermal comfort in the test sun space.

On the other hand, the ratio of exceedance increases for midsummer month. In May and August exceedance is detected for 49% and 90%.

The difference towards an entire day evaluation decreases in terms of May to equilibrium, whereas the situation contrarily turns in terms of August with a 90% exceedance ratio during evening hours. Hence, in particular August shows thermal comfort quality in accordance to the specific comfort band during the entire than during evening hours. In midsummer month June and July, the frequency of comfort band exceedance between 5 to 10 PM increases compared to April and September in such a way, that differences between entire day and evening hour evaluations becomes dispensable. In June, the exceedance of hours was determined with 60%, in July with 73%.

## Summary

---

Thus we can see, that hours with resulting temperatures within the month specific comfort band are limited to two of five or even 1 of four. In conclusion, 100 per cent of hours with satisfying operational temperature was not achievable exclusively with passive solar gains and additional floor heating either for the evening hours or entire days. Moreover, a major fraction (three of four hours at maximum) of at least 80% acceptance was observed in September and in April. Hence, by trend, spring and autumn months, that are established at intermediate climate periods, showed predominant appropriate thermal comfort in evening occupational hours. This statistical evaluation leads to another insight, that in majority of cases the preferred

daily period occupation between 5 to 10 PM showed less frequency of exceedance, thus more often better thermal comfort, than the entire day, except during midsummer months June to August.

Furthermore, except in September and October, the frequency of exceedance in the west flank was observed to be marginally lower than compared to the south flank.

#### § 2.7.5.4 Monthly analysis of comfort chart

---

The dry bulb temperature is monthly related to external dry bulb temperature and indoor relative humidity. Thus, generated graphs allow the analysis of a complex indoor space quality context. Normally, occupants feel comfortable with in a range of relative humidity between 35 to 65 and 75%. EN ISO 15251, 6.4 explicitly stipulates at least 20% relative humidity in order to avoid symptoms like dry eyes, pruritic skin and respiratory irritation. The forthcoming cloud graphs distinguish between the comfortable (optimum) field of special dry bulb temperature and relative humidity

relation and the field of still comfortable. Hours in which floor heating contributed heating are highlighted differently with yellow dots.

In January ([APPENDIX B.5](#)) simply 4 hours are within the optimum comfort field and additional two hours within the still-comfort field. In consequence, six hundred ninety hours of six hundred ninety six hours are surveyed to be out of any ambient air-humidity comfort field.

In February, as Figure 2.47 visualizes, are approximately 30 hours within the optimum comfort field. Still comfortable are another 24 hours of which simply one is provided by additional floor heating. Total floor heating hours are limited in February to only four. As a result, from in total six hundred twenty four hours are 54 within a comfortable range; the rest which accounts for 91,4% is not comfortable. In order to summarize by describing a trend, more than 90% of hours have been much too cold and hence, with relative humidity between 65 and 88 % to humid, respectively clammy.

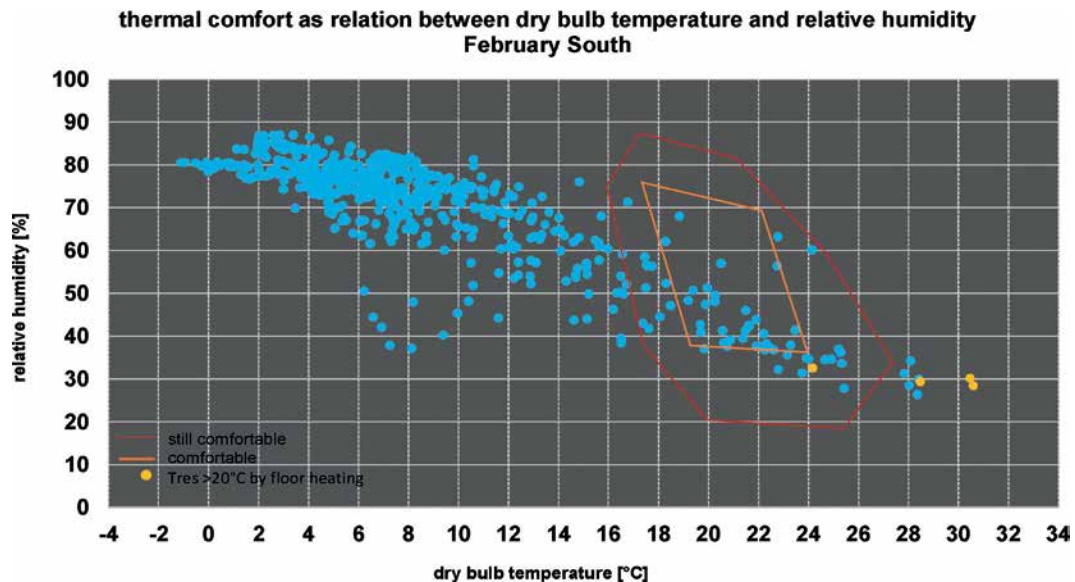


FIGURE 2.47 Comfort chart as cloud diagram February – South

During March ([Appendix B.5](#)) approximately 10 per cent of surveyed 775 hours are within the comfort field. Floor heating did not manage to contribute sufficient temperature for the optimum comfort range, but five hours, which are among the still comfort field. About 25% of 775 hours are comfortable, anyhow. But the major portion of hours are with ambient air temperature of less than 18 or 16°C too cold, and thus, tend to be moderate or too humid. Opposed to the before described monthly surveys, comfort in April (Fig. 2.48) is analysed to be appropriate by majority. About 60 per cent of the measured 408 hours account to be at least still comfortable or even comfortable. Floor heating demonstrably provides a substantial amount of comfortable and still-comfortable hours.

However, a few tend to be too warm. Significant for April is the amount of hours with dry bulb temperature out of comfort fields, since being too cold, but not being too humid. The maximum relative humidity does not exceed 70 per cent. On the contrary, hours which are too warm still are accompanied with relative humidity below 15 per cent. Obviously for May is the major part of hours, about 60 per cent, which aligns within at least the still-comfort range. About one third is even comfortable. This is equal to 20 per cent of 720 hours, respectively, approximately 144 hours. However, the minimum relative humidity under 15%.

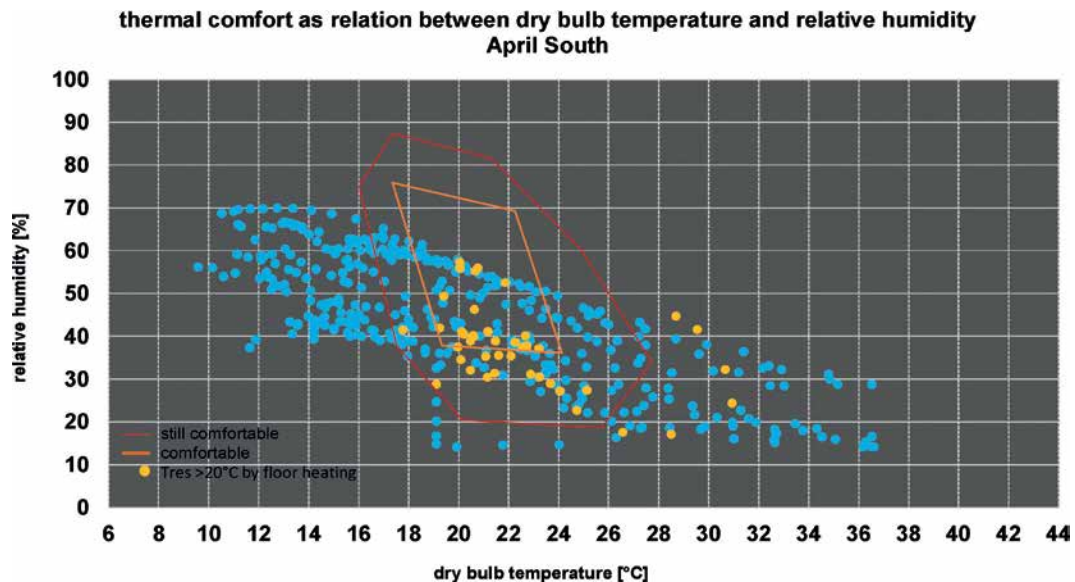


FIGURE 2.48 Comfort chart as cloud diagram April - South

With thirty one hours the floor heating considerably provided additional indoor comfort. The major fraction of floor heating provided hours belongs to the comfort field.

Summarizing, in May firstly the major part of hours were within the comfort range and exceeded 60% of relative humidity for only a little negligible times. Thus, we can state a trend towards a tight and regular dry bulb-humidity relation close the comfort fields.

The amount of hours June within the comfort field is about one fifth of in total 552 being measured. Especially, these hours are in a perfect temperature-humidity relation, and thus in a perfect position within the range.

Namely, by far all hours that were provided with floor heating shows perfect comfort, although the total quantity is less compared to May. A relative humidity of 65% was never exceeded. Opposed to that, half of all hours exceeding 26°C base on relative humidity lower than 30%. Hence, risk of draught and respiratory irritation is high.

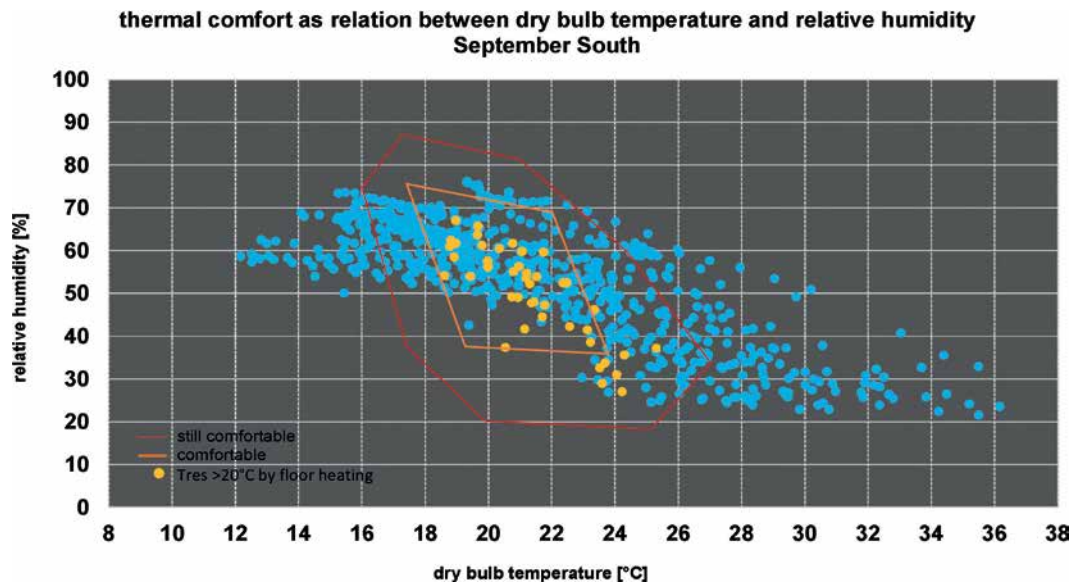


FIGURE 2.49 Comfort chart as cloud diagram September – South

Analysis for July ([APPENDIX B.5](#)) identifies at least one third of measured hours provided comfort-table indoor quality. But, the major part of hours provided ambient air temperature between 28 and 43°C. While the major fraction of hours with ambient air above 26°C was accompanied to a relative humidity between 30 and 50% in June, the body of hours above 26°C goes along with relative humidity between 35 and 60%. We can recognize a tendency towards humid space conditions.

The comfort chart for August exemplifies a tight and homogenous distribution of relative humidity and ambient temperature correlations. Approximately 15% of 648 surveyed hours in August represent comfortable or still-comfortable conditions. Floor heating is considerably represented exclusively within comfort field, but quantitatively less compared to May and April. About the half of all hours show dry bulb temperatures above 26°C.

Maximum temperature accomplishes 48°C, and thus is 4K higher compared to July. The broadest amplitude of represented relative humidity since April is significant for August.

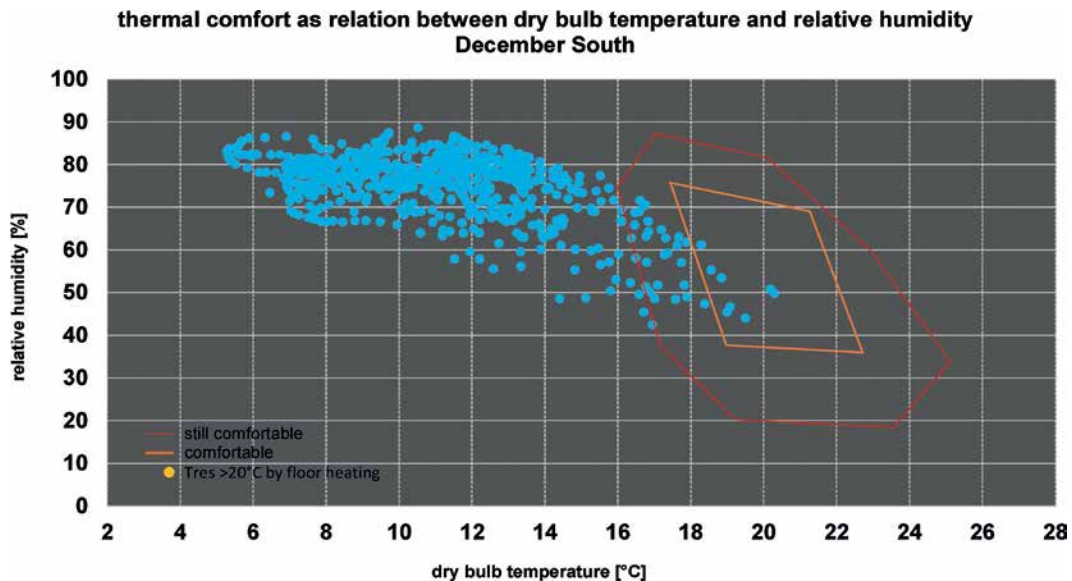


FIGURE 2.50 Comfort chart as cloud diagram December – South

The spread ranges from 12 to 78% relative humidity. Putting emphasis on this, firstly the 25% limit is underran for a considerable amount of hours and secondly analysis reveals a trend towards high relative humidity within the comfort ranges and even exceeding of limits. Regarding September, figure 58 gives an overview over the indoor comfort relationship between dry bulb temperature and relative humidity. It is obvious, that a considerable high fraction of the 696 hours are within the still-comfortable and comfortable range.

About 70 per cent of hours, namely 487, represent high or at least acceptable thermal indoor quality. Compared to the previously discussed monthly comfort charts, in September comfort is predominantly satisfactory. Moreover, thirty six hours with perfect thermal comfort were contributed by floor heating. Another 7 to 10 hours provided still acceptable comfort. Minimum ambient air temperature remained at least 12°C.

Hours with temperatures above 28°C are seldom and do not fall into account. However, more of interest is the fact, that major part of hours are accompanied with relative humidity between 50 and 70%, what for both comfort fields is sufficient. Summarized, September defined a well-balanced indoor comfort.

The comfort chart for October (see Appendix B.5) describes a more inhomogeneous relation of dry bulb temperature and relative humidity. While the comfortable field and the still-comfortable field cover a tremendous portion of hours, approximately the half of 504 surveyed hours show a distribution beyond the comfort field towards cold ambient air zones. The number of floor-heating provided hours is comparably less and limited to 15 to 20. Since the ambient air stronger tends towards cold, logically the relative humidity raised towards 60 and 75% by trend. Furthermore, a specific peculiarity surveyed in October is an over averaged proportion of hours in the upper third level of the comfort field.

Significant for November is only a spare number, approximately 20 hours, of hours within the comfort field. Another 40 hours are show thermal conditions belonging to the still-comfortable range. Moreover ninety per cent of 600 surveyed hours in November are colder and more humid than appropriate for any comfort field. In more details, lowest dry bulb temperatures reaches  $+4^{\circ}\text{C}$  correlated to 80 to 88% relative humidity.

December is plotted in Figure 2.50. Similar to November, only a few and even less hours cover dry bulb temperatures within the comfortable field, contradictive to that, approximately 27 hours can be identified to be still-comfortable. Related to 720 hours in to be surveyed in total were simply 4% comfortable. In consequence, six hundred ninety hours distributed among 5 to  $16^{\circ}\text{C}$  and 50 to 88% relative humidity. Striking for the out of comfortable amount of hours in December is its homogeneity in matter of temperature – humidity relation. As a rule of thumb, the closer single hours are towards comfortable fields, the huger are humidity spreads.

## Summary

---

Summarized, for the months March to October can be identified a considerable number, even elsewise the major fraction of surveyed hours within the comfortable or still-comfortable field. Especially, May and

September showed tremendous portions of hours that can be characterized being comfortable anyhow. However, January, February and November and December are critical months providing no sensible thermal comfort neither by passive solar gains nor by additional floor heating. Starting with May, but not later than June, thermal comfort in the test sun space was governed by overheating with maximum temperatures between  $36$  to  $55^{\circ}\text{C}$ , although being aware of an interior placed sun protection and no natural ventilation by applied fold-works.

Although dry bulb temperatures surveyed in winter month completely overtop +4°C, relative humidity extremely often exceeded 80% in January, November and December.

### § 2.7.5.5 Description and determination of sun space specific inertia

---

Inertia is, as beforehand highlighted by Rempel, Rempel, Gates and Shaw (2016) and Sanchez-Ostiz, Monge-Barrio, Domingo-Irigoyen and Gonzalez-Martinez (2014) in the literature review in section 3.5, a crucial aspect in thermal behavior of sun spaces in general. Thermal mass as trigger of inertia controls charging and discharging periods of building elements during a day.

Configured thermal mass helps balancing energy. Rempel et. al., for example, discovered a floor thickness between 2,5 to 10,2 cm being appropriate either for heat return in evening hours, during night for nocturnal free cooling or for preheating in forthcoming morning hours.

In order to understand thermal behavior of the test set sun space more in detail, the specific inertia has been analyzed. Inertia itself is a reaction of the sun space thermal building mass on external impact in terms irradiation and external temperature. Hence, following thermo-dynamic rules energy within a closed system flows towards parts of less energy. In terms of a inspected specimen as a sun space, building elements absorb energy, if the external source is more rich of energy and emit energy,

if the external source is less of energy. For a sun space does this mean, that charged energy will be released when the difference in internal and external temperature raises.

In consequence, the mean radiant temperature has been set into relation to external temperature. Additionally, the absolute difference of mean radiant and external temperature also has been plotted synchronically.

In order to highlight midterm tendencies, linear trend lines graphically illustrate the effective thermal behavior within the sun space. The thermal behavior will be described and analyzed month-wise in order to generate descriptive knowledge about the location specific sun space inertia.

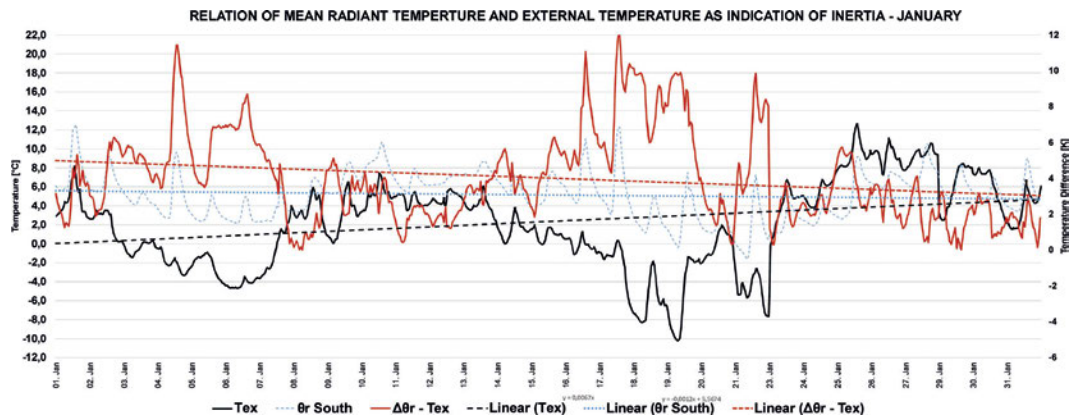


FIGURE 2.51 Month-wise external and mean radiant temperature progression and generated difference – January

Figure 2.51 shows for January a moderate but constant tendency of the external temperature to raise. Although mean radiant temperature predominantly is higher than the external temperature and seldom underrun, opposed to the external temperature, the mean radiant temperature nearly staying constant tends to very slightly decrease. Thus, the difference between external and mean radiant temperature develops a tendency to marginally lower during monthly progression. Figure 2.51 impressively illustrates, that the difference varies extremely with different amplitudes distributed all over the time. Moreover, mean radiant temperature reacts on external temperature time-shifted. It follows with a time lag of several hours, what results in significant temperature difference at certain temporal observations.

That leads to the finding that thermal mass in January compensates daily fluctuations and by trend is getting charged. However, maximum temperature difference could have been determined to be approximately 16 Kelvin.

Thermal behavior specific for February is demonstrated by the plot in Figure 2.52

Although the external temperature amplitudes from +10 to -5°C, the trend line recovers a slight progression of increase. By contrast the mean radiant temperature within monthly progression varies between -0,5 and +26°C. While the tendency of external temperature to raise is moderate but constant, the mean radiant temperature permanently and considerably increases. As a result, the temperature difference also tends to raise, but ascends moderately compared to the radiant temperature.

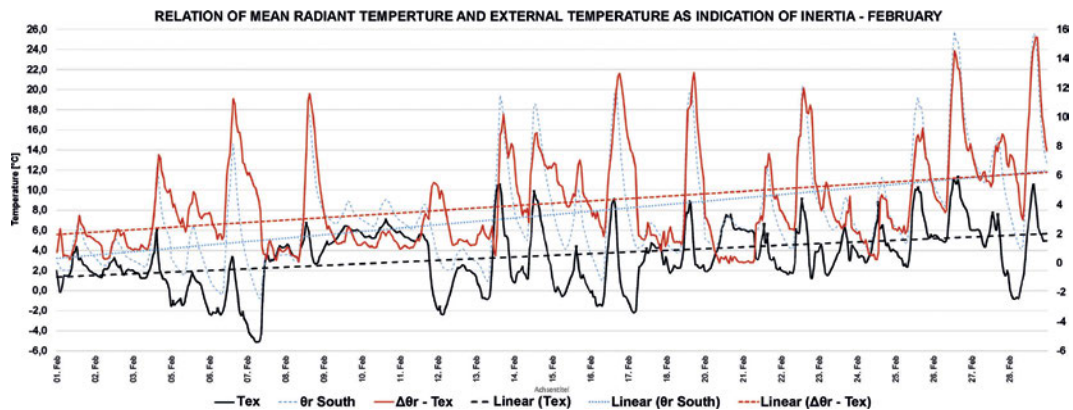


FIGURE 2.52 Month-wise external and mean radiant temperature progression and generated difference – February

Specifically for February, the mean radiant temperature for the most part exceeds external temperature. As finding can be constituted that thermal mass iterated compensates daily fluctuation.

Moreover, thermal mass reaction delay exceeds daily span in February. By trend observation, thermal mass is charged in February and covers maximum temperature differences of 16 Kelvin. Although the linear trend of external temperature for March ([APPENDIX B.6](#)) is observed to be nearly constant, solely imperceptibly raising, the mean radiant temperature shows a strong trend to increase. Consequently, the temperature difference also considerably increases during monthly progression. Summarized, in March thermal mass also compensates temperature fluctuations, and demonstrably often exceeds the lower static comfort set point of 20°C. The positive red dashed lined indicates, that thermal mass is charged permanently during March.

In Figure 2.53 the temperature progression during the month is visualized for April. Notwithstanding, the external temperature raises to maximum 20°C in April, for two time the freezing point is undergone. While mean radiant temperature keeps above 10°C, for several times 30°C is exceeded. In April the linear trend of the external and temperature difference demonstrably diametrically differ.

Whereas the mean external temperature lowers towards end of April, the difference significantly rises. That lead to the insight, that thermal mass meanwhile manage to compensate temperature fluctuations on weekly level. The fact that despite a lowering mean external temperature the lowest thermal comfort limit of 20°C is exceeded

for 2 Kelvin. Thus, since the blue dotted line permanently raises, the thermal mass is charged during

April and inertia is determined by a difference of 12.5 Kelvin. Finally the daily maximum difference of external and mean radiant temperature lowers to 19 Kelvin, 4 Kelvin less compared to March (23K).

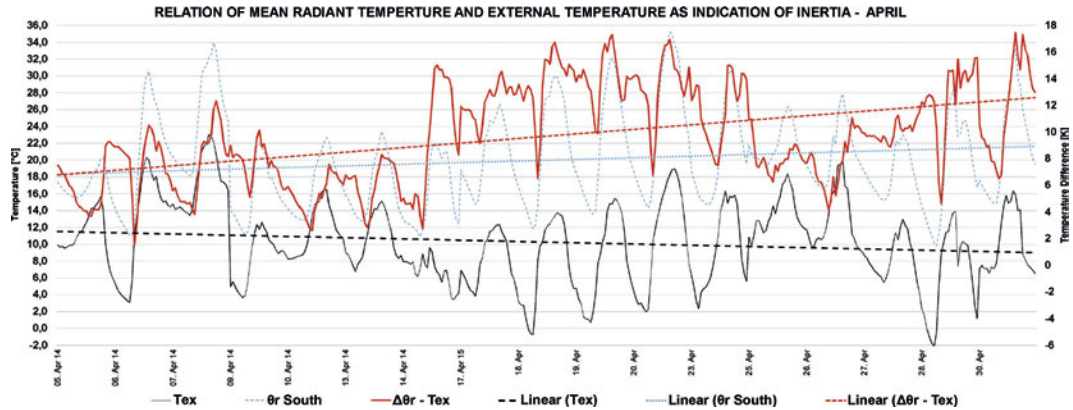


FIGURE 2.53 Month-wise external and mean radiant temperature progression and generated difference – April

While the mean external temperature in May remains constant and falls below 0°C for simply one time, mean radiant temperature varies in a range between 12 to 38°C. The mean radiant temperature and the difference between external and mean radiant temperature slightly decreases by trend, but remains in a band between 22 to 25°C and thus above the lower set point (20°C). However, beside a constant mean external temperature the descending trend of the mean radiant temperature during monthly progression indicates a slightly but permanent discharging of the thermal structure. Finally, the inertia is limited to a temperature difference to 9 Kelvin, that compared to previous month slightly lower.

On the other hand, a temperature difference of maximum 25 Kelvin is observed for May, what counts to be the greatest of the discussed month so far.

June is graphically illustrated in Figure 2.54. Beside exclusively positive external temperature, the mean trend is negative, ergo lowers towards the end of the month

The mean radiant temperature equally lowers by trend, so the difference trend does congruently. Although mean radiant temperature raises in the first triple of March up to 50°C, the trend line weakly lowers. This progression in temperature indicates a discharging of the thermal mass. But, in order to qualify the temperature level of the thermal mass in respect to the charging process during the previous months, the mean radiant temperature by trend is still above 26°C.

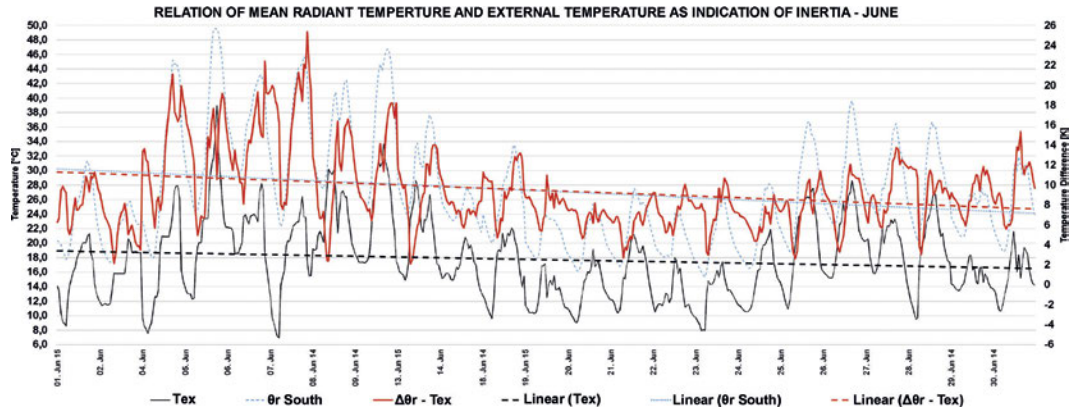


FIGURE 2.54 Month-wise external and mean radiant temperature progression and generated difference – June

Despite July being a midsummer month with the external temperature amplitude including +8°C to nearly 40°C, the monthly trend is demonstrably decreasing. That appears significantly by comparing 24° at the beginning with almost 16°C at the end. In consequence, the mean radiant temperature also lowers strongly by trend.

Since the trend line of the temperature difference slightly but continuously rises, it becomes evident, that thermal mass progressively loses energy during July. While thermal mass strongly discharges, the mean radiant temperature still remains above the upper set point of 26°C by mean of 4 Kelvin. Significant for July is a constant offset to the external temperature trend line of 10 Kelvin. Similar to May and June, the maximum temperature difference recovered for July is 24 Kelvin.

Also August (see [APPENDIX B.6](#)) shows extreme external temperature amplitudes including +8°C and approximately 40°C. In correlation to the external temperature progression the mean radiant temperature trend line decreases. Similar to May and June, the maximum temperature difference recovered for July is 22 Kelvin.

The difference between the means persists to be nearly constant, but slightly decreasing. Thus we can state, that a weak discharging is executed during midsummer month August.

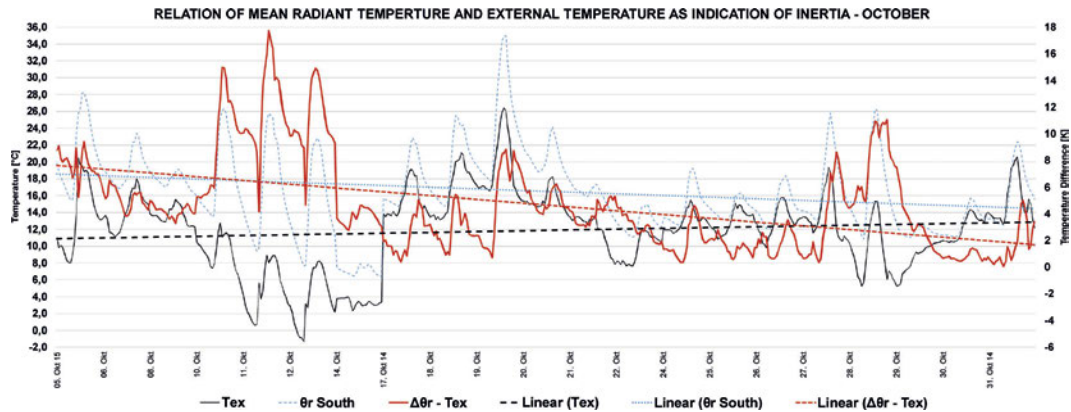


FIGURE 2.55 Month-wise external and mean radiant temperature progression and generated difference – October

Whereas external temperature approximates the freezing point at the end of September, maximum values of 34°C and higher can be inspected at the beginning of the month. Analogously, the radiant temperature reaches comparably high values, it seldom undergoes +12°C. We can recognize a strong tendency of the mean external temperature to ascend towards the end of month. Parallel the mean radiant temperature does with an off-set of approximately 7 Kelvin. Thus the temperature difference remains to be constant. While the thermal mass apparently tends to discharge, it still remains above the lower set point of 20°C for at least two or three Kelvin. The daily maximum temperature difference is identified to be 20 Kelvin.

In Figure 2.55 are described the external and mean radiant temperature for October. While opposed to June, July, August and September the mean external temperature raises by trend, it fluctuates between 11 and 13°C. Freezing point is met for two times, although the external temperature rises to 26°C in mid of the month. Completely disproportional, the mean radiant temperature significantly decreases. It lowers in progress of the month from 19°C to nearly 14°C. The temperature difference strongly decreases towards the end of October. Interestingly, despite the mean radiant temperature and external temperature extremely differs, even time shifted between the

10th and 14th of October and despite radiant temperature accomplishes its monthly maximum of 35°C in the mid of the month, the temperature constantly lowers.

That indicates, that beside a positive and comprehensive trend of external temperature the test sun space in October persistently cools. In consequence, the thermal mass discharges, and undercuts the lower set point of 20°C. Typical for October is, that the temperature difference in opposite to February, March or April extremely lowers to approximately 2 Kelvin, although a maximum difference of 21 Kelvin was detectable.

Since the external temperature for three times lowers the freezing point and diametrically hardly exceeds +18°C, except the mid of month November is predominated by low external temperature. Thermal mass during the month massively discharges, and lowers from 18 to 6°C. Hence, daily solar passive gains are persistently eliminated. Despite this, daily maximum temperature difference figures out to be 16 Kelvin.

In December the external temperature seldom underruns the freezing point and the body despite of some exceptions, was in a range between +4 and +14°C. Beside in September and November the external mean temperature descended, in December the trend is diametrically upwards. Beside a midwinter month the mean radiant temperature permanently raises even stronger than the mean external does. The temperature difference between both tendencies raises from two to three Kelvin. This analysis leads to the finding, that thermal mass is charged in December. The mean radiant temperature consistently has an off-set of at least 2,5 Kelvin to the mean external temperature, thus thermal mass manages to compensate daily fluctuations. The daily maximum difference covers 10 Kelvin.

## Summary

---

Observations and evaluations of sun space inertia is processed with weekly or even monthly interval in order to reveal clear-cut behaviour and tendencies. This section elaborates that even in winter months like January, February and March thermal mass slightly but constantly is charged and manages to compensate temperature fluctuations on daily level.

Especially in April was observed, that inertia was sufficient enough to compensate fluctuations on weekly level. Even in December inertia compensates daily fluctuations. On the contrary, observation evaluates that between May and October thermal mass rather discharges and does rather manage to smooth solar impacts. Parallel to this both observations, November is the month with the most tremendous discharge tendencies and the lowest capability of compensation ever.

### § 2.7.5.6 Monthly analysis of dry bulb temperature related to external temperature and irradiation as indication of inertia

Indoor dry bulb temperature reacts on irradiation. Additionally, ambient temperature lowers or raises in respect to transmission losses to the environment.

For a further analysis of sun space specific inertia, the dry bulb temperature is plotted monthly in relation to irradiation and external temperature in order to determine interrelationships.

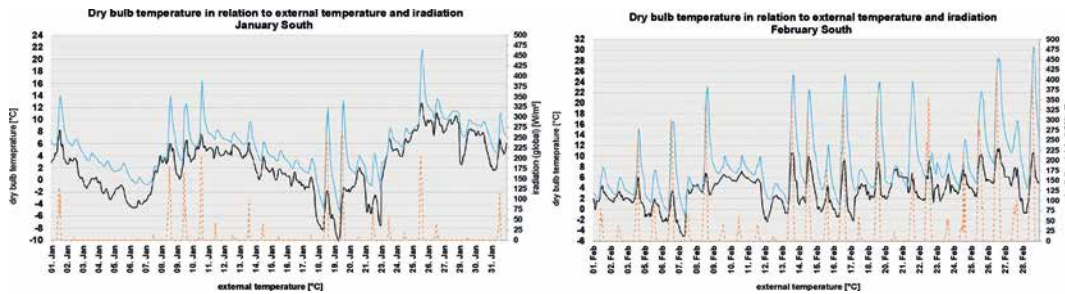


FIGURE 2.56 Month-wise dry bulb temperature progression related to irradiation and external - January + February

Figure 2.56 shows plots of external and dry bulb temperature and irradiation for January and February. The graphs demonstrably show, that in times with approximately no irradiation dry bulb temperature firstly follows decreasing external temperature with simply a little time shift of one or two hours and secondly parallel lowers with a constant off-set of 2,5 to 4 Kelvin. Consequently, external temperature is rarely undercut. Further, when irradiation significantly rises, external temperature dependently synchronically rises, but dry bulb temperature inertly increases.

Dry bulb temperature rises with irradiation changes  $\Delta > 25 \text{ W/m}^2$  distinctly.

When irradiation exceeds  $150 \text{ W/m}^2$  and external temperature is above freezing point, dry bulb temperature dependently increases disproportional compared to external temperature. By contrast, when irradiation outnumbers  $300 \text{ W/m}^2$ , temperature differences between external and dry bulb temperature of more than 16K is possible. The plot at February 20th vividly illustrates, that following a day with very high irradiation ( $350 \text{ W/m}^2$ ) with very low irradiation ( $25 \text{ W/m}^2$ ), external temperature remains stable, while dry bulb temperature essentially undercuts external temperature.

The monthly plots of March and April demonstrate, (see [APPENDIX B.7](#)) that despite daily irradiation maximum of  $200 \text{ W/m}^2$ , dry bulb temperature synchronically to external temperature lowers. On the other hand, the plot of March impressively shows, that after a period of several days with irradiation above  $375 \text{ W/m}^2$  dry bulb temperature simply lowers to a constant low limit, moreover does not cool down such as external temperature. Nocturnal temperature differences between external and dry bulb temperature equal diurnal. That shows us, that a period of over-average irradiation results in a charging of thermal mass, and thus, remain dry bulb temperature on a certain level at nights. An irradiation range between 350 to 500 result in a dry bulb temperature level of 27 to  $40^\circ\text{C}$ .

April additionally interestingly illustrates, that despite of external temperature close to the freezing point at night, dry bulb temperature recovers  $+10^\circ\text{C}$  level and controversially manage to descend to 28 to  $31^\circ\text{C}$  the following day. In the same line, it becomes obvious, that compared to January and February the daily off-set towards the external temperature indicates a charging process of thermal mass.

Significant for May is the observation, that daily diurnal peaks of external and dry bulb temperature are chronologically synchronic, but opposed to that, nocturnal bottoms are timely shifted. Thus, we can conclude that the test sun space heated accordingly to the external temperature, but cooled retardant. Additionally, maximum dry bulb temperature of  $40^\circ\text{C}$  resulted on May 12th related to an irradiation of approximately  $500 \text{ W/m}^2$  following a day with irradiation of  $625 \text{ W/m}^2$ .

Beside significant high irradiation of maximum  $625 \text{ W/m}^2$  and diurnal external temperature of  $27^\circ\text{C}$ , nocturnal natural ventilation via roof sliding window and transmission via the façade result in temperature descends of 8 to 21 Kelvin. Interestingly, the maximum dry bulb temperature in June attains  $55^\circ\text{C}$  by external temperature of more than  $38^\circ\text{C}$  and irradiation maximum of  $625 \text{ W/m}^2$ . After a period of several days, when irradiation was over averaged high with  $> 600 \text{ W/m}^2$  dry bulb temperature exceeds  $50^\circ\text{C}$  even with a daily irradiation of  $440 \text{ W/m}^2$  on June 13th. Similar to May, also in June can be inspected a time shift of external and dry bulb temperature during natural nocturnal free cooling.

In the plot of July (App.) it becomes apparent, that the peaks dry bulb temperature stays permanent within a specific range of 30 to  $40^\circ\text{C}$ . Analogously, nocturnal bottoms range between 16 to  $26^\circ\text{C}$ . Although the external temperature significantly often lowered below  $18^\circ\text{C}$  and thus caused considerable daily temperature amplitudes, the dry bulb band within the test sun space remained stable!

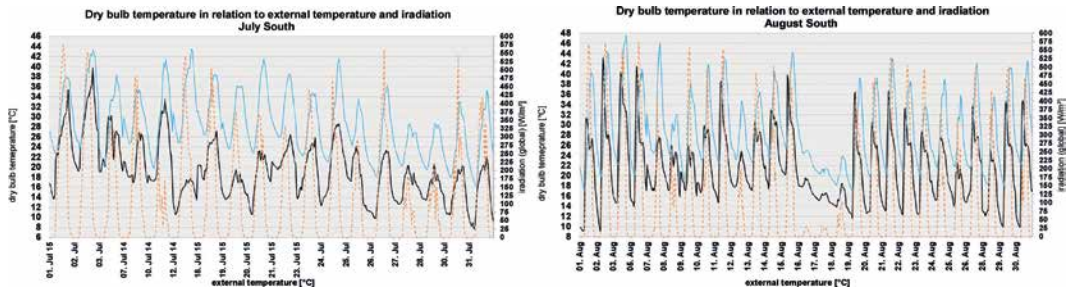


FIGURE 2.57 Month-wise dry bulb temperature progression related to irradiation and external - July + August

Within this observation special attention is called for July 18th, when the external temperature maximum ended with 18°C and dry bulb temperature developed to a daily maximum of 43°C. However, for the first time, compared to the previous months, in August the dry bulb temperature shows a considerable time shift to the external temperature development during sun shine. Observations of months beforehand strengthened the conclusion of a diurnal synchronicity and nocturnal chronological delay, but, nonetheless this changes diurnally since August.

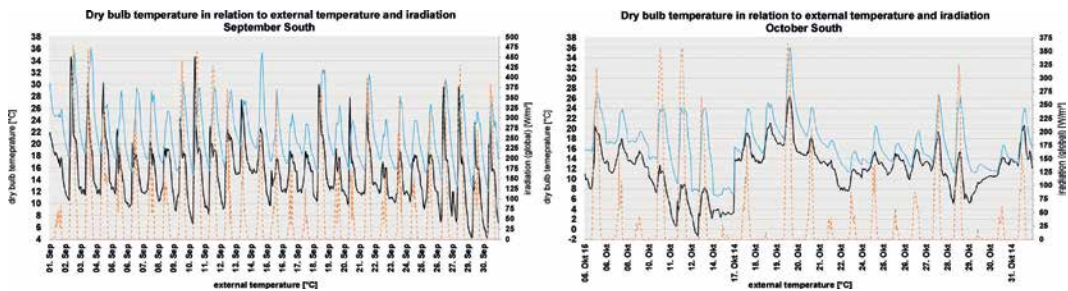


FIGURE 2.58 Month-wise dry bulb temperature progression related to irradiation and external - September + October

Although irradiation reaches 575 W/m<sup>2</sup>, the dry bulb temperature reacts on external temperature delayed in time. In Figure 2.58 the monthly external and dry bulb temperature plots related to irradiation are illustrated for September and October. The progress of dry bulb temperature appears visually, in respect to any statistical evaluation, as a parallel off-set to the external temperature.

In total, the temperature progresses appears homogenous compared to the months beforehand. Daily dry bulb temperature maximum often ranges between 24 to 29 °C.

Despite the irradiation maximum lowers on average by 175 W/m<sup>2</sup>, dry bulb temperature mostly out-weighs external temperature for 8 to 10 Kelvin. Similarly, the plot of October shows in the first half of the month an extraordinary constant level of maximum dry bulb temperature, while opposed to that the external temperature continuously sinks. That is related to the control of natural ventilation openings, which not open until 26 °C dry bulb temperature.

Although the maximum irradiation is limited to merely 350 W/m<sup>2</sup>, the maximum dry bulb temperature rises to 36 °C. From 10th of November to 20th of November irradiation lowers significantly and does not exceed 75 W/m<sup>2</sup>. In consequence, the external temperature by trend descends and parallel dry bulb temperature does. Although from November 21th to the 29th several extreme peaks of irradiation above 200 W/m<sup>2</sup> hardly managed to raise external temperature for about 4 K, but demonstrably influenced internal dry bulb temperature to change from 6 °C close to 20 °C.

In December ([APPENDIX B.7](#)) irradiation predominantly is higher than compared to November, since irradiation majorly exceeded 75 W/m<sup>2</sup>, very often outnumbers 120 W/m<sup>2</sup>. In consequence, external temperature never underrun freezing point, but on the other way round is in a band between 5 to 11 °C. Dry bulb temperature follows external temperature parallel with an off-set of 1,5 to 3,5 K on average, however for seven of all observed days with an off-set of 9 to 10 Kelvin maximum. Compared to November, despite of a smaller off-set of the dry bulb temperature related to the external temperature, the amplitudes of dry bulb temperature are smaller and form a more balanced band of indoor temperature. Temperature close to freezing point are more seldom as in November.

## Summary

---

The inspection of plotted dry bulb temperature shows, that it immediately can react on ex-ternal temperature and irradiation. While dry bulb temperature in January and February in-creases with an off-set of 2,5 to 4K, the inertia already compensates thermal losses and changes. Already in January and February dry bulb temperature raises tremendously, whereas external temperature remains constant.

Thus dry bulb temperature in midwinter always stays above external temperature. Especially in March and April inertia prevents dry bulb temperature to undercut 10 °C,

while few days undergo freezing point. Nocturnal natural ventilation result in cooling of 8 to 21 Kelvin in May and June, what rather reveals with very limited effect and delayed in August. May and June provide maximum dry bulb temperature and distance to external temperature what signals the capacity limits for compensation of the thermal mass. Opposed to that in August, inertia compensates sufficiently, what can be observed by delayed increase in dry bulb temperature.

September and October show very synchronic external and dry bulb temperature progresses, which indicates a balanced thermal behavior of the space in contact with environment. On the contrary, since thermal mass is discharged in November and since irradiation significantly lowers, inertia is not able to compensate any what results in constant temperature ascends.

That can change in the further progress of winter, in particular in December, when irradiation on average raises and inertia manage to stabilized dry bulb temperature levels in the first and second half of month.

---

## § 2.8 Analysis of minor detailed sun space specific local thermal discomfort

---

Former sections analysed frequencies of dry bulb temperature and operative temperature. Operative temperature was either related to each other or plotted as comfort charts related to relative humidity and related to comfort bands, which were generated by the running mean of external temperature. Further, thermal behaviour of the test sun space has been described and evaluated in terms of specific inertia. Since evaluation of predicted mean vote and predicted percentages of dissatisfied occupants by nature are solely meaningful and plausible for mechanically ventilated and actively cooled and heated spaces, this analysis method is only partly appropriate for a sun space evaluation [68].

Calculations of PMV and PPD during this thesis project resulted in either extremely high or low calculated skin temperature and clothing surface temperature ( $\theta_{cl}$  [°C]) [70]. Amplitudes enclosed 35 K by changing from minute to minute. As a result PMV changed into negative values in summer and vice versa. Moreover, the PMV range was limited to “-1,7” and did not cover “-3” (cold) or “+2” (warm). Consequently, PPD values generated appeared without any logic.

Nonetheless, DIN EN ISO 7730 parallel describes alternative methods to analyse thermal comfort by inspecting of local discomfort. Local discomfort analysis focusses on detailed single thermal conditions, which severally do not discredit comfort completely, but give insight in construction and location related correlations, which forces unease and combined result in tremendous uncomfortable perception. Thus, this section focusses on local discomfort in order to detect lacks of sun space thermal-constructional quality, which exceeds simple transmission loss optimization, but concentrates on the interaction of separate building elements.

Local thermal discomfort can be induced by vertical temperature differences of dry bulb temperature, namely striation, (DIN EN ISO 7730, 6.3), cold or warm ceilings (DIN EN ISO 7730, 6.4) or radiation asymmetries of facing building elements (DIN EN ISO 7730, 6.5).

Similar to PMV evaluation, local discomfort evaluation defines limits based on human physiological perception according to thermal comfort quality categories, namely I, II and III. In the context of the empirical test sun space evaluation and theoretical living space analysis, this section accordingly orientates on category II. In order to quantify local thermal discomfort and thereby thermal comfort quality, DIN EN ISO 7730 similarly to PMV procedures introduces calculation methods to determine percentages of dissatisfied (PD), that opposed to PMV are actual and not predicted.

### § 2.8.1 Monthly analysis of dry bulb striation / air temperature gradient

---

Figure 68 illustrates tabular cumulative frequencies of striation recorded in the south flank of the test sun space. As limit value in correspondence to category II (DIN EN ISO 7730) is set 3 Kelvin vertical difference. The table distinguishes between a 0,1m above floor and 1,10m above floor distance and a 1,10 and 1,70m distance, which represents average torso and head height, which Klein and Schlenger, (2008) [71] distinguishes.

Percentage dissatisfied (PD) is solely expressed for the torso-head height investigation.

Furthermore, the table separates between fully day, respectively 0 to 24 hours, and the preferred occupation period between 5 to 10 PM. Thus, the table considers 303 days of a 365-days year. Moreover, the table additionally shows estimated add on hours in a 365 day context.

MONTH	ANALYZED DAYS	ANALYZED HOURS	South Flank													
			STRIATION South >3K 0,1 m to 1,10 m			STRIATION South >3K 5to10PM 0,1 m to 1,10 m			STRIATION South >3K 0,1 m to 1,70 m			STRIATION South >3K 5to10PM 0,1 m to 1,70 m				
			(hours)	303 Days	add on hours for 365 Days	(hours)	303 Days	add on hours for 365 Days	(hours)	303 Days	add on hours for 365 Days	≥ PD>5%	(hours)	303 Days	add on hours for 365 Days	≥ PD>5% 5to10PM
January 2015	29 von 31	696	25	4%	+2	0	0%	+0	34	5%	+2	27	2	1%	+1	2
February 2015	26 von 28	634	109	17%	+8	18	14%	+7	122	20%	+9	72	31	24%	+11	21
March 2015	25 von 31	775	134	17%	+25	10	8%	+12	158	20%	+29	110	25	20%	+29	16
April 2015/14	17 von 30	408	93	23%	+71	11	13%	+40	111	27%	+85	80	20	24%	+73	16
May 2015	30 von 31	720	143	20%	+5	22	15%	+4	233	32%	+8	190	57	38%	+9	42
June 2015/14	23 von 30	552	107	19%	+33	25	22%	+37	156	28%	+47	108	37	32%	+54	26
July 2015/14	18 von 31	432	85	20%	+61	8	9%	+28	123	28%	+89	103	22	24%	+76	17
August 2015	27 von 31	648	147	23%	+22	17	13%	+12	174	27%	+26	136	34	23%	+24	23
September 2015	29 von 30	696	108	14%	+3	1	3%	+0	130	19%	+4	110	14	10%	+2	11
October 2015/14	21 von 31	504	47	9%	+22	0	0%	+0	58	12%	+28	49	5	5%	+11	4
November	25 von 30	600	66	10%	+12	0	0%	+0	69	12%	+14	59	6	5%	+6	3
December	30 von 31	720	23	3%	+1	0	0%	+0	32	4%	+1	21	0	0%	+0	0

FIGURE 2.59 Month-wise analysis of dry bulb striation for entire days and 5 to 10PM focus as PD evaluation – South flank

In January, the entire day analysis reveals a frequency of 25 hours of temperature difference >3K between 0,1 and 1,1 m. That corresponds to 4% of all surveyed days and results in two additional hours of local discomfort in 365-day context. Interestingly, in the time period 5 to 10 PM, in January, any hour of temperature difference > 3K could have been identified. On the other hand, frequency of hours with >3K raises to 34 hours against the background of a 1,10 to 1,70m observation. Thus, the frequency of PD>5% (cat. II) January is 27 hours in an entire day perspective, and simply 2 hours in a 5 to 10 PM perspective. Finally, local discomfort in January concerning torso-head height between 5 to 10 PM occurs for simply 1% of all surveyed hours.

On the contrary, in February, the frequency of hours with a temperature difference in torso-head height perspective raises from 34 to 122 hours in respect of an entire day analysis. Hence, twenty per cent of observed hours showed local discomfort. Another 9 add on hours account in a 365-days perspective. The corresponding number of hours with PD>5% is 72 hours for February. In means if striation from hip to head in the time frame 5 to 10 PM 31 hours showed differences > 3K, what corresponds to 24% of related hours. The accompanied number of hours with PD>5% is 21.

In March can be detected in total 134 hours with striation between 0,1 and 1,10 m greater than 3K for entire day evaluation, thus this trend continues. But, within a 5 to 10 PM separation the frequency compared to February lowers from 18 to 10.

Accordingly, the frequency of hours with temperature difference greater than 3K between torso-head height increases to 158 hours, what corresponds to 20% of observed hours and another 29 hours in a 365-day perspective. In terms of entire day evaluation of percentage of dissatisfied in torso-head height context does this end up into 110 hours. Differently represent the figures for a 5 to 10 PM observation, since simply 25 hours, respectively 20% of hours, result in 16 hours of remarkably local discomfort for category II.

On the opposite, April is the month, that was solely observed by 17 of 30 days in total. But extrapolation of the evaluated values shows a tremendous increase in hours with local dis-comfort by striation. An entire day and 0,1 to 1,10 m observation focus reveals 93 and additional 71 add on hours, 164 hours totally, with temperature differences higher than 3 K. Consequently, this means discomfort for 23% of all entire day hours for sub torso comfort evaluation.

Even in the time slot 5 to 10 PM nearly more than 10% (13%) hours is an apparent frequency of hours with discomfort. For the hip to head investigation the extrapolated number of hours increases to 196 in a full day perspective and will lead to at least 27%, and 80 hours of PD>5%. Similarly, the 1,10 to 1,70m area evaluation in the preferred evening hour period shows 24 % with +73 extrapolated hours with striation >3K, what results in 16 to 30 hours of PD>5% respectively.

For May, beside demonstrably high percentage of hours both in entire day and evening perspective 0,1 to 1,10 m observation with striation >3K of 20 and 15%, especially the torso-to-head height inspection shows high frequencies of local discomfort. One third of hours in an entire day perspective and nearly 40% of all hours between 5 to 10 PM reveal vertical temperature difference greater than 3K. That result in frequency of PD>5% of 190 and 42 respectively.

Figure 2.59 tabulates especially for June high frequencies of hours with striations >3K for 1,10 to 1,70 m field of observation. Even 28% (also in a 365-days context) of hours exceeds a difference of 3K entire-day-wise and for 32 in a 5 to 10 PM perspective. That means, that in June every third hour provided local discomfort. This trend continues in July. While on an entire day and 0,10 m to 1,10 m basis 20% of all hours are detected with temperature differences greater than 3 Kelvin, the number significantly lowers for the 5 to 10 PM time slot towards simply 9%. Opposed to that corresponds 28% day-wise and 24% of hours between 5 to 10 PM for a hip to head investigation with an exceeding of temperature difference. Nearly every third or fourth hour day-wise or in the evening would show in a 365-day context local thermal discomfort in July.

Although for August only 27 of 31 days have been evaluated, an meaningful evaluation is executable without any extrapolation. Also in August the frequencies of hours with detected striation > 3K in day-wise context are higher than the equivalent ones for the evening time frame. Thus more than 23% and 27% of hours day-wise exceeds comfort limits, whereas the frequencies for 5 to 10 PM for either 0,10 to 1,10 m or 1,10m to 1,70m observation are two to ten per cent lower. Generally spoken every fourth hour in August encounters significant striation. In September, striation >3K in context of 0,1 to 1,10m evaluation exceeds for only 14% within surveyed daytime and for merely 1% in the observed evening time.

Opposed to that rises frequencies of hours with limit exceedance for the hip to head observation. Nineteen and ten per cent of hours day-wise, and evening-wise respectively, show striation  $>3K$ , what results in 110 and 11 hours with  $PD>5\%$ .

October the frequencies of hours with exceeded striation limits lowers compared to September. Especially the frequency of hours for the torso-head height investigation in the 5 to 10 PM time slot lowers from 10 to 5%, what actually corresponds to 5 and 11 hours in a 365-day perspective. The evaluated frequencies of hours related to all distinctions of investigation are virtually similar to October, also regarding November with additional four days of surveillance. The number of hours with  $PD>5\%$  exceedance accounts for 55, respectively 3 hours. In December temperature differences, that exceeds 3 Kelvin, exclusively are detected in hip to head perspective, being predominant in the entire-day time frame with simply 32 hours, what equals 4% of all surveyed hours. In contrast to that, in the evening time slot any local discomfort is evaluated at all.

## Summary

---

Summarized, the frequency of hours with striation exceedance generally raised from the beginning of the year in winter month January to May and June and encountered the maximum frequency in midsummer. From midsummer to winter, towards the year's end, the frequency trend was disproportional falling. Limit exceedance was normally higher in entire day perspective than in 5 to 10 PM time frame and for the 1,10 to 1,70 torso-to-head elevation than for the 0,1 to 1,10 m fraction. In particular May, we detected nearly every third or even every second of five hours with local striation discomfort. An analysis of the west flank (Fig. 2.60) shows completely different results compared with the south flank. Analogously, the rule of higher exceedance frequencies in summer than in winter can also be determined in the west flank. Typical for the west flank is identified a stress on the 5 to 10 PM time slot, which opposed to the south flank shows the highest frequencies of hours with temperature differences  $>3K$ .

Thus, we can say, that statistically thermal comfort both generally and in particular between 5 to 10 PM in regard of extreme temperature striation is better in the south flank than in the west flank. Whereas in the south flank relative frequencies of temperature differences  $>3K$  of 20% can exclusively be observed from April to August with peak during midsummer, more than 23% of exceedance can be identified in the west flank already in February and including September and October.

MONTH	ANALYZED DAYS	ANALYZED HOURS	West Flank													
			STRIATION West >3K 0,1 m to 1,10 m			STRIATION West >3K 0,1 m to 1,10 m			STRIATION West >3K 0,1 m to 1,70 m			Σ PD>5%	STRIATION West >3K 0,1 m to 1,70 m			Σ PD>5% StrioPPM
			303 Days	add on hours for 365 Days	Σ PD>5%	303 Days	add on hours for 365 Days	Σ PD>5%	303 Days	add on hours for 365 Days	Σ PD>5%					
(hours)	(hours)	(hours)	(hours)	(hours)	(hours)	(hours)	(hours)	(hours)	(hours)	(hours)	(hours)					
January 2015	29 von 31	696	80	7%	+ 3	2	3%	+ 1	82	7%	+ 4	36	3%	+ 1	1	
February 2015	28 von 28	624	142	23%	+ 11	35	27%	+ 13	183	25%	+ 12	73	40	31%	+ 15	
March 2015	25 von 31	775	208	27%	+ 30	40	32%	+ 46	209	27%	+ 30	115	44	35%	+ 51	
April 2015/14	17 von 30	408	183	38%	+ 117	44	52%	+ 182	167	38%	+ 130	101	44	52%	+ 182	
May 2015	30 von 31	720	318	44%	+ 11	104	69%	+ 17	326	45%	+ 11	262	107	73%	+ 17	
June 2015/14	23 von 30	552	244	44%	+ 74	78	68%	+ 114	248	45%	+ 75	155	81	70%	+ 118	
July 2015/14	15 von 31	432	185	43%	+ 134	61	68%	+ 211	190	44%	+ 237	141	61	68%	+ 221	
August 2015	27 von 31	648	256	40%	+ 38	86	64%	+ 61	263	41%	+ 30	160	87	64%	+ 62	
September 2015	29 von 30	696	222	32%	+ 8	59	43%	+ 30	240	34%	+ 8	181	61	42%	+ 10	
October 2015/14	21 von 31	504	96	19%	+ 46	14	13%	+ 32	105	21%	+ 50	70	18	17%	+ 41	
November	25 von 30	600	79	13%	+ 36	7	6%	+ 7	85	14%	+ 17	46	7	6%	+ 7	
December	30 von 31	720	61	8%	+ 2	0	0%	+ 0	70	10%	+ 2	57	8	0%	+ 0	

FIGURE 2.60 Month-wise analysis of dry bulb striation for entire days and 5 to 10PM focus as PD evaluation – West flank

Interestingly, already in April and lasting to September, the relative frequency of exceedance in the evening time frame is higher than 50% and reaches 71% maximum in May. That means, that striation especially in the torso-to-head area in the evening time causes remarkable local discomfort in every second hour or in two of three hours. Mainly during May, June and July the relative frequency is about 70%.

Reason for this completely different and comparably extreme pattern of local discomfort in the west flank can be the existence of a roof integrated sliding window.

It is intended to open in order to automatically exhaust warm ambient air and to enable free cooling. Thus, as a substantial difference in ambient air context, the ambient air in the west flank is naturally induced by thermal differences and encounters much more intensive exchange and thermal dilution. Whereas indoor air in the south flank mostly remains stabilized striated, striation explicitly develops and causes local discomfort.

### § 2.8.1.1 Monthly analysis cold or warm floor

Reason for local thermal discomfort can be a floor providing a temperature that is either too cold or too warm. Limits are set by DIN EN ISO 7730 less than +19°C and more than +28°C. The empirical floor surface temperature was recorded and analysed for the south and the west flank. Figure 70 tabular shows frequencies of limit exceedance within the surveyed 303 days and additionally extrapolated add on days for a 365-days context of evaluation. Similar to striation, as a quantitative result within this local discomfort evaluation is calculated a percentage of dissatisfied (PD>10%), which beside statistical analysis of frequencies of limit exceedance also considers human metabolism according standard DIN EN ISO 7730.

Thus, the PD values (percentage of dissatisfied, floors: >10%), differ from the simple statistical evaluation and often account slightly better. The table additionally differentiates between entire day and 5 to 10 PM evaluation.

For January Figure 2.61 tables 696 hours of floor surface temperatures below 19°C. This is equal to 100% of all observed hours and can be elongated by +48 add on hours in a 365-days perspective. This figure impressively demonstrates, that the predominant problem in the test sun space south flank in January was local discomfort by too cold floors. The corresponding PD value of more than 10% of dissatisfied is 696 hours or times observed. In consequence, the evaluation of the evening time frame also shows 100% of all hours with floor surface temperatures beneath at least 19°C. This corresponds to 145 hours of PD>10%.

MONTH	ANALYZED DAYS	ANALYZED HOURS	South Flank									
			T <sub>floor</sub> (t) <19°C	T <sub>floor</sub> (tf) >28C	303 Days	add on hours for 365 Days	PD >= 10%	T <sub>floor</sub> (t) <19°C Sto10PM	T <sub>floor</sub> (tf) >28C Sto10PM	303 Days	add on hours for 365 Days	PD >= 10% Sto10PM
January 2015	29 von 31	696	696	0	100%	+ 48	696	145	0	100%	+ 48	145
February 2015	26 von 28	624	624	0	100%	+ 48	610	130	0	100%	+ 48	130
March 2015	25 von 31	775	498	0	64%	+ 93	508	84	0	67%	+ 97	85
April 2015/14	17 von 30	408	170	0	42%	+ 130	178	29	0	34%	+ 106	31
May 2015	30 von 31	720	70	2	10%	+ 2	95	12	0	8%	+ 2	11
June 2015/14	23 von 30	552	11	170	31%	+ 52	189	0	46	40%	+ 67	46
July 2015/14	18 von 31	432	0	203	47%	+ 147	205	0	55	61%	+ 191	55
August 2015	27 von 31	648	1	229	35%	+ 34	234	0	75	56%	+ 53	77
September 2015	29 von 30	696	122	13	18%	+ 4	157	3	0	2%	+ 0	7
October 2015/14	21 von 31	504	366	0	73%	+ 174	375	67	0	64%	+ 153	70
November	25 von 30	600	600	0	100%	+ 120	600	125	0	100%	+ 120	125
December	30 von 31	720	720	0	100%	+ 24	720	150	0	100%	+ 24	150

FIGURE 2.61 Month-wise analysis of too warm or too cold floor temperature with day and 5 to 10PM focus on PD evaluation – South flank

For February, the table illustrates similarly to January no hour of a floor surface temperature >28°C. Nevertheless, 624 of 624 hours surveyed are accompanied with floor temperature below 19°C. The statistically generated 624 hours relate to 610 hours with PD>10% in entire-day perspective.

The inspection of the 5 to 10 PM time slot does not recover different results. In this time slot in February also 100%, namely 145 hours, correlate to floor temperature below 19°C. The figure reveals for March a different results, and hence a change in local comfort quality. The cumulative frequency of hours with floor temperature lower than 19°C is 498 hours in entire-day context. This corresponds to 64% of the observed hours.

In consequence, this means, that one third of all recorded hours provides satisfying floor temperature what causes no local thermal discomfort. The related PD>10% value calculates 508 hours of dissatisfied occupants. An inspection of in particular evening hours reveal a slightly higher number of hours with surface temperatures below 19°C, what correlates to 67% instead of 64% and is equal to 85 hours with PD>10%. Thus, we can conclude so far, that local discomfort by to cold floors are more often in the evening than in entire-day perspective.

In April 170 of in total 408 hours are detected with lower limit exceeding temperatures. This corresponds to 42% of hours in entire-day perspective with local discomfort. Surface temperatures higher than 28°C could not have been observed. Further, another 130 add on hours are calculated that will not fulfil the lower comfort limit.

Since simply 29 hours within 5 to 10 PM perspective are determined with floor surface temperatures below 19°C, the correlated relative figure of 34% significantly differs from 42% for the entire day evaluation. The PD>10% value is 31 and roughly two third smaller than the equivalent for March. Thus, by both inspections we can see, that concerning cold floors the situation changed from frequently more often local discomfort in the evening time to frequently less local discomfort between 5 to 10 PM compared to an entire-day analysis.

In figure 70 the first summer month May is the first, when floor surface temperature of higher than 28°C is observed. That fact is calculated with solely hours. Although the frequency of hours with floor temperature below 19°C is significantly higher than for hours with upper limit exceedance, the total number and related relative percentage tremendously lower towards 70 hours and simply 10% in entire-day perspective. This trend slightly emphasizes for the evening time slot, since the relative frequency lowered to rarely 8%. May is, in order to conclude, the first month analyzed so far with first a dominating high frequency of satisfying local thermal comfort (floor temperature) and second apparently low frequency of limit exceeding floor temperature, respectively 72 hours in total.

For June an analysis reveals simply 11 hours in total in an entire-day inspection context of floor temperature lower than 19°C. Opposed to that 170 hours were detected related to the observed hours that provided floor surface temperature above 28°C. Within the preferred evening occupation time no hour with dissatisfying low temperature, but 46 hours of floor temperature above 28°C were identified.

With a ratio of 31 to 40% local discomfort frequently more often concentrates in the 5 to 10 PM period with predominantly to warm floor. June is the first month, which shows higher frequency of 28°C exceedance than 19°C exceedance.

Nonetheless, beside in June have simply been recorded 23 of 30 days, the total sum of hours with limits exceedance including add on hours for a complete month evaluation accounts for (11+170+52) at least 232 hours of local discomfort. This figure is three times higher than for May. In July is identified no hour with floor surface temperature lower than 19°C, but 203 in total and 55 in particular for the evening time frame with floor temperature exceedance of 28°C. These frequencies are equal to 47 and 61% of observed hours, that can be extrapolated for an entire month evaluation. In the entire-day context 203 hours corresponds to 205 hours of PD>10%, and in 5 to 10 PM perspective 55 hours equals 55 hours with PD>10%.

August is the first month in midsummer, when floor surface temperature lowers 19°C again. Floor surface temperature is in 229 hours higher than 28°C, what equals 35% in entire-day context, whereas the frequency in the evening is about 75 hours and corresponds 56% of hours within this time slot. Both times the correlating PD>10% frequencies of hours are slightly higher than the absolute number of hours.

Opposed to August, September as a late summer month shows floor surface temperatures, that statistically considerably differ from that of August.

In August the frequency of hours with cold floor temperature below 19°C in entire-day context raised from 1 to 122 hours, while the frequency of hours with floor temperature >28°C tremendously minimized from 229 to 13%. Finally, 18% of all hours in September in entire-day context encounter temperature, that is below 19°C, what corresponds to 157 hours with PD>10% in respect to the observed hours. Interestingly, within the 5 to 10 PM time frame, solely three hours are detected, which are correlated to floor temperature <19°C. On the contrary, no hour with upper limit exceedance is identified. Thus, September is beside a higher frequency of hours in entire-day perspective, the month that performed the best during evening times so far, and showed even less hours of local discomfort than May.

In October the frequency of hours with floor surface temperature higher than 28°C lowers to zero, whereas cold floor surface temperature is statistically determined in 366 of in total 504 hours.

That is equal to 73% of all observed hours in entire-day perspective. Since in the evening hours 67 hours are detected with cold floors, 64% of all surveyed hours from 5 to 10 PM provide local discomfort, what results in 70 hours with PD>10%.

November and December, both are predominated from extremely high frequencies of hours with exceedance of the lower limit 19°C. Further, one hundred per cent of hours

provide floor surface temperature of less than 19°C, what does not even improve in the evening time after a day period of sun shine.

The number of hours with PD>10% related to cold floor temperature is each for November and December maximum of the observed amount of hours.

MONTH	ANALYZED DAYS	ANALYZED HOURS	West Flank									
			T <sub>floor</sub> (tj) <19°C	T <sub>floor</sub> (tf) >28C	303 Days	add on hours for 365 Days	PD >= 10%	T <sub>floor</sub> (tj) <19°C 5to10PM	T <sub>floor</sub> (tf) >28C 5to10PM	303 Days	add on hours for 365 Days	PD >= 10% 5to10PM
January 2015	29 von 31	696	696	0	100%	+ 48	696	145	0	100%	+ 48	145
February 2015	26 von 28	624	624	0	100%	+ 48	624	130	0	100%	+ 48	130
March 2015	25 von 31	775	522	0	67%	+ 97	526	93	0	74%	+ 107	90
April 2015/14	17 von 30	408	155	2	38%	+ 119	175	21	2	25%	+ 77	26
May 2015	30 von 31	720	79	9	13%	+ 3	109	10	4	7%	+ 2	12
June 2015/14	23 von 30	552	27	178	32%	+ 54	211	0	57	50%	+ 83	57
July 2015/14	18 von 31	432	0	190	44%	+ 137	191	0	56	62%	+ 194	57
August 2015	27 von 31	648	4	233	36%	+ 35	241	0	100	74%	+ 71	102
September 2015	29 von 30	696	147	6	21%	+ 5	176	0	0	0%	+ 0	0
October 2015/14	21 von 31	504	374	0	74%	+ 178	381	64	0	61%	+ 146	65
November	25 von 30	600	596	0	99%	+ 119	597	123	0	98%	+ 118	123
December	30 von 31	720	720	0	100%	+ 24	720	150	0	100%	+ 24	150

FIGURE 2.62 Month-wise analysis of too warm or too cold floor temperature with day and 5 to 10PM focus on PD evaluation – West flank

Figure 2.62 illustrates the statistical figures of floor surface temperature exceedance month-wise for the west flank. The frequency of hours of limit exceedance in an entire-day perspective does not differ tremendously from the south flank. Until July the frequencies of cold floor perception each a month are generally 5 to 25 hours higher than compared to south. In June and August frequencies of warm floors are slightly higher in the west flank than in the south equivalent. Nonetheless, continuing with September, numbers of hours with cold floor are merely higher than are detected for the south flank. However, calculated relative frequencies vary for not more than 4%.

The comparison of frequencies of the west and south flank in the context of the 5 to 10 PM time frame though reveals demonstrably high differences. While for January, February, March, November and December the frequencies differ for not more than 9 hours and 7 per cent respectively and any cold floor surface cannot be detected for both flanks between June and September, the major differences are detected for warm floor limit exceedance between April and August.

In April, the calculated relative difference accounts for 9%, in June for 10% and in August for 18%. That identified differences indicate, that the west flank in summer tends to more often provide too warm floors than the south floor.

### Summary

---

In terms of local discomfort caused by floor temperature exceedance it can be summarized, that both south and west flank suffer from predominant floor temperature, that is too cold ( $<19^{\circ}\text{C}$ ). Except May, June, July and August all month encounter frequencies of hours with cold floor  $> 120$ , what in extremum ends up into 100% relative fraction. Solely in June, July and August evaluation identifies worth mentioning frequencies of hours with warm floor. From an entire day perspective May, June and September have been identified, in which local discomfort concerning floor temperature for both cold and warm floor parallel occurred. Opposed to that in the evening hours no month is identified with parallel hours of cold and warm floor, thus exclusively simply one limit of exceedance.

#### § 2.8.1.2 Monthly analysis radiation asymmetries

---

While in section 4.5.1 have been analyzed ambient air characteristics and in specific floor temperatures as isolated reasons for thermal local discomfort, section 4.5.3 focusses on thermal discomfort by radiation asymmetries. Focus on radiation asymmetries concentrates on space enclosing surface temperature (Fig. 2.63) and couple-wise differences.

Reason for attentive evaluation gives Figure 2.63, which visualizes temperature peaks of internal surface temperature of roof glazing in summer, midsummer and autumn months. For May are measured approximately  $50^{\circ}\text{C}$  internal surface temperature in the second half of the 22th May, when irradiation reached  $550$  to  $700\text{ W/m}^2$ . Surface and radiation temperature raise to  $58,6^{\circ}\text{C}$  on July the 15th. Even in August are observed surface temperatures between  $54,3^{\circ}\text{C}$  to  $57,5^{\circ}\text{C}$  with irradiation of little less than  $600\text{ W/m}^2$ .

Moreover, on September the 18th the surface temperature increases in the second half of the day towards  $50,8^{\circ}\text{C}$  while irradiation differs between  $450$  and  $550\text{ W/m}^2$  maximum.

Area-intensive surfaces, that are central parts of sun space constructions firstly show very high temperatures and thus account for significant amounts of envelope heat radiation, that are sensible for space occupants and secondly contribute to radiation asymmetries. Such results reason further detailed inspection of surface temperature of building elements and resulting radiation asymmetries. In details, for example floor temperature and rear-wise wall temperature are compared when these building elements enclose for reasonable occupation time since a human occupant choose the space.

Further façade and floor, or roof and façade or roof and rear-wise wall temperature are in focus for analysis. Therefor the building elements are weighted by view factors. View factors relate the distance and dimensions of considered building elements in respect to the occupants position in the space. Moreover view factors consider the building element itself and the relative position or fraction of a building element type (roof, ceiling, wall, parapet area, ribbon-façade window or roof light).

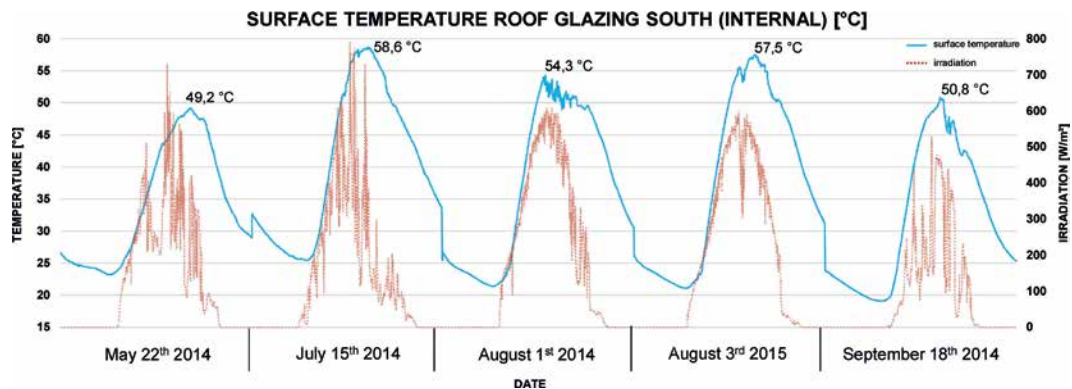


FIGURE 2.63 Selected measured internal surface temperature of roof glazing south

In the context of the test sun space evaluation the following building element couples have been determined :

- wall north / glazing south
- wall north / glazing east
- floor south / wall north

- *wall north / glazed roof south*
- *floor south / glazed roof south*
- *floor south / glazing east*
- *glazing south / glazing east*
- *floor south / glazing south*
- *glazing south / glazed roof south*
- *glazing east / glazed roof south*
- *wall east / glazing west*
- *wall east / glazing north*
- *floor west / wall east*
- *wall east / glazed roof west*
- *floor west / glazed roof west*
- *floor west / glazing north*
- *glazing west / glazing north*
- *floor west / glazing west*
- *glazing west / glazed roof west*
- *glazing north / glazed roof west*

A PD>5%-value as quality standard is similarly to previous local discomfort evaluations constituted according DIN EN ISO 7730. The analysis also distinguishes between entire day and 5 to 10 PM inspection. Between January and April and November to December the evaluation focus is set on cold walls with a radiant temperature difference of >10 Kelvin and cold ceilings specified by a radiant temperature difference of >14 Kelvin. Accordingly, also the PD>5% values are related to the inspection time period, respectively either entire-day or 5 to 10 PM.

Opposed to that, the following month belonging to the summer period are characterized by DIN EN ISO 7730 with different limiting temperature differences : April, May, June, July, August, September and October.

Hence, considering these months, warm wall temperature differences of >23 Kelvin and warm ceiling temperature differences of >5 Kelvin are relevant. Figure 2.64 tabular visualizes for January cumulative frequencies of hours with cold wall and cold ceiling limit exceedance. It becomes obvious that the gross of exceedance is occupied by cold walls than by cold ceilings.

LOCAL DISCOMFORT - RADIATION ASYMMETRIES							
JANUARY							
696 / 145 Hours							
	COLD WALL > 10K	COLD CEILING > 14K	>10K / >14K 5to10PM	PD >5%	>5% in 696h	PD >5% 5to10PM	>5% in 145h
Δtr Wall-North / Glazing-South	78		15	47	7%	7	5%
Δtr Wall-North / Glazing-East	696		145	696	100%	145	100%
Δtr Floor-South / Wall-North	0		0	0	0%	0	0%
Δtr Wall-North / Glazed-Roof-South		158	36	159	23%	36	25%
Δtr Floor-South / Glazed-Roof-South		378	79	379	54%	79	54%
Δtr Floor-South / Glazing-East	696		145	696	100%	145	100%
Δtr Glazing-South / Glazing-East	696		145	696	100%	145	100%
Δtr Floor-South / Glazing-South	216		44	179	26%	33	23%
Δtr Glazing-South / Glazed-Roof-South		0	0	0	0%	0	0%
Δtr Glazing-East / Glazed-Roof-South		0	0	0	0%	0	0%
Δtr Wall-East / Glazing-West	38		7	19	3%	5	3%
Δtr Wall-East / Glazing-North	696		145	696	100%	145	100%
Δtr Floor-West / Wall-East	0		0	0	0%	0	0%
Δtr Wall-East / Glazed-Roof-West		142	33	142	20%	33	23%
Δtr Floor-West / Glazed-Roof-West		452	108	454	65%	108	74%
Δtr Floor-West / Glazing-North	696		145	696	100%	145	100%
Δtr Glazing-West / Glazing-North	676		145	659	95%	145	100%
Δtr Floor-West / Glazing-West	227		45	201	29%	42	29%
Δtr Glazing-West / Glazed-Roof-West		13	3	13	2%	3	2%
Δtr Glazing-North / Glazed-Roof-West		0	0	0	0%	0	0%

FIGURE 2.64 Month-wise radiant temperature difference analysis and PD evaluation in day and 5 to 10PM focus – January

From an entire-day perspective glazing east, glazing west and glazing north are calculated to bear radiant temperature differences to facing walls and floors of greater than 10 Kelvin for 696 hours of entirely observed 696 hours.

That means, that for one hundred per cent of the observed hours, the temperature difference is considerably high to quote for PD>5%. In consequence, it also means, that internal walls and floor always have higher temperatures than the facing investigated ones. Glazing west and glazing south account for 227 and 216 hours of 696 with considerable radiant asymmetries what is equal to 29 and 26% of observed time. On the contrary the glazed roof south and west as horizontal or declined surfaces showed

in comparison to facing building elements remarkably high radiant asymmetries. Glazing roof west accounts with 452 hours and glazing south with maximum 378 hours of in total 696 in entire-day context with difference exceedance of >14 Kelvin. These frequencies are equal to 65 and 54% related to the amount of surveyed hours. In January in particular the 5 to 10 PM context glazing north and glazing east are represented with very high frequencies of radiant asymmetries. They account for 145 of observed 145 hours.

Nonetheless, glazed roof south and glazed roof west as horizontal areas exceeded limits of acceptable radiant temperature differences for 79 and 108 hours, what 54 and 74%. That means that the test sun space roofs are perceived in January in the evening hours for every second or for 3 of four hours as too cold.

In February (see [Appendix B.8](#)) 624 hours on 26 days have been surveyed. Also in February building elements like glazing east and glazing north are represented clear-cut by impressively high frequencies of hours with temperature differences >10K related to counterpart elements. Compared to solid building elements with comparably high specific mass, like wall north or floor south, for these elements is calculated a frequency of 100% of observed entire-day hours.

However, glazing roof south and glazing roof west considerably show radiant asymmetries 433 and 502 hours entire-day-wise, that in particular represent 65 and 78% of the observed evening time. Thus, we can conclude that north and east glazing completely and south and west roof glazing partly for 2 of 3 or even 3 of four hours characterized with surface temperature levels compared with counterpart building elements that induced considerable radiant asymmetries in February. On the contrary, building elements like wall north or east or floor south or west behaved inconspicuously.

LOCAL DISCOMFORT - RADIATION ASYMMETRIES							
MAY	720 / 150 Hours						
	WARM WALL > 23K	WARM CEILING > 5K	>23K / >5K 5to10PM	PD >5%	>5% in 720h	PD >5% 5to10PM	>5% in 150h
ΔBr Wall-North / Glazing-South	0		0	0	0%	0	0%
ΔBr Wall-North / Glazing-East	0		0	0	0%	0	0%
ΔBr Floor-South / Wall-North	0		0	0	0%	0	0%
ΔBr Wall-North / Glazed-Roof-South		0	0	0	0%	0	0%
ΔBr Floor-South / Glazed-Roof-South		0	0	0	0%	0	0%
ΔBr Floor-South / Glazing-East	292		6	1	0%	0	0%
ΔBr Glazing-South / Glazing-East	0		0	0	0%	0	0%
ΔBr Floor-South / Glazing-South	0		0	0	0%	0	0%
ΔBr Glazing-South / Glazed-Roof-South		0	0	0	0%	0	0%
ΔBr Glazing-East / Glazed-Roof-South		709	0	0	0%	0	0%
ΔBr Wall-East / Glazing-West	0		0	0	0%	0	0%
ΔBr Wall-East / Glazing-North	0		0	0	0%	0	0%
ΔBr Floor-West / Wall-East	0		0	0	0%	0	0%
ΔBr Wall-East / Glazed-Roof-West		0	0	0	0%	0	0%
ΔBr Floor-West / Glazed-Roof-West		0	0	0	0%	0	0%
ΔBr Floor-West / Glazing-North	340		8	14	2%	0	0%
ΔBr Glazing-West / Glazing-North	0		0	0	0%	0	0%
ΔBr Floor-West / Glazing-West	0		0	0	0%	0	0%
ΔBr Glazing-West / Glazed-Roof-West		0	0	0	0%	0	0%
ΔBr Glazing-North / Glazed-Roof-West		720	150	720	100%	150	100%

FIGURE 2.65 Month-wise radiant temperature difference analysis and PD evaluation in day and 5 to 10PM focus – May

Reason for that can be solid state and related higher thermal mass and lower thermal conductance as well. Similar to the previously discussed month, glazing east and glazing north account for 100% of hours in the entire-day and evening time frame with radiant temperature differences > 10K. Interestingly, in March glazing south and glazing west are represented with temperature differences >10 Kelvin for simply about half of the observed and calculated hours (317, resp. 336 hours) of glazing east and west. While glazing south and glazing west provide local discomfort in 41 and 42% respectively of the amount of hours in entire-day context, the frequencies lowers to 28 and 24% of hours in the evening.

Thus we can conclude, that vertical glazings facing the sun diurnally induced radiant asymmetries in March in 2 of five hours a day, but opposed to that solely every fourth hour in the evening. Opposed to that, while glazing roof south and west encounters radiant asymmetries for 417 and 450 hours related to 600 hours (70 and 75%) in total in March, the frequency slightly raised (75 and 79%) in the evening time frame.

Similar to the previous months, in April (Appendix B.8) glazing east and glazing north characterizes by 408 of 408 hours in total with temperature differences in relation to counterpart elements. Compared to March, the relative numbers of the glazed roof south and west slightly lowered. On the contrary in a 5 to 10 PM perspective, beside glazing east and west add up to frequencies of 100% of surveyed hours,

frequencies of hours with PD>5% significantly lowers from 50 to 12% and 52 to 11% regarding glazing south and glazing west. This trend is also visible for the glazed roof south and west during evening time. For this case frequencies minimizes from 64 to 46%, and 74 to 61% respectively. Figure 2.65 demonstrates tabular cumulative frequencies of exceedance of radiant temperature differences analysed for May. In May frequencies of radiant asymmetries first extremely lower and secondly cannot be detected for certain building elements any more for the first time within annual progress. Radiant asymmetries for vertical elements can solely be identified for glazing east and glazing north. Glazing east accounts for 41% of hours and glazing north for 47% of in total 720 hours the month. Further, from the evening hour perspective simply 6 and 8 hours could have been detected with PD>5%, which are equal to 4 and 5% respectively. Interestingly, on the contrary, the glazed roof south and west showed for 709 and 720 hours in total as representatives for horizontal or declined building elements radiant asymmetries to facing elements of greater than 5 K. While both elements show high frequencies in entire-day perspective, exclusively the glazed roof west encounters 150 hours and equally 100% of hours with radiant asymmetries in evening time slot. All other inspected building elements, in particular parts of the glazed envelope were inconspicuous.

LOCAL DISCOMFORT - RADIATION ASYMMETRIES							
AUGUST	518 / 135 Hours						
	WARM WALL > 23K	WARM CEILING > 5K	>23K / >5K 5to10PM	PD >5%	>5% in 648h	PD >5% 5to10PM	>5% in 135h
ΔBr Wall-North / Glazing-South	0		0	0	0%	0	0%
ΔBr Wall-North / Glazing-East	1		1	0	0%	0	0%
ΔBr Floor-South / Wall-North	0		0	0	0%	0	0%
ΔBr Wall-North / Glazed-Roof-South		0	0	0	0%	0	0%
ΔBr Floor-South / Glazed-Roof-South		0	0	0	0%	0	0%
ΔBr Floor-South / Glazing-East	328		32	6	1%	0	0%
ΔBr Glazing-South / Glazing-East	0		0	0	0%	0	0%
ΔBr Floor-South / Glazing-South	0		0	0	0%	0	0%
ΔBr Glazing-South / Glazed-Roof-South		0	0	0	0%	0	0%
ΔBr Glazing-East / Glazed-Roof-South		643	135	648	100%	135	100%
ΔBr Wall-East / Glazing-West	0		0	0	0%	0	0%
ΔBr Wall-East / Glazing-North	0		0	0	0%	0	0%
ΔBr Floor-West / Wall-East	0		0	0	0%	0	0%
ΔBr Wall-East / Glazed-Roof-West		0	0	0	0%	0	0%
ΔBr Floor-West / Glazed-Roof-West		0	0	0	0%	0	0%
ΔBr Floor-West / Glazing-North	353		24	5	1%	0	0%
ΔBr Glazing-West / Glazing-North	0		0	0	0%	0	0%
ΔBr Floor-West / Glazing-West	0		0	0	0%	0	0%
ΔBr Glazing-West / Glazed-Roof-West		0	0	0	0%	0	0%
ΔBr Glazing-North / Glazed-Roof-West		648	135	648	100%	135	100%

FIGURE 2.66 Month-wise radiant temperature difference analysis and PD evaluation in day and 5 to 10PM focus – August

Thus, in order to summarize, May is the first month with extreme low and isolated elements with radiant asymmetry and without nearly any in the evening hours. Analogously for June, glazing east and north are the only vertical building elements, for what any worth mentioning frequency of hours with radiant asymmetries was calculated. While the frequencies sum up in the entire-day context for 42 and 48%, they account from 5 to 10 PM for 6, respectively 4% only. Hence, the level of frequencies of radiant asymmetries of glazing east and north do not differ from the level in May. Nevertheless, unlike to previous months, glazed roof south and west do not improve from an entire-day perspective with 99 and 100% to 5 to 10 PM perspective. Related to 432 hours recorded in total, in July ([APPENDIX B.8](#)) glazing east mount up for 44% and glazing north for 51% during the day. Related to the evening time frame, frequencies lower to 19% and 13% respectively. Thus we can see, compared to June, that the number of hours with warm walls and differences higher than 23 Kelvin slightly increases.

Similar to June, the glazed roof south and west account for approximately one hundred per cent of the observed hours in entire-day and evening context with radiant temperature differences  $>5K$  and  $PD>5\%$  respectively.

For August local thermal discomfort in terms of radiant asymmetries have been displayed in Figure 2.66. Within 648 hours that were surveyed, glazing east and glazing north exceeded the difference limit of 23K for 328 and 353 hours.

Exceedance was calculated relatively for 51% and 54% in respect. During evening hours, the relative frequencies lowered to 24% and 18%. In consequence, compared to July, the relative frequencies slightly increased, but however compared to June demonstrably increased. In case of eye-catching horizontal or inclined building elements, exclusively the glazed roofs relatively account for 100% of hours with temperature differences  $>5K$  (too warm) both in entire-day and evening time frame. Thus, relating to simply 5 percent of dissatisfied occupants, 100% of surveyed hours in August were effected.

Considering September (also see Appendix B.8), glazing east and north cumulate frequencies of 305 and 333 hours respectively, what equals 44 and 48% of hours in total. That frequencies demonstrably lowers, when focus is set on evening hours. For the 5 to 10 PM time frame glazing east and north simply provide temperature differences  $>23K$  for 12 and 14% of hours respectively.

LOCAL DISCOMFORT - RADIATION ASYMMETRIES							
100%	504 / 105 Hours						
OCTOBER	WARM WALL > 23K	WARM CEILING > 5K	>23K / >5K 5to10PM	PD >5%	>5% in 504h	PD >5% 5to10PM	>5% in 105h
ΔR Wall-North / Glazing-South	0		0	0	0%	0	0%
ΔR Wall-North / Glazing-East	0		0	0	0%	0	0%
ΔR Floor-South / Wall-North	0		0	0	0%	0	0%
ΔR Wall-North / Glazed-Roof-South		0	0	0	0%	0	0%
ΔR Floor-South / Glazed-Roof-South		0	0	0	0%	0	0%
ΔR Floor-South / Glazing-East	132		16	0	0%	0	0%
ΔR Glazing-South / Glazing-East	0		0	0	0%	0	0%
ΔR Floor-South / Glazing-South	0		0	0	0%	0	0%
ΔR Glazing-South / Glazed-Roof-South		0	0	0	0%	0	0%
ΔR Glazing-East / Glazed-Roof-South		504	105	504	100%	105	100%
ΔR Wall-East / Glazing-West	0		0	0	0%	0	0%
ΔR Wall-East / Glazing-North	0		0	0	0%	0	0%
ΔR Floor-West / Wall-East	0		0	0	0%	0	0%
ΔR Wall-East / Glazed-Roof-West		0	0	0	0%	0	0%
ΔR Floor-West / Glazed-Roof-West		0	0	0	0%	0	0%
ΔR Floor-West / Glazing-North	135		14	0	0%	0	0%
ΔR Glazing-West / Glazing-North	0		0	0	0%	0	0%
ΔR Floor-West / Glazing-West	0		0	0	0%	0	0%
ΔR Glazing-West / Glazed-Roof-West		0	0	0	0%	0	0%
ΔR Glazing-North / Glazed-Roof-West		504	105	504	100%	105	100%

FIGURE 2.67 Month-wise radiant temperature difference analysis and PD evaluation in day and 5 to 10PM focus –October

Thus we can conclude, that compared to August the relative frequencies for September lowered. Likewise the summer month discussed before, the glazed roof south and west show numbers of hours with limit exceedance for an acceptance of more than 95% of occupants of 100%. This is valid for both the entire-day and 5 to 10 PM time frame.

Figure 2.67 illustrates cumulative frequencies of radiant asymmetries calculated for October. In October 504 hours in total were surveyed. Radiant asymmetries were identified simply for a glazing east / floor south configuration and for a glazing north / floor west configuration. They mount up to 132 and 135 hours respectively. They equal in entire-day perspective 26% of hours. Accordingly, for the evening time slot, single hours for a wall warmer than a counterpart element for >23 Kelvin. That figures relate to 105 hours of the evening time frame in 15 and 13%. While there emerges no difference in the evening frequencies compared to September, the difference in entire-day context between 44%, respectively 48% and 26% for October is significant. Similar to the previous month, the roof glazing in south and west direction encounters radiant temperature differences > 5 for 100% of all hours, both for entire-day and 5 to 10 PM perspective.

Inspecting November, completely different to the previously discussed six months is the increased amount of building element couples, for which radiant asymmetries could have been detected. Beside glazing east / floor south and glazing north / floor west, also combinations with wall north or glazing south and wall east and glazing west

account for frequencies of about 100% relative hours. That observation is valid for both entire-day and 5 to 10 PM perspective. In November additionally couples as glazing south / floor south and glazing west / floor west show considerable high frequencies of hours, when temperature differences are higher than 10K.

Thus, thermal local discomfort in terms of radiation asymmetries additionally occur for 25 to 28 % in relation with façade parts which profit from daily sun shine by direction. In terms of a 5 to 10 PM evaluation the relative frequencies of the before mentioned configurations slightly lower to 21 and 23%. Glazed roofs south and west encounter radiant asymmetries for relatively 77 and 89% in entire-day context and 90 and 97% respectively in evening context.

Similar to November can be calculated for December (Appendix B.8) for glazing east and glazing west cumulative frequencies of radiant temperature differences > 10K that account for 100% relatively for the total of hours in a day and a 5 to 10 PM context. Likewise in November glazing south / floor south and glazing west / floor west suffer from considerable hours of insufficient radiant symmetry what equals 37 and 43% in an entire-day context and 27 and 43% in evening time slot. Compared to November, we can conclude that local discomfort in terms of radiant asymmetry raised.

## Summary

---

The evaluation of radiant asymmetries reveals, that east and north facades during the entire year suffer from significant radiation temperature differences compared to facing building elements. This is reasoned by permanent lack of affecting solar irradiation. This observation reinforces the insight that homogeneous irradiation is overaged essential for sun space detailed thermal comfort evaluation. Similar influence to north and east facades and glazed roofs with south and west orientation very often results in considerable radiation temperature differences compared to facing surfaces. Opposed to north and east glazing, roof glazing encounters not that permanent but often during preferred occupational time demonstrable asymmetries.

In particular in the winter months (January and February) the radiation asymmetries between roof glazing and north/east façade glazing are extreme, since roof glazing partly profits from few solar gains, while east and north do not benefit from any.

Opposed to the glazed facades regardless of orientation, massive building elements as floors and walls generally provide higher temperatures, and thus are reasons for significant differences.

Since the floor was partly actively heated (water driven floor heating) and since south and west facing walls benefit from solar gains, losses solely occur towards the space and not like glazings towards environment in principle. Moreover, those described building elements, despite adsorption abilities of glazing, profit from higher thermal mass and determine space specific inertia.

The evaluation especially in summer shows significant high radiation asymmetries between south roof glazing and east facade glazing as well as between west roof glazing and east facade glazing. This relation changes in winter to demonstrable differences between roof glazing and south and west floor respectively.

### § 2.8.1.3 Summary of local discomfort

---

We can summarize, that frequency of especially striation between 1,10 to 1,70 m above the floor, in focused torso-to-head height, is significant high for 8 of 12 month a year. Considerable cumulative frequency already starts with March and endures up to October. In midsummer month every fourth or even every third hour, either in full day perspective or during preferred occupational time, encounters either temperature differences  $>3K$  or  $PD>5\%$ .

Cold floors are a significant problem during the winter months from October to April. In midwinter the frequency can end up into 100% of observed hours. Solely in summer months like May, June, July and August, the frequency of hours with cold floor lowers and thus improves, but diametrically changes into high frequencies with warm floors. Hence, cold and warm floors are a thermal issue during the entire year, what solely resigns in few intermediate months.

Frequencies of radiation asymmetries are tremendously high in midwinter between roof glazings and vertical glazings that are oriented north or east and suffer from any solar gains or in midsummer. Nonetheless, also demonstrably high temperature differences with high frequencies are evident between roof glazing and massive elements like floors and walls in winter months. During midsummer especially radiation asymmetries occur between roof glazings and north or east facing glazing as a matter of irradiation intensity.

## § 2.9 Predicted Mean Vote in long term perspective according EN ISO 15251

Regarding a comprehensive long term evaluation of thermal comfort quality of specific zones, buildings or space archetypes, EN ISO 15251 proposes several homologous methods. Appendix F provides three different methods (A – C), which help valuating the quality of measured or calculated indoor thermal comfort in terms of PMV or operative temperature limit exceedance.

In this line, method A, which concentrates on operative temperature limits exceedance qualifies for winter month evaluations. Opposed to method A, procedure B focusses on degree hours as expression of frequency and intensity of overheating. Both methods are eligible for holistic yearly-based comfort evaluation of naturally ventilated spaces, which offer occupants considerable areas of envelope openings for individual control and adaptation.

Since sun spaces typically exclude mechanical ventilation and conditioning and typically do not belong to working spaces, frequencies of hours with limits exceedance allow greater tolerance than in working spaces.

Whereas Appendix H of DIN EN ISO 15251 limits frequencies of limit exceedance to 3 to 5% for working spaces, naturally ventilated sun spaces allow higher frequencies of exceedance. The fact, that sun space occupants qualify sun space thermal comfort detached from appropriate working productivity conditions, but rather qualify in respect to leisure qualities and are willing to adapt at short notice, widens tolerable limits exceedance to 10 to 15%.

### § 2.9.1 Explanation of method DIN EN ISO 15251, Appendix F or G

DIN EN ISO 15251 exemplifies in Appendix F method A, which evaluates thermal comfort in a comprehensive long term perspective by the calculation of cumulative frequencies of hours with exceedance of lower and upper operative temperature.

As limits of operative temperature are defined  $<18^{\circ}\text{C}$ ,  $<20^{\circ}\text{C}$  and  $>26^{\circ}\text{C}$  in the context of sun spaces and category II. The evaluation distinguishes between entire day inspection and the preferred occupation time investigation.

Method B focusses on hours with exceedance of the daily upper limit of operational temperature calculated with the adaptive comfort algorithm based on the daily mean external temperature. Moreover, the intensity of exceedance is weighted.

This is achieved by calculation of the actual difference of the observed operational temperature towards the daily calculated adaptive comfort upper limit  $T_{op,up,l}$  of, for example 27,3°C (32,7°C-27,3°C =>  $\Delta T_{up,l} = 5,4K$ ). The multiplication of frequency and difference generates degree hours of exceedance. The sum of degree hours within a month interval gives insight in adaptive thermal comfort mismatch.

## § 2.9.2 Winter month evaluation according DIN EN ISO 15251, App. F : method A

Figure 2.68 shows a 100%, respectively 96%, frequency of hours with operative temperature lower than 18°C for January and December respectively in a 24h day perspective for the south flank. That means, that operative temperature is for almost all the time in question below 18°C between December and January. Especially in December the frequency of hours raises to 97 in the preferred occupational time between 5 to 10 PM.

The results of the west flank equals the results of the south flank. In February 117 hours of in total 130 hours represent operative temperature below 20°C during 5 to 10 PM in the south flank.

CUMULATIVE FREQUENCIES OF HOURS WITH EXCEEDING OF LOWER OR UPPER LIMITS - WINTER PERIOD																			
DIN EN 15251, Appendix F :																			
Long term evaluation of thermal comfort conditions, Method A																			
MONTH / DAY PERIOD	ANALYZE D DAYS	ANALYZED HOURS	SOUTH									WEST							
			24 h			5 to 10 PM			24 h			5 to 10 PM							
			$T_{res} < 18^{\circ}C$	$T_{res} < 20^{\circ}C$	$T_{res} > 26^{\circ}C$	$T_{res} < 18^{\circ}C$	$T_{res} < 20^{\circ}C$	$T_{res} > 26^{\circ}C$	$T_{res} < 18^{\circ}C$	$T_{res} < 20^{\circ}C$	$T_{res} > 26^{\circ}C$	$T_{res} < 18^{\circ}C$	$T_{res} < 20^{\circ}C$	$T_{res} > 26^{\circ}C$	$T_{res} < 18^{\circ}C$	$T_{res} < 20^{\circ}C$	$T_{res} > 26^{\circ}C$		
January	29 von 31	696	145	696	100%	696	0	146	145	100%	0	696	100%	696	0	146	145	100%	0
February	26 von 28	624	130	581	93%	601	3	107	117	90%	2	595	95%	611	2	109	122	94%	2
March	25 von 31	775	125	428	55%	465	45	61	75	60%	19	440	57%	481	40	61	75	60%	19
April	17 von 30	408	85	173	42%	229	61	7	16	19%	27	187	46%	242	46	8	17	20%	25
November	25 von 30	600	125	537	90%	557	1	106	119	95%	0	546	91%	567	0	107	120	98%	0
December	30 von 31	720	150	693	96%	696	0	146	146	97%	0	695	97%	696	0	146	146	97%	0

FIGURE 2.68 Cumulative frequencies of hours with exceeding lower and upper limits – winter

This equals 90%, whereas 2 hours are identified to with temperature above 26°C. In the west flank even 94% of all observed hours between 5 to 10 PM encounter less than 20°C indoor temperature.

Further, also in March more than the half of observed hours, precisely 60% of hours between 5 to 10 PM, showed operative temperature less than 20°C in both the south and west flank. Opposed to that benefits the south flank of 465 instead of 481 hours as the west flank of temperature below 20°C in entire day perspective.

On the contrary, hours with operational temperature below 20°C between 5 to 10 PM occur with a frequency of solely 19 and 20% respectively. Thus, 80% of all observed hours in April provided sufficient thermal comfort temperature in the sun space. Nonetheless, the hours with operational temperature above 26°C accounted with frequencies of 25 to 27 between 5 to 10 PM and 61 to 46 hours for the entire day. In November, the frequency of hours with temperature below 20°C assesses for more than 95% in south and west flank in the preferred evening hours, while the frequencies in entire day perspective slightly improve to 95 to 93%. Operational temperature <18°C accounts for 85 to 90% of observed time, either entire day or 5 to 10 PM inspection period.

## Summary

---

The midwinter months November, December, January and February encounter significant frequencies of hours which represent operational temperature either below 20°C or even below 18°C. Thus we can conclude, that despite marginal additional distribution of heating energy by façade integrated solar thermal collectors, passive solar gains and floor heating do in terms of 85 to 90% of observed hours not manage to provide considerable frequencies of hours with sufficient operational indoor temperature. Consequently, the evaluation of indoor thermal comfort is between November until end of February demonstrably unsatisfactory.

Thermal comfort slightly improves in March towards 40% of hours representing thermal comfort. Solely in April, up to 80% of observed hours provide satisfactory thermal comfort. Although evaluation of south and west flank equals, the south flank results overrun for slightly 1%.

Further it is to emphasize, that in particular the south flank suffers from significant frequencies of hours with operational temperature higher than 26°C April. Hence, beside 19% of hours with dissatisfying resulting temperature, overheating for more 27 and 61 hours respectively becomes significant.

### § 2.9.3 Summer month evaluation according DIN EN ISO 15251, App. F : method B

Figure 2.69 illustrates, that for May 35% and 30% respectively of hours between 5 to 10 PM represent operational temperature, that exceed the calculated upper limit. Absolutely, thermal comfort mismatch accounts in the south and west flank for 249 and 216 degree hours. An entire day inspection reveal 1.031 and 1.042 degree hours exclusively in May.

In June the number of degree hours nearly triples in the south flank, whereas it lowers to 179 in the west flank. On entire day basis, degree hours raises to 1.736 for the south and to 1.694 hours for the west flank. In July, the number of degree hours lowers to 466 during evening hours in the south flank and to 219 in the west flank, what equals the number calculated for May. Similarly, degree hours in entire day perspective approximates that level of May with 1.039 in the south flank and 934 for the west respectively. Opposed to that, in August can be recognized the maximum number of degree hours both for the 5 to 10 PM interval and for the entire day interval. Seven hundred sixty five hours in the evening for south and mostly one third 267 hours for the west flank account for August. Notwithstanding, in entire day context the cumulative numbers raise to maximum with 1.622 and 1.481 hours respectively.

<b>DEGREE HOUR EVALUATION - SUMMER PERIOD</b>									
<b>DIN EN 15251, Appendix F :</b>									
<b>Long term evaluation of thermal comfort conditions, Method B</b>									
<b>SUMMER MONTH / PERIOD OF DAY</b>	<b>DEGREE HOURS</b>								
	<b>SOUTH</b>				<b>WEST</b>				
	<b>24 H</b>		<b>5 to 10PM</b>		<b>24 H</b>		<b>5 to 10PM</b>		
<b>May (720 h)</b>	1031	1,43	249	0,35	1042	1,45	216	0,30	
<b>June (552 h)</b>	1736	3,14	736	1,33	1694	3,07	179	0,32	
<b>July (432 h)</b>	1039	2,41	466	1,08	934	2,16	219	0,51	
<b>August (648 h)</b>	1622	2,50	765	1,18	1481	2,29	267	0,41	
<b>September (696 h)</b>	957	1,38	55	0,08	1059	1,52	195	0,28	
<b>October (504 h)</b>	1787	3,55	232	0,46	1872	3,71	480	0,95	

FIGURE 2.69 Weighted degree hours of as deviation from lower and upper limit generated with the daily mean of external temperature

A demonstrably decrease in degree hours for the preferred evening occupation time is observed in September in the south flank. Rarely 55 degree hours cause no worth mentioning mismatch of thermal comfort in the south flank, whereas still 195 degree hours in the west flank quadruplicate the account of the south equivalent. From entire day perspective the amount of degree hours are with 957 and 1.059 significantly high and especially for the west flank outnumber the comparative result for May.

Summarizing, in particular for the south flank the number of degree hours during evening hours is the lowest ever calculated for all summer month, but from entire day perspectives it outruns the level of May.

Contradictive, in October the number of degree hours raises to 232 and 480 in the west flank respectively from 5 to 10 PM in particular. Moreover, 1.787 and 1.872 hours account in an entire day inspection context. That means, that the west flank encounters the highest number of degree hours within summer month especially in the October evening time. The number is 2,7 times higher than compared to the equivalent of June and double the calculated number of degree hours for the entire day of July. With respect to the south flank, the second lowest number of degree hours within the summer period is calculated for the evening hours with 232 hours.

### § 2.9.3.1 Cumulative frequencies of hours with exceeding of category III

---

Additionally to degree hour calculations, this section calculates analogous to winter months the frequencies of hours with daily upper limit exceedance for the summer period. This calculation accessorially helps to identify significant months, when thermal comfort beside adaptive control facilities even outruns PMV levels of + 0,7 and more than 20% of occupants disclaim unsatisfactory thermal comfort. This limits equals adaptive comfort category III of DIN EN ISO 7730 A.1, Tab. A.1.

Figure 2.70 expressively demonstrates, that in the south and west flank based on an entire day perspective from May to September mostly 50 to 57% of hours exceed comfort category III.

Opposed to that, for more than 74% of all observed hours in October the operational temperature in sun space flank south result in more than 20% of predicted dissatisfied occupant and thus exceedance of comfort category III. In case of the west flank, even 77% of observed hours represent operational temperature exceeding the daily calculated upper limit. In terms of the preferred evening occupational time interval between 5 to 10 PM the table in Figure 79 illustrates the highest cumulative frequency

of exceedance for August with both 90% of hours in south and west flank. In July, as midsummer month similar to August, three of four observed hours between 5 to 10 PM represent limit exceedance (73%). Both months are followed by June and October, when approximately 54 to 60%, every second or three of five hours encounter unsatisfactory thermal comfort.

<b>CATEGORY III EXCEEDED, accord. EN ISO 7730 A.1, Tab.A.1,</b>								
<b>SUMMER MONTH / PERIOD OF DAY</b>	<b>Cumulative Frequencies of hours with Exceeding of category III (PMV : +- 0,7; PPD : 20%)</b>							
	<b>SOUTH</b>		<b>SOUTH 5 to 10PM</b>		<b>WEST</b>		<b>West 5 to 10PM</b>	
	absolute [h]	[%]	absolute [h]	[%]	absolute [h]	[%]	absolute [h]	[%]
<b>May (720 h)</b>	370	51%	74	49%	363	50%	68	45%
<b>June (552 h)</b>	306	55%	69	60%	303	55%	69	60%
<b>July (432 h)</b>	231	53%	66	73%	224	52%	66	73%
<b>August (648 h)</b>	371	57%	121	90%	362	56%	121	90%
<b>September (696 h)</b>	372	53%	31	21%	388	56%	37	26%
<b>October (504 h)</b>	375	74%	57	54%	389	77%	59	56%

FIGURE 2.70 Cumulative frequencies of hours with exceeding of category III

On the contrary, especially September and May show cumulative frequencies of observed hours with 21 and 26% respectively, and 49 and 45% of hours with limit exceedance. Thus we can summarize, that all summer month show at least 50% and in particular October more than 74% cumulative frequencies with exceedance of category III on entire day basis. The west flank does not differ significantly from the south flank.

On the other hand, are frequencies of hours with limit exceedance comparably low in the evening hours in September, which account for solely one of five or one of four hours. Opposed to that, the frequencies of hours with category III exceeded considerably outnumber the level of midsummer months from entire day perspective during evenings in July and August. In this case between 70 to 90% of hours provide no tolerable thermal comfort between 5 to 10 PM.

## Summary

---

While most degree hours between 5 to 10 PM could have been calculated for the south flank in June and August, the most degree hours in the west flank for evening hours could have been detected in October. Whereas the south flank suffers from 736 to 756 degree hours in midsummer, the west flank encounters with 480 maximum demonstrably less in October. Both the south and west flank encounter fewest degree hours during evening in September. Similar to the evening period account degree hours on entire day perspective most intensive in June, August and with maximum in October. All months encounter more than 1.480 degree hours, which maximum relocate during midsummer to autumn from south to the west flank.

Parallel, category III is homogeneously exceeded for at least 50% of all entire day hours from May to September, even for more than 73% in October. From 5 to 10 PM perspective, the results differ significantly.

Fewest category III exceedance and thus most frequent satisfying thermal comfort is calculated for September evenings, whereas October evenings encounter 30% more hours with unsatisfying thermal comfort from overheating. Finally, July and August suffer considerably from overheating, when 70 to 90% of hours do not meet any comfort category.

---

## § 2.10 Analysis of effective utilized end energy to auxiliary energy ratio

---

The test set up included façade integrated solar thermal collectors (see Chapter 01 and CH02-1.1.6) in order to collect additional renewable heating energy. The collected heating energy especially for winter months was reviewed in terms of effect on substitution potential. Moreover, this thesis inspects the potential of collected, stored and utilized energy in terms of sun space autarky and potential of surplus energy contribution for an adjacent residential family home. Nonetheless, the amount of net energy, that was required to run the collector and storage system, is to be considered and related to the amount of gained renewable energy.

Moreover, the ratio of required auxiliary energy and gained renewable energy is an expression of system efficiency. This section calculates gained and required auxiliary energy and determines the system efficiency of the tested experimental sun space.

## § 2.10.1 Renewable Energy generated by sun space facades

Figure 2.71 plots the cumulated progress of generated solar thermal energy for 18 months with weekly interval. The histogram additionally plots the summed yield for every month. With subject to system fall outs or maintenance April 2015 generates with considerable distance to the rest the highest monthly yield of 281 kWh. April is followed by May 2015 with 147 kWh and June 2014 with less than the half, respectively 125 kWh. Autumn months like September and October encounter demonstrable periods of system fall out and asses 77 and 33 kWh, and 42 and 28 kWh respectively. From midsummer 2014 to 2015 and from spring 2015 to 2016 is generated 1.091 and 869 kWh respectively. Dynamic thermal simulation calculated a heating energy demand of approximately 1.600 kWh in order to provide sufficient energy for satisfactory operative temperature of  $>20^{\circ}\text{C}$  between 5 to 10 PM from October to April.

Thus, the overall opinion of the author beside the documented monthly yields is, that the system dConsidering September (also see Appendix B.8), glazing east and north cumulate frequencies of 305 and 333 hours respectively, what equals 44 and 48% of hours in total. That frequencies demonstrably lowers, when focus is set on evening hours. For the 5 to 10 PM time frame glazing east and north simply provide temperature differences  $>2\text{K}$  for 12 and 14% of hours respectively. esign for energy generation is designed sufficiently.

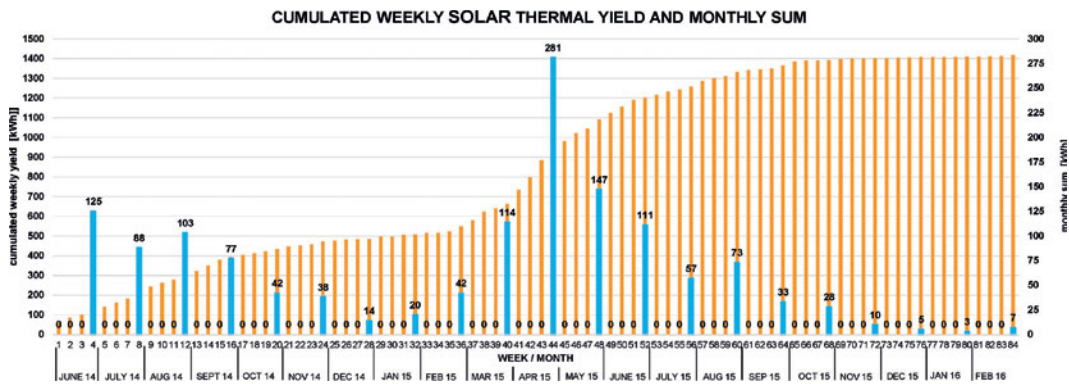


FIGURE 2.71 Cumulated weekly solar thermal yield and monthly sum

Figure 2.72 plots weekly generated cumulated solar thermal energy and monthly sums. Additionally the histogram illustrates the cumulated progress of weekly consumption of the renewable energy. It becomes obvious, that right from the start in June 2014 demonstrably more energy was generated than consumed. That is strongly related to the fact, that energy generated in summer month is not consumed since demand is zero. Opposed to that, shows the parallel progress of energy generation and consumption from November 2014 to end of February 2015 that the few generated renewable energy was consumed immediately. Opposed to the measured energy yield illustrated in Figure 80 the impression of the author during experimental test set up period was, that without too many fall out periods the system normally generates enough energy ( $< 1.600 \text{ kWh/a}$ ) during the year in order to provide 1.060 hours of satisfying thermal comfort.

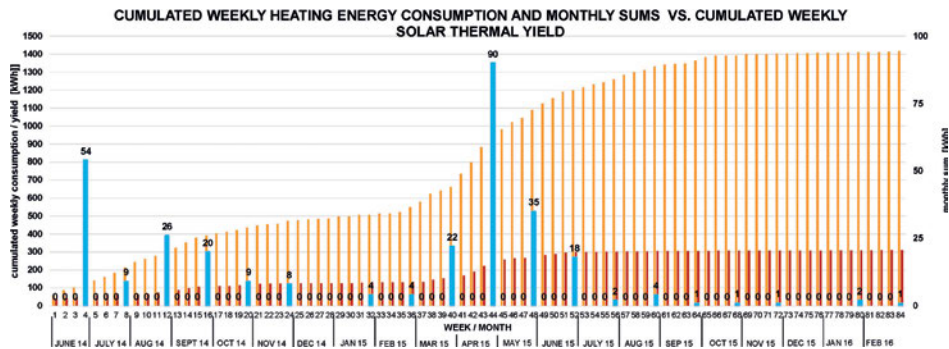


FIGURE 2.72 Cumulated weekly heating energy consumption and monthly sums vs. cumulated weekly solar thermal yield

High system efficiency of course implies the implementation of a loss free seasonal thermal storage. Thus, the overall opinion of the author beside the documented monthly yields is, that the system design for energy generation is designed sufficiently.

Figure 81 plots weekly generated cumulated solar thermal energy and monthly sums. Additionally the histogram illustrates the cumulated progress of weekly consumption of the renewable energy. It becomes obvious, that right from the start in June 2014 demonstrably more energy was generated than consumed. That is strongly related to the fact, that energy generated in summer month is not consumed since demand is zero. Opposed to that, shows the parallel progress of energy generation and consumption from November 2014 to end of February 2015 that the few generated renewable energy was consumed immediately.

## § 2.10.2 Net power consumption as auxiliary energy

Similarly, the parallel but off-set progress of generation and consumption between March and May 2015 demonstrates, that consumption is linked to generation, but more interestingly, either much of the energy generated got lost by transmission losses of the 300L buffer tank and the system itself or was provided simply by passive solar gains. Likewise the figure before, in April was measured the highest consumption. However, in the last month of the winter period and transitional spring month are simply 90 kWh consumed towards 281 kWh generated. That equals nearly one third. Similarity is verified for September 2014, where 77 kWh are generated but solely 20 kWh consumed and for February with 42 and 4 kWh respectively. Auxiliary required power for distribution components within the system can be identified as follows:

- solar thermal circuit pumps ( 2x primary, 2x secondary ) : each 3 Watts,
- solar thermal circuit electromagnetic valves (south, west) : each 5 Watts,
- floor heating pump (1x) : 3 Watts,
- floor heating circuit servos (1x south, 1x west) : each 2 Watts

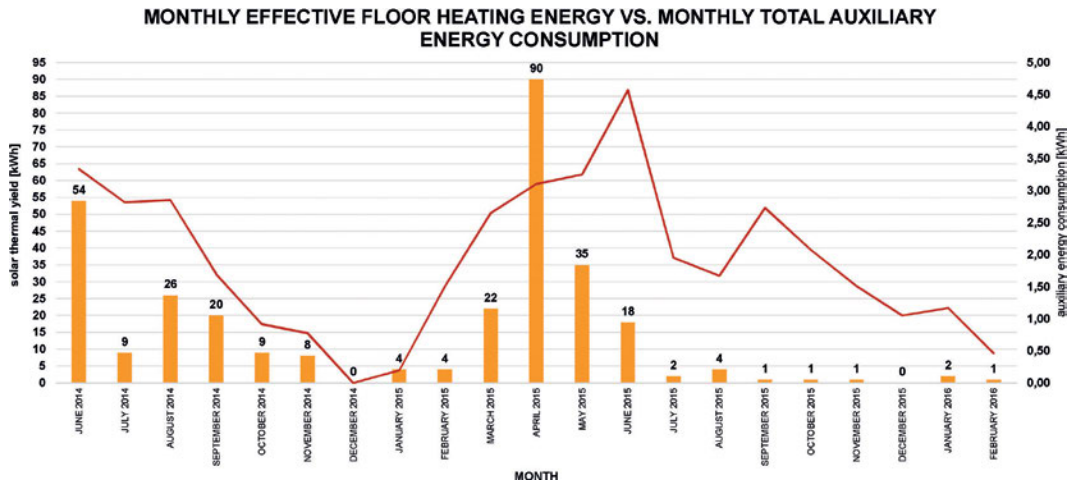


FIGURE 2.73 Monthly effective floor heating energy vs. monthly total auxiliary energy consumption

Valves and servos are normally closed power-off, hence they consume energy exclusively when pumps are in action. In Figure 2.73 required auxiliary energy is plotted against the consumed heating energy.

The graph clear-cut demonstrates, that required auxiliary energy for solar thermal circuit pumps, electromagnetic valves, floor heating pump and the floor heating circuit servos do not fall into worth mentioning account. Thus, the generated solar thermal energy can be considered to be the effective energy gain for further space heating.

### § 2.10.3 Ratio–autarky ratio

---

It was not possible to verify an autarkic operation defined by 1.060 hours of sufficient thermal comfort exclusively by passive solar gains and additional renewable energy during 5 to 10 PM from October to April by the experimental test set combined solely with a sensible heat storage. That was reasoned by too many system fall out during two years of observation. Autarkic operation was furthermore hardly feasible since a sensible water storage provided energy for rarely more than four days.

### § 2.10.4 Summary

---

Yet, an exploratory calculation of monthly yields revealed an feasible approximately annual yield of 1.600 kWh by this installed experimental collector system at location Bissendorf.

Nonetheless, opposed to the observed days, the author is convinced, that the system without any fall out and in combination with a seasonal loss free storage is capable to realize satisfactory thermal comfort for 1.065 hours.

However, the system is limited in capacity in terms of renewable energy generation. The specific test set up configuration is expected not to be feasible for any surplus heating energy contribution for residential heating energy substitution.

## § 2.11 Summary

Theoretical literature research and empirical evaluation of thermal comfort in sun spaces results in manifold findings at the end of this chapter.

Literature review figured out, that improvements of steady-state analysis models to dynamic hourly weather data based models do justice to thermally rapidly reacting sun spaces. Moreover, simulation tools developed in respect to absorption and reflection terms and in regard of modelling vertical striation. Review revealed an overestimation of overheating and cooling loads and diametrically an underestimation of heating demand.

Moreover, the focus of effective sun space planning moved to thermal mass and absorption ability of the separation element as well as thermal mass of floor and massive walls. Thermal mass to façade ratios additionally established as designing tools for sun spaces. Essentially, the question raised to clear-cut define actual utilization behaviour and daily occupation time. Both significantly influence and rule required and recommended thermal mass quality in order to regulate overheating and controlled heat return.

Further, required opening areas are discussed in order to enhance cooling by natural ventilation. Diverse authors limit effective opening to maximum 30% of the entire sun space envelope.

Sun spaces in general have been detected and promoted to be eligible to reduce daily temperature amplitudes, temperature swings and heating energy for adjacent zones and residential buildings respectively. Nonetheless, several authors pointed out, that the effect is significant for the actual adjoining zone, but however, much less for an entire building. Thus, energy saving potential considerably depends on the size of the adjacent zone and its area-wise fraction on the entire net-area.

Sun spaces absolutely save more heating energy for poor insulated estates, whereas they relatively demonstrably improve energy performance of modern residential homes with supreme energetic quality standard.

PMV and PPD models cannot be applied to sun spaces, since assessments of empirical data causes unreliable and unreasonable results. Further evaluation based on adaptive comfort algorithms and calculation of cumulative frequencies of dry bulb and operational temperature, striation and radiation asymmetries as well as progress of radiant temperature as indication of inertia.

Inspection of resulting temperature recovered, that the lower set point limit of 20°C was accomplished solely during midsummer months. Thus, solely by passive solar gains, comfort limit majorly was achieved during June, July and August. However, during November, December, January and partly February the lower set point limits was hardly attained. Nonetheless, September and May and fractions in April showed very well balanced proportions of complied set point limits and overheating, either in respect to cumulative frequencies of resulting temperature or in terms of adaptive comfort bandwidths. April was observed to either lack considerable fractions of satisfying operational temperature, but rather to encounter demonstrably high fractions of hours with overheating. As a conclusion for April, the number of outliers raised while overheating raised.

This first findings allow to draw the conclusion, that prediction of sun space thermal comfort for the experimental test set up was extremely difficult.

The empirical inspection revealed, that diurnal natural ventilation with area-intensive fold-works in midsummer and on sunny spring days was not effective in terms of space cooling. Dry bulb temperature always remained above external temperature with an off-set of 6 to 10 Kelvin. Solely night cooling lowered dry bulb temperature of the internally shaded experimental sun space for 8 to 21 Kelvin.

The empirical evaluation revealed, that cumulative frequencies of hours with satisfying operational temperature during the preferred occupation time between 5 to 10 PM mostly exceed those representing an entire day perspective. That is true for the period March to October, however, except August. Thus, the evening hours established by evaluation to be the most enjoyable once. Interestingly, in the context of adaptive comfort bandwidths evaluations, mostly the south flank of the sun space performed better than the west flank, except during September and October.

Comfort charts, which plot operational temperature against relative humidity, showed, that the major fraction of hours between March and October located in the comfortable or still-comfortable field. On the contrary, the charts diametrically elaborated, that relative humidity very often exceeded 80% during November, December and January. Beside unsatisfactory operational temperature, these months encountered a clammy space environment.

The evaluation of mean radiant temperature in relation to external temperature lead to interestingly insight in respect of sun space specific inertia. During winter months like January, February and March thermal mass tended to slightly but persistently charge. That resulted partly in daily compensation of irradiation fluctuations and in a steady raise of dry bulb temperature. This analysis recovered, that in particular in April inertia

was sufficient to compensate on weekly level. However, during May and November, the thermal mass tended to discharge but managed to provide better balanced thermal comfort. Nonetheless, November was observed as month of significant discharge of thermal mass without any positive influence on resulting temperature. We investigated August when limit of positive effect of thermal mass capacity was reached.

Floor temperature was inspected to be most of the year too cold, exceptionally in June, July and August, when local discomfort resulted oppositional from too warm floors. On the contrary, north and east glazings, which predominantly lack from direct irradiation, reasoned radiation asymmetries with facing surfaces, except during midsummer months. North and west roof glazings as well as vertical glazings either provided too cold or too warm surface temperature. This fact resulted in massive and persistent radiation asymmetries during winter months (November to April) or in particular during midsummer (June to August). Vertical striation in the torso-to-head height between 1,10 m to 1,70 m above floor was detected to be a major and dominant local discomfort phenomenon typical for the experimental test sun space during the entire year.

Finally, a long term evaluation of operational temperature of the test sun space substantiated a principle lack of thermal comfort provided both by solar gains and additional sporadic floor heating during from November until March.

Analogously, in terms of overheating the most degree hours were detected in June and August for the south flank, what changed towards the west flank in October. Nonetheless, the fewest degree hours were observed for both sun space flanks in September and October.



# 3 Literature survey of façade integrated renewable energy collector technology

## § 3.1 Integral façades – from added component to multi-functional layer

The previous Chapter 2 gave definitions of thermal comfort in sun spaces both by literature review and by empirical evaluation. As a result building physical constraints were identified that characterizes thermal comfort in sun spaces. By means of this generated knowledge contribution, the main research question implies an improvement of thermal comfort in sun spaces solely by renewable energy.

Improvements can either be effectuated by enhancements of building physical qualities of sun space envelopes or by implementation of technology in building skins that allow to collect further renewable energy utilized for additional space heating. The latest option seems to the author the only appropriate since sun space envelopes in general do not allow significant improvements in building physical quality related to desired tiny aluminium profile dimensions.

Thus, Chapter 3 elaborates Step B of research by means of investigating on diverse potential building skin integrated renewable energy collector technologies (section 2.1) in terms of a literature review. Section 4.0 and 3.1.2 focusses on various solar thermal and photovoltaic collector technologies. Performance efficiencies and possible negative impact on internal thermal comfort constitute in section 4.0 as key parameters. In particular, the eligibility of a collector technology to be integrated in sun space envelope in order to support sun space heating is predominantly determined by the principle of feasible cascaded energy provision. Moreover, subject in section 6.0 is to detect the technology, that causes least energy and complementary high efficiency what constitutes to be the most appropriate.

This chapter contributes decisive pre-paratory knowledge for chapter 6 and 7, in which a tested product development of a rafter integrated collector will be evaluated and a holistic computational simulation study will be executed as well.

## § 3.2 Specific Effectiveness and Performance of façade embedded collector typologies

Façade integrated collector technologies aim on conversion of environmental energy into utilization energy for specific building management. Environmental energy by principle is primary energy (Weik, 2009, [72]) and bases on irradiation by the sun. Consequently, irradiation generates environmental energy like wind power, warm air and geothermal heat for example. In order to provide warmth for space heating, especially envelope embedded solar thermal collectors convert irradiation and environmental heat, whereas photovoltaic collectors convert irradiation into DC current, what supports either DC or AC power nets in buildings. What technical mechanisms help to optimize energy conversion process and minimizes energy losses to the environment as well are explained in detail for both solar thermal and photovoltaic technologies.

### § 3.2.1 Performance criteria of envelope embedded collectors

Solar thermal collectors actively absorb a specific spectrum range of irradiation and visible light. Especially, the ultra-violet range from 100 nm to 380 nm is compared to the infrared spectrum more intense of atomic energy, what is common known by phenomenon of sun tan. Ultra-violet C and B radiation are the most powerful in order to physically heat up bodies. As well as every common solar thermal collector also envelope embedded ones base on an absorber material, mostly made from copper or alumina sheet, that is specially high-selectively coated.

High performance coatings (Fig.3.1, [73]) can be made from non-selective solar vanish, selective black chrome and highly-selective coating like titan-oxide. The order of the before mentioned coatings improves by the crucial performance ratio of absorption  $\alpha$  to emission  $\epsilon$ . Coatings are technically designed to maximize absorption (95%) and to minimize losses by emission (5%), what results in optimum  $\alpha/\epsilon$  ratio of 19 for Titanate-Sodium-Oxide (TiNOx) in a temperature range of 80 to 100°C. Empirical measurements (Schneider, 2008, [74]) show that applied black chrome on

absorbers nearly achieve comparable performance as TiNOx coatings. Following, the most crucial criteria for optimum collector performance are explained in hierarchical manner. One criteria depends on the directly previously mentioned one. Thus, the amount of irradiation a collectors is enabled to convert depends on the a.) optical collector efficiency rate.

COATING	MANUFACTURING PROCESS	MAJOR SUBSTRATE	coating thickness	ABSORPTION factor	EMISSION factor	$\alpha / \varepsilon$ ratio
solar vanish	solvent application	polymers, metals	-	95%	85%	1,1
black chrome	galvanic tape processing	stainless steel	0,2 to 0,4 $\mu\text{m}$	95%	12%	8,0
black nickel (NiS, ZnS)	galvanic processing	Alumina	-	95%	8%	12,0
"blue coatings" TiNOx	sputtering, physical vapor deposition, chemical vapor deposition, plasma or enhanced vapor deposition	copper , alumina	0,06 $\mu\text{m}$	95%	5%	19,0
Thickness Insensitive Spectrally Selective paints (TISS)	sputtering	polymers	> 0,2 to 0,4 $\mu\text{m}$	-	-	-

FIGURE 3.1 Spectral coatings and  $\alpha/\varepsilon$ -ratios

In principle, solar thermal collectors absorb irradiation to convert into heat. Nonetheless, irradiation is distinguished between diffuse, direct and total or global irradiation. Diffuse irradiation is a disordered variation of irradiation, what causes no shadow. On the opposite, direct irradiation transmits directly energy and causes shadows. Diffuse and direct irradiation in total describe related to perpendicularly oriented receiver surfaces, global irradiation. Seventy per cent of global irradiation occurs in summer time. Normally, diffuse irradiation occupies fractions of global irradiation of 40 to 70% during the year and often exceeds direct irradiation, eventually in summer times. What is more of interest flat plate collectors absorb compared to other collector typologies mainly diffuse irradiation.

The optical efficiency rate  $\eta$  determines the amount of irradiation facing the optical effective collector area (aperture), that can remain as being converted into utilisation heat (Viessmann, 2008, [75]). The efficiency is determined by internal heat conduction of the absorber and lowered thermal losses, e.g. by radiation, convection and transmission, which are specific for a considered collector typology. Thermal losses strongly depends on operation mode and temperature differences between absorber and the ambient air temperature.

Hence, in principle, a collector efficiency lowers with rising operation temperature and decreasing external temperature. Next standing formula is regulated by EN 12975-1:2006+A1:2010 issue 2011-01 [75] and describes mathematically *the optical efficiency ratio* :

$$\eta = \eta_0 - \frac{k_1}{E_g} \Delta T - \frac{k_2}{E_g} \Delta T^2 \quad (16)$$

where is :

$\eta$  = collector optical efficiency ratio [%]

$\eta_0$  = optical efficiency / optical conversion factor [%]

$k_1$  = thermal loss coefficient 1 [W/m<sup>2</sup>K]

$k_2$  = thermal loss coefficient 2 [W/m<sup>2</sup>K<sup>2</sup>]

$\Delta T$  = temperature difference [K]

$E_g$  = irradiation [W/m<sup>2</sup>]

The optical performance of a collector is closely related to the aperture area, which actually is the sum of projective light transmitting area, the sum of absorber area, what easily can exceed the aperture area and the gross or effective area, what is defined by the overall collector case dimensions. Glazed collectors suffer from light reflection and energy absorption by the glass sheet. Reflection causes light transmission losses of 4% by each fraction of a glass surface. This results in 2\*4% by the outer and by the inner surface of a sheet.

Glass thickness additionally causes 1% transmission losses by absorption with every 1mm of glass thickness. For example, a 4 mm glass cover sheet reduces light transmission by (2\*4% + 4 mm \*1% = 12%) 12 to 88% remaining transmission. Optical efficiency of a collector can be improved tremendously by technical qualities of the cover sheet. Qualities in terms of collector cover sheets mainly base on high light transmission, low light reflection, low energy absorption and compensation of solar normal factor losses.

Regarding optimization, different technologies provide optimum cover sheet performance as there is to mention a.) low-iron glass, b.) anti-reflective coating, c.) prismatic surface treatment (Fig.3.2). In particular prismatic cover sheet surface treatment methods have been developed in the last five to ten years, which principally base on glass sheet roller cast processes and chemical acid-treating.

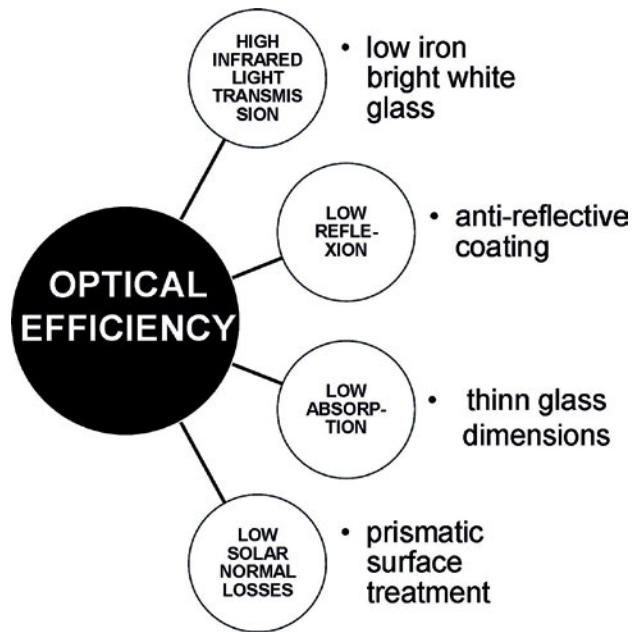


FIGURE 3.2 Parameters of enhanced optical efficiency

Weik (2009, [72]) introduces another performance key parameter : the b.) conversion factor  $\eta_0$ . The conversion factor determines the ratio of irradiation touching the collector and the amount of utilizable heating energy. Besides relative performance characterization parameters, the i.) effective power  $q_{st}$  of a collector informs about the maximal achievable heating power of a collector typology. The effective power is empirically determined by a standardized test procedure, along which the tested collector is orthogonally exposed to artificial irradiation of  $1.000 \text{ W/m}^2$ . In the context of comparison of solar thermal collector with other heat generators diverse international European solar thermal associations confirmed in 2004 to fix a standardized optical efficiency value of solar thermal collectors in general to  $0,7 \text{ kW}_{th}/\text{m}^2$

aligned with a absorber efficiency of 0,9 [72] regardless of any specific collector typology or construction principle.

### Conversion factor $\eta_0$

---

$$\eta_0 [\%] = \tau * \alpha * \eta_a \quad (17)$$

where is :

$\eta_0$  : conversion factor [%]

$\tau$  : transmission factor of glazing [%]

$\alpha$  : absorption degree of absorber [%]

$\eta_a$  : absorber efficiency (F' eff) [%]

(For example :  $\tau = 0,9$ ;  $\alpha = 0,95$  ;  $\eta_a = 0,855$ ;  $0,855 \times F' \text{ eff } (0,9) \gg \eta_0 = 0,77$ )

In this context, Föste, Ehrmann, Giovannetti, Reineke-Koch, Uslu, Krämer and Hesse [77] published in 2013 evaluated averaged reductions of collector conversion factors for 16 vacuum tube, three directly flooded and four recently developed high efficiency flat collectors. Figure 3.3 demonstrably shows a tremendous mean reduction of the conversion factor of vacuum tube collectors after degradation and several stagnation of -11,6%. Opposed to that directly flooded tube collectors and the high efficiency flat collector (HFK) solely account reduction by 1,8 and -1,2%.

As already mentioned before, the collector optical efficiency ratio is in a second step determined by the ability of the absorber sheet and absorber tubing to convert and exchange heat. Thus, c.) the internal conduction value ( $U_{int}$ ) of the absorber defines, what amount of generated heat can actually be exchanged to utilization circuits. Consequently, the internal conduction value is a ratio for the quality of the absorber sheet/tubing system. However, this value is described simply and equal to a conduction value as  $W/m^2K$ .

### Averaged internal conduction value $U_{int}$ [ $W/m^2K$ ]

---

$$U_{int} = Q_{ab} / A * (\delta_{abs} - \delta_{fluid}) \quad (18)$$

where is :

$\delta_{abs}$  = mean absorber temperature [ $^{\circ}C$ ]

$\delta_{\text{fluid}}$  = mean fluid temperature [ $^{\circ}\text{C}$ ]

$Q_{\text{ab}}$  = effective power [W]

$A_{\text{finn}}$  = area of absorber finn [ $\text{m}^2$ ]

$U_{\text{int}}$  = internal conduction value [ $\text{W}/\text{m}^2\text{K}$ ]

(For example :  $U_{\text{int}} = >35 \text{ W}/\text{m}^2\text{K}$  and  $UV = 3,8 \text{ W}/\text{m}^2\text{K} > F' \text{ eff} = 0,9$ )

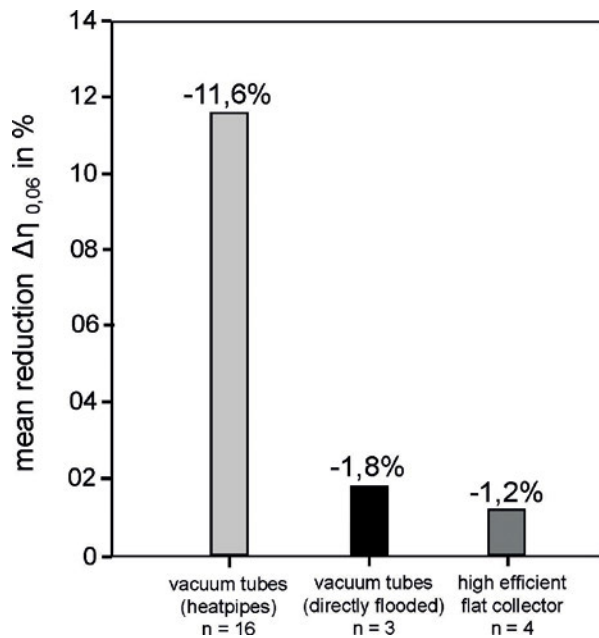


FIGURE 3.3 Averaged reduction of conversion factor  $\eta_{0,06}$  of a.) 16 vacuum tube collectors (heatpipes) b.) three directly flooded vacuum tube collectors and c.) four high efficiency flat collectors

The authors [77] emphasize, that frequent thermal shocks initiated by stagnation reduces the internal conduction value. Moreover, they observe specific dilatations of flat plate absorbers from the middle axis, that in extreme result in direct conductive contact of the absorber with the cover glass or case rear.

These dilations tremendously reduces collector efficiency since conduction and convection within the collector case increase. The authors reveal a close relation between absorber sheet and absorber tubing materials, absorber geometry (harp-shaped or meander -shaped) and absorber temperature. Figure 3.4 illustrates the strong relationship between material-mix absorbers (alumina-copper) and meander-shaped absorbers and remaining distance to front glass or case rear (-4 to -25 mm).

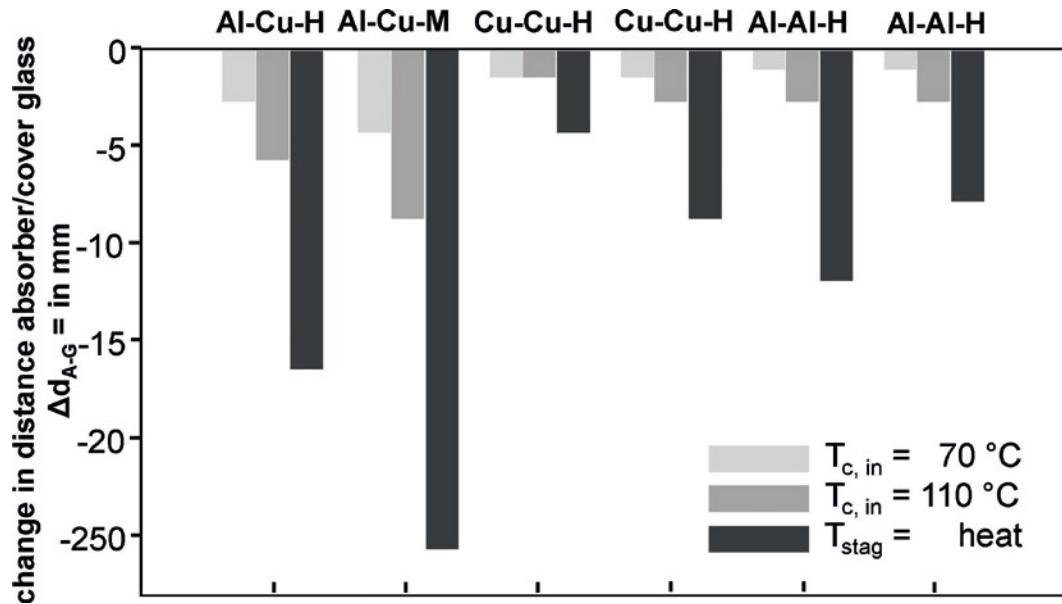


FIGURE 3.4 Variations in distance between absorber and cover glass of inspected absorber with starting feeding temperature 25°C and feeding temperatures of 70°C, 110°C and overheating without working fluid at ambient temperature of 26°C

It additionally call attention for homogenous absorber materials and harp-shaped geometries (Cu-Cu-H: -2 to -4 mm). Summarizing, harp-shaped material-homogenous absorbers causes less dilatations and thus less reduction in collector efficiency by de-formation. Hence, the authors recommend an absorber-casing distance of at least 30 mm in order to respect possible deformation and collision. Furthermore, the authors measured different absorber temperatures along the absorber length. Absorber temperatures can vary between 164 to 264° after two of three of the entire length. Acknowledging this insight, absorber normally suffer from tremendous thermal and, thus induces, mechanical stresses.

Among Giovannetti, Kirchner, Franke, Rohde, Scherer (2014) [78] the internal conduction value can vary between 60 to 110 W/m<sup>2</sup>K. They observed, that several thermal shocks (stagnation) result in a reduction of the internal conduction value of 9 to 12%. Correspondingly, a division of the internal conduction value  $U_{int}$  by the sum of the internal conduction value  $U_{int}$  and the first thermal loss coefficient  $U_v(a_1)$  results in the absorber efficiency ratio  $F'_{eff}$  [%], respectively  $\eta_a$ . Figure 3.5 gives an example in relation to  $U_{int}$  [W/m<sup>2</sup>K].

#### Absorber efficiency ratio $F'_{eff}$ (respectively $\eta_a$ )

---

$$F'_{eff} = \frac{U_{int}}{U_{int} + U_v} \quad (19)$$

where is :

$F'_{eff}$  = absorber efficiency ratio ( $\eta_a$ ) [%]

$U_{int}$  = internal conduction value [W/m<sup>2</sup>K]

$U_v(a_1)$  = thermal loss coefficient 1 [W/m<sup>2</sup>K]

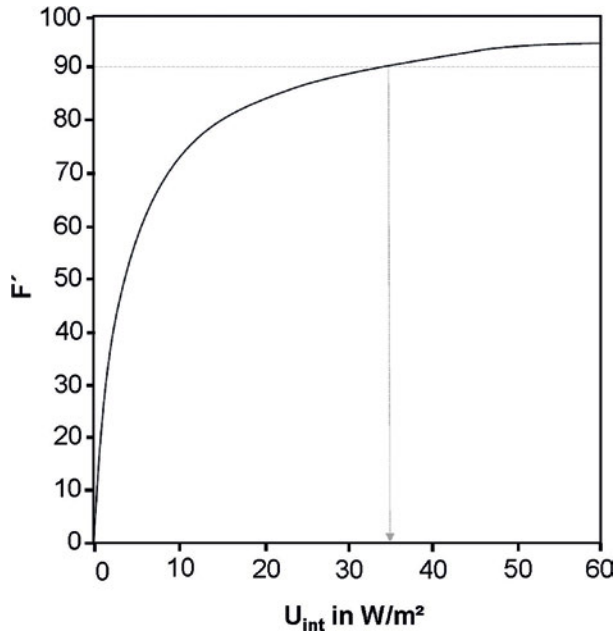


FIGURE 3.5 Example of the absorber efficiency ratio [%]  $F'_{eff}$  of 0,9 in relation to the internal absorber conduction value  $U_{int}$  [ $W/m^2K$ ] of  $35 W/m^2K$

Figure 3.6 illustrates typical optical efficiency ratios of different collector types related to their specific thermal loss coefficients 1 and 2. It becomes obvious, that a flat plate collector with anti-reflecting glass provide better optical efficiency than a vacuum tube collector.

COLLECTOR TYPE	OPTICAL EFFICIENCY RATIO	THERMAL LOSS coefficient 1	THERMAL LOSS coefficient 2
	[%]	[ $W/m^2K$ ]	[ $W/m^2K^2$ ]
flat plate collector	80	4	0,1
flat plate collector with anti-reflecting glazing	84	4	0,1
vacuum tube collector	80	1,5	0,005

FIGURE 3.6 Optical efficiency ratios of different solar thermal efficiency ratios

Another criteria describing the performance of solar thermal collectors is the e.) equivalent  $U_{\text{eff}}$ -value [ $\text{W}/\text{m}^2\text{K}$ ], which is regulated in DIN EN ISO 9806:2014-06 [79]. Different equivalent U-values (Loga, Born, 2012, [80]) of collectors with diverse constructions principle are listed in figure 89 below.

As so far, the technical construction related parameters determining collector efficiency have been explained, similarly external parameters have influence on performance as well. Solar thermal collectors work most sufficient if irradiation touches cover sheet or uncovered absorbers orthogonally. Sufficiency is maximum with less reflections by the cover sheet. Thus, irradiation angle differences from the normal (perpendicular) result in decrease of yield and power. Along this, the term f.) solar normal factor is introduced to define the actual power of a collector related to deviations of perpendicular irradiation (Fig.3.8). The solar normal factor, equal to the incident angle modifier (IAM)  $A \cdot \cos \mu$  corrects the solar recipient area  $A'$ , the aperture, of a collector.

The solar normal factor especially influences performance of optimal vertical façade integrated solar thermal collectors, as they cannot be exposed to the daily sun path. This insufficient exposure fixed to a  $90^\circ$  inclination reduced maximum collector power to solely morning and evening and autumn/spring periods. Deficits in optical manner determined by the solar normal factor can be compensated with anti-reflex coatings (AR, made from Titan-Dioxide or Silicium-Nitride), specialized micro-structuring (prisma) of collector cover glazing or with specialized multi-layer cover sheet including laminated glass, which provides different light fraction indices, and thus, lowers the overall fraction index [72]. Generally, micro-structuring widens the harvesting spectrum towards radiation of extreme angles of incidence.

COLLECTOR TYPE	U <sub>eff</sub> -value
	[W/m <sup>2</sup> K]
a.) uncovered absorber	≈ 20
b.) single-glazed collector	≈ 7
c.) single-glazed collector with selective absorber	≈ 3,5
d.) single-glazed collector with selective absorber + 8 cm transparent insulation	≈ 1,5
e.) double-glazed collector	≈ 4,5
f.) double-glazed collector with selective absorber	≈ 2
g.) vacuum tube collector	≈ 1

FIGURE 3.7 Equivalent effective U-values of different collector typologies

### Solar normal factor

$$A' = A \cdot \cos \mu \quad (20)$$

$$H_n = H_0 \cdot A' = H_0 \cdot A \cdot \cos \mu$$

$$I_\mu = A \cdot H_0 \cdot \cos \mu$$

where is :

A' : corrected recipient area [m<sup>2</sup>]

H<sub>0</sub> : 100% irradiation touching recipient area [W/m<sup>2</sup>]

H<sub>n</sub> : corrected irradiation touching recipient area [W/m<sup>2</sup>]

I<sub>μ</sub> : effective irradiation utilizable by the reduced recipient area [W]

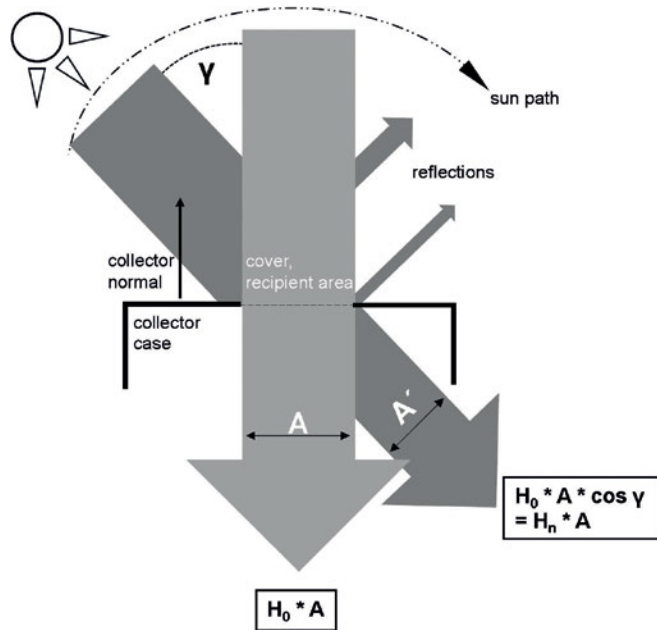


FIGURE 3.8 Effective irradiation power  $I_{\mu}$  in relation to solar normal factor (Weik, 2009)

While the characteristic curve of a collector describes the interdependency between the temperature difference between the absorber and external air temperature, signifies the  $\eta_c$  collector efficiency ratio the interrelationship between a temperature differences related to a specific irradiation  $\Delta\mu/H_n$  and collector efficiency. The collector efficiency in special distinguishes efficiency related to seasonal typical irradiation and thermal losses (Fig.3.9). The efficiency ratio can be plotted by a curve incorporating manifold  $\Delta\mu/H_n$  coefficients. The flatter the curve, the better the efficiency.

### Collector efficiency ratio $\eta$

$$\eta : c_0 - (c_1 * x) - (c_2 * H_n * x^2) \quad (21)$$

where is :

$c_0$  : optical collector efficiency [%] (0,735)

$c_1$  : Ueff-Value of the collector [W/m<sup>2</sup>K] (1,74 W/m<sup>2</sup>K)

$c_2$  : curvature [ $W/m^2K^2$ ] ( $0,016 W/m^2K^2$ )

$\eta_{0,05}$  :  $\eta_x=0,05$  by i.g.  $(\mu_{abs} - \mu_o) = 40K$ , with  $H_n = 800 W/m^2 (=0,615)$

$\eta_{0,1}$  :  $\eta_x=0,1$  by i.g.  $(\mu_{abs} - \mu_o) = 40K$ , with  $H_n = 400 W/m^2 (=0,43)$ ,

typical for autumn/winter with solar normal factor of 0,87

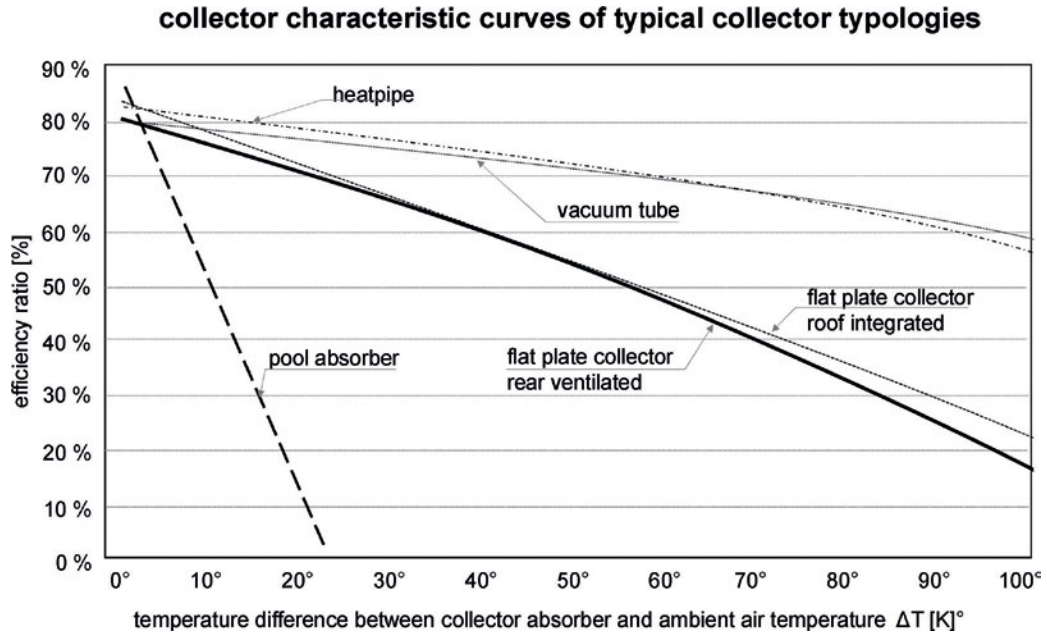


FIGURE 3.9 Characteristic curves of various collector typologies

The optical efficiency ratio combined with the equivalent U-value of each a collector allows to determine the performance in relation to the absorber/external air temperature difference. The better the absorption characteristic combined with thermal insulation is, the better the performance expressed in the h.) characteristic collector curve (see Fig.3.9). Essentially, highly selective absorbers within an evacuated encapsulation show best performances, while they offer comparably high feeding temperatures and less thermal losses.

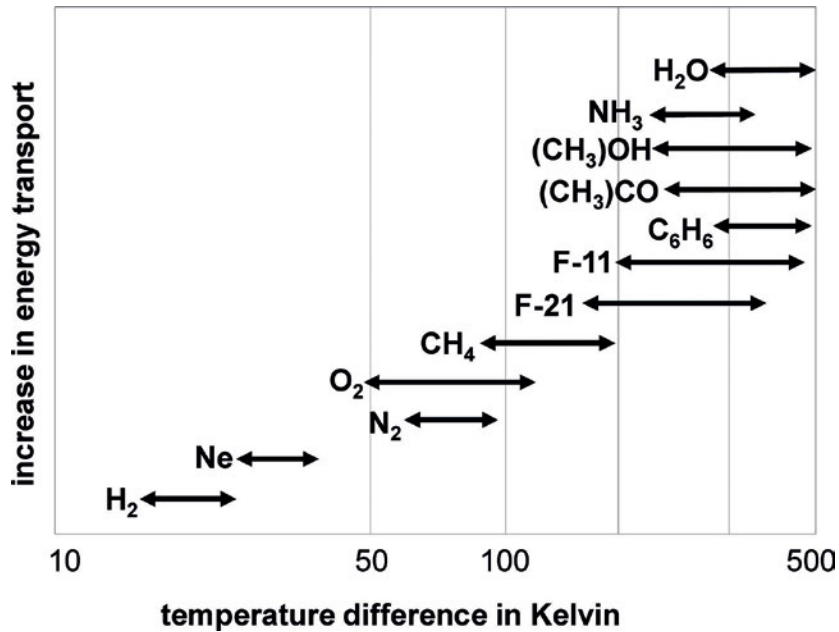


FIGURE 3.10 Energy transfer ratio of working media related to operation temperature by Weidner, 2015

The collector efficiency ratio itself and the system efficiency strongly depend on first the transport medium and secondly on the heat working medium, in particular in closed evacuated tube collectors (heatpipes). While water offers a heat capacity of 3,8 (4,2) kJ/kg, it requires a freeze protection agent, if circulating water risks to come in contact external temperatures below 0°C. In consequence, 30 per cent anti-freeze agent fraction lowers the heat capacity of water to 3,6 kJ/kg. In order to compensate, either the flow-rate needs to be increased or the power of the solar thermal collector needs to be lowered. Regarding the performance of closed evacuated tubes, the sort of working medium and the volume incorporated are crucial parameters.

Groll (1970) [81] and Weidner (2015) [82] inspected different working media appropriate for heatpipes and illustrate different specific heat transfer ratios. In accordance to operation temperature levels and ranges, Figure 91 illustrates different working media. Methane (CH<sub>4</sub>), water (O<sub>2</sub>) and N<sub>2</sub> are the most common working media for an operation temperature range between 50 to 200°C. Nonetheless, for freezy and cloudy days the working media similarly needs to be protected against freezing by anti-freezing agents (Fig.3.10).

## Solar fraction, solar covering ratio

---

Principally, the amount of energy, that has been generated by a solar thermal collector device cannot be used entirely. This mismatch of offer and demand is strongly related to the system efficiency ratio and the efficiency of the applied energy storage. Yet, normally, a sensible water storage is part of the system, especially in summer times a considerable high fraction of generated energy is not used for heating. Solely, in winter and autumn, respectively spring time, offer and demand match and result in a high j.) solar fraction or solar covering ratio.

## Solar fraction ; solar covering ratio $f_a$

---

$$f_a : Q_{\text{solar yield}} / Q_{\text{demand, a}} \quad (22)$$

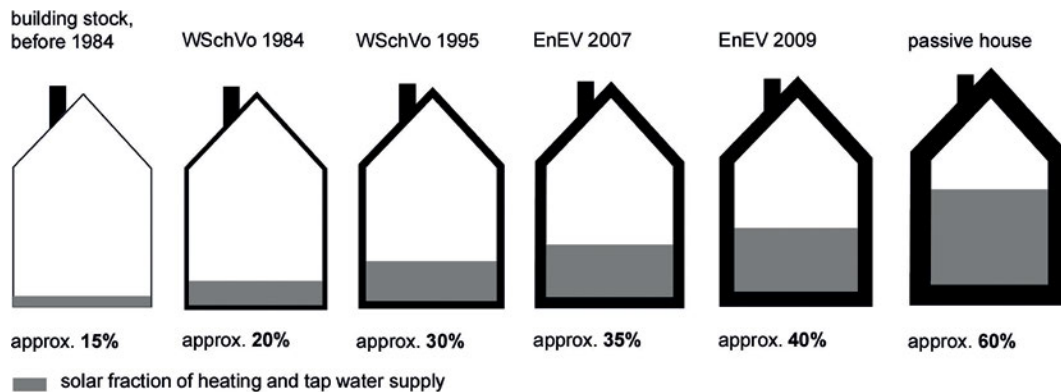
where is :

$Q_{\text{solar yield}}$  : annual solar yield [kWh/a]

$Q_{\text{demand, a}}$  : annual heating demand [kWh/a]

The solar covering ratio is closely related to time shift and the demand in intermediate periods of the year. If the yield in autumn and spring times is expected to be as great as possible, planners attend to maximize the solar thermal collector plant. That maximization leads to increased feeding temperatures and overheating in summer time, the system more often encounters stagnation (Mach, Grobbauer, Streicher, Müller, 2015, [83]), while the sensible buffer tank is completely charged. Correspondingly, stagnation causes thermal stress in the entire collector system.

The solar covering ratio is disproportional to the area specific efficiency of a collector (Viessmann, 2008), hence, the better the collector efficiency the higher is the amount of energy produced in summer, that is not utilized and results in a low solar fraction. In this context, respectively of system efficiency, the size of the buffer tank determines both solar fraction and the amount of “an”ergy, especially in autumn and spring.



**Solar thermal collector plant, 15m<sup>2</sup>,  
combined with 1.000 L buffer tank**

FIGURE 3.11 Solar fraction related to thermally insulation standard and annual heating and tap water demand

On the contrary, solar thermal collectors embedded in vertical, 90° declined facades, work sufficient in autumn and spring with low declined sun. This pre-set allows higher solar fraction and less stagnation (Stark, Gohl, Drück, 2015, [84]). In particular in Europe solar thermal collectors are certified, if by standard test procedure according to DIN 12975 the considered collector gains 550 kWh per year. Opposed to that, an averaged solar yield of 310 kWh per year is close to practice according BDH (2011, [85]). In consequence, the collector annual yield can differ by 40 per cent in practice to standardized test procedures. Nevertheless, BDH (2011) informs about an averaged feasible daily energy yield of 2,5 to 3 kWh/m<sup>2</sup>d by solar thermal collectors in general in summer time, whereas it lowers to 2 kWh/m<sup>2</sup>d in intermediate periods such as autumn and spring. The lower the annual heating energy demand is, the higher solar fraction can be [86]. In particular (see Fig. 3.11), for low-energy-houses with a total heating energy demand less than 70 kWh/m<sup>2</sup> Weiß, Eder, Fink and Streicher (1997) [87] elaborated a incomparably high feasible solar fraction.

Solar fraction definition can be exaggerated towards the total amount of energy for production and operation during the entire life time (life cycle assessment) and the term k.) harvesting factor becomes focus. The individual harvesting factor of each a considered technology relates the amount of energy for production and for running the technology to the energy this device produces (solar fraction) during the entire life span [72]. The harvesting factor enhances, thus rises, correlating with an optimal system control and system efficiency. Hereby, system control includes low-flow run (Friedrich,

2007, [88]), less stagnation if possible and an appropriate activation value regarding temperature difference between device and buffer tank, i.e., heat sink.

Furthermore, system efficiency correlates with an appropriate sensible water buffer tank volume, enhanced buffer tank energy management (stratification), supervised heat exchanger temperature differences [85], low auxiliary energy demand of circulation pumps and location, respectively inclination, of the collectors (Fig.3.12). Moreover, the author emphasizes, that solar fraction and especially collector inclination in means of roof location or vertical façade integration significantly determine the harvesting factor as being explicitly shown in section 3 of this chapter.

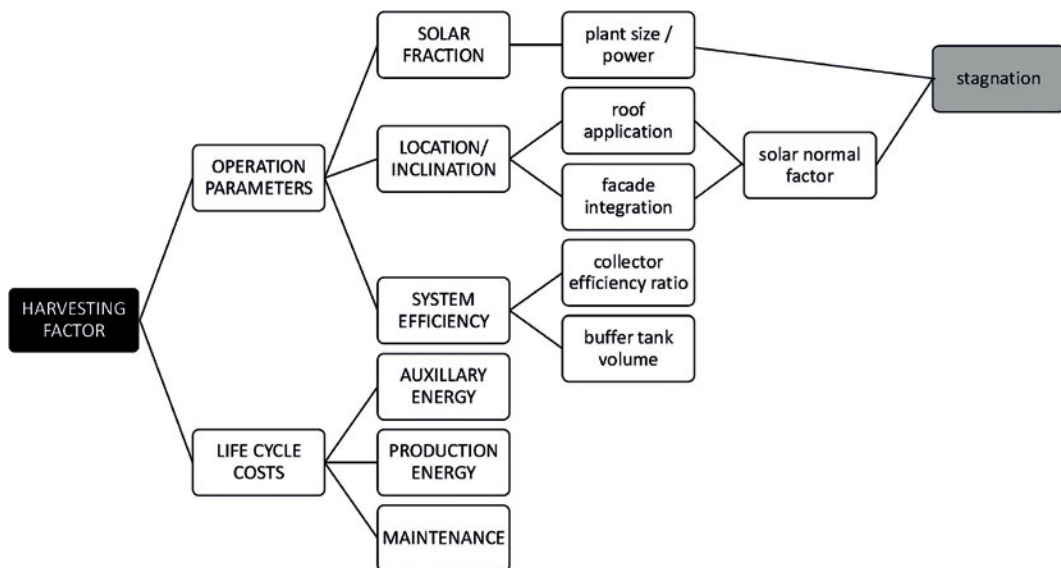


FIGURE 3.12 Harvesting factor defining parameters

Modern collector typologies are characterized by free form design and by implementation into diverse façade typologies. In consequence, the calculation of thermal collector losses and the collector efficiency ratio is difficult, moreover integral dynamic simulation programs are yet not available (Ray-Tracing+Fluid Dynamics) and a two-step post processing is to inaccurate. Zauner, Hengstberger, Reichl et al. (2012) [89] have developed a durability and performance test for free-form, non-planar and façade integrated collector designs. This test procedure also includes inspection and calculation of convective heat losses, detailed split heat losses of case areas and absorber fluid dynamics.

### § 3.2.2 In relation to internal load profile, envelope properties and location

---

The effectiveness of building skin integrated renewable energy collector technology in terms of fossil fuel substitution considerably depends on the efficiency of technology itself. But, moreover, it is a question of the specific energy demand of the building for heating and cooling. In fact, thermal envelope insulation, glazing ratio, geographical location in terms of climate and orientation and consumption behaviour of occupants as well affect energy demand for heating and cooling. Thus, the effectiveness of a specific integral façade solution is determined by diverse independent variables, that are unique for the specific building purpose.

Planning and engineering requires guidelines, experiences and well evaluated cause-effect relations in terms of descriptive knowledge. In any case, empirical measurements and evaluations help to enhance descriptive knowledge, but, characteristically, empirical evaluations are limited to a limited geographical location and climate and to a limited amount of set parameters. Despite this, computer simulations offer the opportunity to enlarge the amount of input parameters, diversity in climate region in matter of geographical location and occupational behaviour as well.

However, Mach, Grobbauer, Streicher and Müller (2015, [83]) evaluated theoretically the effect of thermal envelope insulation, geographical location, glazing and respectively facade integrated collector area by computer simulation. Embedded in “The multifunctional Plug&Play Approach in façade technology” research a study concentrated on an eight level high rise office building, that is heated and cooled electrically, considering also air handled heat and cold recovery. The research aim was to determine the optimum glazing ratio, the required façade insulation quality and feasible autarky ratio in relation to location.

On this account, the authors defined three different capital cities, which represent extrema as well as mean averaged external air temperatures. Hence, Madrid typifies European regions with maximum air temperature during the year, whereas Helsinki represents regions with lowest averaged external temperatures. Likewise, Ljubljana was chosen to incorporate means of European air temperatures. In order to describe the computational models in more detail, glazing ratio changed between 50 and 100%, while overall façade U-values alternated between 2.4 W/m<sup>2</sup>K, 1.2 W/m<sup>2</sup>K, 0.6 and 0.3 W/m<sup>2</sup>K, whereupon the authors considered 0.3 as a target value for the future. PV modules with polycrystalline cells were integrated in the parapet area ( approx. 5.5 m<sup>2</sup>) of each a façade in the context of the 100% transparent façade (approx. 13 m<sup>2</sup>) model variants.

Opposed to that, polycrystalline modules were additionally integrated in the window areas (4.9 m<sup>2</sup>), what results in a 50% decrease of transparent area (6,5 m<sup>2</sup>). Aligned with the façade dimensions, the office floor area was fixed to 25m<sup>2</sup>, corner offices to 26 m<sup>2</sup> and conference room floor area to a multiple of 75 m<sup>2</sup>.

Mach, Grobbauer et al. elaborated by simulation software TRNSYS / TRNBUILD (Solar Energy Lab) different findings, which are merged as clear-cut relationships by the author. Regardless of any location, energy consumption in total for electrical heating and cooling is evaluated to be less for the 50% transparent variants compared to the 100% transparent considerations.

This fact is interpreted besides before mentioned ambitious U-values of glass-alumina façade construction as a crucial and tremendous influence of the remaining thermal solid wall insulation. In case of 50% transparent facades, heating demand exceeds cooling demand if the U-value is above 0.6 W/m<sup>2</sup>K. If this U-value can be undercut, the relationship alternates into a higher cooling energy demand, interpreted as caused by a growing proportion of overheating. In terms of a 100% transparent office room façade, the crucial energetic quality of façade remains the same at 0.6 W/m<sup>2</sup>K, while heating demand exceeds cooling demand with rising U-value. Total energy consumption for conditioning is higher than for the 50% versions with U-value > 0.6 W/m<sup>2</sup>K.

But, by contrast, the total energy demand significantly lowers compared to the 50% transparent models if the U-value of a 100% transparent façade approximate 0.3 to 0.5 W/m<sup>2</sup>K. Regardless transparency ratio, cooling demand generally exaggerates if U-value approximates 0.3 W/m<sup>2</sup>K. What is more of interest, is the autarky ratio, in order to generate knowledge about technology and significant impact of boundary parameters on system efficiency. Similarly in the context of this particular research, the autarky ratio is strongly dependent from thermal insulation quality, glazing ratio and location. The author summarizes the investigational findings as follows:

In general, autarky is more frequently achieved with solely 50% transparent office facades. Further, the more the building is located in southern parts of Europe, the higher the opportunity to realize autarky. This relation is interpreted as being strongly interconnected with less transmission losses on account of moderate averaged external temperatures. Moreover, what describes the effect of thermal insulation quality, is the fact, that a U-value of 1.2 W/m<sup>2</sup>K or lower increases self-supply ratios. The essence of two above mentioned findings can be defined inasmuch as the more south located a building is the worse the façade U-value is allowed to be to still provide mentionable autarky ratio.

Hence, the mean self-supply ratio for south located office buildings can be 4 times higher compared to northern located ones by means of greater extent of sun shine hours during winter. Parallel but not similar investigate Abawi (2014) [90], Shri (2013) [91] and Rennhofer (2014) [92] on feasible autarky for equipment power supply in both office and residential buildings.

While Abawi and Aniel investigate opposed to common AC-power supply on DC-power supply of entire office or residential buildings in order to minimize DC/AC current change losses, Rennhofer puts emphasis on a proper internal load-storage capacity interrelationship. Rennhofer [93] discovers that autarky on power level with given maximum vertical façade area for embedding of PV devices strongly depends on internal equipment power load, on the battery storage capacity and on battery charger efficiency. He empirically elaborated on an office building façade and introduced the boundary load scenarios of internal equipment loads, namely 372 Wh, 774 Wh and 925 Wh per day [94], of which by his test set up hardly the lowest (373 Wh/d) could have been fulfilled.

By contrast, in terms of residential buildings, Weiß, Eder, Fink and Streicher (1997, [87]) evaluated more than 2 decades ago, that low energy house concepts are feasible to be run by solar thermal energy. They argue, that as prerequisites living houses require to have an area specific averaged heating energy demand of less than 70 kWh/m<sup>2</sup> a year. Floor and wall heating are the second prerequisite from which deviated autarky is not possible. The authors above indicate 10 kW heating load as a borderline, which exceeded, causes troubles for feasible solar thermal collector installation area close to building facades. Contradictive to Weiß, Eder, Fink and Streicher the BDH [85] claims, that the worse a residential building is thermally insulated the more fossil energy nominally can be substituted by solar thermal application. Hence, exclusively space heating in winter excluding domestic hot water as main objective raises fossil fuel substitution, but lowers solar fraction.

### § 3.2.3 Summary

---

This section elaborates first crucial items in terms of collector technology and second appropriate power and load management (harvesting factor) in respect to the actual space or building applied. Although facades offer additional area to locate collectors, area-wise maximum yield and minimized losses are essential planning objectives in regard to the space alternatively supplied in question. Beside the technical optimization of the collector itself, the technical planning of orientation and collector

inclination in respect to façade typology and geographical location (north-, mid- or south Europe) is essential for a matching power to load congruency.

Thus, several key parameters were identified, which accomplished help making façade integrated renewable energy collectors efficient. For example, optical and thermal performance criteria can vary in relation to typical location and climatic dependent boundaries like sun height, irradiation intensity and duration. In terms of sun spaces, nonetheless are-wise efficient and insulated collector typologies govern summertime storage related as well as spring and autumn directly utilized yields.

### § 3.3 Systematic planning of yield in context of façade typology and location

Besides technical considerations for planning and designing of solar thermal collectors, more or less defined boundary conditions actually determine solar fraction, annual yield and feasibility of collectors as being incorporated part of building skins. These concrete boundary conditions implement the actual climate, direction and inclination, geometry or aperture dimensions of the collector, the built environment and the applied technology (Fig.3.13) itself at the considered location of application. The figure below draws a picture of hierarchical order and interdependency of those before mentioned conditions. It additionally splits them up into minor aspects independent variables determining the efficiency of a chosen collector typology considered on a specific site.

Thus, along Mach, Grobbauer, Streicher and Müller (2015, [83]) planning and design of envelope integrated collectors include climate, geometry and technology and can be distinguished as following:

Geographical location effects decisively performance and annual yield of a collector in general. In this context, sunshine is defined towards international confirmation as irradiation higher than the boundary value of  $120\text{W}/\text{m}^2$ . Likewise, sunshine duration is the sum of hours with irradiation higher than  $120\text{W}/\text{m}^2$ . Besides that definition, not only sunshine duration in [h/a] but also sun path (azimuth) an sun altitude angle [°] appoint irradiation intensity in [ $\text{W}/\text{m}^2$ ] and solar normal factor regarding aperture inclination. Thus, extreme northern or southern locations significantly differ in terms of sunshine duration and intensity compared to equator sites.

Since sun rotates perpendicular along the equator, irradiation intensity reduction is mainly caused by filtering, reflection and absorption of the atmosphere air mass. Hence, fractions of direct irradiation lowers towards extreme northern or southern location, whereas diffuse light proportions increase.

Although, limited to Germany, hours of direct irradiation in southern parts of Germany exceeds sum of hours in northern parts during winter and intermediate periods, mainly higher cumulated hours of sunshine generally predominate in northern parts of Germany in summer [72].

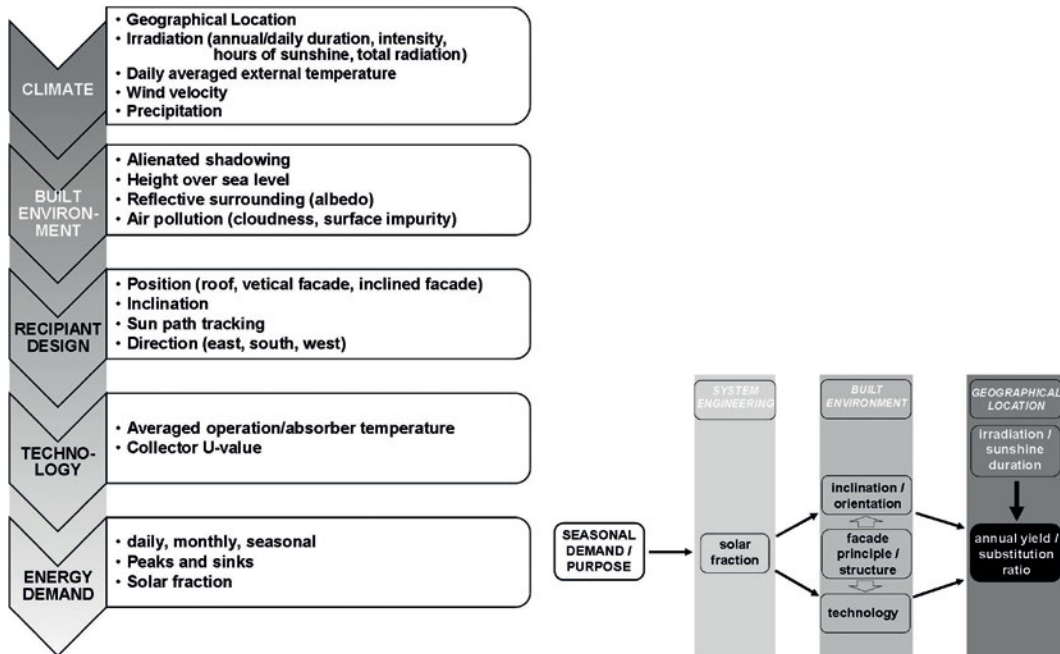


FIGURE 3.13 Hierarchical order of boundary parameters on collector performance

Hours of sunshine in Flensburg and Garmisch in February and December can differ between 59 to 99 (+68%) and 34 to 71 (+208%), while sunshine duration in June can differ between 225 to 154 (-32%) hours. In general sunshine can vary between 1.400 and 1.900 hours per year among Germany. In consequence, this relation essentially determines planning (see also [APPENDIX C.1](#)) of collector position (roof or vertical façade), aperture inclination (0 to 90°) and collector typology (tubed, flat plate, unglazed, etc.(Fig. 3.14)).

Orientation and inclination of the solar thermal plant is the next subordinate step for planning of an optimum performance of the solar thermal collector. Orientation and inclination are especially related to the actual usage, respectively spacial occupation time, solar fraction and provision purpose considering season. If entirely frankly, the recommended orientation of the collectors embedded in facades is defined by the daytime of demand. Furthermore, a collector should be oriented east, if renewable heating energy is required in particular in the morning time.

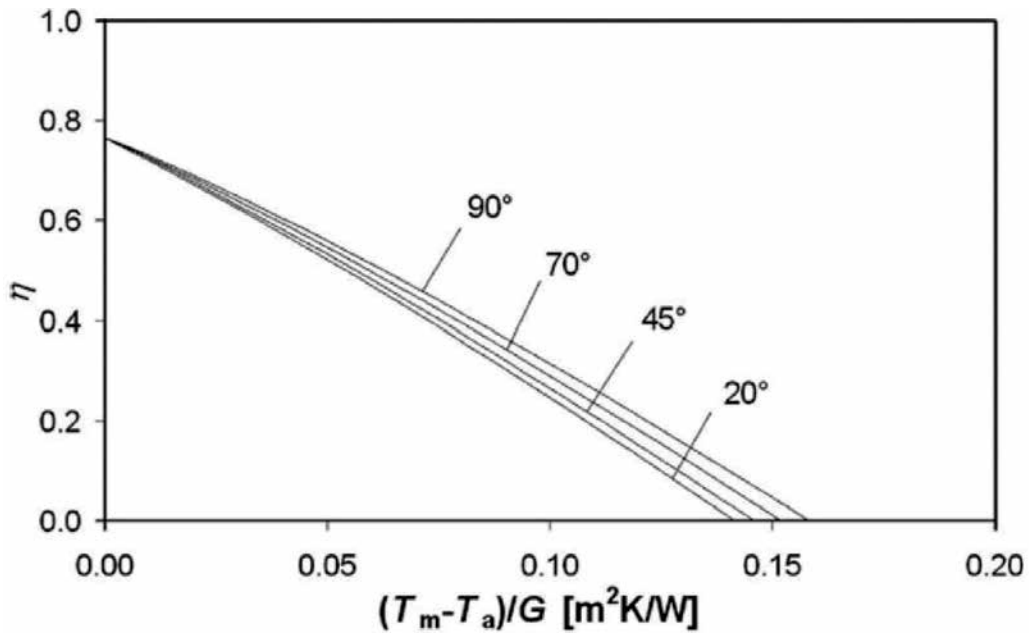


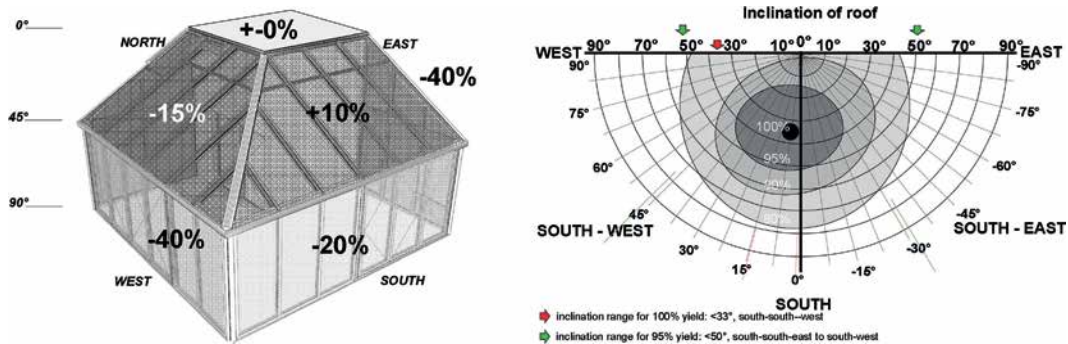
FIGURE 3.14 Annual yield according to technology, inclination related to geographical location and season

Similarly, recommended orientation changes to south or west, if energy provision is requested for the afternoon of evening and night time. However, if renewable energy is buffered sensibly in water tanks, orientation is closely related to the sun azimuth in order to minimize transmission losses and “an”ergy.

Above all, Weik [72] notes that southwest directed apertures compared to southeast oriented apertures of equivalent inclination suffer from less transmission losses.

Even southwest or southeast directed envelope embedded collectors (90°) can compete (Fig.3.15) with roof mounted and less inclined collectors (45 to 90°) in terms of annual yields (Matuska, Sourek, 2006, [95]).

Further, preferred to the framing effect, wind related heat transfer losses are less, because of less wind velocity normal to the façade. The façade framing effect results in a 60 to 80% reduced wind related heat transfer coefficient. Additionally, the heat loss coefficient of back and edge parts of the envelope integrated collector are significantly lowered as consequence of the surrounding conventional wall insulation.



2

FIGURE 3.15 Solar thermal yield and conversion ratio related to geographical location and orientation

In the end, summarizing above mentioned effects, Matuska and Sourek [95] identify almost equal annual earnings of a façade embedded collector with an overall resistance factor of  $6 \text{ m}^2\text{k/W}$  and a solar fraction of  $f = \text{approx. } 70\%$  compared to a roof mounted, free ventilated and less than  $90^\circ$  inclined collector. They figured out a  $275$  to  $265 \text{ kWh/m}^2\text{a}$  yield difference while solar fraction is proceeded by  $70\%$ . While solar fraction is reduced to  $60\%$ , annual yields have been evaluated to improve by  $31$  to  $58\%$  ( $423 \text{ kWh/m}^2\text{a}$  and  $348 \text{ kWh/m}^2\text{a}$ ) and such to differ from each other by  $21,5\%$ . That in particular means, that a façade embedded collector with a  $60\%$  solar fraction provides a higher annual yield, than a roof mounted less inclined variant with  $70\%$  (Fig.3.16) solar fraction. From this we can infer, that collectors intended to provide renewable energy for only a little proportion of tapping water in intermediate and winter time is required are recommended to be inclined towards  $90^\circ$ .

Matuska and Sourek detected a congruency between hot water tapping and heating energy profile and façade integrated façade collectors. This indicates, that

façade integrated collectors superiorly match with actual seasonal heating energy demand profiles.

Thus we can see, since loss free seasonal thermal storage technologies just temporarily emerge and enter the market, solar thermal collectors, that are purposed to contribute renewable heat for intermediate and winter periods for high solar fraction,

are perfectly placed and eligible in 70 to 90° inclined south directed vertical facades. The more heat is intended to be substituted by renewable energy, the more collectors are to be inclined and hence match with vertical façade constructions. In consequence, in matter of construction principles, 70 to 90° inclined collectors matches best in inclined roof constructions (sun spaces), since the same inclination in a 90° inclined façade causes shadowing and eventually limits performance of underneath placed collectors.

According to an orientation-inclination-yield-scheme by Viessmann (2008), we can interpret, that south-east or south-west oriented collector apertures, which are inclined for more than 20°, generally offer 5% higher yields, than a purely south directed horizontal without any inclination. However, as a rule of thumb, the smaller the inclination, the less are differences in daily yield of different orientations. As a result, daily yields of south east, south and south west oriented plants rather approximate with 15° than with 45°. But contrasting that, a plant slightly inclined and purely south directed encounters comparably high losses and stagnation.

<b>PURPOSE / TECHNOLOGY</b>	<b>high solar fraction</b>	<b>vs.</b>	<b>heating in intermediate seasons (and bounded in winter)</b>
flat plate collector	30 to 60°		60 to 70°
evacuated tube collector	20 to 90°		30 to 60°

FIGURE 3.16 Recommended collector inclination related to purpose and technology

In order to summarize the relationship between orientation and inclination Mach, Grobbauer, Streicher and Müller [83] illustrate with a comparative calculation with Meteororm software (2012), that utilizable solar irradiation in kWh/month in Helsinki (Norway) for a 45° inclined south oriented plant from July to September tremendously exceeds a comparable plant in Madrid (Spain) and even a horizontally arranged plant located in Madrid. The calculations parallel remarkably show, that 90° inclined south directed apertures in Helsinki (northern European regions) provide significantly less

yield during summer compared to Madrid (southern regions), but provide substantially longer in autumn month. Figure 98 demonstrates the calculation results of Mach, Grobbauer et al. and was widened out by the author by conversion ratio calculations.

From the figures we can conclude, that in northern European regions horizontal apertures (47;48%) do not provide worth mentioning higher yields than east directed apertures (47,51%). The conversion ratio is similar for Central European located apertures, but on the contrary south directed apertures in Central Europe tend to gain less than horizontally positioned apertures in Northern and Central European regions. Furthermore, the difference between horizontally and south directed solar thermal collectors differ significantly in South European region, in particular by two to four per cent. Moreover, annual yields of apertures located in Southern Europe can exceed gains of northern European placed apertures by 28 to 129%. Especially, east and west directed apertures can exceed by the half or even double. Hess (2012, [98]) describes 100 and 95% yield efficiency in Figure 98 right by an inclination range of  $<33^\circ$  and south-south-west direction and  $<50^\circ$  roof inclination and while orientation can vary between south-south-east and south-west.

Additionally, figure 99 demonstrates recommended collector inclinations, façade or roof inclinations respectively, in dependence to contribution strategy and technology. Likewise, structural inclination of  $30$  to  $60^\circ$  is recommended for high solar fraction, whereas inclination should raise up to  $90^\circ$  for high contribution in intermediate seasons. This planning recommendations can contradict sun space roof inclination, inasmuch as the deeper a sun space is, the flatter the roof constructions is to be designed in order to evite floor exceeding roof annexation points.

Contradictive to that findings, the Viessmann [75] scheme (fig.98) represents differences of annual yield related to direction and zero inclination that are considerably less. Further information on solar thermal yields in Germany as part of Central Europe is given by BDH (2011, [85]) : while an average irradiation of  $1.000 \text{ kWh/m}^2$  is provided,  $350$  to  $550 \text{ kWh/m}^2$  related to solar fraction are achievable. Correspondingly, for  $100$  to  $200$  square meter heated living space approximately  $6,5$  to  $11,5$  square meter collector aperture is required. In conclusion building skin integrated solar thermal collectors can suffer from  $30\%$  less efficiency compared to  $45^\circ$  inclined alternatives, but are enabled to provide more heating energy in intermediate seasons than a  $45^\circ$  inclined collector.

### § 3.3.1 Optimizing Periphery – Optimizing System

---

In section 1 of this chapter the major aspects of efficient solar thermal collectors have been highlighted. Innovative materials and progress in research and development will be exemplified in section 5 this chapter. However, within an entire solar system many components can influence the effective utilization energy for space heating. Hence effective energy can differ tremendously from the actual energy generated by the collector itself. What is more, *modi operandi* such as stagnation, especially in façade embedded solar thermal collectors, causes very high operation temperature, what can have influence on special thermal comfort as well.

This section describes solar systems in general, thus inspects the system periphery in particular. If periphery is engineered properly, incorporated collectors work sufficient and the most possible amount of energy collected is available to support thermal comfort in sun spaces or residential spaces.

In this context it is necessary to identify different components as system periphery, to define a recommended function and to determine the impact poor functionality can have on the system efficiency. System efficiency is defined as the ratio of energy output and component specific efficiencies. All components reduces the maximum energy output to the actual effective energy by specific factors. Consequently, the total system efficiency always is lower than any single part degree.

However, different to the system efficiency is the overall system performance. If a heating system is based on two different heating energy generators (bivalent mode), i.e., a gas heating and a solar thermal collector, the system performance of the gas heater decreases, though the overall system performance enormously increases. Identifying system elements begins with solar thermal collector itself. Besides, the literal collector efficiency can be determined, malfunction related operation can turn high area specific irradiation into not worth mentioning energy output. This especially happens with stagnation. Stagnation is defined as a stop in flow of energy between collector and buffer tank or heat sink, i.e. consumption, although the collector temperature is sufficient in order to contribute energy in the system. Stagnation describes a status, in which a collector extremely exceeds normal and certified operation temperatures, converted energy is not being purged any longer, what finally results in overheating of the collector.

Stagnation can have different technical reasons as to mentioned :

---

- *no power supply for the system*
- *malfunction of circulation pumps*
- *malfunction of distribution valves*
- *no energy demand, especially when buffer tank is charged or tank temperature closed to boiling point (100°C)*
- *obstruction in distribution pipes*
- *leakage of collector or distribution*
- *maintenance*
- *flow-rate of distribution media to low*

If stagnation occurs in a flooded system, converted heat energy causes water or water/ glycol distribution media to evaporate. In this case, temperature and pressure rises within the collector and the distribution system. Consequently, stagnation causes other technical problems within the system :

- *mechanical stress on crucial collector materials such as :*

sealants, connectors, piping , thermal insulation material and temperature sensors

- *mechanical stress such as overpressure and overheating in :*

distribution ducts, valves, gaskets, connections and the pressure equalization vessel

Additionally, stagnation results in energetic and thermal comfort forfeits and conflicts with regulatory offences of such as :

- *decreased solar fraction*
- *(if façade embedded) negative impact (radiation) on living space*
- *ordinance on pressure vessels, gas cylinders and filling plants*

Stagnation has different effects on a solar thermal system. If stagnation temperature of a collector is determined to be above 100°C, boiling temperature of water, stagnation turns distribution media (water) into steam. While water changes the state of aggregate, the volume of the distribution media since being gaseous tremendously increases. Thereby, system pressure rises significantly.

Eventually, exaggerated system pressure causes break down, so as to hot water and hot steam exit the closed distribution system. This exit can have harmful impact on humans and constructions, if collectors are integrated in building skins and adjoin directly to living spaces.

Summarized so far, a proper and optimized periphery is essential for a proper system operation and avoidance of system break-down and harm to human and construction. However, in this context, solar thermal collectors embedded in 90° inclined facades, i.e. vertical facades, are predestined for heating energy generation during intermediate periods of the year, e.g. autumn and spring. Just in autumn and spring solar irradiation in general loses intensity and heating energy inquiry rises. Precisely because of these specific reasons stagnation in 90° inclined facades rarely happens.

Effects of stagnation on the system as already identified as mechanical stresses are defined by Viessmann [75] as a.) maximum steam volume, b.) range of steam and c.) power of steam production. The maximum steam volume  $V_d$  is the evaporated water volume what can be covered by the expansion vessel as part of the system. This volume totally depends on the specific solar thermal customized plant, inasmuch as defined by the sum of duct volume and expansion vessel volume. Insofar, in terms of security, the expansion vessel is to be designed to cover more than maximum steam volume of the defined water volume.

Similar to the maximum steam volume is the range of steam. The range of steam is defined as the length within solar tubing, that is affected by steam in case of stagnation. The length is related to heat losses with a standard 100 per cent thermal insulation that causes condensation within tubing. Is the range of steam higher than the maximum steam volume, the steam will completely fill the expansion vessel and results in destruction. Membranes of expansion vessels normally manage to be in touch to temperatures of maximum 70°C.

*Range of steam*  $DR_{max}$

$$DR_{max} = DPL_{max} \cdot A_{coll} \cdot q_{tube} \quad (23)$$

where is :

$DR_{\max}$  : maximum steam range [m]

$DPL_{\max}$  : maximum power of steam production in [W/m<sup>2</sup>]

$A_{\text{coll}}$  : aperture area in [m<sup>2</sup>]

$q_{\text{tube}}$  : heat transmission losses of tubing in [W/m]

Viessmann (2008) defines additionally the power of steam production, that expresses the power in W/m<sup>2</sup> a solar tubing is effected in case of stagnation. The maximum power is related to the specific drain back behavior of the collectors, the hydraulic design, (serial or parallel) and the collector field geometry.

Stagnation and solar fraction are closely related to each other. Thus, stagnation reduces solar fraction. And conversely, an intended high solar fraction promotes stagnation in general. Thus we can see, that system design strongly determines system efficiency.

### § 3.3.1.1 Thermal losses by distribution piping and string components

---

A different influential factor of system design is thermal insulation of piping and armatures. Armatures by nature show clunky design and dimensions. Additionally, armatures of mostly are made of metal or metal-casts that embody high thermal conductivity. Hence, comparably high thermal losses by radiation are typical for string components. Consequently, effective thermal insulation is indispensable for string components. Similarly, distribution piping besides 100 per cent thermal insulation normally tends to suffer from length specific thermal losses of 25 W/m for 12x1, 5x1 and 18x1 diameters and from 30 W/m for 22x1 and 28x1,5 diameters [75].

That indicates, that a 10 m distribution pipe length from collector to buffer tank per se loses as far as 300W. In terms of vacuum tube collectors, the energy of the first 4 1,00 m evacuated tubes principally is lost in order to compensate thermal losses.

Thus, we can see, that the degree of energy within a solar thermal system rises with every meter of distribution piping.

### § 3.3.1.2 Exergy increase related to operation pressure and modified distribution medium

A conceptual crucial aspect of highly sufficient integral solar thermal façades is the maximum feasible temperature of the distribution medium. The distribution medium solely transports amount of energy in general that prior to this is generated by collectors. Thus, medium temperature never is higher than the actual absorber or condenser temperature, as well as rather lower. In order to increase annual yield, exergy is to be maximized by system efficiency. In residential or commercial low-temperature systems water mainly constitutes the major fraction of a distribution medium. Typically, water evaporates if exceeding 100°C. Hence liquid medium turns into steam, and correspondingly, pressure and steam volume increases in the piping system. Actually, in this moment, the system stagnates, since distribution pumps do not manage to circulate steam. While system temperature increases, in case of solar thermal collectors the exergy above an operating temperature of 100°C decreases.

operation mode vs. exergy and risks	T <sub>max oper.</sub> in liquid state	stagnation	exergy	impact on interior thermal comfort facade distribution	risk for	
					human health	structure
water + minimal pressure (1bar)	0 to 100°C	elevated	limited	X	X	X
water + additives + minimal pressure (1bar)	-15 to 120 °C	limited	elevated	XX	XX	X
water + additives + enhanced pressure (< 3,5bar)	-15 to 150 °C	minimized	optimized	XXX	XXX	XX

FIGURE 3.17 Enhanced exergy by enhanced operation mode in distribution vs. operational risks

The before mentioned context illustrates the necessity to design systems, which work sufficiently even with operation temperatures beyond 100°C. In this context operation pressure and medium additives and modifiers help to preserve the distribution medium in liquid state with defined volumes. Although, water can be replaced by thermal oils in matters of solid liquid state and constant liquid volume, certainly thermal oils typically are apply to systems with system temperature far beyond 250°C. Normally, water is recharged during winter time by alcohols like glycols as anti-freezing agent.

Among this, added polypropylene glycols enable water to be operated in liquid state even with operation temperature of approximately 150°C. Parallel, operation pressure needs to be raised up to 3,5 bar in order to evite evaporation. As a result, water based but recharged distribution medium still operates in liquid state and distributes maximized exergy of the collector system, while preventing the collector and the distribution itself from stagnation.

However, this technically secured exergy results in a massive thermal impact for the distribution system lead through out a building skin structure. Both, high temperature and high pressure cause immediate danger for human, i.e. space occupants, and the bearing construction as well. On account of this persistent risk (Fig.3.17) during operation, in case of average space occupants can firstly be affected by high temperature medium and may suffer from incineration and secondly by pressurisation, that causes physical damage. Moreover, an average may cause the façade structure to collapse, what additionally may affect the bearing structure to be partly devitalized.

Thus, we can see, that system optimization immediately has effect on health and security. In consequence, piping and connections need to be highly pressure-proofed and extremely thermally insulated in order to avoid thermal losses that inferentially thermally stress und weak constructive parts.

### § 3.3.1.3 Circulation pump pulsing determines auxiliary energy efficiency, thermal comfort and yield

---

Energy generated by collectors is distributed to a buffer tank or to consumers by a circulation cycle. Circulation pumps circulate the transport medium, when temperature difference between source and sink is sufficient, in means of normally  $\Delta T > 8-10$  K. If the collector in general do not constantly generate feeding temperatures of sufficient temperature difference, or if the collector is cooled too vast by extraordinary high transport volumes, i.e., a disproportional flow, the circulation pump pulses.

In fact, a solar thermal system in general and alternatively integrated in building envelopes works optimal in manifold aspects, if circulation pumps constantly operate.

Pulsing pumps significantly determine the efficiency ratio of consumed auxiliary energy, minimize annual yield and conversely effect interior thermal comfort. Distribution medium remains locally within the system and cools down. Thus, a constant feeding temperature is not given. By each time, distribution medium starts circulating, cooled down volumes enters the buffer tank or the consumer and decreases

energy. In consequence “a”nergy rises and system efficiency lowers. What is more, the annual yield simultaneously lowers. From this we can infer that, the utilized amount of auxiliary energy for circulation pumps less sufficient compared to a long period running system. The ratio of distributed energy to auxiliary energy is comparably worth.

At the same time, if distribution is incorporated in building envelopes and part of the building skin, distribution medium with continuing changing medium temperature stresses all system components and may cause changes in space adjoined surface temperatures. This changes result in thermal discomfort.

Similar to pulsing the medium flow rate in  $l/m^2h$  or  $kg/m^2h$  is decisive for a collector plant efficiency. Literature and practice distinguish between low-flow and high-flow. Low-flow is limited to 15-20 l per square meter collector plant and hour by Weiß, Eder, Fink and Streicher (1997) [87] that is equal to 8 to 18  $kg/m^2h$ , whereas Viessmann [75] sets limits to 30  $l/m^2h$ . Opposed to that, high-flow is defined as a volume of 30 to 40  $l/m^2h$  or 35 to 70  $kg/m^2h$  [89]. Differently to these two categories “matched flows” often vary between low and high flow, especially if a striation storage tank is applied. Characteristically, lowered low-flow causes overheating and lowers collectors efficiency ratio; causes eventually stagnation. Furthermore, provided that several collectors are hydraulically arranged in serial order, the last collectors tend to overheat and stagnate (Streicher, Heimrath, Zauner, Mach, 2015, [99]), further pressure losses ascend, whereas collector efficiency descends. On the contrary, if collectors are driven with high-flow, exergy and auxiliary energy efficiency ratio decrease. Conversely, a low-flow systems benefits from tiny tube diameters, smaller circulation pump dimensions, circulation pump energy savings and reduction of thermal losses related to pipe diameter.

In conclusion pulsing firstly lowers system efficiency, but additionally, what is crucial for façade embedded collector systems, secondly causes thermal stress for humans and construction. In terms of construction, thermal stress effects the collector itself (joining, sealings, cover glasses), the piping system (connectors, thermal elongation, the surge tank), and the façade construction (elongation of bearing parts and connections).

### § 3.3.2 The f-chart

---

Considering system efficiency, one method has established to tabular illustrate and compare monthly solar gains, heat consumption, auxiliary energy demand, system efficiency and solar fraction. The f-chart by Weik combines all these aspect as being

shown in Figure 3.18. This example shows tap water generation by a 6m<sup>2</sup> flat plate collector plant, what is south directed and 60° inclined. In this example the storage volume contents 300 l, the heat exchanger efficiency is defined with 300 W/K and tap water demand is determined with 200 litre per day.

<b>ENERGY / MONTH</b>	<b>Monthly sum of irradiation [kWh]</b>	<b>Heating Energy Demand [kWh]</b>	<b>Auxiliary Energy [kWh]</b>	<b>Solar Energy Utilisation [kWh]</b>	<b>System Efficiency [%]</b>	<b>Solar Fraction [%]</b>
January	179	238	228	10	5	4
February	277	215	150	64	23	30
March	514	238	87	151	29	63
April	660	230	37	193	29	84
May	826	238	4	233	28	98
June	865	230	0	230	27	100
July	800	238	0	238	30	100
August	804	238	0	238	30	100
September	576	230	46	184	32	80
October	383	238	121	117	30	49
November	215	230	191	39	18	17
December	144	238	238	0	0	0
<b>Annual Sum / Average [kWh]</b>	<b>6.243</b>	<b>2.801</b>	<b>1.102</b>	<b>1.697</b>	<b>Ø 27</b>	<b>Ø 61</b>

FIGURE 3.18 Example for f-chart in account for solar thermal tap water generation [72]

### § 3.3.3 Summary

Stagnation has been identified as a crucial operation modus of solar thermal collectors. Stagnation minimizes collector efficiency as well harms the entire system and what is more in terms envelope embedded solar thermal collectors, actually impacts on the façade construction and indoor thermal comfort.

For that reason several periphery components as well as the collector operation during summer need optimal design and control in dependence to an effective heat sink. This heat sink either can be the actual space to be heated or a short term or long term energy storage. The impact, stagnation can have on the system, becomes significant

in respect to façade construction integrated distribution piping. Thermal stress on construction and space comfort has been detected as crucial design point and requires attentive and dynamic planning.

---

### § 3.4 Concurrent embedded collector technology : status quo

---

As already established in the market for on-roof application, renewable energy collectors are to be categorized in solar thermal, photovoltaic and hybrid technologies. Whereas photovoltaic systems permanently have entered the vertical and declined building skin territory and have become properly integrated solutions within the last 15 years, especially solar thermal collectors solely found sporadic action and constituted isolated projects. Equal to solar thermal solutions are hybrid solutions that are well known for beneficial and synergetic qualities. But so far, hybrid solutions mostly have addressed single projects. That might also relate to difficult and not yet being instituted, but being developing standards for both electrical power and thermal power quality regulations.

This section surveys different solar thermal collector technologies, that firstly are already established in the market for up to forty years and secondly newly especially developed for building envelope integration. Figure 85, 86 and 88 of section 2.1 characterize efficiency and in particular thermal loss behaviour, however, this section specially calls attention for the ability of façade integration.

Integration into vertical or declined façade is to be evaluated by several different qualities, inasmuch there is to be inspected 1.) ability of annual yields [kWh/m<sup>2</sup>a], 2.) risk of thermal impact on interior thermal comfort, 3.) possible level of feeding temperature in regard to thermo-chemical seasonal storages, 4.) level, e.g. layer of façade integration, 5.) ability of façade aligned free form, 6.) ratio of provided perusal [%], 7.) level of thermal insulation, e.g. evacuation, 8.) simplicity of collector construction and design. This survey bases on detection of basic archetypes that acknowledge technical basics and fundamental distinctions. Consequently, advancements and split-off differentiations are determined as variations (e.g., V01.4).



we can infer firstly strengths and weaks and secondly, what is more of interest, concurrent insurmountable contrariness. As a result, the identified contrariness indicates further purposive demand for research and development in façade integrated collector technology. Section 5 reports technical innovations in collector design.

VARIANT	V01.1
STATUS	mass production
RATIO OF PERUSAL	perusal : 0%
TYPOLGY	evacuated flat collector
1. MEDIUM / TRANSPORT FLUID	directly flooded, water-glycols
FRONT COVER	glazed
FRONT COVER QUALITY	anti-reflecting+prismatic cover sheet or anti-reflecting 4 mm tempered low iron
ABSORBER TECHNOLOGY / QUALITY	highly selectiv coated copper absorber
HEAT EXCHANGER TYPOLOGY	meander-shaped copper heat exchang
QUALITY OF VACUUM	evacuate, < 100 mbar
THERMAL INSULATION	back-sided thermal insulation
CASING	alumina case, Krypton filled, 100 mm
TYPE OF ENVELOPE INTEGRATION	0° declined roof, mansard roof solid external wall rear ventilated stck-facade
RATIO OF FLEXIBILITY	standard dimensions, linear
FACADE INTEGRATED STORAGE	none
CONVERSION FACTOR $\eta_0$	0.853 Thermosolar
COLLECTOR EFFICIENCY RATIO $\eta$ at $\Delta T=40K$	0,724
TRANSMISSION COEFFICIENT $a_1$ [W/m <sup>2</sup> K]	3,2 to 4,688
TRANSMISSION COEFFICIENT $a_2$ [W/m <sup>2</sup> K]	0,0043 to 0,008
INTERNAL ABSORBER CONDUCTANCE $U_{int}$ [W/m <sup>2</sup> K]	147
TRANSMISSION COEFFICIENT $a_{1+2}$ [W/m <sup>2</sup> K]	-
SOLAR NORMAL FACTOR	0.95 at K50
EVALUATED SURFACE TEMPERATURE $T_{surf} / T_1$ [°C]	$T_{surf} = ambient, space \Delta T = 0 K$

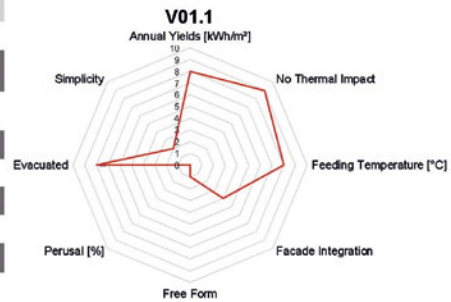
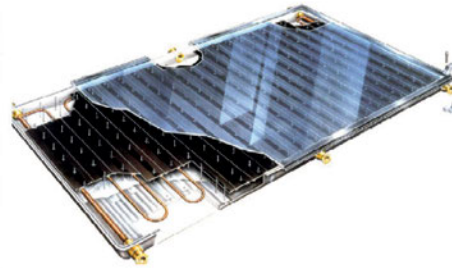


FIGURE 3.20 Performance profile – enhanced evacuated flat plate collector

The contrariness identified in section 4 are preparations for section 5 as well as they commit further subjects of development. Variant V01 represents a premium standard glazed flat plate collector. Premium standard glazed flat plate collector are characterized by front sheet glazing of low-iron and anti-reflectively quality. Front sheets made from solar glass enhances solar transmittance and lowers reflection

by prismatic glass. Anorganic absorbers with selective coatings and high internal conduction values optimize conversion. But, however, related to single front glazing and moderate case backside thermal insulation non-evacuated premium standard flat plate collectors provide moderate performance ( $\eta = 0,27$  to  $0,47$  at  $\Delta T = 60K$ ,  $G = 1.000 \text{ W/m}^2$ ) (Fig. 3.19) due to high thermal losses. While casing depth normally does not exceed 60 to 70 mm, integration into solid building envelope elements normally causes no problems. Considering both limited thermal insulation depth of 50 to 60 mm of common mineral wool insulation and non-evacuated casing, an additional rear ventilation cavity of 60 to 100 mm within the solid building skin is recommended. Significant impact on internal thermal comfort has been verified by different authors (see 3.6.1), inasmuch even rear ventilated solutions causes internal surface temperatures above 32 to 39°C. Integrating premium standard non-evacuated glazed flat plate collectors in post & beam or stick-system facades is manageable within post partitions, but hardly within glazing substitutions. This is related to a 60 mm depth. Further, the construction principle does not allow any perusal or any free-form design at all. Although, this collector type commonly provides advanced annual yields, it is neither the simplest nor provides sufficient feeding temperature for state-of-the-art thermo-chemical seasonal storages ( $< 100^\circ\text{C}$ ).

Standardized glazed flat plate collectors has been enhanced in terms of internal thermal insulation. With Krypton gas filling internal convection has been minimized or even eliminated by case evacuation down to 100mbar remaining pressure. Furthermore a raise in thermal insulation depth up to 70 mm additionally reduces backside transmission losses. This design actions firstly result in considerably higher collector efficiency  $\eta$  with up to 0,72 ( $\Delta T$  40 to 60K,  $1.000 \text{ W/m}^2$ ) and  $a_2$  of  $< 0,008 \text{ W/m}^2\text{K}^2$  and secondly demonstrably higher annual yields (Fig.3.20). Beside façade integration into solid building skin elements acts similarly to V01, integration into post & beam or stick-systems becomes more difficult regarded to higher collector depths (100mm). However, perusal or free-form design aligned to modern architecture is still a drawback.

Nonetheless, above elucidated design advancements inevitably results in higher feeding temperature, but contrarily in no worth mentioning internal thermal impact.

VARIANT	V01.2
STATUS	mass production
RATIO OF PERUSAL	perusal : 0%
TYPOLOGY	<i>ultra high evacuated flat collector</i>
1. MEDIUM / TRANSPORT FLUID	directly flooded, water-thermo-oil
FRONT COVER	glazed
FRONT COVER QUALITY	anti-reflecting, 5 mm low iron float glass
ABSORBER TECHNOLOGY / QUALITY	highly selectiv coated copper absorber, 2 mm
HEAT EXCHANGER TYPOLOGY	laser-welded meander-shaped copper heat exchanger
QUALITY OF VACUUM	<i>highly evacuated &lt; 10mbar</i>
THERMAL INSULATION	backsided thermal insulation
CASING	stainless steel case (62mm)
TYPE OF ENVELOPE INTEGRATION	0° declined roof, mansard roof solid external wall stick-facade, post&beam
RATIO OF FLEXIBILITY	standard dimensions, linear
FACADE INTEGRATED STORAGE	none
CONVERSION FACTOR $\eta_0$	0,765 (0,95 * 0,91 * 0,885)
COLLECTOR EFFICIENCY RATIO $\eta$ at $\Delta T_{=60K}$	0,74 to 0,77 (60 K, 1000 W/m²)
TRANSMISSION COEFFICIENT $a_1$ [W/m²K]	0,508
TRANSMISSION COEFFICIENT $a_2$ [W/m²K²]	0,007
INTERNAL ABSORBER CONDUCTANCE $U_{int}$ [W/m²K]	3,91
TRANSMISSION COEFFICIENT $a_{40 / 60}$ [W/m²K]	-
SOLAR NORMAL FACTOR	0,926 at K50 (0,70 at K70)
EVALUATED SURFACE TEMPERATURE $T_{surf} / T_i$ [°C]	$T_{surf} = \text{ambient, space } \Delta T = 0 \text{ K}$

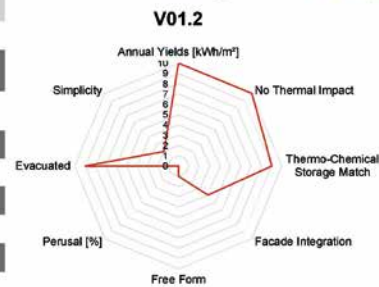
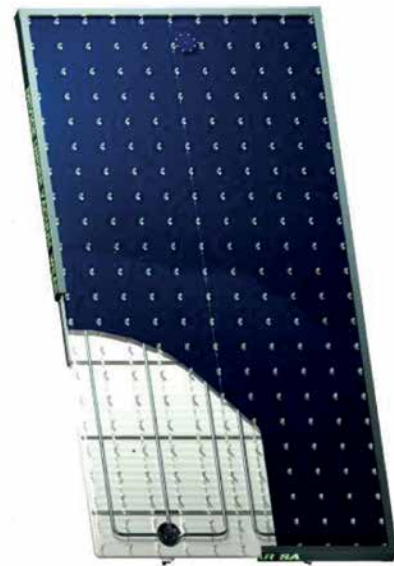


FIGURE 3.21 Performance profile – superior evacuated flat plate collector

Feasible feeding temperature is far above 100°C and, thus, in general appropriate for thermo-chemical storage charging. While this design is explicitly evacuated, the construction principle is far away from simplicity. In regard to evacuation a strict pat-tern of nominal pressure bearing metal pins is required to prevent front glazing from implosion.

VARIANT	V01.4
STATUS	mass production
RATIO OF PERUSAL	perusal : 0%
TYPOLGY	flat collector + reflector CPC
1. MEDIUM / TRANSPORT FLUID	directly flooded, water-glycols
FRONT COVER	glazed
FRONT COVER QUALITY	4 mm anti-reflecting+prismatic low iron cover sheet
ABSORBER TECHNOLOGY / QUALITY	highly selective coated perpendicular copper absorber + rolled and galvanic anodized mirror reflector
HEAT EXCHANGER TYPOLGY	harp-shaped copper heat exchanger
QUALITY OF VACUUM	partly evacuated, 300mbar
THERMAL INSULATION	no backsided thermal insulation, but absorber upheating by CPC mirrors
CASING	alumina case, 65 mm
TYPE OF ENVELOPE INTEGRATION	declined roof, mansard roof solid external wall post&beam
RATIO OF FLEXIBILITY	standard dimensions, linear
FACADE INTEGRATED STORAGE	none
CONVERSION FACTOR $\eta_0$	0,74
COLLECTOR EFFICIENCY RATIO $\eta$ at $\Delta T_{ext}$	-
TRANSMISSION COEFFICIENT $a_1$ [W/m <sup>2</sup> K]	3,3
TRANSMISSION COEFFICIENT $a_2$ [W/m <sup>2</sup> K <sup>2</sup> ]	0,012
INTERNAL ABSORBER CONDUCTANCE $U_{int}$ [W/m <sup>2</sup> K]	20,0
TRANSMISSION COEFFICIENT $a_{t0/80}$ [W/m <sup>2</sup> K]	-
SOLAR NORMAL FACTOR	1,02 at K50°
EVALUATED SURFACE TEMPERATURE $T_{surf} / T_i$ [°C]	$T_{surf} > 45^\circ C$

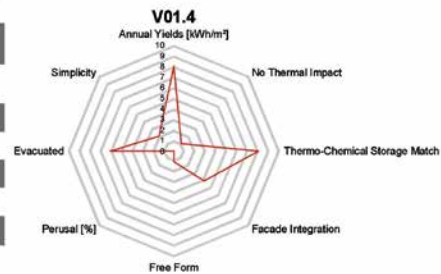
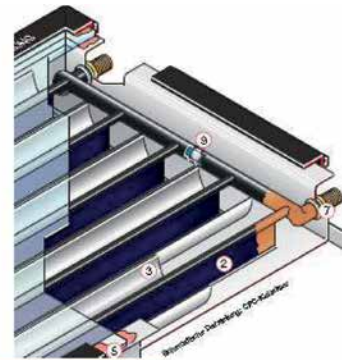


FIGURE 3.22 Performance profile – partly evacuated CPC flat plate collector

The thermal performance of collector type V1.1 can enormously be boosted (Fig. 3.21) by a high level evacuation of the case. Variant V1.2 exemplifies a feasible evacuation level of less than 10 mbar remaining pressure. Thereby, both the efficiency can be raised for 7% up to  $\eta = 0,77$  ( $\Delta T = 60K$ ,  $1.000 \text{ W/m}^2$ ) and  $a_1$  and  $a_2$  can be lowered to  $0,5 \text{ W/m}^2K$  and  $0,007 \text{ W/m}^2K^2$ . These characteristics approximate typical values of

evacuated tube collectors. Especially,  $a_1$  improves for 700 to 800%. Consequently, an improvement in thermal performance leads to comparably higher possible annual yields among higher frequencies of charging eligibility of thermo-chemical seasonal storages.

VARIANT	V01.4
STATUS	mass production
RATIO OF PERUSAL	perusal : 0%
TYPOLOGY	flat collector + reflector CPC
1. MEDIUM / TRANSPORT FLUID	directly flooded, water-glycols
FRONT COVER	glazed
FRONT COVER QUALITY	4 mm anti-reflecting+prismatic low iron cover sheet
ABSORBER TECHNOLOGY / QUALITY	highly selectiv coated perpendicular copper absorber + rolled and galvanic anodized mirror reflector
HEAT EXCHANGER TYPOLOGY	harp-shaped copper heat exchanger
QUALITY OF VACUUM	partly evacuated, 300mbar
THERMAL INSULATION	no backsided thermal insulation, but absorber upheating by CPC mirrors
CASING	alumina case, 65 mm
TYPE OF ENVELOPE INTEGRATION	declined roof, mansard roof solid external wall post&beam
RATIO OF FLEXIBILITY	standard dimensions, linear
FACADE INTEGRATED STORAGE	none
CONVERSION FACTOR $\eta_0$	0,74
COLLECTOR EFFICIENCY RATIO $\eta$ at $\Delta T=40K$	-
TRANSMISSION COEFFICIENT $a_1$ [W/m <sup>2</sup> *K]	3,3
TRANSMISSION COEFFICIENT $a_2$ [W/m <sup>2</sup> *K <sup>2</sup> ]	0,012
INTERNAL ABSORBER CONDUCTANCE $U_{int}$ [W/m <sup>2</sup> *K]	20,0
TRANSMISSION COEFFICIENT $a_{tot / 60}$ [W/m <sup>2</sup> *K]	-
SOLAR NORMAL FACTOR	1,02 at K50°
EVALUATED SURFACE TEMPERATURE $T_{surf} / T_i$ [°C]	$T_{surf} > 45^{\circ}C$

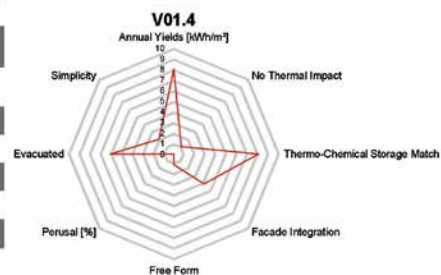
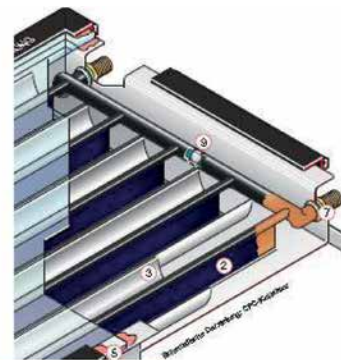


FIGURE 3.23 Performance profile – unglazed uncased free-form flat collector

While the quality of façade integrated perusal and free form remain at zero, in particular post & beam and stick-system façade incorporation offers to be more attractive and capable with 62 mm depth compared to V1.1. Although possible thermal impacts to internal thermal comfort can be neglected, this glazed flat plate collector design represents one of the most complex.

Since, vacuum in collectors degrades and dissolve within several years, possible re-evacuation of façade embedded vacuum collectors results in a substantial effort of maintenance. A completely different flat plate collector technology opposed to variant 01 represent unglazed flat plate collectors. Fundamental trait is the omission of front glazing and casing. The absorber is in direct contact with the environment. This design embodies both benefits and drawbacks in terms of architectural and thermal

performance quality (fig. 3.23). Since front glazing and casing are omitted the absorber on the one hand is free for free forming and for superior integration into building skin envelopes.

VARIANT	V03
STATUS	mass production
RATIO OF PERUSAL	perusal : 0%
TYPOLOGY	<i>polymer absorber flat collector</i>
1. MEDIUM / TRANSPORT FLUID	directly flooded, pure water
FRONT COVER	unglazed
FRONT COVER QUALITY	10 mm twin-walled Polycarbonate sheet, UV-stabilized
ABSORBER TECHNOLOGY / QUALITY	black coated polyphenylene sulfide absorber including heat exchanger
HEAT EXCHANGER TYPOLOGY	absorber = heat exchanger
QUALITY OF VACUUM	not evacuated
THERMAL INSULATION	backsided thermal insulation
CASING	alumina case, anodized, 65 mm <i>drain-back system</i> declined roof, mansard roof solid external wall post&beam
TYPE OF ENVELOPE INTEGRATION	post&beam
RATIO OF FLEXIBILITY	customizeable, linear
FACADE INTEGRATED STORAGE	none
CONVERSION FACTOR $\eta_0$	0,77
COLLECTOR EFFICIENCY RATIO $\eta$ at $\Delta t=60K$	-
TRANSMISSION COEFFICIENT $a_1$ [W/m <sup>2</sup> K]	3,0
TRANSMISSION COEFFICIENT $a_2$ [W/m <sup>2</sup> K]	0,035
INTERNAL ABSORBER CONDUCTANCE $U_{int}$ [W/m <sup>2</sup> K]	80,0
TRANSMISSION COEFFICIENT $a_{40 / 60}$ [W/m <sup>2</sup> K]	-
SOLAR NORMAL FACTOR	-
EVALUATED SURFACE TEMPERATURE $T_{surf} / T_i$ [°C]	$T_{surf} = <40°C$

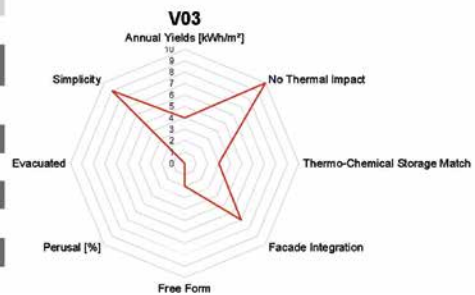
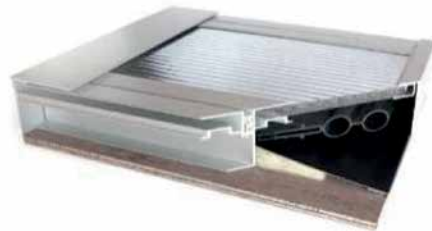


FIGURE 3.24 Performance profile – polymer flat plate collector

The absorber is able to be curved and bended to follow spherical facade outlines. On the other hand the absorber itself composes the buildings skin and thus a weather shield.

A collector design with-out any transparent front cover commonly encounters no optical losses related to fraction, reflection or absorption (>0,99 at K50°), however thermal losses by radiation are tremendous. The power performance of unglazed

lowers by time regarding overaveraged material degradation by oxidation and environmental pollution. Although optical conversion easily exceeds 0,93, the collector efficiency of  $\eta = 0,42$  ( $\Delta T = 60K$ ,  $1.000 \text{ W/m}^2$ ) is significantly lower compared to variant VO1 due to  $a_1 = >9,5 \text{ W/m}^2K$  and  $a_2 = >3,5 \text{ W/m}^2K^2$ . Beside extraordinary benefits covering façade integration and free-form and simplicity, possible annual yields are considerably lower compared to normal glazed flat plate collectors.

While feeding temperatures are far away from being sufficient for thermal-chemical seasonal storages, a possible negative impact on internal thermal comfort is not to be apprehended. Since this collector design, which bases on a single absorber misses any structural strength, a secondary bearing structure is a prerequisite for incorporation and running in building envelopes. That structural circumstance combined with the intransparency of the absorber prohibits any quality of perusal.

Since the above illustrated glazed flat plate collector is simply covered by twin-walled UV-stabilized polycarbonate (Fig.3.24) [100, 101] and bases on a non-selectively coated polymer tailor-made absorber, this collector designed institutes a different typology. Reasons for polycarbonate covering and polymer absorbers are simplicity and customer friendly dimensions. This alumina cased and backsided collector type is easy and labour effective in terms of production, since bulk stock wrought material can be manufactured on demand. Thus, architectural qualities recover to be uncomprably high. Although the conversion factor  $\eta_0$  of 0,77 is considerably high and  $a_1 = 3,0 \text{ W/m}^2K$  and  $a_2 = 0,035 \text{ W/m}^2K^2$  are on superior level, the estimated collector efficiency  $\eta$  of  $< 0,2$  is moderate. Feeding temperature level normally does not exceed  $40^\circ\text{C}$  to  $50^\circ\text{C}$ , what first causes no thermal impact on spacial comfort and secondly is not in account for charging of seasonal thermo-chemical storages. The ability of envelope incorporation is given by a maximum casing depth of solely 65 mm. Especially solid building elements and post&beam partitions benefit from those slim dimensions. However, this design allows either perusal nor free-form integration. Annual yields are expected to excel those of simple pool absorber considerably, but will not compete with simple glazed flat plate collectors by far.

While before exemplified collector typologies distinctively arise from the cased standardized plug-on mass production field, especially this type is strongly determined by façade design and façade parameters. This type bases [102] opposed to cased or tubed mass production derivatives on double or lately on triple glazing (Fig. 3.25). Absorber and heat exchanger are located within a double glazing unit.

Thus, integration in a transparent building envelope is incom-parably higher than contrasted with standardized cased or tube variants. Since being in fact a double glazing, the layer of integration is far away from simply application.

Although the ability of free form in this context is not given, yet collector dimensions can be adapted to the greatest possible extend to individual façade layout. Furthermore, horizontally arranged absorber sheets in double glazing allow a certain quality of perusal. This quality is estimated to 20 per cent.

VARIANT	V04
STATUS	mass production
RATIO OF PERUSAL	perusal : 20%
TYPOLOGY	double glazing as flat collector
1. MEDIUM / TRANSPORT FLUID	directly flooded, water-glycols
FRONT COVER	glazed by double-glazing
FRONT COVER QUALITY	anti-reflecting, low-iron tempered 4 m cover sheet, 85% Argon filled
ABSORBER TECHNOLOGY / QUALITY	highly selectly coated copper shading lamellas utilized as absorber, harp-shaped
HEAT EXCHANGER TYPOLOGY	no heat exchanger
QUALITY OF VACUUM	not evacuated
THERMAL INSULATION	Low <sub>e</sub> -coating #3 as space sided thermal insulation
CASING	not cased, 2 level Polyisobutylene and PUR or PS sealant, window-framed
TYPE OF ENVELOPE INTEGRATION	solid external wall, stick system post&beam, high rise
RATIO OF FLEXIBILITY	customizeable, linear
FAÇADE INTEGRATED STORAGE	none
CONVERSION FACTOR $\eta_0$	0.53
COLLECTOR EFFICIENCY RATIO $\eta$ at $\Delta t=100K$	-
TRANSMISSION COEFFICIENT $a_1$ [W/m <sup>2</sup> K]	4.6
TRANSMISSION COEFFICIENT $a_2$ [W/m <sup>2</sup> K <sup>2</sup> ]	0,0351
INTERNAL ABSORBER CONDUCTANCE $U_{int}$ [W/m <sup>2</sup> K]	6.82
TRANSMISSION COEFFICIENT $a_{40 / 60}$ [W/m <sup>2</sup> K]	
SOLAR NORMAL FACTOR	0.95 at K50° (>0.76 at K70°)
EVALUATED SURFACE TEMPERATURE $T_{surf} / T_f$ [°C]	$T_{surf} = 68^{\circ}C$

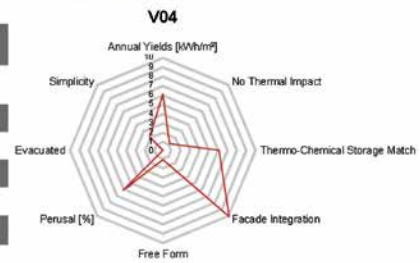
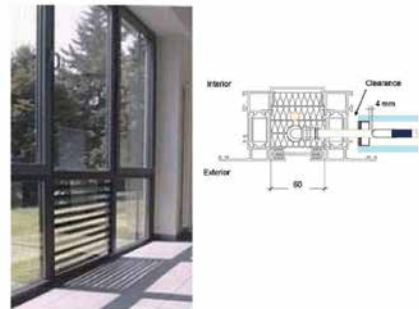
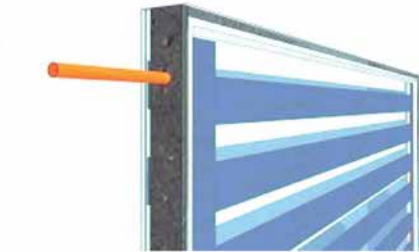


FIGURE 3.25 Performance profile – tripe-glazing collector with limited perusal

However, this collector is neither evacuated nor physically thermally insulated alike cased collectors. Consequently, notwithstanding that feeding temperature during stagnation exceeds 115°C, annual yields are lower than 450 to 500 kWh/m<sup>2</sup> per year.

That is firstly related to the moderate conversion factor of  $\eta_0 = 0,53$ , which expresses under averaged conversion abilities related to aperture area. But secondly, thermal losses to the environment, in particular to spaces have empirically been verified (Ch.02)

by space aligned glass sheet surface temperature of > than 60°C. In consequence, this smart collector design encounters deficits in power and thermal performance by reason of absent thermal insulation. Simply low coatings and 85% inert gas (argon) filling reduces losses in distinct spectral manner.

In this regard the ability to provide sufficiently high feeding temperature in order to charge seasonal thermo-chemical storages is limited. Since piping penetrates spacer and sealant this design is not simple.

### § 3.4.1 Summary

---

Initially to this section several essential key parameters were defined, which help characterizing and validating diverse collector technologies for collectors to be used in building facades. So far, this section elaborated diverse solar thermal collector technologies, which have established on the market and have been successively developed further and enhanced. Either transmission losses or optical performance were subject of improvements and resulted in highly effective but complex collector typologies. Nonetheless, nearly all typologies either were conventional standard-sized solar thermal collectors or essential parts were integrated in façade parts like glazings. However, these demonstrated variants mainly lack from origin eligibility for façade integration, rather have been applied to facades [103].

Thus, the survey illustrates beside proper power efficient solutions, that collectors still encounter holistic planning for facades. Moreover, the major fraction encounters essential key parameters as perusal, free forming, simplicity next to high efficiency and risk of thermal impact.

---

### § 3.5 Thinking about polymers

---

Life cycle consideration [104] on solar thermal collectors helps to design collectors in holistic energy sufficient matter. This section in particular focus on the material component in regard of ecological exploitation of raw material, simplicity in process engineering of wrought material, distribution energy, installation and reliability in respect of life span duration. As crucial components of solar thermal collectors have been identified :

- *transparent cover sheet,*

- *absorber and*

- *heat exchanger*

For glazed collectors transparent cover sheets mainly protects the absorber and its coating from environmental influences. Influences like acids, pollution, mechanical stresses like hail and rain and wind either negatively influence the efficiency of the absorber or the durability. Protection against wind in particular reduces considerably thermal losses by convection and disproportionally enhances efficiency. Commonly, since cover sheets substantially have to provide superb light transmission and mechanical resistance as well, they are made from glass. Glass for collector covering needs to be toughened and tempered. Since glass is an area-wise specific and energy intensive component, application has to be optimized.

The absorber as the core component of solar thermal collectors embodies the main function to convert irradiation into thermal utilizable energy. Therefore the conversion properties are crucial by means of efficiency. At best, absorbers enjoy area-wise optimization and spectrally selective treatment. This treatment bases on an optimum absorption / emission ratio and thus strongly requires advanced process engineering like chemical treatment and electro-magnetic or vacuum deposition sputtering. Heat conduction is the main required purpose of absorbers. The generated heat is to be concentrated to several points where it is exchanged to a transportation liquid. For this reason absorbers are commonly made from metals like copper or alumina. Area-wise optimized absorber sheets and harped- or meander-shaped heat exchanger tubing generally base on copper or alumina coil or tubing ware. Since the exploitation of superiorly conducting metals copper and alumina are labour intensive and

considerably harmful for the environment, they require sustainable and waste optimized utilization. Additionally, since copper resources are finite, application needs to be deliberate and limited. In the context of TASK 39 Solar Heating & Cooling program "SHC Polymeric materials for solar thermal applications" (2015), simulation scenarios reveal that by 2050 the annual copper demand for copper absorbers will be raised to 4.7 million tons what equals 31% of the annual copper mining capacity in 2006. This indicates against the background of the 2020 or 2030 Zero Energy building programme, that first the copper demand for absorbers will tremendously raise and secondly, that at a certain point in the near future copper apportionment for absorbers cannot be in line with the demand.

The consideration above illustrates that cover sheets made from glass and absorbers and heat exchanges made from copper or alumina incorporates massive amounts of primary energy for manufacturing and requires advanced amounts of primary energy for transportation in respect of weight. Köhl, Meir, Fischer and Wallner (2014) [105] determine a cost saving potential of material and manufacturing of overall 26% by polymer. Because of this (Fig.3.26), it is sensible to elicit about substitution of glass, copper and alumina in solar thermal collectors. Thus, researchers identified tremendous potential for polymers to substitute crucial collector components.

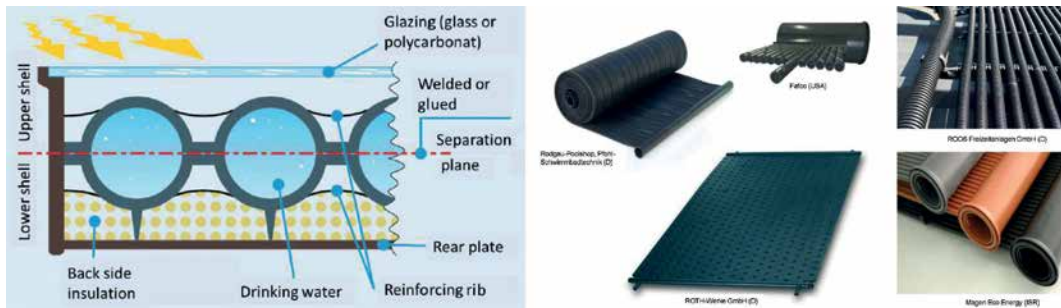


FIGURE 3.26 a.) Integrated collector storage system with injection moulded meandric absorber, SCOOP Newsletter 6/2013 (2013), b.) Holzhaider, K., Wallner, G., Kicker, H., Lang, R., (2015) [106]

Besides diverse benefits of polymer materials as collector components one major drawback has been detected, that complicates and limits the application in thermal collectors. Polymers, especially transparent polymers, encounter limited thermal resistance in regard of solar thermal application.

As elucidated in particular in section 7 absorber temperature in flat plate collectors not seldom exceeds 200 to 260°C and especially evacuated heat pipe absorbers encounter maximum temperature between 170 to 300°C. Most commodity polymer provide temperature resistance comparable to human physiological limits, respectively 30 to 100°C. Advanced technical polymer withstand temperature exposition up to 150°C, before mecha-nical and structural collapse.

Polymers especially designed to be eligible or temperature above 150° present to be cost-intensive, and hence, do not represent monetary attractive alternatives to glass and metals. A different but serious problem of polymers is resistance to ultra-violet irradiation. Most polymers suffer from UV weakness, inasmuch UV radiation

shorten and destroy polymeric molecule chains and thus causes structural dissolution. Exposition to UV radiation in long term perspective of 3 to 10 years inevitably results in yellowing and lowering of light transmission as well.

Whereas polymer provide indisputable resistance to acids, oxides and other corrosives [107] what glass and metals are markedly sensitive for, basic polymers especially show impairment for long lasting harsh environmental exposition.

However, lately, diverse researcher being involved in the TASK 39 Solae Heating & Cooling Program SHC "SHC Polymeric Materials for solar thermal applications" (2015) and being authors of the SCOOP Newsletter June 2013 [108] defined manifold benefits of polymers being applied to solar thermal collectors. The benefits can be categorized according different life cycle phases as being listed below :

#### a) Manufacturing

---

- *simpler constructions*
- *various joining methods : injection molding or extrusion, hot-plate welding, infrared welding*
- *injection molding or extrusion allows complex façade shapes*
- *less spare parts*
- *better customizable, size tailor-made*
- *higher design flexibility*

#### b) Transportation

---

- *light weight components, weight and energy reduction*
- *cost reduction for shipping, handling and installation*

#### c) Performance

---

- *less material related thermal losses related to lower conduction*

- *polymeric collectors offer potential to replace conventional roofs or facades*
- *strengthening of polymers by glass fibre or nano-tube incorporation*
- *absorption performance increase by black carbon pigment incorporation*
- *co-polymers enjoy advanced UV-resistance and comparable light transmission*
- *simple unglazed collectors compete with conventional glazed and complex collectors types due to unique material performance*

#### d) Operation period

---

- *Polymers are resistant to metal-corrosion caused by chlorinated water*

In architectural, energetic and engineering matter, especially benefits concerning manufacturing process, design flexibility and collector performance and finally building skin integration are substantial for further research and development.

### § 3.5.1 Polymer cover sheets and polymer absorbers

---

When thinking about polymers different performance criteria are essential for especially collector cover sheets from polymers and absorbers/exchangers made from polymers (Fig.3.27). The main fundamental difference is defined by the ratio of environmental exposition.

While the polymer cover sheet is affected by rain, wind, irradiation, hail and chemical-aggressive and mechanical-abrasive air pollutions, the absorber principally is protected against these factors. Whereas the cover sheet is affected by temperature differences of mainly 50 Kelvin, the absorber has to withstand differences of 170 Kelvin and higher. Thus, components encounter mechanical stress, but the absorber/exchanger rather thermally involved than pressure or environmental chemistry entailed.

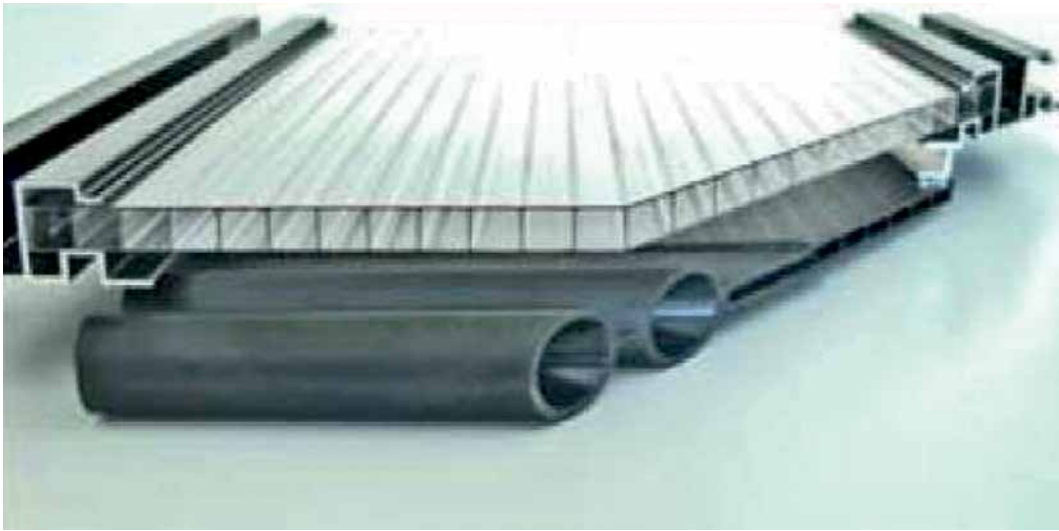


FIGURE 3.27 Construction of entirely polymeric solar thermal collector for envelope incorporation, Köhl (2011)

### § 3.5.1.1 Key performance criteria for polymer cover sheets and absorbers

---

As explained before, cover sheets from polymer ask for different key performance parameter than absorber and heat exchangers. This section firstly determines and secondly quantifies according to essential limits the different key parameters.

Polymeric cover sheets

#### Key parameters :

---

- *light transmittance LT [%]*
- *ultra-violet light resistance structural (in years)*
- *ultra-violet light resistance optical (in years)*
- *fraction index [-]*
- *abrasion resistance : shore hardness*

- *hail resistance : 40 mm*
- *temperature difference in operation  $\Delta T$  [K]*
- *chemical resistance (qualified)*

Polymeric absorbers and heat exchanger

#### Key parameters :

---

- *absorption coefficient  $\boxtimes$  [-]*
- *emission coefficient  $\boxtimes$  [-]*
- *ultra-violet light resistance (qualified)*
- *temperature difference in operation  $\Delta T$  [K]*
- *maximum operation temperature [ $^{\circ}\text{C}$ ]*
- *maximum short-time operation temperature [ $^{\circ}\text{C}$ ]*
- *melting temperature [ $^{\circ}\text{C}$ ]*
- *chemical resistance (qualified)*
- *joining by ultra-sound welding*
- *joining by bonding*

Polymeric absorbers help substituting metals and hence reduce crucial environmental impacts. In the next section most promising polymers as collector covers, hence for glass substitution will be elucidated.

Polyphenylene sulphide (PPS) has been carried out by Kahlen (2010) [109] to benefit from high thermal stability, namely higher than  $200^{\circ}\text{C}$ . Besides absorbers made from NORYL, an amorphous  $\alpha$ -polyphenyle ether polystyrene blend (PPE + PS), two other co-extruded polymers polypropylene (PP) and a polyamide (PA12) have been detected within TASK 39 Solar Heating & Cooling Programme (2015), that have been heat

impact modified and are identified to be “most promising” in solar thermal absorbers. Especially, semi-crystalline Polypropylene (PP) offers according to Holzhaider, Wallner, Kicker and Lang (2014) [106;110] a higher melting temperature of maximum 165° to 170°C. The authors put attention to the ability of Polypropylene, that can be carbon black-pigmented to enhance absorption properties of >95%.

Opposed to that Jorgensen, Brunold, Carlsson, Möller, Heck and Köhl (2003) [111] put a decade before emphasis on fluoropolymers to be used in thin-film collector designs, what have superb optical and thermal qualities, however, they are expensive.

As outstanding film products have been identified Tezel®, (ethylene-tetrafluorethylene copolymer, ETFE), Duralar® (also ETFE), Halar®, Teflon® and Kynar® by the authors with explicit high spectral transmittance of >90% actually after 2 years of extreme weathered operation and accelerated exposure. Ultra-violet stabilized materials are also polyetherimide (PEI) and polyimide (PI), polycyclohexyl-ethylene (PeCHE), notwithstanding are expensive. Most materials suffer from yellowing as result of UV radiation exposure. In this context Jorgensen, Brunold, Carlsson, Möller, Heck and Köhl [111] point out, that Duroglas® PVC degrades to UV light rapidly. Jerman (2010) [112] relegates, that characteristic low polymer absorber  $\alpha/\epsilon$  – ratios can be improved to  $\alpha = 0,9$  and  $\epsilon = 0,25$  ( $\alpha/\epsilon$ -ratio: 3,6) by silane dispersants. This dispersants modify the pigment surfaces to make them compatible with paint polymeric binder.

Jerman additionally highlights the application of thickness insensitive spectrally selective paints (TISS). Compared to conventional coatings TISS offer benefits, since they operate sufficient independently from the coating thickness (less sputter tolerances).

In the field of polycarbonates APEC 5393® from BAYER [113] both convinces with UV and heat resistance (Loumakis, G., Burek, S., Wood, B., 2013, [114]), whereas APEC 9351® is in particular thermally stabilized for persistent 180°C operation temperature and whereas APEC 9353 [115] -especially is UV-stabilized for evaluated temperatures for front sheet applications. Loumakis, Borek and Wood promote simply poor UV resistance and only low heat resistance (90°C) for Polyethylene terephthalate (PET).

On the contrary, Polyethylene Naphthalate (PEN) offers better thermal, mechanical and UV stability, but is more expensive than PET, beside the optical transmittance is low. Acrylics show UV resistance, but firstly are brittle and affective for mechanical impacts as for example hail storms, and secondly are sensitive to temperature, that is characteristic for solar thermal flat collectors.

**HIGHLY TRANSPARENT for cover sheets**

- PEEK : polyetheretherketon
- PPS : polyphenylene sulphide
- PSU : polysulfon
- PFA : perfluoralkoxyalkan
- PI : polyimide
- PEI: polyetherimide
- FEB: perfluorethylenprop
- PPE: a-polyphenyle ether
- MaLon : Makrolon
- PA : polyamide
- PMMA : polymethylmethacrylat
- PC : polycarbonate
- POM : polyoxymethylene
- FP : fluoropolymer
- ABS : acrylnitrilo-butadien-styrol
- PP : polypropylene
- PET : polyethylene terephthalate
- PE-LD : low density polyethylene
- PE-HD : high density polyethylene
- PS : polystyrene
- PVC : polyvinyl chloride

	PFA				PEEK	to 250°C	NOT TRANSPARENT for absorbers/ heat exchanger
	FP PPSU PAI APEC 1803 DP9-9373	FEB			PPS ETFE PPA	to 200°C	
	PES APEC 2097 DP9-9351	DP9-9353 PSU			PP PA 12 PEI PI LCP	to 170°C	high performance polymers
	DP9-9343 APEC 1895 APEC 1897	MaLon2405/7 PC		PVDF	PA 612 sPS PPE	to 150°C	
		PET			PA610 PA6/66 PBT POM SANi	to 130°C	engineering thermoplastic
		PET			PP EPS	to 100°C	
		PS ABS SAN PVC		PE-LD	PE-HD	to 60°C	standard plastics
	> 10 €/kg	> 4 €/kg	> 2 €/kg	> 4 €/kg	> 10 €/kg		

FIGURE 3.28 Transparent and non-transparent polymers with certain operation temperatures and prices for collector glazing and absorbers

Most plastics have been revealed to be partially transparent in near and far infra-red radiation spectrum, what causes higher radiation losses of the absorber to the environment. In consequence, 2011 OENORM EN 12975-3-1 „Thermische Solaranlagen und ihre Bauteile - Kollektoren - Teil 3-1: Qualifizierung der Beständigkeit von Solarabsorberflächen“ [116] was established.

Koch (2010) [117] explains, that modern polymers (absorbers, sealants) provide high-precision tolerances of +- 0,05 mm. Polymeric case profiles are 50% less of weight compared to aluminium cases. Loumakis refers to Dorfling et al [114], who designed a light-weight all-plastic (Aventa, Norway or ALTEN 1°, ALTEN 2A©) solar collectors that absorbers made from low density polyethylene (LDPE) are extruded as a micro-scale multi-tube extrudate with parallel arrays of hollow capillaries which are similar to honey-comb design. Analogously, pool absorber are mostly made from HDPE. This smart polymeric absorber design was in terms of overall heat-transfer performance as sufficient as common metal-based micro-scale heat exchangers (Loumakis, 2013).

Fleck-Vetter (2010) [118] explains in the context of TASK30 SHC a parabolic collector with most parts made from polyamide, polyoxymethylene and polyvinyl chloride (what weathers poorly, fast). On the market are available tube/tube absorbers made from low-cost extruded polyolefine tubes (EPDM) and different injection-molded absorber tubes made from polystyrene and acrylnitrilic-butadien-styrol (PS, ABS).

However, blow- or rotation-formed absorbers with clamped connections or welded tape absorber provide high potential for automated production processes. According to Loumakis, Burek and Wood (2013) [114] some high performance polymers in terms of thermal conductivity are polypropylene with incorporated hollow fibres, which achieve an overall heat transfer coefficient of  $1300 \text{ W/m}^2\text{K}$ . In comparison copper shows a thermal conductance of  $380 \text{ W/m}^2\text{K}$ , whereas conductance of alumina is limited to  $235 \text{ W/m}^2\text{K}$ . The Scottish Plastics and Rubber Association (SPRA) revealed that the conductivity of polymer absorber can be increased for 1000 times from  $0,3 \text{ W}$  to  $350 \text{ W/m}^2\text{K}$  by black carbon fibers (made from complete oil combustion).

Figure 3.28 gives a survey of different polymers on the market that, distinguish maximum feasible operation temperature [ $^{\circ}\text{C}$ ], transparent and non-transparent design and prize per kilogram raw material. Collector cover sheets and collector tubing as well require high light transparency abilities. This ability is equitable to high temperature resistance, namely  $130$  to  $260^{\circ}\text{C}$  absorber temperature and long-time ultra-violet radiation resistance. The figure in APPENDIX C.3 shows a surveyed table of own research results of appropriate polymers which fulfil above listed performance criteria. Polycarbonates, especially DP9-9373<sup>®</sup> and DP9-1803<sup>®</sup> offer UV-resistance and temperature resistance for operation temperature up to  $179$ , respectively  $172^{\circ}\text{C}$ .

This temperature level is adequate for non-evacuated flat plate collectors and heatpipes with auto-cut-off [119] absorber control.

These polycarbonates provide light transmittance of 88% that is very close to low-iron glass without anti-reflectance treatment. Thus, the light transmittance is 3 to 5 points lower than optimal solar glazing on the market. Short-time maximum operation temperature of these transparent polymers is about  $195$  and  $191^{\circ}\text{C}$ . Opposed to that APEC 1897<sup>®</sup> and 2097<sup>®</sup> offer 89% light transmission, that is 1 per cent higher than compared to before mentioned, but nonetheless, the operation temperature is limited to maximum  $150$  to  $157^{\circ}\text{C}$ , respectively, and limited to  $172^{\circ}\text{C}$  in short-time perspective. Makrolon 2405/7<sup>®</sup> provides similar performance criteria. The Vicat maximum temperatures exceed  $200^{\circ}\text{C}$  for DP9-9373<sup>®</sup> and APEC 2097<sup>®</sup>.

Processing procedures as extrusion [120] to tubing was investigated for APEC 2097 and APEC 1803<sup>®</sup>. Likewise interesting are two completely different polymer, which

also offer decisive qualified performances. Perfluorethylenprop (FEB) and Perfluoralkoxyalcane (PFA) persuade by operation temperature of both higher than 200°C, even 260°C for PFA. Short-time operation temperature lies above 250°C, what is interesting for not evacuated or inert gas filled collector designs, and especially perfect for heatpipes in the context of seasonal thermal sorptive storage charging. Both polymers are available with UV-resistant properties.

The light transmission is described in literature with 5 of 5 points, but it is not clear-cut described, what transmittance factor can be provided. Both materials are described to satisfy extrusion and bonding processing abilities.

### § 3.5.1.2 Summary of state-of-the-art polymer performance

---

It has been elucidated, that for further increase and establishing of solar thermal renewable energy collector especially incorporated in facades materials as copper, alumina and glass are in need of alternatives. They need to be substituted in order to reduce harm to environment and energy required for manufacturing, transport and maintenance. Polymer have become prominent as substitution materials, since energy demand for exploitation, manufacturing, transport and maintenance is demonstrably lower compared to metals and glass. Collector cover sheets and absorber components are in focus of substitution. For both components polymer have been detected to provide alternatives. Several polymer offer sufficient temperature resistance, what is required for non-evacuated and especially for evacuated collectors, since generated maximum temperature level of absorbers easily exceed 220 to 250°C.

In particular polycarbonates as well as perfluorethylenprop and perfluoralkoxyalcane have been identified to be especially sufficient for glazing and transparent tubing substitutions. Light transmission has been inspected to be comparable to averaged solar glass qualities. However, polymers so far are not one hundred percent equivalent to solar glass transmission abilities, but competitive. Ultra-violet irradiation resistance is crucial for competitive duration of polymers comparable to glass. Normally polymers, notably polycarbonates, suffer from little UV-resistance and thus, from short exposition properties. Additives, surface treatments and Co-polymer extrusion processes allow to demonstrably increase UV-resistance. Summarized, polymers are attractive alternatives for the design of more sustainable crucial collector components.

## § 3.5.2 Nano-technologies for crucial collector components

---

The survey of market established collector technologies in section 3 demonstrates the strengths and weaks of existing collectors. A critical analysis especially for building skin integrated collectors determined amongst others crucial research and development objectives. Section 4 of this Chapter 03 documents recent and ongoing research and development, which either focus on partly enhancements of physical collector components or on completely new collector typologies. This actual section concentrate on contemporary research insights and developments on smart since not visible collector components.

Hence, this chapter emphasizes development in smart materials and nano-technologies, most innovations belong to the process engineering sector. Besides improvement of physical solid materials this section enlightens the performance of non-visual material treatments like coating, sputtering and etching.

### § 3.5.2.1 Transparent conductive oxides

---

Optical collector efficiency raises with an optimum absorption / emission ratio. Therefor a high light transmission ratio is substantial in order to absorb maximum. Furthermore, thermal collector efficiency, which incorporates optical efficiency, basically is determined by thermal losses of the collector itself.

From that perspective a consortium representing researcher and industry developed in 2013 a flat plate collector (Fig.3.29), that is covered by an insulation double glazing opposed to common single safety glass coverings. Especially by glass sheet coating with transparent conductive oxides (TCO) light transmission was enabled to remain comparably as high as common for single glazed collectors. Moreover, thermal losses by radiation and convection are tremendously lowered by both glazing filling with inert gas and the TCO.

Normally, applied double glazing reduces light transmission resulting from doubled light fraction and light absorption within raised glass sheet mass. Invisible coatings were analysed in order to compensate this unprofitable mechanism. In particular, tin-dopted indium oxides (ITO) have been determined in the past to be sufficient. But, however, the basic element indium is rare, thus expensive and causes considerable harm to environment in matter of exploration.

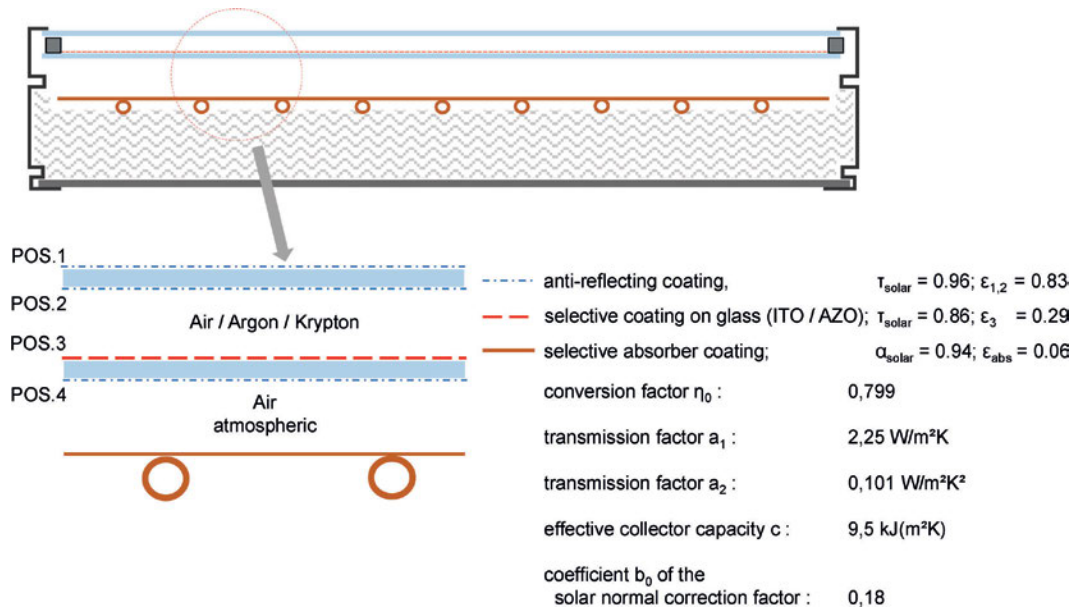


FIGURE 3.29 Construction scheme of TCO treated double-glazed flat plate collector

Furthermore, since collector glazings need to be made of safety glass in order to satisfy safety regulations, standardized and customized collector cover sheets are required to be toughened. Consequently, coatings being applied to toughened collector cover sheets are in account to be heat resistant for more than 200°C. Since cover sheets are made from stack ribbon glass sheets, coatings have to be applied in prior of sheet tailoring and toughening.

### Comparison of optical features of alumina-doped Tin-Oxide (AZO) coated solar collector double-glazing before tempering and after tempering

	solar transmission	solar reflection	IR-emissivity	visual transmission	visual reflection
pre-tempered	76,1%	7,4%	34,1%	79,8%	6,5%
post-tempered	82 - 82,3 %	10,3 - 10,9%	24,0 - 24,5%	92,5%	5,9%

FIGURE 3.30 Optical performance of toughened TCO-treated collector glazing

Thus, Föste, Ehrmann, Giovannetti, Reinike-Koch, Uslu, Krämer and Hesse (2013) [77] evaluate an alumina-doped tin oxide (AZO) to be a promising alternative coating material (Fig. 3.30). Since alumina-doped tin oxide firstly is less expensive, secondly less harmful to environment and finally withstands required safety glass treatment process, it bears three crucial benefits to be applied to double glazing of collectors. According to the researcher [77] flat plate collectors, that are equipped with an AZO coated and argon filled double insulation cover glazing, achieve a conversion factor  $\eta_0 = 0,799$  and transmission factors  $a_1 = 2,25 \text{ W/m}^2\text{K}$  and  $a_2 = 0,010 \text{ W/m}^2\text{K}^2$ . In comparison to a ITO coated double glazing cover sheet  $\eta_0$  increases by 2%, whereas  $a_1$  raises for  $0,22 \text{ W/m}^2\text{K}$  and  $a_2$  for  $0,002 \text{ W/m}^2\text{K}^2$ .

The authors detect a correlation between a raising coating thickness and a resulting decreasing light transmittance and emissivity. The thicker the coating layer the lower the transmission. Hence, the authors determine a sufficient compromise of 83% light transmission and 28% emission. Moreover, they recognize an improvement of transmission if coated cover sheets are toughened.

Thus, the safety glass process improves light transmission and lowers emission (Fig.3.30). Further, to them, invisible defects repair by the toughening process as well.

However, the collector efficiency  $\eta$  of an AZO coated argon filled double glazed flat plate collectors improves or 70% with  $\Delta T = 60\text{K}$  and  $G = 1.000 \text{ W/m}^2$  compared to a standardized single glazed collector (see APPENDIX C.4).

Precisely, collector efficiency  $\eta$  was identified to be 0,47. While the conversion factor significantly improves, calculations verified a feasible required collector area of 25 per cent less compared to common flat collectors. Additionally, the inspections revealed that AZO-double glass collectors being equipped with commonly 50 mm backside thermal insulation first tend to generate higher maximum feeding temperatures, and hence, secondly tend to stagnate more frequently. The authors reveal an optimized operation temperature range of 80 to 110° that is approximately 20 per cent higher than for common single-glazed collectors.

### § 3.5.2.2 Thickness insensitive spectrally selective paints

---

As explained above Föste (2013) [110] recognizes a strong correlation between a decrease in light transmittance and an increase in coating thicknesses. Thus, sufficient AZO coatings require higher quality of process engineering. Opposed to that, Jerman (2010) [112] introduces x paints (TISS). Paints and coating offering this thickness

insensitive quality offer spectrally selective purpose or even enhance self-cleaning qualities of weathered surfaces with less requirements on sputter tolerances.

Hence, as far as TISS offer comparable selective qualities, they are easier to apply and simplify process engineering during collector assembly. More detailed, TISS are multifunctional materials, based on organic macromolecules and additives. TISS manage to include pigments, metallic and metallised flake pigments and polymeric resins as well (SHC Polymeric Materials for solar thermal applications, 2015, [121]). More of interest are silane dispersants which manage to modify pigment surfaces in order to make them compatible to paint polymeric binders (Jerma) [112].

As paints, based on polyhedral oligomeric silsesquioxane (POSS) molecules, they provide UV protection and weathering resistance for especially polymer components of collectors.

### § 3.5.2.3 Nano-tubes and fibres for enhanced strength

---

Nano tubes bases on oblong carbon particles on nano-size level. Used as fillers in polymer components they support tensile and bending strength. Although, nano tubes has not been inspected entirely yet, the use as invisible but multifunctional additive raises enormously. Similar to glass or plastic fibres they can be stirred in organic matrixes in order to advance performance and to give subtle support to structure. Especially in polymer based absorber components and polymer based (polycarbonate) cover sheets nano tubes were introduced to manufacturing processes of wrought materials within the last decade.

### § 3.5.2.4 Co-polymers retard destruction by ultra-violet radiation

---

One of the major drawbacks of light-weight transparent polymer materials that are used in order to substitute heavy-weight glass components in collector technology is the lack of ultra-violet radiation resistance. Ultra-violet radiation, especially UV-C radiation, dissolves long-chained molecular connections between duro-plastic polymers. This results in cracking molecular structures and weakening mechanically the polymer component. Beside mechanical weakening also optical changes go along with exposition to UV radiation. UV radiation exposed polymers, as for example transparent polycarbonate, tends to yellowish and tend to loose transparency.

On the other hand polymethylmethacrylate (PMMA) offers similar transparency qualities, but additionally UV resistance. Polycarbonate that is doped with PMMA improves UV resistance abilities. Thus, one manufacturing process bases on the co-extrusion of mainly a polycarbonate compound to which surface PMMA is added.

PMMA acts like a UV-blocker and prevents polycarbonate from degradation and mechanical collapse. Hence, the method of co-polymerisation (co-polymer) enables several polymers for extraordinary weathered and sun exposed applications.

### § 3.5.2.5 Transparent $low_e$ -coatings substitute opaque backside insulation

---

Management of thermal losses are crucial for efficient solar thermal collectors (ISFH - Institute for Solarforschung Hameln). Optimal conversion factor does not account if thermal losses either to the environment or to a space distinguish converted irradiation.

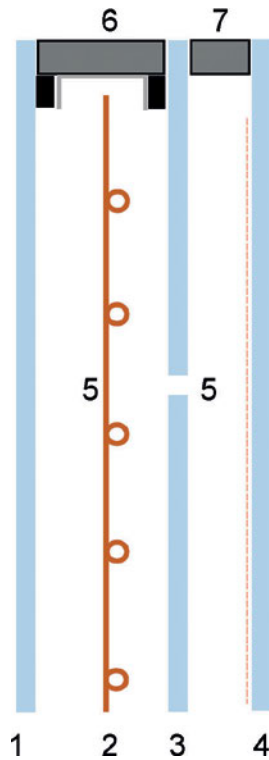
In this context immense thermal losses to spaces irritate thermal comfort as well.

Thus, it is inevitable to equip collectors with thermal insulation. Especially, transparent collector components shall be equipped with transparent insulation properties. Low emission coatings,  $low_e$ -coatings called, are invisible metallic layers which are sputtered on relevant surfaces.

In this context also transparent conductive oxides (TCO) help to control specific transmittance, emission and reflection. Giovannetti, Kirchner, Franke, Rohde and Scherer (2014) [78] developed a solar thermal collector which casing exclusively is a triple or quadruple glazing (Fig.3.31). A copper absorber is placed within the second cavity of triple glazing.

This design enables planers to implement this collector in post & beam facades, stick-systems or simply in window frames of ribbon facades. In order to reduce thermal losses,  $low_e$ -coatings are placed on #5. The cavities are argon filled.

Figures 3.32a shows a comparison of the effective transmission losses [ $W/m^2K$ ] of a triple glazing collector with and without  $low_e$ -coated transparent back sheet.



- 1 float glass, low iron, tempered
- 2 absorber
- 3 float glass, low iron, tempered with drilling hole
- 4 float glass, low<sub>e</sub> coated, tempered
- 5 cavity, Argon filled
- 6 air tight spacer, primary sealing C-profile + Polyisobutyl secondary sealing : silicone
- 7 air tight spacer, primary sealing : Polyisobutyl secondary sealing : silicone

FIGURE 3.31 Construction scheme of entirely glazed (triple-glazed) collector

The graph undoubtedly demonstrates, that a coefficient can be remained on a constant level of  $3,3 \text{ W/m}^2\text{K}$  while ratio of emission on absorber backside increases from 0 to 1,0, whereas the coefficient of a non-coated collector nearly linearly rises from 3,4 to  $3,9 \text{ W/m}^2\text{K}$ . Supporting, the right chart illustrates the normed effective coefficient of transmission losses at a temperature difference between the mean absorber and the ambient temperature of 40 Kelvin in relation to increasing inclination angle (Fig. 3.32b) of the collector (0 to  $90^\circ$ ).

The graph demonstrates that for both a standard and a triple glazing collector the coefficient of transmission losses decreases in dependence of raising inclination. What is more of interest is the impressive decrease of thermal losses for more than 32% towards a  $90^\circ$  inclination for a lowe-coated triple glazing collector. The decrease, and hence, the effective thermal losses of a triple glazing collector compared to a standard collector diminish and differ for more than 19% (69 to 88%) in respect to a  $90^\circ$  inclined mounting.

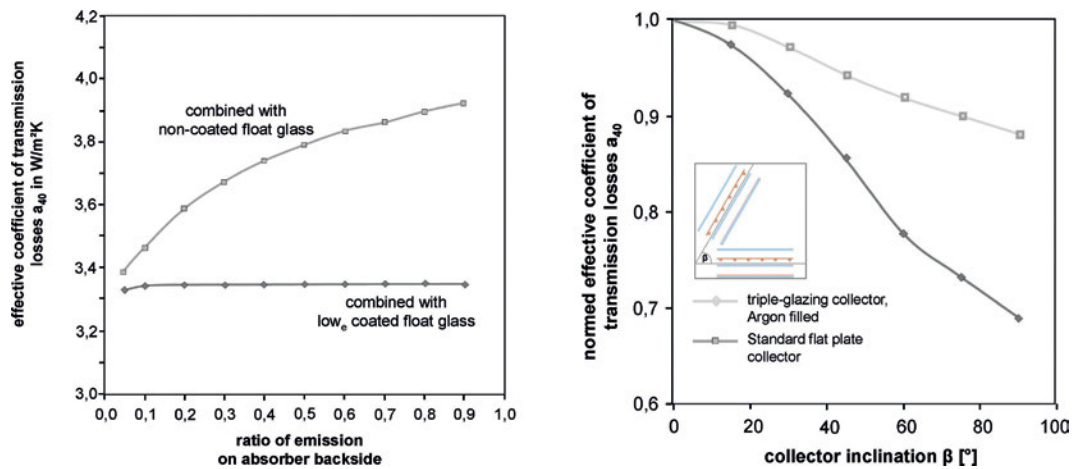


FIGURE 3.32 a.) Effective and normed transmission losses/coefficient in relation to emission ratio and b.) collector inclination

The Figure C.5 in APPENDIX gives a survey of evaluated conversion factors  $\eta_0$ , and transmission losses  $a_1$ ,  $a_2$  and  $a_{40}$ . The evaluation differentiates between triple and quadruple glazing collectors that are either air or argon filled and are either inclined by 45 or 90°.

Argon filling and 90° inclination demonstrably reduce internal filled convection with the case or glazing [122]. Clear-cut essence of the table is a 25 to 30 per cent improvement in thermal performance by argon filling of collectors. A change in inclination by  $\Delta=45^\circ$  and substitution of air by argon lowers  $a_{40}$  by 30%, absolutely for 1,57 W/m<sup>2</sup>K. These results explicitly show, that an effective thermal insulation is practicable by low<sub>e</sub>-coatings for transparent triple-glazing collectors. Especially a combination of low<sub>e</sub>-coating and argon filling with 90° inclination considerably limit thermal losses compared to standard flat plate collectors. As a consequence, transparent triple glazing collectors are eligible for integral implementation in vertical facades.

### § 3.5.2.6 Self-regulating absorbers by spectrally-shutting coatings

Regardless of roof mounted, façade attached or even façade integrated collectors, stagnation is counterproductive for any solar thermal system in respect to efficiency, component duration or even internal special thermal comfort. Stagnation is to be prevented for a sufficient solar thermal system. Normally, when stagnation occurs,

transportation fluid within the piping evaporates. Further, while water turns into steam, volume tremendously increases. Dependent on the steam range, solar pumps, expansion vessels and fluid additives like glycols are directly affected and are in risk to be destroyed. Solely the temperature sensor nearby the collector controls further operation and thus vitality of all components.

Researcher developed an absorber sheet coating that directly reacts on solar irradiation. If solar radiation exceeds specific limits and thus the absorber temperature exceeds limits (75°C), the crystalline structure [123] of the coating changes. With this change also solar transmittance changes. If irradiation and subsequently absorber temperature once again lowers, the crystalline coating structure changes again and becomes spectrally transparent.

This process is unlimited reversible and steady as well [74]. Thus, engineering allows controlling absorber temperatures, and thereby the effect on the solar circuit. Temperature regulation and thereby solar fraction in accordance to stagnation frequency is shifted towards the collector itself. That makes entire solar thermal systems much simpler, more reliable and more efficient.

### § 3.5.3 Enhanced integral collector developments

---

The next section exemplifies recent developments, which incorporate former describes technical innovations.

Transmission losses via collector front glazing has been detected in science as being the crucial ones, since backside losses are commonly reduced by backside insulation. Thus, an thermal enhancement of front glazing in order advance collector efficiency is one major step of design development. Analogously to building skins, flat plate collectors has been covered by a double-glazing unit.

Besides anti-reflecting and lowe-coating and inert gas filling of the double glazing unit, a special transparent conductive oxide (TCO) based on alumina dopted zinc-oxide coating has been developed and evaluated that optimizes light and ultra-violet light transmission. In particular, this TCO development [124] focussed additionally on heat resistance required in safety glass tempering processes in order to enhance safety and freedom of collector dimension-design.

VARIANT	V01.3
STATUS	prototype
RATIO OF PERUSAL	perusal : 0%
TYPOLGY	double-glazed high efficient flat plate collector
1. MEDIUM / TRANSPORT FLUID	directly flooded, water-glycols
FRONT COVER	double-glazed
FRONT COVER QUALITY	twice anti-reflective, low-iron and low <sub>e</sub> TCO (AZO) coated argon-filled tempered double glazing, 3,2 mm
ABSORBER TECHNOLOGY / QUALITY	highly selectiv coated copper absorber
HEAT EXCHANGER TYPOLGY	harp-shaped copper heat exchanger
QUALITY OF VACUUM	not evacuated, hermetically opened
THERMAL INSULATION	backsided thermal insulation
CASING	alumina case, 121 mm
TYPE OF ENVELOPE INTEGRATION	0° declined roof, mansard roof solid external wall rear ventilated stick-facade
RATIO OF FLEXIBILITY	standard dimensions, linear
FAÇADE INTEGRATED STORAGE	none
CONVERSION FACTOR $\eta_0$	0,799
COLLECTOR EFFICIENCY RATIO $\eta$ at $\Delta T_{max}$	0,47 (60 K, 500 W/m <sup>2</sup> )
TRANSMISSION COEFFICIENT $a_1$ [W/m <sup>2</sup> K]	2,25
TRANSMISSION COEFFICIENT $a_2$ [W/m <sup>2</sup> K <sup>2</sup> ]	0,010
INTERNAL ABSORBER CONDUCTANCE $U_{int}$ [W/m <sup>2</sup> K]	27,5
TRANSMISSION COEFFICIENT $a_{t0/60}$ [W/m <sup>2</sup> K]	2,83 (60)
SOLAR NORMAL FACTOR	-
EVALUATED SURFACE TEMPERATURE $T_{surf} / T_1$ [°C]	$T_{surf} = > \text{ambient} + 30K, \text{spacer}=120^\circ$

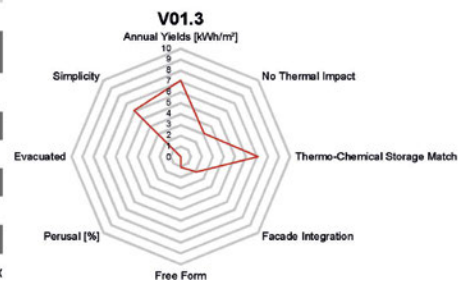
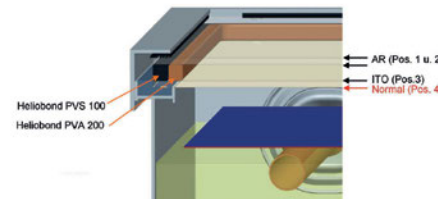
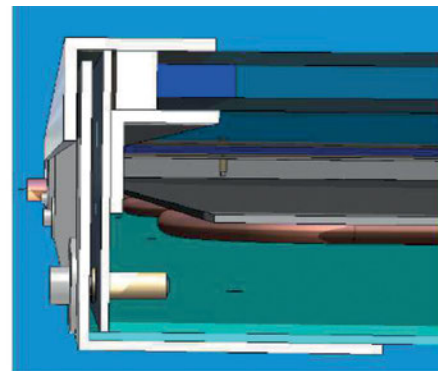


FIGURE 3.33 Performance profile – double-glazed and TCO-treated flat plate collector

Effect of this development is a competitive conversion factor  $\eta_0 = 0,799$  aligned to a collector efficiency of  $\eta = 0,47$ , what constitutes a 70 per cent improvement compared to single glass covered collectors (Fig.3.33). While annual yields approximate to those of partly evacuated single glazed flat plate collectors, and feeding temperatures meet the required level for charging of seasonal thermo-chemical storages, this collector design is complex.

However, the innovative constructive principle results in a collector width of 121 mm. That allows solid wall integration, and scattered post&beam or stick-system integration, but merely window partition substitution.

VARIANT	V01.5
STATUS	prototype
RATIO OF PERUSAL	perusal : 0%
TYPOLOGY	flat collector with auto-cut-off heatpipes
1. MEDIUM / TRANSPORT FLUID	not flooded, heatpipe with butane
FRONT COVER	glazed
FRONT COVER QUALITY	4 mm anti-reflecting+prismatic low iron cover sheet
ABSORBER TECHNOLOGY / QUALITY	highly selectively coated copper absorber, ultrasound-welded auto-cut-off heatpipes
HEAT EXCHANGER TYPOLOGY	auto-cut-off heatpipes with inner rib-structure, stagnation optimized 100 to 125°C
QUALITY OF VACUUM	not evacuated
THERMAL INSULATION	backsided thermal insulation, 50 mm
CASING	alumina case, 65 mm
TYPE OF ENVELOPE INTEGRATION	declined roof, mansard roof solid external wall post&beam, stick-system
RATIO OF FLEXIBILITY	standard dimensions, linear
FACADE INTEGRATED STORAGE	none
CONVERSION FACTOR $\eta_D$	0,68 to 0,79
COLLECTOR EFFICIENCY RATIO $\eta$ at $\Delta T_{\text{net}}$	0,45
TRANSMISSION COEFFICIENT $a_1$ [W/m <sup>2</sup> K]	3,5
TRANSMISSION COEFFICIENT $a_2$ [W/m <sup>2</sup> K <sup>2</sup> ]	0,0107
INTERNAL ABSORBER CONDUCTANCE $U_{\text{int}}$ [W/m <sup>2</sup> K]	49
TRANSMISSION COEFFICIENT $a_{\text{eq}} / a_2$ [W/m <sup>2</sup> K]	-
SOLAR NORMAL FACTOR	-
EVALUATED SURFACE TEMPERATURE $T_{\text{surf}} / T_i$ [°C]	estimated : ambient + 25 K

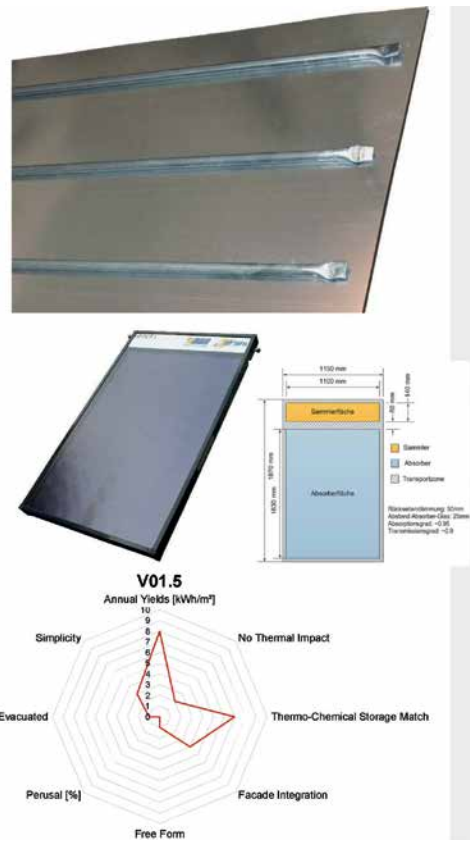


FIGURE 3.34 Performance profile – auto-cut-off heatpipe equipped flat plate collector

Objected to this innovation are firstly zero perusal and secondly considerable impact on thermal comfort. Since the spacer temperature tends to ascend to 120°C and the absorber actually exceeds this level, wall surfaces temperature can increase for more than 30 K. In order to seal the dgu to the case, a two-step sealing agent was developed that manage to withstand operation temperature of maximum 130°C.

Stagnating solar thermal collectors in building envelopes encounter two crucial drawbacks. First overheating causes degradation on absorber, anti-free-zing agent and solar circuit components like pumps, valves and the expansion vessel. These facts reduce effective annual yields, respectively efficiency and elongates amortisation time because of component break-down. For second, overheating solar thermal collectors commonly tend to influence internal thermal comfort negatively, while inner wall surface temperature tremendously rise.

Researcher investigated stagnation and draught border behaviour of different working fluid in heat-pipes [125;126] such as butane and acetone opposed to common water. Such working fluids can be designed and volumetrically applied in order to let heatpipes stagnate slightly above the boiling point of water. That mechanism can be utilized to control heatpipe working phases (Fig.3.34). As a result, heatpipes shut off with maximum condenser or exchanger temperatures of 125 to 140°C, what is much less than commonly 170 to 240°.

Such limited exchange temperatures prevent distribution fluid from evaporating, at least they shorten the steam range considerably. In consequence, components are no longer affected by overheating temperatures, as well as fluid additives like glycol do not tend to crack. Parallel butane or acetone-driven heatpipes with elongated condenser geometries and inner rib-structure enlarges power and efficiency, while they optimally shut-down by stagnation. This mechanism has been transferred to flat plate collectors, inasmuch harped-shaped piping has been exchanged by auto-cut-off heatpipes. This hermaphroditic collectors shows an excellent conversion and internal conduction value and averaged efficiency for flat plate collectors. Although thermal impact is limited, seasonal thermo-chemical storages can be charged.

A further step towards superior envelope integration represents this glazing unit embedded solar thermal absorber. While this approach is similar to the glazing unit collector V04 described in Chapter 04 the major difference is defined by maximization of the aperture area (absorber) and a more complex triple or quadruple glazing composition in respect of thermal performance. Although several glass sheets are low<sub>e</sub>-coated, but not TCO-coating treated, the  $\eta_0$  value is with 0,78 slightly lower than of V01.3.

In respect to any missing physical thermal insulation the transmission coefficient  $a_1$  is 43% higher than in V01.3, but 30% lower than V04. For this design (Fig.3.35) has been evaluated a transmission coefficient of 3,65 W/m<sup>2</sup>K for a temperature difference of 40K and a 90° inclination, what is characteristic for façade integration. Technology related feasible annual yields can be categorized as equal to partly evacuated flat plate collectors. Feeding temperatures are estimated to match with seasonal thermo-chemical storage requirements. Opposed to the cased variant V01.3 this innovation is characterized by a width of 51 to 76 mm depending on the glazing principle and is up to 70 mm leaner than V01.3. In consequence, this design enables to incorporate within window partitions of post& beam or stick-systems or at least in unitized prefabricated curtain wall systems.



VARIANT	V04.2
STATUS	R & D
RATIO OF PERUSAL	translucent (5-10%)
TYPOLOGY	<i>only-glass-collector</i>
1. MEDIUM / TRANSPORT FLUID	directly flooded, water
FRONT COVER	quadruple-glazing, (<50 mm)
FRONT COVER QUALITY	anti-reflective, low-iron, low <sub>e</sub> coated, argon-filled tempered quadruple glazing
ABSORBER TECHNOLOGY / QUALITY	non-selective water-resistant solar vanish coating
HEAT EXCHANGER TYPOLOGY	safety glass pane
QUALITY OF VACUUM	not evacuated
THERMAL INSULATION	Low <sub>e</sub> -coating #3 and #6
CASING	not cased, 2 level Polyisobutylene and silicon sealant, U-profile framed
TYPE OF ENVELOPE INTEGRATION	solid external wall, stick system post&beam
RATIO OF FLEXIBILITY	customizeable, linear
FACADE INTEGRATED STORAGE	none
CONVERSION FACTOR $\eta_0$	0,762
COLLECTOR EFFICIENCY RATIO $\eta$ at $\Delta T_{max}$	-
TRANSMISSION COEFFICIENT $a_1$ [W/m <sup>2</sup> K]	3,98
TRANSMISSION COEFFICIENT $a_2$ [W/m <sup>2</sup> K <sup>2</sup> ]	0,0063
INTERNAL ABSORBER CONDUCTANCE $U_{int}$ [W/m <sup>2</sup> K]	-
TRANSMISSION COEFFICIENT $R_{40/60}$ [W/m <sup>2</sup> K]	-
SOLAR NORMAL FACTOR	0.94 at K50°
EVALUATED SURFACE TEMPERATURE $T_{surf} / T_1$ [°C]	$T_{surf}$ = estimated ref.V4.0/4.1 44-57°C

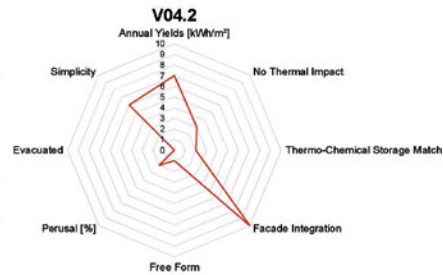
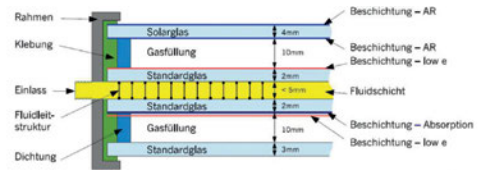


FIGURE 3.36 Performance profile – entire quadruple-glazed and directly flooded no-absorber collector

While the two outer cavities are filled with inert gas and adjoining float panes are low<sub>e</sub>-coated, the inner cavities remains in order to guide a working and transport fluid in once [127]. The inner two panes form a channel cavity which is entirely flooded by a water-glycol solution. Thus, this collector is directly flooded, similar to flat plate collectors. Since, it is made explicitly from glass and requires less than 50 mm width, it perfectly fits in solid ribbon facades, post & beam structures or unitized stick-systems. While the inner cavity is activated for solar thermal utilisation, this design, although it provides simply translucent quality and 5 to 10% perusal, represents the most integral approach of envelope embedded functions (Fig. 3.36).

Doubtlessly, high working temperatures above 100°C causes immense thermal stress for a construction exclusively made from glass. Thus, feasible annual yields and efficiency are estimated to be on average level, comparable to non-evacuated standard flat plate collectors.

VARIANT	V06
STATUS	Prototype
RATIO OF PERUSAL	perusal : 20%
TYPOLOGY	<b>evacuated tube collectors</b>
1. MEDIUM / TRANSPORT FLUID	not flooded, heatpipe
FRONT COVER	tube glazing
FRONT COVER QUALITY	low-iron borosilicate glass
ABSORBER TECHNOLOGY / QUALITY	bifacial highly selective coated copper absorber
HEAT EXCHANGER TYPOLOGY	heatpipe = heat pump tube, heat exchanger in post profile
QUALITY OF VACUUM	<b>evacuated</b>
THERMAL INSULATION	no physical thermal insulation required
CASING	uncased
TYPE OF ENVELOPE INTEGRATION	unitized or stick system post&beam, curtain wall, high rise
RATIO OF FLEXIBILITY	standard dimensions, linear
FACADE INTEGRATED STORAGE	none
CONVERSION FACTOR $\eta_0$	0,69 Apicrus (0,656 HE JIA) to 0,77
COLLECTOR EFFICIENCY RATIO $\eta$ at $\Delta T=60K$	<b>0,53 - 0,57</b> ( $\Delta T=60K$ )
TRANSMISSION COEFFICIENT $a_1$ [ $W/m^2K$ ]	1,38 - 1,505 (2,24 AkaTec)
TRANSMISSION COEFFICIENT $a_2$ [ $W/m^2K$ ]	0,004 - 0,0123 Thermosolar
INTERNAL ABSORBER CONDUCTANCE $U_{in}$ [ $W/m^2K$ ]	10,4
TRANSMISSION COEFFICIENT $a_{10/60}$ [ $W/m^2K$ ]	
SOLAR NORMAL FACTOR	0,93 at K50° (0,97, 0,88 K70° Aka)
EVALUATED SURFACE TEMPERATURE $T_{surf} / T_i$ [ $^{\circ}C$ ]	$T_{surf} = ambient, space \Delta T = 0K$

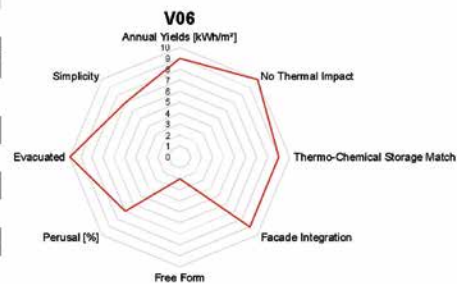


FIGURE 3.37 Performance profile – heatpipe collector facade

The only actions for thermal insulation are non-physical, as they are low-coating and inert gas fillings. Thus, space-ward surface temperatures are estimated to have significant influence on internal thermal comfort. Since maximum working temperatures are limited in re-pect to in-ternal and spacial thermal stress and to a non-selective absorbing area, the quality of charging seasonal thermo-chemical storages is estimated to be strongly limited. Finally, simplicity is partly given, as long as glazing sealing and penetration are in balance.

Obviously, this research proposal satisfies with extraordinary quality of perusal, simplicity and an advanced level of façade integration. Simplicity is given by the non-directly flooded evacuated tube collector principle itself (Fig. 3.37), inasmuch as those tubes represent a high automatization and prefabrication level and easy plug & play

maintenance as well. While the evacuated tube collectors are arranged horizontally and spaced, quality of perusal is higher than compared to V04. Since tube collectors solely offer linear orientation, unitized and prefabricated stick-systems are recommended for embedded designs. Bifacial selective absorber coating (beneficial reflection by the space aligned glazing unit and the superior thermal insulation on account of evacuation) raises the conversion factor up to 0,77 and collector efficiency towards 0,57. Thus, the efficiency is 110 per cent higher than compared to standardized flat plate collectors and 20% higher than compared to double glazed flat plate collectors.

VARIANT	V06.1
STATUS	R & D
RATIO OF PERUSAL	perusal : 100%
TYPOLOGY	evacuated plastic tube collector
1. MEDIUM / TRANSPORT FLUID	not flooded, heatpipe
FRONT COVER	tube glazing
FRONT COVER QUALITY	UV-/mid-temperature stable, highly UV transmitting, Polycarbonat, LT>90%
ABSORBER TECHNOLOGY / QUALITY	highly selective coated copper absorber
HEAT EXCHANGER TYPOLOGY	heatpipe = heat pump tube, heat exchanger in rafter profile
QUALITY OF VACUUM	evacuated
THERMAL INSULATION	no physical thermal insulation required
CASING	uncased, rafter integrated, notch locked
TYPE OF ENVELOPE INTEGRATION	5 to 70° declined roof unitized or stick system post&beam, sun space customizable, linear
RATIO OF FLEXIBILITY	
FACADE INTEGRATED STORAGE	none
CONVERSION FACTOR $\eta_0$	estimated : 0.58 to 0.68
COLLECTOR EFFICIENCY RATIO $\eta$ at $\Delta T=60K$	estimated : 0.52 $\pm$ 3 ( $\Delta T = 60K, 1000W/m^2$ )
TRANSMISSION COEFFICIENT $a_1$ [ $W/m^2K$ ]	estimated : 0.4 to 2.2
TRANSMISSION COEFFICIENT $a_2$ [ $W/m^2K^2$ ]	-
INTERNAL ABSORBER CONDUCTANCE $U_{int}$ [ $W/m^2K$ ]	estimated : 1 to 10
TRANSMISSION COEFFICIENT $a_{40/80}$ [ $W/m^2K$ ]	-
SOLAR NORMAL FACTOR	-
EVALUATED SURFACE TEMPERATURE $T_{surf} / T_i$ [°C]	$T_{surf} = ambient, space + 8 K$

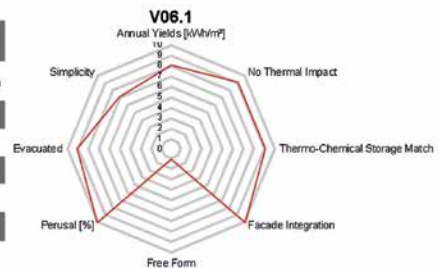
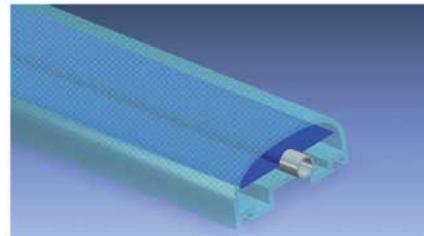
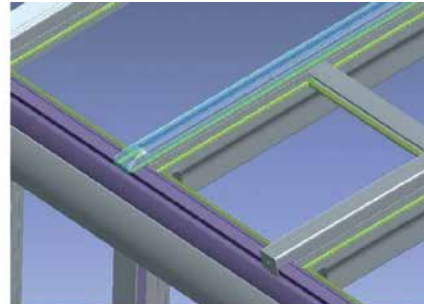


FIGURE 3.38 Performance profile – rafter integrated polymer heatpipe HEATBEAM©

In particular, incomparably low transmission coefficients  $a_1$  and  $a_2$  illustrate the thermal performance both in respect of annual yields and eligibility for seasonal thermo-chemical storage charging.

Depending on design stagnation temperature, evacuated tube collectors offer feeding temperature between 100 to 250°C in order to charge sorptive storages. Disregarded to space separated location in respect of this particular façade design, evacuated tubes commonly do not tend to provide any tube surface temperatures above ambient temperature. Hence, there is no risk of not influence interior thermal comfort anyway.

One hundred per cent perusal is the crucial benefit of this special construction principle. High quality of integration substitutes glazing bars and thus the design even becomes structural. This design bases on polymer tubed and evacuated heatpipes. Opposed to glass-tubed evacuated collectors (heatpipes) the tubing is formed hemispherical and compressed in order to perfectly adapt to rafters of sun space roof constructions.

Since the heatpipes are first evacuated and second mounted to thermally disconnected structural elements, no impact on special thermal comfort is to be estimated. Since the design is in development and part of this thesis optical and thermal parameters are not yet evaluated. Thus, they solely can be derived from other typologies in order to approximate to feasible performance. The tubing is made from extruded and partly ultrasound-welded polycarbonate wrought material with both high light transmission of >89% and temperature resistance > 150°C (Fig. 3.38).

Few spare parts and length-off elements allow tailor-made confection and address a certain quality if simplicity. While the absorber sheet is bi-facial highly selectively coated and thus benefits from light reflections of adjoining roof glazing, the optical conversion factor as well as the collector efficiency is estimated to be comparable with CPC-collector tubes but at least with common heatpipe collectors. Thus, this rafter integrated heat-pipe design offer comparably high annual earnings combined with a feeding temperature level, that is eligible for charging of seasonal sorptive storages. Although, according to rafter axis and distance, the heatpipes are separated from each other and risk to encounter tremendous thermal losses by distribution piping, the thermal losses are countervailed by special polymer tubing. The polymer tubing calls for only a fraction of thermal conduction of corrugated steel tubes.

VARIANT	V07
STATUS	Prototype
RATIO OF PERUSAL	perusal : 10%
TYPOLOGY	evacuated Sidney tube collectors + CPC
1. MEDIUM / TRANSPORT FLUID	directly flooded, Sidney tube, water-glycols
FRONT COVER	tube glazing
FRONT COVER QUALITY	low-iron borosilicate glass
ABSORBER TECHNOLOGY / QUALITY	highly selective coated glass tube inner surface
HEAT EXCHANGER TYPOLOGY	coaxial Sidney tubing, heat exchanger in post profile
QUALITY OF VACUUM	evacuated
THERMAL INSULATION	no physical thermal insulation required
CASING	uncased
TYPE OF ENVELOPE INTEGRATION	unitized or stick system post&beam, curtain wall, high rise standard dimensions, linear
RATIO OF FLEXIBILITY	none
FACADE INTEGRATED STORAGE	none
CONVERSION FACTOR $\eta_{10}$	0.605 to 0.62 Sonnenkraft/ CONSOLAR
COLLECTOR EFFICIENCY RATIO $\eta$ at $\Delta T=10K$	0.56 (40 K, 1000 W/m <sup>2</sup> K) Sonnenkraft
TRANSMISSION COEFFICIENT $a_1$ [W/m <sup>2</sup> K]	0.395 to 0.0850 Sonnenkraft
TRANSMISSION COEFFICIENT $a_2$ [W/m <sup>2</sup> K]	0.01 to 0.02 Sonnenkraft
INTERNAL ABSORBER CONDUCTANCE $U_{int}$ [W/m <sup>2</sup> K]	1,0
TRANSMISSION COEFFICIENT $a_{40/60}$ [W/m <sup>2</sup> K]	-
SOLAR NORMAL FACTOR	0.95 at K50°
EVALUATED SURFACE TEMPERATURE $T_{amb}$ / $T_i$ [°C]	$T_{amb}$ = ambient, space $\Delta T = 0K$

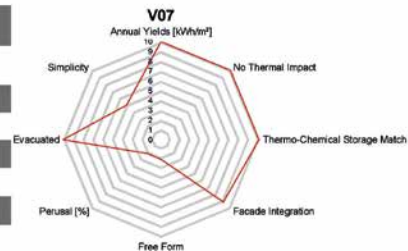
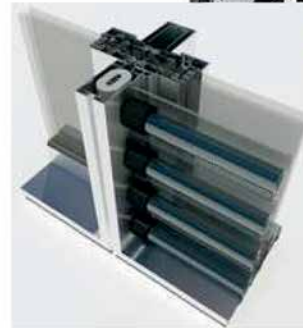
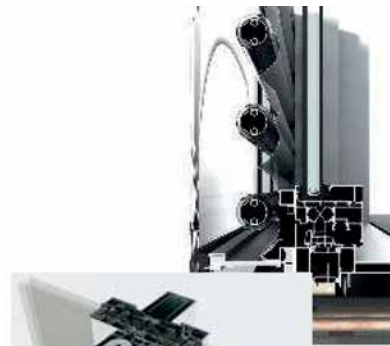


FIGURE 3.39 Performance profile – perforated CPC-mirror equipped evacuated tube collector

This design approach (Fig. 3.39) is a further development of variant V06. Analogue to V06 evacuated tube collectors a horizontally placed in front and separated of an insulation glazing.

This concept equivalently guarantees no thermal impact on interior comfort. Optical and thermal enhancement of performance are achieved by added hemispherical metal mirror sheets, which reflect through passing irradiation on absorber backsides. While the tubes from V06 are exchanged by directly flooded CPC-Sidney tubes, feasible feeding temperature level and also annual yields increase by 10 to 15 per cent. Although the ability to charge a seasonal thermo-chemical storage reaches optimum, simplicity lowers inasmuch directly flooded tubes require more intensive maintenance.

VARIANT	V09
STATUS	R & D
RATIO OF PERUSAL	perusal : 0%
TYPOLOGY	<b>Solid Wall absorber + facade integrated sensible buffer tank</b>
1. MEDIUM / TRANSPORT FLUID	directly flooded (collector+tank=1 element)
FRONT COVER	transparent thermal insulation, selectively coated tank front side
FRONT COVER QUALITY	transparent thermal insulation
ABSORBER TECHNOLOGY / QUALITY	selective solar varnish $\alpha/\tau_{s,vis}$ (Solarlack)
HEAT EXCHANGER TYPOLOGY	no heat exchanger, drain back system
QUALITY OF VACUUM	no vacuum, not evacuated cavities
THERMAL INSULATION	vacuum insulation panels + aerogel mats
CASING	steel and poly carbonate case
TYPE OF ENVELOPE INTEGRATION	solid external wall
RATIO OF FLEXIBILITY	standard dimensions, linear
FACADE INTEGRATED STORAGE	of solid wall depth, sensible, daily, water
CONVERSION FACTOR $\eta_D$	$0,95 * 0,6 * < 1,05 = < 0,6$
COLLECTOR EFFICIENCY RATIO $\eta$ at $\Delta T=40K$	-
TRANSMISSION COEFFICIENT $a_1$ [W/m <sup>2</sup> *K]	Speicher : 7 W/K , (7*9,22m <sup>2</sup> =0,76 W/m <sup>2</sup> *K)
TRANSMISSION COEFFICIENT $a_2$ [W/m <sup>2</sup> *K]	-
INTERNAL ABSORBER CONDUCTANCE $U_{int}$ [W/m <sup>2</sup> *K]	$F_{s+T} = U_{int} / (U_{int} + a_1) = < 0,6$
TRANSMISSION COEFFICIENT $a_{40 / 60}$ [W/m <sup>2</sup> *K]	-
SOLAR NORMAL FACTOR	-
EVALUATED SURFACE TEMPERATURE $T_{surf} / T_i$ [°C]	$T_{surf} = 27-36^{\circ}C$

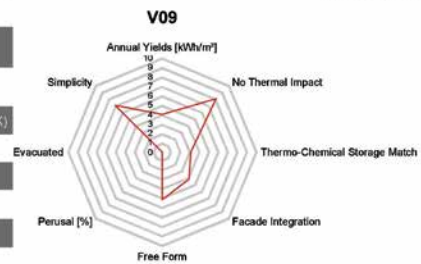
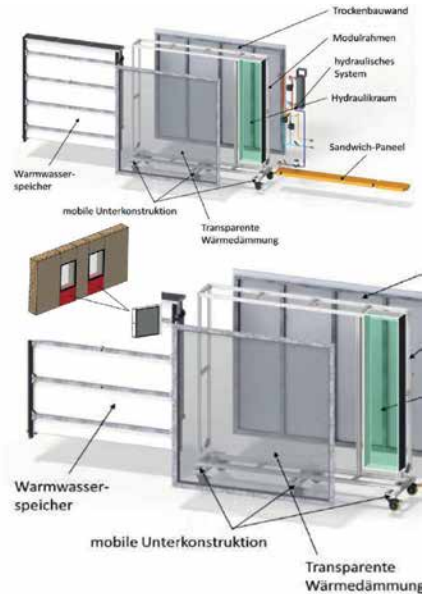


FIGURE 3.40 Performance profile – Sensible storage combined transparent insulation wall integrated flat collector

The incomparable high piping distribution effort of directly flooded tubes parallel asks for different since being bigger post & beam construction to provide sufficient distribution space.

Consequently, this design calls for especially unitized prefabricated façade principles. Since the mirror sheets are solely penetrated by tiny holes, perusal significantly lowers to a percentage, which simply allows contours to be perceived.

Normally, power or thermal collectors are of parts of envelope layers and distribute generated energy to a centralized service point within the building. From that service point renewable energy is distributed on demand to decentralized spaces within in the building again. Thus, common concept follow an intense energy distribution principle.

Researcher developed and evaluated a combined collector/storage design [128], that implemented in building skins, provides the adjacent space directly (Fig. 3.40). Distribution does not occur. Hence, this system principally encounters no distribution losses on account of two times. The design incorporates an irradiation affective weather shield, that is made of a 42 mm double glazing embedding a 30 mm aerogel-mat. This aperture ( $\eta_0 = < 0,6$ ) works as transparent thermal insulation. Backside of the double glazing a selective solar vanish black coated sensible non-pressured polymer water tank is heated up by irradiation transmission. The tank is of forged and planar geometry to be embedded into structural solid wall system or post & beam façade systems. While the tank is all-sided thermally insulated, hydraulic components are also placed within this layer. The rear of the tank is covered with plasterboards and is already the space adjacent finished surface. Besides, the conversion factor  $\eta_0 = < 0,6$  is comparably moderate, the sensible tank encounters an area-specific transmission coefficient of solely  $0,76 \text{ W/m}^2\text{K}$ . Since maximum tank temperatures are evaluated at  $51^\circ\text{C}$ , operation results in tolerable space surface temperatures of simply  $27$  to  $36^\circ\text{C}$ , that do not seriously effect indoor comfort. Although this is a new intensively integrated, simple and condensed design, however, it does of course not allow free form integration, perusal or charging of seasonal thermo-chemical storages. Enhancement of conversion factor and tank striation behaviour can annual yields rise above the standards of pool absorber or polymer absorbers.

Mostly modern building skins hardly manage to adapt to and at best face extreme climatic changes during the year. In consequence, building skins encounter specific transmission losses and involve load peaks for heating and cooling. Thus, energy flux management [129] is an serious issue in contemporary façade design. This approach is complex while being multivalent design in order to better regulate and even balance heat and cooling loads during the day, during the year. While being optimized to response to the different outdoor and indoor climatic conditions (Fig.3.41), the design basically stores energy amounts passing the entire building skin in order to reactivate this energy for cooling or heating at different times. Therefor the design incorporates passive (thermal mass, phase change material) and active (transport fluid, heat exchanger, pumps&valves) strategies and components in an integral and condensed way.

This design is called Advection Based Adaptive Building Envelope (ABABE) and its crucial component is a prefabricated ceramic press-mold and fiber composite reinforced façade tile. While this tile is selectively coated and textured, the location specific geometry design allows perfect adaptation to irradiation and wind vection. Especially, tile geometry simultaneously allows complex solar tracking as well as shaded enlarged radiation losses. Thus, this tile acts both as solar collector and a free cooling device in order to provide heat and cold sinks as well.

VARIANT	V09.1
STATUS	R & D
RATIO OF PERUSAL	perusal : 0%
TYPOLOGY	<i>ceramic collector + heat exchanger-facade cladding tile</i>
1. MEDIUM / TRANSPORT FLUID	directly flooded
FRONT COVER	unglazed
FRONT COVER QUALITY	sun path morphed surface geometries
ABSORBER TECHNOLOGY / QUALITY	ceramic surface, location, sun path and space load optimized texture
HEAT EXCHANGER TYPOLOGY	drain back system
QUALITY OF VACUUM	no vacuum, not evacuated cavities
THERMAL INSULATION	typical multi-level grid facade system with solid insulation layer
CASING	uncased, lapped fixed, injection-molded outer skin
TYPE OF ENVELOPE INTEGRATION	solid external (high-rise) wall
RATIO OF FLEXIBILITY	customizeable, location morphed
FACADE INTEGRATED STORAGE	tile integrated phase change material, latent
CONVERSION FACTOR $\eta_c$	-
COLLECTOR EFFICIENCY RATIO $\eta$ at $\Delta T=60K$	-
TRANSMISSION COEFFICIENT $a_1$ [W/m <sup>2</sup> *K]	-
TRANSMISSION COEFFICIENT $a_2$ [W/m <sup>2</sup> *K]	-
INTERNAL ABSORBER CONDUCTANCE $U_{int}$ [W/m <sup>2</sup> *K]	-
TRANSMISSION COEFFICIENT $a_{40 / 60}$ [W/m <sup>2</sup> *K]	-
SOLAR NORMAL FACTOR	-
EVALUATED SURFACE TEMPERATURE $T_{surf} / T_1$ [°C]	-

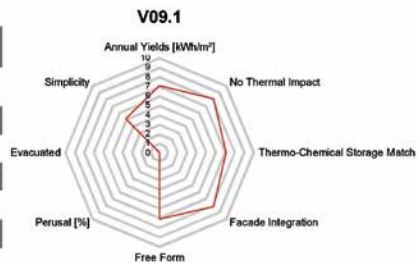
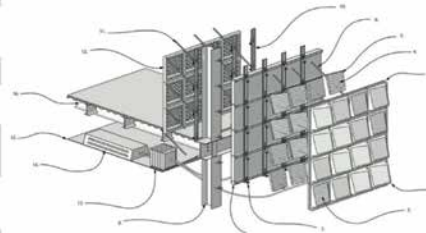
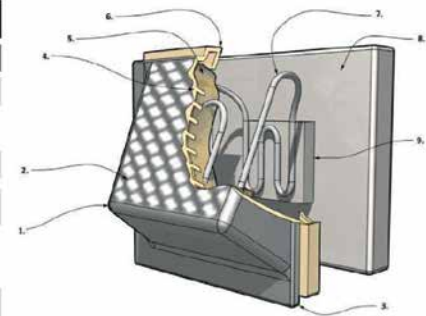


FIGURE 3.41 Performance profile – ceramic heating / cooling façade tile for advanced climatic adaption and energy balance

The modular ceramic tile absorbs, releases, redirects, decelerates and conserves energy fluxes by diverse strategies therewith interior thermal comfort as main driver is optimized.

Summarized, this non-transparent design while still being in engineering development represents a research branch of high façade complexity and integration quality. Actively focussing on interior thermal comfort, this design degrades seasonal storages to be obsolete.

### § 3.5.4 Summary

---

With respect to the established state-of-the-art solar thermal collector typologies in section 3 and the identified lacks of key performance parameters, this section showed recent research and development of game changing polymer and coating technologies.

Polymer have been detected and appropriate in order to substitute essential construction parts of collectors. Cover sheet, absorber, casing and piping as well (see also Chapter 06) profit from competitive polymer alternatives. This development offers a parallel constitution of alternative and less energy intensive construction materials, which, for example, provide less weight and thus shipping effort or lower conductance and hence less transmission losses.

In terms of actually firstly more multifunctional and secondly perusal providing collector types, specific coatings and nano-additives offer enhancement optical performances as well as significant perusal quality. Essentially, coatings promote glazings with collector abilities. Moreover, glazings turn into slim, smart and multifunctional envelope elements.

Further allow modern coatings and additives self-regulating operation of apertures and working mediums. Thus, stagnation can be excluded during operation, what result in highly efficient operation, efficient yields and less heat stress for components, construction and comfort.

---

### § 3.6 Inspection of negative impact on interior thermal comfort

---

Manifold benefits has been demonstrated by the author and other references (Rennhofer, Berger, Abawi, Leidl, 2015 [130]; Gosztonyi, Rennhofer, Zauner, Windholz, 2013, [96]) in section 03 of incorporating renewable energy collectors into vertical building façades. In so far, emphasis is put on considerable enlargement of building specific installation area as well as synergetic building physical benefits by means of weather shell and seasonal active thermal insulation and finally monetary savings in account of façade cladding. However, integral facades, as building envelopes embedding energy collectors need to be regarded, hold significant potential for undesired thermal impact in matter of heat stress on interior spacial thermal comfort.

Continuative, incorporation of renewable energy collectors into building skins may cause additional or even higher auxiliary energy for space cooling than benefits by integral actually balance.

Different researchers have investigated on thermal impact of façade integrated photovoltaic and solar thermal collectors as well, determined severity on well-being of space users and identified strategies for enhanced integral façade and collector designs.

The following sections will cardinaly reflect results of research on solar thermal embedded and photovoltaic embedded technologies. In the field of solar thermal applications will be differentiated between in general flat plate and tube collectors, which are incorporated in massive solid ribbon facades and skeleton unitized metal facades as well.

### § 3.6.1 Impact of solar thermal collectors

---

Normally, surfaces being affected by irradiation absorb electro-magnetic energy split-  
ted in different wavelength. Absorption causes sensible up heating of the absorption  
material. Solely in account of this irradiation can be converted into heating energy or  
power.

As explained in section 01, a collector efficiency is closely related to thermal losses of  
the collector device to the environment. Nevertheless, solar thermal collectors, that are  
embedded in building skins, do not simply loose heating energy to the environment,  
but also towards interior spaces they adjoin to.

Zauner, Sterrer and Gosztanyi (2014) [131] observed during the MPPF (Multif-  
unctional Plug&Play Approach in Façade technology) project temperatures of two  
different absorber materials of office façade embedded solar thermal collectors. On  
a winters day a copper based collector in an entirely mineral wool insulated external  
wall was parallel monitored to a alumina based collector in an external wall, which was  
semi-insulated by mineral wool and aerogel mats (Fig. 3.42).

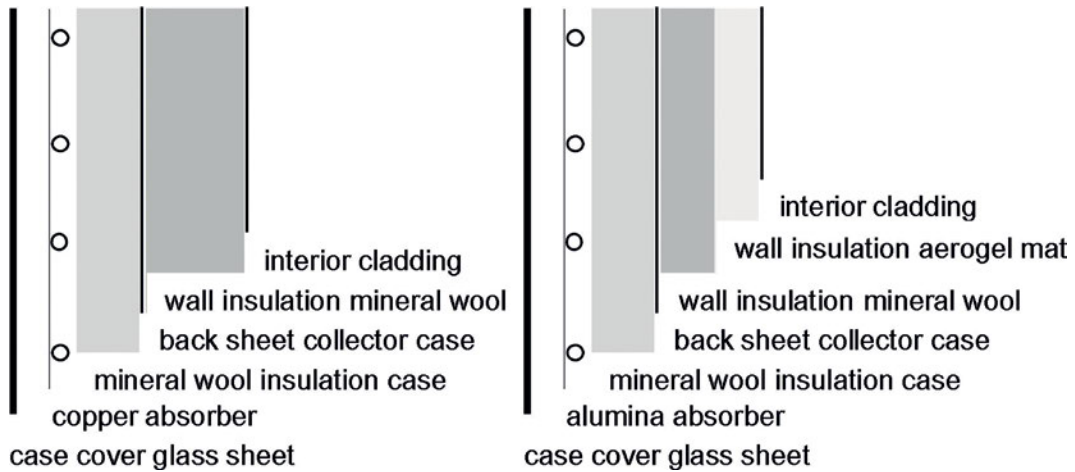


FIGURE 3.42 Material differences of absorber and wall insulation

The irradiation maximum was  $400 \text{ W/m}^2$ , what resulted in maximum absorber temperatures of  $57$  to  $60^\circ\text{C}$ . In consequence, the inner wall surface temperatures of the adjoined space raised to maximum  $25$  to  $26^\circ\text{C}$ . This observation delivers two different findings, inasmuch as during winter period with an irradiation of maximum  $400 \text{ W/m}^2$  building skin embedded solar thermal collectors do not affect interior thermal comfort significantly and, among these observations, aerogel insulation mats offer no thermal insulation benefits at all.

Furthermore, the measured absorber temperatures at max solely slightly differ in account of  $400 \text{ W/m}^2$  irradiation between  $58$  and  $60^\circ\text{C}$ . Both test setups led to clear-cut results measured in the third week of September, in autumn. In particular, while the absorber temperature raised up to  $90^\circ\text{C}$  in terms of  $600 \text{ W/m}^2$  irradiation, ambient temperature and wall temperatures increased significantly. Although, the partly aerogel-mat insulated variant managed to half the energy flow from collector to internal wall surface (Fig.3.43), thermal comfort according to [99] was still not acceptable.

On the other hand, Matuska and Sourek detect 2006 that a homogeneously façade embedded solar thermal collector, significantly participating from the massive brick wall mineral insulation (see APPENDIX C.6) by means of back and edge insulation, causes under certain circumstances a raise in internal surface temperature.

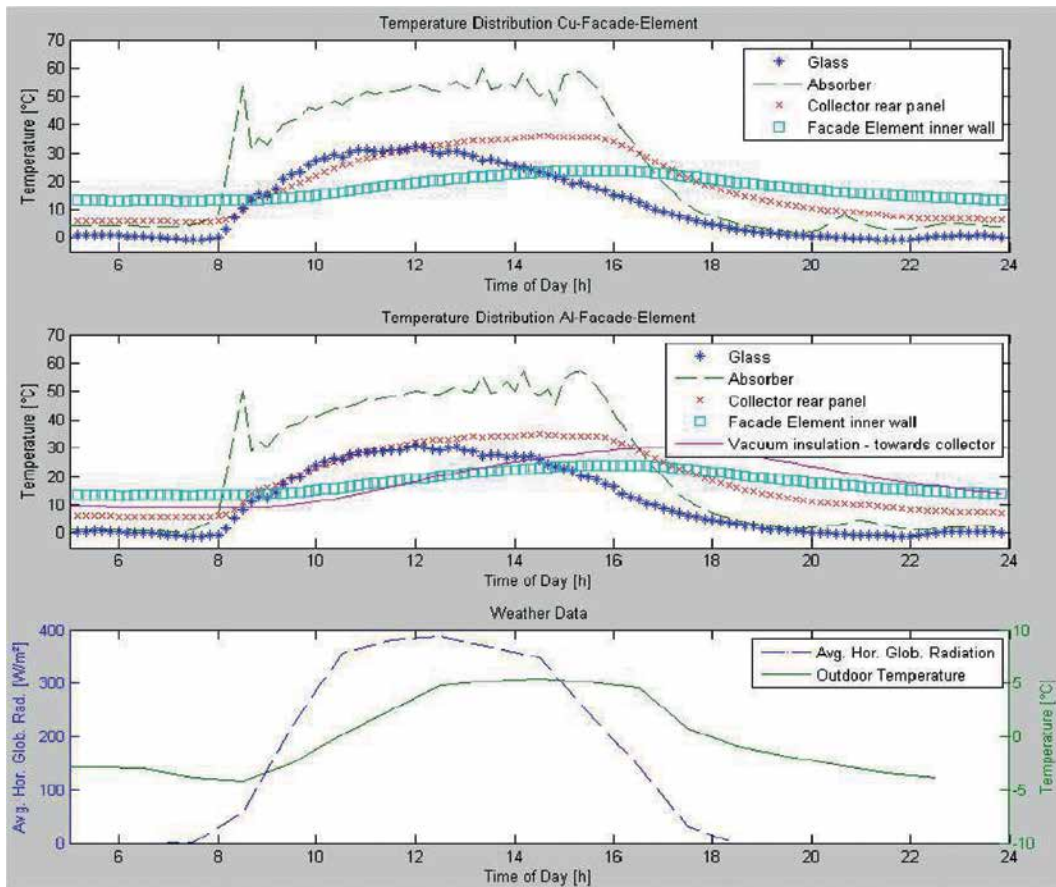


Abb. 4: Temperaturverteilung in unterschiedlichen Schichten in den beiden Modultypen (oben: Cu-Modul, unten: Al-Modul mit Vakuumdämmung). Die Daten wurden am 13.2.2010 aufgezeichnet.

FIGURE 3.43 Observed absorber and interior surface temperature of a copper based, mineral wool insulated solar thermal collector and a alumina based, aerogel insulated collector, by  $400 \text{ W/m}^2$  irradiation, winter day

By computer simulation with KOLEKTOR software and TRNSYS the authors calculated the effect of a south directed,  $90^\circ$  inclined collector on internal ambient air temperature and subsequently on the percentage of dissatisfied space occupants. They investigated the effects both for  $9\text{m}^2$  external middle-weight panel walls with thermal resistance  $R$  of 1, 3 and  $6 \text{ m}^2\text{k/W}$  and for heavy-weight wall with identical thermal resistances, including  $3\text{m}^2$  for windows.

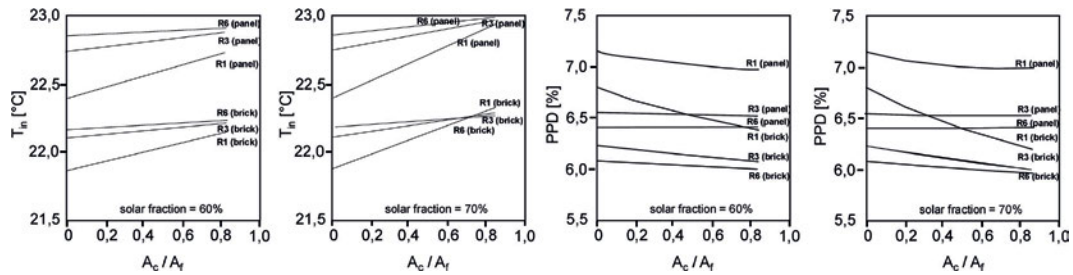


FIGURE 3.44 Average indoor temperature  $T_{in}$  und PPD value in spaces adjoined to facade embedded flat plate collectors during summer (June to August)

The simulation models varied in respect of the thermal resistance or the façade from 1 to 6  $m^2k/W$ , in respect of middle- and heavy-weight, in respect of solar fraction either 60 or 70% and in respect of the area-wise fraction of collector aperture to the wall area (between 0 to 100% of 6 $m^2$ ).

Matuska and Sourek [95] identify a strong correlation between the external wall construction principle (insulated panel wall or insulated brick wall) and the absolute maximum internal air temperature. No matter of solar fraction, internal temperature was always higher (between 22.3 and 22.8°C) among the middle-weight variants compared to the heavy-weight variants (21.8 and 22.3°C).

Further, internal temperature of heavy-weight constructions even did not reached temperature level of middle-weight construction even at area-wise proportion of 100%.

Both interior temperature levels raised linearly in accordance to increasing area-wise fractions of solar thermal collectors of the entire façade area (9 $m^2$ ). Interestingly, they reveal, that considering a solar fraction of 60%, the higher the thermal resistance of the external wall is (max. 6  $m^2k/W$ ) the higher internal temperature rises. Solely, with a solar fraction of 70% the correlation turns into the opposite while exceeding an area-wise collector fraction of 0.75 (75%). Moreover, the more the area-wise collector fraction approximates 80% the smaller the difference between internal temperatures with middle-, or heavy-weight constructions is (< 0,2K). What is more of interest, they show a clear-cut relation between rising internal temperatures and rising area-wise collector proportion and a diametrically increasing influence of thermal resistance of the façade itself (Fig.3.44).

In order to identify the effect of collector radiation on thermal comfort and human perception, Matuska and Sourek parallel determine the percentage of dissatisfied

(PPD) according to DIN EN ISO 7730. In general, solar fraction, either 60 or 70%, has no significant influence on PPD. The percentage of dissatisfied occupants is generally higher with a middle-weight panel façade construction than with a heavy-weight brick construction. Notwithstanding, a poor thermal resistance of  $1 \text{ m}^2\text{k/W}$  for a brick wall mainly causes higher PPD than the heaviest panel constructions. But, interestingly, the authors evaluate a disproportional relationship between a rising proportion of area-wise collector integration and the resulting percentage of dissatisfied. They detect an interrelationship, which asymptotically stabilizes PPD the larger the collector area/wall area proportion is. Matuska and Sourek reveal a PPD during summer time not worse than 7.0 to 7.2% and not better than 6.0 to 6.1% depending on the collector/wall area fraction.

Finally, the authors state that with first an averaged absorber temperature less than  $70^\circ\text{C}$  and second a sufficient thermal insulation, no significant thermal impact for adjoined spaces is to be recognized. Eventually, they conclude, that well insulated façade embedded collectors might simply raise internal room temperature by 1 Kelvin.

Tremendously differing results could have been generated by several researchers representing several building physical and building management disciplines in the five-year-lasting research project Multifunctional Plug & Play Approach in Façade Technology (MPPF) on a real-to-real experimental test set-up ending in 2013. Within a new built two-storey high office building in Stallhofen, Austria, were installed different collectors in order to generate renewable energy. Different approaches of solar thermal flat plate collectors, either rear ventilated or not, (see [APPENDIX C.7](#)) and photovoltaic collector modules of diverse cell technology were incorporated in solid south directed ribbon façades.

Energy distribution was led through the construction and supplied water buffers and electrochemical storages. Further, all external façade area, beside window area, was utilized to incorporate collector technology, regarding vertical opaque and parapet areas as well. The figure in [APPENDIX C.7](#) schematically illustrates wall construction principle and layers. Summarized, all crucial points of collectors, within the façade construction itself, on internal space surfaces and the space temperature have been equipped by sensor to constantly monitor thermal and humidity related effects of collectors in operation during entire years.

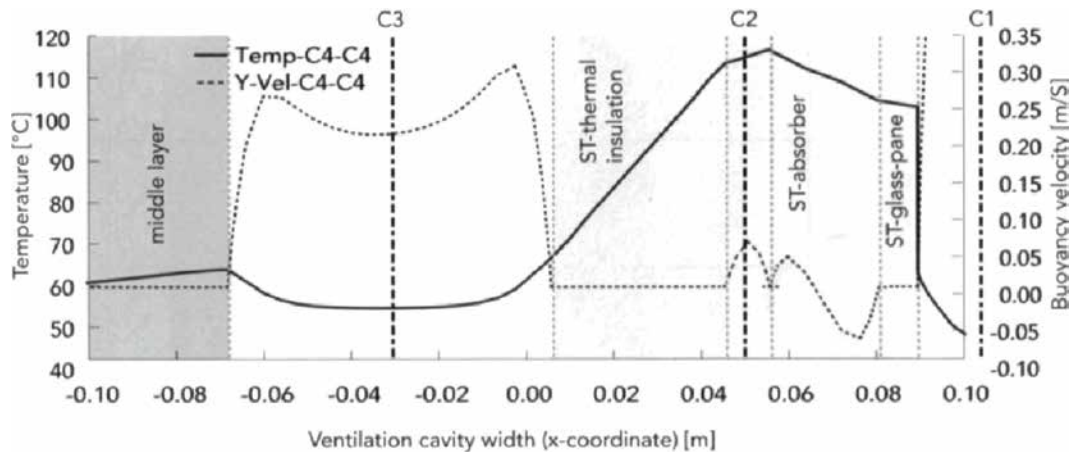


FIGURE 3.45 Temperature profile in ventilation cavities MPPF facade during summer with embedded solar thermal collector

Mach and Brandl (2015) [132] observed temperature profiles within the façade construction on summer days (Fig.3.45). The scheme represents the crucial façade layers, namely a.) collector glazing as whether shell, b.) the solar thermal absorber, c.) solar thermal insulation layer and case back side, d.) the rear ventilation layer (60 mm) and the thermal insulation layer of the solid façade construction.

As indicator of considerable thermal impact as a matter of radiation losses, was additionally plotted the velocity of the induced air within the cavity and within other permeable layers, when possible. The authors evaluate enormous surface temperatures on the collector cover glazing of especially  $>100^{\circ}\text{C}$ , while the absorber temperature reaches approximately  $120^{\circ}\text{C}$ . In consequence of thermal backside insulation the temperature within the collector case decreases towards fairly  $70^{\circ}\text{C}$  on the collector case backside.

Subsequently, a backside temperature of approximately  $70^{\circ}\text{C}$  heats up the 60 mm cavity between case and construction insulation to minimum  $56^{\circ}\text{C}$  and rises on the cavity facing surface of the insulation to approximately  $63^{\circ}\text{C}$ .

Likewise, as the scheme plots solely the first 30mm of apparently 200mm thermal insulation, the temperature decreases by 1K each 10 mm of this layer. This relationship indicates a remaining surface temperature on the wall finish of the adjoining space of at least  $30^{\circ}\text{C}$ .

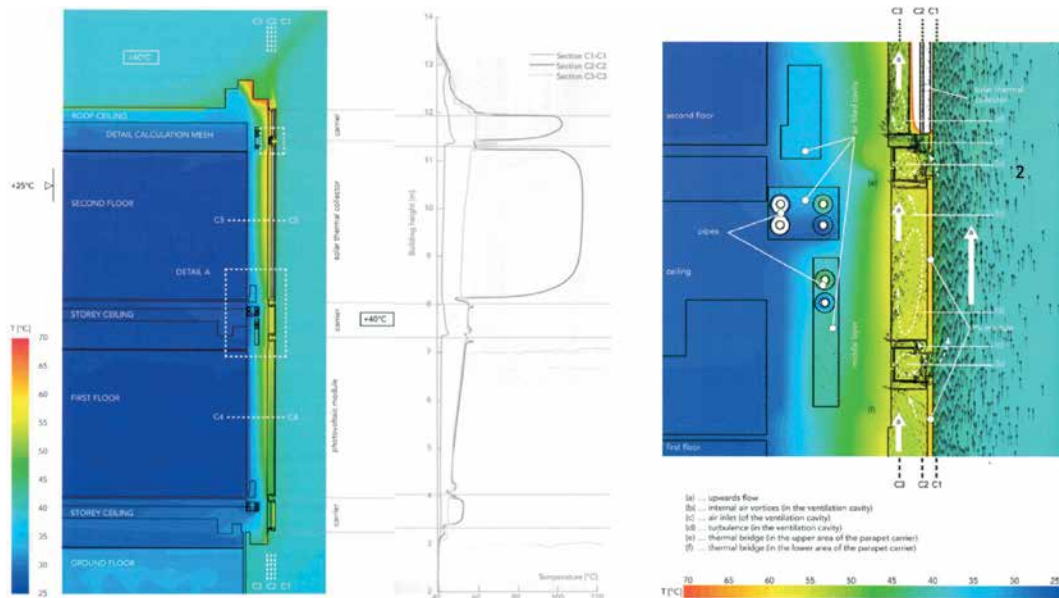


FIGURE 3.46 a.) Temperature patterns and thermal affects of embedded solar thermal collector on case backside, b.) in construction and c.) space during summer

Even though, the building is modern and thermally insulated among modern standards (insulation layer between 160 to 200 mm), the remaining internal surface temperature and hence, the thermal impact of a modern solid façade integrated solar thermal collector appears to be significant. It is worth mentioning, that Mach and Brandl [132] revealed a collector caseback surface temperature of still 63°C while the absorber operation temperature exceeds 115°C. Furthermore, the plot demonstrably shows a rise in air velocity in the rear ventilation cavity from 0 to 0.30 m/s induced by this thermal losses. The smaller the cavity, the higher induced air velocity (Mach, Grobbauer, Streicher, Müller, 2015, [83]).

However, the collector is separated from the bearing construction by a 60 mm cavity, the thermally disconnecting effect is demonstrably poor, since the cavity air temperature differs towards the case backside temperature simply for 3 Kelvin. Since the thermal insulation surface temperature in the middle area continues with 63°C, similar to the collector temperature (70°C), but not tremendously lower, indicates, that the cavity provides simply minor effect on thermal disconnection. In the same line, Figure 3.46 shows three different plots, which, by detailed evaluation, reinforce the thermal impact of a façade embedded collector. The plots represent an embedded solar thermal collector operating summer times.

Layer C1 in the left plot, representing the collector layer within the façade shows operation temperature of maximum 60 to 65°C, whereas layer C2 and C3 as construction areas of the façade still remain temperatures of maximum 38°C.

The inner wall surface areas tend to heat space-wards with temperature up to 32°C. Thus, beside the space ambient air temperature is below 30°C it is significantly affected.

Further, more detailed, the plot in the middle illustrates the temperature profile abroad the two level high façade in the middle layer section C2, beyond the collector, but forward to the space. This plot considerably shows an increase in temperature especially in the section of the collector far above 100°C.

Moreover, the above located carrier as elongated building structure tends to heat up in a similar range as the collector itself, inasmuch as temperature rises towards 100°C. The immediate effect on heat conduction by construction illustrates layer C3, insofar as temperature still remains at least at 45°C, in maximum at 71°C in the carrier area. Nonetheless, the mean temperature in layer C3 within the collector area is 56°C. Similarly, the right plot of Fig.3.46 gives an idea, what temperature range affects the construction between collector backside and interior spacial wall surface. While the collector backside radiates with higher than 70°C, layers of the solid façade construction are still at 32°C.

Overall, these different plots representing all the same situation exemplify a non-negligible thermal impact of envelope embedded thermal collector on the entire construction and subsequently on special surface conditions. This fact demonstrates the counterproductive impact especially in summer times, when in matter of external solar gains, comparably high external air temperature heat up cooled and moderate interior wall surface temperatures. Additionally, Grobbauer and Mach (2013, [133]) inspected on the 29th of July 2013 during the MPPF project stagnation behavior and impact of a building skin incorporated solar thermal flat collector without profiting by any ventilated cavity.

During this inspection day maximum global irradiation was 869 W/m<sup>2</sup> and maximum vertical global radiation was 545 W/m<sup>2</sup> what causes an absorber temperature of 139°C. The authors measured an effective ambient air temperature of at least 36°C (Fig. 3.47) and at maximum at 38.9°C, what is both intolerable by means of indoor thermal comfort either in summer or winter.

A rear ventilation of a facade integrated solar thermal collector is concluded by Mach, Grobbauer, Streicher, Müller (2015), the most appropriate method to thermally disconnect collector from construction and space and thus, to lower thermal impact.

The authors call attention to five different benefits of rear ventilated collector facades :

- *thermal and sound protection layer*
- *vapor pressure barrier if solid internal barrier fails*
- *less impact in case of collector overheating*
- *forced rain protection and drainage cavity*
- *synthetic polymer building elements or ducts are not effected by high temperatures*

Aligned with the arguments above, Grobbauer, Grätzer, Ruckhofer and Müller (2015, [134]) as participant researcher in the MPPF project suggest distributing collector piping within the façade in rear ventilated chambers in order to minimize negative radiation impact to construction and space.

Likewise, Gosztonyi, Rennhofer, Zauner and Windholz (2013) [96] acknowledge necessity of ventilation cavities by the temporal impact a collector can have as an extraordinary heating source within a building skin in relation to envelope incorporated humidity. In fact, a hot collector firstly sucks, but secondly accumulated humidity in construction as well. If the collector is rear ventilated, humidity moves outwards and exits the construction. But, however, if the collector is embedded not rear-ventilated, humidity not consequently leaves the construction.

Moreover, if the collector does not run and is non-rear ventilated, accumulated humidity tends to condensate, what continually harms the construction in terms of corrosion and mould. But as far as the author explained in section 3.1 of this chapter, in case of stagnation the range of steam is a measure to determine the effect stagnation can have on the entire distribution pipe work.

Since, it is not feasible to encapsulate piping completely within façade from conduction by air cavities, and additionally, since the range of steam easily may affect the entire pipe work length, parts of facades will still remain being thermally stressed and initiator of tremendous thermal impacts on thermal comfort.

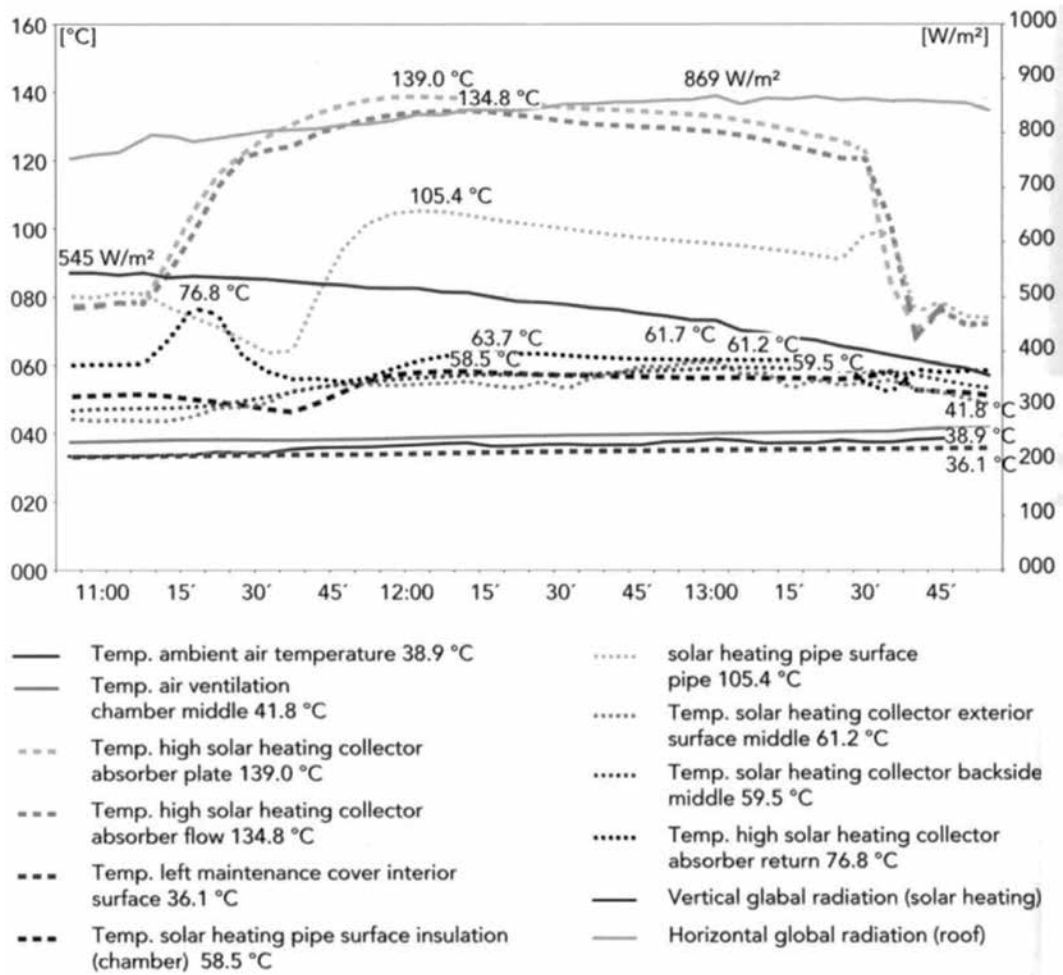


FIGURE 3.47 Temperature profiles of a MPPF embedded solar thermal collector in summer during stagnation

Opposed to those experimental findings explicated above, Matuska and Sourek (2006) emphasize as conclusion of their theoretical computational study, that in general façade integrated solar thermal collector normally do not tend to rise internal ambient air temperature more than 1 K.

Thus, on the contrary, they claim, that collector might not have any worth mentioning influence on interior thermal comfort.

### § 3.6.1.1 Behavior of combined collector-storage systems

Similar results could have been observed by Gohl, Stark and Drück (2015) [135] by measurements of a completely different and innovative envelope integrated collector and storage development (APPENDIX C.8). The development bases on a poly-propylene sensible water buffer tank being incorporated in a massive external building wall, that is coated by solar lack and thus being partly storage and partly absorber by itself. The external surface of the wall is finished by transparent insulation.

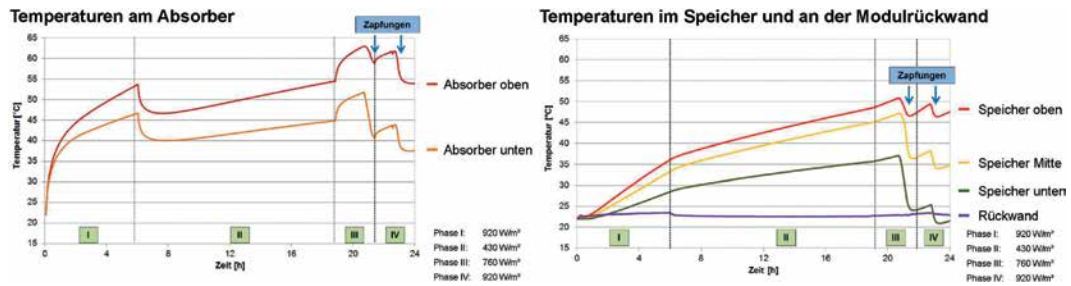


FIGURE 3.48 Absorber-, storage- and interior wall surface temperatures with irradiation between 430 and 920 W/m<sup>2</sup>

The storage tank backside and the flanks aside as well are thermally insulated by aergel insulation mats. The finish towards the occupied space is made by a several centimetre lasting phase change material layer (micro-encapsulated PCM, melting point 25°C) and covered by gypsum plaster boards. This integral wall/storage/collector-construction is called Multi-Komp Façade (APP. C.8). The transparent insulation as collector cover sheet is made of a double glazing with a 30 mm aergel filling.

This construction provides a U-value of 0,6 W/m<sup>2</sup> and a g-value of 0,6 as well (Loose, 2015, [136]). During empirical in-situ measurements and during test booth measurements with irradiation between 600 and 1.000 W/m<sup>2</sup> the storage temperature never exceeded 55°C, beside the absorber temperature reached slightly higher to 63°C. That was related to considerable energy losses of the double glazing cover sheet encountering tremendous proportions of solar reflection and absorption.

However, in spite of moderate absorber and storage temperatures ( $<60^{\circ}\text{C}$ ), the measured internal wall temperature profile ranged between  $23$  to  $27^{\circ}\text{C}$  (Fig.3.48) and raised during operation in August up to  $36^{\circ}\text{C}$  (Gohl, Stark, Drück, Loose, 2015, [137]).

The presented results let conclude that generally during the year especially this wall/storage/collector-construction provides appropriate surface temperatures, which do not effect thermal comfort. Nonetheless, except for August, i.e. mid-summer, surface temperature of  $36^{\circ}\text{C}$  related to comparably low absorber temperatures exceed tolerable limits. Summarized, the impact on thermal comfort by this design is elucidated to be not worth mentioning, yet surface temperatures exhibit to be comparably high in relation to the low system efficiency.

### § 3.6.1.2 Investigations on effects of hybrid-systems

---

Completely oppositional, actually positive synergetic results concerning influence on thermal comfort by integral façade concept have been revealed by Chow, He and Ji (2006) [138] for building skin integrated hybrid collectors (APPEND. C.9). Since, photovoltaic cells tend to predominantly not produce electricity, but warmth compared to area-wise intensity of irradiation, photovoltaic modules absorb irradiation and consistently inevitably heat up.

Up heating of photovoltaic cells results in a decrease of potential power output, what Chow, He and Ji [139] determine to effect on a power decrease of  $0,0045\%$  per K increasing cell temperature.

In consequence, by acknowledging this relationship, many researchers and developers have investigated on combined photovoltaic and solar thermal collectors three decades.

Combined photovoltaic and solar thermal collectors basically work mainly as power generator, while a PV wafer backside arranged water flooded capillary tube or piping grid changes the heat by conduction. Thus, the thermal collector accumulates the heat energy of the PV module and cools.

This collector combination represents hybrid technologies and offers diverse synergetic benefits, inasmuch it provides both power and heat collection, optimized thermal PV module efficiency and a comparably high area-wise system efficiency as well.

Chow, He and Ji inspected indoor thermal comfort in relation to façade integrated PVT hybrid technology by an empirical test set-up, placed in Hong Kong. Next to the test room, a secondary reference room was installed without envelope embedded renewable energy collector. While 6 pieces of 90° inclined PVT collectors approximately covered 80% of a southwest facing façade, the reference room façade was homogeneously solid and opaque.

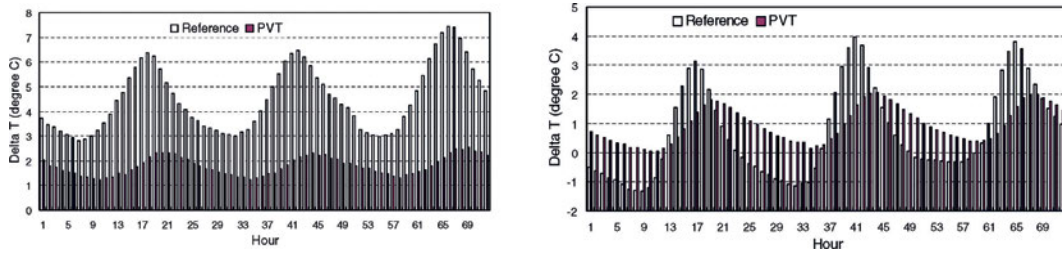


FIGURE 3.49 Caption Interior facade surface temperatures amplitude (delta T) for a hybrid facade and a reference facade for a hot summer (left) and winter period (right)

The external walls characterized having a specific weight of  $>1.300 \text{ kg/m}^2$  and a specific heat capacity of  $840 \text{ J/kg}\cdot\text{C}$ . The authors test PVT collectors naturally driven and forced driven with a mass flow rate of  $0,11 \text{ kg/s}$ . The experimental investigation recovered, that compared to the reference room wall surface temperature amplitudes of maximum  $7,4\text{K}$  could have been reduce to maximum  $2,5^\circ\text{C}$  in summer by running hybrid collectors (Fig. 3.49). What is more of interest, the installed PVT hybrid collectors manage to lower tremendously the temperature amplitudes, although in July 2005 was a very hot summer with city centre air temperatures of maximum  $35.9^\circ\text{C}$ . They additionally observe a time shift of 2 to 3 hours, before the hybrid wall encountered the maximum amplitude compared to the reference wall.

Thus, hybrid collectors, in matter of complex multifunctional derivate of integral facades, stabilize ambient room temperature or rather downsize radiative impact on thermal and stabilize energy fluxes across facades. Resuming from that prospective, façade incorporated hybrid collectors provide thermally active insulation properties (Ji, Han, Chow, Yi, Lu, He and Sun, 2006, [140]).

As a consequence, the authors evaluated significant savings in space heating and especially space cooling demand. They describe savings of thermal loads crossing the hybrid façade of about 59%. From that we can deduce a reduction of energy

consumption for space conditioning to 41%. The authors conclude, that envelope embedded hybrid collectors by means of multifunctional facades provide additional, but renewable energy for building management and reduce building maintenance effort, and on this account are essential components of energy-efficient building concepts.

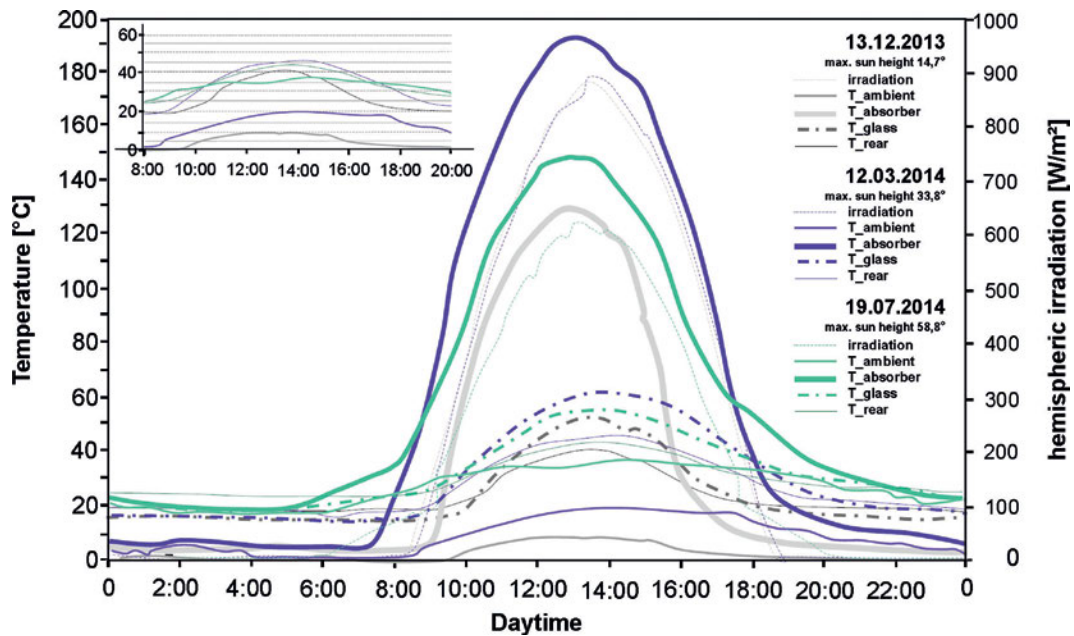


FIGURE 3.50 Temperature profiles of a triple-glazing argon filled collector ( $d=51$  mm,  $\eta_0 = 0,784$ ,  $a_1 = 3,21$  W/m<sup>2</sup>K) with bonded absorber on three different days (seasons) and induced glass surface #6 temperatures

The positive synergetic effect of hybrid collectors on thermal comfort can be explained by analysing both specific construction and operation principle. By reason of photovoltaic cells as being moderate solar thermal absorbers in general, cell temperatures seldom exceed 70°C under normal environmental conditions.

Thus, the absorption property of PV cells is comparable to ordinary not evacuated flat plate collectors. Besides, flat plate collectors are thermally optimized by insulation in order to minimize heat losses by conduction, transmission and convection, the capillary structure of a hybrid collector is poorly insulated.

Rather radiative and convective losses to environment are more likely in order to cool PV cells and contrariwise enhance cell efficiency. Hence, this constructive concept results in markedly moderate distribution fluid temperatures of 30 to 40°C. Additionally, Ji, Han, Chow, Yi, Lu, He and Sun (2006) revealed by numerical simulation, that especially hybrid envelope embedded collectors profit from high working fluid mass flows (0.01 to 0.05 kg/s) up to a critical point in summer time in order to amplify cell cooling and opposed to that minimize thermal impact. Heating sources or gains of this particular moderate temperature level do not have decisive influence the thermal behaviour of external walls in summer, but positive ancillary effect in intermediate or winter periods.

Within a research & development project ending in 2014, Giovannetti, Kirchner, Franke, Rohde and Scherer [97] developed opaque double and triple glazing units, which incorporate selective absorbers and piping.

Thus, they manage to generate glass collectors which perfectly fit into standard window frame systems (see chapter 3.5). Beside measurements of performance and innovative material connection, they reveal specific rear glass (space adjoined glass surfaces) temperatures related to operation temperature. They record for an argon gas-filled triple-glazing collector variant of 51 mm thickness and a bonded absorber a surface temperature on #6 of 57°C. Interestingly, even for a triple glazing unit this temperature undoubtedly will have considerable impact on internal thermal comfort.

On the contrary, an argon-filled quadruple-glazing collector of 76 mm thickness and bonded absorber solely causes 46°C surface temperature, that is expected to virtually have any negative impact in winter time, but explicitly in summer time.

### § 3.6.2 Technical solutions for radiation barriers

---

Above registered research and practical experience show that there is a strong relation between façade integrated solar thermal or photovoltaic collectors and negative undesired impact on interior thermal comfort. Tube collectors show by construction principle as either being installed rear ventilated or at least being evacuated no impact on thermal comfort.

Likewise, envelope embedded hybrid collector encounter simply moderate absorber temperatures, which they attend to diminish either by massive thermal losses or by increased working mass flows.

Thus, remaining radiative potential is lowered to a level not worth mentioning in the context of thermal impacts. Exclusively, as research results above explicate, building skin integrated flat plate collectors bear potential for massive influence and spacial thermal comfort. For this reason, different approaches, which differ in terms of constructive complexity and costs (Fig.3.51) has been investigated in order to eliminate radiation or transmission towards spaces.

TYPOLOGY / LEVEL	LEVEL of COLLECTOR				LEVEL of FAÇADE CLADDING	LEVEL of FAÇADE CONSTRUCTION			LEVEL of SPACIAL WALL CONSTRUCTION			
	aerogel imbedded absorber	OR	case evacuation	OR		thickness enhanced in-case back insulation	rear ventilation	thickness enhanced construction insulation		OR	aerogel-mat / VIP construction insulation	
GLAZED FLAT PLATE COLLECTOR												
<i>effect</i>	++++		+++++		++		+	++		++++		++
EVACUATED FLAT PLATE COLLECTOR	-				rear ventilation	thickness enhanced construction insulation			phase change material			
<i>effect</i>					+	+++++			+++++			
HYBRID PVT COLLECTOR	actively cooled absorber (fluid / hybrid collector)				rear ventilation	-			-			
<i>effect</i>	+++++				+++++							
PHOTOVOLTAIC MODULE	-				rear ventilation	-			-			
<i>effect</i>					+							
TRIPLE GLAZING int. PHOTOVOLTAIC	inert gas filling (Krypton, Argon)	OR	evacuation	OR	highly effective Low <sub>e</sub> -coating on # 3	-			-			
<i>effect</i>	+++		+++++		+							

FIGURE 3.51 Action on different levels to prevent / minimize thermal impact by envelope incorporated collectors on thermal comfort

Tube collectors show by construction principle as either being installed rear ventilated or at least being evacuated no impact on thermal comfort. Likewise, envelope embedded hybrid collector encounter simply moderate absorber temperatures, which they attend to diminish either by massive thermal losses or by increased working mass flows. Thus, remaining radiative potential is lowered to a level not worth mentioning in the context of thermal impacts. Exclusively, as research results above explicate, building skin integrated flat plate collectors bear potential for massive influence and spacial thermal comfort. For this reason, different approaches, which differ in terms of constructive complexity and costs (Fig.3.51) has been investigated in order to eliminate radiation or transmission towards spaces. The figure in [APPENDIX C.10](#) illustrates radiation potential in term of energy flux (transmission losses) of envelope integrated flat plate collectors. The histogram compares different activities to thermally insulate heating source (absorber) within the collector case (a1 to a3) and three activities of construction insulation (b1 to b3). Furthermore, the figure considers three different operation scenarios, which take normal absorber operation temperature (70°C), enhanced absorber operation temperature (120°C) and stagnation temperature (150°C) into account. In this context, stagnation may cause

20W/m<sup>2</sup> radiation potential considering a standardized insulation flat plate collector. For normal conditions a radiation potential of 7,8 W/m<sup>2</sup> is calculated. Collector case evacuation is eligible to reduce the stagnation radiation potential to equivalent radiation potential of normal operation of approx. 8W/m<sup>2</sup>.

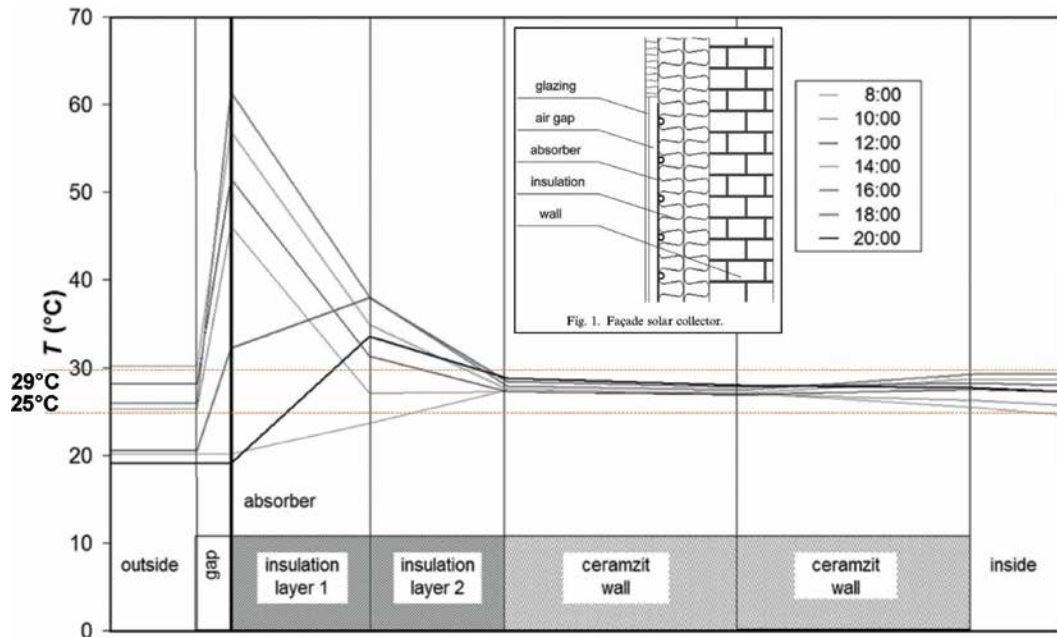


FIGURE 3.52 Temperature profile in an evaluated facade construction on a typical summer day

Moreover, case evacuation bears potential to minimize radiation towards 3,2 W/m<sup>2</sup>. Aerogel mat or vacuum insulation panel integration in the common wall insulation layer represent alternatives for case evacuation, which reduce the standard radiation potential for 44 to 48%. Beside that numeral static inspection neglecting any material specific inertia or heat capacity three different researcher evaluated on enhanced integral façade design. First to mention is Svendsen (1992) [141], who evaluated experimentally and theoretically the collector efficiency of a flat plate collector, what absorber is embedded in two times 20 mm aerogel mat two and a half decades ago.

Although Svendsen does not explicitly document any effect on radiation potential reduction, he exposes enormous efficiency improvement by simply reducing transmission losses by aerogel insulation. He reports an annual performance of a typical

flat plate collector (1992) of 316 kWh/m<sup>2</sup> with 60°C absorber temperature and 183 kWh/m<sup>2</sup> for 80°C. Opposed to that, the aerogel embedded absorber was eligible to escalate annual performance by 221% to 699 kWh/m<sup>2</sup> at 60°C and by 338% to 620 kWh/m<sup>2</sup> at 80°C. Hence, these numbers illustrate tremendous reduction of redundant thermal transmission losses to environment and yet from this we can infer, that façade transmission and equally radiation potential can be reduced significantly. Svendsen additionally elaborates in this context, that enhancement of aerogel dimension higher than 15 mm (20, 25 mm) has simply modest effect of 4 to 8% performance improvement.

Beyond the collector layer itself Matuska and Sourek identify resulting surface temperatures of interior walls of adjoining spaces, which fully incorporate solar thermal flat collectors. The collector that is being inspected, does not profit by any in-case thermal insulation (Fig.3.52), but is totally embedded into two consecutive thermal mineral wool insulation layers of each 100 mm thickness.

The bearing wall construction bases on middle-weight ceramzit wall construction with a specific density of <1000 kg/m<sup>3</sup>. The entire inspected wall construction leads a transmission resistance factor about 6 m<sup>2</sup>k/W. Based upon this configuration the authors recorded a surface temperature variation during the day (between 8 AM to 8 PM) of 25 to 29°C, what results in a collector related radiation impact of 4 K. But continuatively, they state for an alternative heavy brick work (1.600 kg/m<sup>3</sup>) average temperature differences of solely 1 K.

Although Mach, Grobbauer, Streicher and Müller (2015) [82] acknowledge construction surface temperatures of 32 to 35°C resulting from a rear-ventilated façade integrated collector, they conclude that a rear-ventilated collector is the most efficient less affecting solution to prevent any thermal impacts on thermal comfort. They observed resulting interior wall surface temperatures of at maximum 28 to 32°C.

Nonetheless, a rear ventilation of a façade embedded collector avoid massive wall construction from capacitive energy storing, impounding and re-emitting at later time related to material specific inertia.

### § 3.6.3 Impact of photovoltaic collectors

---

Beside solar thermal collectors, envelope integrated photovoltaic modules similarly bear potential to influence spacial thermal comfort. That became exceedingly obvious

in the context of the run sun space test set-up that is located in Bissendorf, Osnabrück. In particular, on a morning in July 2014, the author encounters external surface temperatures of double-glazing embedded a-Si modules, which were installed in the sun space roof. Temperatures reached approximately 60°C at 11 AM (see Figure 3.53), when the author climbed the roof in order to maintain tube collectors. Unendurable surface temperatures of roof incorporated modules hindered the author to stay on the roof and to finish works.

### SURFACE TEMPERATURE ROOF GLAZING SOUTH (INTERNAL) [°C]

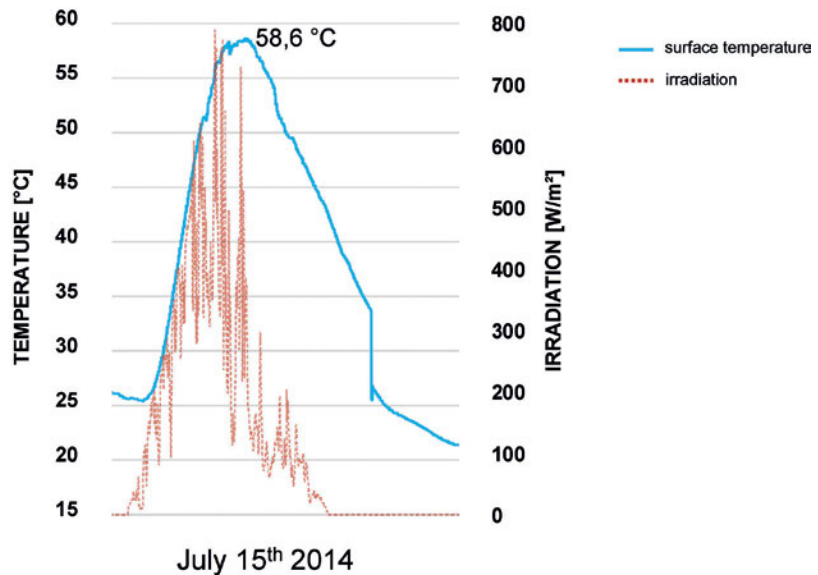


FIGURE 3.53 Internal surface temperature of south oriented PV roof glazing in July

Since, the modules are embedded in the sheltering glazing that sudden adjoins to and further defines the spacial volume, consequentially the modules exert influence on interior thermal conditions. In research different investigators have located differing impact of photovoltaic collectors on thermal comfort. Rennhofer, Berger, Abawi and Leidl (2015) [112] logged module surface temperatures of a non-rear ventilated opaque polycrystalline glass-glass and a semitransparent amorphous silicon thin-film

PV system embedded as a window filling in a post & beam façade, thus with immediate contact to the space in July 2010. Therefor temperature sensors were laminated into the PV modules on various heights. The maximum surface temperature on the

entire PV module (Fig. 3.54) was identified in the top area, what exceeded 90°C at approximately 11 o'clock in the morning. Further, a temperature level of > 50°C was observed in the top module area between 8 AM to 4 PM.

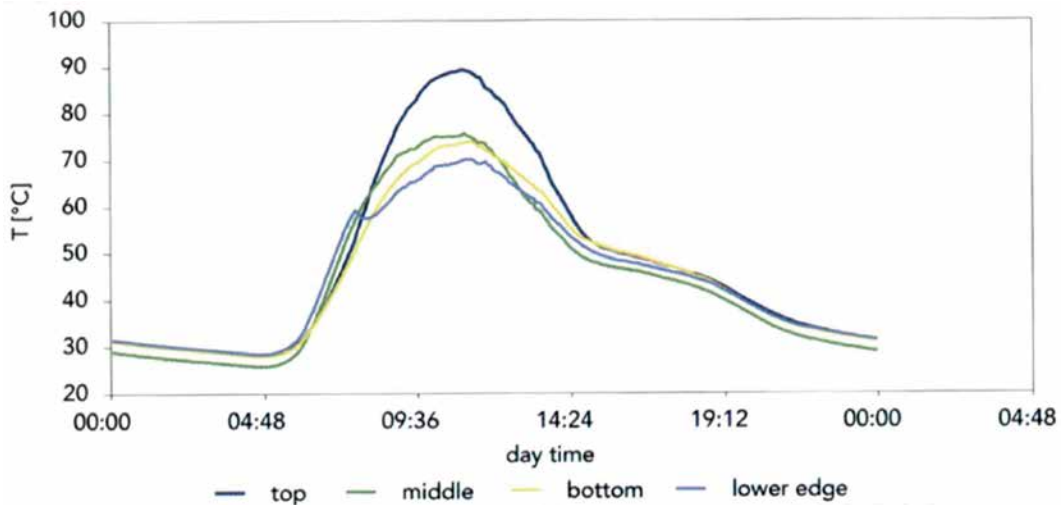


FIGURE 3.54 Facade integrated photovoltaic module surface temperatures on 19.07.2010 (Mach, Grobbauer)

The middle and bottom part of the module even reached temperatures of 76°C, whereas a temperature level >50°C was remained for more than seven and a half hours during sun shine. Interestingly, this figure demonstrates, that the module temperature was already above an assumed maximum ambient air temperature of 35°C at 7 o'clock in the morning.

Despite the authors made experiences, [112] observed maximum temperatures of a-Si thin-film modules, what constitute semi-transparent window fillings without any thermal insulation in a 90° declined façade of solely 40°C. The enormous difference of 30K between 70° and 40°C interprets the author by different irradiation reflection on the façade surfaces (90°C inclination, July; 30°C inclination, September).

Thus, different observations lead to the conclusion of a significant relation between surface temperature of thin-film modules and proportion of solar reflection closely related to sun height angle and façade inclination. Secondly is to mention, the authors reveal for polycry-stalline modules a 25% reduction of power while exceeding 75°C module temperature.

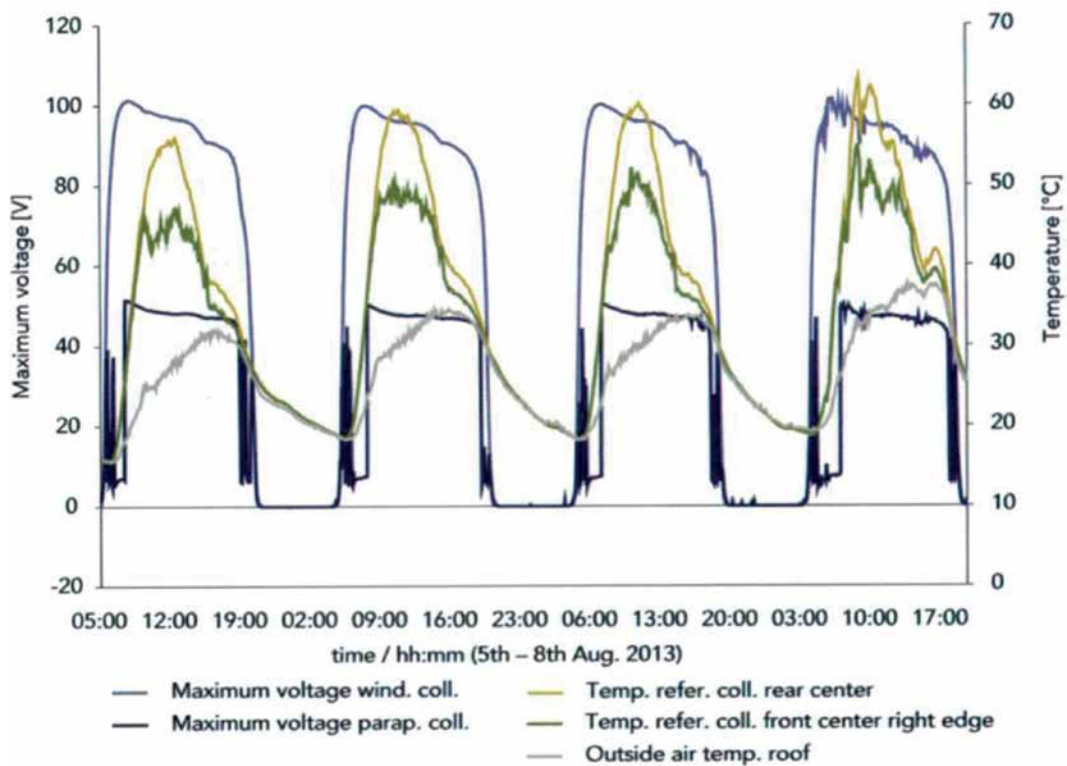


FIGURE 3.55 Facade integrated photovoltaic module surface temperatures on 19.07.2010 (Mach, Grobbauer)

Mach, Grobbauer, Streicher and Müller (2015) investigated on module surface temperature and module efficiency in terms of generated voltage on a facade integrated but rear-ventilated PV system. The authors determined a maximum possible up heating of rear-ventilated center rear module surface of approximately 63°C at 10 o'clock in the morning (Fig.3.55). Parallel, the front surface temperature facing the ambient raised to approx. 54°C.

Moreover, the graph additionally shows, that maximum module temperatures were attained several hours before ambient air temperature scored the max. In the same line Windholz, Zauner, Rennhofer and Schranzhofer (2011) [123] evaluated empirically, that shaded parts of PV modules turns the wafer cells into ohmic resistors, and hence, parts of the module tremendously heat up.

Likewise, Rennhofer, Berger, Leidl et al. (2011) [142] remark, that semi-transparent wafer cells embedded into double-glazing extraordinarily tend to absorb irradiation and thus end to emit significant secondary infrared radiation into the space. Gosztonyi [96] calls attention for a considerable impact on thermal comfort by semi-transparent double-glazing integrated PV modules. She explains, that the entire amount of solar energy passing through the façade and becoming effective in space with semi-transparent modules is less compared to sun protection glazing, but, however causes radiation asymmetries by surfaces.

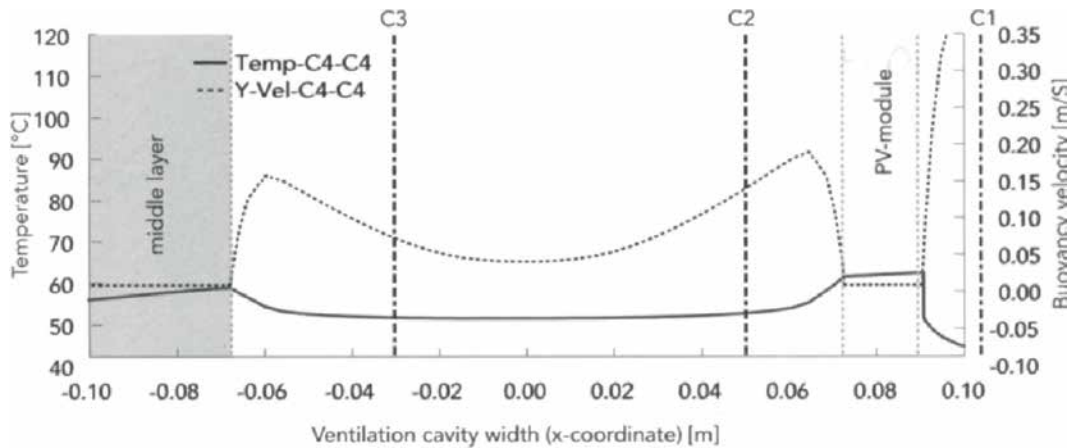


FIGURE 3.56 Temperature profile of facade embedded photovoltaic modules within the construction

In a further step a closer look into the entire façade construction (Fig.3.56) elucidates the above mentioned authors (Mach, et al., 2015), that similar to solar thermal collectors the cavity air temperature solely slightly differs from the collector rear surface temperature (53°C), but, notwithstanding, rises towards the first massive construction layer, namely thermal insulation and remains at 59°C. Thus, the entire massive façade construction is affected effectively by a PV collector with approximately 60°C already merely hours after sun rise. Consequently, a space gets affected negatively in thermal matter by a façade embedded, but rear-ventilated photovoltaic collector at the very beginning of the day.

### § 3.6.4 Summary

---

The diversity of studies and research projects verifies considerations of potential negative impact of envelope embedded collectors either photovoltaic or solar thermal on interior thermal comfort. Potential impact revealed as a question of maximum operation temperature and thermal insulation.

Further, available space for thermal insulation determines either the choice for physical or non-physical insulation by evacuation. Beside evacuation is the most effective and smart solution, nonetheless evacuation turns collector concepts complex. Rear ventilation of collectors has been detected to be indispensable. However, this is not applicable for post & beam or stick system facades, to which sun spaces principally belong.

The field conflict appeals complex. Photovoltaic as well as solar thermal collector, which are embedded in the glazing show significant risk for undesired radiation losses or rather injury. Thus, smart and slim collector types are promoted for the near future, which integrally bases on glazings in order to provide appropriate dimension limits as well as maximum perusal.

---

### § 3.7 Summary

---

Several benefits and arguments plead for incorporation of energy collectors in building skins in order to generate renewable energy for space heating. Not least, facades provide a tremendous amount of surplus installation area compared to conventional exclusive roof area. Further, practical experiences approve for facades, inasmuch vertical installation and collector inclination considerably match more sufficiently with heating demand in autumn-, winter-, spring-time. Consequently, collector efficiency in relation to sun height and temperature differences.

Stagnation has been detected to the most crucial issue in terms of collector operation, annual yield, seasonal collector efficiency and in particular undesired thermal impact on spacial thermal comfort.

This chapter informs about integral facade planning in regard of embedded collectors in respect to location, direction and collector typology. Moreover relationships between

collector efficiency and actual spacial energy loads has been revealed and constituted to be crucial design parameters. In this context, state-of-the-art solar thermal collector typologies has been identified and been categorized in matter of feasible annual yield, eligibility for charging of seasonal thermo-chemical storages, impact on thermal comfort, quality of façade integration as well as ability for free-form adaption, simplicity and perusal.

Consequently, based on the analysis of established collector typologies has been investigated on research and development projects. These projects reflect technological lacks and disadvantages in function, architectural esthetics and adaptation to location.

While for a first approach existing technologies has been applied to facades, in a second research step collectors are designed from the building envelope perspective in order to intensively satisfy structural and constructional requirements. Thus, some research and development projects concentrate on the building structure and weathered transparent skin layers in order to functionalize to absorbers and heat exchangers. Science has recognized a significant technological demand to enhance collectors for charging of seasonal thermo-chemical storages. This subject concerns specific feeding temperature levels as well as designs for combined and enveloped integrated collector and storage systems.

Research determines management of time shift by means of offer and demand, that often exceeds seasonal dimensions, as essential technological postulation for effective integral façade planning. In this context daily operating peak shaving technologies will compete with decentralized combined collector & storage systems.

This chapter additionally analyzed diverse approaches to either limit negative radiation of façade embedded collectors to internal thermal comfort by collector incorporated thermal insulation or by façade layer incorporated insulation. Positive influence in this field has proven research developments on auto-cut-off heatpipes, which by design will not exceed specific operation temperatures and flat plate absorbers coatings with self-adapting irradiation transparency. In terms of facades, these are smart developments, which demonstrate tendencies for a holistic appreciation of both sides of an entire façade.

However, it becomes evident by several investigations, that collector case embedded insulation as well as additional façade layers of rear ventilation and constructional thermal insulation solely manage to prevent collectors from undesired space up heating, if their absorber temperature is demonstrably below 100°C. Since, modern and highly efficient collector typologies encounter absorber temperatures between 170 to 260°C, negative influence on spacial thermal comfort is hardly to prevent.

In this context, tube or case evacuation has been detected to be the most promising technique in order to maintain sufficient annual yields, sorptive storage temperature level and negligible mentioning effect on space as well.

Nonetheless, this chapter elaborates a disproportional correlation between a rising quality of actual façade integration by means of façade layer and a decrease in remaining perusal quality. Hence, it is still a task for research and development to likewise realize façade integration and perusal.

Finally, crucial components of established collector designs have been questioned to be sustainable and cost-effective any longer. While cover sheets made from glass and absorbers and heat exchangers made from metals bear underestimated amounts of grey energy over all life cycles, research focus on polymer for substitution.

Since polymer are more light-weight than glass and metals and require on average less energy for manufacturing, they especially encounter deficits in crucial optical and thermal properties compared to glass and metals. Nevertheless, on-going research will evaluate, what the potential for polymers in future will be.

The next Chapter 4 concentrates on already established technologies and energy storing technologies of the near future. In this part of the thesis will be analyzed, which technologies fit best in order to manage time-shift problems of space heating demand and façade integrated renewable energy collectors.





# 4 Literature survey of seasonal electro-chemical and sorption energy storage technology

---

## § 4.1 Energy storing : logical consequence whilst a chronological offer-demand mismatch

---

We cover our day-to-day energy demand either by energy grids (power, gas) or by decentralized closed-to-consumption stocks (heating oil, natural gas). Although, we intensively promote and implement renewable energy, the fraction of renewable energy contribution worldwide on actual energy mix is concurrently about 2,5 per cent (Albrecht et al. [2]).

Storing energy means dissipating less energy. That is true for both fossil fuel based energy and renewable energy. Storing energy not only enhances security of supply, but also enhances sensible commerce of energy.

Following an extensive empirical analysis of thermal comfort, this chapter concentrates on diverse storage principles and technologies, that are either common use or are promising for an establishment in the near future. This chapter and its essentials justifies its relevance in this thesis least to evaluate potential of fossil fuel energy conservation, but rather on managing the chronological mismatch between offer and demand of renewable, in particular solar thermal energy.

### § 4.1.1 Storing a question of energy conservation

---

Energy can be described as potential to execute action. Energy involves a potential, a kinetic, a chemical or power status, that is higher than compared to another or to the immediate environment.

If energy is not chemically bonded or isolated, it inevitably interacts with the environment. For example heat, cold, or power are potentials compared to the immediate environment and tend to equalize. Whereas heat or cold is relative description of warm potential and heat and cold tend to equalize with environment three dimensional in every direction. Power is a description of ionic charge potential, which directions for equalizing are limited to bilateral.

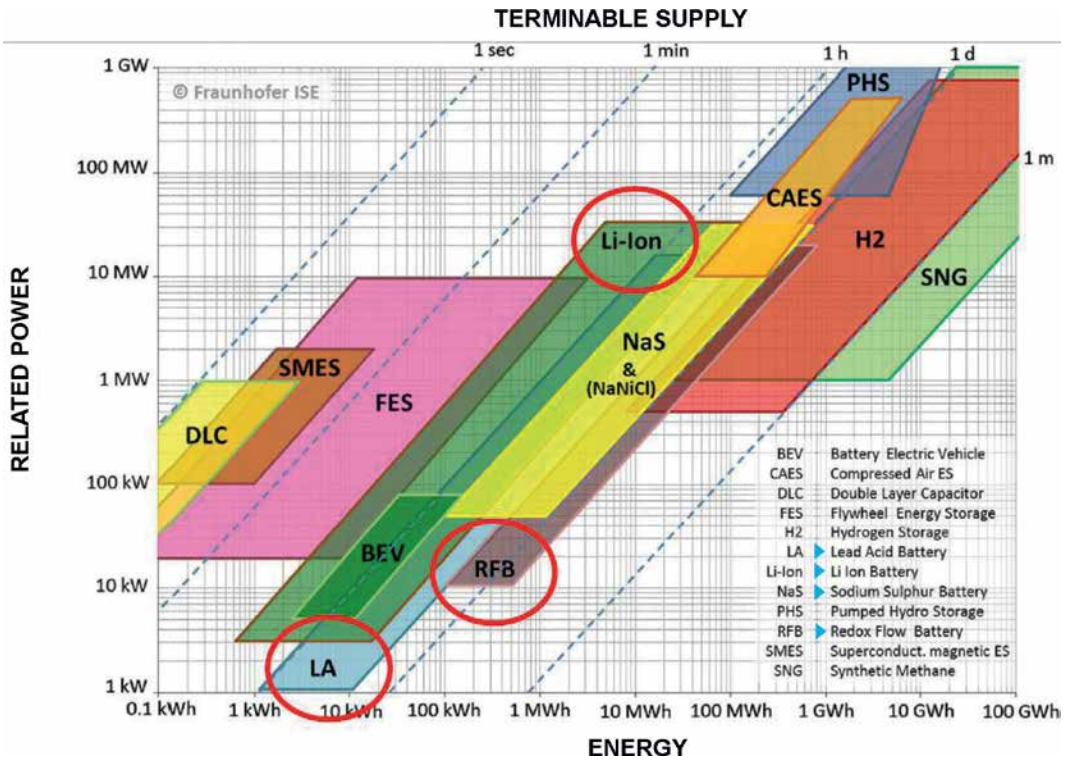


FIGURE 4.1 Technology specific power, energy and limits of terminable supply [143, Fraunhofer]

This fundamental distinction introduces the term of entropy.

A power system with simply bilateral orientation for equalization is ordered on a higher level than a caloric system. Physically and chemically conversion of power to heat is easier and more efficient than a conversion of heat to power. Hence, we say, that a power system profit from a higher entropy and thus higher valence than a caloric system. If we account on the caloric energy sum of a system under specific physical

and chronological conditions, we assess enthalpy. Enthalpy is not static or constant, but rather the stationary determination of heat potential in a clear-cut described system after certain action and before certain action.

Storing of energy in practical terms draw the consequences of decoupling of consumption from energy supply as well as concentrating countable energy on a defined place or defined containment. Providing that, energy storing is energy conservation.

*Appendix D.1* shows a system of diverse practical principles of energy storing. We can distinguish between electrical, electro-chemical, thermal, mechanical and chemical storage principles. All principles offer diverse storage technologies applied in life or being part of the immediate environment as for instance sugar, starch or biomass. The principles differ from each other in respect to storage density, quality of energy conservation regarding losses and application limits as well as efficiency. APPENDIX D.1 categorizes different principles according their related power and terminable supply. Thus, in terms of electrical power several accumulator as well as kinetic storage technologies are exemplified. Interestingly, some storage principles offer beside immense storage density another physical benefit (Fig. 4.1).

Since some storage principles like electrical capacitors or thermo-chemical storages, allow to release the immanent energy on a higher level of potential [Lindner, 2015 [144)] or higher flow rate compared to charging conditions, they function like capacitors or non-mechanical heat pumps.

---

## § 4.2 Key performance criteria of energy storages

---

Since energy storages per definitionem are characterized by firstly a gathering of any sort of energy and secondly the releasing energy, several key criteria determine the performance quality and quality of eligibility for specific utilisation. These key criteria are valid for many different sorts of energy conservation. In particular criteria are valid for electrochemical and sorption storages, which on the one hand represent power and on the other hand represent heat storage technologies.

Although, electrochemical and sorption storages differ in the sort energy eventually provided, these key criteria help comparing on a common level.

Since, as focused in this thesis, in particular electro-chemical and sorption as well as sensible and latent energy storage store either power or heat, a common unit for comparison of power and heat is useful. That is why following expression bases on the unit kilowatt hours.

### § 4.2.1 Volumetric density

---

The volumetric density describes the maximal possible amount of energy, that can be gathered by a storage technology. Energy either occupies a volume of one cubic meter or when greater converted to the unitized value cubic meter. Beside the volumetric density of sorption storages in general is incomparably high, the volume for periphery is not to be underestimated.

Thus, the main unit is derived as :  $kWh/m^3$

### § 4.2.2 Gravimetric density

---

Another crucial key parameter, which represents ones storage energy capacity related to the total weight is the gravimetric density. Since many electrochemical storage bases on metal anodes and cathodes as well as liquid or colloid electrolytes with specific high mass, electrochemical storages often provide comparably low gravimetric densities.

Main unit is derived as :  $kWh/kg$

### § 4.2.3 Charge efficiency

---

The charge efficiency describes the ratio of energy provided and actually being stored. In particular rapid-charging of non-lithium-ion electro-chemical storages causes increased internal ohmic resistance in accumulators.

Increased ohmic resistances in turn result in up heating of the accumulator cell and in thermal losses of the electric power to charge to environment. Reasons for a charge

efficiency of less than 100% are manifold and are closely determined to the storage technology and periphery technique devices.

Here are listed some representative criteria for the main common storage technologies:

• *Sensible buffer tank :*

---

- *feeding temperature level is lower than buffer tank level*
- *mass flow too high causes inefficient heat exchange*
- *poor thermal insulation of buffer tank causes significant thermal losses*

• *Phase change material :*

- *Feeding temperature level is lower than phase change level*
- *Insufficient material utilisation due to poor thermal conductance*
- *Insufficient material utilisation due to poor heat exchanger geometry*

• *Sorption storage :*

---

- *Insufficient material utilisation due to poor heat exchanger geometry*
- *Insufficient material utilisation due to poor thermal conductance*
- *Insufficient material utilisation due to inefficient container volume design*
- *Feeding temperature level is lower than required desorption level*
- *Insufficient evacuation, internal pressure closed to atmospheric pressure*
- *Insufficient physical thermal insulation*
- *Auxiliary energy demand higher than feeding amount*

• **Electrochemical accumulator :**

---

- *Ion quality : lithium ions or lead-acid ions*
- *Poor charge algorithms, i.g., poor MPPT algorithms of PV charger*
- *Exceeding of maximum depths of discharge*
- *Cell degradation due to high sum of executed charge cycles*
- *Inappropriate environment and cell temperature (too warm / too cold)*
- *Inappropriate charge current (too high / too low)*
- *high internal resistant*

Hence, the main unit is derived

as ratio of (in per cent) :  $Q / Q_{s,e} [\%]$

Most electro-chemical storages provide highest charge capacities between 25 and 35°C.

#### § 4.2.4 Discharge / Power supply density

---

Energy provided by a storage can be determined in relation to, for example, time, to mass flow, to providing temperature level, or in relation to the remaining amount of energy and time. The power supply density is often regulated by a maximum possible discharge density. In terms of batteries we make differentiations between “starter” batteries, “power-tool” batteries and back-up batteries for constant loads. According to the purpose of application, the maximum discharge, power supply rate respectively, differs.

A starter battery provides the main proportion of charged energy for a very short period of application, in order to ignite a second consecutively process. Since, tremendous amount of charged energy in provided as high current, starter batteries are discharged after few application. However, since the frequent application recharging requires only straightforward amount of time. Similar to starter batteries provide power-tool

batteries a considerable amount of energy for equal short but higher frequencies of application. Power-tool batteries are in charge of a constant high power for a time span of seconds or minutes for several irregular application. Since, they need to be small, compact and handy, they need high volumetric charge densities.

Opposed to the two before mentioned battery types the back-up batteries are eligible for constant high loads which request a nearly constant power supply for consecutively hours, days or even months. Back-up batteries normally provide a moderate level of current and economize with charge capacity for a long term perspective. Anode and cathodes as well as electrolytes and separators are designed for long-life and reliability. Thus, back-up batteries are the most appropriate battery technology for a decentralized or off-grid building service provision.

Thus, the main units related to time are derived as :  $kWh/h$ ,

related to mass flow are derived as :  $kWh/m^3$

related to volume and time are derived as :  $kWh/m^3*s$

related to mass and time are derived as :  $kWh/kg*s$

#### § 4.2.5 Monthly losses related to environmental conditions

---

Nearly all technologies suffer from frequent losses to the environment. For example, electro-chemical storages encounter monthly losses due internal chemical conversion processes and discharge to humid atmospheric air. Similar, sensible water buffer tanks suffer from daily transmission losses to the environment. Thereby, the higher the temperature difference between tank temperature and ambient air is the higher transmission losses are. Regarding an efficient energy conservation in respect of seasonal time shift between charging and recalling, daily and monthly losses are requested to be as minimal as possible.

Whereas lithium-ion batteries naturally suffer from 1 to 2% losses of charge capacity per months, sorption storages suffer from less losses indicated by undesired adsorption, if vacuum can automatically be controlled and maintained. Since humidity in ambient causes dried sorption material to absorb, stored heating energy will be released from the material. Either it remains as sensible heat within the storage

containment or transmits to the environment. Thus, thermal insulation of sorption storage containment focus rather evacuation than on physical insulation.

#### § 4.2.6 Charge cycles – life span

---

One decisive criterion for decentralized heat or power storage technologies for building and space conditioning is the life span and maximum possible charge cycles. Whereas power tools as hand workshop tools or even solely the power pack can easily be replaced or renewed, a incomparably more weight or volume intensive domestic storage device is requested to function and outlast for at least one or two decades. That request is justified by building specific economic and transport aspects.

Whereas the lead-acid batteries provide 500 to 1.000 charge cycles before significant and even total decrease in charge capacity, lithium-ion batteries compete with 5.000 to 10.000 charge cycles. High charge cycles call for attention, if the amount of energy utilizable by one cycle of discharge does not almost meet the cumulated heating demand of a heating season (October to April).

Thus, the multiple product of the maximum storage capacity and standardized evaluated minimum charge cycles are an indicating key factor for the eligibility for an application in buildings. Normally, lithium-ion batteries outnumbers lead-acid batteries with higher volumetric densities by factor three to five and by life cycles by at least factor ten to fifteen. On the contrary, sorption storages and sensible water storages as well encounter no degradation in charge cycling, when certain subjects are respected. The maximum number of charge cycles of sorption storages mainly depends on cleanliness of the adsorbed humidity. Consequently, impurities like lime scale lowers porosity and also conductance of the heat exchanger surfaces.

#### § 4.2.7 Availability of crucial key materials

---

From the perspective of sustainability are the key materials essential for each an energy storages technology. In this context ecological and economic consequences for the storage construction as well as for plant maintenance define the efficiency and stainability of technology. Against the background of fossil fuel substitution in buildings, it is crucial to apply storage technologies, which do not eliminate the annual

substitutions potential simply by the cumulated amount of energy for exploration, manufacturing, transport and dis-mounting. Likewise, a storage technology is not efficient if spare parts costs distinguish any feasible payback period.

In this context especially sorption storages convince by mainly natural sorption volume materials like silica or zeolite and any derivatives. Additives seldom are organic, what might inforce potential of harm for environment, related to poor thermal conductance qualities.

In contrast, electrochemical storages content many essential materials, that either requires demonstrable amounts of energy for exploitation of processing. For example, anodes and cathodes are made from primary energy intensive raw materials like titanate, as well as electrolytes mainly bases on acidity. Considered separately or combined, these materials incorporate significant potential of harm for the environment, especially purity of phreatic water.

#### § 4.2.8 Safety and environmental impact

---

As already described in 17.7 the potential of harm to environment determined the sustainability of the energy storage itself and its intended application context, like a building or a mobile. Quality of safety during application, service, transport and decommissioning additionally values.

Whereas opened lead-acid batteries evaporate acid vapor and thus requires ventilation of disposition space in order to prevent chemical burn of respiratory passages and risk of explosion, lithium-ion batteries in particular threat to explode if being charged after absolute discharge. However, a development of improvement was reached with the design of closed lead-acid batteries.

These batteries are hermetically closed and separated from the atmosphere. If the acidity volumes increases due to increase in temperature or charge progress, an incorporated expansion valve and vessel regulate gauge pressure. Since, they do not lose any acidity vapor to the ambient air, they do not need to be refilled. Hence, they are called "dry-fit" batteries. Risk and maintenance effort is reduced by this design. Likewise, sodium-nickel-chloride batteries, also known as ZEBRA (Zero Emission Battery Research Activity) batteries follow this design, although sodium and chloride are chemical substances which intensively react with the immediate environment.

## § 4.3 Electro-chemical storages

Whereas the first discoveries of electrical voltage made Luigi Galvani and the first developments of batteries were made by Alesandro Volta (1745-1827), the first re-chargeable battery was invented by Johann Wilhelm Ritter in 1803. While Humphry Davy (1778–1829) detected the ability of calcium as the fifth most abundant element by mass in the earth shell to enhance the mechanical strength of lead plates in lead acid accumulators, the first documented lead-acid battery was invented between 1850 and 1886. In that time, it was Thomas A. Edison, who lived from 1847 to 1931, who concentrated on the development of a nickel-iron battery and resulted in 1901 the first nickel-iron accumulator.

In 1817 Johan August Arfwedson experimented with the soft and light silver and white alkali metal lithium for alkali batteries. Where all batteries until than required liquid electrolytes, Paul Schmidt finished 1901 his developments of the first dry battery. More than a hundred years later it was Wilhelm Peukert, who described and calculated the battery capacity by the discharge rate and constituted the Peukert Law as value to describes battery specific losses.

### § 4.3.1 Current research on electro-chemical storages: improvement of details

Vetter [145] detects several fields concerning the application of electro-chemical storages and power supply in residential buildings. While he highlights the limited life span of lead-acid accumulators with maximum 10 years, he makes beside pay-off concern aware of the eco-logical scope of accumulator technologies at all.

Specific potential of improvement Vetter exemplifies in anode, cathode and electrolyte material research. Innovative materials and new material alloys or doping as well both enhances performance in terms of power, life span and charge efficiency as well ecological characteristics. To him, lithium-titanate as anode material or phosphate-based cathodes are beneficial for enhancing robustness against mechanical and thermal stress, namely thermal runaway effect. Further, Vetter detects the beneficial potential of Redox-Flow accumulators and high temperature sodium-sulfur and sodium-nickelchloride accumulators in respect of higher specific storage densities.

Opposed to Vettors ecological long term concern, the Wemag Company reuses Japanese lithium-manganate electro bicycle accumulators [146] with a rest charge capacity of 80% for residential power blocks.

While the used accumulators do not satisfy the standards for electro bicycles, lithium secondary cells are still eligible for residential use. Since the cell blocks are typically designed compact in the e-mobility sector, residential storage can be configured extremely modular with recycled cells.

Winter [147] from Research Centre MEET/Institute of Physical Chemistry of the University of Münster concentrates on graphitic carbon used as interstitial material in order to fill cavities at the cathodes and to advance electrical conductance. Beside graphite is cost-effective, it enhances safety in accumulators. Another focal point are ionic liquids which replace common acid electrolytes. Moreover, Vogel [148] experiments with sugar as reduction material for carbon coated cobalt-oxide particles and with carbon coated titan oxide (TiO<sub>2</sub>) nano particles [149] as anodes.

These recently invented nano particle insertion methods aim an enhancement of electrical conductance and hence on better charge and discharge performance of lithium-ionen cells. The improvement includes advanced cycle strength of Co<sub>3</sub>O<sub>4</sub> anodes.

Additionally, these alternative electrode compositions enlarge mechanical stress robustness and enhance the cell intrinsic safety level, in particular interesting for automotive application. Especially, carbon coated iron oxide and zinc ferrite particles in combination with carboxy methyl cellulose (CMC) as binder [150] allows higher charge capacities and cycle strength aligned with environmental harmless lithium-ion cell design. Moreover, Vogel investigated on electrodes, which both store ions, which emitted are attracted by the opposite electrode. This process of dual intercalation requires organic electrolytes and salt melt [151]. The result is an environmental friendly lithium-titanate-oxide accumulator, which excludes fluoride composites, while it resists higher operational temperature and provides 3,5V cell voltage.

On electrolyte level, unconventional fluorinated Ketones as additives in a propylene carbonate electrolyte [152] generate a solid electrolyte interphase (SEI) and protects electrodes from degradation and thus remain cell capacity. These additives provide thermal stability, enhances passive intrinsic safety and enlarges cycle strength. In particular, lithium-ion accumulator suffer collaterally from over charging. T

Thus, active battery management by the digital battery management system is in-avoidable for long cell life. In order to avoid impact of over charging or the risk of the active digital management to fall out, a chemical passive over charge protection was invented.

This passive over charge protection bases on NCN carbon adducts as additives in electrolytes [153], which compensates elevated voltage. Compared to the state-of-art these additives do not limit the cell performance at all.

Obeidi, 2012, [154] explains that mechanical and chemical safety of lithium-ion accumulators in e-mobility applications is essential. Lithium cells, which separator tapes in case of an accidents or very low discharge cannot effectively separate anode from cathodes or dendrites to grow, represents crucial risks (thermal run away).

Thus, the development of inorganic non-flammable micro porous separator tapes well promote an effective transfer of ions, but vital prevent contact of electrode even with ambient temperature higher than 200°C.

Opposed to lithium-ion accumulators liquid metal batteries as for instant sodium-nickelchloride (ZEBRA) accumulators, experiences technical improvements. Major problem of this thermal batteries is a dispersion of the anode, cathode and electrolyte what is defined as the Tayler-instability, actually distinguishes capacity. An inner vertical catalyst tube [155] directs the cell flow and remains the material striation. This invention promotes larger cell and capacity design, higher cell efficiency, as well as considerably reduced conversion losses.

Similarly, redox-flow batteries have been developed by Schubert, Janoschka und Hager [156,157] at University of Jena with electrolyte of polymer and sodium-chloride. Since this highly corrosive composition destroys special separation membranes within short period of time, redox flow accumulators are cost intensive. This development makes compared to conventional vanadium-sulphur-acid-composition environmental harm-less and enables a cost effective run. Additionally, the sodium-chloride polymer redox flow battery provides a cycle strength of 10.000 cycles 10 kWh/m<sup>3</sup>. Although, this volumetric density cannot even compete with the simplest lead-acid battery, it benefits from zero monthly losses and a separate control of capacity and power output.

#### § 4.3.1.1 DC or AC systems : tumble of a dogma

---

Research and practical experiences have shown, that DC systems in residential buildings are sensible, since they profit from higher efficiency ratios. Opposed to that, in a AC system power was converted for three times and remains with 15% less efficiency, according to Tappeser (2015) [158]. Beside Tappeser argues that lead-acid-gel accumulator are no longer sensible for decentralized residential storing, he promotes DC systems supplied by a high voltage lithium-ion accumulator to assure maximum

system efficiency. He also puts emphasis on significant less converter losses of the higher the battery system voltage is. Considering mono- or polycrystalline pv modules with closed circuit voltage between 45 to 95 Volts, the battery system voltage should range likewise between 48 to 96 Volts.

Correspondingly, Shri (2013 [91], concurrently) remarks the contemporary complexity of power grids since it has become practice to feed in renewable power. Beside, public power grids were configured to transmit power mono-directional from high power supply to lower power consumers, with decentralized renewable power fed-in the net has become bi-directional. That makes capacity control and primary energy efficiency difficult.

Thus, Shri concentrates in research on net level on the development of solid-state-transformers as well as on decentralized estate level on exclusively DC/DC nets. He identified in particular benefits of domestic DC/DC nets in demonstrably lowered system losses (heat) and in simpler converter and controller architecture.

#### § 4.3.1.2 DC/AC converter : despite tri-phase - a nonessential efficiency choke

---

Koenemann (2015) [159] explains that commonly a one-phase DC/AC converter has to store the entire energy provided by the pv modules during the voltage zero crossing. In order to provide that, electrolyte capacitors are used. They often risk to dry and induces converter fall out, beside the rest of technique is well. Hence, a one-phase converter risks to lose considerable amount of energy. Thus tri-phase converters have become utilizable since 2012, in order to transform energy at any time with demonstrably less losses. Moreover, the less the converter lose in terms of heat, the less the energy amount for converter cooling.

Modern silica carbon (SiC) diodes and transistors switch faster and result in slightly less switching losses. That goes along with higher frequencies that allow smaller choking coils. In the end, the efficiency coefficient is higher.

However, concurrently SiC diodes are still cost intensive for converters, what results in a long payback time for 1 or one and a half percent points higher efficiency.

Since the maximum efficiency coefficient strongly relates to climate region and orientation, many DC/AC converters frequently work in part load field. The efficiency coefficient of data sheets are far away from practice. For that reason the European efficiency coefficient has been established, which considers European weather

conditions. This coefficient normally is 2 to 5 points lower than the common maximum one. While in 2013 the maximum efficiency coefficient was about 97,8% [160], the European very close to, in 2015 listed converters obtained 98,7% maximum, but the according to the European coefficient 93,0 to 98,7% [161].

### § 4.3.2 Accumulator types : space heating - a question of discharge-power

---

The typology of accumulators or secondary cells which concerns on short maximum power supply or constant long-term provision has been exemplified in section 3.4. By contrast, this section concentrates on diverse battery designs and materials which originate specific performance. As main electrochemical accumulator types can be identified three different related to their specific anode-cathode material. Hence, we can distinguish between common lead-acid accumulators, lithium-ion accumulators and nickel accumulators, which all profit in performance diversification by key material additives and derivatives. Along the nickel accumulator technology the sodium-nickel-chloride accumulator constitute a special variant. Additionally vanadium based redox-Flow battery has become interesting for decentralized off-grid application, which once revolutionized common accumulator working principle.

Figure 141 surveys the major accumulator typologies according their cell materials differentiating between normally low or high voltage technology (> 52 V) and considering ranges of gravimetric and volumetric densities (Wh/kg; kWh/m<sup>3</sup>), the charge efficiency [%], the feasible depth of discharge (DoD [%]) for remaining 80% capacity after 500 to 5.000 cycles, the average monthly loss rates without consumption [%] and the cycle life. Next to this, specific characteristics of performance are additionally are quoted.

This survey was conducted by both literature research and a market analysis of especially off-grid back-up accumulators in 2017. Thus, the table is a reasonable survey of theoretical and actually applicable status of technology. That fact justifies more than one slightly more conservative performance value.

SPECIFIC ENERGY DENSITY, CHARGE EFFICIENCY AND MONTHLY DISCHARGE RATES : scaled to 12 V Units												
TYPE OF ACCUMULATOR (secondary cell block)	LOW or HIGH VOLTAGE TECHNOLOGY	GRAVIMETRIC DENSITY [Wh/kg]	VOLUMETRIC DENSITY [Wh/m <sup>3</sup> ]	CHARGE EFFICIENCY [%]	DEPTH OF DISCHARGE DoD [%]	MONTHLY SELF- DISCHARGE [%]	CYCLE LIFE	CHARACTERISTICS				
LEAD	Lead-Water	L	33-49	63-103	80-85 <sup>9</sup>	50-60 <sup>9</sup>	3 <sup>6</sup> , 8-10% <sup>7</sup>	12000-2800 <sup>6</sup>	cost-efficient, no memory-effect,			
	Lead-Acid valve-regulated (VRLA)	L	25-178	50-97					-			
	Lead-Calcium	L	35-102	75-215					high safety quality, less maintenance, low monthly self-discharge			
	Lead dryfit AGM	L	40	25-30					long life, no maintenance, lower DoD than liquid lead acid			
LITHIUM	Lithium-Ion Cobalt-Oxid (LiCoO <sub>2</sub> )	L / H	120-210	50-185	92-98 <sup>2</sup>	80-90 <sup>9</sup>	< 2 %	5,000 <sup>7</sup> - 8,000	fast-charging eligible, extremely low self-discharge, highest energy density, non-ecological materials			
	Lithium-Ion-Polymer	L	80-120	100-115	90-97				0,5%	5,000	intrinsically safe, ecological materials, inflammable, non-explosive	
	Lithium-Iron-Phosphate (LiFePO <sub>4</sub> )	L	30-100	20-90	92-94 <sup>2</sup>				0,5 <sup>6</sup> - 4 % <sup>2</sup>	6,000 <sup>7</sup>	8,000	long life, fast-charging eligible, high current-ability, intrinsically safe
	Lithium-Titanate (NCO Titanate, Li <sub>2</sub> TiO <sub>5</sub> )	L	70-90	25-30	94-98 <sup>2</sup>				2-4 % <sup>2</sup>	15,000 <sup>4</sup>		extraordinary safe and tolerant against overcharging, fast-charging eligible
	Lithium-Ion Nickel-Manganese-Cobalt (LiNiMnCoO <sub>2</sub> )	L	45-68	25-30	-				-	-	8,000	-
NICKEL	Sodium-Nickelchloride ("Zebra-Battery")	H	100-140 <sup>3</sup>	260-280	82-88 <sup>2</sup>	70-80%	0,5 <sup>9</sup>	800-1.400	no self-discharge, low cost materials, simple construction, T <sup>opt</sup> : 270 to 350°C			
	Sodium-Sulphur	L	120-220	-	70-85				-	750-1.100	no self-discharge	
	Nickel-Iron	L	40	-	65-75				-	-	extreme robust for overcharging and deep discharge, longer life than lead-acid accu	
	Nickel-Cadmium	L	40-60	100-190 <sup>10</sup>	70				10%	1.500-2.000	vapor light, advanced cycling endurance, cold robust, long life, memory effect, lazy-effect	
	Nickel-Metal-Hydrate (NiMeH)	H	60-110	190-380 <sup>10</sup>	70				15-25%	> 1.200	long life, high cycling endurance, excellent volumetric/gravimetric density, memory effect	
	Nickel-Hydrogene	L	60	-	75				-	-	-	-
	Nickel-Zinc	L	50 <sup>2</sup>	-	65 <sup>2</sup>				-	-	< 700	short life reasoned by increased tend for dendrites

FIGURE 4.2 Main accumulator typologies and their specific energy densities, charge performance and life span

Figure 4.2 shows, that especially lithium-ion and sodium-nickel-chloride accumulators are eligible for high voltage energy storages. High voltage design enhances the power supply and increases volumetric density. Thus, automotive accumulators profit from high voltage accumulators by high power with low string diameters. As figure 4.2 further illustrates, the gravimetric capacity density is with lithium-ion cell technology the highest in competition and is followed by nickel+X technologies. Opposed to that, the volumetric energy density of nickel-based accumulators was identified to be greater than for lithium-ion or lead-acid cell technologies. Although some lead-based accumulators cannot compete with high performance lithium-cobalt or lithium-polymer accumulators in terms of volumetric density, lead-water, valve-regulated lead-acid and lead-calcium technologies outnumber lithium-phosphate, lithium-titanate and lithium-manganate-nickel-cobalt technologies. In respect of charge efficiency, what is a key issue for area-wise limited façade-integrated collector technologies, lithium-ion technology provides clear-cut competences with at least 90%, followed by improved lead-acid technology with 80 to 85% and followed by nickel-X accumulators with 65 to 88%. Analogously, lithium-ion accumulators provides high performance depth of discharge by far, which enables 90 to 100% of capacity utilization. Nickel+X technologies contribute 70 to 80% of capacity without encountering any performance forfeits, ultimately followed by lead-acid technology known for maximum 50 to 60% of discharge depth.

For that reason, lead-acid accumulators claim nearly the double of capacity for reliable and durable performance what results in comparably intensive volume and weight. Considering monthly inevitable losses without consumption, lead-acid and nickel+X technologies stipulate between 3 to 10%, in case of nickel-metal-hydrate actually 15 to 25%. In fact, such demonstrably high losses in combination with charge efficiencies of simply 70% requests reasonability of such a accumulator technology applied for a critical annual space energy demand-façade yield ratio.

Durability in respect of charge-discharge cycle strength significantly varies between the technologies and in the scope of each a technology. Cycling strength of lithium-ion technology at least covers 5.000 cycles, but oppositional can cover up to 15.000 cycles. Commonly, life span ranges between 6.000 to 8.000 cycles for lithium-ion, what qualifies lithium-ion as durable and sustainable technology. On the contrary, cycle strength of lead-acid accumulators is limited to 2.800 cycles and normally ranges between 500 to 1.500 cycles. Nickel+x technologies cannot convince better with 700 to 2.000 cycles maximum. Outstanding benefits of especially closed lead-AGM and lead-calcium technology cover high intrinsic safety, exclusion of memory effect, low monthly self-discharge ratio comparable to lithium-ion technology and high current with low voltage what enables for efficient DC/DC systems. Lithium-ion on the other hand profits from long life, no effort for maintenance and volumetric and gravimetric high capacities and in respect of lithium-titanate and lithium-polymer technology from high intrinsic safety and ecological materials.

On the opposite, nickel-metal-hydrate and nickel-cadmium benefits from competitive high volumetric densities, no monthly self-discharge and high tolerance for over-charging and discharge with low ambient temperature.

### § 4.3.3 Cell type specific performance tendencies : key skills of accumulators

---

The literature research and the market analysis as well helped to identify performance and eligibility tendencies of major applicable secondary cell block technologies.

In this context by the authors complemented radar plots [BMZ 2012] help to visualize in qualitative matter the main ad- and disadvantages. Visualized ad- and disadvantages reveal durable and powerful technologies, that can compete with sorption storage technology. Consecutively to the quantitative evaluation of diverse common and appropriate accumulator technologies, a qualitative analysis was elaborated in order to highlight key performance and focal points from the perspective of a space heating by power storage.

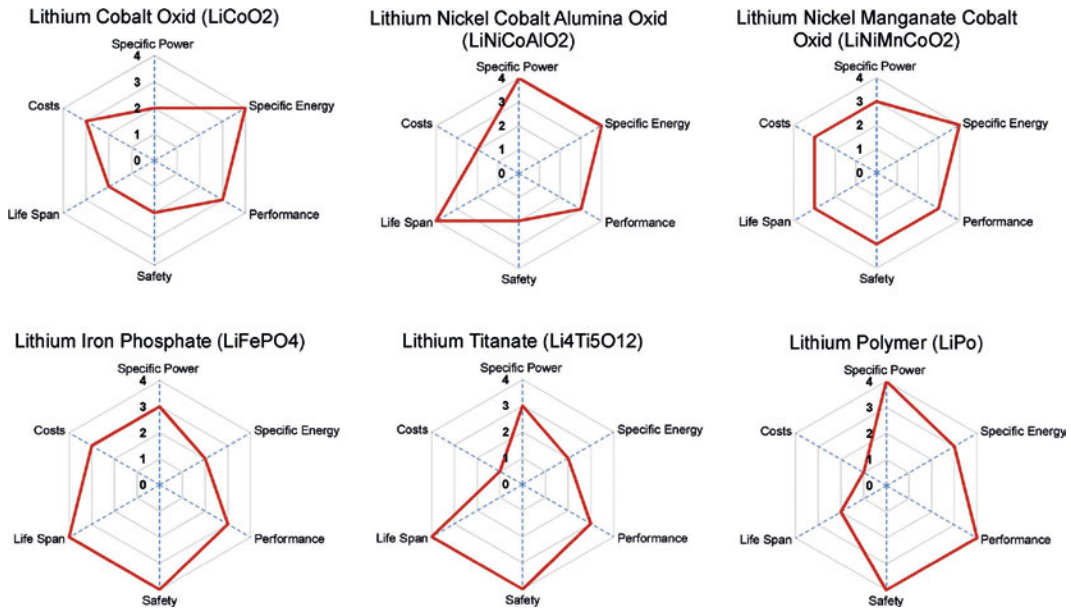


FIGURE 4.3 Performance focus of lithium-ion accumulator types

Essentially, a power storage for electrical heating has to provide an extraordinary high charge efficiency and low self-discharge rate (performance), as well as sufficient high (power) discharge current in ampere hours and high capacity (specific energy density) what ensures straightforward rack space and transportation feasibility.

Figure 4.3 demonstrates qualitatively, that lithium-polymer and lithium-cobalt-oxide as well as lithium-nickel-cobalt-alumina-oxide accumulators provide the pre-requisites. Opposed to that, especially certain valve-regulated lead-acid (VRLA) (see Fig. 4.4) accumulators can compete in specific power and specific energy with lithium-ion accumulators.

However, lead-acid suffers in terms of performance from lower charge capacities, what for compensation requires the pv plant to be being enlarged, and lower cycle strength, what requires exchange after a shorter period of application.

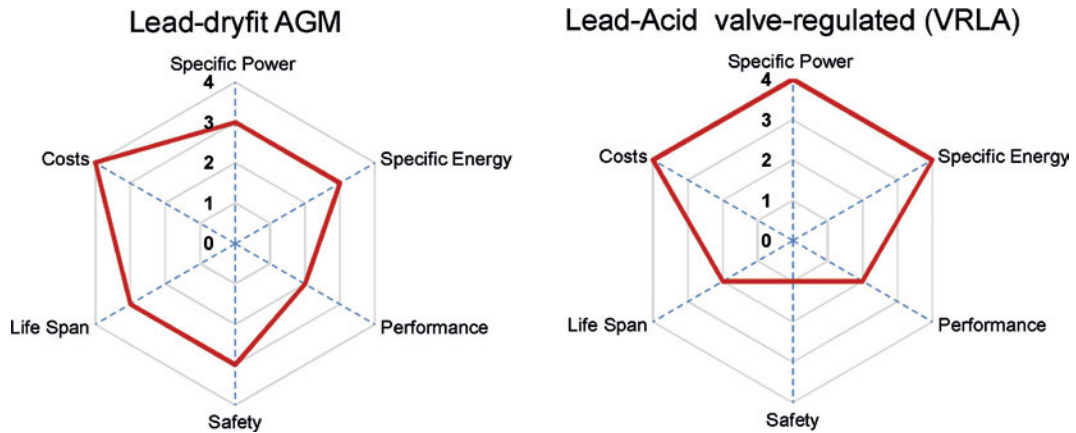


FIGURE 4.4 Performance focus of lead-acid accumulator types

Interestingly, all the evaluated nickel-technology encounters moderate lower power, what is decisive for sufficient electro-chemical space heating in winter. Although the sodium-nickel-chloride accumulator provides very high specific energy, it conversely requires constant ambient temperature of 270 to 350°C, what somehow eliminates the specific energy.

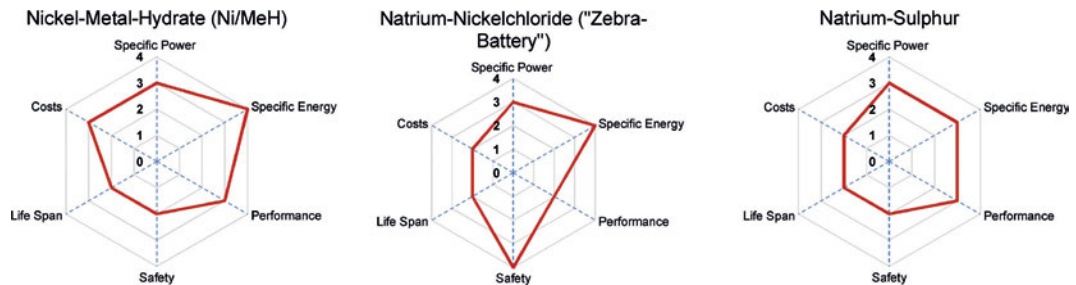


FIGURE 4.5 Performance focus of nickel accumulator types

But nickel-metal-hydrate accumulators (Fig. 4.5) convince with over average high specific power and energy and performance. Right at the start of this thesis project, a survey of established and semi-established automotive high-voltage accumulator systems for mono- and bivalent operation mode was conducted.

What is of interest is the fact, lithium-ion and nickel-technologies are applied as result of high gravimetrical energy densities.

In fact, electrical mobility requires lightweight and powerful accumulators. However, some the weight of some designs is enlarged by more than 400 kilogram. Interestingly, some car designs incorporate accumulators with 600 to nearly 7.000 connected single cells. Typical for automotive accumulator designs and e-mobile designs (APPENDIX D.2) are high operational voltages of 202 to 400 Volts. High voltage reduces wire diameter and weight. This survey serves as a reference in terms of manageable capacity and power.

Thus, we can see, that single designs profit from 55 to 92 and up to 1.130 kWh of energy supply and benefit from 50 to 800 kW power. Hence, we derive, that high volumetric and gravimetric energy density is a question of cell and voltage design. Moreover, is the system efficiency comparably high due to DC-motors, which require no current conversion and thus causes no losses.

The analysis of this system design raises the question of a transformation into the building sector.

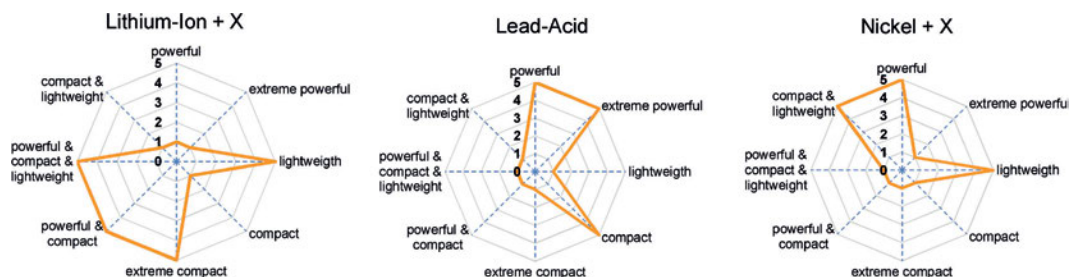


FIGURE 4.6 Weight and volume related power performance focus for building application

### § 4.3.4 Most eligible secondary cell block typologies for sun space seasonal power storages

---

#### Summary

---

Finally, a volumetric and gravimetric analysis of the three common technologies, as shown in Figure 4.6, illustrates advantages for lead-acid technology, when façade area for collector installation and volume for storage deposition is without problems. If these aspects are crucial for design, lithium-ion technology alternatively provides solutions which are powerful, compact and lightweight simultaneously.

### § 4.4 Thermo-chemical sorption storages

---

Storing of energy either helps to conserve surplus energy or waste energy, and thus, to enhance system efficiency. Or, energy storing helps to compass the time mismatch of energy offer and energy demand. In context of heating energy substitution by renewable energy, the inevitable time shift between disproportional offer of solar gains in summer and the alternated demand in winter, makes heating energy storages crucial for a sustainable building maintenance. Considering a low energy and solar driven single family homes relying on envelope integrated solar thermal collector and seasonal long term storages, Drück (2013) [162] highlight beside 5 to 10% higher invest costs decisive benefits like 1.) security of energy supplies, 2.) security of running and energy costs as well as 3.) energy supply autarky.

Electro-chemical storage technologies, although providing power instead of heat, have been discussed previously. Despite, exemplified accu technologies temporarily suffer from little monthly loss rates, accumulator technology cannot reasonably provide considerable amounts of energy for space heating.

On the contrary, established heat energy storages like water or phase change materials either encounter comparably low storage densities or significantly high daily or weekly losses. At least these two aspects causes sensible water and latent phase change materials to remain questionable storage technologies.

Essentially, space heating with renewable energies requires high storage density and loss-free storage technologies. Opposed to electro-chemical thermo-chemical storages allow two to three times higher storage densities than water (Kerskes et al., 2013, [163]) and have been evaluated to provide charged energy loss-free (Abedin, Rosen, 2011 [164], Kerskes et al, 2013, [163], Mugele, Stach, Jänchen, 2012, [165]) in at least seasonal but even longer perspective of time.

Research and application of thermo-chemical storages within the last four decades illustrate their seminal potential, whereas Shigeishi, Langford and Hollebone in 1979 [186] already confirmed their eligibility even for solar thermal application with defined demarcation of 300°C operation temperature between low and high temperature systems. Although the authors above at that time promoted the reasonability of thermo-chemical storages, they identified considerable demand for material research as well as Kerskes (2013) emphasizes, that concurrent reactor systems still occupy two times the volume of conventional natural gas boilers.

Nonetheless, Drück [166] emphasized 2013 in the context of change of energy supply, that research will generate interesting developments and design of heating energy storage in the near future.

#### § 4.4.1 Storage principal of desorption

---

According to Eichler, Mack and Hirth, 2015 [167] thermo-chemical heat storage technology is based on a reversible chemical reaction. In the case of charging two reaction partners are chemically separated with even the amount of energy to be stored. On the contrary, an intended local and chronological association of previously separated reaction partners releases the stored amount of energy. While this happens, the reaction runs exothermic (Dicaire and Tezel, 2012 [168]) and offers utilizable energy.

The storing process and in particular the loss-free effectiveness is maintained as long as the reaction partners are locally disassociated. Thermo-chemical processes base on materials, that tend to adsorb molecules of liquids. These materials behave adsorptive due to their natural molecular lattice what provide manifold pores. Sorptive materials provide up to 1.000 m<sup>2</sup> of inner surface with pores.

The more porous sorptive materials are and the larger these pores are, the more adsorptive and convenient these materials are for thermo-sorptive applications (Hauer, 2002, [169]). Figure 4.7 visualizes the reaction principles. The sorptive material under

natural circumstances contains water. By the energy to be stored, the water by heating is segregated from the material.

This endothermic procedure is called desorption and results in a quasi-latent thermal charging of the solid material. Water exits as water vapor and needs to be dislocated and cooled down in order to condensate with considerable less volume.

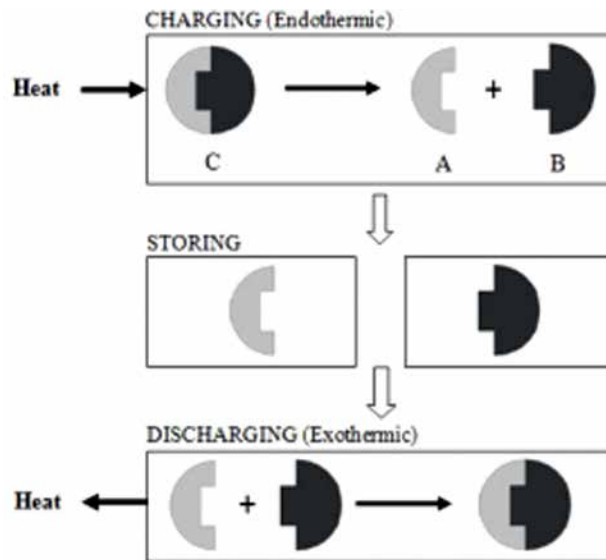


FIGURE 4.7 Charge- store- and discharge principle of thermo-chemical storing

As long as the desorbed solid sorptive material is hindered to associate with water again, the heating energy remains stored. Reversibly, when water is evaporated and contacts the desorbed material, the reaction begins with the sorption material to adsorb the water vapor. On molecule level, water vapor ions are adhered and close gaps within the solid material lattice.

This adsorption results in freeing of binding energy and water vapor enthalpy. In principle, A as the solid component can be hydroxide, ammoniate, carbonate or hydrate, while B as the liquid component can be water, carbon, ammonia, hydrogen (Abedin, Rosen, 2011, [164])

## § 4.4.2 Competitive storage performances

---

After the explanation of the working principle in the previous section, this section focus on comparison of different heating energy storage technologies. For heat storing we can differentiate between sensible, latent and thermo-chemical storage principles. The major difference between these principles is the gravimetric or volumetric storage density. However, we can describe and distinguish between those three principles with performance parameters as Abedin and Rosen (2011, [164]) tabular examines (see Fig.4.8). Performance parameter include temperature range, storage densities, which are closely related, lifetime, technology status and ad- as well as disadvantages.

While common sensible heat storages, as water buffer tanks for instance, provide low densities of maximum  $0,2 \text{ GJ}/\text{m}^3$  and require a high temperature range from  $50$  to  $500^\circ\text{C}$  (case of concrete), latent storages cover  $0,3$  to  $0,5 \text{ GJ}/\text{m}^3$  abroad much tighter temperature intervals between  $40$  to  $80^\circ\text{C}$ .

In terms of applicability and efficiency latent storage principles outnumber sensible. Moreover, compared to sensible latent storage principles manage to store heat loss-free within certain temperature ranges as long as certain temperature limits are not underrun.

Whereas latent storage principles outnumber sensible in terms of compactness and volumetric density, nevertheless they encounter disadvantages like material degradation, higher frequency of corrosivity and low conductivity what limits geometries. Normally, costs exceeds those of simple sensible storage principles.

Oppositional, thermo-chemical principle provide the highest comparable storage density of  $0,5$  to  $3 \text{ GJ}/\text{m}^3$ , what easily outnumber that of water for two to four time, as Kerskes (2013, [163]) exemplifies. Likewise Shigeishi, Langford and Hollebone 1979 already exemplified that for example ammonia-bromide ( $\text{NH}_4\text{Br}$ ) stores in respect to the mass nine times more heat energy than water ( $1.901 \text{ kJ}/\text{kg}$ ,  $209 \text{ kJ}/\text{kg}$ ) and

26 times more heat energy than water in respect to volume ( $5.540 \cdot 10^3 \text{ kJ}/\text{m}^3$ ;  $209 \cdot 10^3 \text{ kJ}/\text{m}^3$ ) with less than one fourth of weight and less than 5% of volume.

Thermo-chemical storages are applicable in a wide range of operational temperature between  $20$  to  $200^\circ\text{C}$  (Fig.4.8). The main advantages in regard to latent storages are higher densities for potential long storage periods without any losses. However, these principles are rarely commercially available and yet encounter comparably high costs and technical complexity. In that context Decaire and Tezel (2012) [168] argue that

thermo-chemical energy adsorption storages are feasible for energy long-term storing and volumetrically comparably to with two natural gas boilers.

Performance Parameter	Type of Thermal Energy Storage		
	Sensible TES	Latent TES	Chemical TES (Sorption and Thermo-chemical)
Temperature range	Up to: 110 °C (water tanks) 50 °C (aquifers and ground storage) 400 °C (concrete)	20-40 °C (paraffins) 30-80 °C (salt hydrates)	20-200 °C
Storage density	Low (with high temperature interval): 0.2 GJ/m <sup>3</sup> (for typical water tanks)	Moderate (with low temperature interval): 0.3-0.5 GJ/m <sup>3</sup>	Normally high: 0.5-3 GJ/m <sup>3</sup>
Lifetime	Long	Often limited due to storage material cycling	Depends on reactant degradation and side reactions
Technology status	Available commercially	Available commercially for some temperatures and materials	Generally not available, but undergoing research and pilot project tests
Advantages	Low cost Reliable Simple application with available materials	Medium storage density Small volumes Short distance transport possibility	High storage density Low heat losses (storage at ambient temperatures) Long storage period Long distance transport possibility Highly compact energy storage
Disadvantages	Significant heat loss over time (depending on level of insulation) Large volume needed	Low heat conductivity Corrosivity of materials Significant heat losses (depending on level of insulation)	High capital costs Technically complex

FIGURE 4.8 Compared performance parameter of sensible, latent and thermos-chemical / sorption storages [Abedin/Rosen]

Nonetheless, the potential high storage densities combined with long term loss-free operation time make them promising approaches for compact and powerful seasonal and loss-free heat energy storages. Against the background of thermos-chemical storage solutions we can determine general advantages and requisitions :

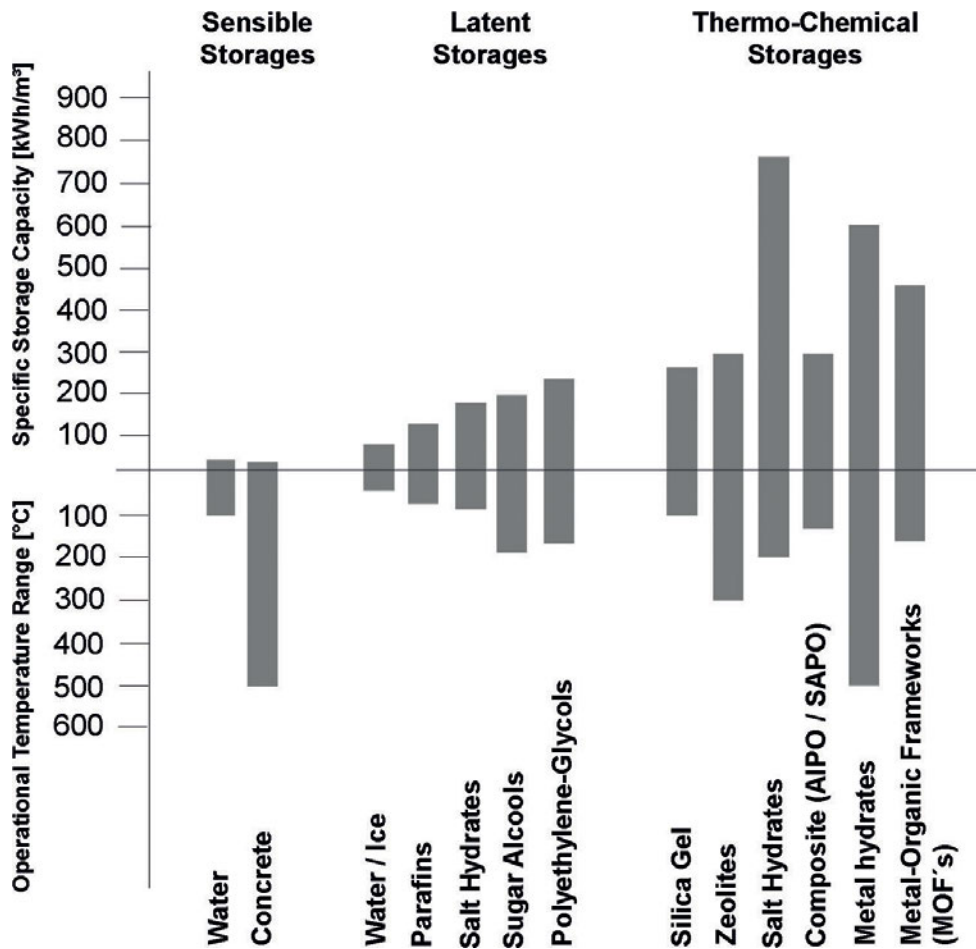


FIGURE 4.9 Specific storage densities [kWh/m<sup>3</sup>] and maximum operational temperatures [°C] of different thermal energy storage material groups (Accd. Hauer, 2012, Kerskes, 2013, Meinert, Kieback 2015, Lottner 2004 and Deaire and Tezel 2012)

#### Advantages :

- flexible operating temperatures
- no energetic losses during storage phase
- no intrinsic material degradation > high cycle stability
- compensates supply fluctuations of renewable energy sources

In the context of storage mechanisms we can differentiate for sensible, latent and thermo-chemical principles :

- *phase change materials (heat of fusion)*
- *surface effects (heat of adsorption)*
- *chemical reaction (heat of reaction)*

Figure 4.9 illustrates the range of average densities and operational temperature for the three different determined storage principles. (Kieback 2015, Lottner 2004 and Deaire and Tezel 2012). Finally, we can identify principal relevant factors for the choice of material in the context of sufficient and effective seasonal thermal energy storages for sun space application :

- *Availability / Costs*
- *Cycling behavior (material degradation)*
- *Toxicity, environmental behavior*
- *Corrosiveness, safety*
- *Specific Energy density*
- *Reaction temperatures defines eligibility for solar thermal feeding*
- *Integration quality into residential technical systems*

Nonetheless, energy storing calls for more than a stationary consideration in respect to building energy consumption profiles. Moreover is a consideration of energy flows and balancing all over the year the appropriate method. Thus, the next section inspects the effectiveness of thermos-chemical storages in respect to load profiles.



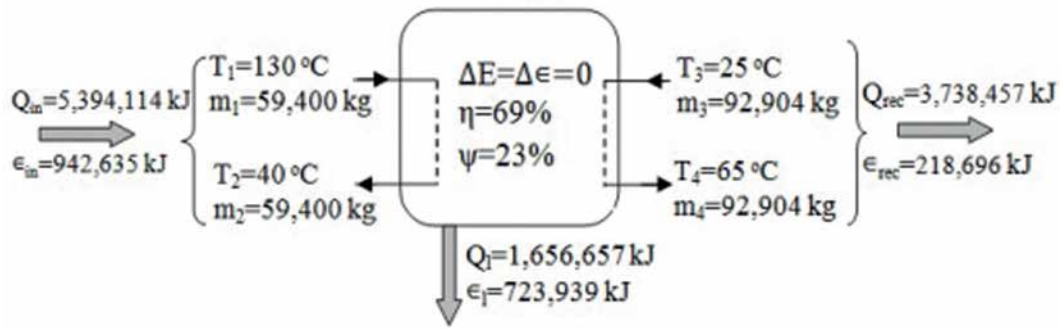


FIGURE 4.11 Energy and exergy expressions of an overall open-system storage process

However, Abedin and Rosen argue, that this consideration is either comprehensive nor meaningful. From their perspective an exergy evaluation (see Fig. 4.11) is more consistent and comprehensive. They figure out two arguments, that are closely related to the system principally. The first concentrate on the regeneration energy cycle-wise and the second on the actually utilizable released energy determined firstly by the rest remaining charging capacity and secondly for the specific heating system.

Thus, both researcher concentrate on each cycle and determine exergy efficiency by

1. *the required material specific temperature level for 95% dehydration*
2. *the provided temperature level for desorption,*
3. *the actual adsorption status, namely absolute and relative adsorbents bed humidity,*
4. *the actual disproportional charging velocity related to previous hydration*
5. *related sensible losses during adsorption and desorption as well as*
6. *the provided adsorption temperature level*
7. *the adsorption humidity level*
8. *pressure drop in the reactor*
9. *with discharge decreasing release temperature*

## 10. the required temperature level for the specific space heating system

### 11. and thus resulting amount of energy

Hence, Abedin and Rosen do not follow a static theoretical equation of best case values under optimal boundary conditions, but incorporate all potential losses and weight the input energy by the actual released energy referencing the remaining utilization factor for the effective application. Thus, with every cycle the amount of energy changes according regeneration temperature and duration, remained charge status, decreasing heat transfer ratio and gained temperature in related to heating system requirements.

The major terms of a differentiated consideration for energy efficiency were determined as :

$$\eta_o = \frac{\text{energy gained by adsorbent}}{\text{energy input}} = \frac{\Delta H_{ds}}{\Delta Q_{in}} \quad (23)$$

$$\eta_c = \frac{\text{useful output energy}}{\text{input energy}} = \frac{\Delta H_{ds}}{\Delta Q_{in}} \quad (24)$$

, whereas the terms for exergy were elaborated to be :

$$\psi_c = \frac{\text{exergy stored in desorption}}{\text{exergy input}} = \frac{\Delta \epsilon_{ds}}{\Delta \epsilon_{in}} \quad (25)$$

$$\psi_d = \frac{\text{exergy recovered by air}}{\text{exergy released in adsorption}} = \frac{\Delta \epsilon_{rec}}{\Delta \epsilon_{ad}} \quad (26)$$

This becomes demonstrably crucial, when a thermochemical storage is incorporated in a domestic heating or cooling system with mechanically ventilation, what rigidly narrows the range of operational temperature set points (Heier, Bales and Martin, 2015) [171]. The potential raise in energy is disproportional to the tight set point interval.

To them, in particular exergy evaluations are helpful in order to detect locations and reasons of losses within the observed TES system. Especially, the standard chemical exergy of a component is inevitable to be incorporated. The differentiated calculation of an open-system revealed an energy efficiency of 93% for charging, while exergy was calculated with 84%, whereas discharging energy efficiency constituted with 74%, nonetheless the exergy counterpart with simply 28%.

The overall product for energy efficiency resulted in 69%, whereas opposed to that the exergy accounted for simply 23%.

#### § 4.4.4 Beneficial side effect : evaporative cooling

---

Thermo-chemical storages executing adsorption profit from a side-effect, that often is disregarded while concentrating on heating energy performance. Adsorption of water vapor requires the aggregation of water to vapor. The evaporation inevitably requires energy, that consumed within the system effects cooling. Thus, evaporation always effectuates cooling. This cooling effect at that place or the cooling energy can be utilized at another place with in a system. Since the cooling effect is not desired within the storage device, precisely in the condenser / evaporator unit additional energy is required in order to compensate and remain optimal operation temperature. The figure in APPENDIX D.3 shows the progress of increasing evaporation energy, cooling energy respectively, that is generated after a few seconds (a 41 kg zeolite bed in closed system, TNO, The Netherlands). A cooling power of 2kW is already available after 90 seconds of initial evaporation with a packed bed of 41 kg zeolite 5A and a evaporated temperature of 5 to 15°C in a closed evacuated system.

For energy or exergy considerations potential cooling energy, if exploitable, is to be considered. Consequently, if cooling energy is not utilizable, heating energy for comprehension, lowers the overall system efficiency.

#### § 4.4.5 Research projects and practical experiences

---

We profit from various research projects and single prototypes developments in the context of thermo-chemical sorption storages of the last one and a half decades. This section highlights appropriate and interesting projects in order to determine the current status of technical development. The projects are reported rough by bullet points in order to report essentials and to simplify differentiation.

1) ZeoSys GmbH [Lass-Seyoum,2012 [172]] and Fraunhofer IGB developed a 750 L storage material closed and evacuated containment 2012. Aim was to increase the maximum effective storage density to 220 kWh/m<sup>3</sup> by the overall conductivity of material and within the bed. The scaling from the 1,5 labor test rig to the 750L

prototype delivered satisfactorily results. The control and process was observed to be adaptable to different heat source and heat consumers. Thus, solar thermal heat source was validated to be suitable.

- 2) Hauer and Lävemann elaborated, that an open zeolite system achieved a storage density of  $124 \text{ kWh/m}^3$ , what is three times higher of what a water tank could store at  $130^\circ\text{C}$  charging temperature [173]. The scientists calculated a payback period of 6 to 7 years for an open system with 150 heating and 100 cooling cycles a year.

Compared to phase change materials, Hauer and Lävemann call attention for a two to four times higher charge- and discharge capacity related to the liquid-gaseous phase change, compared to the solid-liquid phase change. Thus an open system provide  $120$  to  $150 \text{ kWh/m}^3$ , compared to an solid-liquid ice-system with  $70$  to  $90 \text{ kWh/m}^3$ .

- 3) Gartler, Jähnig, Purkathofer and Wagner evaluated in 2007 [174] an energy output of  $115$  to  $123 \text{ kWh/m}^3$  silica gel storage material for two different closed evacuated storage containments. They encountered a difference to simulation results ( $150 \text{ kWh/m}^3$ ) of about  $35$  to  $27 \text{ kWh/m}^3$ . Summarized, the value the overall storage density of commercially available silica gel as rather insufficient.

- 4) Heier, Bales and Martin (2015) [171] report of the EMPA project, Switzerland, when a NaOH salt hydrate provided  $250 \text{ kWh/m}^3$ . Beside enormous cycle-strength the storage was successful with 7 cubic meters of total system volume to supply a passive house standard single family home.

- 5) Kerskes et al. (2013) [163] developed an integrated sorption storage – sensible buffer tank design for tap water heating and supply (see Fig. 4.12). Heating energy is intended to be freed from the seasonal sorption storage fractionally to heat the sensible buffer tank on demand. The benefit of this integrated system are justified by sensible heat losses of the sorption storage during desorption, that are not irretrievably lost to environment, but remain utilizable for a certain time as sensible energy until increased energy prohibits any other utilization. Thus, buffering sensible losses raises the total system efficiency.

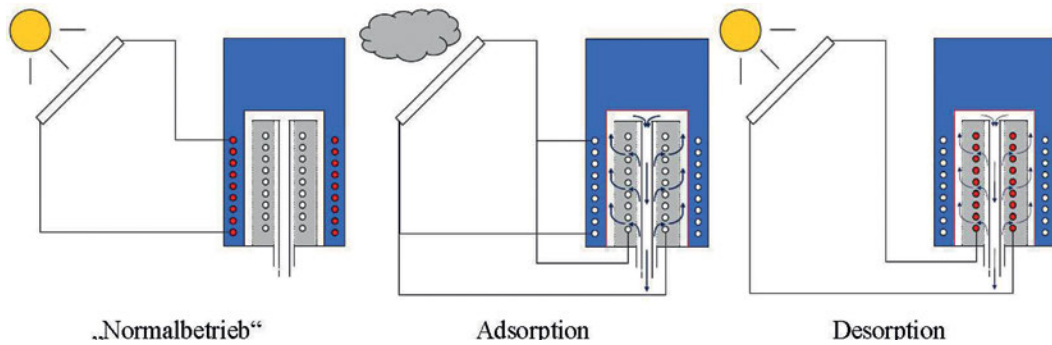


FIGURE 4.12 Operating scheme of the buffer tank integrated seasonal sorption storage

Figure 4.13 shows tabular results of the integrated sorption storage-buffer tank combined with a 6m<sup>2</sup> CPC vacuum tube collector plant for fractionized energy saving, post-heating days between June and August and hours of stagnation.

The short choice of research projects shall illustrate, what research and development have achieved so far in respect to actual domestic application and which questions are still to be answered.

Speicher	anteilige Energieeinsparung	Nachheiztage Juni–August	Stagnationszeit
	%		h
Referenz 230 I <sub>WWS</sub>	70,5	11	592
Referenz 330 I <sub>WWS</sub>	71,9	8	484
Referenz 400 I <sub>WWS</sub>	72,2	7	426
230 I <sub>WWS</sub> + 100 I <sub>SWS</sub>	72,9	4	174
200 I <sub>WWS</sub> + 130 I <sub>SWS</sub>	72,7	5	211

FIGURE 4.13 Results of entire year simulation with climate Würzburg, 6m<sup>2</sup> CPC evacuated tubes, hot tap water demand 2.945 kWh/y

Overall, the projects validate, that with respect to technical details, certain system configurations ZeoSys GmbH and 5) Kerskes et al.) meet the requirements and provide sufficient and elaborated solutions which are closed to ready-to-market. Solar thermal heat source has been verified to be effectual and efficient.

The following section concentrate on diverse thermo-chemical sorption materials in order to clarify weaks and strengths and to identify eligible candidates.

---

## § 4.5 Storage materials for sorption storages

---

For thermo-chemical storage processes the materials group of suitable materials is extensive. Suitable materials differ in storage density, water, respectively more general liquid adsorption and specific binding behavior, in desorption behavior, in durability, in performance degradation, in availability and costs.

The next sections give a survey of detected material groups and further material developments which aim on the improvement of single material properties.

### § 4.5.1 Material groups

---

Since storage density depends on the chemical ability to bind water molecules in the existing molecule lattice, what is a question of pores, and the storage system efficiency on the energy amount to release the water, molecular structure is a key concern of thermo-chemical sorption materials.

Thus, we need adsorption materials with large pore volumes. In general the natural material group of zeolites has been detected to be extraordinary performing. Zeolites are rocks and can be processed to ceramics. Within zeolite structures alumina-oxide and silica-oxide molecules form sodalith-cages (Fig. 4.14). Several sodalith-cages form a macro-structure with pores. This macro structure contains up to 700 to 1.000 m<sup>2</sup> of pores per gram of zeolite and tends to bind liquids.

For zeolites have been detected the types A, X and Y as beneficial, as well as chabasit (Schmidt, 2006, [175]).

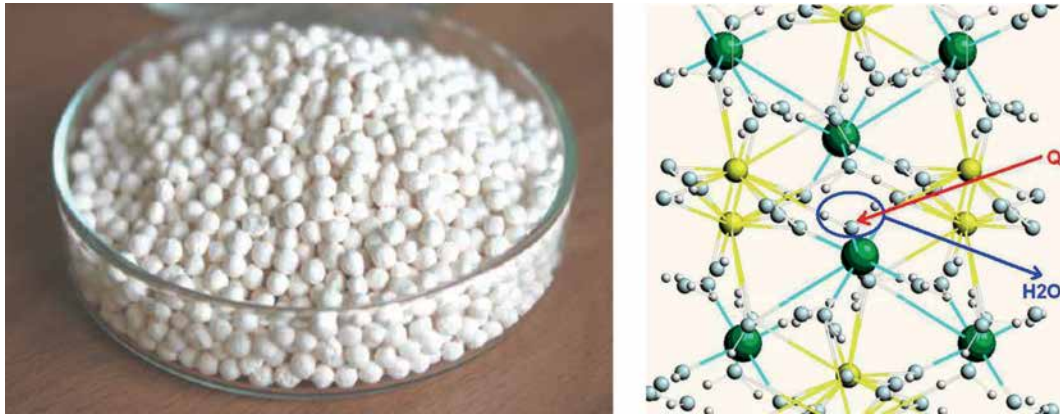


FIGURE 4.14 a.) Synthetic zeolite beads, b.) molecular lattice

As common materials in commercially available and large quantities have been detected 1979 by Shigeishi, Langford and Hollebone, 1979 :

- *alumina oxide (alumina gel, activated alumina)*
- *poro-tecto- alumina-silicons (zeolite)*
- *carbon (charcoals, activated coal)*
- *silica gel*
- *crystalline zeolites-aluminosilicates (pellets, spheric form)*

They profit from being chemical inert and resistant to deterioration.

In terms of working temperatures for solar thermal applications on low-temperature level especially silica gel qualifies with 40 to 100°C, zeolites with 130 to 300°C and metal-hydrates with 280 to 500°C operating temperature range. For effective storages a material choice requires focus on intensive polar molecules. High polarity enforces dispersion, polarization and quadrupole contributions to the van der Waals forces. By this higher temperatures during adsorption and larger adsorbate-adsorbent affinity is attained. Furthermore, the lower the evaporation temperature of the adsorbens (water) is, the more adsorbens will be adsorbed. The closer it evaporates to the specific material boiling point the less will be adsorbed. Nevertheless, Gantenbein, 2004 [176] remarks, that common silica gel 490 degrades after exceeding a desorption temperature of 120°C. That fact promotes investigations on more powerful and resistant materials.

Further research and synthetic material development extended the group of eligible materials by :

- *MCM-41 materials*
- *composite adsorbens : hydrate salts on carrier structures*
- *phosphate composite : silicon-alumina-phosphates (SAPOs) and alumina-phosphates (AIPOs)*
- *metal-organic hollow structures (metal organic frameworks = MOF's)*

Shigeishi, Langford and Hollebhone 1979 already exemplified for common available synthetic zeolites 4A and 13X:

- *Heat of adsorption (average) J/mol H<sub>2</sub>O adsorbed : 79,4 (molecular sieve), 79,4 (13x)*
- *Energy density [kJ/kg] : 1.020 (4A molecular sieve), 1.370 (13x)*
- *Energy density [kJ/m<sup>3</sup>] : 796\*103 (4A molecular sieve), 823\*103 (13x)=228 kWh/m<sup>3</sup>*
- *Weight required [kg] : 4.080 (4A molecular sieve), 3.050 (13x)*
- *Volume required [kg] : 6.0 (4A molecular sieve), 5.1 (13x)*
- *Readsorbed water 110°desorpt. [kgH<sub>2</sub>O/kg]: 0,053 (4A molecular sieve), 0,086 (13x)*
- *Readsorbed water 150°desorpt. [kgH<sub>2</sub>O/kg]: 0,052 (4A molecular sieve), 0,091 (13x)*

This list demonstrates, that zeolite 13X mostly outnumbers 4A. Beside published theoretical storage densities of common synthetic zeolites ranges between 200 and 250 kW/m<sup>3</sup>, experiments and practical assessments revealed actual densities between 90 to 150 kWh/m<sup>3</sup>

### § 4.5.1.1 Designing material towards specific application : solar thermal heat source

---

Beside synthetic composite materials, common synthetic materials can be designed in respect to concerned application, reaction behavior or heat source and supply characteristic. Thus, adsorption performance can be enhanced and designed by changes in the ratio of silica and alumina in the crystal lattice. Since, we cannot ensure constant and high temperature desorption conditions with, for example, solar thermal heat sources, we need materials with less hydrophilicity, with less alumina in the lattice.

We call this designing dealumination. Instead of alumina ion and cations (positive ion) the gaps in the lattice remain unfilled and do not provide attractive positions in the lattice any-more for water. Thus, the lattice encounters less binding and adherence power, what eases desorption (Schmidt, 2006 [M]). Detailed understanding of ion positions in the lattice can be gained with X-radiation and neutron deflection experiments. On the contrary, if cations can be positioned in the smaller sodalite-cages, water molecules are inevitably caught in the “super-cage” and thus easier to release.

Slightly dealuminated NaY-Zeolites (NAY-1 ( $\text{Na}_{56}[(\text{AlO}_2)_56(\text{SiO}_2)_{136}]$ ); NAY-3 ( $\text{Na}_{15}[(\text{AlO}_2)_{15}(\text{SiO}_2)_{177}]$ ) are powerful and eligible for thermo-chemical sorption storages in the temperature range of 70 to 120°C typical for low temperature solar thermal feeding [Y; M]. On the contrary, composites as SAPO<sub>4</sub>-34 and AIPO<sub>4</sub>-18 [171] as well as AIPO-17 and AIPO-18 [175] with micro-porous structures are powerful with solar thermal charging temperatures between 100 to 150°C. They outnumber the storage capacities of NaLSX, NaX and NaY-1 at comparable charging temperatures. Metal Organic Frameworks (MOF's) provide high specific storage densities and adsorptions capacities (discharge temperature and energy density), if treated with water.

Moreover, also selective water sorbents (sws-materials) have been developed since the nineteen nineties. A hygroscopic salt is embedded in a meso-pore lattice. Water is adsorbed by the salt and the cavities in the lattice as well.

For example calcium-chloride is embedded into meso-porous silica. In 2003 experiments in a reactor showed a strong tendency for washing and dissolving [177].

### § 4.5.1.2 Composite materials

Composite materials have been developed in order to diminish material drawbacks like low conductivity, high water binding forces or pore size. Normally, composite materials base on common zeolites that are used as basic structure. To these zeolites are high conductive nano-particles. For example, alumina-phosphates (AIPOs) and silicon-alumina-phosphates (SAPOs) contain alumina and phosphate in rigid alternating structures.

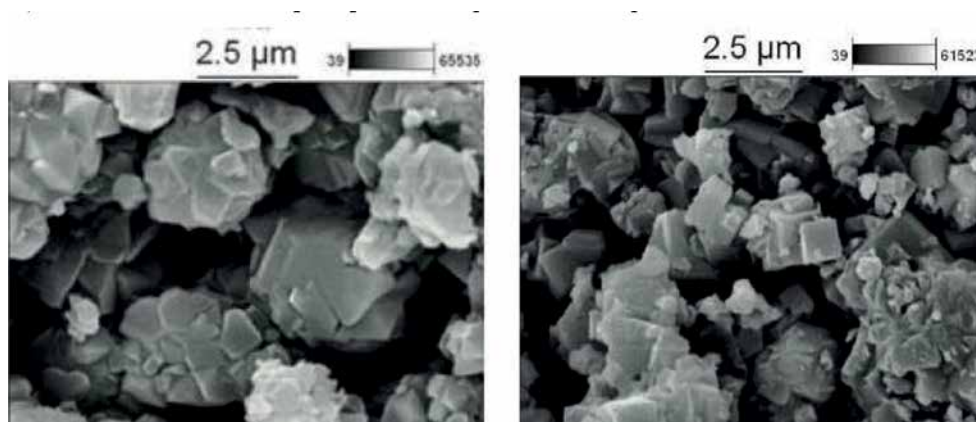


FIGURE 4.15 Surface molecular sieve 13XBF (left) and 4ABF (right) (van Helden, 2012 [178])

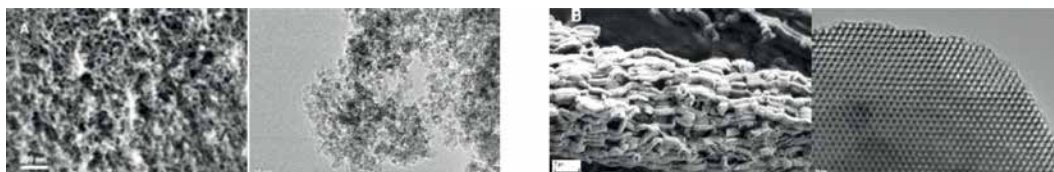


FIGURE 4.16 CaCl active carrier matrix (alumino-phosphates), Fraunhofer IGB, (van Helden , 2012 [178])

TH Wildau concentrated on the development of binder-free zeolites 13XBF and zeolite 4ABF (Fig. 4.15) , since binder reduces performance (van Helden, 2012, [178]). Further have been inspected and developed metal-organic matrix materials (MOF's)

like Cu-BTC which adsorption characteristics are similar to AIPOs. The University of Mainz evaluated a possible charging hub of 36%. However, since this material is highly porous and instable, it does not provide high cycling strength. ZeoSys GmbH and Fraunhofer IGB developed composite Poolkohl and Attapulgit (Fig. 4.16) with 30% of CaCl<sub>2</sub> as matrix [Lass-Seyoum, 2012 [I]]. That composites profit from doubled and higher water adsorption at lower temperature than common zeolites.

Sorption material	Bead size/Pellet $\varnothing$ [mm]	Bulk density [g/l]	Adsorption capacity (static) at RH = 75%/100% [g/g]	Adsorption capacity (dynamic) [g/g]
<b>Zeolites</b>				
NaMSX-CWK (I)	1.6 – 2.5	650	0.275/0.301	0.272
NaMSX-CWK (II)	2.5 – 3.5	670	0.282/0.286	0.268
NaMSX-CWK (III)	2.5 – 5.0	651	0.204/0.230	0.196
NaMSY	2.5 – 3.5	754	0.206/0.223	0.142
4ABF	1.5 – 2.5	612	0.248/0.252	0.242
4AK	1.5 – 2.5	688	0.218/0.232	0.206
<b>Composites</b>				
Poolkohl (pellet)	-	643	0.512/0.566	0.450
Attapulgit (pellet)	3.0 – 3.2	950	0.420/0.601	0.316

FIGURE 4.17 Adsorption capacities of composite materials [Lass-Seyoum, 2012 [172]]

Schmidt reports of developments of the University of Leipzig, who treated active charcoal, that normally is extraordinary hydrophobic, with nitric acid and measured a charging hub of 19% for a charging interval of 105 Kelvin (140°C/35°C). That modified charcoal is much less cost intensive than AIPOs and SAPOs, what makes market feasibility more attractive.

Figure 4.18 shows, that all adsorbents need a desorption temperature of higher than 90°C for a sufficient charging and provision of a low-temperature space heating system. AIPO-18 provide the largest charging hub of 0,25 to 0,31. That is twice as high as with Na-Y. Is a desorption cycle applied with simply 95°C, SAPO and AIPO provide demonstrably higher charging hubs. That is related to less hydrophilic tendency.

Schmidt states 2006 AIPOS and SAPOS still to be cost intensive. Although, research on composite material development have been carried out for than a decade, Kerskes (2013, [163]) in 2013 reinforced that alumino-phosphates and silicon-phosphates are still cost intensive and misses stability and cycling strength.

Further Schmidt inspected the charging hubs of different common and composite materials.

- *Na-Y : nano-crystalline zeolite Y (faujasite), containing sodium as cations*
- *Li-LSX : "low silica X", zeolite X (faujasite), little fractions of silica/alumina, enhanced by ion exchange with lithium for high >95% lithium cation fraction*
- *Ni-Y : zeolite Y, ion exchange with nickel*
- *Li-Y : zeolite Y, silica/alumina ratio 2,5, ion exchange with lithium*
- *AIPO and SAPO*

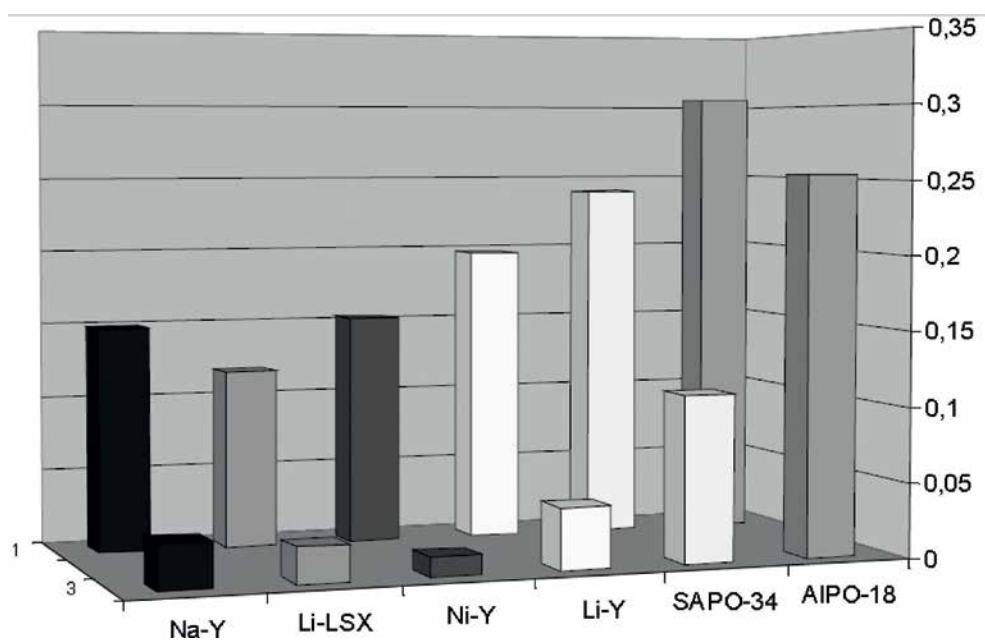


FIGURE 4.18 Charging hubs for different adsorbents with evaporation 10°C, condensation 35°C, front bars: desorption 95°C, adsorption 40°C, rear bars : desorption 140°C, adsorption 30°C

### § 4.5.1.3 Salt Hydrates

Salt hydrates are powerful thermos-chemical storage materials. In terms of process, salt in solid form is solved in water vapor, whereby the solving enthalpy is utilized as storage enthalpy. The resulting adsorption state is a salt hydrate, which may provide hundreds of kWh storage capacity per cubic meter volume. Applicable salts are  $\text{MgSO}_4$ ,  $\text{CaCl}_2$  and  $\text{SrBr}_2$ .

Salt hydrates are in particular eligible for open and fluidized reactor and process designs. Beside advanced storage densities, Mette (2012) [179] explains, that thermal performance of salt hydrates is strongly related to the specific systems of pores, the carrier matrix and its water adsorption properties. D'Ans, Hohenauer, Courbon, Frere, Degrez and Descy [180] investigated on thermal conductivity of matrix-salt composites as seen in figure 158.

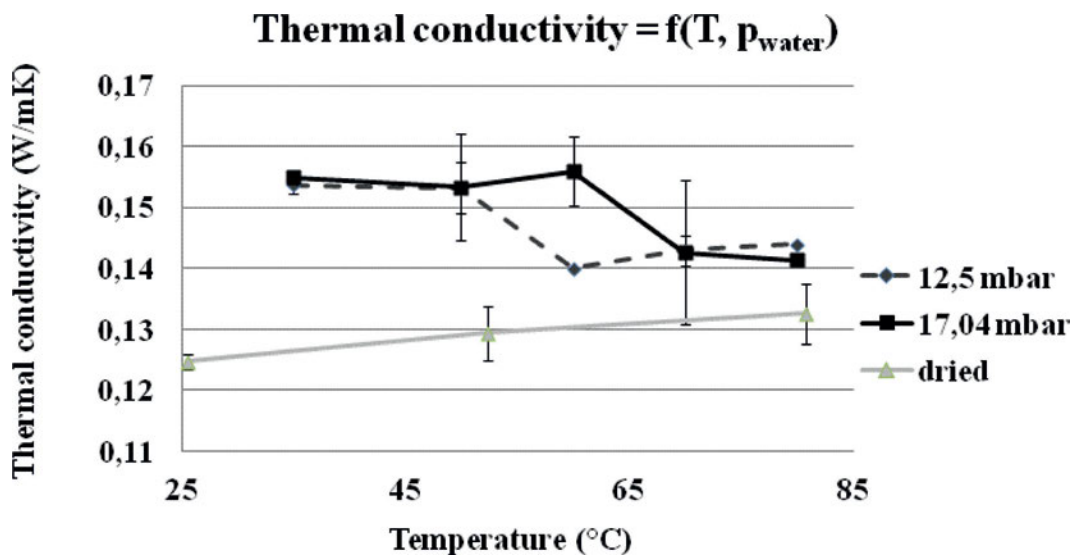


FIGURE 4.19 Resulting thermal conductivity of matrix-salt composite in relation to relative humidity

The authors measured thermal conductivity of matrix salt composites in dried phase, and recognized, that thermal conductivity of salts is relatively independent from temperature, but strongly related to humidity level. Figure 4.19 plots thermal conductivity in W/mK as a function of material temperature and material relative humidity.

The plot shows, that both lines of differently humidified matrix salts decrease in relation to temperature. Thus, conductivity decreases with decreasing relative humidity.

The author conclude, if temperature increases or water pressure decreases thermal conductivity descends, since the salt loses molecules of water. Moreover, they detected a temperature range between 35 to 60°C as being crucial during adsorption. Thus, consequently adsorption below 35°C is likely to enhance reaction and heat transfer performance.

Parallel, van Essen and Zondag [181] 2009 identified substantial decrease in performance of salt, if the required discharge temperature is too high. However, salt hydrates suffer from two major drawbacks during cycling that influence cycling strength and storage density. Pure treatment causes structural modifications and degrade thermal performance as well reversibility of process as D´Ans, Hohenauer, Courbon, Frere, Degrez and Descy (2013) [181] emphasize.

Thus, they call attention for a encapsulation of the salts into porous solid carrier matrixes. That matrixes can be provided by zeolites, carbon or silica gel. Salts like MgSO<sub>4</sub>, CaCl<sub>2</sub> or CuSO<sub>4</sub> in pure, or powder form respectively, suffer from limited process control, agglomeration or melting since reaction kinetics strongly depend on flow characteristics (Kerskes, 2013 [163]). Trausel, de Jong and Cuypers (2014) [182] remark, that Na<sub>2</sub>S salt hydrate causes toxic gases. Na<sub>2</sub>SO<sub>4</sub> needs very high humidity to hydrate >75%. MgSO<sub>4</sub>, although cheap and capacitive, tends to melt since the melting point of the salt is lower than dehydration temperature. However, toxicity, corrosiveness (Heier, Bales and Martin, 2015 [171]) and by-products of the salts have to be inspected in terms of safety and health. In order to enhance physical stability, cycle strength and conductivity as well as thermal transfer, salt should be encapsulated in water vapor permeable polymers.

Moreover, in particular the deliquescence humidity is a limit in the context of salts, that should be complied in order to avoid solutions [175]. Opposed to that provides magnesia-chloride or magnesia-sulphate that is embedded into a foam glass a stable, durable and cost effective composite solution.

Hence, encapsulated salts miss the above mentioned drawbacks and profit from comparable cycle strength. Since being encapsulated they belong to composite materials. Nonetheless, even encapsulated salts encounter drawbacks like limited conductivity, and thus, reduced reaction kinetics. Since not for all salt hydrates Clausius-Clapeyron diagrams exist, thermogravimetric analyses (TGA) help to identify humidity and temperature relation and hydration and dehydration behavior of materials.

Thereby phase diagrams can be generated for better storage system planning and process control.

## § 4.5.2 Storage densities and operation temperatures

The feasible energy density of a storage material is limited by the enthalpy storage capacity of the material. More detailed, the storage density is a maximum potential material property, that depends on previous external thermal material treatment. Hence, the power input during desorption, respectively the maximum temperature for material drying, as well as duration actually determine the resulting charge status of the material (Hauer, 2002 [169]).

Batch #	Material	C-Start	C-Ende	$\Delta m$ -Wasser	H	h-Adsorbens	h-Adsorbat
		[% Wasser]	[% Wasser]	[kg]	[kWh]	[kJ/kg]	[kJ/kg Wasser]
1	Zeolith 4A	5,9	18,6	8,65	7,86	538	3271
2	Zeolith 4A	6,0	18,4	8,42	7,72	530	3299
3b	Zeolith 4A	8,6	19,6	7,64	6,93	480	3263
4	Zeolith 4A	8,2	19,1	7,65	6,88	479	3236
5	Zeolith 4A	2,7	19,3	10,74	10,46	744	3508
6	Zeolith 13X	1,5	21,5	12,73	11,92	871	3369

FIGURE 4.20 Survey of measured adsorption enthalpies of zeolite 4A and 13X

Gartler, Jähnig, Purkathofer and Wagner (2007) [174], explain, that the heating energy of a seasonal thermo-chemical storage, namely the released adsorption enthalpy, is the sum of the evaporation enthalpy of the working fluid and the molecule binding energy of the adsorption couple. Moreover, in terms of process control, the demonstrable temperature difference between desorption (75 to 300°C) and the adsorption (15 to 30°C) a thermo-chemical sorption storage principally works like a chemical heat pump. In that context, according to Hauer, the binding enthalpy amounts to only 18-25% of the total adsorption enthalpy. Detailed information about required charging temperature and impact is exemplified in section 7.1. This section explicitly focus static and maximum material related storage densities.

Since several researcher reported considerable differences between theoretical storage density values and actually evaluated in experiments or by practical experiences, likewise Dicaire and Tezel, 2012, [168] (theoretical storage densities of 200 to 250 kWh/m<sup>3</sup>, whereas practically simply realizable 125 to 150 kWh/m<sup>3</sup>), for planning and design a conservative strategy is rather reasonable. From reported projects the effective storage densities for different material groups have been conducted and listed in the table in APPENDIX D.4. Parallel to the conducted reported values, Zettl, Englmaier, Steinmaurer and Reichl (2014, [T]) measured the storage densities for zeolite 4A and 13X in an opened system (Fig.4.20).

### § 4.5.3 Conductivity and reaction kinetics

Conductivity of the single beads within a packed bed is crucial for a homogeneous and fast reaction. Conductivity also determines controllability of a bed reaction. An efficient volume utilization equires high heat transfer through the bed towards the heat exchanger and vice versa.

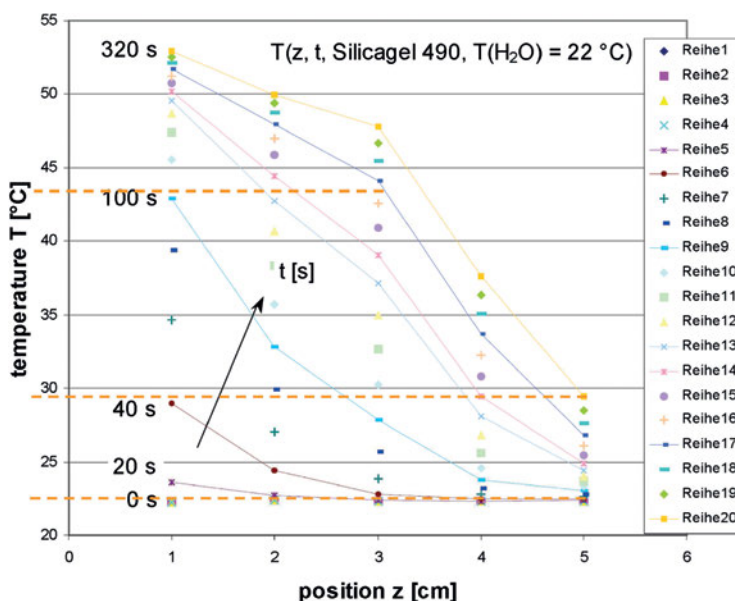


FIGURE 4.21 Adsorption temperature distribution in a silica gel 490 packed bed as function of time and fest bed thickness

Gantenbein [176] investigated 2004 (see Figure 4.21) on a packed bed of silica gel 490 and measured temperature at different points in the bed. Sensors were distributed with maximum distance of 60 mm. Figure 160 illustrates that after 40 seconds the temperature of a 5 cm bed has risen for 7 Kelvin, after 10 seconds for 21 Kelvin in a 3 cm bed and after 320 seconds for 30 Kelvin in a 1 cm bed. The graph demonstrates, that even after 5 minutes temperature of 5 cm distanced material raised for solely seven Kelvin by conductivity. Thus we can conclude, that material distanced simply a few centimeters from the heat source is affected only little by heat from the heat source by conductivity and disqualifies for adsorption, and effective discharging respectively. This insight calls for attention for both material development in terms of conductivity improvement and space efficient heat exchanger geometry.

---

## § 4.6 Reactor design and prerequisite for process control

---

While for instant geothermal heat remains on constant temperature level and assure constant supply, solar energy fluctuates hourly, daily and monthly. For that reason thermal energy storage technology is requested to provide volumetric physical design, control and mechanics that optimize process and reaction. Since solar irradiation changes in power and duration, thus in intensity, reactor design is asked to come to terms with that independent variable. This is asked, either in terms of portioned affected bed volume in order to enhance solar power to volume ratio or in terms of highly efficient volume-wise and thermal loss free distribution of the power.

Following, several different reactor and especially heat exchanger designs are explained. However, prior to that these section clarifies two fundamental reactor systems.

### § 4.6.1 Opened & Closed systems

---

In terms of reactor design and thus substantially in terms of reaction conditions we can differentiate between two fundamental designs. We can differentiate between the opened and closed design. Thereby the heat source can be identical, for example solar thermal heat. If space heating and cooling is managed by mechanical ventilation, air handling and heat recovery as well as mechanically provided fresh air is key issue of

the predominant system an opened system can be applied. That is often fundamental technical concept of a low energy, zero energy or passive house.



FIGURE 4.22 Closed sorption storage system (ZeoSys GmbH, Fraunhofer IGB)

If mechanical air handling is not the case, rather occupants enjoy natural ventilation, space heating rather bases on floor or surface radiative heating. These circumstantial conditions promote a closed system. Figure 4.22 illustrates a 0,75 m<sup>3</sup> closed reactor system in non- thermally insulated status.

The main difference between an opened and closed system is the question, how adsorption humidity is supplied and how powerful the heat source is. Since opened systems utilize the humidity in ambient air the amount of air and humidity is not limited.

Hence, these systems profit from inexhaustible amounts of ambient air. On the contrary, closed systems bases on a hermetically closed containment system and consume a clear-cut defined amount of recycling water. Further the reactor containments of closed systems are evacuated.

Evacuation helps to evaporate water at lower temperature than under atmospheric pressure. Thus, less evaporating energy is required. On the contrary, opened systems consume much more energy and higher desorption and adsorption temperatures in order to evaporate water.

In this context, Gartler, Jähnig, Purkathofer, and Wagner, [174] recommend a containment remaining pressure of 10 to 50 mbar, what equals recommended vacuum of 10 to 25 mbar by Lass-Seyoum, Blicher, Borozdenko, Friedrich and Langhof [172].

In consequence, closed systems discharging performance is much better to control than the performance of opened systems. Further, subject to the actual storage material, closed systems require less energy and lower temperature for desorption and adsorption processes than opened systems. While opened systems exchange heat to ambient air, which heat capacity is lower than of water, normally closed systems exchange heat to water driven systems.

#### § 4.6.1.1 Advantages & Disadvantages

---

System configurations, ad- and disadvantages are formulated below in bullet points.

##### Open Systems :

---

- *atmospheric pressure*
- *water vapour transport limited, high air change volume required*
- *often fluidized or floating, rotating bed : auxiliary energy required*
- *higher adsorption temperature required, lower solar fraction*
- *comparably lower storage density (90 to 120 kWh/m<sup>3</sup>)*
- *lower system efficiency*
- *filling of solid (zeolite, silica gel) or liquid adsorbents (hydrated salt solutions as lithium-chloride or calcium-chloride) [Hauer, Lävemann,2006 [173]]*
- *sensible losses to ambient air can be recovered or directly used*

- *92% of stored energy can be recovered for space heating*

#### Closed Systems :

---

- *low pressure*
- *vacuum tight containment*
- *water vapour transport requires no mechanical support*
- *mostly packed bed with no additional mechanical treatment, auxiliary energy demand*
- *lower adsorption temperature required, higher solar fraction*
- *especially solid bed reactors require a free low temperature waste heat source for adsorption process initialization*

Streicher et al. (2013 [184]) compares closed and opened sorption storage systems for space heating that are supplied by a evacuated tube plant in terms of annual process and operation. He refers to TRNSYS simulations of a low energy residential building (30 kWh/m<sup>2</sup>\*a) with a 35m<sup>2</sup> vacuum tube collector plant and a 7,5 t sorption storage tank with 13XBF binder-free zeolite. To him, annual savings of more than 90% are realistic.

The results show, that a closed system is enabled to provide a higher annual solar fraction, since reaction is run in vacuum mostly with moderate collector temperature. The opened system needs 180°C collector temperature to operate, that limits solar fraction and annual operation duration as well. Opposed to that the maximum collector temperature is reached in closed systems at the end of summer and autumn. Consequently, desorption operation of closed systems starts already in spring, whereas desorption for opened systems is as recently as possible with collector temperature of 180°C solely in March, but however predominantly in summer.

Opened systems require additional heating at the beginning of the heating period, since heating capacity is limited by the ventilation system and the amount of water provided.

On the other hand, closed systems suffer from significant sensible losses during desorption and require thermal insulation. Opposed to that opened systems could recover that sensible losses if heat recovery in the service room air handling unit is

applied. Although Kerskes (2013 [163]) argues, that the storage density of sorption storages compared to other storage technologies is higher, nonetheless, the benefit he evaluated with an opened system for especially tap water heating was low.

He relates that to the required periphery of technical devices and to the limited effective substitution potential for required tap water energy.

## § 4.6.2 Mechanical reaction systems

---

Since a packed bed of sorption material suffers from pressure drop of evaporated water and demonstrably reduced heat transfer, several different methods and devices have been developed to enhance reaction kinetics. Likewise, Gantenbein (2004, [176]) describes the maximal potential difference in pressure was likely the pressure in the adsorbents bed. Hence, the process is determined by the partial pressure of the solvent.

Several reactor designs developed regarding either the general type of storage system or the aggregate of the adsorbents. According to the aggregate, reactor design differentiations can be identified as

### 1) Mechanical adsorbent bed configuration and treatment:

---

*a.) solid bed, b.) floating bed, c.) stirring bed, d.) fluidized bed :*

Since a solid or packed bed encounters significant pressure drop and low heat transfer, a floating or fluidized bed optimizes heat, water vapor and adsorbents contact. Alternatively or parallel a stirring of the bed optimizes direct heat transfer. All three mechanical treatments require auxiliary energy and causes complex hydrodynamics. On the contrary fluidized bed reactors suffer from corrosion of device components.

### 2) Separated (salt hydrates) vs. integrated reactor (solid bed) :

---

An integrated reactor normally maps a closed system. Thus, the adsorbents bed needs sensible preheating. An integrated reactor allows no apportionment of the adsorbent. If heat source is limited, the frequency of adsorbents not being heated to desorption temperature rises. Opposed to that,

separated reactor containments either enables highly efficient desorption and adsorption of the actually demanded amount of adsorbends for heating or the highly efficient reaction of a smaller amount of adsorbends apportioned for the actual solar gain. Since integrated reactors affect but unutilized material (Zondag, 2009, [181]), they encounter higher sensible losses. While processes run slower and stop neither completely desorpted nor adsorpted, process control is difficult and insufficient. Separated reactors are most appropriate for solvents and salt hydrates.

### 3) Reactor separated from buffer tank vs. Reactor in buffer tank (Kerskes):

The released heat immediately needs to be utilized in order to gain maximum exergy. If floor or surface heating systems are applied, released heat complicates direct utilization with high temperature. Either a mixer, heat exchanger or a buffer tank is required in order to bridge the gap of different temperature levels. Every device in between heat source and heat sink causes thermal losses and lowers system efficiency. Thus, researcher developed a reactor being incorporated into a sensible thermally insulated buffer tank in order to recover sensible losses by desorption and release storage heat directly to the heat sink.

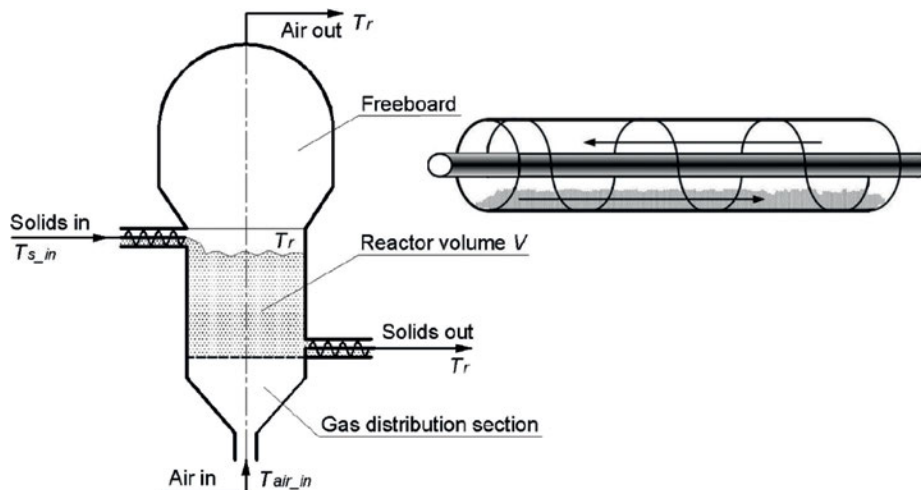


FIGURE 4.23 a.) Fluidized bed reactor, b.) extruder reactor, c.) bulk reactor by Zondag et al. [181], 2009

#### 4) Bulk vs. drum reactor or extruder reactor :

A bulk reactor (Fig. 4.23) commonly contain a solid bed, that enters above and exits at the bottom. Thus, material flow can be controlled by friction in a gravimetric down-wards flow and specific heat transfer along heat exchanger plates. Opposed to that allows a drum or extruder reactor (Fig. 4.24) a horizontal control of reaction process by rotation, velocity and inclination and improves adsorbents bed mixture.

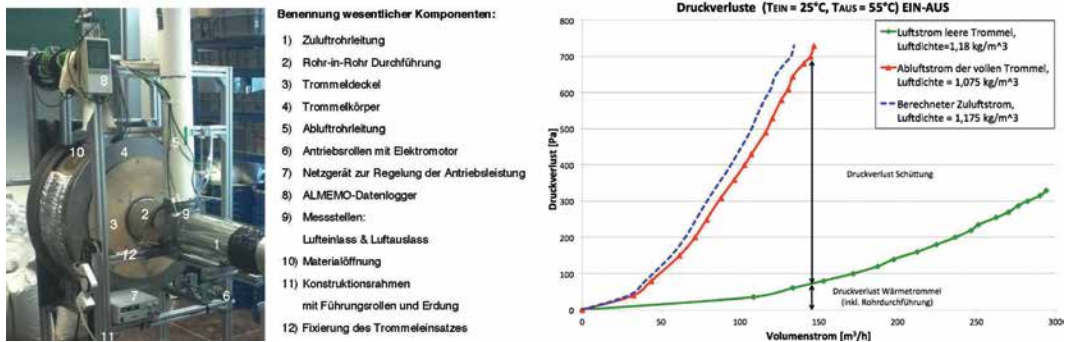


FIGURE 4.24 a.) Drum reactor and, b.) measured pressure drop of air volume [183]

Zettl, Englmaier, Steinmaurer and Reichl. (2014, [183]) published results of a measured drum reactor. Major benefit of the drum reactor is a persistent homogeneous intermixture and a negligible pressure drop (see Fig. 4.24b) what result in optimized humidity saturation of adsorbents material.

#### § 4.6.3 Heat exchanger geometry

As previously already explained in section 2.2 reaction kinetics are closely related to heat and humidity transfer across the sorptive material. Since thermal conductivity of sorptive material is commonly poor, likewise phase change material, heat transfer throughout the bed is limited. See again Gantenbein (2004) [176] in section 2.2 who determined time intensive and restricted temperature rise in bed solely 3 to 5 cm from the heat source.

For that reason, Gärtler, Jähmig, Purkathofer and Wagner (2007, [174]) call explicit attention for heat exchanger design in closed evacuated reactor.

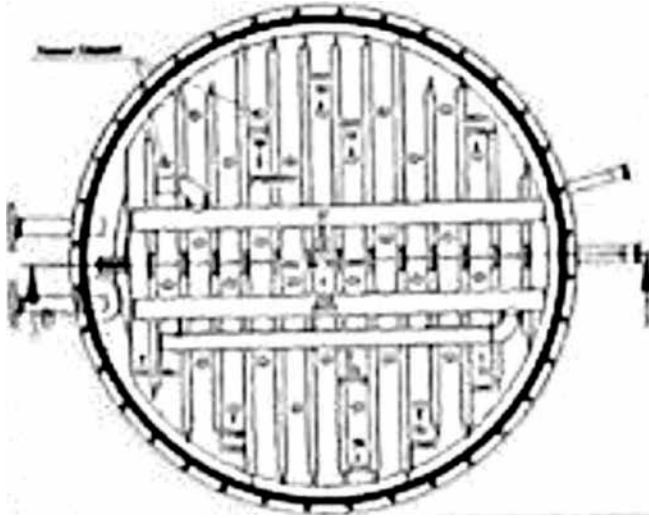


FIGURE 4.25 Space efficient vertical and concentric U-shaped tube register heat exchanger (Lass-Seyoum et al., 2012)



FIGURE 4.26 Tubular finned heat exchanger for closed systems (TNO), fixed bed heat exchanger, (ECN), The Netherlands, rotating drum heat exchanger, ASIC and TU Vienna, Austria, (van Helden, 2012, [178])

Moreover, Hauer and Lävemann [173] evaluated a practical heat exchanger performance of simply 30% in an open system, what was calculated to be 90%.

Parallel, if closed systems with solid bed are applied where the bed does not profit from gravimetrically induced intermixing, a smart heat exchanger geometry is indispensable and decides about reaction inertia. Lass-Seyoum emphasizes a 60% better reaction performance by an improved vertical matrixed tube register (Fig. 4.25), which allows adaption to the given bulk geometry and approximates the bulk envelope (see Figure 4.22 [172]).

Distances between the tubes shall not exceed the double the mean maximum achievable heat conduction bed width to assure a homogenous heat transfer. Several geometric developments of heat exchanger have been realized so far that will roughly be sketched in order to call attention for this influencing factor and to give an overview (Fig.4.26) :

#### 1) Finned heat and mass exchanger

---

- *Drawback : adherence of zeolite to exchanger fins*

#### 2) Fixed bed heat and mass exchanger

---

- *compact bed, pressure drop*

#### 3) Rotating drum

---

- *efficient, but complex hydrodynamics*

#### 4) Spiral plate heat exchanger (adsorber)

---

- *improved heat transfer, but lacks in center area*

#### 5) Plate fin exchanger (evaporator/condenser)

---

- *Drawback : freezeed condensate (water to ice) tends to dilate the plate fins*

## 6) Concentric tube register of U-shaped tubes

---

- *tight matrix of heat exchange surfaces, enhanced area to volume ratio, time effective enhanced reaction*
- *regular heat distribution, no striation*
- *adaptable to many reactor geometries*

Opposed to mechanical developments, Kerskes et al. (2013, [163]) investigate the concept of integrating sorption materials into border areas, which suffer from the highest distance from heat exchangers and encounters lower temperature levels. Since these materials profit from lower specific desorption temperature, despite lower storage densities reaction starts anyhow. This concept helps activating and utilizing material and reactor volume with less energy and rises volume specific system efficiency.

---

## § 4.7 Specific process characteristics and detected aspects for further research

---

Since thermo-chemical storages by principle work on molecular level, that rather can be observed, analyzed and partly controlled on laboratory level, this storage technology is promised to be part of future domestic energy systems. Thus they need to be fool proof and reliable to work durably without any maintenance. The processes itself are requested to be simplified on a level, that they work routinized on a non-molecular but more or less physically observed level.

For that reason, a further insight and descriptive knowledge is necessary to make control feasible and reliable and to ensure system efficiency. This section concentrate on power input and output and informs about gained descriptive knowledge.

## § 4.7.1 Required energy source and temperature for desorption

For charging sorptive material requires being dried. Incorporated water is to be freed and thus lattice and molecular binding energy is to be overpowered. Figure 4.27a.) demonstrably plots the effect of different desorption temperature of 180 and 230°C on zeolite 4a and 13X.

Zettl, Englmaier, Steinmaurer and Reichl, 2014, [183] measured a drying rate of 6% of zeolite 4A after 72 hours and of 4,5% for zeolite 13X after 58 hours with 230°. Thus, for solar thermal application zeolite 13X is more adequate. The more the adsorbents is dried the better is the charging performance as figure cx shows [183].

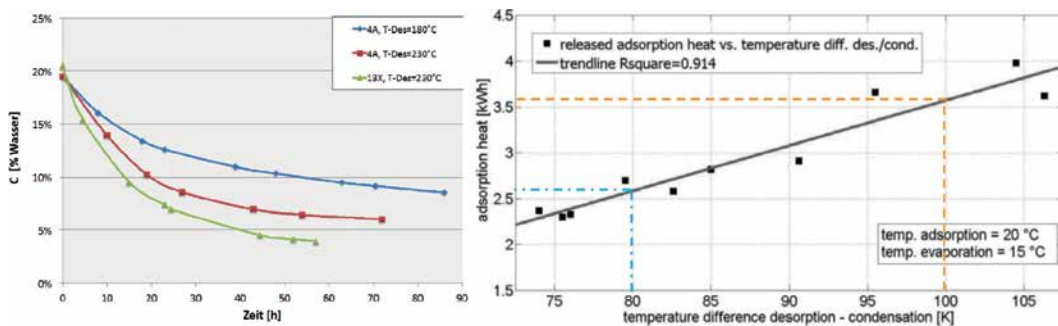


FIGURE 4.27 a.) Desorption curves as a function of time for zeolite 4A and 13X [183], b.) adsorbed heat as a function of desorption to condensation temperature difference with zeolite 5A, TNO

Figure 4.27b.) impressively illustrates the linear relation between increased temperature difference between condensation and desorption temperature, dehydration temperature respectively, and adsorbed heat in kWh for a 41 kg zeolite 5A bed. Considering the off-set of 72 K, a temperature difference of 20 Kelvin results in a difference of adsorption heat of 1 kWh.

Decaire and Tezel (2012) [168] confirm that regeneration (desorption) is a non-linear process, since effective material drying proceeds asymptotically. At some point, when material is not already 100% dried, desorption energy faces a disproportional ratio of drying. The ratio of applied desorption energy to increase in material drying is highly ineffective, consequently the energy will not be stored and is better used for sensible buffer tank heating.

## § 4.7.2 Potential temperature and released energy by adsorption

Adsorption releases the stored energy. It is a question of material, absolute humidity in the vapor flow and flow velocity, mass flow respectively, on how effective reaction process and efficient energy release is. Several researchers have investigated on the process and displays either adsorption temperature, effective utilizable flow temperature or power.

Figure 4.28 shows adsorption temperature of four different materials. On the hand zeolite 4A, 13X and binder-free 13XBF show maximum temperature of 75 to 80°C for zeolite after the first hour of adsorption, whereas on the other hand silica gel 490 shows a released temperature increase from 22 to 56°C within 580 seconds, what equals 9,6 minutes. During the process a released temperature of 50°C was obtained for 38 minutes, >40°C for approximately 80 minutes. The graphs demonstrate, that pressure and humidity influences the process and thus the temperature. Binder-free 13XBF zeolite reacts inertly.

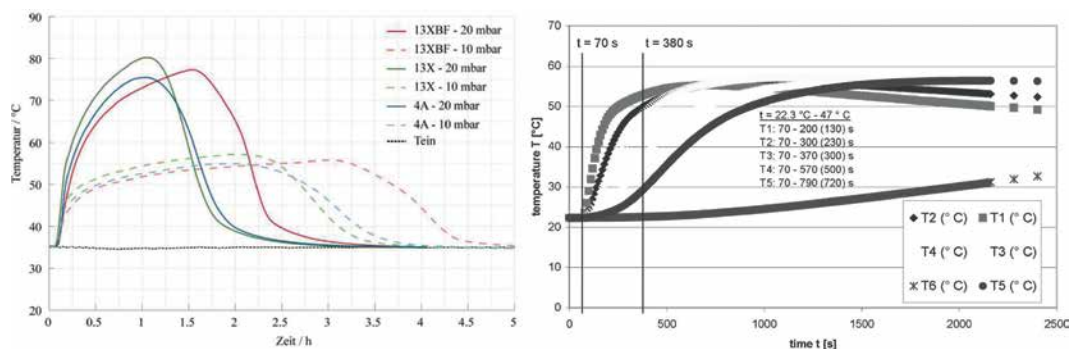


FIGURE 4.28 Measured zeolite 4A, 13X and 13XBF temperature, different water vapour pressures (Kerskes, 2013 [163]) and released temperature progress of silica gel 490 (Gantenbein, 2006 [176]) fest bed with 25 mbar remaining pressure

Lass-Seyoum et al. (2012 [172]) measured reaction and packed bed temperatures of around 150°C in a 750 L volume (Fig. 168), what resulted in a transportation oil temperature of 80 to 100°C. During a adsorption process duration of 6 hours a released temperature of > 60°C was observed. Here, the temperature differences between the temperature sensors in the reactor are more or less low, what indicates a homogeneous temperature distribution, heat transfer and reaction of the bed volume. Compared to a 1,5 L test rig (180-240 Wh/kg), the estimated heat storage capacity is

150 to 220 Wh/kg and the power (45-66 W/kg) about 19 to 50 W/kg [172]. The process of 6 hours of duration the power output started with 55kW and raised to 122 kW. A constant power output higher than 80 kW was observed for more than five hours.

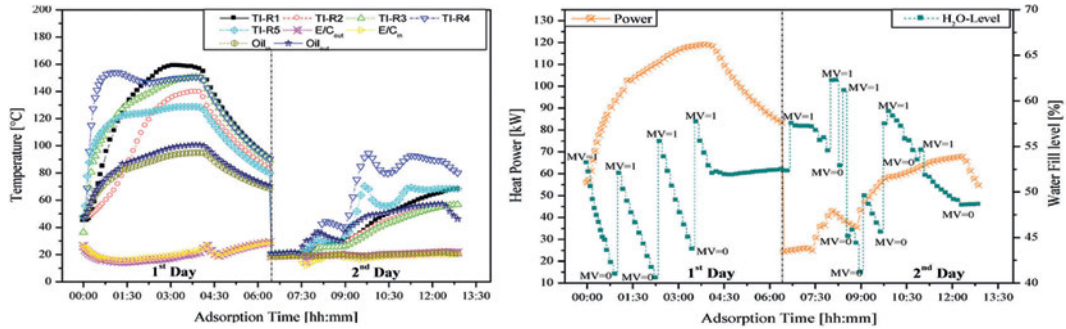


FIGURE 4.29 a.) temperature progress and b.) released power/heat of 750L reactor [172]

Similarly, Finck, Henquet, van Soest, Oversloot, de Jong, Cuyper and van 't Spijker, 2014, [185], evaluated a raise in adsorption released power up to 980 W for a 41 kg zeolite 5A reactor bed within the initial 1400 sec. (23 min.).

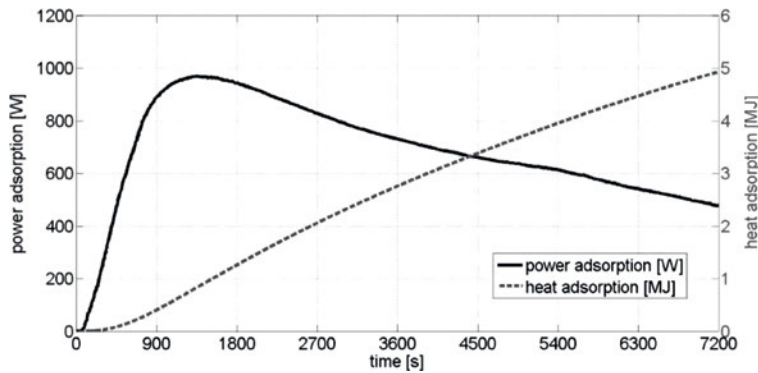


FIGURE 4.30 Increase in output heating power of a 41 kg zeolite 5A bed within 23 min

Likewise, after 120 minutes (2 hours) a cumulated effective heating energy of 1,4 kWh was released. As can be seen in the graphs above (Fig. 4.30), the released temperature and power respectively decreases in further progress of the adsorption process. Thus, material and reactor design determine the period of time when output is sufficient, the point in process when adsorption is longer efficient.

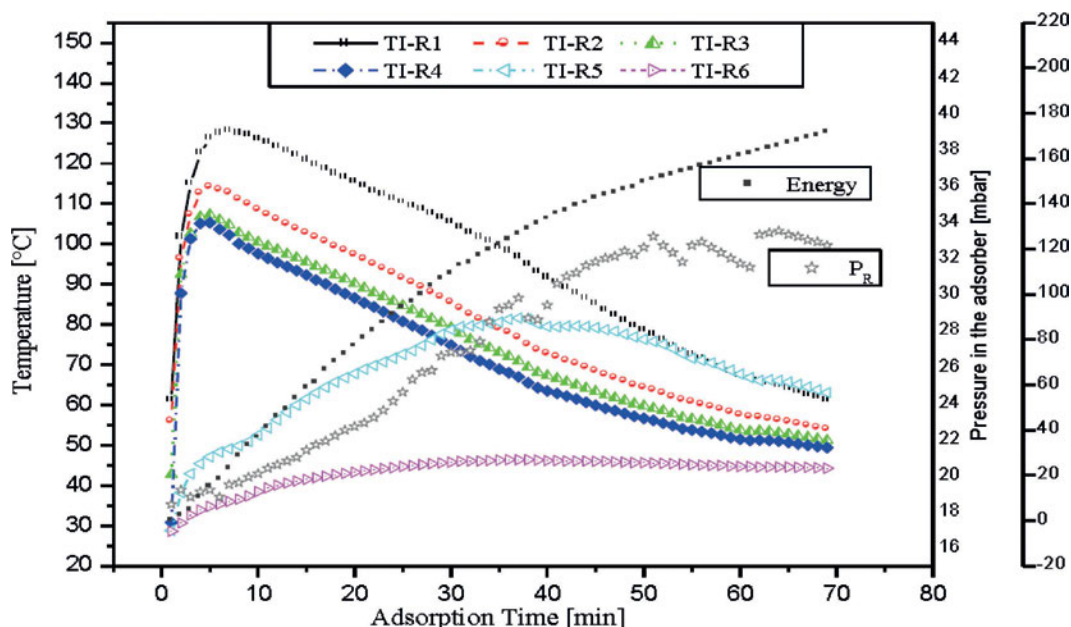


FIGURE 4.31 Released temperature, heating power of bed as function of time [1]

Lass-Seyoum et al. observed, that temperature in reactor in bed rises (Fig.4.31), when adsorbent becomes saturated during adsorption (discharge). In consequence the bed releases less energy (heat) and reaction lowers, hence becomes inefficient. Likewise, Dicaire and Tezel [168] highlight a clear-cut relation between release power and relative humidity and flow rate for integrated closed systems. Since a system suffer from over averaged sensible losses and reduced released power (temperature) when being adsorpted with lowered relative humidity and choked flow rates, reaction process runs inefficient.

Parallel, towards Shigeishi, Langford and Holebone (1979) molecular sieves need bed cooling during adsorptions. If bed temperature rises, the adsorption abilities significantly decreases.

Especially, molecular sieve 13x turns from adsorption into desorption when bed temperature of 150°C is exceeded.

Schmidt, 2004, [187], explains, that the ability of adsorbents materials to adsorb water and to release water is a crucial and critical material quality. He exemplifies, that water during adsorption could be adsorbed likely weak in the lattice, that simply a little rise in adsorption temperature in the adsorbents bed and reactor, what according to Lass-Seyoum [172] is inevitable during satisfactory discharge, is adequate to change adsorption into desorption. Schmidt calls this material characteristic energetic heterogeneity, that is closely related to chemical surface structure and pore size of the material. Thus, materials are high performance materials in terms of process control, which provide a large effective temperature difference during adsorption and desorption. Finally, he scrutinizes the positive effect of dealumination of zeolites, since he argues dealumination promotes less natural binding of water and lowers desorption temperature, hence temperature difference.

Nevertheless, Mette (2012, [179]), emphasizes a huge specific storage capacity [kWh/m<sup>3</sup>], high reaction kinetics in terms of high discharge rates [kWh/h] and high power [kW] supply as crucial for effective and efficient thermo-chemical storages for space heating. From the design perspective she calls attention for high scaling properties without significant forfeit in performance as well as modularity. Modularity in particular promotes a sufficient adaptation to the actual application (space heating, material drying) and circumstantial conditions (heat source, heat sink).

---

## § 4.8 Summary thermo-chemical storages

---

Thermo-chemical sorption storage technologies have been identified to be the most eligible for seasonal long term storing of solar thermal heat. That preliminary implies both compatibility and sufficiency. Different storage reactor typologies and different sorption materials have been inspected in respect of comprehensive performance features as well as cycling strength and costs. Although research and development still have to resolve technical details, fundamental eligibility has been verified versatile so far. As crucial finding of the literature research has been detected the insight of a considerable difference between theoretical calculated volumetric densities and actual applicable.

Further research needs to concentrate on modular storage design and controllability in order to enhance market mature prototypes which meets customized energy demand and load profile.

---

## § 4.9 Summary

---

This chapter inspected diverse energy storage technologies and in particular evaluated contemporary volumetric and gravimetric storage densities of electro-chemical and thermo-chemical storage systems.

Although this thesis focuses on heating energy management for space heating, this chapter focuses on technologies which represent caloric as well as power storages. Power storages have been parallel inspected, firstly since in terms of entropy power can be beneficially converted to heat and secondly since the volumetric storage densities of some single electro-chemical storage typologies are interestingly high and outnumber (Fig. 4.32) those of latent phase change technologies in this context.

Since the two major decisive key parameters of eligible energy storages focus on overall average high storage density and loss-free storing thermo-chemical storages have been intensively investigated.

Although practical experiences of thermo-chemical sorption storage densities are considerably lower than literature and theoretical examinations have told so far, the effective storage densities still outnumber those of alternative phase change or electro-chemical storage technologies. The most dominant drawback of this technology is the lack of commercial availability and thus the concurrent research and development status of prototypes. But, nonetheless, evaluation has verified the promising incomparable performance and compatibility with solar thermal heat sources.

Summarized, we can say, that despite several remaining technical details to solve, thermo-chemical storages are the most efficient and thus the first choice of thermal loss-free seasonal energy storage technology in the context of this thesis.

Nevertheless, it is sensible to include in particular lithium-ion accumulators in this sun space research context to alternatively evaluate the system efficiency.

## CATEGORICAL OVERVIEW OF VOLUMETRIC AND GRAVIMETRIC DENSITIES

storage technology	volumetric storage density [kWh/m <sup>3</sup> ]	gravimetric storage density [kWh/kg]
electro-chemical accumulators	ca. 11,8 to 100,0 (plumbum-acid, dryfit gel-c120)	ca. 0,150 (plumbum-acid)
	ca.100 to 115 (lithium ion-polymere)	ca. 0,040 (dryfit gel-c120)
	ca. 20,0 to 80,0 (lithium-ion-ironphosphate)	ca. 0,085 to 0,1 (lithium-ion)
thermal-chemical by desorption	ca. 150 (desorption - zeolith)	ca. 0,280 (desorption - zeolith)
	+ ca. 75,0 (sensible - zeolith)	+ ca. 0,11 (sensible - zeolith)
thermal-physical by phase change	ca. 53,0 (parafin, ?T = 20 K)	ca. 0,067 (parafin, ?T = 20 K)
	ca. 97,0 (salt hydrates, ?T = 20 K)	ca. 0,052 (PEG, ?T = 20 K)
		ca. 0,065 (salt hydrates, ?T = 20 K)
thermal-sensible e.g. water	ca. 60,0 (sensible)	ca. 0,0625 (water T=100°C, 1bar)



FIGURE 4.32 Categorical overview of different technologies: related ranges of volumetric and gravimetric storage densities

Thus, further theoretical calculations in terms of numerical simulation will consider both high efficient thermal-chemical and high efficient electro-chemical storages in order to elaborate differences in system efficiency.





# 5 Description & evaluation of BIPV combined with electro-chemical storage for sunspace heating

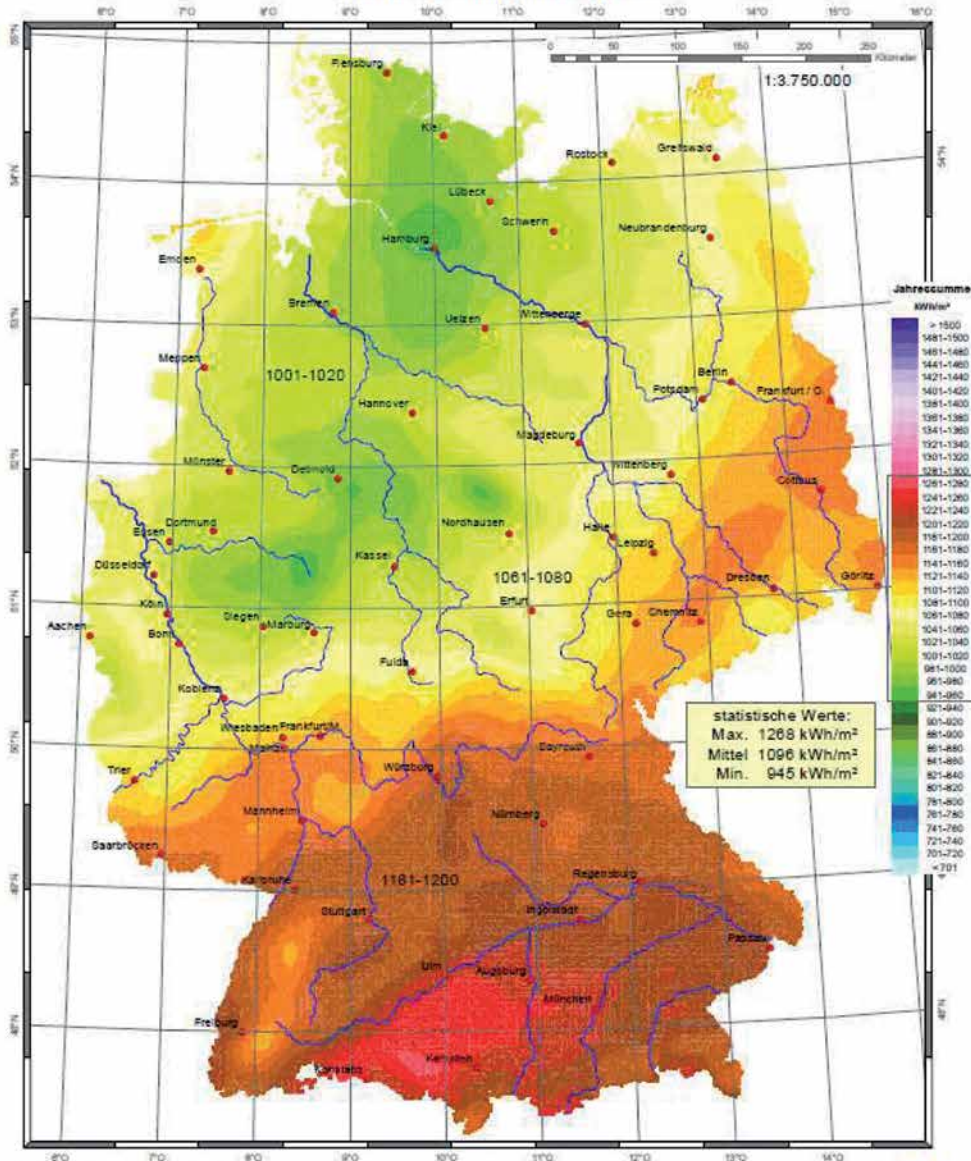
## § 5.1 Power-to-heat: sun space envelope integrated photovoltaic for space heating

After a literature review of collector and storage technology, this chapter describes a sun space test set-up and evaluates the system efficiency of a photovoltaic battery system for sun space conditioning. One alternative to façade embedded solar thermal collectors are envelope integrated photovoltaic (BIPV) generators. Comparative research in this thesis lays the focus on BIPV.

Therefore, the glazing of the experimental test sun space was replaced with glass-glass photovoltaic modules in 2012. Generated power was stored seasonally in electro-chemical storage components to be utilized in autumn and winter for ohmic resistant space heating. Dynamic simulation determined the annual heating energy demand for the test sun space to be 1.600 kWh per year for a preferred occupation time between 5 to 10 PM.

According to the map of global radiation in Germany for 2012 (Fig. 5.1) published by Deutscher Wetterdienst (DWD) [188], the maximum annual sum of irradiation for Osnabrück was determined to be 1.001 to 1.040 kWh/m<sup>2</sup>. Thus, planning required an effective area of gross 15.4 to 20.0 m<sup>2</sup> of building integrated photovoltaics with a mean efficiency of 10% in order to meet the annual consumption. The designed system including all implemented components as well the effect and efficiency will be explained in the next sections.

# Globalstrahlung in der Bundesrepublik Deutschland Jahressummen 2012



Wissenschaftliche Bearbeitung:  
 DWD, Abt. Klima- und Umweltberatung, Pf 30 11 90, 20304 Hamburg  
 Tel.: 069 / 8062 6022; eMail: klima.hamburg@dwd.de



FIGURE 5.1 Potential of fossil fuel substitution by irradiation related to county in kWh/m² and year: scenario "norm" (related to effective living area [m²])

## § 5.2 The System – components and constraints

The system is based on photovoltaic wafer cells that were laminated into the sun space glazing. In order to maintain a specific quality of perusal, two different wafer technologies were investigated. First, thin film cells of amorphous silicon (a-Si) were embedded in PVB and EVA tapes, and, secondly, mono-crystalline cells were embedded into glazing in order to provide 10% remaining transparency. In parallel, the modules were connected to groups in order to not only maintain a moderate module voltage but rather to enhance the current. Different charge controllers transformed voltage and current into the maximum charge load in order to charge a 12 V, 13.6 kWh nominal lead-acid battery rack. Battery monitor and shunt as well as diverse temperature sensors managed and controlled sufficient battery status and performance. In charge of consumption, separate load controllers [189] fed KNX-actuator controlled devices with 12 volt voltage; but rejected loads, when the battery charge status goes down to 50% depth of charge. Space heating was provided by surface embedded ohmic resistant panel heating mats, which radiated in the infrared spectrum. Hence, infrared radiation is perceived as warmth and results in less cold stress by cold space enclosing surfaces.

### § 5.2.1 Glass-to-glass photovoltaic: envelope integrated power generator



FIGURE 5.2 a.) Semi-transparent a-Si thin film modules in vertical facades and roof area, b.) Mono-crystalline in ridge area

In order to provide a remaining quality of daylight provision and perusal semi-transparent glass-glass modules have been incorporated into vertical east façade and

east gable, into vertical south façade and south roof, into vertical west façade and west roof and as well in the north facing vertical façade and gable. In particular, roof glazing was constructed to fulfil overhead safety requirements. Eighteen of a total of twenty-three modules based on amorphous silicon cells as thin film technology.

<b>SURVEY OF TECHNOLOGY, STRINGS AND PERFORMANCE</b>							
<b>No.:</b>	<b>TECHNOLOGY</b>	<b>FIELD/ ORIENTATION</b>	<b>CHARGE CONTROLLER</b>	<b>VOLTAGE MODULE (Volt)</b>	<b>MAXIMUM CURRENT [Ampere]</b>	<b>MAXIMUM POWER [W] (STGT 000, 1.5AM)</b>	<b>MAXIMUM VOLTAGE PRO STRING [V]</b>
<b>GENERATOR, MODULE</b>							
01	a-Si-THIN FILM, overhead glass-glass with PVB tape	A (south grout)	L-1	92	0,9	57	97
02	a-Si-THIN FILM, overhead glass-glass with PVB tape	A (south grout)	L-1	85	0,5	30	
03	a-Si-THIN FILM, overhead glass-glass with PVB tape	A (south grout)	L-1	97	1,4	102	
04	a-Si-THIN FILM, overhead glass-glass with PVB tape	A (south grout)	Dummy				
05	a-Si-THIN FILM, overhead glass-glass with PVB tape	C (west grout)	L-2	92	0,9	57	97
06	a-Si-THIN FILM, overhead glass-glass with PVB tape	C (west grout)	L-2	85	0,5	30	
07	a-Si-THIN FILM, overhead glass-glass with PVB tape	C (west grout)	L-2	97	1,4	97	
08	a-Si-THIN FILM, overhead glass-glass with PVB tape	C (west grout)	Dummy				
09	a-Si-THIN FILM, glass-glass	G (east gable)	L-3	83	0,47	28	90
10	a-Si-THIN FILM, glass-glass	G (east gable)	L-3	83	0,47	28	
11	a-Si-THIN FILM, glass-glass	G (east gable)	L-3	90	1,8	117	
12	a-Si-THIN FILM, glass-glass	G (east gable)	Dummy	-	-		
13	a-Si-THIN FILM, glass-glass	G (east gable)	Dummy	-	-		
14	a-Si-THIN FILM, glass-glass	H (north gable)	L-4	112	0,74	56	113
15	a-Si-THIN FILM, glass-glass	H (north gable)	L-4	113	1,9	154	
16	a-Si-THIN FILM, glass-glass	H (north gable)	Dummy	-	-		
17	Mono-Crystalline, overhead glass-glass with PVB tape	B (south attic)	L-5	70	7,8	451	70
18	Mono-Crystalline, overhead glass-glass with PVB tape	D (west attic)	L-6	30	7,8	193	30
19	a-Si-THIN FILM, glass-glass	E (south edge)	L-7	112	0,74	56	112
20	a-Si-THIN FILM, glass-glass	F (west edge)	L-8	75	1,8	98	83
21	a-Si-THIN FILM	south attic	L-9	84,5	0,103	9	84,5
					<b>sum : 1.563 Wp</b>		

FIGURE 5.3 Survey of installed photovoltaic cell technology, strings and voltage

The mean solar efficiency of amorphous silicon thin film technology is rated with a 5 per cent conversion factor. Notwithstanding, roof glazing close to ridges was, as Figure 5.2 b.) shows, divergently to amorphous silicon cells equipped with mono-crystalline cells. In contrast to the amorphous cell technology the mono-crystalline wafers provide

a solar conversion factor of 17.4 per cent. Figure 5.3 illustrates the different modules and location of incorporation into the sun space envelopes as well as performance features like module voltage and module current determined under standardized test conditions. The modules were grouped area-wise in accordance to orientation and exposure to the sun to enhance performance. The PV generators generally circled parallel due to limited string voltage but enhancing string current.

Finally, nine strings were constituted, which consequently required nine different charge controllers. The strings were successfully integrated in the sun space profiles and have not encountered any short-circuit or delay during the project. Besides the PV plant consisting of nine different fields with six different orientations and inclinations towards the sun, the installed BIPV accounted for a maximum potential power of 1.563 Watt peak. Thus, considering all losses and discount in power, the plant provided one third of the maximum required heating power of 4,500 Watt.

## § 5.2.2 Circuitry and charge controller extent

---

As Figure 5.3 demonstrates, at least five modules were based on 95 Volt and higher, and nearly all exceeded 60 Volt.



FIGURE 5.4 PV battery charge controller set for diverse PV circuits

Further, for an appropriate evaluation of efficiency, charge controllers were in charge which firstly provided MPPT tracking algorithms for optimal power point managing, secondly managed voltage up to 113 Volt, thirdly managed 12 Volt battery charging, and lastly provided software and interfaces for a real-time power and charge performance analysis. In fact, these feature requirements limited the amount of approximately 50 available charge controllers on the market to solely three being appropriate.

Figure 5.4 shows the arrangement of ten MPPT 12 Volt charge controllers, each eligible for 45 ampere total charge current with RS-232 and USB/Serial DB9 ports for real-time data access.

Moreover, the charge controllers are based on modern charge algorithms which consider the three different charge phases (absorption, conservation and equilibrium charge phase) typical for lead-acid batteries.

### § 5.2.3 Lead-acid accumulator: more than monthly storage, the sole power supplier

---

Since the author had to consider the extraordinary amount of power needed for space heating and the charge capacity specific prices for different available electro-chemical accumulators, the choice was either a conventional lead-acid or a lithium-ion battery. Whereas one kWh capacity lead-acid battery cost approximately 400 Euro in 2012, the lithium-ion technology was cost 800 to 1,000 Euro per kWh capacity.

Therefore, a 12 Volt closed lead-acid battery was installed which provided 27 kWh capacity, respectively a nominal capacity of 13.5 kWh regarding a depth of discharge limit of 50%. Thus, twelve 2 Volt cells with a maximum discharge current of 1250 Ah were serially connected to two separate 12 Volt blocks, and consequently serially connected to provide 13.5 kWh effectively.

Figure 5.5 demonstrates the battery block, which had a total weight of 960 kilo grams. Hence, the battery provided a gravimetric charge capacity of 0.0141 kWh/m<sup>2</sup> and a volumetric charge capacity of 11.62 kWh/m<sup>3</sup>. The charge status and battery health was monitored by a battery monitor, which calculated the remaining capacity by considering the cell temperature measured by 12 different temperature sensors, the remaining voltage and internal resistant by a 500A shunt. The monitor provided a 10 mA definition, but showed differences to a reference monitor of up to 15% 3 weeks after the latest calibration, reset at 100% charge status respectively.



FIGURE 5.5 Rack of 12 Volt, 13,6 kWh Cnom lead-acid off-grid accumulator with Bat-fuse

The charge status was recallable in real-time as .csv-data file on a personal computer via a RJ12 net port. Analogously, as power supply control were installed three 12 Volt - 60 Ampere and one 12 Volt - 45 Ampere DC-load controller with load-rejection at remaining voltage of 11.3 Volt. Although by principle the battery provided nearly 15,000 W per hour ( $12 \times 1.250\text{Ah}$ ), the maximum available DC power per hour was limited to 2,700 W ( $[3 \times 60\text{A} + 1 \times 45\text{A}] \times 12\text{V} = 2700 \text{ Watt}$ ). Parallel to the DC load controller, a 1,500 W DC/AC converter was installed in order to provide 1.5 kW AC power.

This DC/AC converter was also programmed to reject loads at 11.3 Volt remaining battery voltage. An interesting factor of this PV battery system was that the maximum power was not supplied by the PV plant itself, but by the battery. Since the entire PV plant is separated into ten different fields, which all generate with different efficiencies to a specific time, the maximum power peak was far below the power peak of 1,563 Watt. Hence, the maximum power revealed in May 2013 rather turned out to be 750 Watt.

## § 5.2.4 Heating system: ohmic resistant mats as radiant panel heating

Space heating that utilizes power, was realized with infrared emitting heating mats. Polyethylene (PET) foils of 0.6 m width and 5 m length incorporate oppositional electrical conductance stripes. Due to carbon fibres and filling material in the PET foil, closed circuit voltage converted power into heat. Thereby, surface temperatures of 34°C were applicable while the heating power ranged between 50 to 150 W/m<sup>2</sup>, depending on the voltage.



FIGURE 5.6 Screed and wall plaster embedded ohmic resistant panel heating mats

Four PET heating mats with dimensions of 0.6 x 2.25 m were incorporated into the screed of the south flank, four mats with dimensions of 0.6 x 5.85 m were incorporated in the screed of the west flank. Thus, with a voltage of 12 Volt and 7 Ampere current the heating power was equal to 50 W/m<sup>2</sup>. Additionally, three mats with dimensions of 0.6 x 2.50 m were embedded in the wall plaster of the north and two mats into the plaster of the east wall. In contrast to the floor mats, the wall mats were driven by 24 Volt and 15 Ampere, which resulted in 52 W/m<sup>2</sup>.

In summary, the mats – when driven synchronically – provided heat with 1,960 Watt maximum, which equals nearly 44% of the maximum required heating load. Subsequently to the load controller, four galvanic isolated DC/DC converters were installed in the system to provide DC power especially for the heating mats.

Each controller, on a 12 Volt basis and 30 Ampere current, provided 360 Watt power at maximum. Four DC/DC controllers [Fig. 5.6 allowed a maximum power supply for heating of 1,440 Watt. Thus, the maximum heating power installed was effectively limited to 1,4 kW, which equals 32% of the maximum load. Figure 5.7 visualizes the incorporation of mats into space enclosing surfaces.

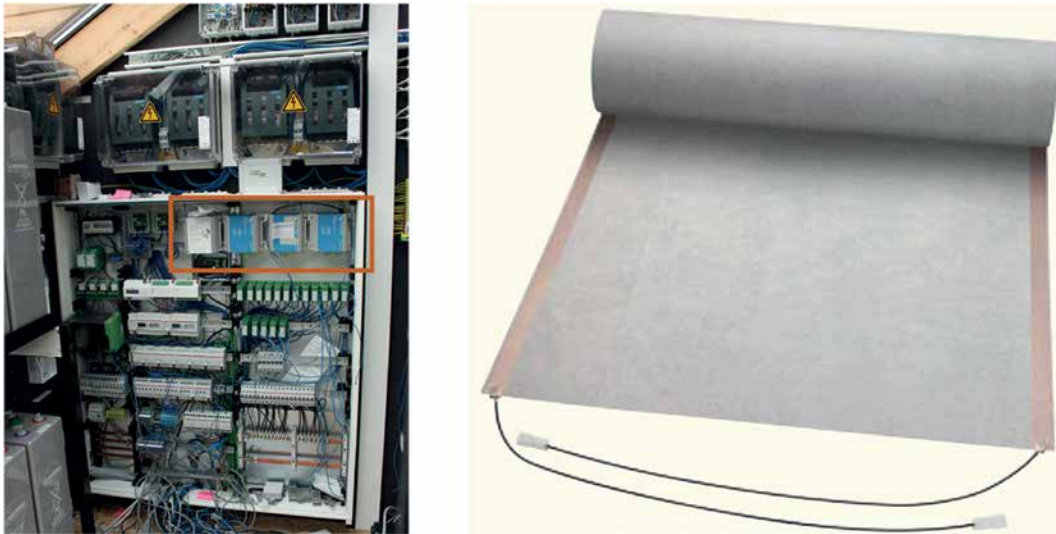


FIGURE 5.7 AC/DC switch cabinet with KNX relays and actuators and 30 ampere DC/DC converter

#### § 5.2.4.1 Source related measurement of radiative heating: additional sensors

Infrared radiating heating mats caused problems for temperature measurements. Since radiation in the infrared spectrum only warms and heats ambient air insignificantly and cannot be perceived on clothed parts of the body, additional temperature conductance sensors had to be installed directly on the mats. The mats themselves were not allowed to be penetrated by objects larger than 70 by 70 mm, otherwise shortcuts in the mats caused burns (Fig.5.6). While common combi-surface temperature sensors mounted to the north and east wall covered the sensor with a casing that exceeded 70 by 70 mm, the mats were placed beside the sensors in order to evade penetration and burn.

For that reason, additional sensor heads were mounted to the wall mats to avoid significant penetration that would have logged especially the mats surface temperature.

## § 5.2.5 Additional provided functions and consumers

---

In summary, the mats – when driven synchronically – provided heat with 1,960 Watt maximum, which equals nearly 44% of the maximum required heating load. Subsequently to the load controller, four galvanic isolated DC/DC converters were installed in the system to provide DC power especially for the heating mats. Each controller, on a 12 Volt basis and 30 Ampere current, provided 360 Watt power at maximum. Four DC/DC controllers [Fig. 5.7] allowed a maximum power supply for heating of 1,440 Watt. Thus, the maximum heating power installed was effectively limited to 1,4 kW, which equals 32% of the maximum load. Figure 5.6 visualizes the incorporation of mats into space enclosing surfaces.

### § 5.2.5.1 Source related measurement of radiative heating: additional sensors

---

Infrared radiating heating mats caused problems for temperature measurements. Since radiation in the infrared spectrum only warms and heats ambient air insignificantly and cannot be perceived on clothed parts of the body, additional temperature conductance sensors had to be installed directly on the mats. The mats themselves were not allowed to be penetrated by objects larger than 70 by 70 mm, otherwise shortcuts in the mats caused burns (Fig.5.7). While common combi-surface temperature sensors mounted to the north and east wall covered the sensor with a casing that exceeded 70 by 70 mm, the mats were placed beside the sensors in order to evite penetration and burn. For that reason, additional sensor heads were mounted to the wall mats to avoid significant penetration that would have logged especially the mats surface temperature.

## § 5.2.6 Additional provided functions and consumers

Diverse DC and AC devices were also installed beside heating mats. These devices covered functions like natural and forced ventilation, artificial lighting, internal sun shading and active cooling. Figure 5.8 lists additional electrical consumers which either run with 12 Volt or 24 Volt voltage. Power and current are highlighted, as is the assignment to one of the four load controllers, respectively DC/DC converter.

FUNCTION / CONSUMERS / PERFORMANCE / LOAD CONTROLLER								
No.:	FUNCTION	CONSUMER / DEVCE	POSITION	VOLTAGE [V]	CURRENT I [A]	POWER P [W]	measured/observed currents [A]	LOAD CONTROLLER
01	HEATING	ohmic resistant panel heating mat	South - floor	12 (DC)	6,9 (x4,paral.)	83,0 (x4,paral.)	5,93	LC-01 / 02
02			West - floor	12 (DC)	15,2 (x4,paral.)	182,0 (x4,paral.)	10,62	LC-01 / 02
03			North - wall	24 (DC)	15,0 (x3,paral.)	180,0 (x3,paral.)	37,80	LC-03
04			East - wall	24 (DC)	15,0 (x2,paral.)	180,0 (x2,paral.)	37,80	LC-04
05	COOLING	converter split unit	East - wall, flank south	230 (AC)	15	3.500	-	AC/DC converter
06	NATURAL VENTILATION	roof sliding window	West - roof	24 (DC)	3	72	14,60	LC-04
07		tilt window	East - gable	24 (DC)	2,25	54	0,70	LC-04
08		ventilation flap	East - socket	24 (DC)	1,67	40	-	LC-04
09	MECHANICAL VENTILATION	radial fan	West - roof	24 (DC)	1,67	40	-	LC-04
10	INTERNAL SUN SHADING	roller carvas blind	South - internal	12 (DC)	1,15 - 5,9	72	1,62	LC-02
11			West - internal	12 (DC)	1,15 - 5,9	72	1,62	LC-02
12	ARTIFICIAL LIGHTNING	LED bars	South + West ridge	12 (DC)	1,60	19,2	1,55	LC-01
13			South - flank	12 (DC)	3,62	43,4	2,90	LC-04
14			Grout	12 (DC)	4,40	52,8	4,53	LC-01
15			West - flank	12 (DC)	3,68	44,2	2,90	LC-04

FIGURE 5.8 Table with function related consumers, performance and load controller assignment

The fact, that the maximum power supply of 14 kW was limited to 2.7 kW by load controllers and further was limited to 1.44 kW by DC/DC converters, required a load management. The load management grouped oppositional consumers/functions, which eliminated the risk of maximum duty. Thus, the sliding window and ohmic floor heating as well as internal roller blinds and artificial lighting were grouped together. But then, similar consumers were disseminated on diverse controllers to disperse loads.

### § 5.2.6.1 Cooling system: AC split cooling (optional)

---

The question, whether power consuming active space cooling could also be provided by PV power, was also considered and met by the installation of a 3.5 kW AC converter split unit. The unit allowed to be run on three different power levels with a maximum cooling power of 3.5 kW. Therefore a 1,500 W DC/AC converter was integrated; thus, the maximum cooling capacity was limited to 1.5 kW. The split cooling unit was located in front of the north wall in the sun space west flank. The outlet of the forced-air cooling was positioned at a height of 1.30 m above the floor to accomplish an effective ambient air intermixture.

### § 5.2.7 Control parameters

---

Since the considerable high heating and cooling load with respect to limited battery capacity was not applicable, heating by panel heating mats and split unit cooling was reduced to manual and intended activation. Since overnight control and overnight malfunction could have led to tremendous depth of discharge far below the limit of 50% remaining charge, heating mats were activated manually on site for a limited time.

In contrast, natural and mechanical ventilation as well as internal sun shading and artificial lighting were controlled by logics. Accordingly, the sliding window, tilt window and ventilation flap opened at an operational temperature above 23°C and simultaneously an external temperature of 8 Kelvin lower than indoors, provided that heating and cooling devices were off and it did not rain. The radial fan started on maximum power level 10, independently of the windows for natural ventilation when ambient air temperature exceeded 28°C.

---

## § 5.3 Performance evaluations

---

After a holistic description of the test set-up, an inspection of the performance follows. The inspection includes the measured monthly yields of the BIPV plant, the battery charging, energy consumption and load management, energy efficiency, and effect on thermal comfort.

An evaluation of these parameters simultaneously will show how effective such a system incorporated in sun spaces performs, beside monetary aspects.

### § 5.3.1 Monthly evaluation of power yield: PV performance

As described, the 23 PV generators have been grouped in order to comply with maximum input voltage limits of the charge controller, and to minimize performance losses due to single shaded modules within a string. Figure 5.9 illustrates the cumulated yields of each string between the measurement periods of December 2012 to April 2013 and May 2013 to November 2013. Thus, we can see, that the mono-crystalline modules at the ridge of the south roof and west roof produced by far the highest amount of energy, respectively power.

SURVEY OF BIPV POWER YIELD RELATED TO STRING/FIELD AND SEASON 2012/13									
BIPV - FIELDS / FEATURES	PV-Field: Grout South	PV-Field: Grout West	PV-Field: Gable East	PV-Field: Gable North	PV-Field: Ridge South	PV-Field: Ridge West	PV-Field: Edge South	PV-Field: Edge West	PV-Field: Atbc South
ANNUAL BRUTTO SINGLE YIELD [kWh]	112 kWh	77 kWh	30 kWh	9 kWh	394 kWh	266 kWh	40 kWh	20 kWh	3 kWh
ANNUAL BRUTTO TOTAL YIELD [kWh]	951 kWh								
FRACTION ON TOTAL YIELD [%] Dec.12-April13:	16,5%	8,1%	2,8%	0,4%	38,0%	17,3%	14,6%	2,0%	0,2%
FRACTION ON TOTAL YIELD [%] May.13-Nov.13:	11,0%	8,0%	3,2%	1,0%	42,0%	29,7%	2,6%	2,2%	0,3%
WAFER TECHNOLOGY	a-Si Thin Film glass-glass	Mono-Crystallin glass-glass	Mono-Crystallin glass-glass	a-Si Thin Film glass-glass	a-Si Thin Film glass-glass	a-Si Thin Film			
total effective aperture area [m²]	2,88	2,27	2,63	2,77	2,73	1,39	1,89	1,89	0,14
total minimum power accor. flasher protocol [P <sub>1</sub> ] [W]	183	186	166	210	451	193	114	117	9

FIGURE 5.9 Total annual yield separated by power strings and season

The south ridge string produced 394 kWh in total and the west string produced 266 kWh within this one year period. The mono-crystalline strings are followed by the amorphous cell technology that was implemented into the south roof close to the grout with 112 kWh oriented south and 77 kWh oriented west. Single field strings in the vertical south façade produced 40 kWh and the opposing west oriented field generated 20 kWh. In contrast, east and north oriented PV generator strings provided a total of 30 and 9 kWh. In total, the entire PV plant provided 951 kWh within months.

Thus, we can see, that mono-crystalline façade integrated PV generators oriented south or west generated more than 70% of the cumulated annual power yield. In terestingly, according to the table the amorphous cell technology generated approximately the same amounts of power, regardless of the season. The relative share of power generation in winter from December to April does not differ considerably from the share during the summer and autumn months May to November. A significant dif-ference is obvious for the envelope embedded mono-crystalline cell technology between winter and summer and autumn of 12.4%. Moreover, the south directed vertical façade integrated a-Si module generated in the shorter winter period 5 times more power than in the summer and autumn months. That can be interpreted by a lower solar angle and thus less reflection of irradiation during winter, and additionally by reflections during winter by the high-albedo snow covered ground.

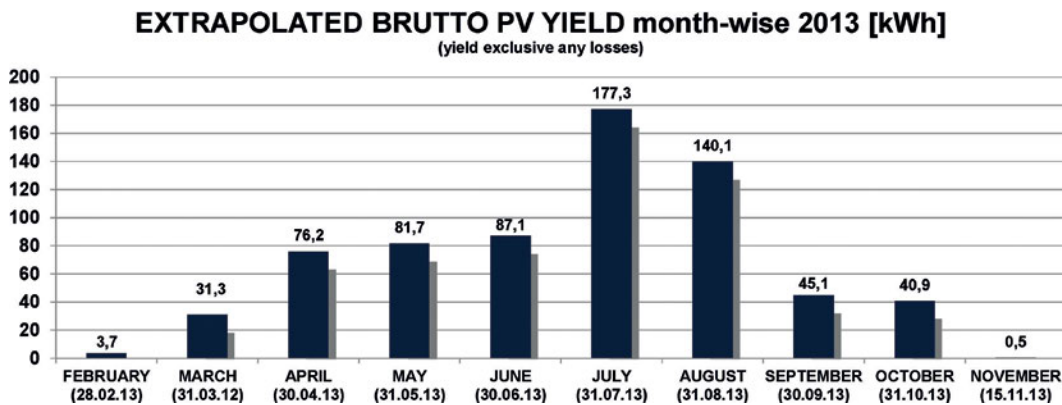


FIGURE 5.10 Monthly extrapolated gross BIPV yield [kWh] 2013

However, related to the relative high amount of amorphous PV modules in the north and east facing facades, the annual yield is not worth mentioning. Thus, it can be concluded, that amorphous cell modules are not sensible for such orientations and are recommended to be excluded. The PV yield has been extrapolated diminishing any system fall outs and was plotted in Figure 5.10 between February and November 2013.

The major share of the PV yield was recorded in July and August (Fig. 5.10). That, actually opposing calculations in literature and common sense, seems extraordinary, since May or June are typically the months with the highest PV yield. Indeed, 46.3% of the plotted cumulated yield were generated in July and August 2013.

This, with respect to an efficient power storage in seasonal terms, is beneficial, since the later the major share of PV power is generated, the later it is stored and the longer power will be available in autumn months.

Interestingly, the levels of monthly yields in the early summer months April, May and June are roughly equal at 80 kWh per month, likewise in September and October, where the yields were similar with about 40 to 45 kWh. Finally, Figure 129 demonstrates that PV yield is not worth mentioning between November and February.

### § 5.3.2 Monthly energy consumption, load profiles and battery charge status

Before we discuss the monthly mean battery charge status, we will have a look at the recorded monthly energy consumption and load profiles between February and November. Figure 5.11 exemplifies that energy consumption was the highest in July and August, synchronic to the before reported highest PV yields. Similar to the PV yield analysis, the energy consumption between April and June was nearly constant with a slight increase towards mid-summer, however lower but constant in the autumn months September and October.

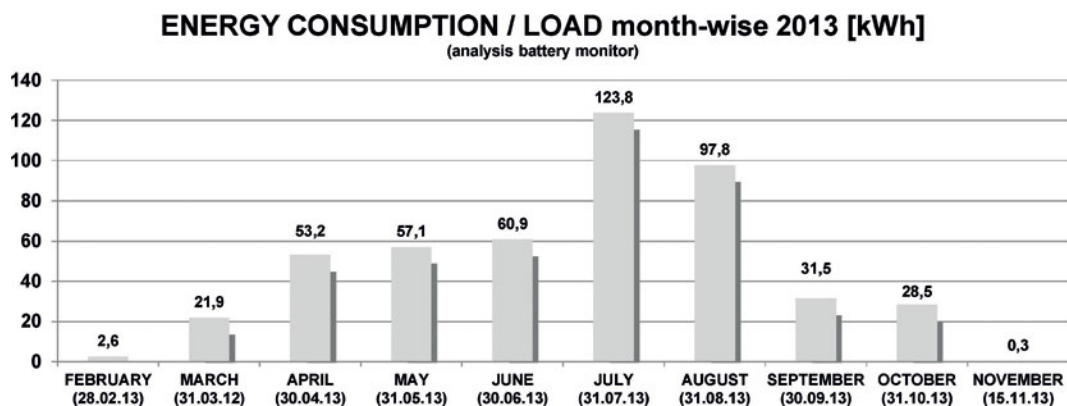


FIGURE 5.11 Monthly energy consumption / loads 2013

Comparing Figures 5.11 and 5.12, we can see, that PV yields persistently were 13 to 20 kWh higher than the monthly consumption. Furthermore, in particular during July and August the surplus of generated PV power was up to 40 kWh higher than consumption.

Figure 5.12 plots the mean monthly battery charge status between February and November 2013. Although the plot shows firstly weak monthly PV yields and secondly proportionally high energy consumption for heating, it is obvious that the mean battery charge status was the highest in April, March and May. This fact calls for attention, since we recognized before in Figure 181 that the PV yield was most sufficient rather in July and August than from March to May. This is the result of less heating effort in April to May than compared to February, when the heating energy demand was high and the PV yield was disproportional low.

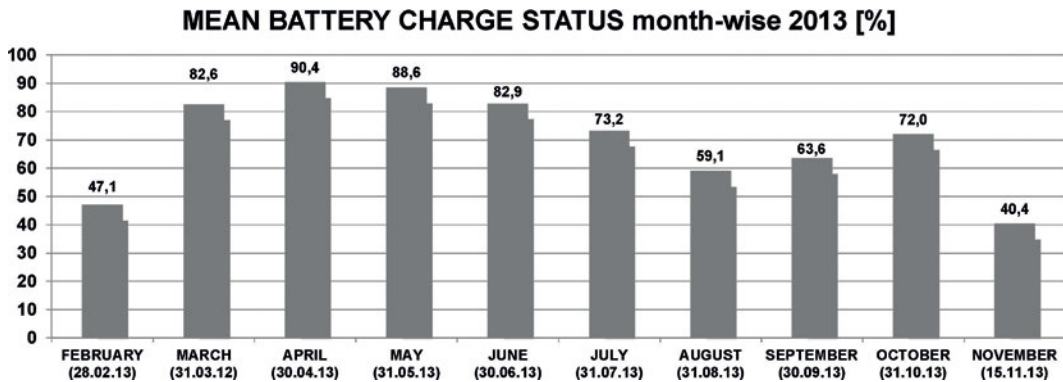


FIGURE 5.12 Monthly mean battery charge status [%] 2013

Thus, Figure 5.12 shows for February a mean charge status below the limit of depth of discharge, namely 50%. On the contrary, the mean battery status in July, August and September lowered from 73 to 59% since the active cooling by the split unit has been activated frequently and heating demand increased in September and October. Proportionally to the limited PV yields in September and October of about 40 kWh, the potential capacity supply decreased, thus energy consumption for heating and sun protection decreased by approximately 30 kWh per month. Since the sun space profited from passive solar gains and overheating turned to be secondary, adapting to preferred operational temperatures turned into less space conditioning effort. For that reason, the mean battery charge status increased by 12% compared to August. Finally, in November, due to not worth mentioning PV yields of 0.5 kWh, the battery capacity

was exploited and resulted in a mean charge status of 40.4%. Since the energy demand in November was insignificant low, potential energy consumption that led to the described low battery status is to be allocated to October.

### § 5.3.3 Battery charge performance

While previously the battery charge status was analysed in relation to PV charging and discharging by consuming space conditioning devices, this section concentrates on the long-term, respectively seasonal, storage performance. An analysis of the seasonal storage performance requires consideration of the components intermediately adjoined to the battery as well. Because charge efficiency and utilization efficiency load controllers as well as consumers also determine the utilization efficiency of gained PV power in the long run.

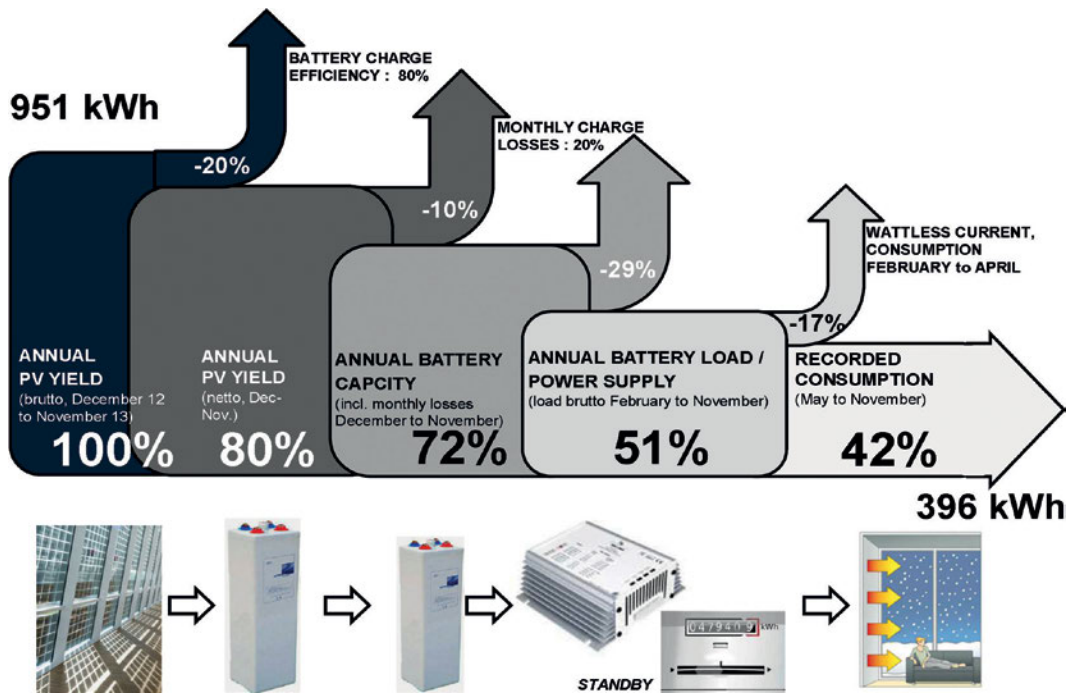


FIGURE 5.13 Relative progress of charge and load profiles, watt-less losses

Thus, Figure 5.13 illustrates the main different steps of power generation, power charging, power storing, power recalling and finally power consuming. Figure 5.13 highlights the specific component efficiencies and thus resulting energy losses within the system in terms of heat generation and losses to the environment. Originally, the gross amount of power generated by the PV strings was determined to be about 951 kWh from December 2012 to November 2013. Even though the PV charge controller profited from the MPPT tracking algorithm, the effective power actually stored by the lead-acid battery rack was 20% less than the energy once generated. Thus, the first losses in the system are related to the lead-acid battery technology and determined at 20%. That, as Figure 185 explains, resulted in a net remaining stored energy amount of 761 kWh.

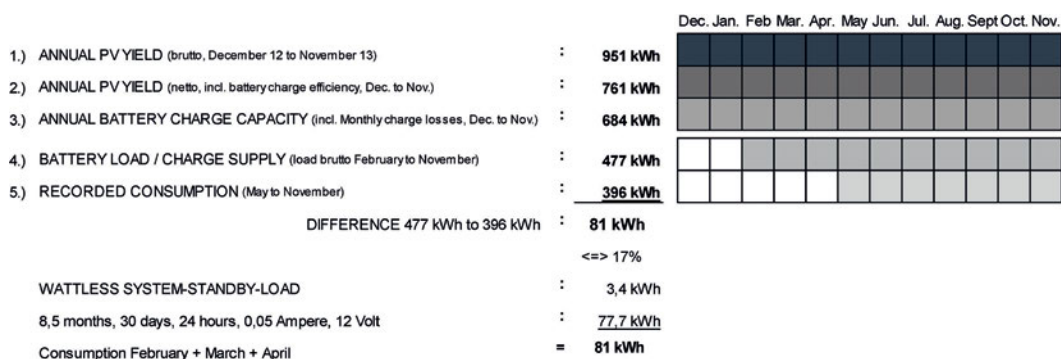


FIGURE 5.14 Absolute progress of charge and load profiles, watt-less losses

Since lead-acid batteries commonly suffer from 10 to 20% of monthly losses due to temperature and humidity changes in the battery environment, the effective utilizable amount of power is reduced by a total of approximately 80 kWh to 684 kWh. To that point, the gross generated amount of energy supplied by the building integrated photovoltaic is reduced to remaining 72%.

Furthermore, while consuming energy, the load controller, DC/DC converters as well as the devices themselves caused watt-less losses and system-standby-losses during the consumption period of February to November 2013. This amount has been calculated to be about 81 kWh, which equals 17% an effective net usable energy amount of 684 kWh. The consideration of system related losses resulted in an effectively utilized amount of power of 396 kWh for space conditioning between May and November (Between point 3.) and 4.) of Figure 5.14 exists a difference of 207 kWh between 684

kWh and 477 kWh. This difference is allocated to consumed energy by eaves gutter heater. These eaves gutter heater had a total heating power of 1,100 W. They have not been part of the interior space comfort evaluation, but were repeatedly tested during year under real conditions. Nonetheless, ultimately nearly 400 kWh of the originally generated (961-207=754 kWh) were free for consuming, which equals a utilization factor of 53%. That shows that beside a predominantly low area PV generator efficiency, a lead-acid battery system suffers from significant system losses throughout the year, which considerably lowers the effective amount of power for space conditioning.

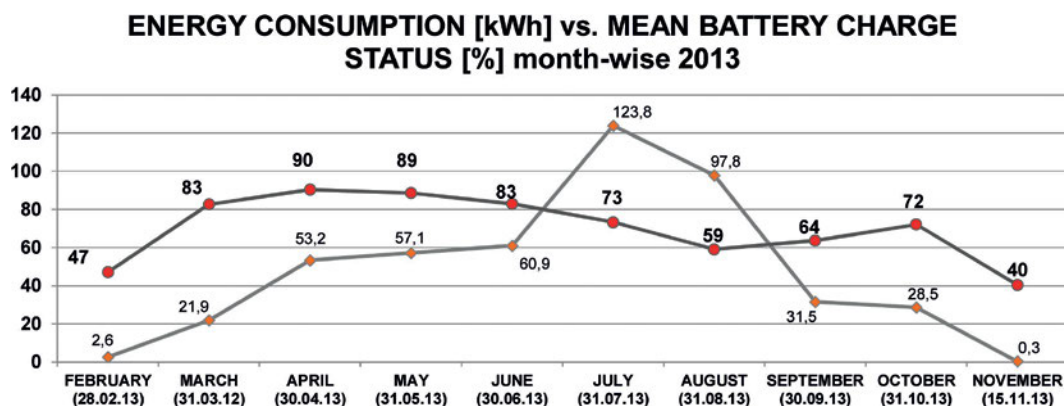


FIGURE 5.15 Monthly energy consumption [kWh] vs. mean battery charge status [%] 2013

Figure 5.15 plots the monthly energy consumption against the monthly mean battery charge status. It becomes obvious that due to high solar yield in July and August the potentially possible consumption can be comparably high, whereas in autumn months like September, October and November potential consumption for cooling or heating are considerable limited due to the restricted battery performance.

This graph also indicates that a comparably large battery of 13.5 kWh nominal capacity is not an eligible seasonal storage medium for extensive space conditioning, especially heating, during autumn and winter months.

### § 5.3.4 Limits of heating power: effect

Figures 5.16 and 5.17 show representative days in October, when wall heating was activated. An activated east wall heating provided 360W heating energy, similarly the north wall 540W heating energy. Figure 5.16 impressively illustrates the surface temperature increase from 16°C to 32°C within five hours. The graph also demonstrates that the wall surface temperature significantly rose within 20 min, followed by a period of four hours with moderate but constant increase.

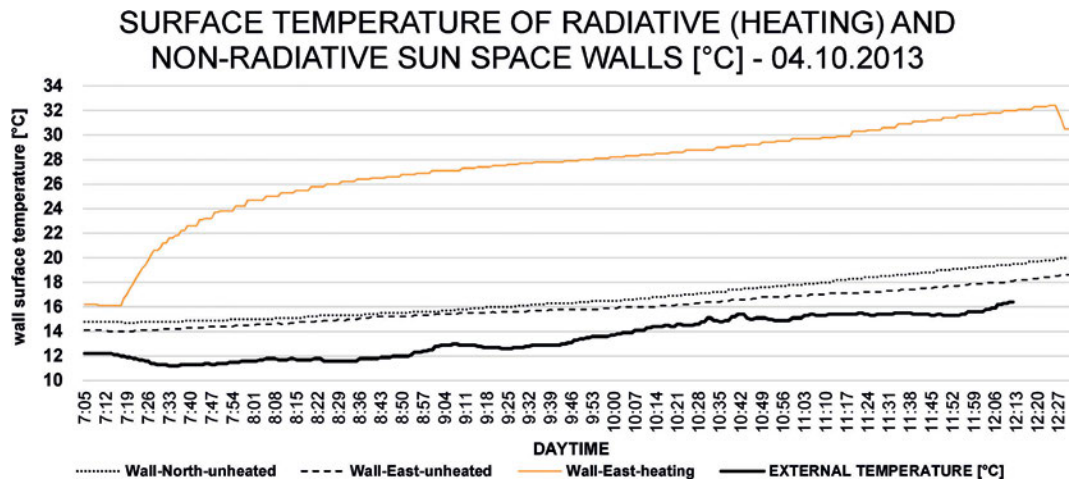


FIGURE 5.16 Surface temperature increase and space heating effect of wall-east panel heating mats

The increase rose parallel to the surface temperature ascend of the unheated parts of the eastern wall and the unheated northern wall. A maximum temperature difference to external temperature was 16 Kelvin. Within this observed period also the external temperature rose from 11 to 16.2 °C. The maximum temperature difference between the heated east wall and the unheated east or north wall is less than 25 Kelvin, the according PD value (percent of dissatisfied) of 5% is not exceeded and thus, category II is still complied with. In case of activated wall heating on October 14th, the surface temperature of the north and east walls reached a maximum of 20°C, whereas unheated parts of these walls remained at 11°C surface temperature.

A maximum temperature difference of 9 Kelvin also correlates to less than 5% PD, wherefore in terms of local discomfort category II is accomplished.

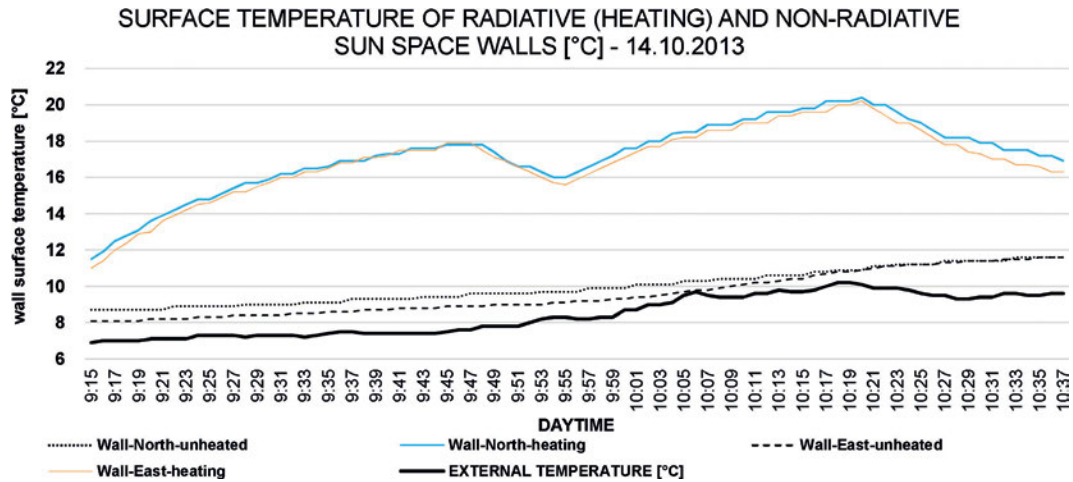


FIGURE 5.17 Surface temperature increase and space heating effect of east wall and north wall panel heating mats

In summary it can be stated that surface heating and thus active space heating in the autumn months was possible exclusively with renewable power generated by the building integrated photovoltaic. Storing and recalling was possible to the end of October at the latest. However, the frequency of activation was strictly limited to only a couple of days from late summer to end of autumn.

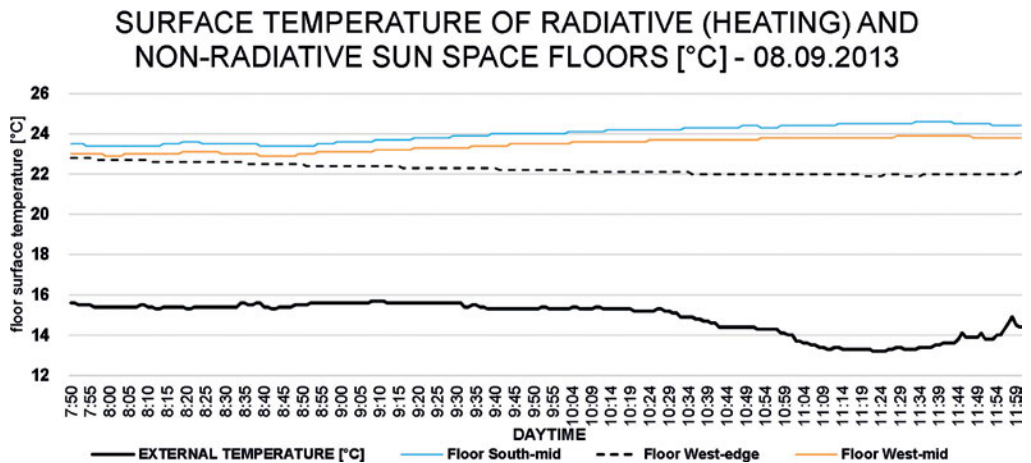


FIGURE 5.18 Surface temperature increase and space heating effect of floor-south and floor-west panel heating mats

Also, the number of hours were limited related to mismatch of provided battery capacity and the enormous amount of required heating energy. Heating from November to March was not feasible. And the potential maximum surface temperature of heated building elements was limited with respect to the limited output power of load controller and DC/DC converter. According to the inevitable large charging cycles, as a rule of thumb active cooling and active heating was possible every two to three weeks twice every 5 hours from March to mid-October.

### § 5.3.5 Limits of cooling power: effect

The test sun space was equipped with an active AC-cooling split unit. The maximum nominal cooling power of 3.5 kW was limited by the limited AC output of the DC/AC-converter to 1.5 kW. Besides that the AC-cooling split unit modulated continuously three power levels with a frequency-regulated converter, the maximum cooling power was 1,500 Watt. Figure 5.19 shows an observation of the interior dry bulb temperature aside the entirely closed sun space façade for July, 2nd 2013. Split unit cooling was activated at ca. 9:30 AM.

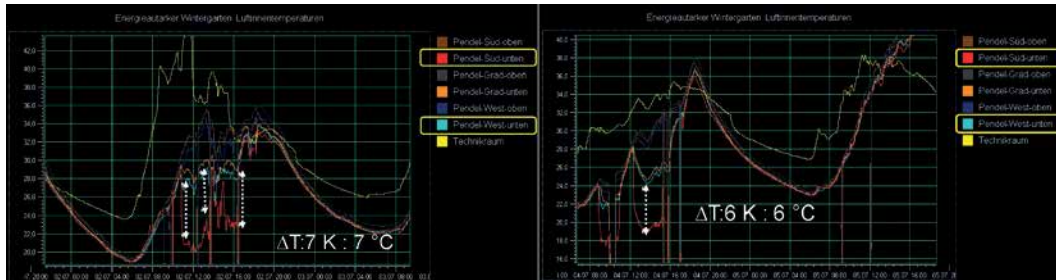


FIGURE 5.19 Observation of interior dry bulb temperature lowering by active split cooling, decreased by 6 to 7 Kelvin

The effect of the 1.5 kW cooling is visible by the direct comparison of the affected dry bulb temperature measured by the sensor “Pendel-Süd-unten” in the south flank and the sensor “Pendel-West-unten” in the west flank. Within a few minutes the dry bulb temperature in the south flank decreased from 28 °C to 21 °C, which equals a temperature difference of 7 Kelvin. A difference of 6 to 7 Kelvin was achievable, despite continuous mean irradiation of 404 W/m<sup>2</sup> with a maximum of 723 W/m<sup>2</sup> irradiation

as well as mean 23,1 °C and a maximum 27.1 °C external temperature between 9:30 to 16:30 o’clock and increasing dry bulb temperature in the west flank. That was repeated two days later, on July, 4th at 2 PM and resulted in a cooling of the dry bulb temperature from 24.4 to 18.3 °C. A difference of 6 Kelvin was attainable, while mean irradiation of 241 W/m<sup>2</sup> ascended to a maximum of 515 W/m<sup>2</sup> and resulted in a mean external temperature of 23.4 °C with a maximum of 26.8 °C.

## § 5.4 Summary

The empirical test set-up exemplified that the incorporation of building skin integrated photovoltaic in terms of construction regardless of technology is feasible without any worth mentioning constraints or confinements. Furthermore, amorphous cell technology caused immense effort in time and planning to be provided by appropriate battery charge controller, which managed the related high module voltage. Moreover, the evaluation shows that 70% of the annual yield was generated by mono-crystalline cell technology, that was underrepresented considering the entire area.

Thus, we can conclude that amorphous cell technology from the perspective of a system configuration effort and effective yield contribution is reasonable for application in sun space envelopes with regard to significant high energy amount for space conditioning.

Finally, the annually required amount of energy for space heating from 5 to 10 PM between October to April of 1,600 kWh was not yielded. Nearly 60% of the demand was generated. Moreover, the system itself, concerning the battery and load controller system suffered from significant high monthly, respectively system related losses. Half of the gross amount of power generated by BIPV was applicable for space conditioning.

Decisive in this context is the overall charge efficiency of the lead-acid battery of solely 80%, which predominantly diminished considerable amounts of laboriously generated power by BIPV. In general, we can conclude that the sun space suffered from a tremendous energy demand and collector-integration envelope area mismatch. In particular, PV power proved to be inefficient when compared to solar thermal power.

Although the battery encounters considerable losses in capacity in autumn months, the test set-up demonstrated that the energy can be utilized in late autumn to power wall and floor incorporated heating devices.

Notwithstanding, the power and thus performance was limited by the system configured performance, surface temperature clearly increased whereas external temperature was low. However, energy amount and power was dissatisfactory. On the contrary, in summer months, active cooling was eligible to decrease indoor air temperature by 7 Kelvin. Resulting indoor air turbulences and cooled air resulted in satisfactory ambient air temperature. As a rule of thumb, from spring to autumn active cooling and active heating was feasible every two to three weeks twice for 5 hours.

As reasons were identified three major aspects of the system: first, the extremely low power of the split envelope - in terms of orientation - incorporated PV plant, secondly, the unsatisfactory battery capacity with respect to the demand, and thirdly, the un-economic and restricted output power of the load controller, DC/DC converter and the DC/AC converter as well.





# 6 Description and evaluation of the product development “HEATBEAM®”

---

## § 6.1 HEATBEAM - A collector becomes constructional component of a sun space rafter

---

### Intention / Prologue

---

The quality and quantity of indoor thermal comfort in sun spaces is in question and has been evaluated in Chapter 02. Empirical measurements and evaluations showed that beside the quality of thermal comfort in terms of local discomfort concerning building physical improvement of buildings elements, quantitative comfort in terms of cumulative hours are to improve as well.

Thus, this thesis also inspects technical possibilities to gain additional heating energy via façade components beside solar gains. As elaborated in Chapter 03, manifold solutions of façade integrated collector technologies are developed. With respect to generating heat, solar thermal technologies are more in favour than power generators. This chapter describes the product development of a sun space envelope integrated collector technology and an experimental test set-up, and analyses empirical data. Empirical research in this context includes measurements of the monthly yield of the development, respectively efficiency, feeding temperature in respect of feasibility to charge seasonal sorption storages and transmission losses, namely surface temperature facing the interior sun space volume in order to analyse and detect undesired negative impact on indoor thermal comfort.

Latest research in the field of science of building skin and solar thermal collector offers manifold reasons and arguments for the development and investigation in façade integrated solar thermal collectors. While Corradini (2013) [190] inspects and verifies the potential of retroactive equipping single-unit residential buildings with solar thermal collectors (Fig. 6.1), he makes us aware of the considerable amount of final energy consumption and its share of the total final energy demand in the building sector of such small types of buildings, but he also illustrates the enormous effect of a comparably simple technology on fossil fuel substitution.

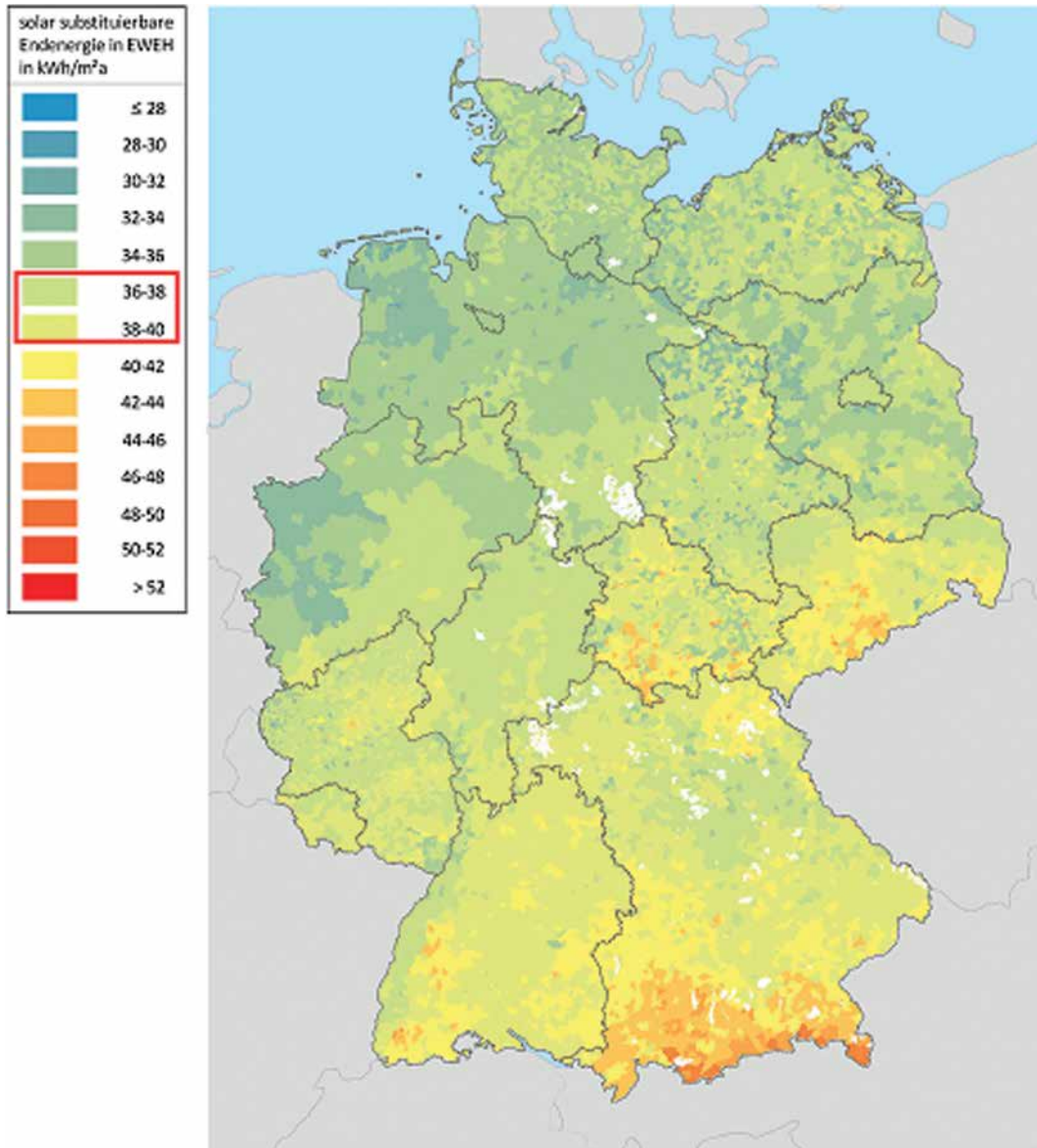


FIGURE 6.1 Potential of fossil fuel substitution by solar thermal plants related to county in kWh/m<sup>2</sup> and year: scenario "norm", (related to effective living area [m<sup>2</sup>])

Indeed, as exemplified in Chapter 03, Weiss, Fink, Haslinger, Strasser and Wörgetter (2014) [191] explicate as members of the Austrian Federal Ministry for Traffic, Innovation and Technology that building envelope integrated solar thermal collector technology combined with sorption storage technology occupies research and

technology justification in Austria until 2025. Alongside manifold research and development projects (see Chapter 03), which achieve different depths of façade integration and multi-functionality, designs for the Solar Decathlon in Europe in particular inform about feasible dimensions, practicability and efficiency by monitoring.

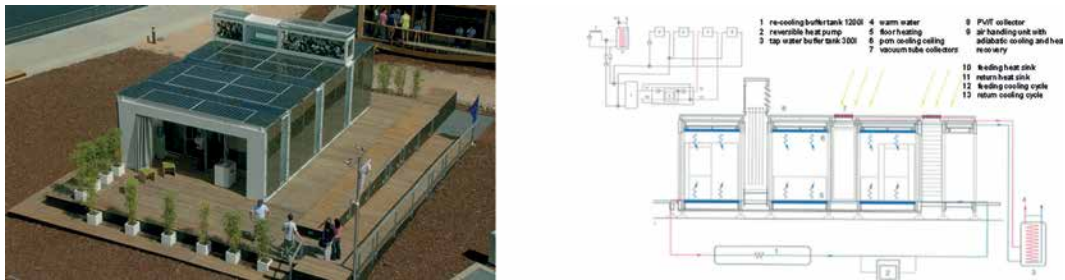


FIGURE 6.2 Contribution of University of Techniques Stuttgart to Solar Decathlon , Spain, 2010

For example, the contributions of University of Technology in Stuttgart [192] (Fig. 6.2) as well The Ekihouse [193] (Fig. 6.3) demonstrate the imperative of façade planning if such components shall play an appreciable role in the entire building management system.

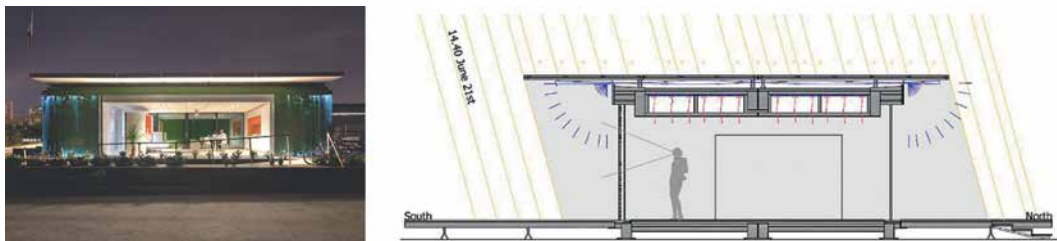


FIGURE 6.3 Basque contribution : Ekihouse to Solar Decathlon , Spain, 2012

Moreover, the author recently illustrated the need for integral façade design with respect to zero-energy-houses 2020 and the relation between decentralized multi-functional design [106] and resulting benefits for ground floor design [194]. Façade

quality is no longer a question of the quality of each of its separate components, but of integral capabilities. Nonetheless, the inspected designs still lack multi-functionality that increases their quality beyond the key faculty of energy generation. Thus, in this chapter will be exemplified the design of a sun space rafter integrated solar thermal collector, that – beside collecting – manages making glazing bars obsolete and hence becomes constructional.

### § 6.1.1 Requirements for an efficient operation in order to verify Hypothesis II

---

The main purpose of an envelope integrated solar thermal collector is to generate energy, which is directly utilized in the building in order to substitute fossil fuels. Considerations are justified as to whether an envelope integrated collector contributes considerable amounts of heating energy and either makes the space maintenance greener or enhances indoor thermal comfort. Enhancement of thermal comfort can either mean reduction of local thermal discomfort or an increase in hours with at least acceptable operational temperature. However, beside this, the main challenge an efficient collector design has to face are diverse constructional requirements. If these constructional requirements are not met, the most powerful collector forfeits efficiency.

A hypothesis is formulated with regards to a less technical but means-end definition of operation efficiency. Hypothesis II below ministers as methodological bridge and defines the scope of research of this Chapter 06.

#### Hypothesis II

---

*Cumulated frequencies of hours of resultant temperature > 20°C between 5 to 10 PM in order to determine indoor thermal comfort in SL80 Solarlux sun space according to DIN EN 15251-A regarding south direction and 25 m<sup>2</sup> sun space dimensions in 15 different climate regions in Germany provided with renewable heating energy by solar gains and additionally by facade integrated technologies are annually closer to but not actually 1.060 hours during autumn to spring time (Oct.-April).*

Thus, the aim of the evaluation is to define the number of annual hours, which represent adequate internal operative temperatures in addition to hours provided by passive solar gains that are contributed by a floor heating directly supplied by façade

integrated collectors. More precisely, the effect is weighted by the maximum possible number of hours from October to April between 5 to 10 PM each a day, namely 1060 hours.

The scope of research is defined by independent variables like space size (15, 25, 35 m<sup>2</sup>), space orientation (south-east, south, south-west) and 15 climate regions in Germany. The aim of an investigation within this scope is the verification of basic properties as fundamental design basis for an expansive numerical study.

## § 6.1.2 Decisive performance features based on literature review

---

An efficient façade integrated solar thermal collector is determined by several individual technical properties, which distinguishes the solar thermal collector from others. These individual technical properties are defined explicitly in this section, and they merge into standardized performance coefficients. Although the performance features and coefficients have been elaborately exemplified in Chapter 03 by literature review, crucial aspects for a sun space rafter design are highlighted in this section again.

Although unglazed collector technology exists, generally the efficiency of glazed collectors in terms of annual yield and feeding temperature is higher. In order to maximize the amount of irradiation passing through the glazing and affecting the absorber area, cover glazing profits from low thickness for minimal losses through optical fraction and absorption, as well as from anti-reflection coating or from prismatic surface treatment. As Föste, Ehrmann, Giovannetti, Reineke-Koch, Uslu, Krämer and Hesse (2013) [77] evaluated, tempering of cover glazing enhances solar transmission.

High radiation conversion into heat requires a high absorption factor  $\alpha$  [%], a low emission factor  $\epsilon$  [%] and a high internal conduction factor  $U_{\text{int}}$  [W/m<sup>2</sup>K] of the absorber itself. Best selective coatings provide a  $\alpha/\epsilon$ -ratio of (96/5)  $\approx$  19. Also the fixing of the absorber to the heat exchanger or heat pipe provides advantages and disadvantages in terms of conductance, balanced heat distribution and shape retention of the absorber sheet, as Giovannetti, Kirchner, Franke, Rohde and Scherer [78] investigated in 2014. In addition to ultra-sound welding, laser-welding and soldering, practical solutions are gluing and positive locking by applying heat-conductive paste.

If the heat exchanger is not intended to be drained-back during winter month and thus forms a closed 365-day operating first working cycle, the transport medium needs to be protected against freezing.

Adding an anti-freezing agent for a 70 to 30% water-glycol mixture, the specific heat capacity lowers from 4.2 kJ/kg to 3.65 kJ/kg. Likewise, in the context of a heat pipe, if the working fluid is based on water also a little amount of anti-freezing agent is added, whereas if organic or alcoholic working fluids are used freezing is usually not an issue.

The collector case in combination with cover glazing is at least to be sealed against rain, water, acids and precipitation in general to prevent heat losses by conductance and convection. Furthermore, the high-selective coating is to be protected against atmospheric influences to eliminate degrading efficiency. In contrast, Föste, Ehrmann, Giovannetti, Reinike-Koch, Uslu, Krämer and Hesse (2013) as well as other manufacturers consciously provide air exchange ports in the collector case, which, on the one hand demonstrably enforces convective losses and thus renders vacuum insulation impossible and degradation of selective coating. However, on the other hand water vapor and solvent evaporation of physical thermal insulation within the case are in equilibrium with the atmosphere and thus cause no light transmission reduction by condensation on the cover glazing backside.

Finally, the absorbing and heat conversion space, namely the casing, requires thermal insulation in order to at least minimize or even distinguish heat losses by transmission. Thermal insulation can either be achieved with physical thermal insulation material like mineral wool or polyurethane or expanded polystyrene on the backside and flank sides. Although physical thermal insulation is the easiest concept to insulate, it exhibits drawbacks and restrictions. Thus, key properties of physical insulation material in solar thermal collectors eligible to charge sorption storages or to gain high amounts of exergy, are thermal heat resistance up to 260°C and deformation resistance. Moreover, Zauner, Lager and Hohenauer [195] (2010) detected temperature influenced solvent and binder evaporation of mineral wool and organic insulation material, which deposits on the backside of the cover glazing. If the case by design provides no space or only little space for physical thermal insulation, which makes physical insulation obsolete, a space evacuation to a remaining pressure of 10 to 100 mbar presents an alternative solution.

While evacuation is a smart and effective alternative of thermal insulation, it requires high quality pressure proved sealants and non-air permeable materials. Since perpetuation of efficient under pressure (vacuum) is extremely complicated from a constructional perspective, a valve for frequent re-evacuation within the case envelope and sufficient space for easy maintenance are mandatory.

Main design parameters like conversion factor  $\eta_0$ , the collector efficiency ratio  $\eta_{60}$  in relation to a temperature difference of 60 K of operational and external temperature, the transmission coefficient  $a_1$  [W/m<sup>2</sup>K] and  $a_2$  [W/m<sup>2</sup>K<sup>2</sup>] as well as stagnation temperature [°C] are crucial for a proper design.

### § 6.1.3 Constraints regarding façade integration and distribution and assembly

---

Since a rafter integrated collector is a part of the building element – even if only generating energy – integration and distribution of the transport fluid and assembly, either preassembled or at the latest on site, need to be considered and planned.

With respect to façade integration, especially fixation allowing thermal expansion and sealing are the main crucial points. A collector normally tends to raise [UE1] with rising temperatures. Inevitably, this leads to thermal elongation of several temperature affected components. Thus, a design must consider the maximum possible thermal elongation related to a reference length. However, in the context of customized sun spaces, roof length and hence rafter length depends on space depths and roof inclination. Thus, a rafter integrated collector can vary from 2.5 to 4.5 m in length. In consequence, possible thermal elongation needs to be managed by the construction itself.

Since a collector is an add-on or even incorporated component in a constructional element, the construction itself has to be protected from humidity and precipitation. Presumably, thermal elongation exacerbates proper sealing additionally.

In the context of distribution, piping and conjunctions for the transport fluid require to be guided throughout the entire roof construction. Therefore necessary effective inner pipe diameter and bending radius are required to be complied with in order to maintain minimum fluid flow rates and flow itself. Moreover, similarly to the prerequisites of integration in case of distribution are to maintain thermal elongation and thermal insulation. The latter is most important in order to prevent the construction from thermal impact by the heated or cooled transport fluid itself in order to avoid mechanical stress and condensation or dissolving of organic compounds. What is more, sufficient thermal insulation of the distribution piping is essential in terms of yield conservation and system efficiency.

Finally, the assembly of an entire customized roof construction requires standardized and planned joining points.

Distribution piping needs to be easily inserted into roofing profiles and further adjoining transmission building elements like a ridge, eaves or hollow layers of fair face masonry. Jointing points require a faultless, accurate and true to size standardization of couplings, bows, diversions or block valves.

In this context, the design quality benefits from prefabrication of the most standard and difficult elements in order to minimize distribution and jointing efforts on site. Since distribution piping of liquid transportation fluid is mainly based on metallic and non-metallic materials or alloys like alumina, copper and brass, joints require soldering or welding. Thus, processing steps during assembly include the presence of enormous heat or even fire. While normally "roof makers" belong to carpenters by trade or metal worker, the production of soldered or welded joints bears risks on site. For that reason, it is essential to think about joints and sealants, which are technically based on positive locking or a mechanical pinch. Normally, these connections require few working steps or profit from being industrialized.

The requirements mentioned above define the constructional constraints regarding integration, distribution and assembly.

### § 6.1.3.1 Constraints regarding impact on thermal comfort

---

Parallel to intentions of maximized annual yield and appropriate high feeding temperature, a collector as part of the construction bears the risk of having considerable influence on indoor thermal comfort simply by transmission losses.

The higher the feeding temperature and the longer the period of high operational temperature below a stagnation temperature, the more intensive and durable radiative losses can be. Beside the intensity and constancy of undesired radiative impact, the geometry of radiation directly determines local thermal discomfort in such a limited space volume as a sun space.

Since, in contrast to building integrated photovoltaic modules the collectors are arranged not area-wise, but axially and grid-oriented, disproportional high radiation appears not as an disturbing area, but rather punctually. Consequently, such a grid-wise and punctual radiation asymmetry is above all more difficult to localize and hence more difficult to adapt to than a singular hot spot.

According to the human kind of perception this discomfort pattern might cause significant uneasiness and insecurity.

Moreover, since DIN EN ISO 7730, Tab. A.4 limits local discomfort resulting from “warm ceilings” to solely 5 Kelvin difference towards facing surfaces in order to comply with category II requirements, the maximum possible surface temperature is demonstrably restricted. Furthermore, an inadvertent heat source located in the roof space may foster striation and a hot spot. It is therefore important to design the collector in a way that thermal losses to the environment are minimized. However, since the collector is integrated into a sun space rafter, space for physical thermal insulation is more than limited, but mandatory to incorporate.

The before mentioned aspects define serious constraints with regard to the design from a thermal comfort perspective.

---

## § 6.2 Concept/construction of a rafter integrated solar thermal collector HEATBEAM®

---

This section describes two designs of sun space rafter integrated solar thermal collectors. The first design (Heatbeam I®) is based on a aluminium case and was empirically evaluated at a test-site under real conditions for a year. The second design (Heatbeam II®) is based principally on the first, but was further developed for a completely transparent polymeric design. The rafter integrated evacuated tube collectors HEATBEAM I® and HEATBEAM II® were developed by Solarlux.

Applicability, efficiency and lessons learned were elaborated with the first design. The second design is object for the numerical simulation and analysis in Chapter 08.

### § 6.2.1 Physical and technical description HEATBEAM I

---

Since the roof glazing area of a sun space in terms of desired transparency is not predestined for embedding opaque solar thermal collectors, the idea is an integration into rafters. Since a rafter is an axial oriented building element and offers limited space for absorption area and heat exchanger, an area-wide collector typology is required.

Rather, we noticed that exchange and maintenance without any considerable effort as well as an undisturbed transport cycle are crucial requirements for an applicable

design. Therefore, the author decided to focus on heat pipe technology that works like hermetically closed heat tubes on the principle of a non-mechanical heat pump.

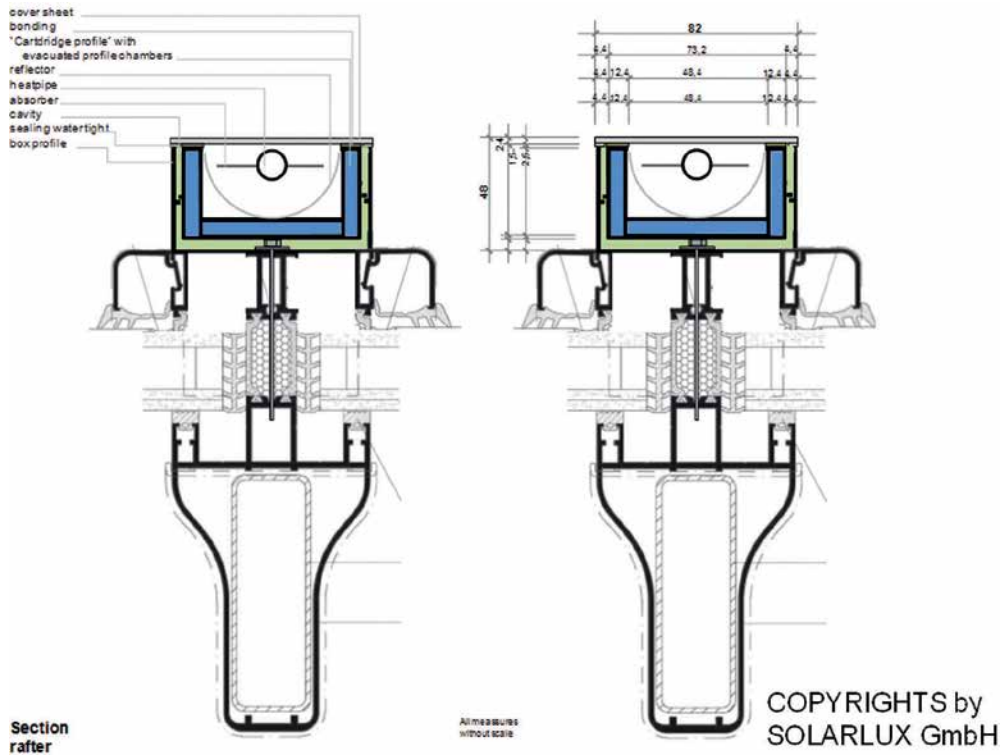


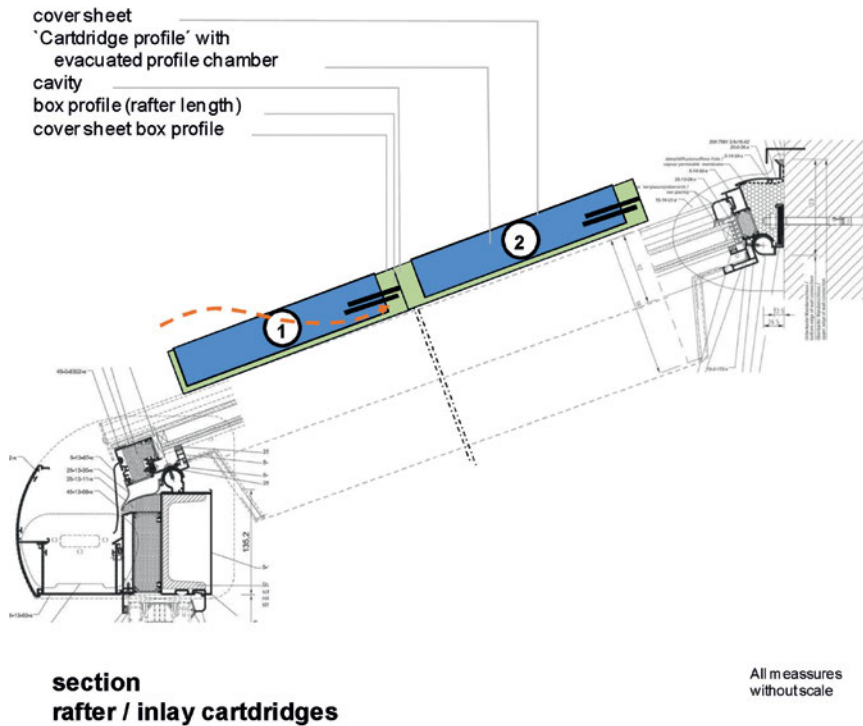
FIGURE 6.4 Sections of HEATBEAM I© design

Since the main elements like absorber sheet, adjacent heat pipe and condenser usually are slender components, they are eligible for rafter integration (Fig. 6.4). Common designs place the condenser outside of the evacuated glass tube; accordingly, the heat exchanger also works outside the tube.

### § 6.2.1.1 Casing

When developing heat pipes integrated into customized, i.e. flexible length rafter elements, working with standardized heat pipe lengths causes difficulties in terms of the construction area and construction length. Thus, the design is principally based on a

1.5m long heat pipe module that, by coupling individual modules, allowed sufficient utilisation of the customized offered rafter length (3m, 4.5m, 6m).



COPYRIGHTS by SOLARLUX GmbH

FIGURE 6.5 Construction scheme and cartridge concept / longitudinal section of HEATBEAM I©

By concept, the heat pipe was encased in a U-shaped powder-coating on the outside, and a press-bright 1.5 mm aluminium casing on the inside that was covered on top by a slender glass sheet (Fig. 6.4). This hermetically closed aluminium-glass encased heat pipe was called cartridge. The cartridge itself was inserted into a U-shaped profile, which was mounted outside on the existing SL80 nobles rafter profile beyond the glazing layer (see Fig. 6.5).

The U-shaped profile, called box profile, in turn was screwed on top of the thermally disconnecting rack of the profile and sealed by dry sealing gaskets towards the roof glazing. The box profile worked as the adapter for the cartridge to the entire roof construction. Cartridge and box profile were distanced by a circular air cavity of 4 mm.

Consequently, cartridge and box profile were sealed with each other by dry rubber gaskets, whereby the contact was intensified by forced closure of the screwing. Thus, the cartridge could be removed for maintenance without disassembly of the rafter itself. The U-shaped aluminium cartridge profile, 2,000 mm long, 82 mm wide and 48 mm high, was welded on all sides to provide air tightness.

### § 6.2.1.2 Cover sheet

---

The length of the cover glazing equalled the outer dimensions of the casing. The glazing was made from 4 mm tempered, low iron-oxide float glass with seamy edges. Since the glass sheet was that thin (3mm), narrow (82mm) and long (2,000mm), commission for tempering revealed to be technically complex and time intensive but not impossible.

Although, the comparably thin 4 mm glass sheet was manufactured and tempered at that length, it encountered no breaking neither during adhesion to the profile nor during testing in environment until the project end. The light transmission factor was calculated with equation (27) as follows:

$$LT = 1 - (3\text{mm} \cdot 0.01 + 2 \cdot 0.04) = 0.89 (= 89\%) \quad (27)$$

The 3 mm tempered low-iron and not anti-reflectively coated glass sheet provided light transmission of  $LT = 89\%$ .

### § 6.2.1.3 Sealings

---

Since special absorber sheets develop operational temperatures of up to  $260^{\circ}\text{C}$  (Giovannetti, Kirchner, Franke, Rohde and Scherer, 2014), and a heat pipe by principle develops high operational temperatures of  $>150^{\circ}\text{C}$ , organic sealants of aluminium-glass connections require more than average high thermal resistance.

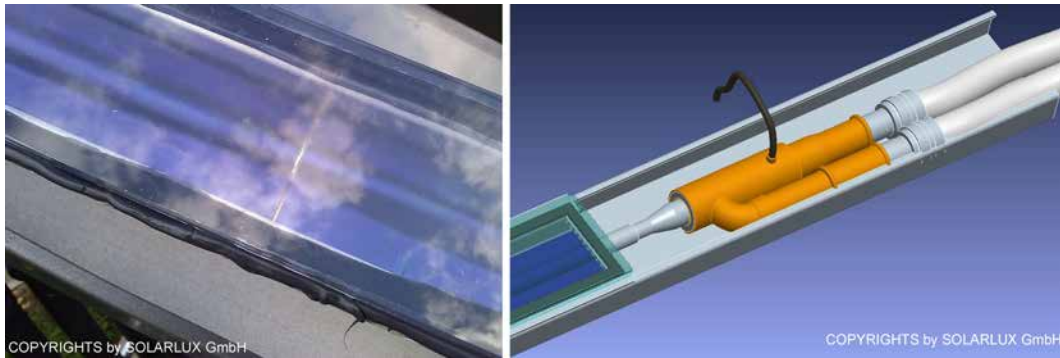


FIGURE 6.6 a.) HEATBEAM applied handmade two level sealing system, b.) Cartridge – casing – heat exchanger situation

In order to achieve an air tight and temperature durable connection between the cover glazing and the aluminium casing, a 2-levelled sealant system for high thermal applications in the solar field was applied. This system compounded by an outer wet applied 2-component silicon sealant and an inner high temperature resistant oxygen reactive 3 mm butylene tape (Fig. 6.6). Usually, this system is applied automatically by machine for 100% performance, but for first fundamental prototyping and testing 3mm x 26mm tape and silicon was cut and applied by hand.

Thus, the 2,000 mm by 64 mm tempered glass sheet was applied to the casing circumferential contact flanks (6 mm) with 2,000 mm wooden ledges and bar clamps. After 5 days of setting time the clamps and ledges were removed.

#### § 6.2.1.4 Condenser penetration

While by principle a heat pipe is a hermetically closed system, generated heat requires heat exchange in order to be utilized. A heat pipe (copper tube) ends with a condenser. In context of the design the condenser penetrated the slim top flank of the 48 mm high cartridge casing in the upper third. Subsequently, remaining cavities between casing and copper tube were sealed air tight and heat resistant with a 2-component resin dry adhesive.

### § 6.2.1.5 External Linear Heat exchanger

---

Due to the fact, that a heat pipe collector was developed for axial rafter application in contrast to common heat pipe collectors, the heat exchange changed from centralized to decentralized by concept. Commonly, collector fields are based on one single heat exchanger that is arranged perpendicularly to the heat pipes axis. In case of the heatbeam design, a single decentralized heat exchanger was to be developed, that opens to the condenser linearly, axis-wise (Fig. 6.7), and not orthogonally. Moreover, the new heat exchanger required maximum dimensions to fit into the U-shaped box profile, namely within 60 mm inner width.

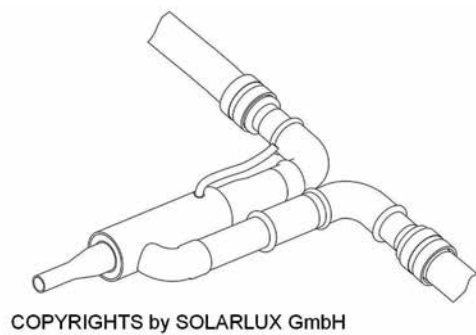


FIGURE 6.7 a.) Box profile – ridge situation : heat exchanger, b.) 3D linear heat exchanger rendering

Therefore, a tube-in-tube concept was developed. An inner tube, slightly wider than the outer dimensions of the condenser jacket, was centrally inserted in a tube with an inner diameter 8 mm wider than the inner tube.

The cavity between one end was closed by soldering. The inner diameter of both tubes was reduced to 15 mm with adapter nipples. Whereas the wider tube obtained 15 mm junctions rectangular to the main axis on both opposite sides, the tube-in-tube system was finally closed at the top end with a soldered cap. Thus, the system was water tight and ready to be flushed thoroughly, while enclosing a condenser over the entire length. With dimensions of 190 mm length and 62 mm maximum width the linear heat exchanger could be placed tilted, exploiting the diameter width within the adapter box profile. Cavities required physical thermal insulation.

### § 6.2.1.6 Unconventional piping and connection

---

The author investigated alternative piping material. Reasons here for were diverse. Commonly, piping for transport fluid distribution is made of stainless steel corrugated tube.

Since it is made from steel, it is not only rather expensive but also encounters considerable heat losses by conduction. Normally, corrugated steel tubes need welding or soldering for any type of tight connection. However, simple positive locking or crimping is always preferable; even for a high preassembly rate. Moreover, a corrugated surface texture complicates feeding through tiny aluminium profiles, which is inevitable for a façade integrated collector system.

For these four reasons, the authors searched for and found a specific sort of polymer tube as an appropriate and beneficial alternative. The identified polymer tubing was temperature resistant up to 230°C, ultra-violet radiation stable and chemical resistant. In particular, resistance to freezing agents like glycol was proven for two years (2015-2017) without any apparent impact.

Since the thermal conductance value of the polymer tubing is  $\lambda = 0.24 \text{ W/m}^2\text{K}$  compared to  $21,0 \text{ W/m}^2\text{K}$  for V2A stainless steel, thermal losses are 87 times lower. Moreover, the polymer tubing offered a tight bending radius (80 mm, 90°C) and smooth inner and outer tube surfaces, which facilitates feeding through aluminium profiles and lowers flow resistance. It also offered easy, error-free and fire-free clamping connections to rafter and heat exchanger, even on site.

### § 6.2.2 Physical and technical description HEATBEAM II – beneficial integral design

---

While Heatbeam I is based on a composite casing, the second design Heatbeam II benefits from a homogeneous polymer casing material. The polymer was proven for operational temperatures up to 150°C, with possible short time peaks up to 172°C. It showed UV-resistance and a light transmission factor of 89% (see Chapter 03, [APPENDIX C.3](#)).

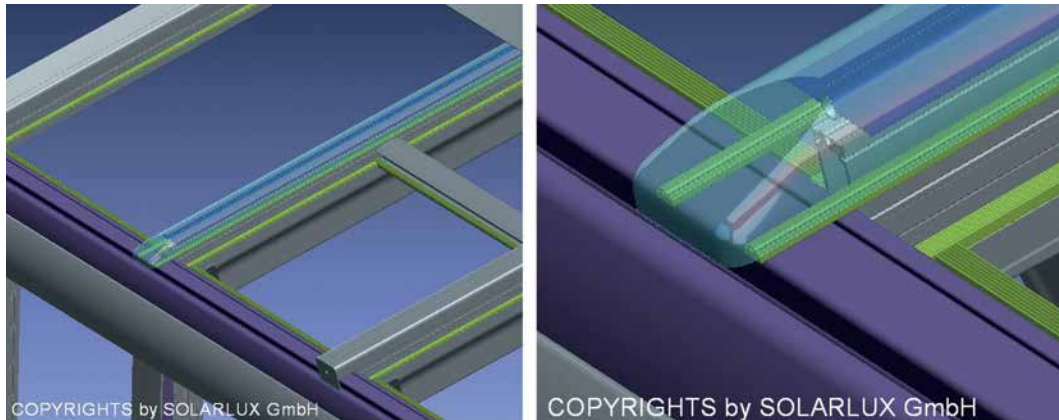


FIGURE 6.8 a.) 3D rendering of HEATBEAM II application align in rafter axis, b.) Eave junction

Since it can be extruded to 2 mm thickness the main body of maximum 30 mm height can be made from 6 to 10 m wrought material. This wrought ware allows for customer specific roof lengths. The top and end was hermetically closed with formed end caps; on the top with a penetration opening to solder the condenser later on. The caps were polymer-welded to the body. Thereby a homogenous and transparent curved tubing provided physical, optical and constructional benefits. Due to its transparent and curved appearance (h: 30 mm, Fig.6.8; 6.9), HEATBEAM II was less noticeable than the 48 mm structure of HEATBEAM I.

The entire tubing was evacuated to 10 mbar remaining pressure. Such a remaining pressure level provided considerable thermal insulation quality; comparable to standardized OEM tubes. A needle valve, incorporated on the top end, allowed for subsequent re-evacuation. The heat exchanger was placed in the ridge area of the sun space roof. exchanging port was incorporated into a covering rafter profile and into the regular sun space ridge profiles as well.

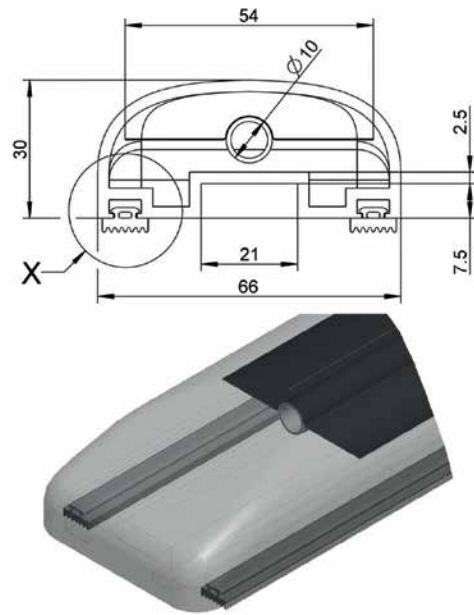
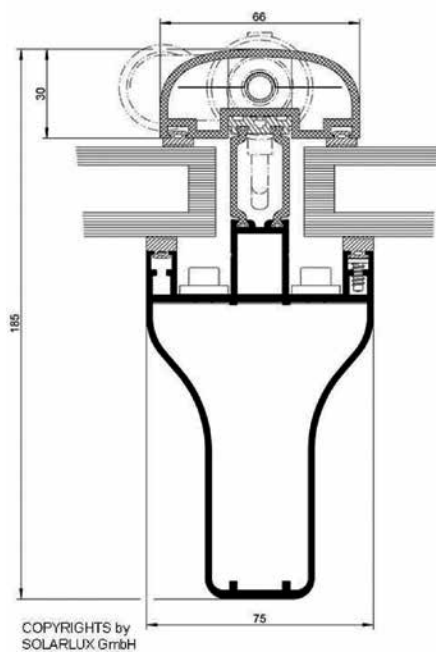


FIGURE 6.9 a.) Section : HEATBEAM II as glazing bar, b.) Eave end cup, section with incorporated heat pipe

Since it aligned with the main axis of the polymer tubing the heat Feeding and return diversions of the heat exchanger were lead perpendicular to the rafter axis and parallel to the ridge profiles (Fig. 6.8). Thermal insulation and ducts were integrated in hollow spaces of the ridge profiles and allow serial coupling in terms of vicinal rafters. The tubing incorporated screw channels alternate on both sides every 400 mm.

The channels allowed to fix the tubing by force closure to the thermally insulating grouser of the rafter. Thus, illustrated in Figure 6.9, the polymer tube allowed to fix and clamp the sun space roof glazing. While the polymer tubing provided notches in the bottom side facing the glazing, rubber gaskets could be integrated, which provided contact pressure and water tightness.

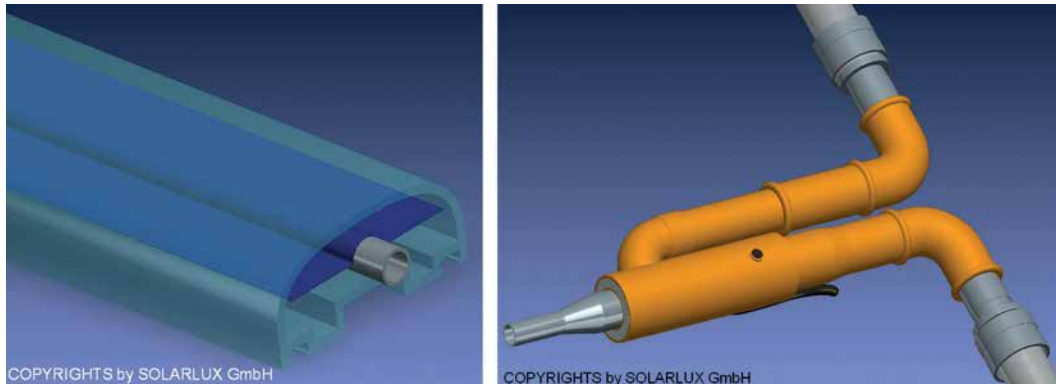


FIGURE 6.10 a.) 3D section of case inserted heat pipe, b.) Linear heat exchanger with perpendicular piping

This design considered the requirements of the ETAG 006 [196] and the recently established DIN 18008-2, 2010-12 [197] and DIN 18008-5:2013-07 [198] in terms of mechanically fixed roof sealing and linearly fixed walk-on-able overhead glazing.

### § 6.3 Description of the experimental test set-up: HEATBEAM

The experimental set-up HEATBEAM was installed in the immediate vicinity of the test sun space on the former Solarlux headquarter site in Bissendorf. A durable and stable foundation was made from four euro pallets, which were fixed to a plane slab with oriented strand boards. A front and a backside rack of different heights mounted at a 1.6 m distance simulated eave and ridge points and enabled a sample installation with 30° inclination, exemplifying the common roof inclination of interest.

The heatbeam test sample, including adapting box profile and cartridge element was installed with south orientation and 30° inclination (Fig. 6.11). A buffer tank with decelerated thermal insulation was closely installed as heat sink. Hydraulic and electrical components like valves, pumps, heat meter and KNX-controlled actuators were installed within a wooden box nearby. The linear heat exchanger was inserted in the top area of the box profile. Feeding and return tubing was clamped on as well. Subsequently, the HEATBEAM heat pipe, in detail, the condenser was inserted in the heat exchanger. Thus, a smart closed test circle was established. The AC-pumps were activated by KNX-actuators which were controlled by the Eisbaer software via KNX-bus net.



FIGURE 6.11 a.) Real life weathered euro pallet experimental test set-up with 4000 mm HEATBEAM I, b.) Vacuum equipment

A reference vacuum tube of 2,000m length with  $\eta_0 = 0.75$ ;  $a_1 = 1.12 \text{ W/m}^2\text{K}$  and  $a_2 = 0.004 \text{ W/m}^2\text{K}^2$  was installed additionally. The highly selective coated copper absorber assured a stagnation temperature of  $160^\circ\text{C}$ . The maximum power at STG  $1,000 \text{ W/m}^2$  and  $1,5 \text{ AM}$  was confirmed with  $76 \text{ W}$  [199],  $58 \text{ W}$  with  $\Delta T = 40 \text{ K}$ , respectively.

### § 6.3.1 Sensing + Monitoring

For the feeding temperature measurements, a temperature T-130 sensor with KNX T6-UN-B4 unit was inserted into the immersion sleeve of the heat exchanger. Additionally, a T-130 sensor was attached on the outside of the cartridge profile and the box profile (see Figure 6.12) in order to measure surface temperature resulting from heat losses. In this way, potential undesired thermal impact on the comfort of a sun space could have been detected and evaluated in relation to radiation and feeding temperature of the heat pipe. Three different temperature sensors were placed in the top area, mid area and bottom area, respectively, of the sensitive 300L buffer tank. Although the heat meter data exchange was KNX-based and implemented in the net, for this test set-up the data was recorded analogously and sporadically for one week at a time.



FIGURE 6.12 a.) Test set-up : heat sink, feeding and surface temperature monitoring, reference tube, b.) Pumps and heat meter and actuators

### § 6.3.2 Variants of investigation

HEATBEAM I was configured in different test variants. The author wanted to also investigate mechanical and optical performance of the cover glass at 2,000 and 4,000 mm length in relation to thickness and float glass quality (tempered, polymer, laminated safety glass). In addition, the author tested standardized heat pipes re-filled with water instead of the original working fluid. No cover glass was additionally low-coated, anti-reflectively coated or prismatic treated; it was simply based on low-iron basic float glass.

Thus, the experimental set-up contained seven variants, differing mainly as follows:

- *V01: 6 mm extra bright white float glass, standard heat pipe*
- *V02: 4 mm extra bright white tempered glass, standard heat pipe*
- *V03: 3 mm extra bright white tempered glass, standard heat pipe*
- *V04: 3 mm extra bright white tempered glass, standard heat pipe water re-filled*
- *V05: 3 mm extra bright white tempered glass, standard heat pipe, acrylic casing*
- *V06: 2x3 mm polyvinyl-butylral tape laminated float glass, standard heat pipe*
- *V07: 4 mm polycarbonate sheet, standard heat pipe*

In addition, two HEATBEAM I variants of V03 with a length of 4.000 mm were constructed and tested. For the V03-4000 variants the heat pipe itself was constructed by a 3,900 mm x 12 mm aluminium tube which was filled with a few millilitre acetone and glycol, and both end closed by end caps.

Highly selective absorber sheets of 400 mm length were strained in an omega shape and punctually glued on top of the heat tube with heat conductive paste. All casings were equipped with a T-shape DN-KF 16 vacuum bead with ball valve and analogue barometer. Underpressure was generated by a rotary vane pump for 10-3 mbar effective vacuum.

### § 6.3.3 Meteorological background

---

Irradiation maximum was detected on a monthly basis as follows:

- *July 2015:* 746 W/m<sup>2</sup>
- *August 2015:* 728 W/m<sup>2</sup>
- *September 2015:* 647 W/m<sup>2</sup>
- *October 2015:* 434 W/m<sup>2</sup>
- *November 2015:* 330 W/m<sup>2</sup>
- *December 2015:* 298 W/m<sup>2</sup>
- *January 2016:* 307 W/m<sup>2</sup>
- *February 2016:* 487 W/m<sup>2</sup>
- *March 2016:* 609 W/m<sup>2</sup>
- *April 2016:* 709 W/m<sup>2</sup>
- *May to July 2016:* 710 W/m<sup>2</sup>

### § 6.3.4 Monitoring and Control rules

---

The pumps were controlled via KNX-bus net to start whenever illumination was >50 Lux and the difference between the heat pipe feeding temperature and the bottom area of the 300L sensitive buffer tank greater than 10 Kelvin. The pumps were set to provide a volume flow of 0.15 m<sup>3</sup> per hour; equalling a power of 3 Watt per hour. The pumps were off-set with a time delay of 15 seconds when the temperature distance decreased below 10 Kelvin. Data points within the KNX-bus net were sent at 1 minute frequency or by change of more than 0.3°C.

## § 6.4 Results (descriptive knowledge)

---

All nine HEATBEAM I variants including V03-4000 I und V03-4000 II were sealed with a two-level bonding system especially developed for temperature impacted solar thermal applications.

### § 6.4.1 Vacuum duration and collector performance

---

For variant V04 (3 mm tempered glass sheet and water re-filled standard heat pipe) and V03-4000 II (4,000 mm long casing with 3 mm tempered glass sheet and acetone/glycol filled aluminium heat pipe) an under-pressure (sufficient low vacuum) of 10 to 25 mbar remaining was generated as well. Subsequently, it changed on average:

- *within the first two days only 50 mbar,*
- *within 7 seven less than 190 mbar,*
- *within 14 days 410 mbar and*
- *after 22 days evacuation 540 mbar to a remaining pressure of 590 mbar,*
- *after 6 weeks the under-pressure had eliminated towards atmospheric pressure*

The under-pressure stayed constant for at least 6 hours.

The under-pressure stayed constant for at least 6 hours. Thus, two of the nine simple handmade prototypes (V04 and V03-4000 II) provided a vacuum quality sufficient for thermal insulation application and for the duration of a few weeks. A rough rule-by-thumb daily pressure elimination of 25 mbar/d can be derived from the evaluated mid-step evacuation levels.

## § 6.4.2 Monthly yields

Variant V03 has been revealed to be the best performing handmade prototype. Although variant 03's sealing quality was not sufficient to be evacuated either towards 10 mbar under-pressure or to any other constant pressure level for any duration of time worth mentioning, the combination of 3 mm tempered bright white glass and standard encased heat pipe performed comparably best. Thus, variant 03 is compared to the reference standardized tube in terms of monthly cumulated yield. Figure 6.13 shows the recorded period between June 2015 to November 2016; covering 18 months of real-life testing and highlighting the phases (days) when the test set-up was out of order due to maintenance or KNX system fall out.

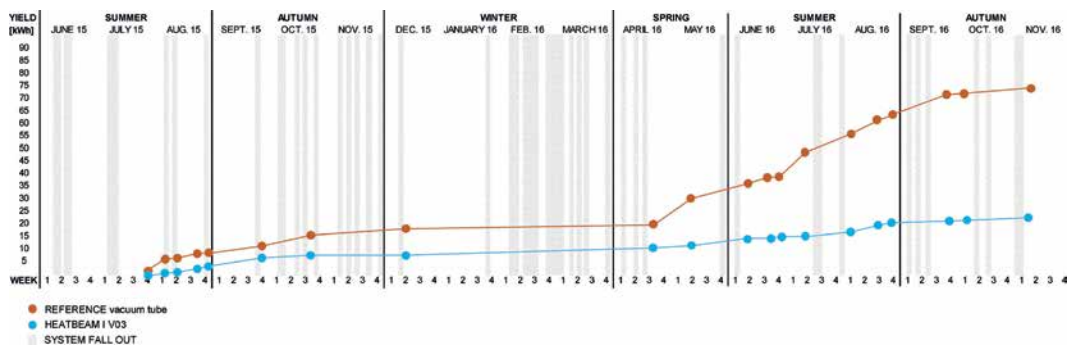


FIGURE 6.13 Monthly yield of HEATBEAM I variant 03 in relation to reference vacuum tube

Figure 6.13 demonstrates the yield performance in kWh of V03 from July 2015 to May 2016 as a parallel process to the reference tube, drawing an off-set right from the

beginning. The off-set grows especially between October and November 2015 up to 10 kWh. The yield process stagnates between the winter months December to April. Continuing from April 2016 to November 2016 the yield progress of the reference tube is nearly constant, while the progress of variant O3 does not continue with the previous off-set, but more plainly.

In summary, variant O3, although not evacuated, generates constant heat successfully. In the second summer of investigation, measurements show that the performance gradient of variant O3 compared to the reference is good. Essentially, within 18 months or real-life irradiation and weathering, variant O3 generates approximately 23 kWh, while the reference tube accomplishes 75 kWh.

Thus, the first HEATBEAM I prototype of a potentially rafter integrated solar thermal collector exhibits one third the efficiency of a standardized high quality evacuated tube. Reasons for measured lowered yield performance of V03 compared to a high quality reference tube are identified as follows:

- 1. no sufficient and durable vacuum, no thermal insulation: high thermal losses*
- 2. higher degradation of absorber selective coating due to missing vacuum and exposure to atmosphere*
- 3. limited impact angle of irradiation related to opaque casing construction principle (see Figure 132)*

Since evacuation of variant O3 was not sufficient during the 18 months of observation (1.), thermal losses in relation to increasing operation temperature increased. Hence, the collector efficiency was actually comparable to a glazed ventilated collector type.

Moreover, the ventilation, even when limited in respect of the existing two-level sealing system, enabled atmospheric gases and humidity to enter the case and to oxidize (2.) the selective coating. Oxidation leads to degradation of the original absorption/emission properties of the highly selective coating. That might either have reduced the absorption ability or increased the emission properties. The third major reason for lower annual yield performance of variant O3 was construction related.

Figure 204 illustrates the maximum effective irradiation angle (3.) of variant O3 compared to the reference tube, that impacts the absorber. Since evacuation of variant O3 was not sufficient during the 18 months of observation (1.), thermal losses in relation to increasing operation temperature increased. Hence, the collector efficiency was actually comparable to a glazed ventilated collector type.

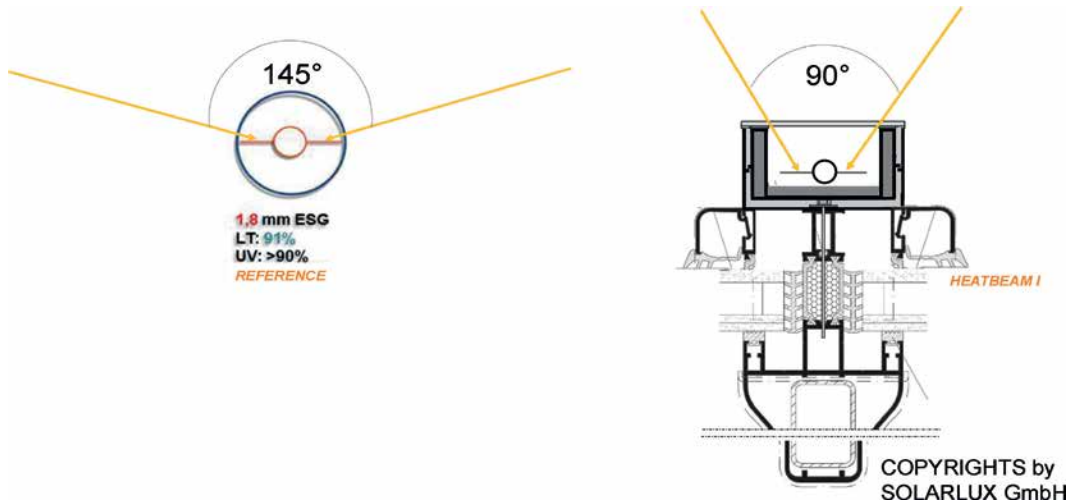


FIGURE 6.14 Different construction-related maximum irradiation impact angle

Moreover, the ventilation, even when limited in respect of the existing two-level sealing system, enabled atmospheric gases and humidity to enter the case and to oxidize (2.) the selective coating. Oxidation leads to degradation of the original absorption/emission properties of the highly selective coating. That might either have reduced the absorption ability or increased the emission properties. The third major reason for lower annual yield performance of variant 03 was construction related. Figure 6.14 illustrates the maximum effective irradiation angle (3.) of variant 03 compared to the reference tube, that impacts the absorber. Resulting from the opaque aluminium casing as well as the bottom level position of the absorber, the maximum irradiation angle was 90°, whereas the reference tube profited from approximately 145°.

According to the design phase on HEATBEAM I, there should have been implemented a hemispheric irradiation mirror sheet in the aluminium casing in order concentrate irradiation on the absorber.

During assembly, this was not implemented, which changed the proposed standard heat pipe position from the upper third to the lower third of the casing height. This significantly reduced the effective impact angle, and thus the duration of effective irradiation impact per day.

Especially the last reason as being a constructional constraint exemplifies the need of design improvement and justifies the re-design of HEATBEAM I to an entirely transparent and pleasing derivate (h=30mm) HEATBEAM II.

### § 6.4.3 Maximum feeding temperature – collector performance

---

A comparison of the synchronic feeding temperature of variant O3 related to the reference tube additionally helps to determine the potential performance of the design. Thus, within the observed 13-month period from July 2015 to July 2016 the monthly maximum reference tube feeding temperature has been identified, to which the equivalent feeding temperature of the HEATBEAM I was plotted. Furthermore, Figure 205 shows two things; the accompanied V03 temperature to the monthly maximum reference tube and the accompanied reference tube temperature to the detected maximum V03 feeding temperature.

Additionally, the synchronic cartridge temperature and box profile temperature are listed too, in order to demonstrate potential radiation impact on the thermal comfort of the interior space.

Although by construction, the radiative collector component is outside the space, i.e. beyond the glazing and what is more the entire rafter is thermally decoupled by a thermally disconnecting grouser, the temperature was recorded in order to estimate potential impact (Fig. 61.5). Cell E1 and F1 demonstrate that the V03 temperature in July is 91.9°C, which is very close to the reference temperature of 92.7°C.

On the contrary, when the cartridge temperature was at 48.9°C due to missing vacuum (G2), the reference tube and the V03 temperature were at 34.6 and 37.1°C, respectively. Interestingly, in March and April the reference tube reached a maximum of 143.2 and 147.3°C, respectively, with irradiation of 555 and 573 W/m<sup>2</sup>. In contrast, the feeding temperature of V03 only increased to 25.5 and 45.5°C. Thus, a tremendous difference in performance in spring becomes obvious. The maximum temperature generated by V03 did not exceed 62.0°C, while the cartridge temperature rose towards 43°C. In May, once at the beginning and once at the end of the month, V03 and reference tube maximum temperature were on a comparative level of 70 to 80°C (E22, F23). Thus, we can conclude that the ability to convert irradiation to heat was comparably high for both collectors in May. Resulting cartridge temperature exceeded 55.0°C and increased considerably. In June, the competitive temperatures of E24 and F24 were equally high, whereas the temperature listed in F24 of 72.4°C for V03 illustrates the performance potential with irradiation of 553 W/m<sup>2</sup>.

MAXIMUM MONTHLY FEEDING AND SURFACE TEMPERATURE OF HEATBEAM V03 AND REFERENCE								
MONTH	DAYTIME	EXTERNAL TEMPERATURE [°C]	IRRADIATION [W/m <sup>2</sup> ]	Temp. Feed. REFERENCE [°C]	Temp. Feed. V03	Temp. Cartridge V03	Temp. Box Profile V03	
	A	B	C	D	E	F	G	H
1	JULY 15	24.7.12:32	29,5	481	92,7	91,9	41,72	35,70
2		2.7.16:36	35,2	386	34,60	37,10	48,9	42,1
3	AUGUST 15	15.8.14:24	30,40	383	101,5	93,1	50,32	39,30
4		31.08. 14:14	29,50	455	98,72	91,84	55,0	46,0
5	SEPTEMBER 15	21.9.11:52	27,0	438	66,0	57,2	34,70	25,10
6		21.9. 12:13	26,2	430	19,1	62,0	36,50	25,30
7	OCTOBER 15	26.10. 14:43	11,40	164	71,3	23,70	20,70	19,50
8		11.10. 12:19	9,80	339	53,7	42,9	21,50	11,70
9		5.10. 13:37	19,8	352	23,80	35,10	30,4	25,9
10	NOVEMBER 15	01.11. 14:18	14,20	236	56,5	23,30	22,70	23,40
11		01.11. 12:26	13,50	307	14,50	42,4	30,00	25,6
12	DECEMBER 15	6.12. 12:49	11,0	231	44,9	23,4	18,4	14,7
13		8.12. 12:06	11,5	217	29,1	30,7	23,3	20,3
14	JANUARY 16	18.1. 12:45	- 2,1	251	58,9	17,8	11,9	8,5
15		25.1. 12:38	12,4	188	56,9	34,9	25,6	18,6
16	FEBRUARY 16	27.2. 12:49	4,3	353	72,7	49,2	27,8	11,5
17		27.2. 12:14	4,6	344	70,9	50,1	28,2	16,1
18	MARCH 16	17.3. 14:02	10,5	83	143,2	25,5	19,7	18,0
19		6.3. 11:14	13,1	354	19,8	45,8	28,7	25,1
20	APRIL 16	1.4. 12:50	18,2	555	147,3	41,5	25,9	22,0
21		22.4. 12:42	19,0	573	33,9	61,9	43,7	31,7
22	MAY 16	1.5. 15:00	15,1	465	79,3	41,1	30,9	24,4
23		22.5. 11:46	34,7	618	36,8	71,8	55,0	38,1
24	JUNE 16	7.6. 12:32	39,0	634	46,2	46,9	38,7	38,6
25		5.6. 14:22	28,8	553	44,3	72,4	55,9	44,5
26	JULY 16	17.7. 15:47	26,8	441	77,2	37,1	31,6	31,9
27		4.7. 13:47	29,4	647	40,2	73,0	55,8	38,0

FIGURE 6.15 CMaximum monthly feeding and surface temperature HEATBEAM I V03 related to reference tube

More of interest, in contrast to the measured maximum temperatures in July 2015 (92.7 and 91.9°C with 481 W/m<sup>2</sup> irradiation), the maximum feeding temperatures of both collectors never exceeded 77.2 and 73°C, re-spectively, in the context of 441 and 647 W/m<sup>2</sup> irradiation.

In summary, from the data it can be derived that the handmade not evacuated aluminium-cased rafter integrated collector design was able to compete with standardized high quality evacuated tube in terms of maximum feeding temperature.

Especially in midsummer months like May, June, July and August the maximum potential temperature level was comparable. On the contrary, the maximum temperature level of V03 significantly lowered during intermediate times between September and October and March and April, when the temperature level especially for this design is proposed to be comparably high for the first or last charging phases of sorption storages or direct daily gain utilisation.

The described specific performance deficit is likely related to the limited angle of irradiation impact and not that much to enforced transmission losses due to a lack of evacuation. From that perspective, the design does not satisfy the expectations of potential feeding temperature levels. However, the maximum achievable temperature of 92°C in midsummer indicates the design's performance potential even against the background of the 4.2 detected technical constraints. Finally, the detected cartridge surface reaches up to 56°C.

Since the collector is placed outside the living space and separated by double-glazing and a thermal decoupling grousse, the effect on interior thermal comfort is likely to be ignorable. Nonetheless, 56°C is a serious surface temperature; the author expects to enhance non-physical thermal insulation by evacuation, and thus to significantly lower resulting surface temperature to the external temperature level.

#### § 6.4.4 Potential sorption storage charging performance vs. potential local discomfort

---

Beside the evaluation of potential maximum feeding temperature and thus resulting cartridge surface temperature, the annual number of hours of specific collector power is of interest, too. Thus, cumulative frequencies of hours with specific measured feeding temperature of the HEATBEAM V03 related to the reference tube was evaluated and analysed. Figure 6.16 illustrates monthly cumulative frequencies of hours with feeding temperatures higher than 120°C, 100°C and 75°C.

## CUMULATIVE FREQUENCIES OF HOURS WITH SPECIFIC FEEDING TEMPERATURE

	A	B	C	D	E	F	G
	MONTH	FEEDING TEMPERATURE LEVEL	Temp. Feed. REFERENCE [°C]	Temp. Feed. V03	Temp. Cartridge V03	Temp. Box Profile V03	HOURS OF SYSTEM FALL OUT
1	JULY 15	> 75°C	3,3	1,4			312 42%
2		> 100°C	0	0			
3		> 120°C	0	0			
4		> 34°C (29°C+5K)					
5	AUGUST 15	> 75°C	59,9	22,1			48 6%
6		> 100°C	0,6	0			
7		> 120°C	0	0			
8		> 34°C (29°C+5K)					
9	SEPTEMBER 15	> 75°C	0	0			24 3%
10		> 100°C	0	0			
11		> 120°C	0	0			
12		> 34°C (29°C+5K)					
13	OCTOBER 15	> 75°C	0	0			216 29%
14		> 100°C	0	0			
15		> 120°C	0	0			
16		> 34°C (29°C+5K)					
17	NOVEMBER 15	> 75°C	0	0			120 17%
18		> 100°C	0	0			
19		> 120°C	0	0			
20		> 34°C (29°C+5K)					
21	DECEMBER 15	> 75°C	0	0			24 3%
22		> 100°C	0	0			
23		> 120°C	0	0			
24		> 34°C (29°C+5K)					
25	JANUARY 16	> 75°C	0	0			24 3%
26		> 100°C	0	0			
27		> 120°C	0	0			
28		> 34°C (29°C+5K)					
29	FEBRUARY 16	> 75°C	0	0			528 79%
30		> 100°C	0	0			
31		> 120°C	0	0			
32		> 34°C (29°C+5K)					
33	MARCH 16	> 75°C	30,7	0			552 74%
34		> 100°C	16,9	0			
35		> 120°C	0	0			
36		> 34°C (29°C+5K)					
37	APRIL 16	> 75°C	47,8	0			168 23%
38		> 100°C	26,6	0			
39		> 120°C	0	0			
40		> 34°C (29°C+5K)					
41	MAY 16	> 75°C	0,1	0			120 16%
42		> 100°C	0	0			
43		> 120°C	0	0			
44		> 34°C (29°C+5K)					
45	JUNE 16	> 75°C	0	0			216 30%
46		> 100°C	0	0			
47		> 120°C	0	0			
48		> 34°C (29°C+5K)					
49	JULY 16	> 75°C	0	0			384 52%
50		> 100°C	0	0			
51		> 120°C	0	0			
52		> 34°C (29°C+5K)					

FIGURE 6.16 Cumulative frequency of hours with feeding temperature levels and local discomfort exceeding (asymmetries : roof cat. II: DIN EN ISO 7730

These temperature levels are crucial boundary levels, enabling statements about the complete drying (desorption) of sorptive storage material volume, 50% of volume or even the boundary for high-tech hybrid sorption materials (Lass-Seyoum, 2012), whose desorption threshold is detected to be around 75°C.

Moreover, the table in figure 206 shows cumulative frequencies of hours, when there is a risk of local discomfort caused by overhead radiation asymmetry. According to DIN ISO 7730, the maximum acceptable floor surface temperature in category II is 29°C in order to prevent “warm floor”. The allowed temperature difference between a ceiling (sunspace roof) and a floor is less than 5 Kelvin. Thus, the limitation of a roof temperature of 34°C is established in order to identify risks of radiation impact by the rafter integrated collector to interior thermal comfort. Figure 206 demonstrates for July 2015 a total of 3.3 hours of feeding temperature higher than 75°C provided by the reference tube.

In August, the reference temperature reached 101.5 and 98.72°C, which synchronically resulted in feeding temperatures of 93.1 and 91.8°C (F3, F4), respectively, for V03. The V03 temperature differed to the reference for seven to eight Kelvin. Related cartridge temperatures of 50.3 and 55.0°C were measured irradiation of 383 and 455 W/m<sup>3</sup>, respectively.

In September, the reference tube reached a maximum temperature of 66.0° and the V03 feeding temperature of 57.2°C in relation to a comparably high irradiation of 438 W/m<sup>2</sup>. The difference in feeding temperature is marginal. On September 21th, at 12:13, the V03 also reached the temperature level of 62.0°C, which resulted in a cartridge surface temperature (G6) of 36.5°C.

In October 2015, the synchronic V03 feeding temperature was considerably lower than the reference tube temperature, which became obvious on October 11th and 26th. The difference between both plotted to be roughly 11 and up to 47 Kelvin. This information illustrates that the HEATBEAM I design performed not as sufficiently as a standard reference tube; especially in the preferred autumn time, when roof integrated and inclined solar thermal collectors are very good in generating renewable energy for direct use (see chapter 03). In October, related cartridge temperatures varied between 20 and 30°C. From November to January, the inspected maximum feeding temperatures of the reference tube always were demonstrably higher than those of variant 03. The cartridge surface temperatures ranged between 20 to 30°C.

Significant for February 2016 was that the reference maximum feeding temperature with 72.7 and 70.9°C (E16, E17) was 20 Kelvin higher than the V03 feeding temperatures in every case. Cartridge temperatures in February were close to 30°C.

Likewise, the evaluated cumulative hours provided by V03 above this temperature boundary was 1.4 hours. During approximately 32 cumulative hours, the cartridge temperature was above 34°C, the box profile surface for 18.3 hours, respectively. These figures have to be evaluated against the background of about 40% of missing hours caused by system fall out.

In contrast, in August, the reference tube provided about 60 hours with feeding temperatures above 75°C, the HEATBEAM I variant 03 about 22 hours. Moreover, the reference tube was only able to achieve 0.6 hours with temperatures above 100°C, in the case of V03 the cumulative frequency was zero. Since in August rarely 6% of hours were related to system fall out, nearly 150 hours were obtained with cartridge surface temperatures above 34°C, 80 hours with respect to the box profile.

On the contrary from September to February, the feeding temperature of the evacuated tube and variant 03 neither reached 120 nor 75°C at all. Consequently, the surface temperature of the cartridge and box profile also showed no limit exceedance.

Although system fall out was present in autumn during the intermediate months September and October for 3 and 29% of all hours, temperatures above 75°C was not even observed for the high-quality standardized vacuum tube. In contrast, during the spring intermediate months March and April 2016 with 74 and 23% of system fall out, the reference tube provided feeding temperatures above 75°C for 30 hours, and above 100°C for at least a total of 17 hours. The HEATBEAM I variant 03 provided no temperatures above these limits.

Similarly, in April the reference tube managed to supply 75°C and higher feeding temperatures for a total of 47.8 hours, 100°C for 26.6 hours. On the contrary, the aluminium-cased variant 03 generated temperature only below the 75°C border, but nonetheless induces 7.5 hours cumulated with cartridge temperatures above 34°C.

Interestingly, in May, June and July 2016 neither variant 03 nor the reference tube accomplished feeding temperatures higher than 75°C. Compared to July 2015, however, when the system fall out was comparably high with 42% (July 2016: 52%), the yield of temperatures above 75°C was at least 1.5 to 3 hours for the reference tube as well as for V03.

However, no required temperature level for sorption storage charging was complied with from May to July, the resulting cartridge temperature above 34°C was evident for 94 hours in May, for 112 in June and 35 hours in July. As a conclusion, we can say that the cumulated number of hours with feeding temperatures above 75°C by HEATBEAM I variant 03 was about 23.5 hours, whereas the reference tube managed about 142

cumulated hours under equal conditions. Variant O3 neither managed to provide feeding temperatures noticeable above 100°C nor 120°C. However, the reference tube managed 100°C and higher for 43.5 hours in total. Despite predominating feeding temperatures below 75°, the cartridge surface temperature raised above 34°C for 94.4 hours in May and for 111.7 hours in June.

---

## § 6.5 Summary

---

This chapter introduced the integral product development HEATBEAM I of a solar thermal collector, integrated into a sun space rafter. This building element was tested under real conditions in terms of power (maximum temperature °C), annual yield (collected energy amount in kWh), eligibility for charging of sorption storages (cumulative frequency potential hours with determined temperature levels) and resulting surface temperature as indicator for potential negative radiative influence on space interior thermal comfort. All parameters in questions were validated synchronically by a reference evacuated tube.

As a result, during the midsummer months the maximum achievable feeding temperature was slightly lower, but comparable to that of the reference tube. Differences in months with high impact angle were about 10 to 15 Kelvin or relatively spoken less than 10%.

This was observed even with the non-evacuated variant V03. However, in intermediate seasons and winter, when the demand for additional directly utilized energy is high, the feeding temperature was demonstrably lower compared to the reference. Essentially, the temperature of V03 was up to 60% less than that of the reference. The author identified the narrowed effective irradiation impact angle due to the low position of the absorber on the opaque aluminium casing to be the reason for lower maximum temperatures and less annual yield in seasons with a steep sun angle.

While the reference tube managed to provide more than 75°C feeding temperature for 142 hours a year, and higher than 100°C for 44. hours, the performance of V03 was restricted to 23.5 hours and zero hours, respectively. Thus, firstly the performance was limited to temperatures between 75 to 100°C, and secondly only covered 17% of the reference tube. However, the rafter integrated evacuated tube causes more than 390 hours a year with cartridge temperatures above 34°C. The surface temperature by construction does not have a direct negative influence on indoor thermal comfort,

since being outside, but is an indicator for the effect or lack thereof of physical or vacuum thermal insulation.

Nonetheless, although the performance of annual yield, frequency of hours with feeding temperature above 100°C and the cartridge surface temperature need to be improved, the test set-up gave essential insight in the first HEATBEAM I design and its variants. Thus, these results justify the further development of the HEATBEAM I design and shows that improvements considering transparent aperture area is a crucial issue of rethinking.

Finally, in order to verify Hypothesis II, it is to state: although Figure 6.16 shows no cumulated hours of temperatures above 75°C between October and April, Figure 6.15 shows maximum feeding temperatures of at least 30 to 43°C between October to January, and even 50 to 62°C in February and April. Notwithstanding, simple potential maximum temperatures reveal nothing about the potential energy amount; the maximum temperatures in midwinter months like November, December and January even meet the required floor heating feeding temperatures already.

Essentially, this empirical evaluation beside detected aspects of improvement, justifies elaboration in this field of integral façade development.



# 7 Parametrization and algorithms for comfort and annual energy yield modelling in Chapter 08

## § 7.1 Dynamic Thermal Simulation Software

Computer aided dynamic thermal modelling was executed with TAS – Thermal Analysis Software, Copyright 2015 EDSL U.K., in version 9.3.3. Especially passive solar gains were modelled with TAS 3D Modeller, TAS Building Simulator and TAS Result Viewer. Furthermore the models (see Fig. 7.1) were equipped with photovoltaic and solar thermal collectors configured with TAS Systems.

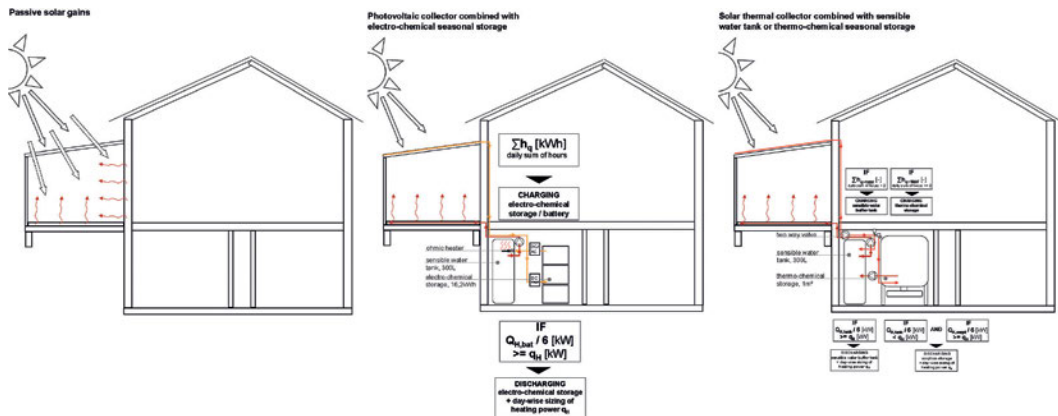


FIGURE 7.1 Operational schemes of three different inspection variants : a.) Passive solar gains, b.) PV collectors+battery, c.) Solar thermal collector+sorption storage

Hourly values of yield and power were reported in TAS macros

- TAS macro SHW output v2.3 from 18.01.2012
- TAS macro PV output v1.4 from 25.02.2011

Finally, the results of operational temperature, surface temperature and hourly generated power were imported into Microsoft Office Excel for further analysis and post processing.

---

## § 7.2 Software Limits – Additional Post processing

---

Since TAS does not enable to simultaneously model daily yields and storing of renewable energy as well as utilization for an improvement of operational temperature, modelling had to be separated. The methodology will be explained in 2.1.

### § 7.2.1 Methodology

---

The reference variant was a sun space adjacent to a single family home without any incorporated collector and storage technology. With reference models we analysed the effect of exclusively passive solar gains on thermal comfort. All generated hourly values of operational and surface temperature were exported to Excel (Fig.7.2). The 3D models were equipped by configured collectors, weather and controls which resulted in tsd.files. Based on the tsd.files the macros SHW output v2.3 and PV output v1.4 calculated hourly (8760 hours) values of power and yield.

In Excel all 8760 hourly values of each of the five photovoltaic variants (TRY 01; 04; 05;13) and five solar thermal variants were listed and inspected. We put emphasis on the analysis of the hourly values of operational temperature between 5 to 10 PM each a day. If demand for heating ( $T_{op} > 20^{\circ}\text{C}$ ) within these 5 daily hours was evident, the parallel hourly inspection of collector yield and storage charge status was inspected. If energy was available, this evident day exclusively was simulated a second time. Therefore floor heating was sized according to estimations of required power ( $Q_n = q \cdot 6$  hours), but maximum sized by the power available either from sensible,

thermo-chemical or electro-chemical storage. The results of operational temperature was imported into Excel again and replaced data from the reference model.

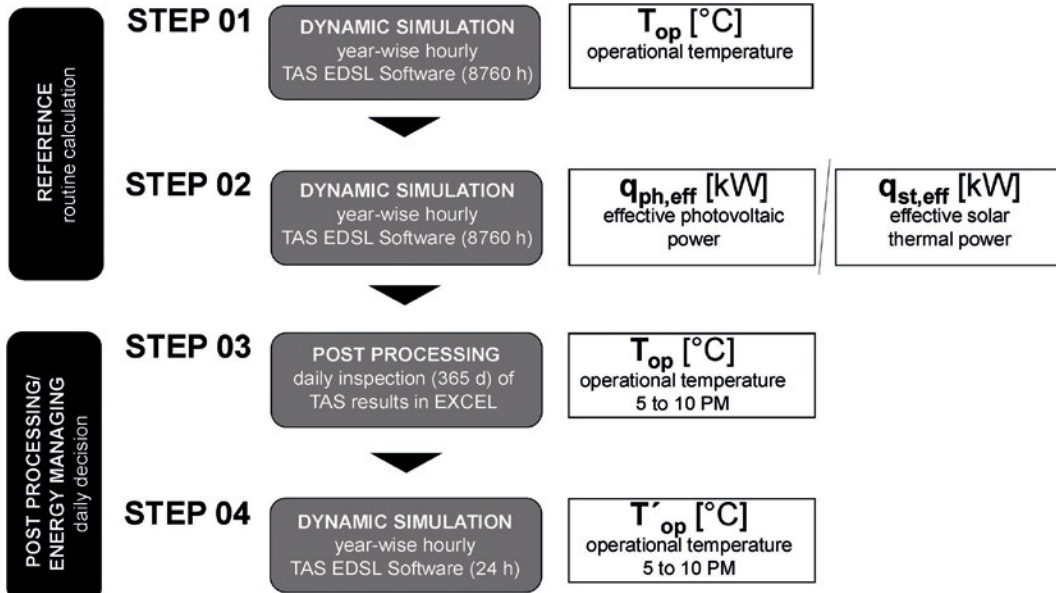


FIGURE 7.2 Modeling and post processing scheme

### § 7.3 Weather – climate regions according DWD

For external weather conditions the Test Reference Year (TRY) from Deutscher Wetterdienst (DWD). For 2010 normal weather has been applied. The 15 test reference years covers the 15 climate regions in Germany defined by DWD. The author relinquished on application of extreme winter or extreme summer test reference years.

## § 7.4 Residential home

The residential home is configured to cover the living and working behaviour of both a typical four head family with children with compulsory schooling as well as active mostly retired but persons who daily take care for their grandchildren in their home.

### § 7.4.1 Calendar

Simulations covered an entire year period with 365 considered days. Thus a calendar was defined considering four different types of days, which differ in occupational presence. The calendar

bases on the four *day types* :

1.) *Wochentag (week day)*

2.) *Wochenende (week end)*

3.) *Abwesend/U. (absent, vacation)*

4.) *Urlaub daheim (rest (time) at home)*

The calendar (see Fig.7.3) considers typical statutory holidays in Germany and a mean vacation time at turn of the year, Easter holidays, summer and autumn holidays.

Woche	Montag	Dienstag	Mittwoch	Donnerstag	Freitag	Samstag	Starten Sonntag
1							Urlaub dahoam
2	Urlaub dahoam	Wochenende	Wochenende				
3	Wochentag	Wochentag	Wochentag	Wochentag	Wochentag	Wochenende	Wochenende
4	Wochentag	Wochentag	Wochentag	Wochentag	Wochentag	Wochenende	Wochenende
5	Wochentag	Wochentag	Wochentag	Wochentag	Wochentag	Wochenende	Wochenende
6	Wochentag	Wochentag	Wochentag	Wochentag	Wochentag	Wochenende	Wochenende
7	Wochentag	Wochentag	Wochentag	Wochentag	Wochentag	Wochenende	Wochenende
8	Wochentag	Wochentag	Wochentag	Wochentag	Wochentag	Wochenende	Wochenende
9	Wochentag	Wochentag	Wochentag	Wochentag	Wochentag	Wochenende	Wochenende
10	Wochentag	Wochentag	Wochentag	Wochentag	Wochentag	Wochenende	Wochenende
11	Wochentag	Wochentag	Wochentag	Wochentag	Wochentag	Wochenende	Wochenende
12	Wochentag	Wochentag	Wochentag	Wochentag	Wochentag	Wochenende	Wochenende
13	Wochentag	Wochentag	Wochentag	Wochentag	Wochentag	Wochenende	Wochenende
14	Wochentag	Wochentag	Wochentag	Wochentag	Wochentag	Wochenende	Wochenende
15	Wochentag	Wochentag	Wochentag	Wochentag	Wochentag	Wochenende	Wochenende
16	Urlaub dahoam	Wochenende	Wochenende				
17	Wochentag	Wochentag	Wochentag	Wochentag	Wochentag	Wochenende	Wochenende
18	Wochentag	Wochentag	Wochentag	Wochentag	Wochentag	Wochenende	Wochenende
19	Wochentag	Wochentag	Wochentag	Wochentag	Wochentag	Wochenende	Wochenende
20	Wochentag	Wochentag	Wochentag	Wochentag	Wochentag	Wochenende	Wochenende
21	Wochentag	Wochentag	Wochentag	Wochentag	Wochentag	Wochenende	Wochenende
22	Wochentag	Wochentag	Wochentag	Wochentag	Wochentag	Wochenende	Wochenende
23	Wochentag	Wochentag	Wochentag	Wochentag	Wochentag	Wochenende	Wochenende
24	Wochentag	Wochentag	Wochentag	Wochentag	Wochentag	Wochenende	Wochenende
25	Wochentag	Wochentag	Wochentag	Urlaub dahoam	Urlaub dahoam	Wochenende	Wochenende
26	Wochentag	Wochentag	Wochentag	Wochentag	Wochentag	Wochenende	Wochenende
27	Wochentag	Wochentag	Wochentag	Wochentag	Wochentag	Wochenende	Wochenende
28	Wochentag	Wochentag	Wochentag	Wochentag	Wochentag	Wochenende	Wochenende
29	Wochentag	Wochentag	Wochentag	Wochentag	Wochentag	Wochenende	Wochenende
30	Wochentag	Wochentag	Wochentag	Wochentag	Wochentag	Wochenende	Wochenende
31	Urlaub dahoam	Wochenende	Wochenende				
32	Wochentag	Wochentag	Wochentag	Wochentag	Wochentag	Wochenende	Wochenende
33	Wochentag	Wochentag	Wochentag	Wochentag	Wochentag	Wochenende	Wochenende
34	Urlaub dahoam	Wochenende	Wochenende				
35	Urlaub dahoam	Urlaub dahoam	Wochentag	Wochentag	Wochentag	Wochenende	Wochenende
36	Wochentag	Wochentag	Wochentag	Wochentag	Wochentag	Wochenende	Wochenende
37	Wochentag	Wochentag	Wochentag	Wochentag	Wochentag	Wochenende	Wochenende
38	Wochentag	Wochentag	Wochentag	Wochentag	Wochentag	Wochenende	Wochenende
39	Wochentag	Wochentag	Wochentag	Wochentag	Wochentag	Wochenende	Wochenende
40	Wochentag	Wochentag	Wochentag	Wochentag	Abwesend/U	Abwesend/U	Abwesend/U
41	Abwesend/U	Urlaub dahoam	Wochentag	Wochentag	Wochentag	Wochenende	Wochenende
42	Wochentag	Wochentag	Wochentag	Wochentag	Wochentag	Wochenende	Wochenende
43	Wochentag	Wochentag	Wochentag	Wochentag	Wochentag	Wochenende	Wochenende
44	Wochentag	Wochentag	Wochentag	Wochentag	Wochentag	Wochenende	Wochenende
45	Wochentag	Urlaub dahoam	Urlaub dahoam	Wochentag	Wochentag	Wochenende	Wochenende
46	Wochentag	Wochentag	Wochentag	Wochentag	Wochentag	Wochenende	Wochenende
47	Wochentag	Wochentag	Urlaub dahoam	Wochentag	Wochentag	Wochenende	Wochenende
48	Wochentag	Wochentag	Wochentag	Wochentag	Wochentag	Wochenende	Wochenende
49	Wochentag	Wochentag	Wochentag	Wochentag	Wochentag	Wochenende	Wochenende
50	Wochentag	Wochentag	Wochentag	Wochentag	Wochentag	Wochenende	Wochenende
51	Wochentag	Wochentag	Wochentag	Wochentag	Wochentag	Wochenende	Wochenende
52	Wochentag	Wochentag	Wochentag	Wochentag	Wochentag	Urlaub dahoam	Urlaub dahoam
53	Abwesend/U	Urlaub dahoam	Abwesend/U	Abwesend/U	Abwesend/U	Urlaub dahoam	Urlaub dahoam

FIGURE 7.3 Yearly calendar

## § 7.4.2 Building physics – Residential home

The residential building is a four-head family home with 174,7 m<sup>2</sup> heated living area (see Fig.7.4/7.5). It is designed in accordance with the Energieeinsparverordnung (EnEV) 2016 [200]. Thus, all building elements full fill the requirements of Anlage 3, Tab. A1, for indoor temperature  $T_i > 19^\circ\text{C}$  [201].

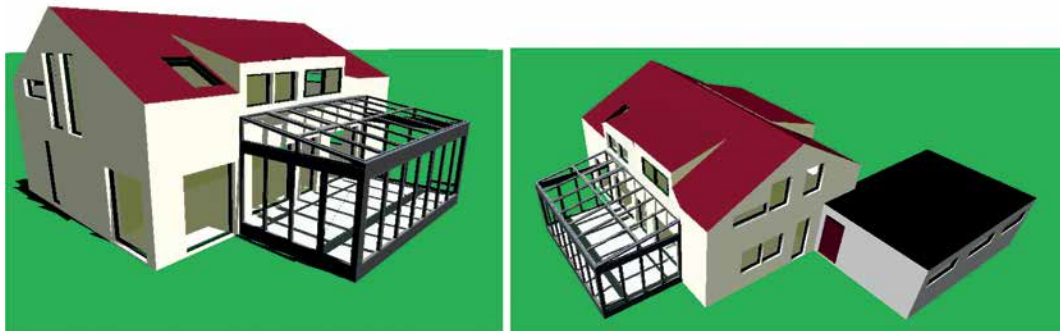


FIGURE 7.4 3D model of simulation model : reference variant

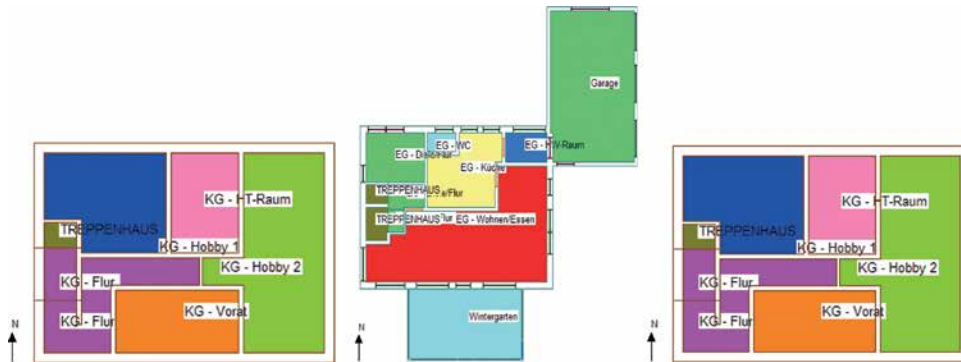


FIGURE 7.5 Functional ground floor schemes, zoning : basement, ground floor, 1. level

The overall H't value for buildings build in 2016 has to undergo the H't value of a reference building required for 2014 (0,51 Wm<sup>2</sup>K) for 25%. This results in a mean transmission value of the entire heat transmitting envelope area of 0,38 W/m<sup>2</sup>K.

The building profits from a basement, a ground floor and a first level. A car garage is aligned on the east side connected with the utility room.

The *transmission values (U-value in W/m<sup>2</sup>K)* for the building elements delineate as follows:

• <i>Bottom slab :</i>	<i>0,149 W/m<sup>2</sup>K</i>
• <i>Elevating walls touching ground (basement) :</i>	<i>0,162 W/m<sup>2</sup>K</i>
• <i>External walls :</i>	<i>0,160 W/m<sup>2</sup>K</i>
• <i>Window panes, double :</i>	<i>1,00 W/m<sup>2</sup>K</i>
	<i>LT : 73% ; g : 62%</i>
• <i>Window panes, double shaded externally:</i>	<i>1,00 W/m<sup>2</sup>K</i>
	<i>LT : 8,5% ; g : 10%</i>
• <i>Windows :</i>	<i>1,30 W/m<sup>2</sup>K</i>
• <i>Main entrance door :</i>	<i>1,80 W/m<sup>2</sup>K</i>
• <i>Floor slabs :</i>	<i>0,49 W/m<sup>2</sup>K</i>
• <i>Double pitch roof :</i>	<i>0,130 W/m<sup>2</sup>K</i>
• <i>Dormer roof :</i>	<i>0,186 W/m<sup>2</sup>K</i>
• <i>Pitch window :</i>	<i>1,90 W/m<sup>2</sup>K</i>

### § 7.4.3 Sun Protection

---

Sun protection was applied as external roller blind with a distance to #1 of 80 mm. All windows are shaded from 08 to 21 o'clock in the period from April to end of September.

### § 7.4.4 Zone Conditioning

---

All zones in the residential home as well the sun space are determined by internal gains [202,203] and heating controls. Internal gains are defined each a zone as follows:

*Infiltration :* all 0,1 (24 hours)  
Pidgeon 2,5 (24 hours)

*Lighting :* living / kitchen 5W/m<sup>2</sup>  
(weekend, vacation home 7-8; 20-23)  
(week 6-8;18-22)  
0W/m<sup>2</sup> (vacation away 19-8)

bathes 10W/m<sup>2</sup>  
(weekend, vacation home 8+23)  
(week, 7+22)

0W/m<sup>2</sup> (vacation away 0)

kitchen 10 W/m<sup>2</sup>  
(weekend, vacation home 8-9; 19-20)  
(week 7-8; 18-19)

0 W/m<sup>2</sup> (vacation home)

sleeping 3 W/m<sup>2</sup> (weekend, vacation home 8+23)  
(week 7+22)

0 W/m<sup>2</sup> (vacation away)

sleeping guest/children 5 W/m<sup>2</sup> (weekend, vacation home 7+22)

0 W/m<sup>2</sup> (week, vacation away)

stairways, corridors 3 W/m<sup>2</sup> (weekend, week, vacation home  
6-8;18-22)

3 W/m<sup>2</sup> (vacation away 6-8;18-8)

*Sensible Gains Occupants :*

living 5W/m<sup>2</sup> (weekend, vacation home 8-9;  
17-23)  
(week 6-8;18-22)

0W/m<sup>2</sup> (vacation away 24 hours)

kitchen 7W/m<sup>2</sup> (weekend, vacation home 8-9; 19-  
20)  
(week 7-8;18-19)

0W/m<sup>2</sup> (vacation away 24 hours)

bathes 15W/m<sup>2</sup> (weekend, vacation home 8+23)  
(week, 7+22)

0W/m<sup>2</sup> (vacation away 0)

sleeping 8 W/m<sup>2</sup> (weekend, vacation home 0-8)  
(week 23-6)

0 W/m<sup>2</sup> (vacation away)

sleeping guest/children 6 W/m<sup>2</sup> (weekend, vacation home 0-8)  
0 W/m<sup>2</sup> (week, vacation away)

stairways, corridors 3 W/m<sup>2</sup> (weekend, week, vacation home  
6-8;18-20)

0 W/m<sup>2</sup> (vacation away 24 hours)

### Equipment:

living	2W/m <sup>2</sup> (weekend, vacation home 8-9; 17-23) (week 7-8;20-23)
	0W/m <sup>2</sup> (vacation away 24 hours)
kitchen	120W/m <sup>2</sup> (weekend, vacation home 8-9; 19-20) (week 7+22)
	0W/m <sup>2</sup> (vacation away 24 hours)
bathes	60W/m <sup>2</sup> (weekend, vacation home 8+23) (week, 7+22)
	0W/m <sup>2</sup> (vacation away 0)
sleeping	0 W/m <sup>2</sup> (24 hours)
sleeping guest/children	0 W/m <sup>2</sup> (24 hours)
stairways, corridors	0 W/m <sup>2</sup> (2 hours)

#### § 7.4.4.1 Thermostats

---

Living room, kitchen, the utility room and the bath rooms, corridors and stair ways as well as the guest rest room profit from 20°C set point [204] temperature during the year. If occupants are on vacation, the set point is set to 16°C. The sleeping rooms up-stairs are set on 16°C during occupation, on 12°C minimum on vacation. The rooms in the basement profit from 16°C during the year without occupation and from 20°C with occupation.

## § 7.5 Sun Space

The sun space is an alumina-extruded profile construction (Fig. 7.6), which profiles are thermally decoupled. All construction jointing of the frame construction to adjoining constructional elements are sealed airtight according requirements of DIN 4108 in order to eliminate infiltration.



FIGURE 7.6 3D model of sun space simulation model : reference variant

### § 7.5.1 Building physics – sun space

- *Bottom slab :* 0,162 W/m<sup>2</sup>K
- *Vertical glazing, double glazing :* 1,10 W/m<sup>2</sup>K  
LT : 73% ; g : 62%
- *Vertical glazing, double glazing, shaded externally :* 1,10 W/m<sup>2</sup>K  
LT : 8,5% ; g : 10,2%

• <i>Inclined roof glazing, double, safety, 30° :</i>	1,62 W/m <sup>2</sup> K
	LT : 62%; g : 51%
• <i>Inclined roof glazing, double, safety, shaded internally, 30° :</i>	1,62 W/m <sup>2</sup> K
	LT : 4,6%; g : 4,2%
• <i>Inclined roof glazing, double, safety, shaded externally, 30° :</i>	1,62 W/m <sup>2</sup> K
	LT : 4,6%; g : 8,1%
• <i>Window, double glazing, see above :</i>	1,30 W/m <sup>2</sup> K
• <i>Tilt window, double glazing, see above :</i>	1,62 W/m <sup>2</sup> K
• <i>Door window, double glazing, see above</i>	1,60 W/m <sup>2</sup> K
• <i>Fold-works, three-part :</i>	1,60 W/m <sup>2</sup> K
• <i>Fold-works, four-part :</i>	1,60 W/m <sup>2</sup> K
• <i>Ventilation flap :</i>	1,75 W/m <sup>2</sup> K
• <i>Roof sliding window (Aaero : 0,29 m<sup>2</sup>) :</i>	1,92 W/m <sup>2</sup> K
• <i>Separation element (door window):</i>	1,60 W/m <sup>2</sup> K

### § 7.5.1.1 Aperture opening rules

The sun space contains three different element groups for natural ventilation. These groups have different functions and yet are controlled by specific control rules. The first group considers a door window of (0,8\*2,11 m) Ageom = 1,69 m<sup>2</sup> opening area and Aaero = 1,10 m<sup>2</sup> free aerodynamic opening area.

The second group covers an automatically controlled ventilation flap located in the socket of a sun space vertical side façade and a sliding window placed in the upper half of the glazed and 30° inclined roof. The ventilation flap profits from (0,6\*0,1 m)  $A_{\text{geom}} = 0,06 \text{ m}^2$  opening area and  $A_{\text{aero}} = 0,04 \text{ m}^2$  free aerodynamic opening area, while the sliding window accounts for (0,6\*0,8 m) effective  $A_{\text{geom}} = 0,48 \text{ m}^2$  opening area and  $A_{\text{aero}} = 0,317 \text{ m}^2$  free aerodynamic opening area. Sliding window in combination with the opposed located ventilation flap always simultaneously open in order to establish laminar flow with sufficient naturally induced suction.

The third group covers to different fold-works being part of the main south, respectively west, oriented vertical façade and the 90° turned side façade. The main façade in the 3D model contains a four-part fold-work with W/H = 4,0m x 2,10m, resulting in an effective  $A_{\text{geom}} = 7,8 \text{ m}^2$  opening area and  $A_{\text{aero}} = 5,07 \text{ m}^2$  free aerodynamic opening area. Opposed to that, the side façade incorporated a three-part fold-work with W/H = 3,0m x 2,10m, resulting in an effective  $A_{\text{geom}} = 5,76 \text{ m}^2$  opening area and  $A_{\text{aero}} = 3,74 \text{ m}^2$  free aerodynamic opening area.

## Opening controls

---

### A.) The door window in separate wall

The door window in the separation wall between sun space and adjacent living room functions as entrance and logically opens first exclusively in accordance to the presence of the space occupants and secondly in between rational occupational time between 6 AM and 11 PM. The door is closed during nights.

Living space dry bulb temperature is remained on 20°C by thermostat. The door window is exclusively opened by space occupants, when sun space dry bulb temperature exceeds 22°C. This rule ensures no heat losses by air movements from the living to the sun space, but rather enforced preheating benefits of the sun space for the living room.

If sun space dry bulb temperature exceeds 28°C, the doors closes.

### B.) The sliding window + ventilation flap

The sliding window and the ventilation flap opens automatically every day a year if raining is excluded. The aperture open when dry bulb temperature exceed 22,0°C and a wind velocity < 10 m/s is assured.

### C.) The fold-works

Fold-works are opened exclusively on schedule days with space occupants being present. Fold-works are opened by the occupants by hand during 6 o'clock in the morning and closes the late at 23 o'clock in the evening. The fold-works are opened solely in time with no precipitation, when interior sun space dry bulb exceeds  $23,5^{\circ}\text{C}$  and external temperature is lower dry bulb temperature. This rule promotes natural cooling of the sun space in risk of overheating instead of further up heating by external temperature. The fold-works are latest closed when air velocity exceeds 10 m/s

## § 7.5.2 Sun Protection

---

Sun protection was applied on every glazed sun space surface. In the reference models, which calculate passive solar gains, sun protection was applied on the outer surfaces of glazing, as well as in the rafter integrated solar thermal collector models. In case of the roof glazing integrated photovoltaic modules, sun protection was applied on the inner surfaces.

Sun protection was established as roller blinds [205]. For each a sun space orientation the schedules were configured in order to optimize passive solar gains and minimizing hours with overheating.

Fabric blinds were applied which provided an radiation transmission value of 0,07, an radiation reflection value of 0,4 what results in an  $F_c$ -value of 0,15. The glazing-blind combination profits from a resulting gtotal value for inclined units of 0,08 and 0,10 for vertical units respectively.

### § 7.5.2.1 Schedule of sun protection (substitute element schedules)

---

<i>For south orientation :</i>	day 90 to 120 : 8AM to 15PM	(31.03. – 30.04.)
	day 121 to 150 : 8AM to 18PM	(01.05. – 30.05.)
	day 151 to 242 : 8AM to 22PM	(31.05. – 30.08.)
	day 243 to 272 : 12AM to 16PM	(31.08. – 29.09.)

*For east orientation :*

day 91 to 120	: 10AM to 14PM	(01.04. – 30.04.)
day 121 to 243	: 8AM to 22PM	(01.05. – 31.08.)
day 244 to 273	: 10AM to 14PM	(01.089. – 30.09.)

*For west orientation :*

day 91 to 120	: 10AM to 15PM	(01.04. – 30.04.)
day 121 to 150	: 11AM to 22PM	(01.05. – 30.05.)
day 151 to 242	: 8AM to 22PM	(31.05. – 30.08.)
day 243 to 274	: 11AM to 16PM	(31.08. – 01.10.)

### § 7.5.3 Zone Conditioning

---

*Infiltration :* all 0,25 (24 hours)

*Lighting :*

*Summer*

4W/m<sup>2</sup> (weekend, vacation home 21-23)  
(week 21-23)

*Winter*

4W/m<sup>2</sup> (weekend, vacation home 8-11;  
17-22)

(week 6:30-7:30;17-22)

0W/m<sup>2</sup> (vacation away 19-8)

Internal gains were in accordance with [202] and [201].

### *Sensible Gains Occupants :*

7W/m<sup>2</sup> (weekend, vacation home 8-11; 13-23)  
(week 6:30-7:30;17-22)

0W/m<sup>2</sup> (vacation away 24 hours)

### *Equipment :*

6W/m<sup>2</sup> (weekend, vacation home 8-11; 13-23)  
(week 6:30-7:30;17-22)

0W/m<sup>2</sup> (vacation away 24 hours)

#### § 7.5.3.1 Thermostats

---

For the sun space thermostats were not configured since heating bases on passive solar gains and contribution by façade integrated collectors. Since renewable energies suffer from fluctuations, provision strongly depends daily contributions and storage capacities and thus thermostats are not reasonable.

#### § 7.6 Sun space floor heating

---

The floor heating of the sun space is established as an individual zone volume beneath the actual space volume separated from solid and conductive building mass (60mm screed, 20mm natural stone floor tiles). The floor heating zone covers the entire space area and constitutes with 100mm width a total volume of approx. 2,5m<sup>3</sup>

Beneath the zone a typical construction layers 20 mm screed, 65 mm solid thermal insulation, 160 mm concrete and 120 mm solid thermal insulation, hence models a typical thermally insulated floor heating/ground slab construction.

## § 7.6.1 Zone Conditioning

---

In TAS the radiant proportion is set to 0,65, while the view coefficient is set to 0,26, in order to specifically model a surface heater device, floor heating respectively. Likewise, the TAS convection coefficient accounts for 4 W/m<sup>2</sup>C.

TAS thermostat control is activated with 2 Kelvin control band.

In order to simulate and analyse a day specific heating power (heating energy in kWh) dependant from remaining storage capacity, the zone heating power is always set on "non-sized" in order to size individually in accordance to capacity.

In case of the solar thermal direct supply or sorption storage supply the specific heat capacity of the flow mass is reduced since from both solar thermal collector and sorption storage the heat is freed by either a (70%/30%) water/glycol agent or a thermo-oil.

Thus the gravimetric heat capacity of the source firstly reduced from 4,2 kJ/kg\*K to 3,65 kJ/kg\*K and secondly reduced by 75% in order to model the efficiency of a required water/oil or water/water-glycol heat exchanger.

## § 7.6.2 Inter-zonal Air Movements (IZAMS)

---

Running the floor heating is realized in the TAS models via inter-zonal air movements (IZAMs). Since the floor heating zone actually represents a single zone with specific volume, this functions allows air volumes that are up heated in a origin "boiler" zone to enter the floor heating zone secondly, to exchange heat to the floor heating surfaces and finally to exit the floor zone secondly again.

Thus, a mass flow can be modelled heating up the floor heating zone. The mass flow can be configured in kilogram per seconds (kg/s). Since this TAS function handles on "air" volumes, the specific density of water is to be applied to actually simulate water mass flow. With applying the water specific heat capacity of 4,2 kJ/kg\*k a specific mass flow of 0,058 kg/s has been evaluated by test to be the most realistic and effective one for the models.

In consequence, the models were programed with

*1.) IZAM Boiler-in : feeding the boiler zone with outside air mass flow 0,058 kg/s*

*2.) IZAM Floor Heating-in : feeding the floor heating zone with heated air mass flow 0,058 kg/s from the boiler zone*

*3.) IZAM Floor Heating-out : freeing the floor heating zone from cool air mass flow 0,058 kg/s to outside*

All IZAMs are scheduled from 4 to 10PM in order to preheat the floor heating zone one hour of the preferred occupational time in front.

---

## § 7.7 Collector systems

---

The inspected versions for climate region (TRY) 01 (Bremerhaven), 04 (Berlin), 05 (Köln) and 13 (München) consider two different façade integrated collector technologies. Photovoltaic wafers are incorporated in inclined roof glazing, while evacuated tubes are integrated in sun space rafters.

### § 7.7.1 Sun space roof glazing embedded photovoltaic modules

---

The entire roof glazing is substituted by glass embedded photovoltaic modules (Fig. 7.7). Mono-crystalline cell technology is chosen in order to provide maximum possible area-related yield and power. The cell architecture bases on squared wafers with back bars and backside passivation layer for maximum yield. The glazing as overhead glazing is made from safety and tempered glass on the space adjacent side. Safety glass is required to prevent fall down in case of glass collapse. Hence, wafers are embedded between pane 2 and 3, between #4 and #5 and are distanced in order to provide 20% remaining transparency.

Transparency factor in the 3D model is realized by first homogeneous pv areas and related areas of common overhead glazing (20%).

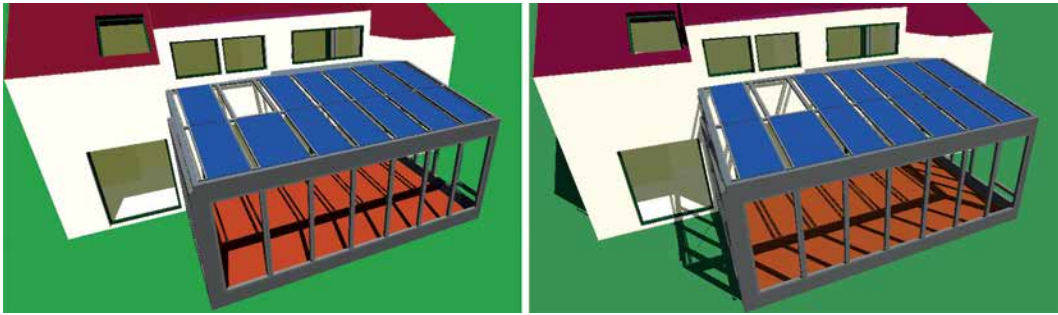


FIGURE 7.7 3D model of sun space variant equipped with roof glazing incorporated photovoltaic modules

Each a module assesses with standard test conditions an area-wise maximum power output of 140 W/m<sup>2</sup> at irradiation STG 1.000 W/m<sup>2</sup> and 1,5 AM (air mass).

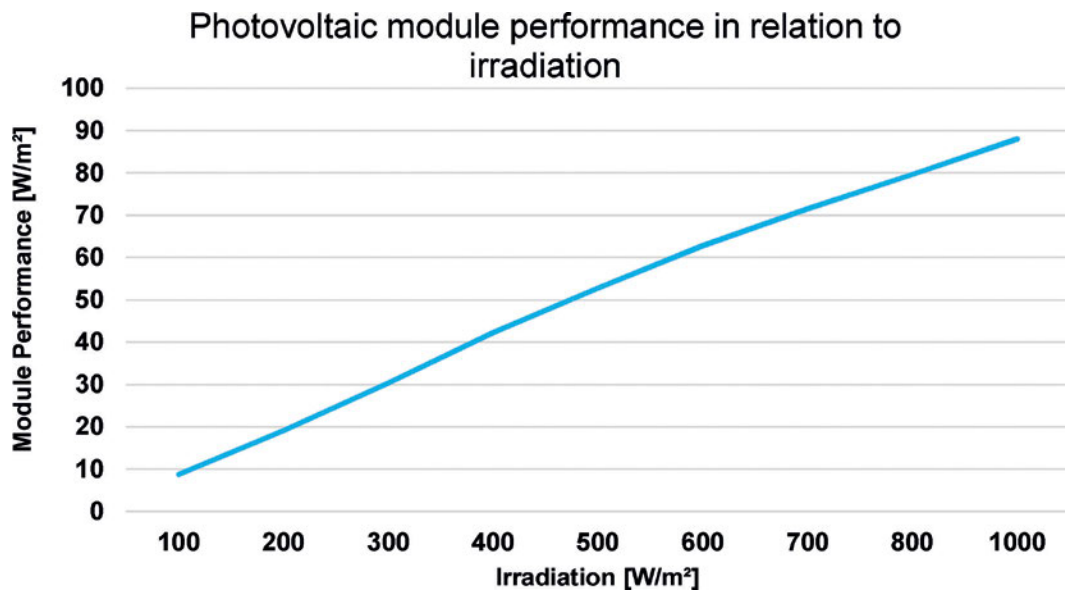


FIGURE 7.8 Module performance [W/m<sup>2</sup>] in relation to irradiation [W/m<sup>2</sup>]

Cell efficiency of 18,2% at 25°C module temperature is reduced by a mean reduction factor of 7% for environmental pollution, 3% for wiring and diodes. Potential induced cell degradation (PID) accounts annually with 0,55%. The remaining cell efficiency after 5 years operation accounts in total with 87,5%. Cell efficiency further changes, decreases respectively, by module temperature increase. Hence, the efficiency lowers for -0,45% for each Kelvin difference above 25°C reference temperature (Fig.7.8).

The hourly output of the pv plant is calculated based on the .tsd-file with TAS macro "PV output v1.4" from 11-25-2011. In terms of calculation the cell efficiency is linearly reduced related to irradiation with "0" W/m<sup>2</sup> at 0 W/m<sup>2</sup>, "51" W/m<sup>2</sup> at 500 W/m<sup>2</sup> and "89" W/m<sup>2</sup> at 1.000 W/m<sup>2</sup> irradiation.

### § 7.7.2 Sun space rafter integrated evacuated solar thermal tube collector

The second modelled collector system bases on the product development previously described in chapter 06. Thus, the main technical key parameter are given in chapter six. They will be repeated and added by the performance criteria listed below. Figure 7.9 visualizes the physical arrangement and appearance of the HEATBEAM II© integrated into the sun space roof. To each a rafter a collector is accompanied. The visualization also demonstrates, that the corner rafters profit from two collectors since their width offers enough space. The effective length and aperture area of the solar thermal collector is limited by true (effective) the rafter length to 3750 mm.

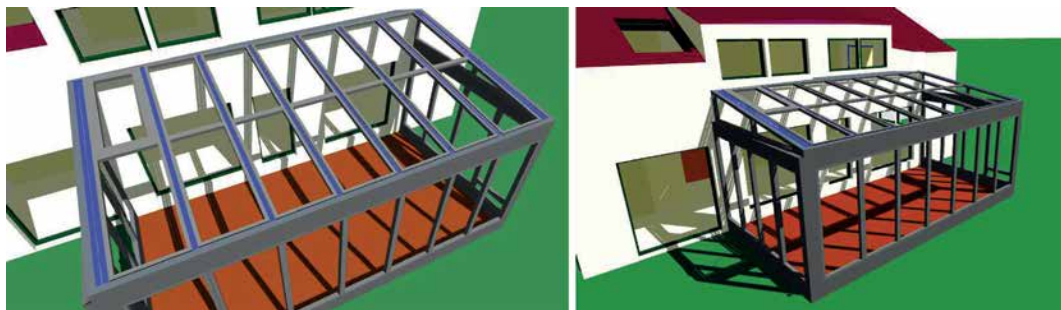


FIGURE 7.9 3D model of sun space variant equipped with rafter integrated evacuated tube collectors and heat exchanger

The applied *performance parameters* in the model are as following:

- *Absorber absorption/emission ratio* :  $\alpha/\varepsilon = 96/5 = 19$
- *remaining pressure absorber cavity* :  $p : 10 - 50 \text{ mbar}$
- *light transmission polymer cover* :  $LT = 89\%$
- *internal conductance of the absorber sheet* :  $U_{int} = \approx 50 \text{ W/m}^2\text{K}$
- *collector conversion factor* :  $\eta_0 = 70\%$
- *transmission factor 1. order* :  $a_1 = 1,12 \text{ W/m}^2\text{K}$
- *transmission factor 2. order* :  $a_2 = 0,004 \text{ W/m}^2\text{K}^2$
- *maximum power* :  $q_{th, L3750} = 146 \text{ W}$  at  $STG : 1.000 \text{ W/m}^2\text{K}$ ,  $AM 1,5$
- *heat capacity transport fluid (water/glycol:70/30%)*  $C : 3,65 \text{ kJ/Kg}^*K$

In sum the 25m<sup>2</sup> sun space incorporates 10 HEATBEAM© units with in total (0,06m\*3,75m) 2,25 m<sup>2</sup> aperture area and with each P<sub>th,peak</sub> = 146 Watt. The total plant power is approximately 1.460 Watt.

---

## § 7.8 Seasonal energy storage systems

---

Two different storage technologies were applied and investigated in terms of seasonal performance. First, an electro-chemical battery storage and second a loss-free thermo-chemical sorption storage. Performance criteria a described in this section.

## § 7.8.1 Electro-chemical storage

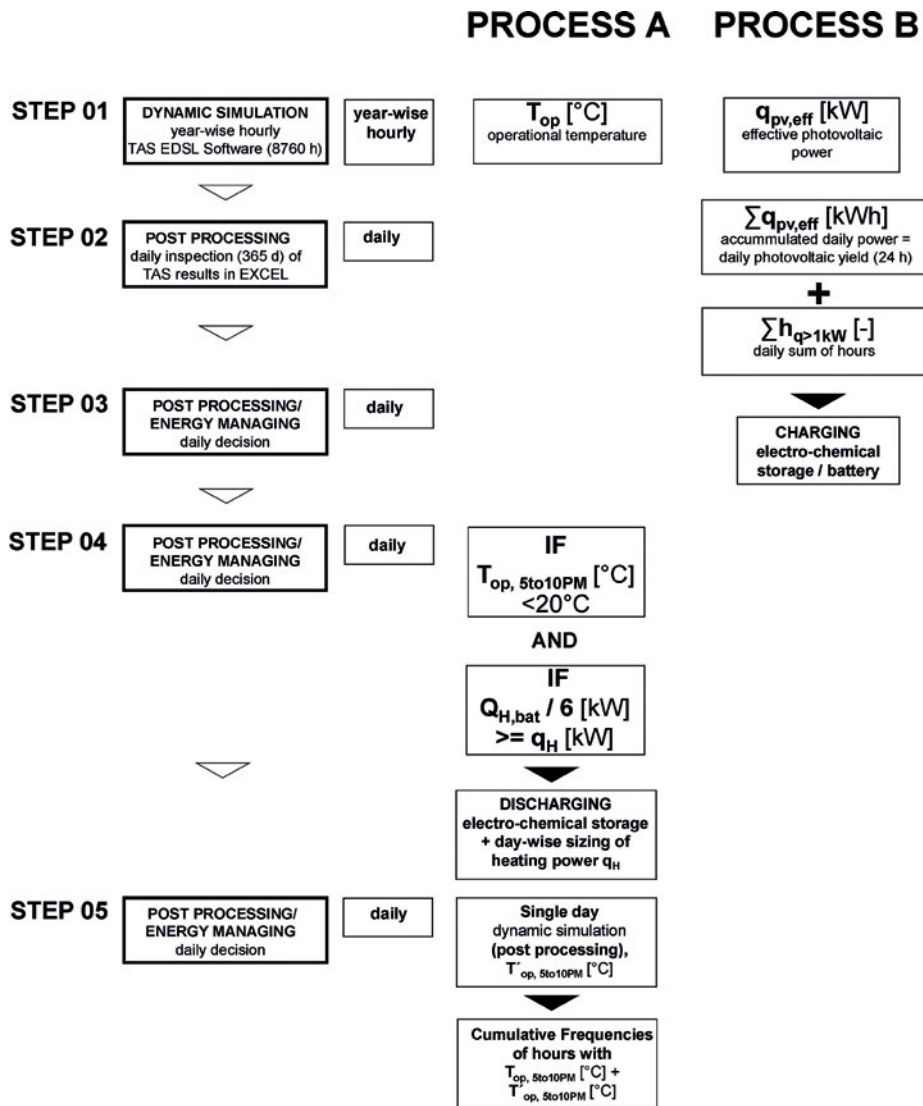


FIGURE 7.10 Post processing scheme for improvement of operational temperature with photovoltaic collector and battery storage system

As electro-chemical storage was chosen a lithium-ion secondary cell pack. One module provides a storage capacity of 6,8 kWh. The accumulator rack can be enlarged modular. The storage contains 3 modules and covers a total capacity of 20,4 kWh. Figure 7.10 visualizes the post processing routine of battery charging, discharging, running the ohmic heater in the sensible water storage and feeding the floor heating.

The electro-chemical accumulator is technically determined by the following *performance parameter* :

1. Operational voltage :	55 Volts
2. Nominal capacity 1C [Ah] :	121,5 Ah
3. Storage capacity total rack [kWh <sub>nom</sub> ] :	20,4 kWh
4. Depths of Discharge (DoD) >SOH = 80% :	20%
5. Effective storage capacity total rack [kWh <sub>eff</sub> ] :	16,2 kWh
6. Charge efficiency [%] :	97%
7. Specific Peukert´scher Exponent :	ca. 1,05
8. Monthly loss rate [%] :	3%+(1%*m)
9. Maximum discharge current/energy 1C (1h):	121,5 Ah, 16,0 kWh
Maximum discharge current/energy 0,2C (5h):	24,3 Ah, 3,2 kWh
Maximum discharge current/energy 0,1C (10h):	12,1 Ah, 1,6 kWh

### § 7.8.1.1 DC/AC converter

Battery DC power is converted into AC power by a DC/AC converter in order to run an ohmic heater for tank water heating. The DC/AC converter manage to provide 3 phases of each a power output of 1.500 Watts.

Thus, the maximum output power of the converter is 4.5 kW<sub>peak</sub>. The converter is suitable for a photovoltaic plant peak power up to 2,25 kW<sub>p</sub> and for a battery capacity of 25 kWh. The maximum efficiency coefficient accounts for 96%, whereas the European efficiency coefficient considering European climate and irradiation changes is limited to 94,5%.

The ohmic heater efficiency is given with 98%.

In order to calculate the effective heating power reliable for the water tank the battery power output (capacity) is reduced by first by 5,5% (converter) and second by 2% (ohmic heater). Consequently, the actual required power is enlarged by firstly 1,058 and secondly by 1,021 and finally multiplied with 6 in order to figure the required energy demand (kWh) for a preheating from 16 to 17 o'clock and for further 5 hours (5 to 10PM) supply. Auxiliary energy consumed by the converter is already considered with the losses.

### § 7.8.1.2 Applied pv module-converter-battery algorithms

---

Hourly calculated power is summed each a day. The sum is reduced by a module efficiency factor 0,99 considering dirt and pollution and by an battery charger efficiency factor of 0,98. Effectively, 97,02% of the generated power is charged. The battery spends maximum 16,2 kWh of electrical power, since 4,2 kWh of capacity needs to remain in order to assure 20% of 20,4 kWh base charge, depth of discharge respectively (DoD = 20%). Power charged in the electro-chemical storage encounters monthly losses of once 3% and additional 1% each a month.

That results in total in 9% charge losses of the lithium-Ion battery within six month. Related to day level, the lithium-ion accumulator encounters losses of 0,0008% per day.

In summer time or periods without any demand the losses account day-wise and accumulate until power is requested. The DC/AC converters manages to convert 94,5 % of the required power into DC power. The Ohmic heater heating up the sensible tank water itself manages to convert 09% of the power into heat. Hence, power in questions always is limited by 5,5% and subsequently by 2%, hence the requested power is enlarged by 1,08 respectively.

Since power for heating is required for 5 hours (5 to 10 PM) and the hour beforehand for preheating, the energy demand is calculated by :

$$Q_h = p_{h,eff} * 1,08 * 6 \quad [\text{kWh}] \quad (28)$$

While the reduction of power generated and effectively utilized energy is calculated by :

$$Q_h = \Sigma p_{eff,n} * 0,99 * 0,98 * (0,9992 * n + 1) * 0,945 * 0,98 * 6 \quad [\text{kWh}] \quad (29)$$

## § 7.8.2 Thermo-chemical storage

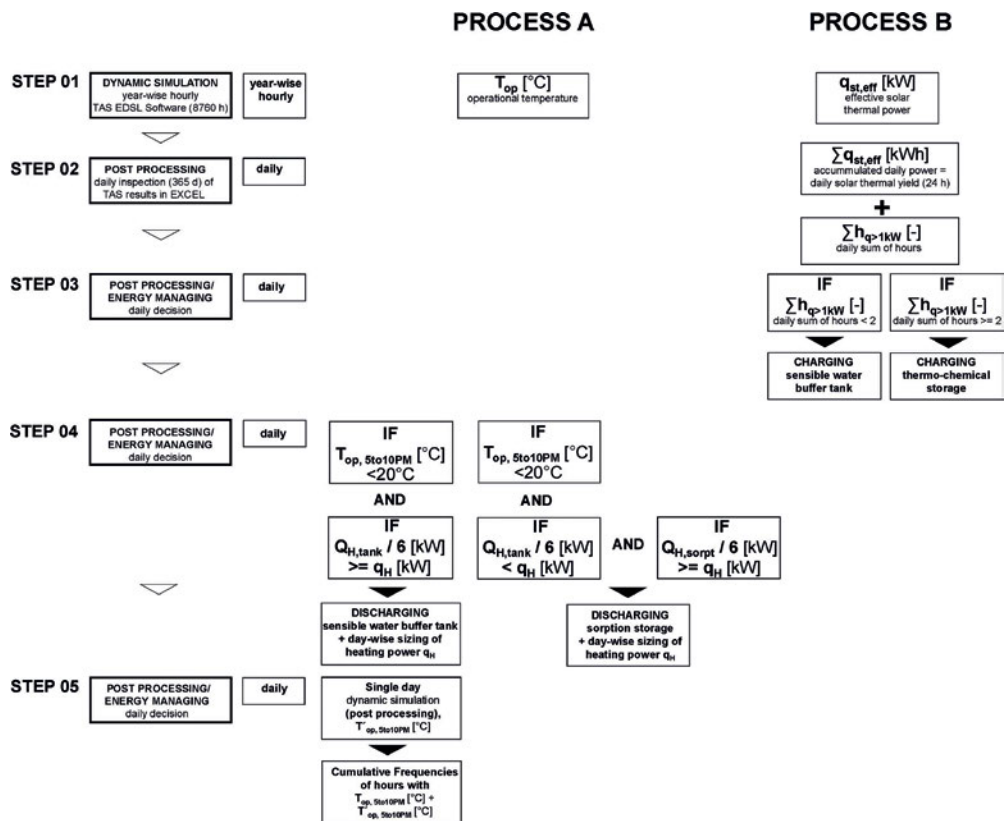


FIGURE 7.11 Post processing scheme for improvement of operational temperature with solar thermal collector and sorption storage system

Key issue of the thermo-chemical sorption storage technology that is focuses on in this investigational project is loss-free thermal energy storing. For that reason a sorption storage model was developed in Excel. This model applied in a post processing routine (Fig. 7.11) does not gain on a detailed calculation in order to model the entire physical process or to give detailed insight in any process step, but on conservation of 99% to 100% of the thermal energy that is generated in summer up to the winter period. Thus, the model reduces the amount of supplied thermal energy by the evacuated tube collector by several reduction ratios which represent different steps in the entire process in order to calculate the effective thermal energy that can be utilized for space heating in winter.

In this context literature review helped to identify rules and values to determine losses and degrees of efficiency. The model and the simulation calculations do not aim on a the complex modelling of a complex process, but on a conservative and reliable estimation of potential effective utilizable thermal energy. Auxiliary energy, that accounts for sorption processes much more intensive than for electro-chemical storage processes was calculated and reported separately.

### § 7.8.2.1 Charging and discharging strategy of sensible and thermo-chemical storage

---

The system allows alternative charging of a sensible water buffer tank and a loss-free thermos-chemical sorption storages. The choice which storage to charge depends first on the actual sensible water temperature of the sensible water tank and second on the number of hours with effective solar thermal power above 1.000 Watt.

The maximum acceptable sensible temperature of the sensible tank is limited to 95°C in order to avoid boiling and hence increase of internal pressure and volume exceedance. In order to define the actual storage capacity of the sensible tank, the water volume is heated by the effective solar thermal heating power. That calculation results in an actual water temperature. If water temperature is still below 95°C and the sun space continuously demands heating, solar heat heats the tank. If demand lowers in spring and summer months and the number of hours with solar thermal power exceeds 2, the energy is used to charge the sorption storage. If the sorption storage is charged during the day, hourly transmission losses of the sensible water tank continuously reduce water temperature and thus heating power.

During post processing water temperature and related maximum heating power of the 300L water volume is expressed hourly. Starting the day requires an inspection of the operational temperature between 5 to 10 PM. If heating demand occurs and the power

multiplied by six hours (kWh) can be covered by the sensible tank, the water volume is involved. Otherwise the sorption storage re-maining capacity is in question Heating demand and remaining charging capacity of both the sensible and the sorption storage are calculated hourly, respectively daily.

### § 7.8.2.2 The solar thermal collector cycle

The hourly solar thermal power calculated by TAS Shw output v2.3 has to be reduced to the effective solar thermal power that either can charge a sensible water buffer tank or a thermos-chemical sorption storage. Thus generation losses by environmental pollution (0,01%) and transmission losses for the piping ( $0,01 \text{ W/m}^2\text{K} * 6,0 \text{ m} * (T_{st} - T_{ex})$ ) are considered. The trans-mission value for the piping has been reduced from  $0,2 \text{ W/m}^2\text{K}$  [1] to  $0,01 \text{ W/m}^2\text{K}$  since the piping according to the HEATBEAM II© design bases on polymer tubing with comparably low conductance values (1/87 of stainless steel).

The transport fluid water in the solar thermal collector system is added by 30% anti-freezing agent (glycol). For that reason the specific energy capacity of  $\approx 4,2 \text{ kJ/kg}^*\text{K}$  is reduced to  $\approx 3,65 \text{ kJ/kg}^*\text{K}$ .

### § 7.8.2.3 The physical storage systems

Sensible water buffer tank For daily and sensible heat storage is selected a sensible water tank covering 300 litre effectively. The tank is thermally insulated superior that results in hourly thermal transmission losses of  $7 \text{ W/m}^3^*\text{K}$ . The temperature difference is calculated to a reference room temperature of  $20^\circ\text{C}$ . The actual water temperature is calculated and documented hourly. According to the water temperature a potential heating capacity in kW is expressed by the volume, the specific energy capacity and the difference of the water temperature towards a room temperature of  $20^\circ\text{C}$ . The maximum power divided by six hours of heating supply results in the actual maximum possible heating power and vice versa in the maximum potential heating energy demand.

$$T_{t10} [\text{°C}] = ((P_{st10} * 0,99 - (6\text{m} * 0,01\text{W} * P_{st10} * 0,057)) / 1000 / 300) \quad (30)$$

$$0,00101389 + (T_{t09} \text{°C} - ((7\text{W} * 0,3\text{m}^3 * (T_{t09} \text{°C} - 20^\circ\text{C})) / 1000 / 300 / 0,001166))$$

where :

$T_{t10}$  : actual water tank temperature (e.g. at hour 10)

$P_{s_{t10}}$  : effective power [W] (heat) generated by collector (e.g. at hour 10)

Efficiency ratio due to efficiency reduction by pollution : 0,99 (99%)

length of transport tubing (roof to basement) : 6 m

Heat losses of polymer transport tubing : 0,01 W/mK

Interpolation factor  $T_{coll,max}$  : 100°C;  $T_{house,min}$  : 20°C;  $\Delta T = 80K$ ,  $P_{max} = 1.406W$ ;  
 $80K/1.406W = 0,057$

Heat capacity transport medium water/glycol : 3,65 kJ/kg\*k = > 0,0010389 kWh/kg\*K

$T_{t9}$  : water tank temperature of the previous hour (e.g. at hour 9, respectively  $n-1$ )

hourly heat loss factor of 300L buffer tank : 7 W/m³K\*h

service room temperature : 20°C

Buffer tank volume : 0,3 m³ (300l)

Heat capacity of buffer tank water : 4,20 kJ/kg\*k = >0,001166 kWh/kg\*K

### § 7.8.2.4 Physical description of the thermo-chemical sorption storage

The storage contains an effective material volume of 1m³. Although a determination of material offers variability in a little range, the main criteria for material selection was high volumetric storage density, a charging temperature range between 100 and 180°C and cycle strength For that last reason the author excluded modern innovative composite material, that have been detected by literature review but concentrated on Zeolite 13X. Zeolite 13X allows 50% of volume to be dried (desorpted) with 100°C. Zeolite 13X is identified to provide a storage density of 220-250 kWh/m³.

Lass-Seyoum detected an effective storage density of 220 kWh/m² within a 1m³ storage project. The author considers a specific volume within the 1m³ storage material volume not to be affect by any thermal input related to limited material conductivity

and limited heat exchanger exchange capacity. This amount of material, that is thermally not included in the process is determined to be 15%, thus the effective volume is multiplied with 0,85. Since half of the material volume is desorptable with 100°C desorption temperature and another 50% requires 100 to 180°C, we decided, that the first half can be desorpted with simply losses of 5% (multiplication with 0,95), whereas the next half requires higher temperature and longer period of time is accounted with 15% losses (multiplication with 0,85). The author refer to the finding of Zettl, Englmaier, Steinmaurer and Reichl, 2014, who demonstrate the drying of the last 20-25% of the material volume requires extraordinary amounts of power and time. Thus, the desorption (drying) process in terms of time approximates asymptotic. For that reason we decided to consider 25% of the material volume as extreme energy intensive and hence not worth drying. In the consequence the effective volumetric storage capacity is reduced by another 25%. Finally, we consider an effective volumetric storage capacity of 150 kWh/m<sup>3</sup>.

#### § 7.8.2.5 Periphery equipment : pumps, heat exchanger, flow heater and free cooler

---

Between the water/glycol collector cycle and the storage heat exchanger is included another water/glycol–thermo oil heat exchanger. Lass Seyoum reports of a heat exchanger development, that was enhanced by 60% efficiency. Since heat exchanger efficiency of 100% is not realistic, we assumed an origin heat exchanger of 50% [206], that improved by 60% ends up in a heat exchanger efficiency of 75%, what finally is extraordinary good. An thermo oil pump pumps thermos oil of the second cycle into the storage containment onto the internal heat exchanger. The pump performance and pump power is regulated modular by an electronic frequency converter with a power demand of 25 Watt.

#### § 7.8.2.6 The Adsorption process

---

Since during adsorption the water evaporation causes cooling on the evaporator/condensator structure, additional heat is required to prevent the evaporator/condensator from freezing. For this a flow heater with a heating power of 1.200Watt is installed. A rotary pump pumps heated water into the evaporator, which consumes 460 Watt. In total for the adsorption process an electric power (25 Watt+1.200 Watt+460 Watt) of 1.685 Watt is required. Since an adsorption process is the most effective within the first 45 minutes, thus is modelled to last no longer than one single hour the total required auxiliary power accounts for 1.685 kWh per adsorption process (a day).

### § 7.8.2.7 The Desorption process

---

During desorption process heating the material by solar thermal heat causes material drying. Thus encapsulated water is freed and condensates in the evaporator/condensator device. This causes up heating and an increase in system pressure. An tremendous increase in system pressure is not desired, since it stops evaporation. Hence, the heated condensated water is re-cooled by a free cooler. This process lasts as long as desorption occurs (\*hours) and consumes additional 30 Watt for the pressure-free free-cooler ventilator. In total the desorption process including thermo-oil pump (25 Watt) and the rotary pump (460 Watt) consumes 515 Watt per hour. Each single day hours have been identified with >1.000 effective solar thermal power. Desorption exclusively starts on days with at least two hours of >1.000 Watt effective solar thermal power. The required auxiliary energy was calculated with 515 Watt multiplied with the number of hours with solar thermal power >1.000 Watt.

### § 7.8.2.8 Applied Sorption storage algorithms

---

#### Desorption (Chargin) :

---

If  $\Sigma h$  with  $p_{st,eff} > 1.000 \text{ W} >= 2$  :

*If storage volume charge status <50%*

$$Q_{ch,sorpt} [\text{kWh}] = \Sigma n_{0-24} P_{st,eff} * \epsilon_{ch'} < 50\% * \eta_{he,ch}$$

$$Q_{ch,sorpt} [\text{kWh}] = \Sigma n_{0-24} P_{st,eff} * 0,95 * 0,75$$

*If storage volume charge status >50%*

$$Q_{ch,sorpt} [\text{kWh}] = \Sigma n_{0-24} P_{st,eff} * \epsilon_{ch'} > 50\% * \eta_{he,ch}$$

$$Q_{ch,sorpt} [\text{kWh}] = \Sigma n_{0-24} P_{st,eff} * 0,80 * 0,75$$

where :

$Q_{ch,sorpt}$  = remaining heating energy charge [kWh]

$\Sigma n_{0-24} P_{st,eff}$  = daily accumulated effective solar thermal heating power [kW]

$\eta_{chr} < 50\%$  = charge efficiency with charge status <50% [%]

$\eta_{chr} > 50\%$  = charge efficiency with charge status >50% [%]

$\epsilon_{he,ch}$  = heat exchanger efficiency

### Adsorption (Discharging) :

---

$$Q_{disch,sorpt} \text{ [kWh]} = Q_{ch,sorpt} - q_H * d * \epsilon_{he,dis}$$

$$Q_{disch,sorpt} \text{ [kWh]} = Q_{ch,sorpt} - q_H * 6(h) * 1,25$$

where :

$Q_{disch,sorpt}$  = required discharged heating energy [kWh]

$Q_{ch,sorpt}$  = remaining heating energy charge [kWh]

$\epsilon_{he,dis}$  = compensation of heat exchanger losses, efficiency

$q_H$  = heating power

$d$  = durance in [h]



# 8 Comfort and yield analysis of dynamic modelling of passive and active sun space facades

## § 8.1 Evaluation of effectiveness of façade embedded collectors combined with seasonal storages

The thesis is structured by five constituted hypotheses. The hypotheses help gaining further descriptive knowledge about the potential of sun spaces to provide thermal comfort. Thermal comfort can be enhanced beside passive solar gains by additional collector technologies embedded in sun space envelopes.

This chapter analyses dynamic model based computed information in order to evaluate the quality of thermal comfort. Therefore, in the following, the five hypotheses are phrased again in order to remind:

5 Hypotheses :

I

*Cumulated frequencies of hours of resultant temperature > 20°C in order to determine indoor thermal comfort in SL80 Solarlux sun spaces according to DIN EN 15251-A regarding south directed 25m<sup>2</sup> dimensioned sun spaces in 15 different climate regions in Germany provided by renewable heating energy exclusively by solar gains are annually less than 1060 hours during autumn to spring time (Oct.-April).*

II

*Cumulated frequencies of hours of resultant temperature > 20°C in order to determine indoor thermal comfort in SL80 Solarlux sun spaces according to DIN EN 15251-A regarding south directed 25m<sup>2</sup> dimensioned sun spaces in climate region -1-, -4-, -5-*

*and -13-, representing four major cities in Germany, provided by renewable heating energy exclusively by solar gains and additionally by facade integrated technologies are closer to but not actually 1060 hours a year during autumn to spring time (Oct.-April).*

### III

---

*Cumulated frequencies of annually 1060 hours of resultant temperature >20°C are realizable regarding indoor thermal comfort in SL80 Solarlux sun spaces according to DIN EN 15251-A regarding south directed 25m<sup>2</sup> dimensioned sun spaces in climate region -1-, -4-, -5- and -13-, representing four major cities in Germany, provided by renewable heating energy exclusively by solar gains and additionally by facade integrated technologies in combination with seasonal thermal storage technologies in order to generate renewable energies.*

### IV

---

*The sum of solar gains and additional renewable energies, which are generated by facade integrated collector technologies and seasonally stored with sorption storage technologies provide in climate region -1-, -4-, -5- and -13-, representing four major cities in Germany, at least 20°C resultant temperature based heating energy autarkic operation from 5 to 10 PM in 25m<sup>2</sup> dimensioned south directed SL80 sun spaces during autumn to spring time (Oct.-April).*

### V

---

*10 per cent of the sun space adjacent residential houses effective heating energy demand can be substituted by surplus of solar gains and additional renewable energy that is generated by sun space facade integrated collector technologies and seasonally stored by sorption storage technologies of 25m<sup>2</sup> dimensioned and south directed SL80 sun spaces.*

By computer aided dynamic simulation hypothesis I is proven in section 2. Hypotheses II, III and V will be verified in section 3 and 4 of this chapter. Especially section 4 focuses on the verification of hypothesis IV. Beside this primary investigation, the demand of auxiliary energy will be inspected and cumulated frequencies and maximum values of internal space adjacent façade surface of embedded collectors will be detected. This inspection allows a differentiated evaluation of the effectiveness of the chosen typologies of sun space façade integrated collectors.

## § 8.2 Evaluation of dynamic simulation of operative temperature exclusively by passive solar gains

Figure 8.1 tables cumulative frequencies of hours with operative temperature  $>18^{\circ}\text{C}$ ,  $>20^{\circ}\text{C}$  and  $>32^{\circ}\text{C}$  in an unheated  $25\text{m}^2$  sized modelled sun space. Operative temperature results from passive solar gains, thermal mass and transmission losses. Simulation scope was enlarged to additional east and west orientations for the 15 different climate regions (Test Reference Years [TRY]) in Germany defined by the Deutscher Wetterdienst (DWD). Figure 218 separates between daily 5 to 10 PM and 10 to 5 PM analysis and winter and summer period.

For climate region 01 the table reveal the highest cumulative frequency of hours with Top  $>20^{\circ}\text{C}$  in winter between 5 to 10 PM with 180 hours for east orientation. Opposed to that south and west oriented sun spaces benefit from solely 12 to 17 hours less. Frequencies of hours with Top  $>18^{\circ}\text{C}$  are at least 221.

The cumulative frequency of hours with Top  $>20^{\circ}\text{C}$  are slightly higher for climate region 02. In particular south oriented sun spaces provide the highest frequency with 195 hours during winter. At least 237 hours of Top  $>18^{\circ}\text{C}$  could have been inspected for west oriented sun spaces.

Climate region 03, representing “Nordwestdeutsches Tiefland”, results in considerable less cumulative frequencies of hours with Top  $>20^{\circ}\text{C}$ . East oriented sun spaces provide with 133 hours the highest amount of hours in winter, whereas west oriented provide with 113 hours simply half the amount of hours compared to regions 01 and 02.

South oriented sun spaces were detected to provide 181 hours of Top  $>20^{\circ}\text{C}$  in climate region 04. East and west directed spaces benefit from slightly less hours, from 178 and 174 hours respectively. The cumulative frequencies of hours with Top  $>20^{\circ}\text{C}$  evaluated for climate region 05, “Niederrheinisch-Westfälische Bucht und Emsland”, are with 115 hours for south oriented sun spaces comparably low as for climate region 03. The highest verified frequency of hours assess east oriented spaces with 147 hours. Operative temperature of  $>18^{\circ}\text{C}$  was evaluated for 219 hours for east oriented spaces.

Similarly to region 05, in climate region 06 especially east oriented sun spaces provide by passive solar gains the highest amount of hours with Top  $>20^{\circ}\text{C}$ . The amount is limited to 127 hours, what is comparable to region 03. In particular south oriented spaces profit from simply 84 hours with Top  $>20^{\circ}\text{C}$  in winter, whereas opposed to that west orientation provides 13 hours more. Summarized, operative temperature of  $18^{\circ}\text{C}$  and higher is applicable for 168 hours maximum in west sun spaces.

CR 01	Nordsüdseite	Winter		Summer		Winter		Summer	
		5PM 10PM	10PM 5PM	5PM 10PM	10PM 5PM	5PM 10PM	10PM 5PM	5PM 10PM	10PM 5PM
		[905]	[3439]	[920]	[3496]	[905]	[3439]	[920]	[3496]
	>18°C	249	995	916	3424	219	927	916	3461
	>20°C	163	610	877	3204	151	656	929	3210
	>32°C	0	0	0	43	0	0	0	1
	>18°C	225	967	916	3398	187	916	916	3397
	>20°C	180	704	845	3176	178	867	863	3152
	>32°C	0	8	0	17	0	9	1	40
	>18°C	221	880	915	3403	209	759	915	3378
	>20°C	168	590	863	3222	174	600	857	3062
	>32°C	0	2	0	17	0	14	1	38
CR 02	Ostseite	Winter		Summer		Winter		Summer	
		[905]	[3439]	[920]	[3496]	[905]	[3439]	[920]	[3496]
	>18°C	273	964	916	3438	217	961	911	3417
	>20°C	196	691	871	3201	115	812	872	3143
	>32°C	0	2	0	59	0	1	0	23
	>18°C	298	923	909	3393	219	1017	908	3405
	>20°C	174	664	868	3120	147	718	854	3130
	>32°C	0	3	0	20	0	0	0	13
	>18°C	237	854	912	3414	206	907	906	3409
	>20°C	168	612	866	3155	153	668	852	3112
	>32°C	0	0	0	13	0	0	0	17
CR 03	Nordwestdaches Tiefand	Winter		Summer		Winter		Summer	
		[905]	[3439]	[920]	[3496]	[905]	[3439]	[920]	[3496]
	>18°C	212	777	916	3411	159	720	878	3169
	>20°C	124	511	804	3090	84	465	773	2859
	>32°C	0	10	0	16	0	0	0	13
	>18°C	212	809	915	3379	186	769	858	3195
	>20°C	158	574	873	3098	127	578	753	2946
	>32°C	0	10	0	22	0	0	0	3
	>18°C	193	695	913	3354	168	660	851	3201
	>20°C	113	472	865	2956	97	473	794	2910
	>32°C	0	8	0	10	0	1	0	3
CR 04	Nordostdaches Tiefand	Winter		Summer		Winter		Summer	
		[905]	[3439]	[920]	[3496]	[905]	[3439]	[920]	[3496]
	>18°C	219	927	916	3461	219	927	916	3461
	>20°C	151	656	929	3210	151	656	929	3210
	>32°C	0	0	0	1	0	0	0	1
	>18°C	212	871	916	3397	212	871	916	3397
	>20°C	178	607	863	3152	178	607	863	3152
	>32°C	0	9	1	40	0	9	1	40
	>18°C	209	759	915	3378	209	759	915	3378
	>20°C	174	600	857	3062	174	600	857	3062
	>32°C	0	14	1	38	0	14	1	38
CR 05	Westdaches Winkelsteil und Einland	Winter		Summer		Winter		Summer	
		[905]	[3439]	[920]	[3496]	[905]	[3439]	[920]	[3496]
	>18°C	217	961	911	3417	217	961	911	3417
	>20°C	115	812	872	3143	115	812	872	3143
	>32°C	0	1	0	23	0	1	0	23
	>18°C	219	1017	908	3405	219	1017	908	3405
	>20°C	147	718	854	3130	147	718	854	3130
	>32°C	0	0	0	13	0	0	0	13
	>18°C	206	907	906	3409	206	907	906	3409
	>20°C	153	668	852	3112	153	668	852	3112
	>32°C	0	0	0	13	0	0	0	13
CR 06	Nordliche u. Westl. Mittelsüdge- Bergsteil	Winter		Summer		Winter		Summer	
		[905]	[3439]	[920]	[3496]	[905]	[3439]	[920]	[3496]
	>18°C	159	720	878	3169	159	720	878	3169
	>20°C	84	465	773	2859	84	465	773	2859
	>32°C	0	0	0	13	0	0	0	13
	>18°C	186	769	858	3195	186	769	858	3195
	>20°C	127	578	753	2946	127	578	753	2946
	>32°C	0	0	0	3	0	0	0	3
	>18°C	168	660	851	3201	168	660	851	3201
	>20°C	97	473	794	2910	97	473	794	2910
	>32°C	0	1	0	3	0	1	0	3
CR 07	Nordliche u. Westl. Mittelsüdge- zentral Bersteil	Winter		Summer		Winter		Summer	
		[905]	[3439]	[920]	[3496]	[905]	[3439]	[920]	[3496]
	>18°C	257	1012	910	3373	257	1012	910	3373
	>20°C	177	703	863	2989	177	703	863	2989
	>32°C	0	0	0	2	0	0	0	2
	>18°C	266	1033	919	3341	266	1033	919	3341
	>20°C	208	749	815	2947	208	749	815	2947
	>32°C	0	2	1	19	0	2	1	19
	>18°C	247	897	901	3332	247	897	901	3332
	>20°C	173	629	854	2983	173	629	854	2983
	>32°C	0	0	0	23	0	0	0	23
CR 08	Oberhalb Schwarzfeld	Winter		Summer		Winter		Summer	
		[905]	[3439]	[920]	[3496]	[905]	[3439]	[920]	[3496]
	>18°C	156	607	853	3104	156	607	853	3104
	>20°C	78	449	724	2921	78	449	724	2921
	>32°C	0	0	0	9	0	0	0	9
	>18°C	149	704	840	3069	149	704	840	3069
	>20°C	94	536	676	2511	94	536	676	2511
	>32°C	0	1	0	0	0	1	0	0
	>18°C	135	579	848	3036	135	579	848	3036
	>20°C	78	418	673	2424	78	418	673	2424
	>32°C	0	0	0	4	0	0	0	4
CR 09	Nüringer Becken und Schönhaas Lage	Winter		Summer		Winter		Summer	
		[905]	[3439]	[920]	[3496]	[905]	[3439]	[920]	[3496]
	>18°C	184	846	909	3361	184	846	909	3361
	>20°C	97	618	859	3016	97	618	859	3016
	>32°C	0	7	0	75	0	7	0	75
	>18°C	168	826	906	3315	168	826	906	3315
	>20°C	93	629	816	2933	93	629	816	2933
	>32°C	0	12	0	49	0	12	0	49
	>18°C	151	714	914	3364	151	714	914	3364
	>20°C	87	485	850	2989	87	485	850	2989
	>32°C	0	6	0	32	0	6	0	32
CR 10	Südliche Mittelsüdge bis Topp	Winter		Summer		Winter		Summer	
		[905]	[3439]	[920]	[3496]	[905]	[3439]	[920]	[3496]
	>18°C	189	686	850	3154	189	686	850	3154
	>20°C	114	481	736	2659	114	481	736	2659
	>32°C	0	0	0	1	0	0	0	1
	>18°C	179	780	850	3146	179	780	850	3146
	>20°C	121	559	738	2686	121	559	738	2686
	>32°C	0	3	0	9	0	3	0	9
	>18°C	172	636	840	3053	172	636	840	3053
	>20°C	112	459	729	2601	112	459	729	2601
	>32°C	0	0	0	6	0	0	0	6
CR 11	Erzgebirge, Böhmer- und Schwarzfeld	Winter		Summer		Winter		Summer	
		[905]	[3439]	[920]	[3496]	[905]	[3439]	[920]	[3496]
	>18°C	85	442	617	2272	85	442	617	2272
	>20°C	48	322	428	1541	48	322	428	1541
	>32°C	0	24	0	42	0	24	0	42
	>18°C	106	515	561	2250	106	515	561	2250
	>20°C	45	400	378	1327	45	400	378	1327
	>32°C	0	21	0	18	0	21	0	18
	>18°C	70	372	544	2050	70	372	544	2050
	>20°C	32	277	334	1333	32	277	334	1333
	>32°C	0	6	0	19	0	6	0	19
CR 12	Oberhängeboden und unteres Meckartal	Winter		Summer		Winter		Summer	
		[905]	[3439]	[920]	[3496]	[905]	[3439]	[920]	[3496]
	>18°C	343	1334	914	3474	343	1334	914	3474
	>20°C	264	946	910	3339	264	946	910	3339
	>32°C	0	28	5	116	0	28	5	116
	>18°C	315	1266	915	3450	315	1266	915	3450
	>20°C	246	849	827	3087	246	849	827	3087
	>32°C	0	20	5	100	0	20	5	100
	>18°C	308	1133	916	3453	308	1133	916	3453
	>20°C	232	824	908	3292	232	824	908	3292
	>32°C	0	13	4	62	0	13	4	62
CR 13	Schwäbisch-fränkisches Mittelland/Alpenvorland	Winter		Summer		Winter		Summer	
		[905]	[3439]	[920]	[3496]	[905]	[3439]	[920]	[3496]
	>18°C	209	892	914	3334	209	892	914	3334
	>20°C	111	641	861					

During winter east oriented sun spaces benefit in climate region 07 from cumulative frequencies of hours with  $\text{Top} > 20^{\circ}\text{C}$  of maximum 206 hours.

In “Nördliches und Westliches Mittelgebirge – zentrale Bereiche” south and west oriented sun spaces profit from 177 and 173 hours in total. At least 247 hours have been detected for west orientation with  $\text{Top} > 18^{\circ}\text{C}$ .

Sun spaces placed in “Oberharz and Schwarzwald”, climate region 08 respectively, encounters the lowest cumulative frequencies of hours with  $\text{Top} > 20^{\circ}\text{C}$  so far. Solely 78 hours for south and west oriented sun spaces could have been evaluated, however, east sun spaces benefit from 94 hours.

South oriented sun spaces in climate region 09, “Thüringer Becken und Sächsisches Hügelland”, benefit from simply 97 hours with  $\text{Top} > 20^{\circ}\text{C}$  during winter, east and west directed sun spaces account for 93 and 87 hours respectively. With 184 hours south oriented sun spaces account the maximum potential hours with  $\text{Top} > 18^{\circ}\text{C}$  during winter months.

In climate region 10, representing “Südöstliches Mittelgebirge” bis 1.000m, evaluated cumulative frequencies of hours with  $\text{Top} > 20^{\circ}\text{C}$  and comparable to the frequencies for region 03. West oriented sun spaces provide with 112 hours the lowest cumulative frequency, while frequencies turn into 129 hours maximum for east directed spaces. At least 172 hours with  $\text{Top} > 18^{\circ}\text{C}$  during 5 to 10 PM are attainable with west facing sun spaces.

Climate region 11, covering “Erzgebirge, Böhmer- and Schwarzwald”, provides the demonstrably lowest cumulative frequencies of hours with operative temperature  $> 20^{\circ}\text{C}$  detected so far. West oriented sun spaces benefit from simply 32 hours in total during winter, east oriented from 45 hours and south oriented sun spaces from maximum 48 hours with satisfying thermal comfort exclusively by passive solar gains. That equals solely 3 to 4,2% of the entire sum of hours between 5 to 10 PM during winter (1.060 hours). Operative temperature of  $> 18^{\circ}\text{C}$  is achievable for 106 hours in east directed spaces.

Opposed to that profit sun spaces located in climate region 12, representing “Oberrheingraben and Unteres Neckartal”, from at least 232 cumulated hours with operative temperature  $> 20^{\circ}\text{C}$  for west oriented spaces. Maximum cumulative frequencies of hours with  $\text{Top} > 20^{\circ}\text{C}$  are attainable with south oriented sun spaces, which benefit from 264 hours exclusively by solar gains during winter. Operative temperature of  $> 18^{\circ}\text{C}$  have been evaluated between 5 to 10 PM for 343 hours in south oriented spaces.

**CUMULATIVE FREQUENCIES OF OPERATIVE TEMPERATURE BY PASSIVE SOLAR GAINS**  
**SUN SPACE - 25 m<sup>2</sup> - SOUTH**

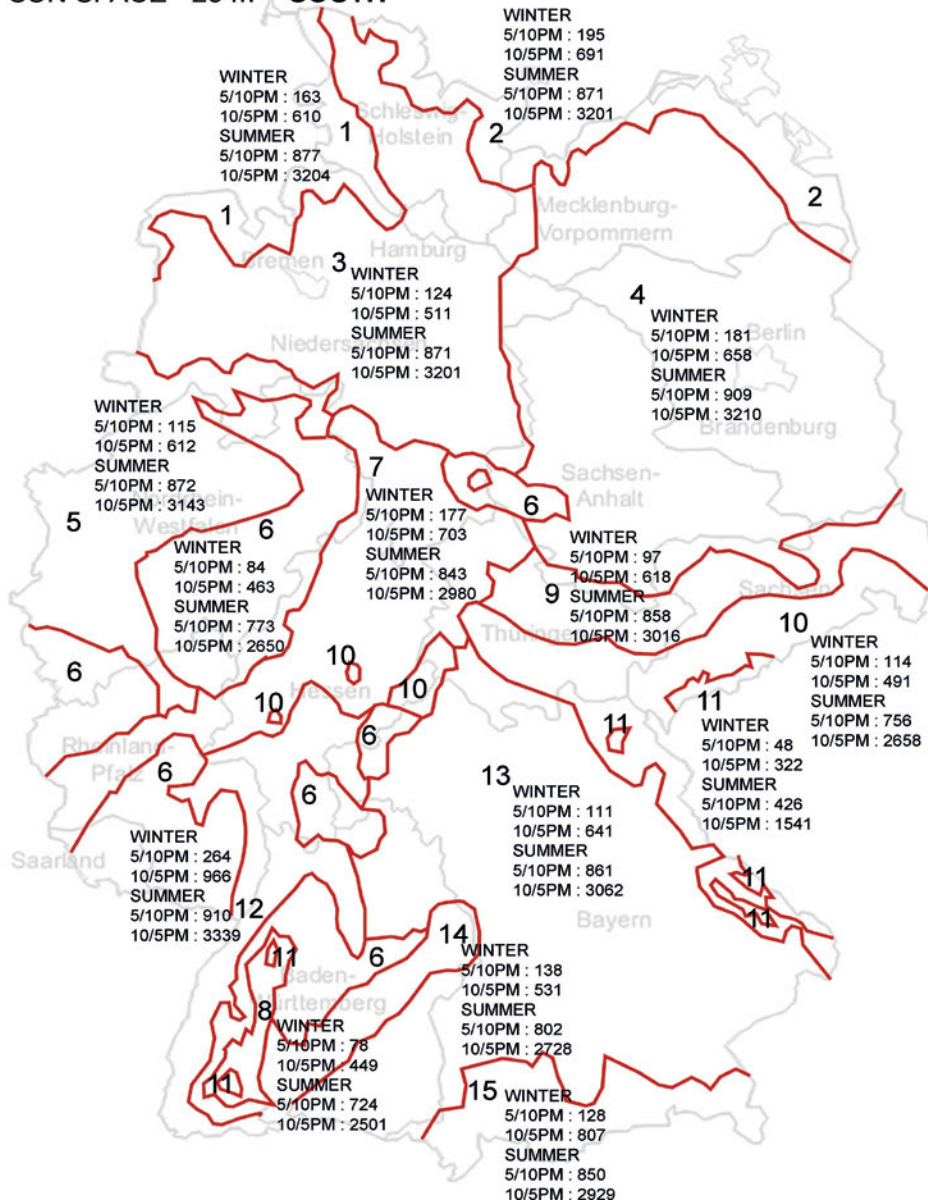


FIGURE 8.2 Cumulative frequencies of operative temperature Top > 20°C for south orientation by exclusively passive solar gains between 5 to 10 PM and 10 to 5 PM for 15 different climate regions

Sun spaces located in "Schwäbisch-Fränkisches Stufenland and Alpenvorland" profit from 111 hours with  $T_{op} > 20^{\circ}\text{C}$  in south directed, from 127 hours in west directed and from 149 hours in east oriented sun spaces. Opposed to that can operative temperature of  $18^{\circ}\text{C}$  and higher be evaluated for 209 hours in south directed spaces.

Climate region 14 causes east oriented sun spaces to provide 146 hours with operative temperature above  $20^{\circ}\text{C}$ , south directed to provide 138 and west oriented to provide 123 hours with satisfactory resultant indoor temperature. Thus, the climate region "Schwäbische Alp und Baar" resembles climate region 13. Operative temperature  $> 18^{\circ}\text{C}$  is evaluated to be achievable for 202 to 235 hours during preferred evening occupation hours in winter.

Cumulative frequencies of hours with  $T_{op} > 20^{\circ}\text{C}$  account for 154 hours in east sun spaces located in climate region 15, "Alpenrand und -täler", for 128 hours in south and for 116 in west facing sun spaces. Interestingly, the amount of hours with  $T_{op} > 18^{\circ}\text{C}$  is related to  $20^{\circ}\text{C}$  frequencies with 270 for south spaces comparably high. East and west oriented spaces profit from 248 and 229 hours respectively.

In this context could have been evaluated the lowest cumulative frequency of  $T_{op} > 20^{\circ}\text{C}$  during winter in entire day perspective from 10 to 5 PM of 372 hours in west oriented sun spaces located in "Erzgebirge, Böhmer- und Schwarzwald" (climate region 11).

On the contrary accounts "Oberrheingraben–Unteres Neckartal" for the highest cumulative frequency of  $T_{op} > 20^{\circ}\text{C}$  from 10 to 5 PM during winter with 1334 hours. This equals 33% of the entire amount of 4028 hours. The range is defined by the specific difference of 962 hours.

Opposed to that reveals the evaluation of the operative temperatures  $> 32^{\circ}$  during preferred occupation time (5 to 10PM) in summer minimum cumulative frequencies of zero hours and maximum cumulative frequencies of 5 hours in south and west oriented sun spaces in climate region 12. During 10 to 5 PM regarding entire day perspective, minimum cumulative frequencies account in summer month for zero and at least 3 hours in east and west facing sun spaces located in climate region 06, "Nördliche und Westliche Mittelgebirge, Randgebiete".

Maximum cumulative frequencies of operative temperature  $> 32^{\circ}$  was evaluated in south facing sun spaces for 3.474 hours in climate region 12, "Oberrheingraben und Unteres Neckartal" respectively. Thus, resultant temperature of  $32^{\circ}\text{C}$  and higher is calculated for 86% of the summer time from 22 to 17 o'clock solely by passive solar gains.

**CUMULATIVE FREQUENCIES OF  
OPERATIVE TEMPERATURE BY  
PASSIVE SOLAR GAINS  
SUN SPACE - 25 m<sup>2</sup> - EAST**

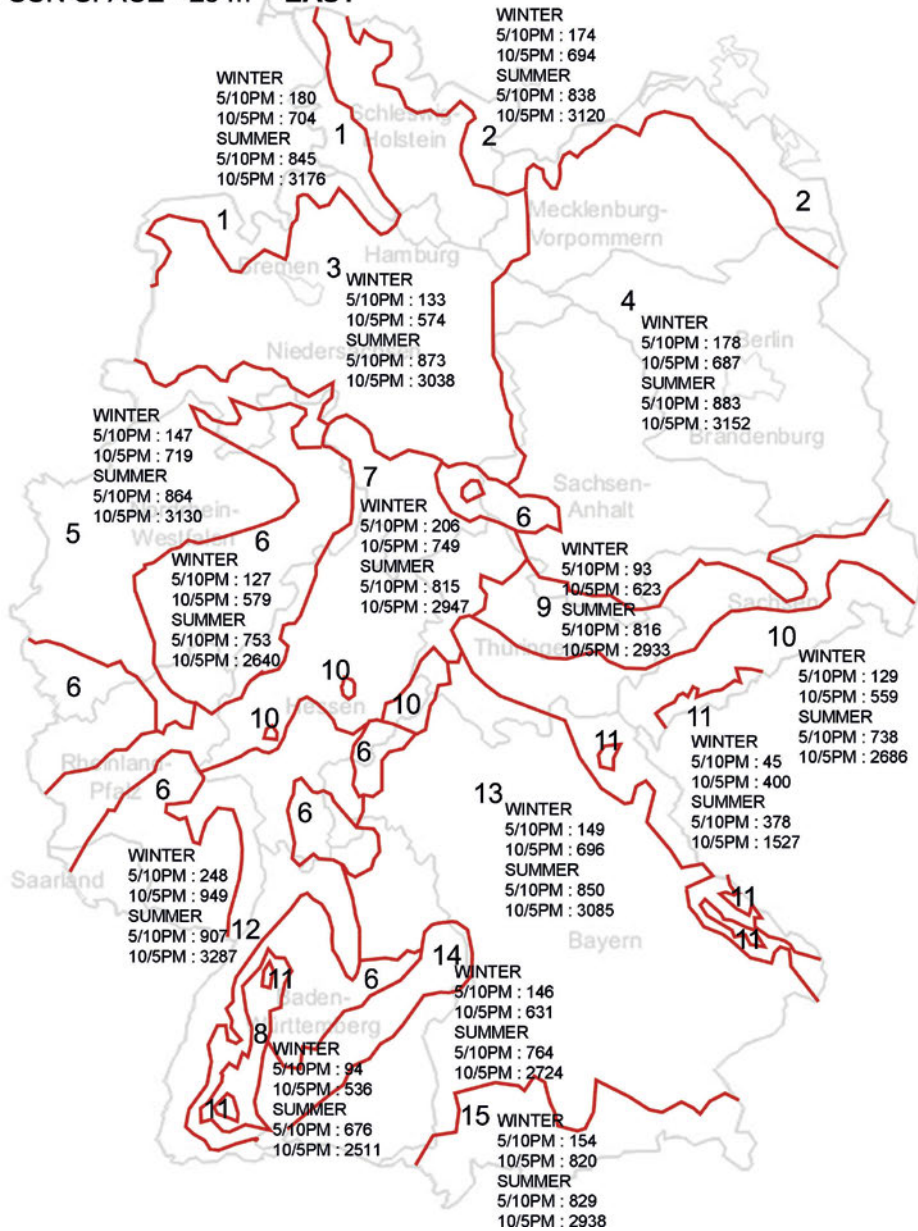


FIGURE 8.3 Cumulative frequencies of operative temperature Top > 20°C for east orientation by exclusively passive solar gains between 5 to 10 PM and 10 to 5 PM for 15 different climate regions

Summarized, we can state, that according to computed dynamic modelling, operative temperature of  $>20^{\circ}\text{C}$  between 5 to 10 PM during winter exclusively by passive solar gains is possible for at least 32 to maximum 264 hours. Mostly, in 10 of 15 climate regions east oriented sun spaces (Fig. 8.3) provide the highest cumulative frequencies of  $\text{Top}>20^{\circ}\text{C}$ . Opposed to that provide west oriented sun spaces (Fig. 8.4) in 10 of 15 climate regions the lowest frequencies of hours with  $\text{Top}>20^{\circ}\text{C}$ .

Operative temperature  $>18^{\circ}\text{C}$  is achievable for maximum 343 hours in south directed sun spaces located in "Oberrheingraben and Unteres Neckartal".

The geographical schemes in Figure 8.2 to 8.4 illustrate separated by orientation (east, south, west) maximum cumulative frequencies of hours with  $\text{Top}>20^{\circ}\text{C}$  between 5 to 10 PM and 10 to 5 PM in summer and winter. Whereas south oriented sun spaces satisfy with high cumulative frequencies in south, west regions like "Hessen and north west Baden-Württemberg" with more than 260 hours, as well as in coastal parts of "Schleswig-Holstein and north and north-east of Mecklenburg Vorpommern" with 195 and 181 hours between 5 to 10 PM during winter, sun spaces located in "Erzgebirge, Böhmerwald and Schwarzwald as well as at Schwäbische Alp and Baar" cannot convince with high cumulative frequencies.

In terms of east oriented sun spaces promotable regions beside "Hessen and north west Baden-Württemberg" change to "Deutsche Nordseeküste and especially Nördliches and Westliches Mittelgebirge-Zentrale Bereiche" with 180 and 206 hours respectively. Most climate regions (CR 01,03,05,06,07,10,12,13,14,15) profit in terms of an enlargement of hours with satisfying thermal comfort by a  $90^{\circ}$  turn from south to east orientation. Especially climate region 06, north-east and south-east of "Nordrhein-Westfalen" benefits from a change from 84 to 127 hours significantly.

East orientation is especially beneficial for northern-west coastal parts of "Schleswig-Holstein and Niedersachsen", south-east regions of Germany covering "Sachsen and north-east of Bayern", as well as the "Alps with its Alp socket areas and valleys" and northern part of "Hessen".

On the contrary causes west orientation compared to east orientation in 13 of 15 climate regions reduction of cumulative hours with  $\text{Top}>20^{\circ}\text{C}$ .

However, sun spaces in climate region 2 and 4 covering the northern coastal areas of "Schleswig-Holstein and Mecklenburg-Vorpommern" as well as entire "Mecklenburg-Vorpommern, Berlin-Brandenburg and Sachsen-Anhalt" and eastern parts of "Niedersachsen" profit significantly from either south or west orientation.

**CUMULATIVE FREQUENCIES OF  
OPERATIVE TEMPERATURE BY  
PASSIVE SOLAR GAINS  
SUN SPACE - 25 m<sup>2</sup> - WEST**

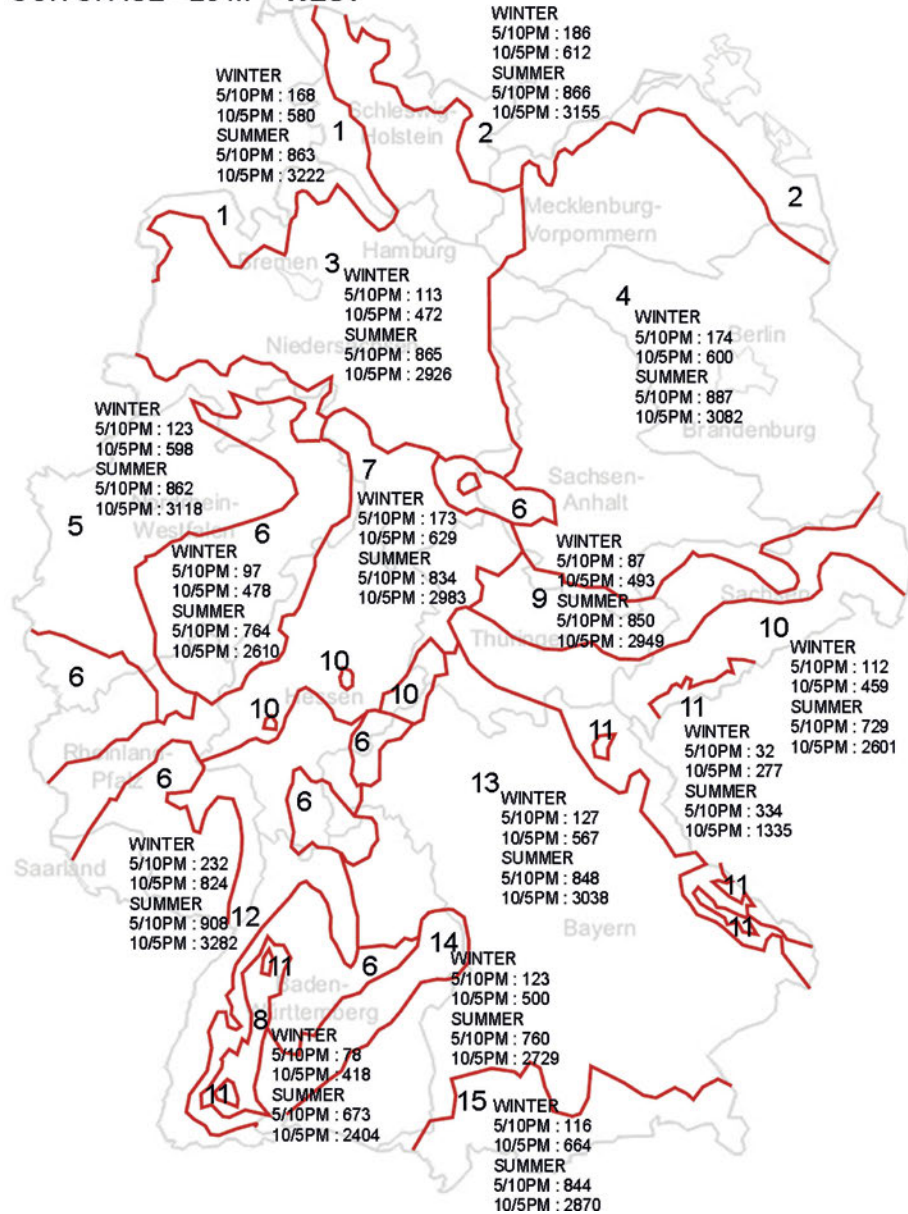


FIGURE 8.4 Cumulative frequencies of operative temperature Top > 20°C for west orientation by exclusively passive solar gains between 5 to 10 PM and 10 to 5 PM for 15 different climate regions

## § 8.2.1 Bandwidths of cumulative frequencies of hours with focused operative temperature

---

The figures in [APPENDIX H.1](#) table evaluated bandwidths of achievable cumulative frequencies of hours separated to south, east and west orientation and differentiated month-wise. The tables unambiguously show, that during winter months December and January from 5 to 10 PM neither 20°C nor at least 18°C operative temperature is attainable exclusively by passive solar gains regardless any orientation.

That slightly changes for the daily time interval from 10 to 5 PM, as for in particular south directed sun spaces in December 93 hours with 18°C and in January 67 hours with 18°C are calculated for maximum. In terms of 20°C operative temperature the maximum cumulative frequencies lower to 61 and 46 hours respectively (see [APPENDIX H.1](#)).

For November and February also south directed sun spaces are eligible to provide maximum frequency of hours with 18 and 20°C. While in March once again south directed sun spaces manage to provide 138 and 128 hours with operational temperature of 18°C and 20°C respectively, in particular in April east and west oriented sun spaces account higher cumulative frequencies of hours than south directed ones.

This relation is notably true for the time interval 10 to 5 PM in April in case of east oriented sun spaces. On the contrary in September and October south directed sun spaces assess higher frequencies of hours abroad all operative temperature bands and time intervals.

Interestingly, the tables demonstrate maximum frequencies of hours with operational temperature >26°C during summer months. Maximum frequencies from June to August are limited to 35 to 44 hours from 5 to 10 PM and to 108 to 189 hours for 10 to 5 PM respectively. This maximum amount of hours is thoroughly acceptable and related to the extension of especially external sun shading in the digital models to also vertical facades. The experimental test set up did not profit from this additional and external sun shading.

## § 8.2.2 Cumulative frequencies of hours with focused operative temperature

---

The tables in [APPENDIX H.2](#) in detail show cumulative frequencies of hours with focused operative temperature exclusively by passive solar gains with different orientations in 15 different climate regions. For the winter and separately summer period the hours were summed finally.

Considering the summed hours for the interval 5 to 10 PM during winter months helps to verify [Hypothesis I](#).

*Hypothesis I can be validated.*

Operational temperature of 20°C cannot be achieved from during winter months from 5 to 10 PM for 1.060 hours exclusively by passive solar gains.

---

## § 8.3 Operative temperature feasible with embedded PV collectors combined with electro-chemical storage and floor heating

---

This section exemplifies the effect of façade integrated photovoltaic modules. A floor heating is driven by battery stored power and the frequency and effect on operational temperature is evaluated in order to verify hypothesis II<sub>pv</sub> and III<sub>pv</sub>.

Figure 8.5 shows geographically mapped the cumulated frequencies of hours with resulting temperature between 5 to 10 PM and 10 to 5 PM during winter and summer months. According to time intensive post processing that is explained in Chapter 7 for an evaluation four climate regions representing four major cities and region have been chosen.

The following major cities represent *the following climate regions* :

- *Emden, Flensburg, St. Peter Ording* : climate region 01, German northern coastal region
- *Berlin, Magdeburg, Dresden* : climate region 04, eastern Germany
- *Köln, Essen* : climate region 05, western Germany

• *München* :

*climate region 13, southern Germany,  
foothills of the Alps*

The comparison of Figure 8.5 with Figure 8.2 reveals, that the cumulative frequency of hours with operational temperature  $> 20^{\circ}\text{C}$  does not improve for any of the chosen climate zones. All sums of hours in Figure 8.5 are at least slightly or even significantly lower than the sum of hours of sun spaces computed dynamically with exclusively passive solar gains. Especially sun spaces with envelope embedded pv collectors in northern coastal regions of Germany, namely climate region 01 suffer from 46 hours less between 5 to 10 PM and from 228 hours less in the 10 to 5 PM interval.

In particular the comparison of the 10 to 5 PM interval demonstrates the essential drawback of sun space roof glazing integrated pv modules on thermal behavior of the sun space. Hence, the differences between Figure 8.2 and 8.5 extend to 248 hours for climate region 5 covering western parts of "Nordrhein-Westfalen", south-west parts of "Niedersachsen" and northern parts of "Rheinlandpfalz". That relation clear-cut demonstrates, that roof integrated pv modules firstly tend shade sun spaces and demonstrably reduces passive solar gains. This is extremely evident for the 10 to 5 PM interval, when floor heating was not active.

Secondly, the difference show, that pv modules provide energy for fossil fuel free heating, but however, the combination of envelope embedded pv modules and electro-chemical storage does not manage to compensate the reduction in passive solar gains and to provide at least equal sum of hours with  $\text{Top} > 20^{\circ}\text{C}$ .

Thus, we can conclude, that neither *Hypothesis IIpv* nor *Hypothesis IIIpv* is validated.

*Hypothesis IIpv is to be rejected.*

And further

*Hypothesis IIIpv is to be rejected.*

In the following Figure 8.6 to 8.15 table cumulative frequencies of hours with operational temperature  $> 16^{\circ}\text{C}$ ,  $> 18^{\circ}\text{C}$ ,  $> 20^{\circ}\text{C}$ ,  $> 26^{\circ}\text{C}$  and  $> 32^{\circ}\text{C}$  for each of the selected climate regions, for south oriented sun spaces for winter and summer in the time intervals 5 to 10 and 10 to 5 PM. Each a pair of 2 table allow to identify first the improvement of the situation by additional pv power powered floor the heating and second the remaining distance to the reference variant without any embedded pv and optimized solar passive gains.

**CUMULATIVE FREQUENCIES OF  
OPERATIVE TEMPERATURE BY  
FACADE INTEGRATED PV+BATTERY  
SUN SPACE - 25 m<sup>2</sup> - SOUTH**

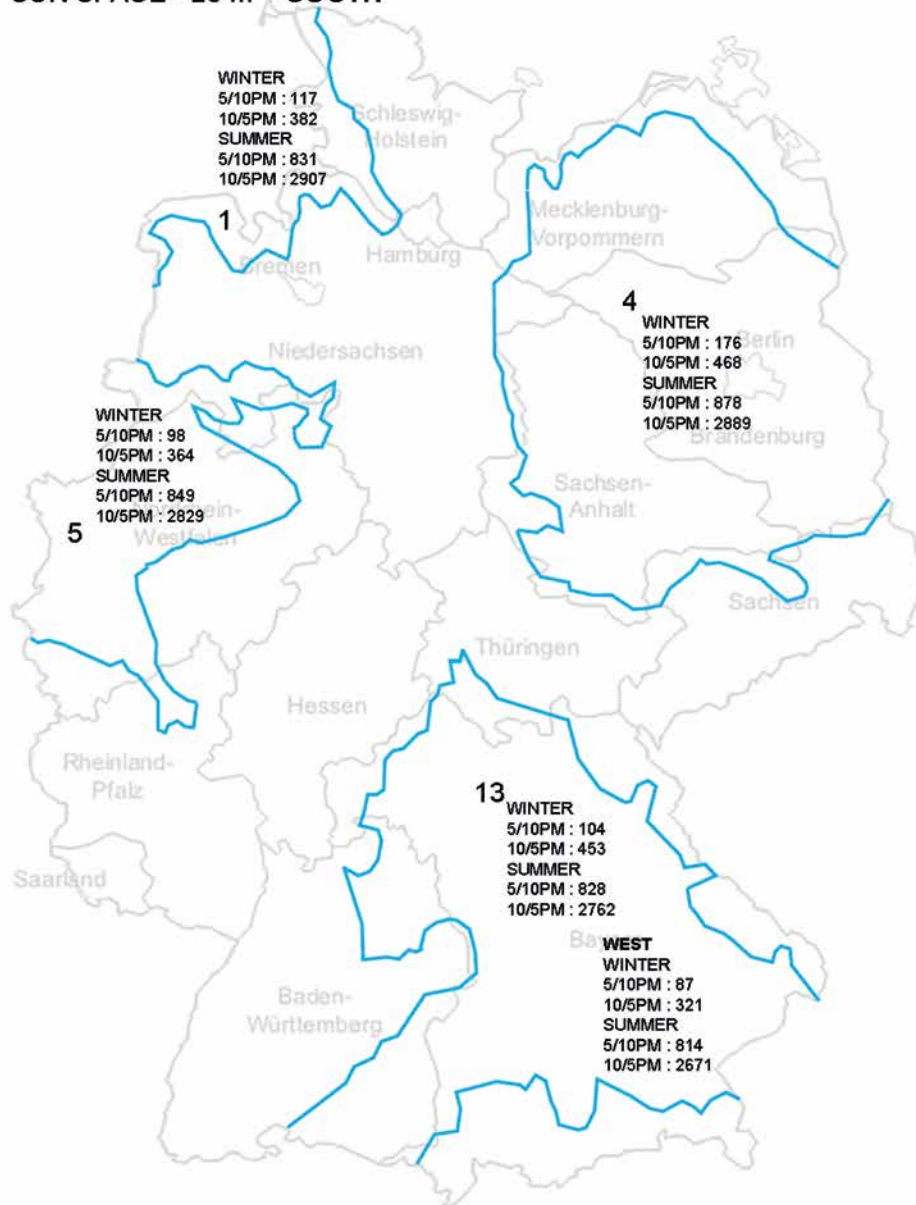


FIGURE 8.5 Cumulative frequencies of operative temperature Top > 20°C for south orientation by passive solar gains and additional façade integrated photovoltaic and battery between 5 to 10 PM and 10 to 5 PM for 15 different climate regions

25m <sup>2</sup> - South - CR 01		WINTER							SUMMER						
Embedded PV - With FLOOR HEATING		November	December	January	February	March	April	SUM	May	June	July	August	September	October	SUM
MONTH/ Cumul. Frequency															
5PM to 10PM T <sub>op</sub> [°C]	>16°C	46	0	0	10	70	146	272	155	150	155	155	150	151	916
	>18°C	4	0	0	2	44	125	175	155	150	155	155	150	126	891
	>20°C	0	0	0	0	19	98	117	130	150	155	155	150	91	831
	>26°C	0	0	0	0	0	1	1	1	8	6	13	4	0	32
	>32°C	0	0	0	0	0	0	0	0	0	0	0	0	0	0
10PM to 5 PM T <sub>op</sub> [°C]	>16°C	165	8	2	85	248	471	979	585	570	589	589	570	529	3432
	>18°C	82	0	0	40	164	359	645	538	570	589	589	570	455	3311
	>20°C	31	0	0	17	111	223	382	386	500	589	583	530	319	2907
	>26°C	0	0	0	0	1	5	6	13	23	64	78	71	29	278
	>32°C	0	0	0	0	0	0	0	0	0	0	2	9	1	12

FIGURE 8.6 Cumulative frequencies of hours with focused operative temperature with façade integrated PV- with active floor heating in climate region 01 – south orientation

25m <sup>2</sup> - South - CR 01		WINTER							SUMMER						
Passive solar gains		November	December	January	February	March	April	SUM	May	June	July	August	September	October	SUM
MONTH/ Cumul. Frequency															
5PM to 10PM T <sub>op</sub> [°C]	>16°C	60	0	0	16	121	150	347	155	150	155	155	150	151	916
	>18°C	30	0	0	1	68	150	249	155	150	155	155	150	151	916
	>20°C	0	0	0	0	41	122	163	142	150	155	155	150	125	877
	>26°C	0	0	0	0	0	0	0	1	8	7	14	6	0	36
	>32°C	0	0	0	0	0	0	0	0	0	0	0	0	0	0
10PM to 5 PM T <sub>op</sub> [°C]	>16°C	271	23	15	115	398	557	1379	589	570	589	589	570	586	3493
	>18°C	158	9	2	88	286	452	995	565	570	589	589	570	541	3424
	>20°C	83	1	0	60	172	294	610	452	560	589	589	570	444	3204
	>26°C	0	0	0	0	19	40	59	14	34	86	89	143	84	450
	>32°C	0	0	0	0	1	2	3	0	0	0	2	32	9	43

FIGURE 8.7 Cumulative frequencies of hours with focused operative temperature exclusively by passive solar gains in climate region 01 – south orientation

The comparison of Figure 8.6 and 8.7 representing climate region 01 demonstrates, that both in December and January target resulting temperature cannot be met. However, pv power powered and battery supplied floor heating slightly enhances the sum of hours with Top >20°C in March and April. Nonetheless November and April do not profit from pv power and electrochemical seasonal storages. The sum of hours can be increased during summer months in May and October.

The comparison with the reference sum of hours in doubtlessly shows that best performance is achievable without roof integrated photovoltaic. The sum of hours without embedded pv is 50 hours higher in November (see APPENDIX H.2), 60 hours higher in March and 70 hours higher in April considering the 10 to 5 (overnight) interval. Interestingly, in the context of comparison of cumulated frequencies of hours with Top>20°C in climate region 04 solely in March roof embedded pv outnumbers the reference sum of 54 hours with 61 hours by 7 hours. However, the rest of the year the concept cannot manage to improve the reference situation.

25m <sup>2</sup> - South - CR 04																
Embedded PV - With FLOOR HEATING		WINTER							SUMMER							
MONTH/ Cumul. Frequency		November	December	January	February	March	April	SUM	May	June	July	August	September	October	SUM	
5PM to 10PM	T <sub>op</sub> [°C]	>16°C	7	0	1	9	73	138	228	155	150	155	155	150	151	916
		>18°C	5	0	0	7	68	125	205	155	150	155	155	150	151	916
		>20°C	0	0	0	5	61	110	176	148	148	155	155	150	122	878
		>26°C	0	0	0	1	0	0	1	5	10	20	17	2	0	54
		>32°C	0	0	0	0	0	0	0	0	0	0	0	0	0	0
10PM to 5 PM	T <sub>op</sub> [°C]	>16°C	80	14	51	36	287	478	946	586	570	589	589	570	556	3460
		>18°C	38	11	26	28	199	368	670	557	554	589	589	555	453	3297
		>20°C	24	5	12	20	142	265	468	454	495	584	584	476	296	2889
		>26°C	0	0	0	4	18	9	31	33	100	113	106	65	25	442
		>32°C	0	0	0	0	0	0	0	1	0	9	12	7	3	32

FIGURE 8.8 Cumulative frequencies of hours with focused operative temperature with façade integrated PV- with active floor heating in climate region 04 – south orientation

25m <sup>2</sup> - South - CR 04																
Passive solar gains		WINTER							SUMMER							
MONTH/ Cumul. Frequency		November	December	January	February	March	April	SUM	May	June	July	August	September	October	SUM	
5PM to 10PM	T <sub>op</sub> [°C]	>16°C	25	0	2	10	104	150	291	155	150	155	155	150	151	916
		>18°C	5	0	0	7	70	137	219	155	150	155	155	150	151	916
		>20°C	5	0	0	4	54	118	181	152	150	155	155	150	147	909
		>26°C	0	0	0	0	2	3	5	15	13	21	17	5	1	72
		>32°C	0	0	0	0	0	0	0	0	0	1	0	0	0	1
10PM to 5 PM	T <sub>op</sub> [°C]	>16°C	160	22	75	69	352	530	1208	589	570	589	589	570	589	3496
		>18°C	85	14	48	43	281	456	927	577	568	589	589	570	558	3451
		>20°C	53	10	28	27	208	332	658	506	530	589	589	547	449	3210
		>26°C	1	0	1	10	63	48	123	45	132	151	115	136	90	669
		>32°C	0	0	0	4	9	0	13	0	0	8	15	24	11	58

FIGURE 8.9 Cumulative frequencies of hours with focused operative temperature exclusively by passive solar gains in climate region 04 – south orientation

A comparison of the pairs figure 8.8 and 8.9, 8.10 and 8.11, as well as 8.12 and 8.13 and 8.14 and 8.15 underline the before mentioned relation and finding.

25m <sup>2</sup> - South - CR 05																
Embedded PV - With FLOOR HEATING		WINTER							SUMMER							
MONTH/ Cumul. Frequency		November	December	January	February	March	April	SUM	May	June	July	August	September	October	SUM	
5PM to 10PM	T <sub>op</sub> [°C]	>16°C	27	0	0	22	79	127	255	155	150	155	155	150	143	908
		>18°C	5	0	0	6	37	95	143	155	150	155	155	148	122	885
		>20°C	0	0	0	4	24	70	98	143	149	155	155	142	105	849
		>26°C	0	0	0	0	0	0	0	4	6	23	16	2	0	51
		>32°C	0	0	0	0	0	0	0	0	0	0	0	0	0	0
10PM to 5 PM	T <sub>op</sub> [°C]	>16°C	130	11	27	142	277	431	1018	587	570	589	589	564	536	3436
		>18°C	66	4	11	86	180	285	632	546	570	589	589	561	455	3310
		>20°C	30	2	4	48	116	164	364	416	481	569	578	497	288	2829
		>26°C	0	0	0	0	5	4	9	20	48	85	82	56	18	309
		>32°C	0	0	0	0	0	0	0	1	0	2	6	3	0	12

FIGURE 8.10 Cumulative frequencies of hours with focused operative temperature with façade integrated PV- with active floor heating in climate region 05 – south orientation

25m <sup>2</sup> - South - CR 05															
Passive solar gains		WINTER							SUMMER						
MONTH/ Cumul. Frequency		November	December	January	February	March	April	SUM	May	June	July	August	September	October	SUM
5PM to 10PM	>16°C	55	0	0	55	140	149	399	155	150	155	155	150	151	916
	>18°C	10	0	0	7	81	119	217	155	150	155	155	150	146	911
	>20°C	0	0	0	0	33	82	115	149	145	155	155	147	121	872
	>26°C	0	0	0	0	0	1	1	7	6	23	16	7	0	59
	>32°C	0	0	0	0	0	0	0	0	0	0	0	0	0	0
10PM to 5 PM	>16°C	234	20	40	187	423	496	1400	589	570	589	589	570	583	3490
	>18°C	111	9	26	142	294	379	961	566	565	589	589	563	545	3417
	>20°C	66	4	13	105	210	214	612	458	528	584	585	550	438	3143
	>26°C	0	0	0	1	22	23	46	29	60	102	88	125	78	482
	>32°C	0	0	0	0	1	0	1	0	0	0	2	17	4	23

FIGURE 8.11 Cumulative frequencies of hours with focused operative temperature exclusively by passive solar gains in climate region 05 – south orientation

25m <sup>2</sup> - South - CR 13															
Embedded PV- With FLOOR HEATING		WINTER							SUMMER						
MONTH/ Cumul. Frequency		November	December	January	February	March	April	SUM	May	June	July	August	September	October	SUM
5PM to 10PM	>16°C	20	0	2	4	81	118	225	155	150	155	155	150	150	915
	>18°C	1	0	1	1	54	94	151	146	150	155	155	150	123	879
	>20°C	0	0	0	0	34	70	104	132	146	153	155	148	94	828
	>26°C	0	0	0	0	0	0	0	8	11	24	26	1	0	70
	>32°C	0	0	0	0	0	0	0	0	0	0	1	0	0	1
10PM to 5 PM	>16°C	112	13	67	63	285	383	923	566	568	589	589	570	492	3374
	>18°C	69	3	49	42	211	301	675	518	558	589	589	552	406	3212
	>20°C	44	0	31	28	150	200	453	393	495	560	576	448	290	2762
	>26°C	0	0	0	0	9	2	11	57	96	146	135	64	45	543
	>32°C	0	0	0	0	0	0	0	0	8	13	18	2	4	45

FIGURE 8.12 Cumulative frequencies of hours with focused operative temperature with façade integrated PV- with active floor heating in climate region 13 – south orientation

25m <sup>2</sup> - South - CR 13															
Passive solar gains		WINTER							SUMMER						
MONTH/ Cumul. Frequency		November	December	January	February	March	April	SUM	May	June	July	August	September	October	SUM
5PM to 10PM	>16°C	61	0	0	5	148	131	345	155	150	155	155	150	151	916
	>18°C	17	0	0	2	78	112	209	153	150	155	155	150	151	914
	>20°C	0	0	0	1	38	72	111	135	146	155	155	150	120	861
	>26°C	0	0	0	0	0	0	0	8	12	26	24	3	1	74
	>32°C	0	0	0	0	0	0	0	0	0	0	1	0	0	1
10PM to 5 PM	>16°C	195	22	100	86	380	446	1229	585	570	589	589	570	579	3482
	>18°C	118	15	63	62	310	324	892	543	561	589	589	568	484	3334
	>20°C	84	7	45	46	242	217	641	434	523	571	586	540	408	3062
	>26°C	2	0	0	5	52	20	79	60	120	166	139	140	106	731
	>32°C	0	0	0	0	2	0	2	0	0	1	14	20	12	47

FIGURE 8.13 Cumulative frequencies of hours with focused operative temperature exclusively by passive solar gains in climate region 13 – south orientation

25m <sup>2</sup> - WEST - CR 13		WINTER							SUMMER						
Embedded PV - With FLOOR HEATING		November	December	January	February	March	April	SUM	May	June	July	August	September	October	SUM
MONTH/ Cumul. Frequency															
5PM to 10PM T <sub>op</sub> [°C]	>16°C	8	0	0	7	64	119	198	155	150	155	155	150	150	915
	>18°C	2	0	0	3	39	88	132	145	150	155	155	150	104	859
	>20°C	0	0	0	2	19	66	87	137	145	154	155	145	78	814
	>26°C	0	0	0	0	0	0	0	8	10	25	23	0	0	66
	>32°C	0	0	0	0	0	0	0	0	0	0	2	0	0	2
10PM to 5 PM T <sub>op</sub> [°C]	>16°C	83	0	26	45	257	370	781	573	568	589	589	570	444	3333
	>18°C	49	0	10	24	177	275	535	517	558	589	589	548	369	3170
	>20°C	25	0	3	8	116	169	321	384	491	549	567	420	260	2671
	>26°C	0	0	0	0	2	2	4	47	83	130	118	47	24	449
	>32°C	0	0	0	0	0	0	0	0	5	7	16	1	2	31

FIGURE 8.14 Caption Cumulative frequencies of hours with focused operative temperature with façade integrated PV- with active floor heating in climate region 13 – west orientation

25m <sup>2</sup> - West - CR 13		WINTER							SUMMER						
Passive solar gains		November	December	January	February	March	April	SUM	May	June	July	August	September	October	SUM
MONTH/ Cumul. Frequency															
5PM to 10PM T <sub>op</sub> [°C]	>16°C	39	0	0	2	111	141	293	155	150	155	155	150	151	916
	>18°C	4	0	0	1	55	125	185	155	150	155	155	150	150	915
	>20°C	0	0	0	0	28	99	127	148	149	155	155	143	98	848
	>26°C	0	0	0	0	0	0	0	12	12	25	21	0	0	70
	>32°C	0	0	0	0	0	0	0	0	0	0	0	0	0	0
10PM to 5 PM T <sub>op</sub> [°C]	>16°C	145	1	44	59	330	508	1087	589	570	589	589	570	555	3462
	>18°C	97	0	23	38	272	394	824	576	567	589	589	563	428	3312
	>20°C	55	0	6	20	206	260	567	523	542	569	585	485	334	3038
	>26°C	2	0	0	0	35	32	69	154	107	149	118	82	77	687
	>32°C	0	0	0	0	1	0	1	24	0	1	9	4	5	43

FIGURE 8.15 Caption Cumulative frequencies of hours with focused operative temperature exclusively by passive solar gains in climate region 13 – west orientation

### § 8.3.1 Internal surface temperature by façade embedded PV collector

The dynamic simulation additionally calculated resulting space adjacent internal surface temperature of the roof embedded photovoltaic collectors. The results are helpful for an evaluation of the surface temperature and potential negative impact on spacial thermal comfort. Figure 233 shows cumulative frequencies of calculated surface temperature T<sub>surf</sub> [°C] for sun spaces in climate region 01,04,05 and 13, also in 13 with west orientation.

This table identifies cumulative frequencies for selected temperature like >30°C, >40°C, >50°C and >70°C as well as the maximum ever detected surface temperature.

Additionally the surface temperature >32°C were also calculated in regard to a resulting limit temperature for a remaining percentage of dissatisfied of less than 5 percent, that is mandatory for compliance of category B according DIN EN ISO 7730

in terms of local discomfort. The maximum surface temperature of 32°C results from a combination of the limited allowed maximum floor temperature of 28°C in order to accomplish less than 10 percent of dissatisfied (PD) in context of warm floors and a radiant asymmetry of maximum 5K between floor and ceiling to comply thermal comfort category B in ISO 7730.

CUMULATIVE FREQUENCIES OF SPACE FACING SURFACE TEMPERATURE OF FAÇADE EMBEDDED PHOTOVOLTAIC MODULES										
CLIMATE REGION / $T_{surf}$ [°C]	TRY01 Bremerhaven		TRY04 Berlin/Potsdam		TRY05 Köln/Essen		TRY13 München		TRY13 München WEST	
	5 TO 10 PM	10 TO 5 PM	5 TO 10 PM	10 TO 5 PM	5 TO 10 PM	10 TO 5 PM	5 TO 10 PM	10 TO 5 PM	5 TO 10 PM	10 TO 5 PM
$T_{surf} > 30^{\circ}\text{C}$	30	1071	85	1516	66	1215	78	1700	87	1569
$T_{surf} > 32^{\circ}\text{C}^1$	16	807	52	1314	42	1013	57	1505	63	1373
$T_{surf} > 40^{\circ}\text{C}$	1	277	3	565	8	379	11	861	18	747
$T_{surf} > 50^{\circ}\text{C}$	0	69	0	113	1	65	0	334	0	269
$T_{surf} > 70^{\circ}\text{C}$	0	3	0	2	0	1	0	19	0	14
MAX $T_{surf}$ [°C]	40.1	72.8	43.2	71.5	51.2	76.8	47.8	85.1	49.8	81.0

FIGURE 8.16 Cumulative frequencies of space adjacent surface temperature of façade embedded PV modules

Figure 8.16 demonstrably illustrates, that potential maximum surface temperature of 70°C and higher is possible. For a south oriented sun space in climate region 13 (München) even 85,1°C was calculated. Moreover, obviously the maximum temperature level of 70°C and higher is representative for the 10 to 5 PM interval.

Maximum surface temperatures during the preferred occupational evening hours do not exceed 51,2 °C.

Nonetheless, this temperature level is far away from either being harmless or non-effective on thermal comfort.

### § 8.3.2 Influence on thermal comfort by façade embedded PV collector

However, surface temperature higher than 32°C, which have demonstrably causes local discomfort and result in more than 5% of dissatisfied (category III) were calculated between 5 to 10 PM for at least 16 to 63 hours.

Essentially, in terms of impact on thermal comfort the frequency of hours ranges in entire year context between less than 1% and 3,4%. That means that for maximum 3,4 per cent of all evening hours are affected by surface temperature above 32°, what is negligible. On the contrary, account frequencies of surface temperature above 32°C of 807 to 1.505 hours in potential impact on thermal comfort on entire day basis for at least 11,6% to maximum 21,7%. As conclusion, roof embedded photovoltaic collectors have significant impact on thermal comfort on every eighth or fifth hour.

Moreover, in terms of risk of injury by tangency surface temperature above 50°C occur between 65 and 334 hours a year.

### § 8.3.3 Auxiliary energy consumption

---

In the context of a comprehensive energy balancing also auxiliary energy for system components need to be considered. Regarding photovoltaic modules, battery charger and DC/AC converter auxiliary energy solely accounts in terms of losses related to efficiency coefficients. Explicit additional energy to “run” components is not required. Singly power to run floor heating pumps and servo drives is required, but as already exemplified in Chapter 2, section 6.0, accounts for a few kilowatt hours per anno to run such a system.

Thus, we can conclude, that auxiliary energy requirement for a façade embedded photovoltaic module and battery combination and pv powered floor heating system is negligible.

### § 8.3.4 Surplus energy of PV collector – contribution to residential building

---

Since the storage capacity of the electro-chemical storage was limited to 20,2 kWh and 16,2 kWh effectively, a significant amount of power generated by pv collectors during summer months could not be stored. Consequently, these amounts of pv power was surplus and free for residential utilization. This section evaluates monthly surplus energy amounts. Therefore figure 234 visualizes monthly heating energy consumption supplied by photovoltaic and resulting surplus energy for residential fossil fuel substitution.

This section aims on the verification of Hypothesis Vpv.

Prior to any evaluation we have to acknowledge, that photovoltaic plants supply power but not heat, that is gained within this thesis. Thus, we both have to value the surplus power as potential energy for power-to-heat systems as well as potential power for residential housing.

In this context we propose an annual heating demand for

1. *An old fashioned residential home build in the 1960ties, respectively very poor building energetic standard with :*  $Q_h = 45.000 \text{ kWh/a}$

2. *A modern residential home build in 2016 (EnEV 2016), respectively supreme low energy building energetic standard with :*  $Q_h = 6.500 \text{ kWh/a}$

an annual power demand for

3. *A four head residential home with standard power consumption*

with :  $Q_p = 6.000 \text{ kWh/a}$

While the summed heating power supply ranges between 348 and 473 kWh, firstly Figure 8.17 illustrates, that the amount of surplus energy the combination of the envelope embedded pv and battery with floor heating generates always exceeds the effective applied power to additionally heat.

For example 779 kWh of surplus power in climate region 01 (TRY 01) outnumber 370 kWh effectively converted to heat. That indicates firstly, that a power storage with 16,2 kWh effectively is not sufficiently dimensioned to make generated power available in winter when heating demand is apparent.

MONTHLY SUN SPACE HEATING CONTRIBUTION BY PHOTOVOLTAIC COLLECTOR AND RESIDENTIAL SURPLUS ENERGY CONTRIBUTION															
	TRY 01 - BREMERHAVEN			TRY 04 - BERLIN / POTSDAM			TRY 05 - KÖLN / ESSEN			TRY 13 - MÜNCHEN			TRY 13 - MÜNCHEN WEST		
	Q <sub>H</sub> [kWh]	Σd <sub>QH</sub>	Q <sub>surpl</sub> [kWh]	Q <sub>H</sub> [kWh]	Σd <sub>QH</sub>	Q <sub>surpl</sub> [kWh]	Q <sub>H</sub> [kWh]	Σd <sub>QH</sub>	Q <sub>surpl</sub> [kWh]	Q <sub>H</sub> [kWh]	Σd <sub>QH</sub>	Q <sub>surpl</sub> [kWh]	Q <sub>H</sub> [kWh]	Σd <sub>QH</sub>	Q <sub>surpl</sub> [kWh]
JANUARY	-	-	-	15,6	1	-	14,7	1	-	31,2	2	-	15	2	-
FEBRUARY	43,7	3	-	39,0	3	-	45,0	3	4,9	31,2	2	10,6	45,6	2	3,0
MARCH	72,6	5	1,2	83,4	7	7,3	63,6	5	5,3	83,4	6	12,8	78,0	5	10,5
APRIL	95,1	7	57,7	60,4	7	110,7	64,8	5	59,0	106,2	8	14,2	101,4	9	13,1
MAY	70,2	5	95,6	28,2	3	173,0	72,6	6	93,2	36,0	4	157,9	57,9	8	127,4
JUNE	-	-	166,7	6,0	1	205,1	15,6	1	160,9	29,4	4	158,9	30,0	4	153,8
JULY	-	-	179,3	-	-	186,6	-	-	181,8	9,0	1	185,3	12,0	2	175,6
AUGUST	-	-	157,6	-	-	165,6	-	-	151,9	-	-	166,4	-	-	158,5
SEPTEMBER	-	-	98,5	10,2	1	105,8	15,6	1	81,7	24,0	1	92,5	33,0	1	75,9
OCTOBER	42,0	4	22,5	65,1	9	20,3	47,4	4	31,8	61,8	8	16,7	53,9	10	16,2
NOVEMBER	31,2	2	-	27,2	2	-	28,8	2	-	15,6	1	18,1	31,2	2	-
DECEMBER	15,6	1	-	13,8	1	-	15,0	1	-	24,6	2	-	15,6	1	-
	<b>370,4</b>	<b>27</b>	<b>779,1</b>	<b>348,8</b>	<b>35</b>	<b>974,4</b>	<b>383,1</b>	<b>29</b>	<b>770,5</b>	<b>452,4</b>	<b>39</b>	<b>833,4</b>	<b>473,6</b>	<b>46</b>	<b>734,0</b>
			<b>68%</b>			<b>74%</b>			<b>67%</b>			<b>65%</b>			<b>61%</b>

FIGURE 8.17 Monthly sun space heating contributed by façade integrated photovoltaic collector, cumulated extra days of heating and residential surplus energy contribution

Secondly, the limited capacity causes poor system performance in November, December and essentially in January. We can see, that the effective heating energy provision is on a nearly equal level of 360 kWh for climate region 01, 04 and 05. Opposed to that the south directed pv plant in climate region 13 provides 452 kWh effectively and 473 kWh with west orientation respectively. Although the total sum of effectively provided heating power and surplus power accounts for 1207 kWh for western “Munich version”, compared to the south directed “Berlin/Potsdam version” with 1322 kWh, the system manages providing significant higher proportions (39/61%) for effective floor heating.

Thus, the southern Germany west oriented variant performs best with regard to the prior aim of enhancing thermal comfort. The table additionally demonstrates, that power supply and additional heating is manageable in from November until April in all climate regions, except climate region 01, “Bremerhaven”, since January is missed. Disproportional to demand account highest amounts of supply represented in March and April for all climate regions. Thus best system performance, but moderate effect, is achieved in intermediate spring months. Analogously, the spring and autumn months profit from the highest amount of supply days with up to nine days. In total a combined sun space façade embedded pv and battery system performs with 27 to 46 additional days a year with enhanced thermal comfort. This equals 7 to 12% of the entire year.

On the contrary, annual surplus power yield of 734 to 974 kWh contributes between 1,6 to 2,1% of heating energy of an energetically poor residential home (1.), substitutes between 11,3 and 14,9% of heating energy of a modern low energy house or substitutes between 12,3 to 16,2% of the annual power demand with renewable energy.

*Hypothesis Vpv* can be verified on this generated insight.

Thus, in terms of a modern low energy house (2.) with subject to a second sufficient electro-chemical storage

*Hypothesis Vpv can be validated.*

Hence, in terms of an energetically poor residential building (1.; 1960ties)

*Hypothesis Vpv is to be rejected.*

---

## § 8.4 Operative temperatures by passive solar gains and façade embedded solar thermal collectors combined with sorption storage and floor heating

---

Section 4 inspects the effect of façade integrated evacuated solar thermal collectors. The floor heating is driven by solar thermal heat, that is seasonally stored in a loss free sorption storage. Analogously to section 3 the frequency and effect on operational temperature is evaluated in order to verify hypothesis II<sub>st</sub> and III<sub>st</sub>.

The comparison of figure 8.18 and 8.2 shows the effect in terms of enhanced cumulative frequencies of hours with  $T_{op} > 20^{\circ}\text{C}$  by additional sun space rafter integrated solar thermal collectors. In all four selected climate regions the sum of hours with  $T_{op} > 20^{\circ}\text{C}$  could have been enhanced by solar thermal heat provided by a loss free sorption storage.

Sun spaces in climate region 13 (Munich) benefit from at least additional 30 hours with  $T_{op} > 20^{\circ}\text{C}$ , while sun spaces in climate region 4 (Berlin) profit from additional 38 hours, in climate region 01 (Bremerhaven, Flensburg) from another 41 hours and sun spaces in climate region 05 (Köln/Essen) from additional 78 hours.

As a consequence, disproportional to this improvement hours with  $T_{op} > 20^{\circ}\text{C}$  between 10 to 5 PM decrease between 60 and 120 hours.

The comparison of figure 8.19 to 8.26 reveals the effect of solar thermal collectors and loss-free thermal seasonal storage in detail. An evaluation aims on the verification of Hypothesis II<sub>st</sub>, III<sub>st</sub> and IV. Figure 8.19 compared to Figure 8.20 illustrates, that the sum of hours with  $T_{op} > 20^{\circ}\text{C}$  between 5 to 10 PM during winter in climate region 01 can be improved by 41 hours from 163 to 204 hours. Further, cumulative frequencies of hours with  $T_{op} > 20^{\circ}\text{C}$  between 5 to 10 PM during summer months were calculated to be raised from 877 in the reference model to 903 in the solar thermal model.

Hence, additional 26 hours in summer provide satisfactory indoor thermal comfort. As a consequence, the cumulative hours with  $T_{op} > 20^{\circ}\text{C}$  in the time interval 10 to 5 PM decreases. In the winter this decrease accounts for 59 hours and in summer for 50 hours.

A closer look comparing Figure 8.21 and 8.22 additionally detects a decrease in hours with  $T_{op} > 18$  and  $T_{op} > 16^{\circ}\text{C}$  when floor heating is fed by solar thermal collectors and seasonal thermal loss-free storage.

**CUMULATIVE FREQUENCIES OF  
OPERATIVE TEMPERATURE BY  
FACADE INTEGRATED HEATPIPE+SORPTION STORAGE  
SUN SPACE - 25 m<sup>2</sup> - SOUTH**

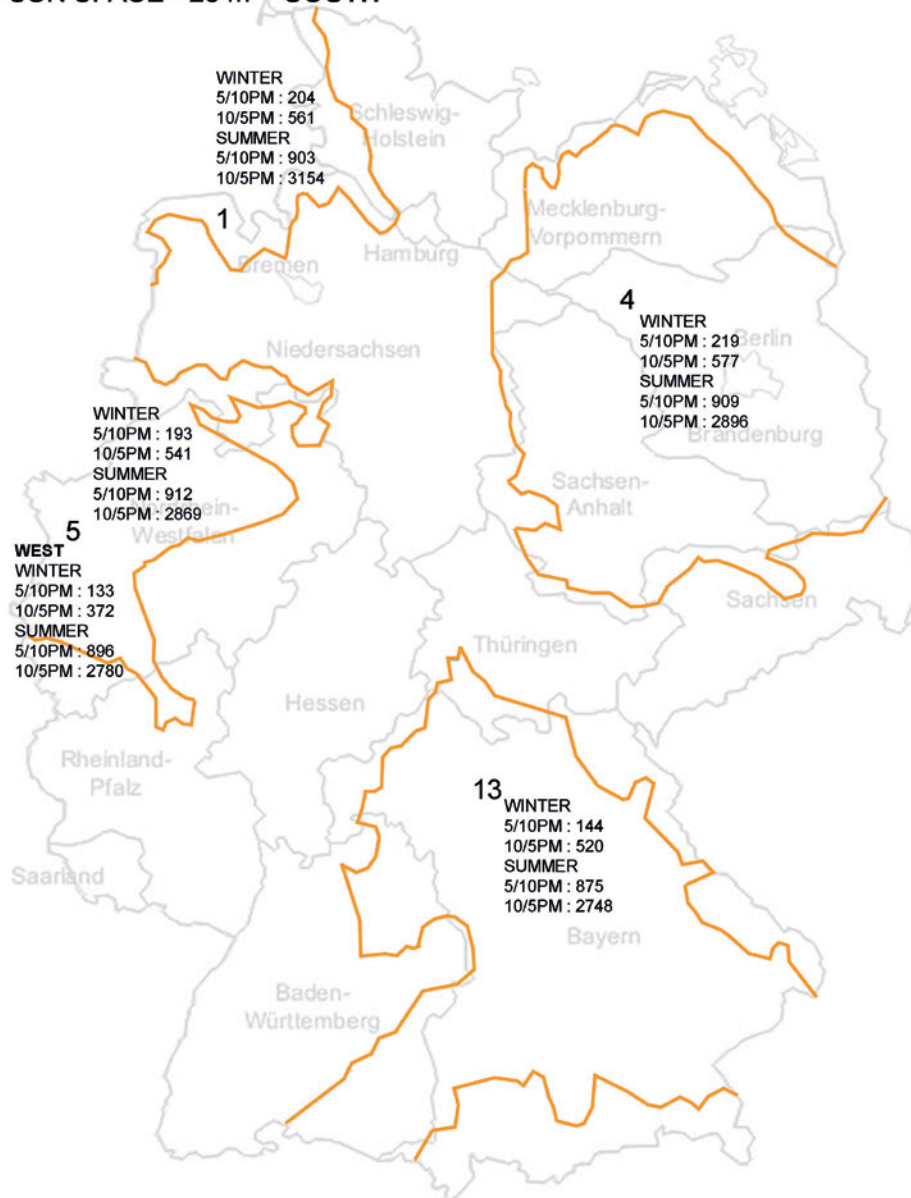


**FIGURE 8.18** Cumulative frequencies of operative temperature  $T_{op} > 20^{\circ}\text{C}$  for south orientation by passive solar gains and additional façade integrated heatpipe and sorption storage between 5 to 10 PM and 10 to 5 PM for 15 different climate regions

25m <sup>2</sup> - South - CR 01		WINTER							SUMMER							
HEATBEAM - With FLOOR HEATING		November	December	January	February	March	April	SUM	May	June	July	August	September	October	SUM	
MONTH/ Cumul. Frequency																
5PM to 10PM	T <sub>op</sub> [°C]	>16°C	46	0	0	15	88	150	299	155	150	155	155	150	151	916
		>18°C	24	0	0	1	66	148	239	155	150	155	155	150	151	916
		>20°C	11	0	0	0	55	138	204	152	150	155	155	150	141	903
		>26°C	0	0	0	0	1	7	8	2	11	7	37	9	6	72
		>32°C	0	0	0	0	0	0	0	0	0	0	3	0	0	3
10PM to 5 PM	T <sub>op</sub> [°C]	>16°C	208	15	14	108	338	537	1220	588	570	589	589	570	583	3489
		>18°C	129	3	1	84	239	429	885	562	570	589	589	570	524	3404
		>20°C	70	0	0	54	159	278	561	448	543	589	585	569	420	3154
		>26°C	2	0	0	0	45	81	108	50	88	148	194	224	139	843
		>32°C	0	0	0	0	5	15	20	1	0	4	38	72	28	143

FIGURE 8.19 Cumulative frequencies of hours with focused operative temperature with façade integrated heatpipe - with active floor heating in climate region 01 – south orientation

25m <sup>2</sup> - South - CR 01		WINTER							SUMMER							
Passive solar gains		November	December	January	February	March	April	SUM	May	June	July	August	September	October	SUM	
MONTH/ Cumul. Frequency																
5PM to 10PM	T <sub>op</sub> [°C]	>16°C	60	0	0	16	121	150	347	155	150	155	155	150	151	916
		>18°C	30	0	0	1	68	150	249	155	150	155	155	150	151	916
		>20°C	0	0	0	0	41	122	163	142	150	155	155	150	125	877
		>26°C	0	0	0	0	0	0	0	1	8	7	14	6	0	36
		>32°C	0	0	0	0	0	0	0	0	0	0	0	0	0	0
10PM to 5 PM	T <sub>op</sub> [°C]	>16°C	271	23	15	115	398	557	1379	589	570	589	589	570	586	3493
		>18°C	158	9	2	88	286	452	995	565	570	589	589	570	541	3424
		>20°C	83	1	0	60	172	294	610	452	560	589	589	570	444	3204
		>26°C	0	0	0	0	19	40	59	14	34	86	89	143	84	450
		>32°C	0	0	0	0	1	2	3	0	0	0	2	32	9	43

FIGURE 8.20 Cumulative frequencies of hours with focused operative temperature exclusively by passive solar gains in climate region 01 – south orientation

25m <sup>2</sup> - South - CR 04		WINTER							SUMMER							
HEATBEAM - With FLOOR HEATING		November	December	January	February	March	April	SUM	May	June	July	August	September	October	SUM	
MONTH/ Cumul. Frequency																
5PM to 10PM	T <sub>op</sub> [°C]	>16°C	25	0	5	10	81	144	265	155	150	155	155	150	151	916
		>18°C	21	0	3	10	75	135	244	155	150	155	155	150	151	916
		>20°C	13	0	1	9	70	126	219	154	149	155	155	150	146	909
		>26°C	0	0	0	1	4	5	10	9	11	20	17	4	0	61
		>32°C	0	0	0	0	0	0	0	0	0	1	0	0	0	1
10PM to 5 PM	T <sub>op</sub> [°C]	>16°C	140	20	72	63	327	498	1120	586	570	589	589	570	570	3474
		>18°C	92	13	46	36	240	390	817	558	558	589	589	555	484	3333
		>20°C	52	8	26	26	180	285	577	446	500	577	574	476	323	2896
		>26°C	1	0	1	9	50	37	98	34	107	116	101	116	70	544
		>32°C	0	0	0	4	5	0	9	0	0	7	14	18	9	48

FIGURE 8.21 Cumulative frequencies of hours with focused operative temperature with façade integrated heatpipe - with active floor heating in climate region 04 – south orientation

25m <sup>2</sup> - South - CR 04															
Passive solar gains															
MONTH/ Cumul. Frequency		WINTER						SUMMER							
		November	December	January	February	March	April	SUM	May	June	July	August	September	October	SUM
5PM to 10PM	>16°C	25	0	2	10	104	150	291	155	150	155	155	150	151	916
	>18°C	5	0	0	7	70	137	219	155	150	155	155	150	151	916
	>20°C	5	0	0	4	54	118	181	152	150	155	155	150	147	909
	>26°C	0	0	0	0	2	3	5	15	13	21	17	5	1	72
	>32°C	0	0	0	0	0	0	0	0	0	1	0	0	0	7
10PM to 5 PM	>16°C	160	22	75	69	352	530	1208	589	570	589	589	570	589	3496
	>18°C	85	14	48	43	281	456	927	577	568	589	589	570	558	3451
	>20°C	53	10	28	27	208	332	658	506	530	589	589	547	449	3210
	>26°C	1	0	1	10	63	48	123	45	132	151	115	136	90	669
	>32°C	0	0	0	4	9	0	13	0	0	8	15	24	11	58

FIGURE 8.22 Cumulative frequencies of hours with focused operative temperature exclusively by passive solar gains in climate region 04 – south orientation

The comparison of Figure 8.21 and 8.22, which represent climate region 04 (Berlin/ Potsdam) exemplifies in increase of hours with  $T_{op} > 20^{\circ}\text{C}$  of 38 hours from 181 to 219 hours in winter. Opposed to figure 8.19 (CR 01) additionally cumulative frequencies of hours with  $T_{op} > 18^{\circ}\text{C}$  considerably improves.

Likewise solar thermal system manage to improve cumulative frequencies from January to April for operational temperature  $< 20^{\circ}\text{C}$  compared to the reference passive solar gain model.

In climate region 05, representing major cities like “Köln, Essen” and covering “Nieder-rheinische Bucht and Emsland”, the sum of hours with  $T_{op} > 20^{\circ}\text{C}$  in the evening is significantly improved from 115 to 193 hours in winter and also from 872 to 912 hours during summer months. The improvement covers 78, respectively, 40 hours. Interestingly, the cumulative frequencies of hours with  $T_{op} > 16^{\circ}\text{C}$  lowers from 399 to 314, on the contrary the cumulative frequencies with  $T_{op} > 18^{\circ}\text{C}$  raises from 217 to 231.

Notwithstanding, thermal comfort situation for midwinter months December and January does not improve.

Figure 8.25 and Figure 8.26 table the results for a west oriented 25m<sup>2</sup> sun space located in climate region 05.

Although the west oriented sun space suffers from less hours in preferred occupational time with satisfactory operational temperature according category B, after integrated collector combined with a loss free sorption storage manage to improve the comfort situation.

25m <sup>2</sup> - South - CR 05		WINTER							SUMMER						
HEATBEAM - With FLOOR HEATING		November	December	January	February	March	April	SUM	May	June	July	August	September	October	SUM
MONTH/	Cumul. Frequency														
5PM to 10PM	>16°C	37	0	0	31	108	138	314	155	150	155	155	150	150	915
	>18°C	11	0	0	16	71	133	231	155	150	155	155	150	150	915
	>20°C	6	0	0	12	57	118	193	155	150	155	154	150	148	912
	>26°C	0	0	0	0	0	1	1	6	7	23	16	7	0	59
	>32°C	0	0	0	0	0	0	0	0	0	0	0	0	0	0
10PM to 5 PM	>16°C	151	16	38	176	375	515	1271	587	570	589	589	570	587	3492
	>18°C	98	7	21	140	281	405	952	556	568	586	589	562	540	3401
	>20°C	51	4	8	95	182	201	541	409	465	564	562	499	370	2869
	>26°C	0	0	0	1	17	19	37	17	46	90	74	99	65	391
	>32°C	0	0	0	0	1	0	1	0	0	2	3	12	2	19

FIGURE 8.23 Cumulative frequencies of hours with focused operative temperature with façade integrated heatpipe - with active floor heating in climate region 05 – south orientation

25m <sup>2</sup> - South - CR 05		WINTER							SUMMER						
Passive solar gains		November	December	January	February	March	April	SUM	May	June	July	August	September	October	SUM
MONTH/	Cumul. Frequency														
5PM to 10PM	>16°C	55	0	0	55	140	149	399	155	150	155	155	150	151	916
	>18°C	10	0	0	7	81	119	217	155	150	155	155	150	146	911
	>20°C	0	0	0	0	33	82	115	149	145	155	155	147	121	872
	>26°C	0	0	0	0	0	1	1	7	6	23	16	7	0	59
	>32°C	0	0	0	0	0	0	0	0	0	0	0	0	0	0
10PM to 5 PM	>16°C	234	20	40	187	423	496	1400	589	570	589	589	570	583	3490
	>18°C	111	9	26	142	294	379	961	566	565	589	589	583	545	3417
	>20°C	66	4	13	105	210	214	612	458	528	584	585	550	438	3143
	>26°C	0	0	0	1	22	23	46	29	60	102	88	125	78	482
	>32°C	0	0	0	0	1	0	1	0	0	0	2	17	4	23

FIGURE 8.24 Cumulative frequencies of hours with focused operative temperature exclusively by passive solar gains in climate region 05 – south orientation

25m <sup>2</sup> - WEST - CR 05		WINTER							SUMMER						
HEATBEAM - With FLOOR HEATING		November	December	January	February	March	April	SUM	May	June	July	August	September	October	SUM
MONTH/	Cumul. Frequency														
5PM to 10PM	>16°C	17	0	0	18	94	126	255	155	150	155	155	150	146	911
	>18°C	6	0	0	10	51	100	167	155	150	155	155	150	145	910
	>20°C	3	0	0	7	31	92	133	154	148	155	154	150	135	896
	>26°C	0	0	0	0	1	1	2	5	6	21	18	6	0	56
	>32°C	0	0	0	0	0	0	0	0	0	0	0	0	0	0
10PM to 5 PM	>16°C	114	7	17	135	311	426	1010	587	570	589	589	570	572	3477
	>18°C	60	3	6	88	242	305	704	553	564	586	589	581	519	3372
	>20°C	23	0	1	49	143	156	372	395	448	549	556	485	347	2780
	>26°C	0	0	0	0	9	17	26	10	40	77	70	71	32	300
	>32°C	0	0	0	0	0	0	0	0	0	0	0	8	1	9

FIGURE 8.25 Cumulative frequencies of hours with focused operative temperature with façade integrated heatpipe - with active floor heating in climate region 05 – west orientation

Summarized, the figure of hours from 5 to 10 PM in winter improves for solely 10 hours, but nonetheless, cumulative frequencies of hours with lower operational temperature demonstrably lower.

25m <sup>2</sup> - West - CR 05															
Passive solar gains															
MONTH/ Cumul. Frequency		WINTER						SUMMER							
		November	December	January	February	March	April	SUM	May	June	July	August	September	October	SUM
5PM to 10PM	>16°C	44	0	0	16	130	150	340	155	150	155	155	150	151	916
	>18°C	2	0	0	1	61	142	206	155	150	155	155	150	141	906
	>20°C	0	0	0	0	24	99	123	155	145	155	155	142	110	882
	>26°C	0	0	0	0	0	3	3	5	7	20	18	4	0	54
	>32°C	0	0	0	0	0	0	0	0	0	0	0	0	0	0
10PM to 5 PM	>16°C	174	9	20	150	371	534	1258	589	570	589	589	570	574	3481
	>18°C	89	3	8	99	264	444	907	586	565	589	589	556	524	3409
	>20°C	36	0	2	60	179	321	598	519	521	584	584	528	382	3118
	>26°C	0	0	0	0	18	32	50	80	46	84	71	56	39	376
	>32°C	0	0	0	0	0	0	0	8	0	0	0	7	2	17

FIGURE 8.26 Caption Cumulative frequencies of hours with focused operative temperature exclusively by passive solar gains in climate region 05 – west orientation

Likewise the frequencies of hours for the time interval 10 to 5 PM do.

Summarized, the figure of hours from 5 to 10 PM in winter improves for solely 10 hours, but nonetheless, cumulative frequencies of hours with lower operational temperature demonstrably lower. Likewise the frequencies of hours for the time interval 10 to 5 PM do.

Finally, the evaluation of cumulative frequencies of hours for climate region 13 (Munich) show a considerable increase in hours with  $T_{op} > 20^\circ\text{C}$  for evening hours both in winter and summer (Fig. 8.27 and 8.28). Improvement in indoor temperature by rafter integrated solar thermal collector covers November, February, March, April and May. Interestingly, this variant also illustrates the potential to improve operational temperature in the late autumn month October considerably

Summarized, the cumulative frequency of hours with  $T_{op} > 20^\circ\text{C}$  in preferred evening time at maximum reaches 219 hours.

As result of this evaluation, *Hypothesis IIst, IIIst and IV* can be verified.

The table in this section evident, that the cumulative frequencies of hours with  $T_{op} > 20^\circ\text{C}$  can be improved exclusively by rafter integrated solar thermal collectors combined with a common sensible water buffer tank. This is especially evident in the early spring months, when the seasonal thermal loss-free sorption storage is still complete discharged and provides not yet any heating energy.

*Hypothesis IIst can be validated.*

The tables in Figure 8.19 to 8.28 exemplify, that cumulative frequencies of hours with  $T_{op} > 20^\circ\text{C}$  in the 5 to 10 PM time interval during winter never reaches 1.060 hours.

25m <sup>2</sup> - South - CR 13		WINTER							SUMMER						
HEATBEAM - With FLOOR HEATING		November	December	January	February	March	April	SUM	May	June	July	August	September	October	SUM
MONTH/	Cumul. Frequency														
5PM to 10PM	>16°C	22	0	0	5	99	123	249	155	150	155	155	150	151	916
	>18°C	8	0	0	5	68	111	192	146	150	155	155	150	143	899
	>20°C	6	0	0	4	51	83	144	138	141	155	155	149	137	875
	>26°C	0	0	0	0	0	1	1	8	12	25	24	1	1	71
	>32°C	0	0	0	0	0	0	0	0	0	0	1	0	0	1
10PM to 5 PM	>16°C	129	20	78	80	340	401	1048	569	567	589	589	570	540	3424
	>18°C	95	11	58	58	296	289	777	526	556	588	589	548	460	3267
	>20°C	61	3	36	43	204	173	520	379	436	551	546	455	319	2748
	>26°C	2	0	0	4	44	13	63	56	106	146	125	110	91	634
	>32°C	0	0	0	0	2	0	2	0	1	2	15	16	10	44

FIGURE 8.27 Caption Cumulative frequencies of hours with focused operative temperature with façade integrated heatpipe - with active floor heating in climate region 013 – south orientation

25m <sup>2</sup> - South - CR 13		WINTER							SUMMER						
Passive solar gains		November	December	January	February	March	April	SUM	May	June	July	August	September	October	SUM
MONTH/	Cumul. Frequency														
5PM to 10PM	>16°C	61	0	0	5	148	131	345	155	150	155	155	150	151	916
	>18°C	17	0	0	2	78	112	209	153	150	155	155	150	151	914
	>20°C	0	0	0	1	38	72	111	135	146	155	155	150	120	861
	>26°C	0	0	0	0	0	0	0	8	12	26	24	3	1	74
	>32°C	0	0	0	0	0	0	0	0	0	0	1	0	0	1
10PM to 5 PM	>16°C	195	22	100	86	380	446	1229	585	570	589	589	570	579	3482
	>18°C	118	15	63	62	310	324	892	543	561	589	589	568	484	3334
	>20°C	84	7	45	46	242	217	641	434	523	571	586	540	408	3062
	>26°C	2	0	0	5	52	20	79	60	120	166	139	140	106	731
	>32°C	0	0	0	0	2	0	2	0	0	1	14	20	12	47

FIGURE 8.28 Caption Cumulative frequencies of hours with focused operative temperature exclusively by passive solar gains in climate region 13 – south orientation

For that reason

*Hypothesis III is to be rejected.*

Since the maximum cumulative frequency of hours with  $T_{op} > 20^\circ\text{C}$  during winter month in the time interval 5 to 10 PM reaches 219 hours at maximum, the hypothesized cumulative frequency of 1.060 hours is not accomplished.

Thus, an autarkic operation assuring 1.060 hours with  $T_{op} > 20^\circ\text{C}$  with the in chapter 7 defined collector and limited seasonal sorption storage design is not feasible.

For that reason

*Hypothesis IV is to be rejected.*

## § 8.4.1 Internal surface temperature by façade embedded solar thermal collector

---

A holistic thermal comfort evaluation calls for a detailed analysis of resulting internal surface temperature of any façade embedded collector technology. Analogously to section 3.1 also the rafter integrated solar thermal heatpipe collector HEATBEAM II© is to be evaluated.

However, since the absorber and heatpipe firstly is evacuated, secondly located outside the space upon the basic rafter construction and thirdly thermally decoupled by a low conductive polymer separator, heat transfer and radiation towards the space is considered to be nearly zero and hence negligible.

### § 8.4.1.1 Influence on thermal comfort by façade embedded solar thermal collector

---

Solar thermal absorber have been observed in Chapter 2 to generate temperature of 260 to 300°C. Although such solar thermal collectors belong to medium temperature level collectors (Mitteltemperatur-Kollektoren), any radiant temperature above 40°C impacts thermal comfort and any surface temperature above 50°C causes risk of injury by tangency.

Based on the concept of an evacuated tube collector, that is additionally thermally decoupled from further construction and from the occupation space, any impact on thermal comfort is not expected and thus not further inspected.

## § 8.4.2 Evaluation of energy management

---

Since also the seasonal thermal loss-free sorption storage is limited in terms of storage capacity, solar heat generated in midsummer months is neither consumed by the sun space nor can be stored for winter. Thus, parallel to the photovoltaic-battery concept, the rafter integrated collector-sorption storage combination generates specific amounts of surplus heating energy. This surplus heating energy is free for consumption by the adjacent residential home. Figure 246 tables both effectively consumed heating energy and surplus energy. Since the sorption storage system requires considerable amounts of auxiliary energy in terms of power and heat as well, the cumulated amount of surplus energy is reduced by cumulated auxiliary energy.

Thus, the tables documents the effective surplus heating energy  $Q_{surpl,eff}$  in kWh for a climate zone.

### § 8.4.2.1 Surplus energy related to required auxiliary energy

Similar to the pv system the surplus energy is related to the overall heating energy consumption. The ratio is plotted on the bottom of the table (Fig. 8.29).

MONTHLY SUN SPACE HEATING CONTRIBUTION BY SOLAR THERMAL COLLECTOR, RESIDENTIAL SURPLUS ENERGY CONTRIBUTION AND AUXILIARY ENERGY CONSUMPTION																				
	TRY 01 - BREMERHAVEN				TRY 04 - BERLIN / POTSDAM				TRY 05 - KÖLN / ESSEN				TRY 05 - KÖLN / ESSEN WEST				TRY 13 - MÜNCHEN			
	$Q_{L}$ [kWh]	$\Sigma E_{Dp}$	$Q_{aux}$ [kWh]	$Q_{surpl}$ [kWh]	$Q_{L}$ [kWh]	$\Sigma E_{Dp}$	$Q_{aux}$ [kWh]	$Q_{surpl}$ [kWh]	$Q_{L}$ [kWh]	$\Sigma E_{Dp}$	$Q_{aux}$ [kWh]	$Q_{surpl}$ [kWh]	$Q_{L}$ [kWh]	$\Sigma E_{Dp}$	$Q_{aux}$ [kWh]	$Q_{surpl}$ [kWh]	$Q_{L}$ [kWh]	$\Sigma E_{Dp}$	$Q_{aux}$ [kWh]	$Q_{surpl}$ [kWh]
	HEAT		POWER		HEAT		POWER		HEAT		POWER		HEAT		POWER		HEAT		POWER	
JANUARY	18.0	2	-	-	12.6	1	-	-	-	-	-	-	-	-	-	-	-	-	-	-
FEBRUARY	28.0	2	-	-	19.5	2	-	-	32.4	2	-	-	35.1	2	-	-	15.6	1	-	-
MARCH	70.9	6	-	-	78.6	7	-	2.06	56.4	6	-	0.5	60.6	6	-	-	87.7	7	-	2.1
APRIL	87.0	11	-	-	11.85	69	9	-	1.2	24.2	113.5	9	-	3.2	11.8	100.3	8	-	1.2	8.7
MAY	93.0	8	-	-	13.4	77.4	8	-	26.6	89.4	10	-	2.0	11.8	106.62	12	-	2.4	11.27	90.9
JUNE	18.0	3	110.0	-	11.85	18.0	2	253.0	-	-	33.4	4	-	20.1	26.4	4	22.1	-	16.5	88.2
JULY	-	-	227.7	-	-	-	-	229.4	-	-	-	-	215.7	-	-	-	210.6	-	1.5	24.0
AUGUST	-	-	199.8	-	-	-	-	201.8	-	-	-	-	189.9	-	-	-	2.4	1	181.6	-
SEPTEMBER	-	-	137.2	-	-	-	-	149.9	-	-	-	-	123.9	-	-	-	128.4	-	-	18.0
OCTOBER	111.0	9	66.6	6.0	2.4	79.8	11	36.4	7.2	2.9	177	13	-	8.4	3.4	200.16	16	30.5	9.6	
NOVEMBER	76.2	8	-	3.6	1.45	63.0	4	-	3.6	1.5	22.8	2	-	-	-	26.4	3	-	1.2	
DECEMBER	-	-	-	-	-	-	-	-	-	-	-	-	-	-	-	-	-	-	-	-
			<b>9.6</b>	<b>41.8</b>				<b>12.0</b>	<b>57.6</b>				<b>13.6</b>	<b>57.6</b>			<b>14.4</b>	<b>52.4</b>		<b>12.0</b>
	<b>502.1</b>	<b>47</b>	<b>749.2</b>	<b>-50.6 kWh</b>	<b>428.4</b>	<b>45</b>	<b>649.6</b>	<b>-89.5 kWh</b>	<b>557.9</b>	<b>49</b>	<b>529.6</b>	<b>-61.2 kWh</b>	<b>573.0</b>	<b>51</b>	<b>573.2</b>	<b>-56.8 kWh</b>	<b>652.6</b>	<b>60</b>	<b>470.0</b>	<b>-60.2 kWh</b>
<b><math>Q_{surpl,eff}</math> [kWh]</b>	<b>689.7</b>			<b>60%</b>	<b>800.1</b>			<b>67%</b>	<b>468.4</b>			<b>49%</b>	<b>516.5</b>			<b>50%</b>	<b>409.8</b>			<b>42%</b>

FIGURE 8.29 Monthly sun space heating contributed by façade integrated photovoltaic collector, cumulated extra days of heating, auxiliary energy and residential surplus energy contribution

The sun space roof integrated solar thermal collector and seasonal sorption storage system manages to provide a south oriented and 25m<sup>2</sup> sized sun space located in climate zone 01 with in total 502 kWh effectively consumed heating energy. The system requires approximately 50 kWh auxiliary energy, what reduces 740 kWh surplus energy to 689 kWh effective surplus energy.

For climate region 04 (Berlin/Potsdam) is calculated an effective consumed amount of 428 kWh. Opposed to that accounts auxiliary energy for 69,5 kWh, resulting in an effective surplus energy amount of 800 kWh. The system supplied the floor heating in climate region 05 (Köln/Essen) with 558 kWh effectively consumed heating energy. Auxiliary energy is calculated with 61 kWh. This results in an effective surplus energy amount of 468 kWh for climate region 05. A west orientated sun spaces in climate

region 05 profits from 570 kWh effectively consumed heating energy, while auxiliary energy accounts with 57 kWh. The resulting surplus energy assesses with 516 kWh.

In Munich, in climate region 13, 652 kWh can be effectively consumed for comfort improvement, whereas auxiliary energy sums with 60 kWh. The sun space-collector-sorption storage system provides 410 kWh surplus energy for the residential home.

The table shows, that heating energy ranges between 428 and 626 kWh. Auxiliary energy demand remains on a level of approximately 60 kWh per year. The resulting effective surplus energy ranges for the solar thermal and sorption storage system between 410 and 800 kWh. Thus, dependant on the climate zone the surplus energy can double compared to climate zone 13.

Figure 8.29 additionally illustrates, that heating energy supply for the sun space includes the winter month January exclusively for climate region 01 and 04. Supply is limited to November and misses December for all climate zones. Opposed to that heating energy supply for the sun space floor heating is also required in September for climate zones 04, 05 and 13.

A sun space in climate region 01 benefits from 47 additional days of heating energy supply, a space in 04 from 45 additional days, in climate 05 south from 49 and 51 for west oriented respectively. Deviating from this mean of 47 days, a sun space in climate zone 13 profits from 60 additional days of renewable heating energy. Although the calculated variant in climate region 13 accounts for the comparably lowest total sum of consumed and surplus energy (1062 kWh), the number of days with effective heating supply accounts with 60 the highest ranked. The system effects a consumed/surplus energy-ratio of 42%, what is the lowest in contest.

Thus, the system, although utilizing the lowest amount of solar thermal energy works the most efficient in terms of sun space heating energy supply of all investigated. The system achieves the lowest efficiency ratio in respect to the main aim of sun space supply in climate region 04 with a ratio of 67% surplus energy and a total sum of potential utilizable solar thermal energy of 1248 kWh.

#### § 8.4.2.2 10% energy substitution by surplus energy - Verification of Hypothesis Vst

---

Since the storage capacity of the seasonal loss-free thermal thermos-chemical sorption storage was limited to 220 kWh/m<sup>3</sup> and to 150 kWh effectively, a significant amount of solar thermal heating energy generated during summer months could not be stored.

Consequently, these amounts of heating energy was surplus and free for residential utilization. After explanation and evaluation of computer aided dynamic modelling results, this section aims on the verification of Hypothesis Vst.

In this context we similar to 3.4 propose an annual heating demand for

1. An old fashioned residential home build in the 1960ties, respectively very poor building energetic standard with :  $Q_h = 45.000 \text{ kWh/a}$

2. A modern residential home build in 2016 (EnEV 2016), respectively supreme low energy building energetic standard with :  $Q_h = 6.500 \text{ kWh/a}$

Prior to any evaluation we have to consider, that the storage capacity of the sorption storage in the models was limited to effectively 150 kWh. If this technically in terms of volumetric density and economically could significantly improve, could double or triple for instance, the amount of effective heating energy for the sun space floor heating will improve and the effective potential surplus energy demonstrably lower.

Hence, any analysis of potential surplus energy for the residential building has to be weighted against the background of the selected limited storage capacity of 150 kWh.

Figure 246 exemplifies surplus heating energy ranging from 410 to 800 kWh. In terms of the old fashioned and poor thermally insulated residential building (1.) at least 10% of the assumed annual heating energy amount that equals 4.500 kWh cannot be met in any of the calculated climate regions. In case of an modern residential building with supreme energetic building physical quality 10% equals 650 kWh per year. In this context a sun space equipped with rafter integrated solar thermal evacuated tube collectors and combined with a seasonal loss-free sorption storage generates sufficient surplus energy, if located in climate region 01 or 05.

In context of *a poor thermally insulated residential building* built in the 1960ties

*Hypothesis Vst is to be rejected.*

In context of *a modern contemporary and supreme insulated residential building* with regard to climate region 01 and 04

*Hypothesis Vst can be validated,*

but with regard to climate region 05 and 13

*Hypothesis Vst is to be rejected.*

## § 8.5 Effect comparison of the two different collector and storage combinations

After detailed evaluation of each an investigated collector-storage system both systems can be compared and analysed with regard to the major aim and secondary benefits.

First we can summarize, that the photovoltaic-battery system was not eligible to improve thermal comfort in comparison to the passive solar gain reference. Roof implemented and area-intensive photovoltaic modules cause shading and demonstrably hinder transmission of irradiation, thus reduce passive solar gains. Generated pv power does not manage compensating the lack of passive solar gains, what results in less cumulative frequencies of hours with satisfactory operational temperatures.

Opposed to the roof embedded pv modules, rafter integrated evacuated tube collectors simply slightly shadow sun spaces and thus have negligible impact on passive solar gains. Hence, the second system based on area-efficient evacuated tubes combined with a seasonal loss-free thermo-chemical storage manages improving thermal comfort compared to the reference.

The rafter integrated solar thermal collector-storage system is the only effective system.

On the contrary, direct comparison of the energy management performance tabled in figure 234 and 246 demonstrates, that the pv-battery system manages effectively providing 348 to 473 kWh of additional heating energy, while the evacuated tube-sorption storage system effectively provides 428 to 652 kWh.

In order to conclude, the evacuated tube-sorption storage system manage to provide 80 to 180 kWh more additional heating energy than the pv-battery system. Moreover, the direct comparison of summed days with additional heating recover a range of 27 to 46 days for the pv-battery system, but 45 to 60 days for the evacuated tube-sorption storage system. Disproportionally, the pv-battery system allows a surplus energy utilisation between 734 to 974 kWh. The tube-sorption storage system offers less, only energy amounts in a range of 410 to 800 kWh.

Although already explicated, that the pv-battery system does not manage improving thermal comfort, a direct comparison of the summed effective energy to utilize (heating energy+surplus energy) identifies for the pv-battery system a range between 1.149 and 1.322 kWh in total and for the evacuated tube-sorption storage system a range between 1.025 and 1.248 kWh in total.

As a conclusion we can state, that the evacuated tube-sorption storage system is first the only effective and second the more efficient system. Since the pv-battery system slightly offers a higher amount of heating and surplus energy, but does not manage to effectively utilize the major part it convinces more with demonstrative amounts of surplus energy for residential consumption, but not with effective thermal comfort improvement.

Moreover, calculations indicate, that high surface temperature of the modules firstly impacts negatively thermal comfort and secondly give rise for risks of injury.

---

## § 8.6 Summary

---

This chapter answers many questions. Questions include thermal comfort quality by exclusively passive solar gains including all 15 climate regions in Germany, effectiveness and efficiency of two different façade integrated collector systems combined with seasonal energy storages as well as potential surplus energy and undesired negative impact on interior thermal comfort by outlying surface temperatures of the façade embedded collectors.

Providing operational temperature of  $>20^{\circ}\text{C}$  in winter between 5 to 10 PM exclusively by passive solar gains is maximum possible for 248 hours, what equals nearly 25% of the total sum of hours (1.060). This level of hours can be enhanced for several hours (45 to 60) by a façade implemented solar thermal collector system that is combined with a thermo-chemical sorption storage.

Autarkic operation of a sun space by passive solar gains and embedded collectors and storages is not possible with respect to the limited storage capacities, which either are contemporary feasible or economic. Despite obvious amounts of auxiliary energy consumption, the rather integrated evacuated tube collector and loss-free sorption storage system exclusively manages improving thermal comfort instead of worsening it.

The system has been evaluated to be only efficient one, since it manages providing higher amounts of heating energy when heating energy is requested.

In regard to one climate region, the system nearly manages doubling the days the pv-battery system is eligible to provide additional heating energy.





epimmos hamos  
ubris-ain as

...de beste manier om de toekomst te creëren.

...de beste manier om de toekomst te creëren.

"Als er een wind van verandering

"De beste manier om de toekomst te creëren."

## 9 Conclusion

This thesis project successfully investigated on potential thermal comfort in sun spaces. The project elaborated in detail relevant findings and extensive insights both based on empirical as well as on theoretical data relevant for the entire German federal territory.

Both detailed empirical and theoretical analysis inspected cumulative frequencies of hours with required operational indoor temperature, especially for an preferred occupational time between 5 to 10 PM during winter. Further, an experimental test set-up allowed to analyse detailed reasons, frequencies and impact of local discomfort month-wise.

### Major insights and deliverables

---

The research question as well as the five established hypothesis could be answered or verified respectively.

Starting with *Hypothesis*,

#### *I*

*Cumulated frequencies of hours of resultant temperature > 20°C in order to determine indoor thermal comfort in SL80 Solarlux sun spaces according to DIN EN 15251-A regarding south directed 25m<sup>2</sup> dimensioned sun spaces in 15 different climate regions in Germany provided by renewable heating energy exclusively by solar gains are annually less than 1060 hours during autumn to spring time (Oct.-April).*

we detected any climate region, in which a sun space provided 1.060 hours with operational temperature above 20°C between 5 to 10 PM from October to April. For south oriented sun spaces were calculated maximum 264 hours in climate region 6 (Nördliche und Westliche Mittelgebirge – Randgebiete), covering parts of Rheinlandpfalz and Saarland.

Thus, *Hypothesis I was validated.*

Calculations of photovoltaic and solar thermal collectors, which are incorporated into sun space envelopes, helped to verify the second *hypothesis*:

## II

*Cumulated frequencies of hours of resultant temperature > 20°C in order to determine indoor thermal comfort in SL80 Solarlux sun spaces according to DIN EN 15251-A regarding south directed 25m<sup>2</sup> dimensioned sun spaces in climate region -1-, -4-, -5- and -13-, representing four major cities in Germany, provided by renewable heating energy exclusively by solar gains and additionally by facade integrated technologies are closer to but not actually 1060 hours a year during autumn to spring time (Oct.-April).*

Solar thermal collectors helped to improve cumulative frequencies of hours with operational temperature >20°C fractionally, but not significantly in order to verify Hypothesis I. In contrast to solar thermal collectors, photovoltaic collectors firstly caused considerable shading what resulted in demonstratively less solar gains and secondly did not manage to compensate the lack of solar gains. Consequently, photovoltaic collectors generated energy, that was insufficient in order to improve the reference variant (Hypothesis I).

On the contrary, solar thermal collectors showed slightly better performance.

Hence, *Hypothesis II was validated*.

Numerical calculations elaborated results to verify the third *hypothesis*:

## III

---

*Cumulated frequencies of annually 1060 hours of resultant temperature >20°C is realizable regarding indoor thermal comfort in SL80 Solarlux sun spaces according to DIN EN 15251-A regarding south directed 25m<sup>2</sup> dimensioned sun spaces in climate region -1-, -4-, -5- and -13-, representing four major cities in Germany, provided by renewable heating energy exclusively by solar gains and additionally by facade integrated technologies in combination with seasonal thermal storage technologies in order to generate renewable energies.*

The combination of envelope embedded solar thermal collectors and seasonal loss-free sorption heat storages significantly increased the cumulative frequencies of hours with resulting temperature >20°C. However, the maximum frequency of 1.060 hours was never met.

Photovoltaic collector combined with electrochemical storages resulted in less cumulative frequencies of hours with operational temperature of >20°C between 5 to 10 PM.

For that reasons *Hypothesis III was refuted*.

This findings positively accounted in terms of answering the origin research question:

*“To what extend can energy collectors and seasonal energy storages provide thermal comfort in sun spaces?”*

Both the empirical and theoretical inspections helped to identify the range of additional cumulative frequencies of hours realizable with solar thermal collectors integrated into sun space facades and combined with seasonal sorption storages . In terms of the empirical assessment in Bissendorf collectors provided approximately 50 additional hours, whereas the theoretical evaluation in combination with a loss-free seasonal sorption storage provided at maximum 78 additional hours in climate region 5 (Niederrheinische Bucht/partly Niedersachsen).

In order to conclude for the main research question, we can say, that solar thermal collectors embedded in sun space facades which are combined with sorption storages positively influence the cumulative frequency of hours at preferred occupational day times. Thus, in respect to the selected climate regions, this combination of technology in the research field of energy facades was evaluated to add on 7,3 % of the prerequisite defined amount of 1.060 hours.

By answering the origin research question, one sub-question formulated in *Hypothesis IV* could subsequently be verified:

#### IV

---

*The sum of solar gains and additional renewable energies, which are generated by facade integrated collector technologies and seasonally stored with sorption storage technologies provide in climate region -1-, -4-, -5- and -13-, representing four major cities in Germany, at least 20°C resultant temperature based heating energy autarkic operation from 5 to 10 PM in 25m<sup>2</sup> dimensioned south directed SL80 sun spaces during autumn to spring time (Oct.-April).*

Since the additional amount of hours with operational temperature  $>20^{\circ}$  between 5 to 10 PM calculated for the selected climate regions -1-, -4-, -5- and -13- resulted in effective cumulative hours less than 1.060 hours. For that reason a complete autarkic operation of a sun space exclusively by renewable energies was not feasible.

However, the technology concept enlarged the amount of hours with sufficient thermal comfort in the preferred evening hours between November to end of April.

Hence, the *Hypothesis IV was refuted*.

Moreover, investigations focussing on the main research question delivered information in order to verify Hypothesis V, what reformulated rises another sub-question:

#### V

---

*10 per cent of the sun space adjacent residential houses effective heating energy demand can be substituted by surplus of solar gains and additional renewable energy that is generated by sun space facade integrated collector technologies and seasonally stored by sorption storage technologies of 25m<sup>2</sup> dimensioned and south directed SL80 sun spaces.*

Simulation results exemplified that the amount of surplus energy either power or heat often exceeded the amount of effective additional energy for sun space heating. Considering solar thermal collector and storage systems, surplus energy generated in climate region 4 (Nordostdeutsches Tiefland) managed to provide 13%, thus more than 10% of the average annual heating demand for modern low energy residential buildings. In terms of photovoltaic and electrochemical storage systems, the five investigated climate regions profited from surplus energy that equals 11,3 to 15% of annual heating demand of low energy buildings.

Against this background, we can conclude, that sun space envelope integrated collectors, in particular combined with seasonal storages of limited storage capacity, actually rather manage providing surplus energy during summer for a residential building than heating energy for a sun space in winter month.

In terms of power substitution, the power systems managed to substitute 12,3 to 16,2% of an average annual power consumption of 6.000 kWh typical for a four head family home. However, considering the alternative reference of a poor thermally in-

sulated family home accounting for an annual heating energy demand of 45.000 kWh, no system provided surplus energy significantly close to 10%.

As a conclusion, rather residential buildings that profit from an extraordinary high energetic standard, benefit from the investigated systems than family homes, that encounter a poor energetic standard.

For that reason, the Hypothesis V was partly validated, considering the low energy houses and persistently refuted in terms of family homes encountering a poor energetic standard.

The system performances strongly depended on each the limitation of storage capacity than on the system peak power. The author calls for attention, that a doubled or tripled thermo-chemical storage capacity or an electro-chemical storage capacity equal to that will influence the results significantly.

So far, we can conclude, that this thesis project was effectual in order give answer to the main research question and to verify the five hypotheses which represent subordinate questions.

### Further minor findings

---

As we can conclude, literature research recovered firstly additive insight and information about both constructive and theoretical planning tools in order to increase cumulative hours with sufficient thermal comfort as well to lessen overheating. In particular, a façade area-floor area ratio, building physical properties of the separation element between sun space and living room as well as thermal mass significantly determine heat return, overheating, transmission losses, residential energy savings and balancing and thus thermal comfort.

From this we can derive, that comprehensive constructional and building physical planning and design is crucial for thermal comfort.

Furthermore, literature research revealed diversified collector technology and seasonal storage technology being appropriate for building skin integration. We can implicate, that high operational feeding temperature of high performance evacuated solar thermal tube collectors and low desorption temperature of seasonal sorption storages are essential for a high annual yield, solar fraction respectively and minimized stagnation. Since research and development has already identified these technical

bottlenecks and offer first solutions, we can deduct, that system efficiency will demonstratively enhance in the near future.

Moreover, literature research discovered both for photovoltaic and non-evacuated solar thermal collectors a tendency to negatively influence interior thermal comfort by undesired radiation.

We can draw the conclusion, that this fact does not eliminate eligibility but rather reasons a distinguished constructional planning of façades with respect to cavities, rear ventilation and physical thermal insulation.

In contrast to that, from empirical measurements with internal shading we can conclude that local discomfort is a substantial matter in terms of vertical striation of ambient air in the comfort sensitive height between 1,10 and 1,70 m. Likely, radiation asymmetries accounted as local discomfort between roof glazing and floor and walls and vertical glazing between solid walls. Especially, warm floors as a matter of inertia related heat return dominate in respect of cold glazing surfaces in winter and warm glazing surfaces facing moderate floor temperatures in summer.

Having vertical striation in mind, we can deduce and conclude from empirical observations, that natural ventilation either provided by limited aerodynamic openings of roof integrated sliding windows or by significant area-intensive fold-works is not sufficient in order to compensate overheating. Since, we empirically inspected overheating already at the end of March until end of

October, overheating is even present in months when thermal comforts lacks satisfying operational temperature between 5 to 10 PM.

From product development and empirical testing we can conclude, that integration of evacuated high performance solar thermal tube collectors in sun space rafter is reasonable, feasible as well as efficient in terms of yields and comfort.

### Future Research

---

Nonetheless, this thesis project lacks investigations on local discomfort caused by increased air velocity. Increased air velocity in sun spaces is especially induced by convection and striation.

Further, the author is convinced that indoor thermal comfort is predictable by inspection of the relation of the mean radiation and irradiation duration and external temperature.

In particular these parameters rule the ratio of potential passive solargains and effective transmission losses, which superordinate determine thermal comfort.

In respect to overheating, especially sun spaces could profit from surface coatings for glazing in order to regulate radiation emission. Thus, investigation on internal emission performance of sun space glazing both for winter and summer performance will contribute solving local discomfort.

Aside building physics, further research in innovative composite sorption materials, which provide a lower required charging temperature range, will allow higher solar fraction and enhances system efficiency. This reasons further research in lately developed composite materials, which still suffer from short cycle strength.

Notwithstanding, sun spaces as naturally ventilated spaces provide living space enlargement with active options for individual control of thermal comfort from early spring to late autumn.

Moreover, the simple façade concept allows space heating primarily by the sun. If required, hours with enjoyable thermal comfort can be raised with additional façade integrated collector and combined storage technology.

## Outlook

---

The next generation of sun spaces, what is a promising and feasible solution in the near future, combines supreme thermally insulated sun space envelopes with stagnation optimized evacuated high performance solar thermal tube collectors and enhanced volumetric sorption storage densities. Living spaces already benefit from simple and conventional sun spaces by the conventional thermal buffer function and by heating energy savings resulting from controlled inter-zonal movements of preheated sun space air.

Opposed to that, the next generation of sun spaces approximates autarkic operation depending on the local climate and develops to a game changer in the context of a fossil fuel driven residential space heating.

Finally, as we can conclude in the end of this thesis project, sun spaces are eligible facade systems to contribute in various ways to the energy transition.



# References

- [1] BdeW-Bundesverband der Energie- und Wasserwirtschaft, e.V. (2013)
- [2] Albecht, B., Abuel, H., Baratta, M. von, Brander, S., Ell, R., Engler, P., Hartwig, M., Intemann, G., Kiegel, H., Kraft, E., Lotz, B., Manig, B.O., Rudolf, M. (2015). Der neue Fischer Weltalmanach 2016–Zahlen, Daten, Fakten. Fischer Taschenbuch, Frankfurt am Main, S. 659
- [3] International Energy Agency, IEA, Paris
- [4] Potsdam-Institut für Klimafolgenforschung (PIK), e.V., Potsdam
- [5] Knaack, U.. (2008). Grenzen des Machbaren–Ein Versuch, Fassaden neu zu interpretieren, VDI Berichte 203
- [6] Vollen, J., Winn, K.. (2014). Advection based adaptive building envelopes: Component surface morphology and entropy management of a ceramic building façade, Center for Architecture, Science and Ecology
- [7] Rudolph, M.. (2013). Climate Interfaces – From Buildings to Cities, Façade Value–The Future Envelope 7, Conference on Building Envelopes, Delft University of Technology, Faculty of Architecture, Conference 6 June 2013, S.24
- [8] Klein, T.. (2009). Scenarios for Future Building Envelopes–Students Designs, Façades-The Making Of –The Future Envelope 3, Conference on Building Envelopes, Delft University of Technology, Faculty of Architecture, Symposium 14 May 2009, 53
- [9] Durst, A.. (2013). Fassadenkollektoren mit Durchblick-Fenster mit integrierten Vakuumröhren gewinnen solare Wärme, spenden Schatten und leuchten Räume gleichmäßig aus, bine projektinfo 07/2013
- [10] Gosztonyi, S., Rennhofer, M., Zauner, C., Windholz, B.. (2013). Architectural benefits of virtual and experimental assessments of active components in multi-functional façades, AIT Austrian Institute of Technology, AIT, Energy Department
- [11] World Health Organization–WHO, United Nation Specialized Agency, Geneva
- [12] Boucher, B.. (1994). Palladio–Der Architekt in seiner Zeit, Hirmer Verlag, München
- [13] Lahti, L.. (2004). Alvar Aalto–Paradies für kleine Leute, Taschen GmbH
- [14] Auer, T., Lauter, M., Olsen, E.. (2009). High Comfort–Low Impact, Transsolar Climate Engineering, Transsolar Energietechnik
- [15] Hausladen, G., de Saldanha, M., Liedl, P.. (2006). ClimateSkin–Building-skin concepts that can do more with less energy, Birkhäuser Verlag, Berlin
- [16] Henning, H. M.. (2013). 100 percent renewables for electricity and heat–the role of storage in a future German energy system.
- [17] Hohmeyer, O.. (2013). Scenarios of our future energy supply and energy storage technologies, S.24
- [18] Bluysen, P.. (2009). The Indoor Environment Handbook–How to make buildings healthy and comfortable, earthscan, U.K.
- [19] Heller, E.. (2002). Wie Farben wirken – Farbpsychologie, Farbsymbolik, Kreative Farbgestaltung, Rowohlt Verlag
- [20] DIN EN ISO 15251 : 2012-12, Eingangsparmeter für das Raumklima zur Auslegung und Bewertung der Energieeffizienz von Gebäuden-Raumluftqualität, Temperatur, Licht und Akustik
- [21] EN ISO 7730:2005, Ergonomie der thermischen Umgebung-Analytische Bestimmung und Interpretation der thermischen Behaglichkeit durch Berechnung des PMV- und des PPD-Indexes und Kriterien der lokalen thermischen Behaglichkeit (ISO 7730:2005); Deutsche Fassung EN ISO 7730:2005
- [22] Taleghani, M., Tenpierik, M., van den Dobbelaer, A.. (2012). The effect of different transitional spaces on thermal comfort and energy consumption of residential buildings, Proceedings of 7th Windsor Conference : The changing context of comfort in an unpredictable world, Network of Comfort and Energy Use in buildings, 2012
- [23] Yang, L., Yan, H., Lam, J. C.. (2014). Thermal comfort and building energy consumption implications–A review, Applied Energy 115 (2014), 164-173
- [24] ASHRAE Standard 55, 2010–Thermal Environmental Conditions for human Occupancy
- [25] Zürcher, C., Frank, T.. (2014). Bauphysik – Bau & Energie, vdf Hochschulverlag AG, ETH Zürich, 4. Edition

- [26] deDear, R.J., Brager, G.S.. (2002). Thermal comfort in naturally ventilated buildings : revisions to ASHRAE Standard 55, *Energy and Buildings* 34, 549 - 561
- [27] McCartney, K.J., Nicol, F.J.. (2002). Developing an adaptive control algorithm for Europe, *Energy and Buildings*, 623-635
- [28] Borgeson, S., Brager, G.. (2011). Comfort standards and variations in exceedance for mixed-mode buildings. *Building Research & Information* 39, 118-133
- [29] Oliveti, G., Arcuri, N., De Simone, M., Bruno, R.. (2012). Solar heat gains and operative temperature in attached sunspaces, *Renewable Energy* 39, 2012, 241-249
- [30] Chun, C., Tamura, A.. (2005). Thermal comfort in urban transitional spaces, *Building and Environment* 40 (2005), 633-639
- [31] Glässel, J., W.. (1979). Urban Sunspaces–Ecology of Atria and Arcades for Northern Climates, Master Thesis submitted to Massachusetts Institute of Technology (MIT)
- [32] Hauser, G.. (1983). Verglaste Baukörper zur passiven Sonnenergienutzung, *Bauphysik* 5 (1983), 147-152
- [33] Parsons, B., K.. (1983). The Simulation and Design of Building attached Sun- spaces, Master Thesis submitted to University of Wisconsin-Madison
- [34] Rabenstein, D.. (2005). Energetische und wirtschaftliche Optimierung von Glasvorbauten am Beispiel eines Wintergartens, *Bauphysik* 27 (2005), Heft 1
- [35] Lumbis, A. J.. (1988). Operational strategies for attached sunspaces in Canada, Master thesis submitted to the College of Graduate Studies and Research, Department of Mechanical Engineering, University of Saskatchewan, Canada
- [36] Chen, W., Liu, W.. (2004). Numerical and experimental analysis of convection heat transfer in passive solar heating room with greenhouse and heat storage, *Solar Energy* 76 (2004), 623-633
- [37] Sanchez-Ostiz, A., Monge-Barrio, A., Domingo-Irigoyen, S., Gonzalez-Martinez, P.. (2014). Design and experimental study of an industrialized sunspace with solar heat storage, *Energy and Building* 80, (2014), 231-246, Elsevier
- [38] Achad, P., Gicquel, R.. (1986). European Passive Solar Handbook: Basic Principles and Concepts for Passive Solar Architecture, *Method 5000-5000 Maisons Solaires*, Commission of the European Communities: Brussels, Belgium, 1986
- [39] Mottard, J. M., Fissore, A.. (2007). Thermal simulation of an attached sunspace and its experimental validation, *Solar Energy* 81 (2007), 305-315, ScienceDirect
- [40] Passerini, F.. (2012). Sunspaces for passive building heating–calculation models and utilization of empirical data, Doctoral Thesis in Environmental Engineering submitted to Faculty of Engineering, University of Trento
- [41] DIN EN ISO 13790 : 2008 Energieeffizienz von Gebäuden-Berechnung des Energiebedarfs für Heizung und Kühlung (ISO 13790:2008)
- [42] Wall, M.. (1997). Distribution of solar radiation in glazed spaces and adjacent buildings. A comparison of simulation programs, *Energy and Buildings* 26 (1997), 129-135
- [43] Laouadi, A., Atif, M.R., Galasiu, A.. (2003). Methodology towards developing skylight design tools for thermal and energy performance of atriums in cold climates, *Building and Environment* 38 (2003), 117-127
- [44] DIN EN 832 : 2003-06, Wärmetechnisches Verhalten von Gebäuden-Berechnung des Heizenergiebedarfs–Wohngebäude, subducted
- [45] DIN EN ISO 13790:2008-09, Energieeffizienz von Gebäuden-Berechnung des Energiebedarfs für Heizung und Kühlung (ISO 13790:2008)
- [46] DIN V 4108-6:2003-06, Wärmeschutz und Energie-Einsparung in Gebäuden - Teil 6 : Berechnung des Jahresheizwärme- und des Jahresheizenergiebedarfs, revised by DIN V 4108-6 Berichtigung 1:2004-03
- [47] Oliveti, G., De Simone, M., Ruffolo, S.. (2008). Evaluation of the absorption coefficient for solar radiation in sunspaces and windowed rooms, *Solar Energy* 82 (2008), 212-219
- [48] Oliveti, G., Arcuri, N., Bruno, R., De Simone, M.. (2011). An accurate calculation model of solar heat gain through glazed surfaces, *Energy and Buildings* 4 (2011), 269-274
- [49] Asdrubali, F., Cotana, F., Messineo, A.. (2012). On the Evaluation of Solar Greenhouse Efficiency in Building Simulation during the heating period, *energies* 5, 2012
- [50] Oliveira Pnao, M.J.N., Camelo, S.M.L., Goncalves, H.J.P.. (2012). Solar load ratio and ISO 13790 methodologies : Indirect gains from sunspaces, *Energy and Building* 51 (2012), 212-222, Elsevier

- [51] Babae, F., Fayaz, R., Sarshar, M.. (2015). The optimum design of sunspaces in apartment blocks in cold climate, *Architectural Science Review*, DOI: 10.1080/000338628.2015. 1077326, Taylor & Francis
- [52] Ignjatovic, D., Popovic, M. J., Kavran, J.. (2015). Application of sunspaces in fostering energy efficiency and economic viability of residential buildings in Serbia, *Energy and Buildings* 98 (2015), 3-9
- [53] Monge-Barrio, A., Sanchez-Ostiz, A.. (2012). Energy efficiency and thermal behavior of attached sunspaces, in the residential architecture in Spain. *Summer Conditions, Energy and Buildings* 108 (2015), 244-256
- [54] Rempel, A., Rempel, A.W., Gates, K. R., Shaw, B.. (2016) Climate-responsive thermal mass design for Pacific Northwest sunspaces, *Renewable Energy* 85 (2016), 981-993
- [55] Aelenei, D., Leal, H., Aelenei, L.. (2014). The use of attached-sunspaces in retr-fitting design: the case of residential buildings in Portugal, SHC 2013, International Conference on Solar Heating and Cooling for Buildings and Industry, Sep.23.25, 2013, Freiburg, Germany, *Energy Procedia* 48 (2014) 1436-1441, ScienceDirect
- [56] Taleghani, M., Tenpierik, M., van den Dobbelsteen, A.. (2013). Energy performance and thermal comfort of courtyard/atrium dwellings in the Netherlands in the light of climate change, *Renewable Energy* 63 (2014), 486-497, Elsevier
- [57] Pitts, A.C., Saleh, J. B.. (2007), Potential for energy saving in building transition spaces, *Energy and Buildings* 39, 815-822
- [58] Aldawoud, A., Clark, R.. (2007). Comparative analysis of energy performance between courtyard and atrium in buildings, *Energy and Building* 40 (2008), 209-214, Elsevier
- [59] Mihalakakou, G., Ferrante, A..(1999). Energy conservation and potential of a sunspace: sensitivity analysis, *Energy Conversion & Management* 41 (2000), 1247-1264
- [60] Tan, M.. (1997). Opposite Sunspaces passive solar air heating system, *Solar Energy Vol. 60*, S. 127- 134, 1997, Elsevier 1997
- [61] Holford, J. M., Hurt, G.R.. (2003). Fundamental atrium design for natural ventilation, *Building and Environment* 38 (2003), 409-426
- [62] Wang, F., Pichatwatana, K., Roaf, S., Zhao, L., Zhu, Z., Li, J.. (2013). Developing a weather responsive internal shading system for atrium spaces of commercial building in tropical climates, *Building and Environment* 71 (2013), 259-274, Elsevier
- [63] Abdulla, A. H., Wang, F.. (2011). Design and low energy ventilation for atria in the tropics, *Sustainable Cities and Society* 2 (2012), S.8-28, Elsevier
- [64] Oliveti, G., Arcuri, N., De Simone, M., Bruno, R.. (2012). Solar heat gains and operative temperature in attached sunspaces, *Renewable Energy* 39, 2012, 241-249
- [65] Bewertungssystem Nachhaltiges Bauen (BNB)–Neubau Büro- und Verwaltungsgebäude, Thermischer Komfort im Winter, Steckbrief 3.1.1., Bundesministerium für Verkehr, Bau und Stadtentwicklung, 2009, A3
- [66] EnEV : 2016 - Verordnung über energiesparenden Wärmeschutz und energiesparende Anlagentechnik bei Gebäuden (Energieeinsparverordnung-EnEV), 24.07.2007, amended 24.10.2015, Die Bundesregierung
- [67] Mihalakakou, G.. (2001). On the use of sunspace for space heating/cooling in Europe *Renewable Energy* 26 (2002), 415-429
- [68] Pisello, A. L., Goretti, M., Cotana, F.. (2012). A method for assessing building´s energy efficiency by dynamic simulation and experimental activity, *Applied Energy* 97 (2012), 419-429, Elsevier
- [69] Gorgolewski, M., Grindley, P.C., Probert, S.D.. (1996). Energy-efficient renovation of highrise housing, *Applied Energy* 53 (1996), 365-382
- [70] Lee, K. H., Schiavon, S.. (2013). Influence of three dynamic predictive clothing insulation models on building energy use, HVAC sizing and thermal comfort, Center for the Built Environment, University of California, Berkeley, 2013
- [71] Klein, O., Schlenger, J.. (2008). *Raumkonditionierung–Basics*, Birkhäuser Verlag AG
- [72] Weik, H.. (2006). *Expert Praxislexikon–Sonnenenergie und Solare Techniken*, 2.Edition, 5
- [73] Schoofs, S.. (1999). Selektive Absorberbeschichtungen in Solarkollektoren, bine projektinfo 5/99, bine Informationsdienst–FIZ Karlsruhe
- [74] Schneider, B.. (2008). *Thermische Solaranlagen–Studentenwohnheime*, bine projektinfo 06/08, bine Informationsdienst–FIZ Karlsruhe, 2

- [75] Viessmann, M.. (2008). Planungshandbuch Solarthermie-climate of innovation, Viessmann Deutschland GmbH, 39
- [76] DIN EN 12975-1:2011. Thermische Solaranlagen und ihre Bauteile-Kollektoren-Teil 1: Allgemeine Anforderungen, Deutsche Fassung EN 12975- 1:2006+A1:2010
- [77] Föste, S., Ehrmann, N., Giovannetti, F., Reineke-Koch, R., Uslu, F., Krämer, M., Hesse, G.. (2013). Hocheffiziente Flachkollektoren mit selektiv beschichteten Zweischiebenverglasungen „HFK Low-e“, Abschlussbericht, Institut für Solarenergieforschung GmbH Hameln (ISFH)
- [78] Giovannetti, F., Kirchner., M., Franke., M., Rohde., N., Scherer, C.. (2014).Entwicklung eines Isolierglaskollektors für eine flexible, objektbezogene Gebäudeintegration
- [79] DIN EN ISO 9806:2014-06, Solarenergie-Thermische Sonnenkollektoren-Prüfverfahren (ISO 9806:2013), Deutsche Fassung EN ISO 9806:2013
- [80] Loga, T., Born, R.. (2012). Hessisches Ministerium für Umwelt, Energie, Landwirtschaft und Verbraucherschutz-Brauchwasserbereitung mit Sonnenenergie, Energiesparinformationen 14
- [81] Groll, M.. (1970). Wärmerohre als Bauelement in der Energietechnik, 85
- [82] Weidner, H.. (2015). Graph: "Evaporating temperature of fillings for heat pipes", Datei: Verdampfungsbereiche.gif (German Wikipedia). Lizenziert unter Gemeinfrei über Wikimedia Commons
- [83] Mach, T., Grobbauer, M., Streicher, W., Müller, M.. (2015). MPPF–The multifunctional Plug&Play Approach in facade technology, Verlag der Technischen Universität Graz, 55
- [84] Stark, S., Gohl, N., Drück, H.. (2015). Forschungsprojekt „Multi-Komp-f“ – Entwicklung von multifunktionalen Gebäudekomponenten (Gebäudeintegrierte Solarthermie), Institut für Thermodynamik und Wärmetechnik (ITW), 23.10.2015,4
- [85] BDH.. (2011). Solare Heizungsunterstützung, Teil 2 : Praxistipps zur Planung und Installation, BDH-Bundesindustrieverband Deutschland Haus-, Energie- und Umwelttechnik e.V., 03-2011, 6
- [86] Hessisches Ministerium für Umwelt, Energie, Landwirtschaft und Verbraucherschutz.. (2012). Brauchwasserbereitung mit Sonnenenergie, Energiesparinformationen 14,
- [87] Weiß, W., Eder, M., Fink, C., Steicher, W.. (1997). Heizen mit der Sonne, Teil- solare Raumheizung & Solaranlagen mit Schichtspeicher im low flow Betrieb, ARGE Erneuerbare Energien, Forschungsforum, BMWV, Österreich, 2-3
- [88] Friedrich, U.. (2007). projektinfo 11/07, 2007, Thermische Solaranlagen–Rehaklinik, BINE Informationsdienst–FIZ Karlsruhe, 3
- [89] Zauner, C., Hengstberger, F., Reichl. C., Lampersberger, P., Helminger, F.. (2012). Simulation, Entwicklung und Prüfung von Mitteltemperaturkollektoren, AIT–Austrian Institute of Technology, Energy Department, 2
- [90] Abawi, Y.. (2014). Analysis of Direct DC-Power Usage of facade-integrated photovoltaics in a test façade, Loughborough University, U.K.
- [91] Shri, A.. (2013). A solid-state transformer for interconnection between the medium- and the low-voltage grid, Master Thesis in Electrical Engineering, Mathematics and Computer Science, Electrical Power Processing, Delft University of Technology, 2013
- [92] Rennhofer, M.. (2014). multifunctional integration of vertical BIPV, AIT–Austrian Institute of Technology, 19
- [93] Rennhofer, M., Allmer, A., Berger, K., Wascher, H., Aichinger, M.. (2014). DC-Energieversorgung direkt aus fassaden-integrierter PV, Austrian Institute of Technology, Giefingstraße 2, Austria, 3
- [94] Abawi, Y., Allmer, A., Berger, K., Wascher, H., Aichinger, M.. (2013). Elektrisch autarke Versorgung über fassadenintegrierte PV, Energy Department, AIT–Austrian Institute of Technology
- [95] Matuska, T., Sourek, B.. (2006). Facade solar collectors, ScienceDirect, Solar Energy 80, 1
- [96] Gosztonyi, S., Rennhofer, M., Zauner, C., Windholz, B.. (2013). Architectural benefits of virtual and experimental assessments of active components in multifunctional facades, AIT Austrian Institute of Technology, AIT, Energy Department, 1
- [97] Giovannetti, F., Kirchner., M., Franke., M., Rohde., N., Scherer, C.. (2014). Entwicklung eines Isolierglaskollektors für eine flexible, objektbezogene Gebäudeintegration
- [98] Hess, S.. (2012). Thermische Solaranlagen für Warmwasser und Heizung–Stand der Technik, Systeme im Überblick, Fraunhofer Institut für Solare Energiesysteme ISE, 3
- [99] Streicher, W., Heimrath, R., Zauner, C., Mach, T.. (2015). Integration of solar thermal applications-MPPF –The multifunctional Plug&play Approach in facade technology, Verlag der Technischen Universität Graz, 49

- [100] Wallner, G., Grabmeyer, K., Povacz, M., Kicker, H., Holzhaider, K., Fischer, J., Lang, R., Preiß, D., Fink, C.. (2014). SHC, TASK 39, Polymerwerkstoffe für Solarthermische Anwendungen, 34/2015, Final Presentation 10/2014
- [101] www.aveno.no, 2016-02-26
- [102] Robin, J.. (2013). Technical Documentation Solar thermal Glass-Vitrage Solaire Thermique, Robin Sun, V01/2013
- [103] Lang, J.. (2015). „Kollektoren von der Baubranche aus neu denken“, bine Informationsdienst, bine 11-2015
- [104] Lang, R.. (2013). Polymerwerkstoffe und die Transformation des Energiesystems, Innviertler VDI-Dialog: Energie Effizienz Denken, Technologische Ansätze zur industriellen Nachhaltigkeit, 28
- [105] Köhl, M., Meir, M., Fischer, S., Wallner, G.. (2014). Polymeric Material for Solar Thermal Applications – 2006-2014, Final Presentation
- [106] Holzhaider, K., Wallner, G., Kicker, H., Lang, R.. (2014). 100% Renewable Energy Scenarios–Relevance of Plastics for Solar thermal technologies, SHC, TASK 39, Polymerwerkstoffe für Solarthermische Anwendungen, 34/2015, A1-43
- [107] Köhl, M.. (2011). Polymere Materialien für solarthermischen Anwendungen, Task 39 des ´Solar Heating and Cooling Programme´ der International Energy Agency (IEA), Fraunhofer Institut für Solare Energiesystem Freiburg, Deutschland, 10
- [108] Novel materials, ideas and designs for solar thermal collectors made by polymers.. (2013). Scoop Newsletter June 2013, 3
- [109] Kahlen, S.. (2010). Review: Structural Polymeric Materials for Solar thermal Applications Newsletter SHC Task39, 2010, 5
- [110] Holzhaider, K., Wallner, G., Kicker, H., Lang, R.. (2015). SHC, TASK 39, Polymer werkstoffe für Solarthermische Anwendungen, 34/2015, Subtask A, final presentation 10/2014
- [111] Jorgensen, G., Brunold, S., Carlsson, B., Möller, K., Heck, M., Köhl, M.. (2003). Durability of polymeric glazing materials for solar application, Conference paper, First European Weathering Symposium, Czech Republic, 2
- [112] Jerman, I.. (2010). Newsletter SHC Task 39, Summary and outlook on spectrally selective coatings for polymeric absorbers, 2010, S.7
- [113] BAYER. (2013). Apec/Makrolon Typenübersicht – Typische Werte/Verarbeitung. BAYER Material Science AG, Business Unit Polycarbonates
- [114] Loumakis, G., Burek, S., Wood, B.. (2013). A review of solar thermal applications using polymer materials, Athens, ATINER´S Conference Paper Series, No.: ENV2012-0027
- [115] COVESTRO.. (2016). APEC 1803 Polycarbonate, www.matweb.com, 04.08.2016
- [116] OENORM EN 12975-3-1:2011-09: Entwurf, Thermische Solaranlagen und ihre Bauteile-Kollektoren - Teil 3-1: Qualifizierung der Beständigkeit von Solarabsorberflächen
- [117] Koch, J.. (2010). Newsletter SCH Task 39, Presentation of Technoform Kunststoffprofile GmbH (TKP) at Blumau Conference, 3
- [118] Fleck-Vetter, M.. (2010). Newsletter SCH Task39, Parabolic through collector made from polymeric materials, 2010, 3
- [119] Jack, S., Kantenbrink, N., Partefal, J., Giovannetti, F., Rockendorf, G.. (2013). Wärmerohre in Sonnenkollektoren–Wärmetechnische Grundlagen und Optimierung sowie neue Ansätze für die Integration, Institut für Solarenergieforschung GmbH Hameln (ISFH)
- [120] BAYER Material Science AG, Business Unit Polycarbonates.. (2015). Optinova–Medical tubing for World Class Producers-Optical Properties of Makrolon and Apec for non-imaging optics, Material Guides for custom extrusion 2014
- [121] ..(2015). SHC Polymeric Materials for solar thermal applications, 2015, TASK 39 Solar Heating&Cooling Programme, 7
- [122] Leibbrandt, P., Schabbach, T., Dölz, M., Rhein, M.. (2016). CFD–Untersuchung zu konvektiven Wärmeverlusten in Scheibenzwischenräumen im großen Seitenverhältnis, RET–Institut für Regenerative Energietechnik
- [123] Beckmann, M.. (2016). Climate of Innovation–Neue Flachkollektoren mit Temperaturabschaltung ThermProtect, Viessmann Group
- [124] Föste, S.. (2013). Flachkollektoren mit selektiv beschichteter Zweischeibenverglasung, genehmigte Dissertation an der Gottfried Wilhelm Leibniz Universität Hannover, Fakultät für Maschinenbau

- [125] Föste, S., Schiebler, B., Giovannetti, F.. (2016). Steigerung der Leistungsfähigkeit von Wärmerohren für Kollektoren mit reduzierter Stagnationstemperatur, Institut für Solarenergieforschung GmbH Hameln (ISFH)
- [126] Jack, S., Föste, S., Schiebler, B., Giovannetti, F.. (2014). Neuartige Kollektoren mit Wärmerohren zur Begrenzung der Stagnationstemperatur und Reduzierung der Systemkosten, Institut für Solarenergieforschung GmbH Hameln (ISFH)
- [127] Rhein, M., Schabbach, T., Leibbrandt, P., Dölz, M.. (2016). Strukturanalyse eines Nurglaskollektors unter Berücksichtigung statischer und dynamischer Lasten, RET-Institut für Regenerative Energietechnik
- [128] Stark, S., Gohl, N., Loose, A., Drück, H.. (2015). Entwicklung eines kompakten fassadenintegrierten Moduls zur solaren Trinkwassererwärmung, Institut für Thermodynamik und Wärmetechnik (ITW)
- [129] Vollen, J., Winn, K.. (2013). Climate Camouflage : Advection based adaptive building envelopes, The center for Architecture, Science and Ecology, Rensselaer Polytechnic Institute New York, U.S.A, 3
- [130] Rennhofer, M., Berger, K., Abawi, Y., Leidl, R.. (2015). Integration of photovoltaic applications in multifunctional building skins, MPPF–The multifunctional Plug&Play Approach in facade technology, Verlag der Technischen Universität Graz
- [131] Zauner, C., Sterrer, R., Gosztonyi, S.. (2014). Verhalten innovativer Solarthermischer Fassadenkollektoren im Rahmen des Forschungsprojektes MPPF, Austrian Institute of Technology, Austria, 5
- [132] Brandl, D., Mach, T.. (2015). Flow characteristics of multifunctional facade constructions, MPPF–The multifunctional Plug&play Approach in facade technology, Verlag der Technischen Universität Graz, 115
- [133] Grobbauer, M., Mach, T.. (2015). Design and implementation of the physical prototypes, MPPF–The multifunctional Plug&play Approach in facade technology, Verlag der Technischen Universität Graz, 221
- [134] Grobbauer, M., Gratzner, J., Ruckhofer, A., Müller, M.. (2015). Measurement based evaluation of Prototype II, MPPF–The multifunctional Plug&play Approach in facade technology, Verlag der Technischen Universität Graz, 245
- [135] Stark, S., Gohl, N., Drück, H.. (2015). Forschungsprojekt „Multi-Komp-I“ –Entwicklung von multifunktionalen Gebäudekomponenten (Gebäudeintegriert Solarthermie), Institut für Thermodynamik und Wärmetechnik (ITW), 23.10.2015, 4
- [136] Loose, A.. (2014). Effiziente Allianzen-Multivalente Heizsysteme Wärmepumpe plus X, Sonne, Wind, Wärme 04-2014
- [137] Gohl, N., Stark, S., Loose, A., Drück, H.. (2015). Messtechnische Untersuchung eines modular aufgebauten solarthermischen Fassadenelements, OTTI Symposium Thermische Solarenergie 2015, Bad Staffelstein
- [138] T.T. Chow, W. He, J. Ji.. (2006). An experimental study of facade-integrated photovoltaic/water-heating system, Applied Thermal Engineering 27 (2007), 1, ScienceDirect
- [139] T.T. Chow, W. He, J. Ji.. (2006). An experimental study of facade-integrated photovoltaic/water-heating system, Applied Thermal Engineering 27 (2007), ScienceDirect, 1
- [140] Ji, J., Han, J., Chow, T.T., Yi, H., Lu, J. He, W. Sun, W.. (2006). Effect of fluid flow and packing factor on energy performance of a wall-mounted hybrid photo-voltaic/water-heating collector system, Energy and Building 38, 2, ScienceDirect
- [141] Svendsen, S.. (1992). Solar collector with monolithic silica aerogel, Journal of Non-Crystalline Solids 145, 1992
- [142] Rennhofer, M., Berger, K., Leidl, R.; Kubicek, B., Popovac, M., Gosztonyi, S., Gerstmann, H., Prankovic, M., Wascher, H., Aichinger, M.. (2011). Lichttechnische Bewertung von Photovoltaischen Verschattungselementen, AIT Austrian Institute of Technology, AIT, Energy Department
- [143] Vetter, M.. (2013). Battery system development–from cells to complete solutions, Energy Storage conference, Düsseldorf, 9th March 2013
- [144] Lindner, M.. (2015). Thermochemical Systems–heat transformation, Deutsches Zentrum für Luft- und Raumfahrt, Institut für Technische Thermodynamik, 2015
- [145] Vetter, M.. (2012). Lithiumbatterien bieten große Chancen–Speicherbatterien werden sich lohnen, wenn die Strompreise weiter steigen, Intersolar Europe Messezeitschrift–Interview, Messe Intersolar, München, 2012
- [146] Ossenbrink, R.. (2013). Recycling-Speicher für Solarstrom, Sonne Wind & Wärme 07/2013
- [147] Winter, M.. (2013). Dual-ion battery technology, from Research Centre MEET/Institute of Physical Chemistry of the University of Münster, pv magazine 04/2013

- [148] Vogel, T.. (2012). Anodenmaterialien für Li-Ionen-Batterien–Herstellung kohlenstoffbeschichteter Cobaltoxid-Partikel, Research Centre MEET/Institute of Physical Chemistry of the University of Münster, Provendis GmbH, 2012
- [149] Vogel, T.. (2012). Anodenmaterialien für Li-Ionen-Batterien–Kohlenstoffbeschichtete TiO<sub>2</sub>-Nanopartikel als Anodenmaterial, Research Centre MEET/Institute of Physical Chemistry of the University of Münster, Provendis GmbH, 2012
- [150] Vogel, T.. (2012). Anodenmaterialien für Li-Ionen-Batterien–Herstellung kohlenstoffbeschichteter Eisenoxid- und Zinkferrit-Partikel, Research Centre MEET/Institute of Physical Chemistry of the University of Münster, Provendis GmbH, 2012
- [151] Vogel, T.. (2012). Batteriesysteme mit dualer Interkalation–Einlagerung von Ionen aus Salzschnmelzen und organischen Elektrolyten, Research Centre MEET/Institute of Physical Chemistry of the University of Münster, Provendis GmbH, 2012
- [152] Schaefer, T.. (2012). Li-Booster–SEI bildender Elektrolytzusatz für Lithium-Ionn Batterien, Research Centre MEET/Institute of Physical Chemistry of the University of Münster, Provendis GmbH, 2012
- [153] Schaefer, T.. (2012). Li-Protect–Chemischer Überladungsschutz für Lithium-Ionn Batterien, Research Centre MEET/Institute of Physical Chemistry of the University of Münster, Provendis GmbH, 2012
- [154] Obeidi, S.. (2013). Neuartige mikroporöse Separatorfolien für Lithium-Ionen-Batterien, Research Centre MEET/Institute of Physical Chemistry of the University of Münster, Cluster EnergieForschung.NRW , Ministerium für Innovation, Wissenschaft und Forschung des Landes Nordrhein-Westfalen
- [155] Bleiweiss, L.. (2012). Verfahren und Anordnung zur Herstellung großer Flüssigbatterien durch die Vermeidung von Instabilitäten, Sächsisches Patent und Verwertungs-Agentur
- [156] Pesche, T.. (2015). Redox-Flow Batterie aus Kunststoff, Sonne Wind & Wärme 09/2015
- [157] Dötsch, C.. (2013). Redox-Flow-Batterien zur Speicherung elektrischer Energie, Fraunhofer UMSICHT, Cluster EnergieForschung. NRW, Ministerium für Innovation, Wissenschaft und Forschung des Landes Nordrhein-Westfalen
- [158] Tappeser, J.. (2015). Wir haben uns von der Blei-Gel-Technik verabschiedet, photovoltaik 03/2015
- [159] Koenemann, D.. (2015). Kleine Alleskönner-Wechselrichter, Sonne Wind&Wärme 03/2015
- [160] Application&Installations /Market overview inverters, 2013, pv magazine 04/2013, 66-73
- [161] Ossenbrink, R.. (2015). Marktübersicht Wechselrichter für häusliche Anlagen (Auswahl), Sonne Wind&Wärme 03/2015, 64
- [162] Drück, H.. (2013). Intersolar Bericht Wärmespeicher
- [163] Weber, R., Asenbeck, S., Kerskes, H.. (2013). Entwicklung eines kombinierten Warmwasser-Sorption-wärmespeichers für thermische Solaranlagen, - KoWass-, Forschungsbericht BWPLUS, Institut für Thermodynamik und Wärmetechnik (ITW), Universität Stuttgart
- [164] Abedin, A., H., Rosen, M. A.. (2011). A critical review of thermochemical energy storage systems, the Open Renewable Energy Journal 04/2011, 42-46
- [165] Mugele, J., Stach, H., Jänchen, J.. (2012). Neue Arbeitsmaterialien für die thermo-chemische Speicherung solarer Niedertemperaturwärme, ZeoSys GmbH Berlin, 2012
- [166] Drück, H.. (2013). Bei Speichern wird es interessante Entwicklungen geben–mit dem Wandel der Energieversorgung werden sich Wärmespeicher ändern, Intersolar Europe Messezeitschrift 2013, Wärmespeicher, 24-25
- [167] Eichler, M., Mack, S., Hirth, T.. (2015). Evaluation of liquid absorption heat storage by isothermal flow calorimetry, University Stuttgart, IRES 2015 Poster Exhibition, 9th International Renewable Energy Storage Conference, Düsseldorf
- [168] Dicaire, D., Tezel, F. H.. (2012). Study of adsorbent energy density and regeneration for long term thermal energy storage of solar and waste heat, University of Ottawa, Department of Chemical and Biological Engineering, Ontario, Canada
- [169] Hauer, A.. (2002). Beurteilung fester Adsorbentien in offenen Sorptionssystemen für energetische Anwendungen
- [170] Abedin, A. H., Rosen, M.A.. (2012). Energy and Exergy analysis of open thermo-chemical energy storage system : methodology and illustrative application, University of Ottawa, Institute of Technology Oshawa, Faculty of Engineering and Applied Science, Canada, The Open Renewable Energy Journal, 05/2012, 41-48
- [171] Heier, J., Bales, C., Martin, V.. (2015). Combining thermal energy storage with buildings–a review, Renewable and Sustainable Energy Review 42/2015, 1305-1325, ScienceDirect

- [172] Lass-Seyoum, A., Blicher, M., Borozdenko, D., Friedrich, T., Langhof, T.. (2012). Transfer of laboratory results on closed sorption thermo-chemical energy storage to a large-scale technical system, *SciVerse ScienceDirect–Energy Procedia* 30/2012, 310-320
- [173] Hauer, A., Lävemann, E.. (2006). Möglichkeiten offener Sorptionsspeicher zum Heizen, Klimatisieren und Entfeuchten, Bayerisches Zentrum für Angewandte Energieforschung, ZAE Bayern
- [174] Gartler, G., Jähniq, D., Purkathofer, G., Wagner, W.. (2007). Development of a high energy density sorption storage system, AEE-INTEC, Austria, 2007
- [175] Schmidt, F.. (2006). Neue Materialien und Systemkonzepte für Adsorptionsspeicher–Ergebnisse des BMBF-Netzwerkes, Fraunhofer-Institut für Solare Energiesysteme ISE
- [176] Gantenbein, P.. (2004). Sorptionsspeicher, Sorptionsmaterial/Studie Temperaturprofile&Sorptionsmodelle, Jahresbericht 2004, Institut für Solartechnik SPF, Hochschule für Technik Rapperswil HSR, Austria
- [177] Mugele, J.. (2005). Optimierung von Speichermaterialien für den Einsatz in geschlossenen thermochemischen Wärmespeichern für gebäudetechnische Anwendungen, VDI-Verlag, 2005
- [178] Van Helden, W.. (2013). Results of 4 years R&D in the IEA Task 4224 on Compact Thermal Energy Storage : Materials Development for System Integration, Renewable Heat, The Netherlands
- [179] Mette, B.. (2012). EnErChem–Entwicklung und Erprobung eines Chemisch-Sorptiven Langzeitwärmespeichers für die Gebäudebeheizung, ITW-Institut für Thermodynamik und Wärmetechnik-Universität Stuttgart
- [180] D´Ans, P., Hohenauer, W., Courbon, E., Frere, M., Degrez, M., Descy, G.. (2013). Monitoring of thermal properties of a composite material used in thermo-chemical heat storage, Eurotherm Seminar 99, Advances in Thermal Energy Storage
- [181] Zondag, H. A., Kalbasenka, A., van Essen, M., Bleijendaal, L., Schuitema, R., van Helden, W., Krosse, L.. (2009). First studies in reactor concepts for thermo-chemical storage, ECN–Energy Research Centre of the Netherlands, Petten, TNO, Appeldorn
- [182] Trausel, F., de Jong, A.J., Cuypers, R.. (2014). A review on the properties of salt hydrates for thermo-chemical storage, SHC 2013, International Conference on Solar Heating and Cooling for Buildings and Industry, September 23-25, 2013, Freiburg, Energy Procedia 48/2014, 447-452, ScienceDirect
- [183] Zettl, B., Englmaier, G., Steinmaurer, G., Reichl, C.. (2014). Entwicklung eines offenen Adsorptionsprozesses in einem Trommelreaktor, Austria Solar Innovation Center-ASIC, Wels, Austrian Institute of Technology–AIT, Wien, Solar 2014, Gleisdorf
- [184] Streicher, W., Mauthner, G., Jähriq, D., Basciotti, D., Monsberger, M., Zettl. B., Steinmaurer, G., Heinz, A., Schranzhofer, H.. (2013). Task 42: Fortschrittliche Materialien für kompakte thermische Energiespeicher 2010-2012, Projektbericht nachhaltigwirtschaften bmvit-Bundesministerium für Verkehr, Innovation und Technologie
- [185] Finck, C., Henquet, E., van Soest, C., Oversloot, H., de Jong, A.J., Cuypers, R., van ´t Spijker, H.. (2014). Experimental results of a 3 kWh thermochemical heat storage module for pace heating application, SHC 2013, International Conference on Solar Heating and Cooling for Buildings and Industry, September 23-25, 2013, Freiburg, Energy Procedia 48/2014, 320-326, ScienceDirect
- [186] Shigeishi, R. A., Langford, C. H., Hollebone, B. R.. (1979). Solar Energy storage using chemical potential changes associated with drying of zeolites, *Solar Energy* 23/1979, 489-495
- [187] Schmidt, F. P.. (2004). Optimizing Adsorbents for Heat storage applications: estimation of thermodynamic limits and Monte Carlo simulations of water adsorption in nanopores, Dissertation an der Fakultät für Mathematik und Physik, Albert-Ludwigs-Universität Freiburg im Bressgau
- [188] www.dwd.de
- [189] TriStar T-60 manual German, Morningstar Corporation, 2012
- [190] Corradini, R., 2013, Regional differenzierte Solarthermie-Potenziale für Gebäude mit einer Wohneinheit, Dissertation zur Erlangung des Grades Doktor-Ingenieur, Fakultät Maschinenbau, Ruhr-Universität Bochum
- [191] Weiss, W., Fink, C., Haslinger, W., Strasser, C., Wörgetter, M.. (2014). Forschung und Innovation für Heizen und Kühlen mit Erneuerbaren–Berichte aus Energie- und Umweltforschung 28/2014, bmvit Bundesministerium für Verkehr, Innovation und Technologie, Österreich
- [192] Cremers, J., Fiedler, S., Röttinger, C.. (2011). Solararchitektur4 –Die deutschen Beiträge zum Solar Decathlon Europe 2010, DETAIL Green Books, Institut für internationale Architektur-Dokumentation GmbH & Co. KG

- [193] Irulegi, O., Tores, L., Sierra, A., Mendizabal, I., Hernandez, R.. (2012). The Ekihouse: An energy selfsuffici-ent house based on passive design strategies, Energy and Buildings, 2014
- [194] Wiegel, C.. (2016). ...towards the layer it actually occurs–Integral facades vs. symptomatic building man-agement, Engineered Transparency 2016, Glass in Architecture and Structural Engineering, Schneider, J., Weller, B., Wiley–Ernst&Sohn GmbH & Co. KG, First Edition
- [195] Zauner, C., Lager, D., Hohenauer, W.. (2010). Thermophysikalische und Spektroskopische Methoden zur Analyse von Isolationsmaterialien für Solartherme Anwendungen, Austrian Institute of Technology
- [196] ETAG 006:2000-12 : Systems of mechanically fastened flexible roof waterproofing
- [197] DIN 18008-2, 2010-12 : Glas im Bauwesen-Bemessungs- und Konstruktionsregeln-Teil 2: Linienförmig gelagerte Verglasungen, inkl. Berichtigung zu DIN 18008-2:2010-12
- [198] DIN 18008-5:2013-07 Glas im Bauwesen-Bemessungs- und Konstruktionsregeln-Teil 5: Zusatzen-forderungen an begehbare Verglasungen
- [199] [www.narva-bel.de](http://www.narva-bel.de)
- [200] Energieeinsparverordnung (EnEV)–Verordnung über energiesparenden Wärmeschutz und energiespar-ende Anlagentechnik bei Gebäuden, Novellierung 2016, zuletzt geändert 24.10.2015, Bundesministe-rium für Wirtschaft und Technologie und das Bundesministerium für Verkehr, Bau und Stadtentwick- lung, Anlage 3, Tab. A1,  $T_i > 19^\circ\text{C}$
- [201] DIN V 18599-10: 2011-12, Energetische Bewertung von Gebäuden–Berechnung des Nutz-, End- und Primärenergiebedarfs für Heizung, Kühlung, Lüftung, Trinkwarmwasser und Beleuchtung – Teil 10, 17 - Nutzungsrand- bedingungen Wohngebäude
- [202] DIN V 18599-10: 2011-12; Energetische Bewertung von Gebäuden–Berechnung des Nutz-, End- und Primärenergiebedarfs für Heizung, Kühlung, Lüftung, Trinkwarmwasser und Beleuchtung–Teil 10 - Nutzungsrandbedingungen Wohngebäude, interne Wärmequellen, 17
- [203] DIN V 18599-10: 2011-12, Energetische Bewertung von Gebäuden–Berechnung des Nutz-, End- und Primärenergiebedarfs für Heizung, Kühlung, Lüftung, Trinkwarmwasser und Beleuchtung – Teil 10, Tab.A.1, 33 - Nutzungsrandbedingungen Einzelbüro, interne Wärmequellen
- [204] DIN EN 15251-2007, Eingangparameter für das Raumklima zur Auslegung und Bewertung der Energieeffizienz von Gebäuden–Raumluftqualität, Temperatur, Licht und Akustik; Deutsche Fassung EN 15251:2007, Tab. A3, Wohngebäude Kategorie II
- [205] DIN V 18599-2:2007-2; Energetische Bewertung von Gebäuden – Berechnung des Nutz-, End- und Primärenergiebedarfs für Heizung, Kühlung, Lüftung, Trinkwarmwasser und Beleuchtung–Teil 02, Nutzenergiebedarf für Heizen und Kühlen von Gebäudezonen, 66, Tab.05
- [206] Recknagel, H., E., Schramek, E. Sprenger.. (2013). Taschenbuch für Heizung+Klima Technik, Prof. Dr- Ing. Ernst-Rudolf Schramek, Edt., 76. Auflage, Edition -Recknagel, 1242





# Appendix A Chapter 01

BUILDING ELEMENT	ELEMENT/ PART	SPECIFIC U-value [W/m <sup>2</sup> ·K]; [W/m <sup>2</sup> ·K]	AREA SPECIFIC TRANSMISSION LOSSES [WK]	AREA [m <sup>2</sup> ]	AREA SPECIFIC U-value [W/m <sup>2</sup> ·K]	BUILDING ELEMENT SPECIFIC TRANSMISSION LOSSES PER TEMPERATURE DIFFERENCE [WK]
<b>ROOF SOUTH</b>						
1	DWS-01	SL Nobles Roof + a-Si PV-DGU	3,39	2,71	0,80	1,96
2	DWS-02	SL Nobles Roof + a-Si PV-DGU	2,51	4,42	1,75	
3	DWS-03	SL Nobles Roof + a-Si PV-DGU	2,64	3,75	1,42	
4	DWS-04	SL Nobles Roof + a-Si PV-DGU	3,14	2,13	0,68	
5	DS-01	SL Nobles Roof + Cristall PV-DGU	2,30	3,73	1,62	
6	DS-02	SL Nobles Roof + Cristall PV-DGU	2,44	3,20	1,31	
7	DS-03	SL Nobles Roof + Cristall PV-DGU	2,35	3,75	1,59	
8	DS-04	SL Nobles Roof + 1.1 DGU	1,78	3,17	1,78	
9	DS-05	SL Nobles Roof + 1.1 DGU	1,91	2,76	1,44	
10	DS-06	SL Nobles Roof + 1.1 DGU	1,82	3,18	1,75	
11	T-S	Eave South	0,33	2,01	1,53	
12	RS-O	Aside Rafter East	0,16	0,53	0,68	
13	WA-S	Attos Profile South	0,23	0,71	0,32	
14	GS	Grouf Rafter	1,49	1,20	1,61	

BUILDING ELEMENT	ELEMENT/ PART	SPECIFIC U-value [W/m <sup>2</sup> ·K]; [W/m <sup>2</sup> ·K]	AREA SPECIFIC TRANSMISSION LOSSES [WK]	AREA [m <sup>2</sup> ]	AREA SPECIFIC U-value [W/m <sup>2</sup> ·K]	BUILDING ELEMENT SPECIFIC TRANSMISSION LOSSES PER TEMPERATURE DIFFERENCE [WK]
<b>ROOF WEST</b>						
15	DW-01	Roof Sliding Window+1.1 DGU	2,12	3,59	1,69	1,93
16	DW-02	Mdt. Drum Vent	1,88	0,98	0,52	
17	DW-03	SL Nobles Roof + Cristall PV-DGU	2,62	2,33	0,89	
18	DW-04	SL Nobles Roof + Cristall PV-DGU	2,21	3,39	1,41	
19	DW-05	SL Nobles Roof + 1.1 DGU	1,76	3,31	1,88	
20	DW-06	SL Nobles Roof + 1.1 DGU	1,88	2,90	1,55	
21	DW-07	SL Nobles Roof + 1.1 DGU	1,88	2,90	1,55	
22	DWS-01	SL Nobles Roof + a-Si PV-DGU	3,39	2,71	0,80	
23	DWS-02	SL Nobles Roof + a-Si PV-DGU	2,51	4,42	1,75	
24	DWS-03	SL Nobles Roof + a-Si PV-DGU	2,64	3,75	1,42	
25	DWS-04	SL Nobles Roof + a-Si PV-DGU	3,14	2,13	0,68	
26	T-W	Eave West	0,33	2,01	1,53	
27	RS-N	Aside Rafter West	0,16	0,53	0,68	
28	WA-W	Attos Profile West	0,23	0,71	0,32	
29	GS	Grouf Rafter	1,49	1,20	1,61	

BUILDING ELEMENT	ELEMENT/ PART	SPECIFIC U-value [W/m <sup>2</sup> ·K]; [W/m <sup>2</sup> ·K]	AREA SPECIFIC TRANSMISSION LOSSES [WK]	AREA [m <sup>2</sup> ]	AREA SPECIFIC U-value [W/m <sup>2</sup> ·K]	BUILDING ELEMENT SPECIFIC TRANSMISSION LOSSES PER TEMPERATURE DIFFERENCE [WK]
<b>FACADE SOUTH</b>						
30	VS-02	SL 80 + 0,8 DGU	1,20	2,76	2,29	1,27
31	VW/VS-03	SL 80 + 1.1 Heating Pane	1,38	3,01	2,18	
32	VW/VS-04	SL 80 + a-Si PV-DGU	1,58	4,00	2,53	
33	VS-01	SL 80 Fold Works 3-4 + 0,8 DGU	1,20	7,80	6,50	
34	ES-O	Corner Column East	0,33	0,37	0,21	
35	ES-SW	Corner Column SouthWest	0,27	0,61	0,21	

BUILDING ELEMENT	ELEMENT/ PART	SPECIFIC U-value [W/m <sup>2</sup> ·K]; [W/m <sup>2</sup> ·K]	AREA SPECIFIC TRANSMISSION LOSSES [WK]	AREA [m <sup>2</sup> ]	AREA SPECIFIC U-value [W/m <sup>2</sup> ·K]	BUILDING ELEMENT SPECIFIC TRANSMISSION LOSSES PER TEMPERATURE DIFFERENCE [WK]
<b>FACADE WEST</b>						
36	WV-01	SL 80 Fold Works 4-4 + 0,8 DGU	1,20	10,55	6,80	1,27
37	VW/VS-03	SL 80 + 1.1 Heating Pane	1,38	3,01	2,18	
38	VW/VS-04	SL 80 + a-Si PV-DGU	1,58	4,00	2,53	
39	ES-SW	Corner Column SouthWest	0,33	0,37	0,21	
40	ES-N	Corner Column North	0,27	0,61	0,21	

BUILDING ELEMENT	ELEMENT/ PART	SPECIFIC U-value [W/m <sup>2</sup> ·K]; [W/m <sup>2</sup> ·K]	AREA SPECIFIC TRANSMISSION LOSSES [WK]	AREA [m <sup>2</sup> ]	AREA SPECIFIC U-value [W/m <sup>2</sup> ·K]	BUILDING ELEMENT SPECIFIC TRANSMISSION LOSSES PER TEMPERATURE DIFFERENCE [WK]
<b>FACADE ATTIC EAST</b>						
41	VO-01	SL 80 + a-Si PV-DGU	1,77	0,82	0,47	1,64
42	VO-02	SL 80 Tie Window + a-Si PV-DGU	1,76	1,71	0,97	
43	VO-03	SL 80 + a-Si PV-ISO	1,87	1,91	3,21	
44	VO-04	SL 80 + a-Si PV-ISO	1,71	0,73	0,43	

FIGURE APP.A.1

BUILDING ELEMENT	ELEMENT / PART		SPECIFIC U-value [W/m <sup>2</sup> K]; [W/m <sup>2</sup> K]	AREASPECIFIC TRANSMISSION LOSSES [W/K]	AREA [m <sup>2</sup> ]	AREASPECIFIC U-value [W/m <sup>2</sup> K]	BUILDING ELEMENT SPECIFIC TRANSMISSION LOSSES PER K TEMPERATURE DIFFERENCE [W/K]
<b>FACADE EAST</b>							
45	VO-05	SL 80 Door + a-Si PV-DGU	1,94	4,15	2,14	<b>1,47</b>	<b>10,12</b>
46	VO-06	SL 80 + 0,8 DGU	1,22	2,61	2,14		
47	VO-07	SL 80 + 0,8 DGU	1,24	2,12	1,71		
48	VO-06	Ventilation Flap	1,89	0,63	0,33		
49	ES-O	Corner Column East	0,27	0,61	0,21		

BUILDING ELEMENT	ELEMENT / PART		SPECIFIC U-value [W/m <sup>2</sup> K]; [W/m <sup>2</sup> K]	AREASPECIFIC TRANSMISSION LOSSES [W/K]	AREA [m <sup>2</sup> ]	AREASPECIFIC U-value [W/m <sup>2</sup> K]	BUILDING ELEMENT SPECIFIC TRANSMISSION LOSSES PER K TEMPERATURE DIFFERENCE [W/K]
<b>FACADE ATTIC NORTH</b>							
50	VN-01	SL 80 + a-Si PV-DGU	1,54	3,00	1,95	<b>1,59</b>	<b>4,14</b>
51	VN-02	SL 80 + a-Si PV-DGU	1,75	1,14	0,65		

BUILDING ELEMENT	ELEMENT / PART		SPECIFIC U-value [W/m <sup>2</sup> K]; [W/m <sup>2</sup> K]	AREASPECIFIC TRANSMISSION LOSSES [W/K]	AREA [m <sup>2</sup> ]	AREASPECIFIC U-value [W/m <sup>2</sup> K]	BUILDING ELEMENT SPECIFIC TRANSMISSION LOSSES PER K TEMPERATURE DIFFERENCE [W/K]
<b>FACADE NORTH</b>							
52	VN-03	SL 80 + a-Si PV-DGU	1,46	4,69	3,21	<b>1,28</b>	<b>8,18</b>
53	VN-04	SL 80 Hub-Sliding Door	1,09	3,50	3,21		

BUILDING ELEMENT	ELEMENT / PART		SPECIFIC U-value [W/m <sup>2</sup> K]; [W/m <sup>2</sup> K]	AREASPECIFIC TRANSMISSION LOSSES [W/K]	AREA [m <sup>2</sup> ]	BUILDING ELEMENT SPECIFIC TRANSMISSION LOSSES PER K TEMPERATURE DIFFERENCE [W/K]
<b>INTERMEDIATE WALLS / FLOORS</b>						
54	BE-01	Floor on Ground	0,15	3,90	25,85	<b>3,90</b>
55	TW-01	Intermediate Wall to heated room	0,09	2,30	24,99	<b>2,30</b>

FIGURE APP.A.2

# Appendix B Chapter 02

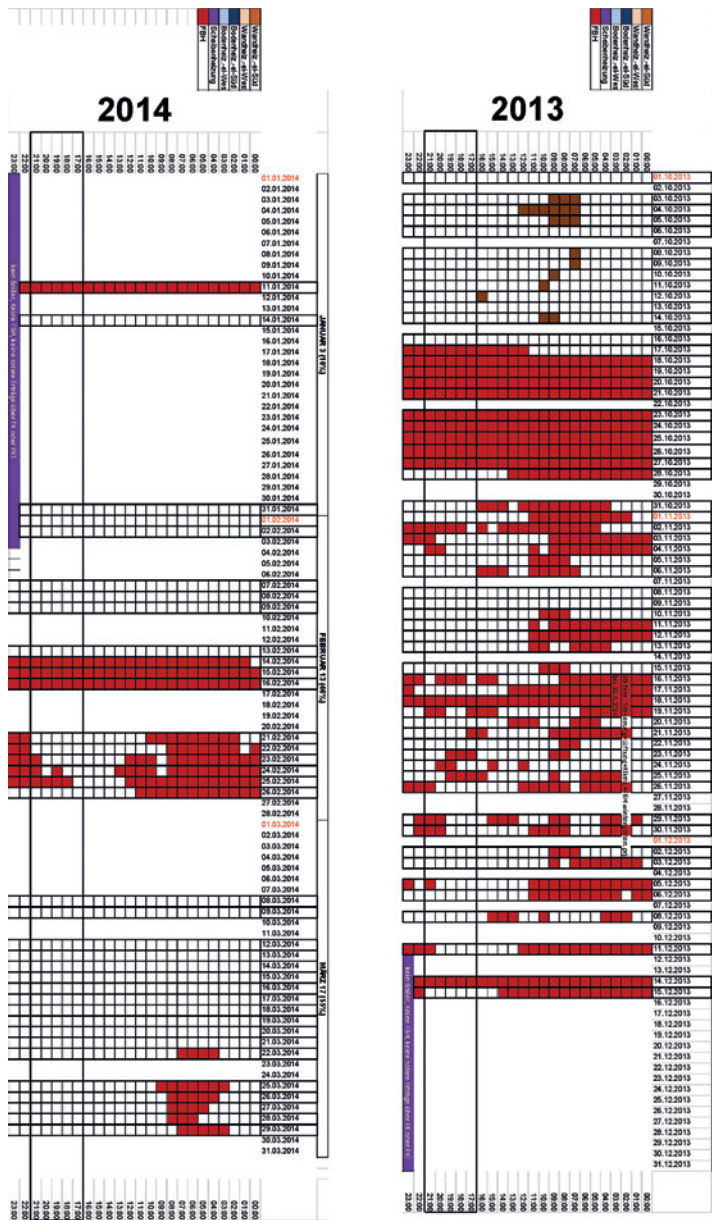


FIGURE APP.B.1



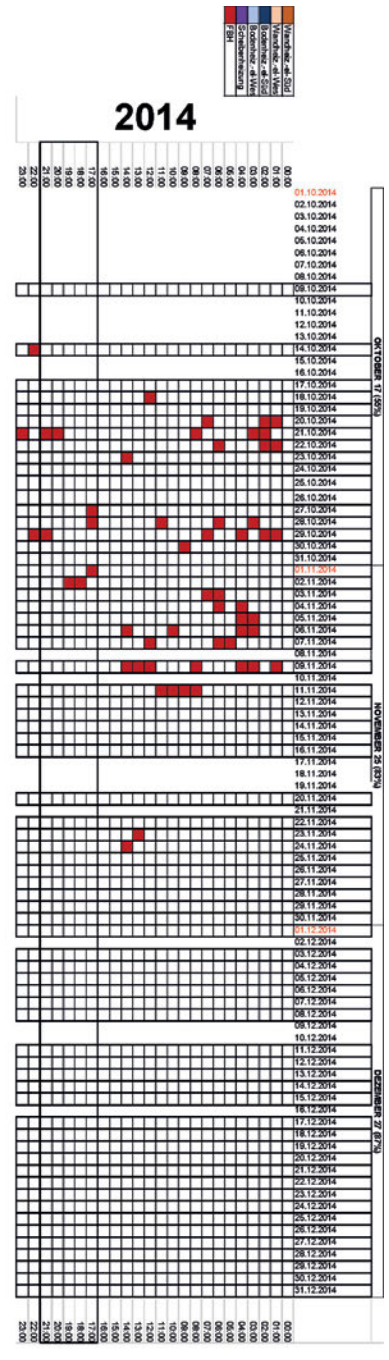
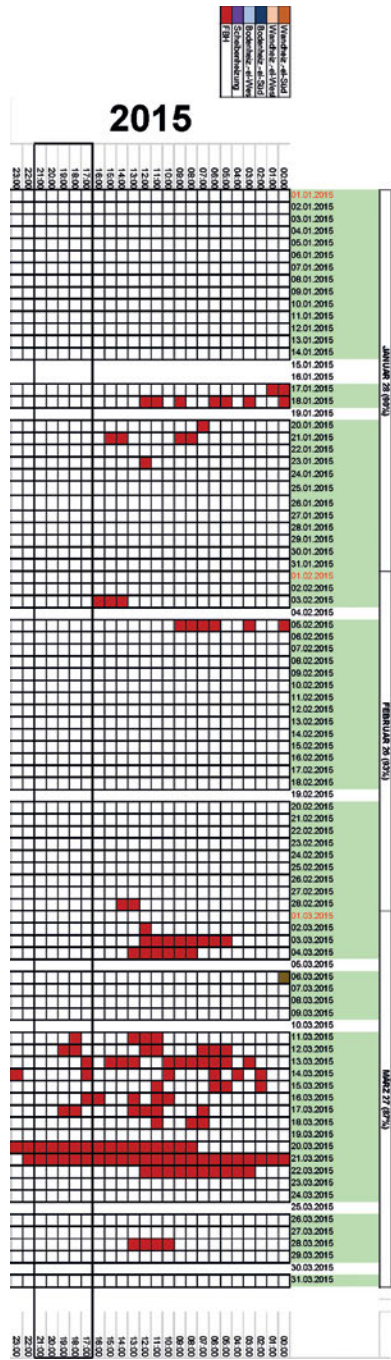


FIGURE APP.B.3



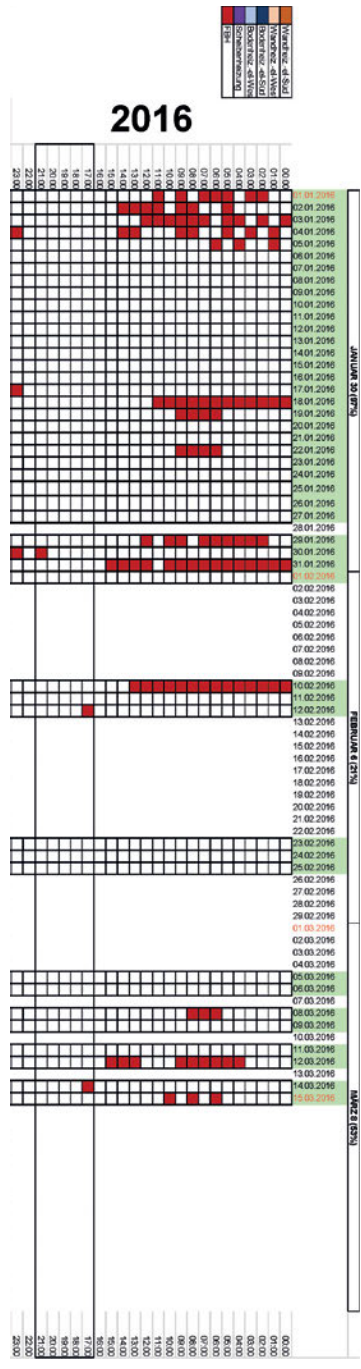


FIGURE APP.B.5

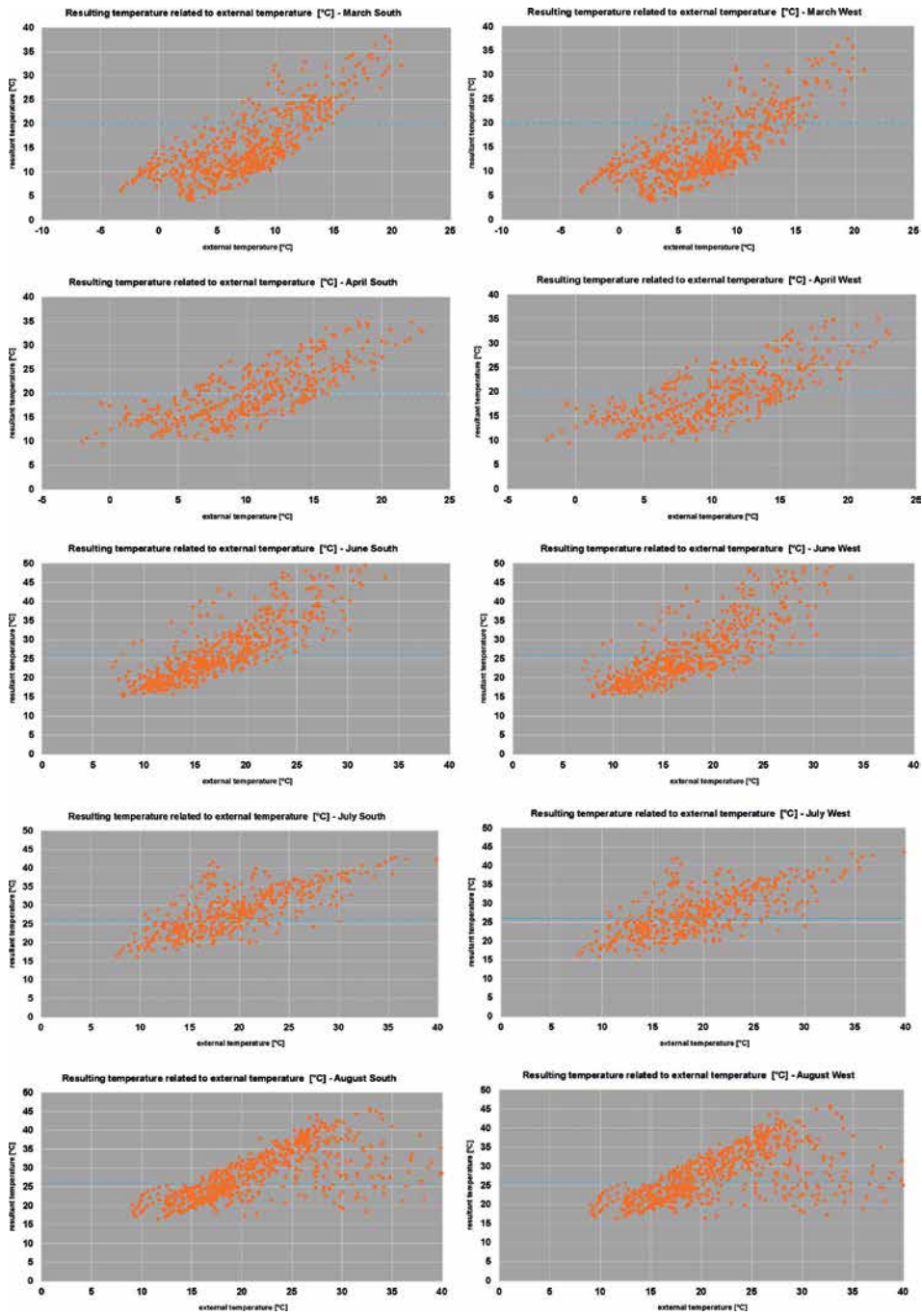


FIGURE APP.B.6

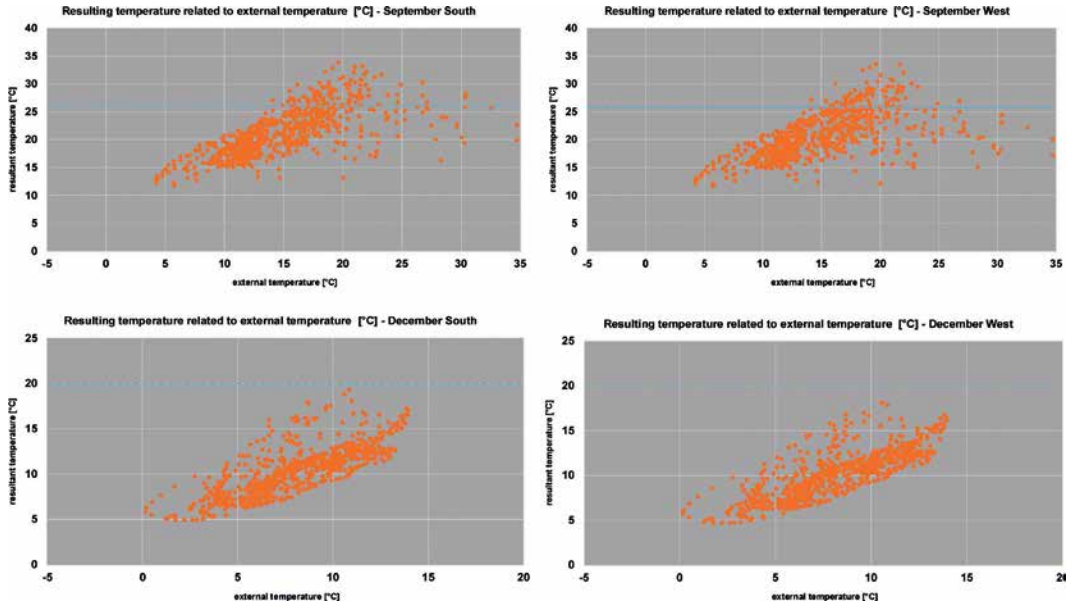


FIGURE APP.B.7

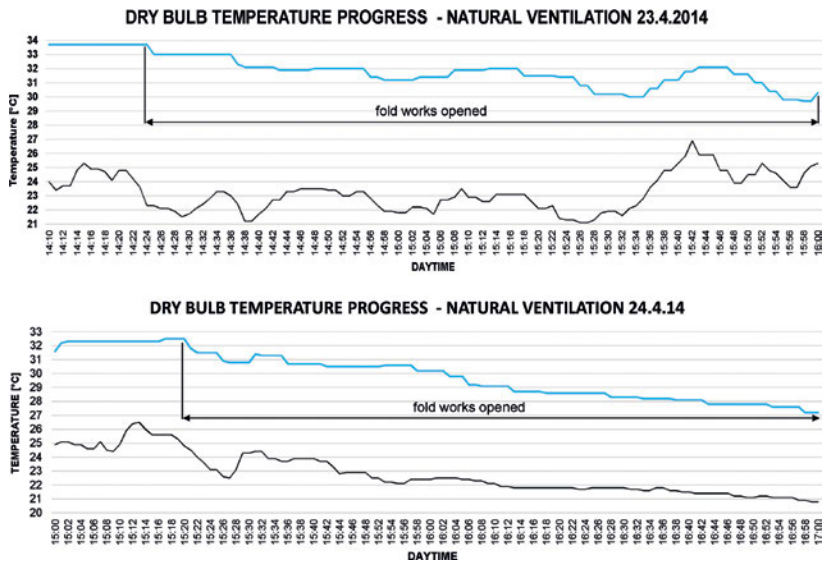


FIGURE APP.B.8

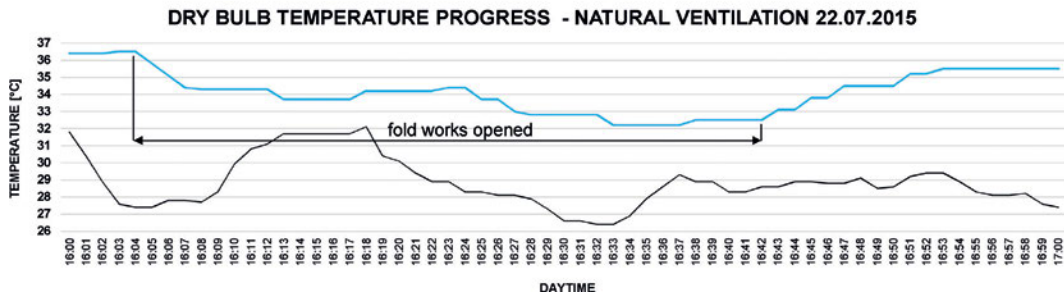
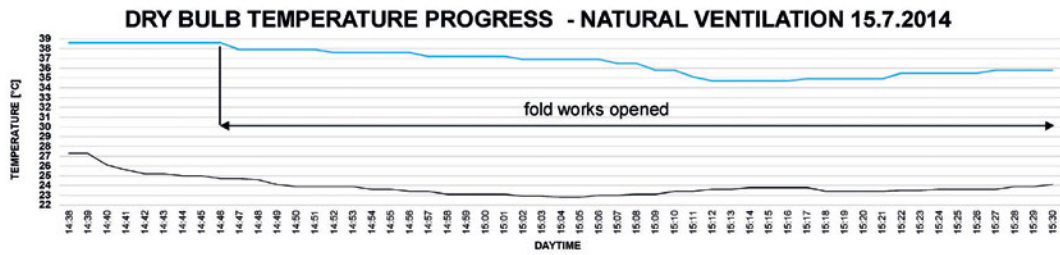
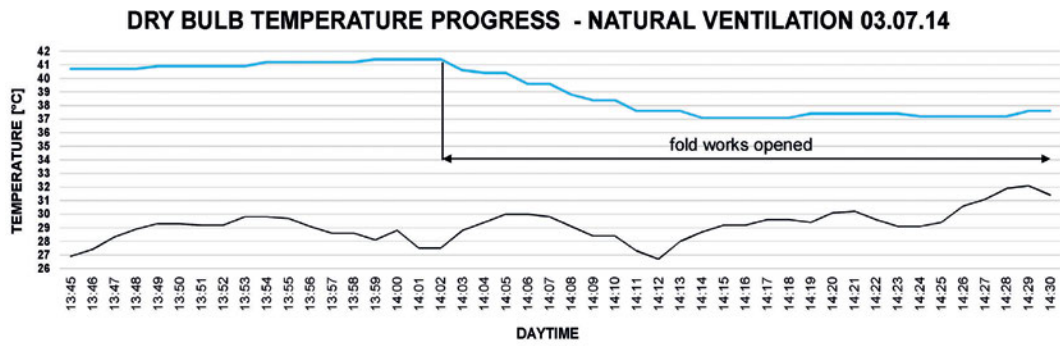


FIGURE APP.B.9

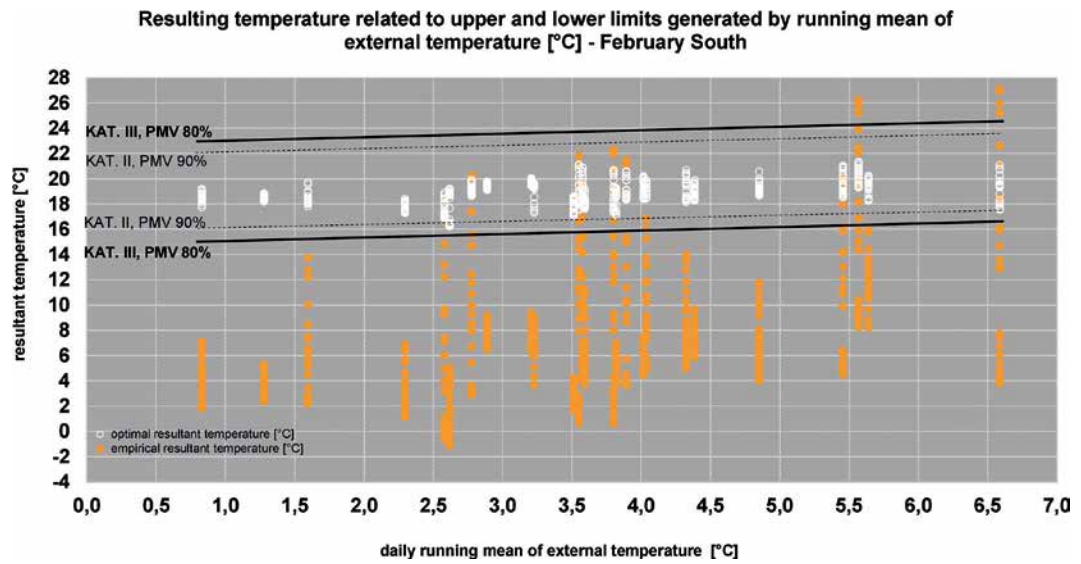


FIGURE APP.B.10

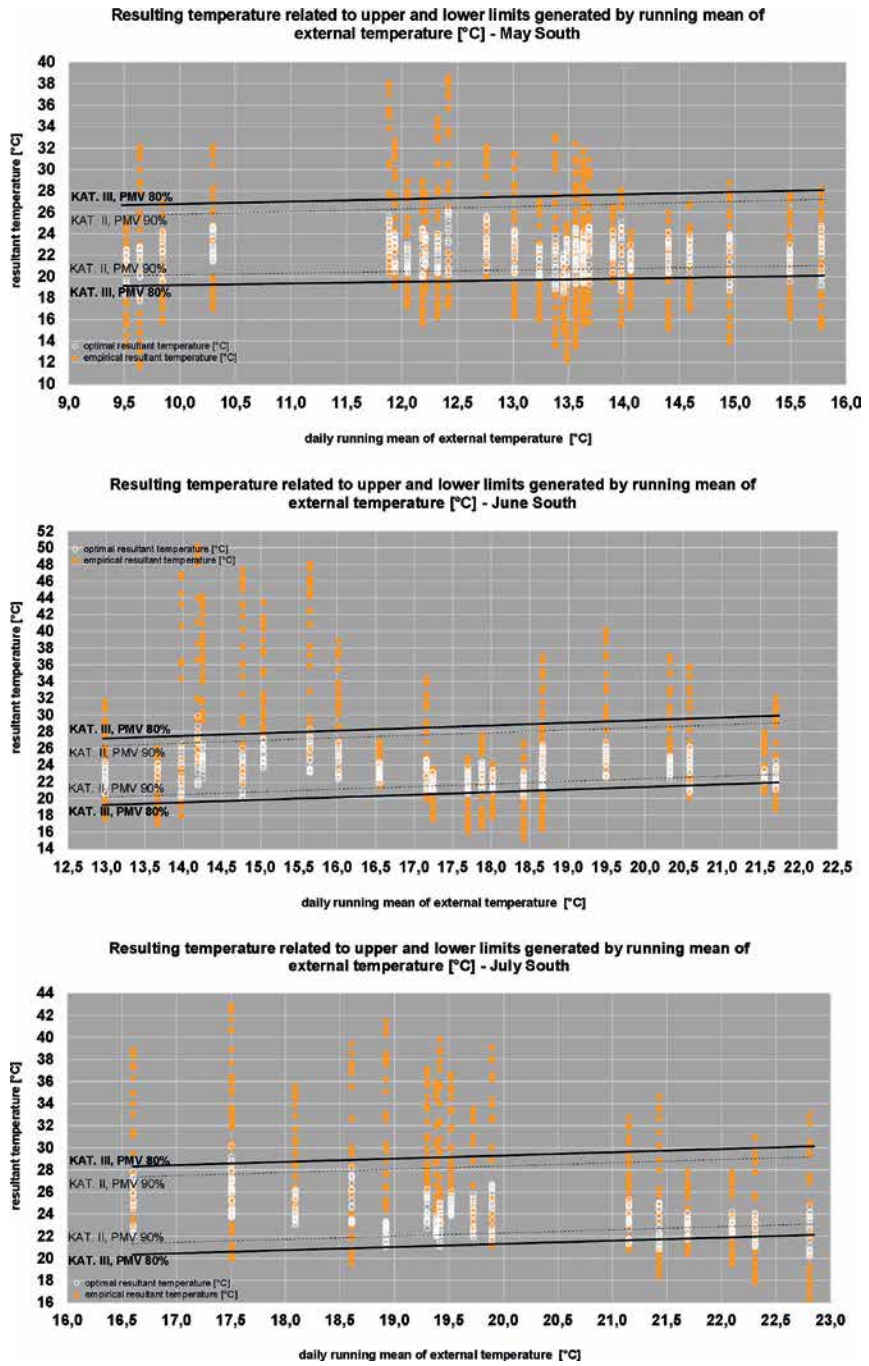


FIGURE APP.B.11

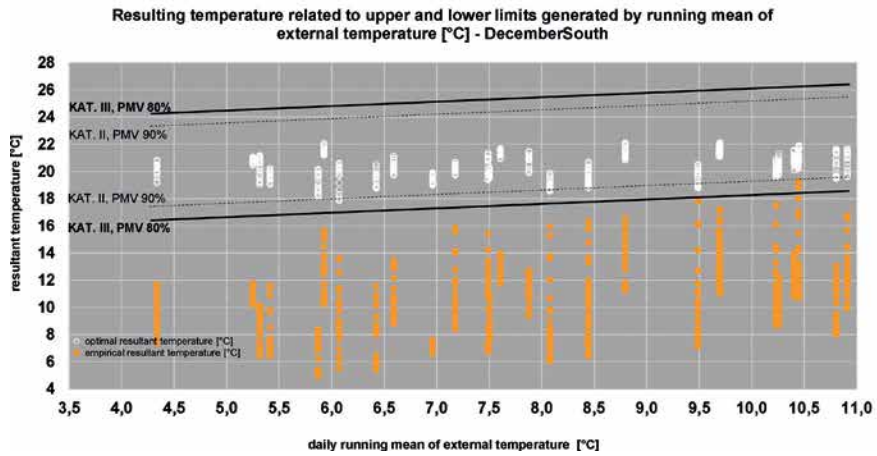
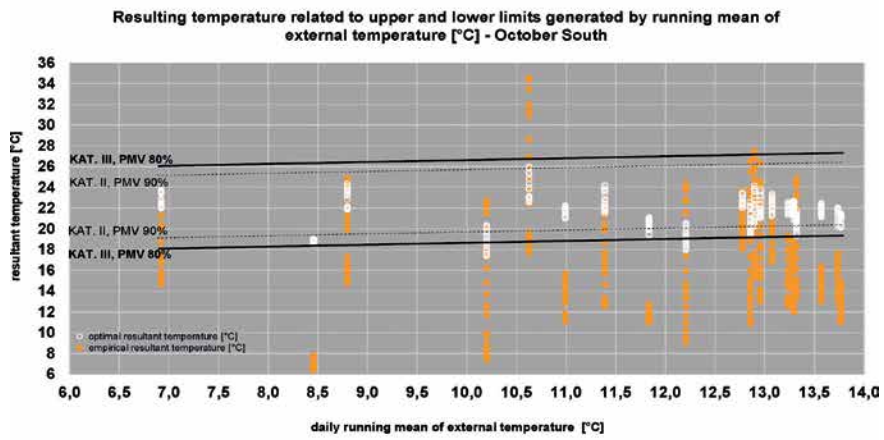
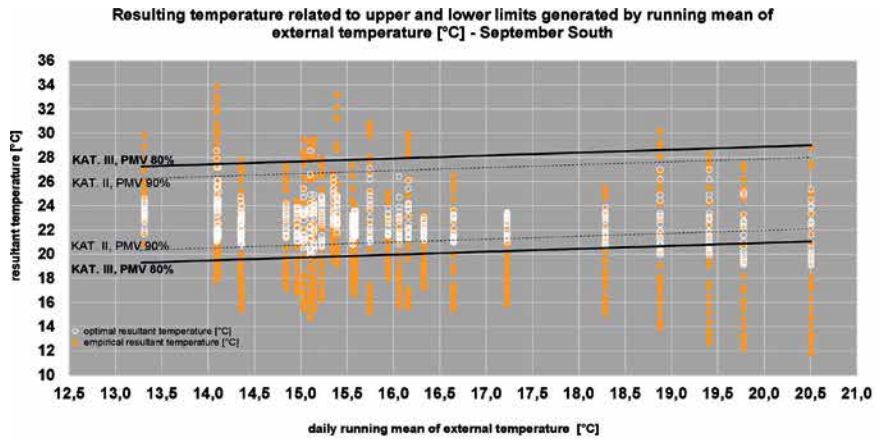


FIGURE APP.B.12

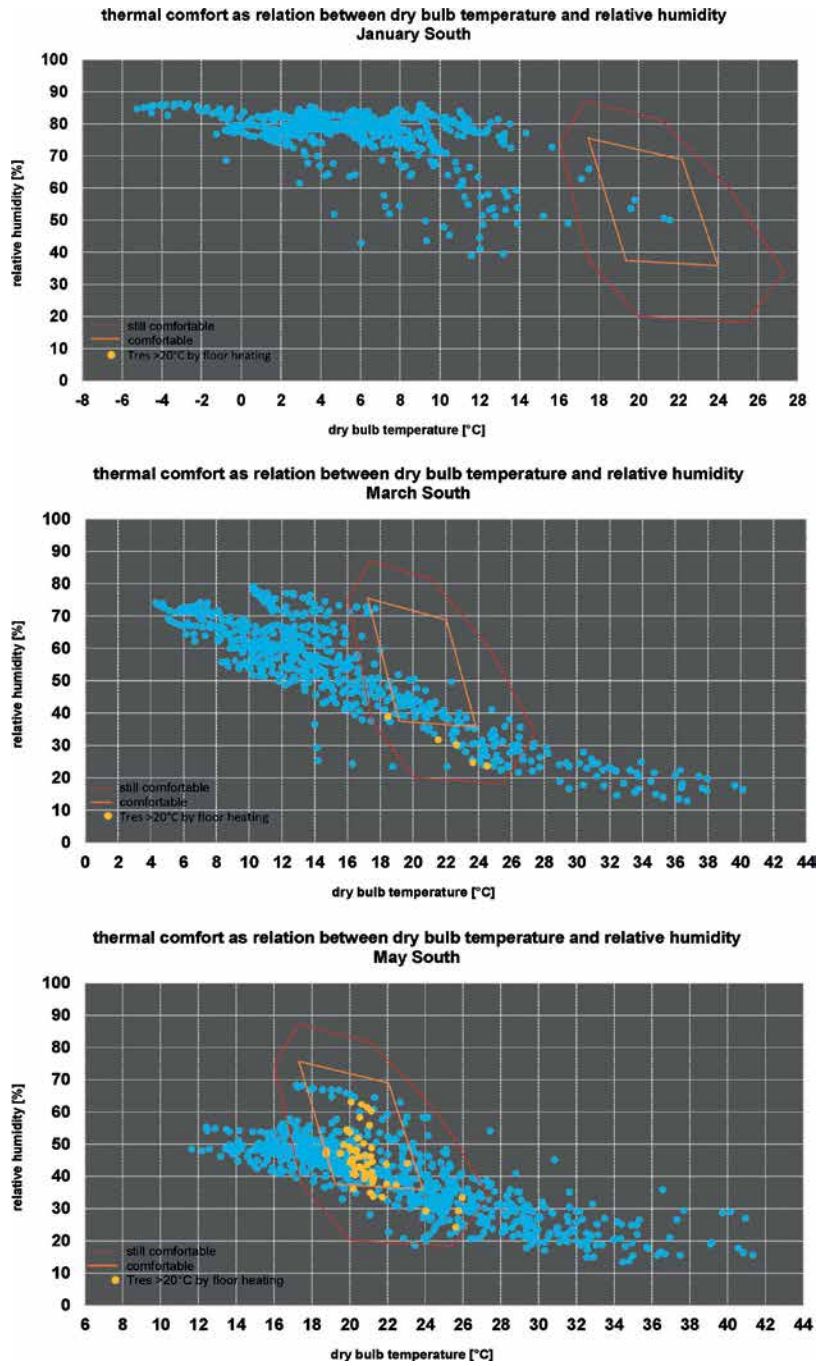


FIGURE APP.B.13

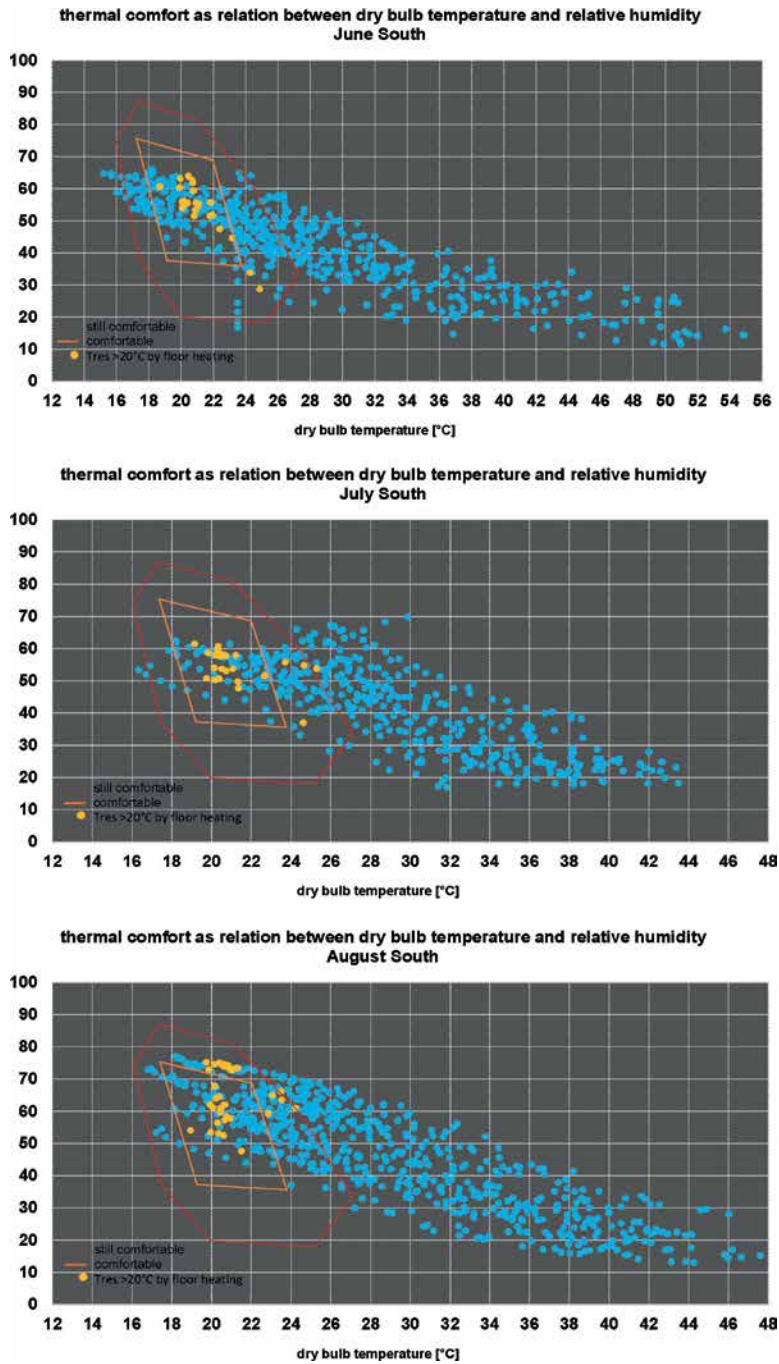


FIGURE APP.B.14

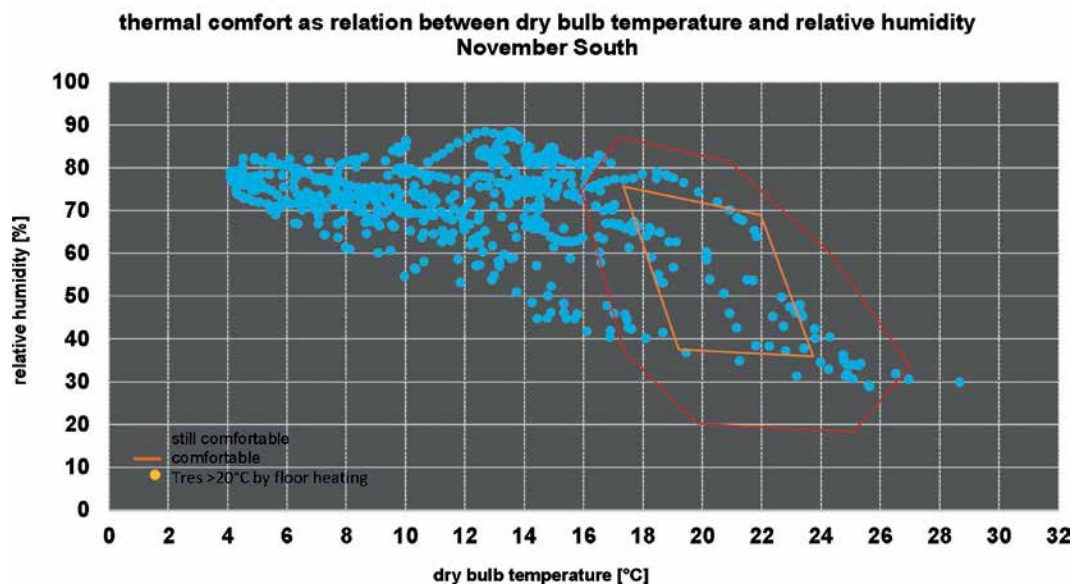
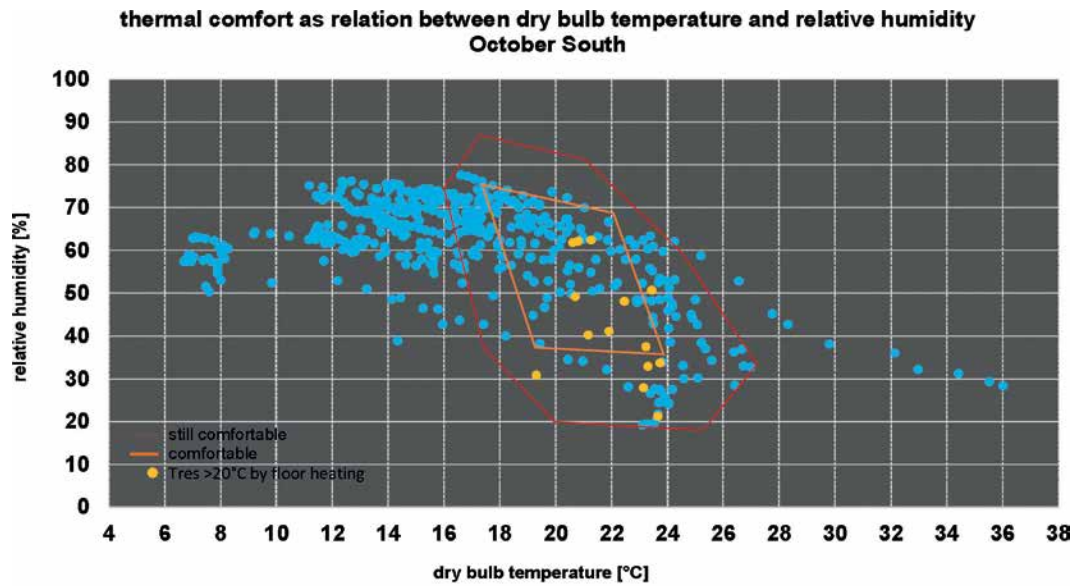


FIGURE APP.B.15

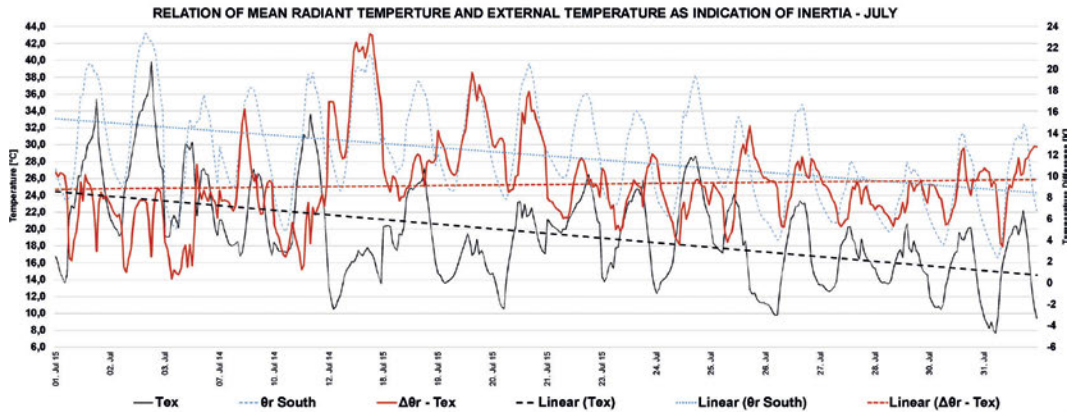
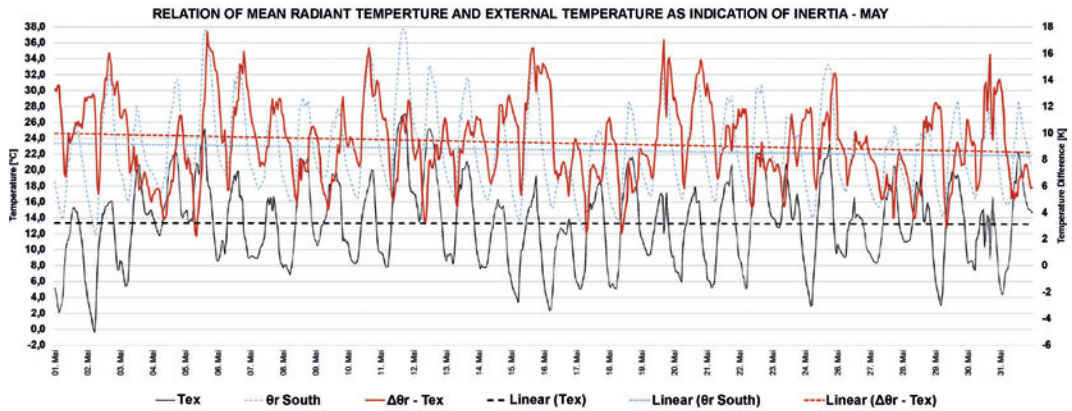
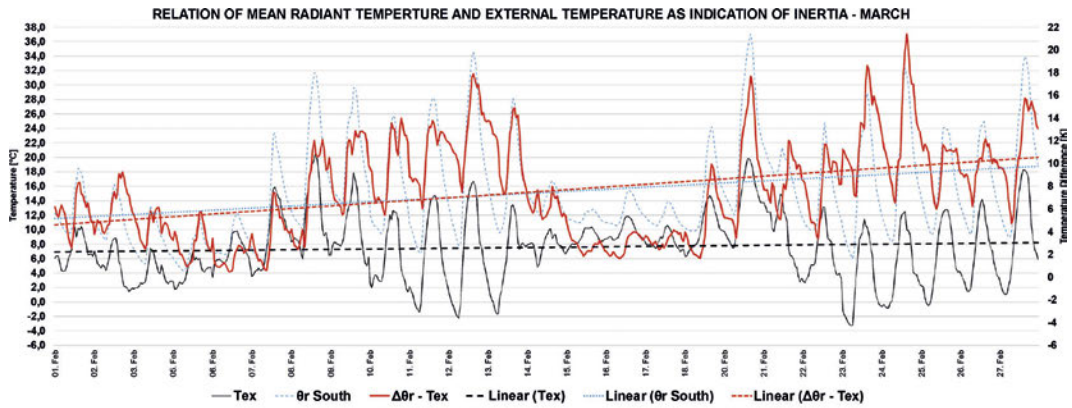


FIGURE APP.B.16

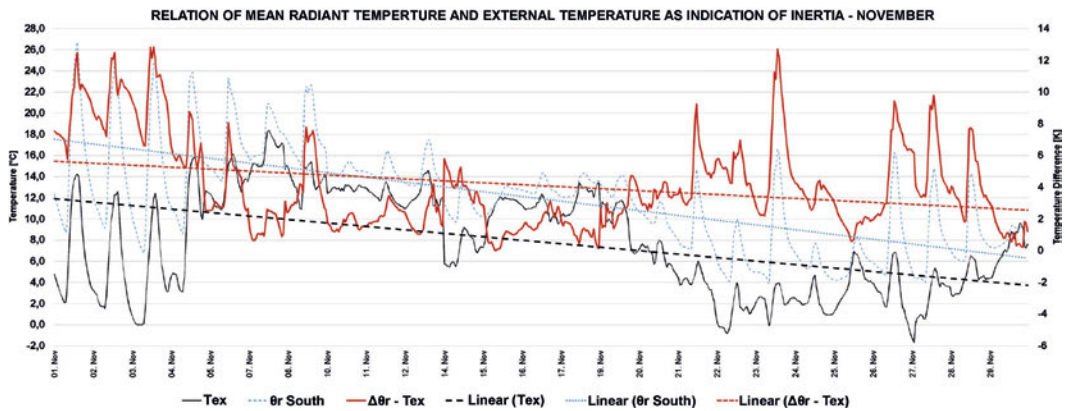
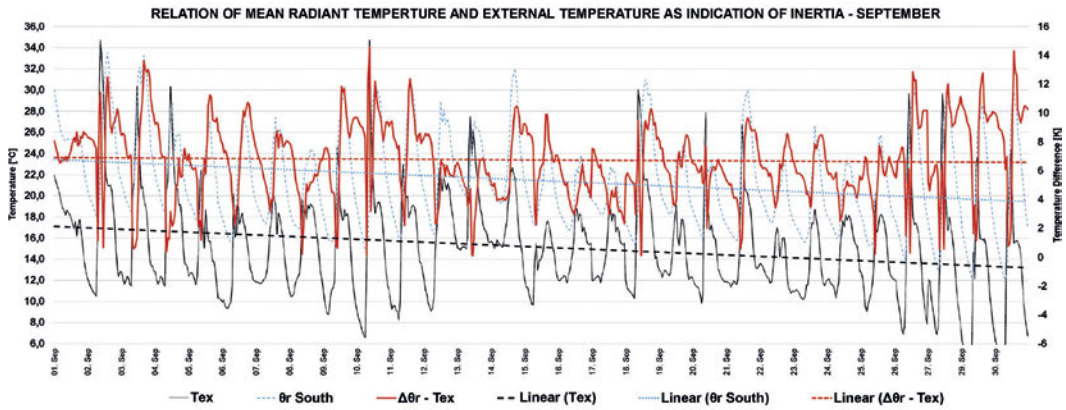
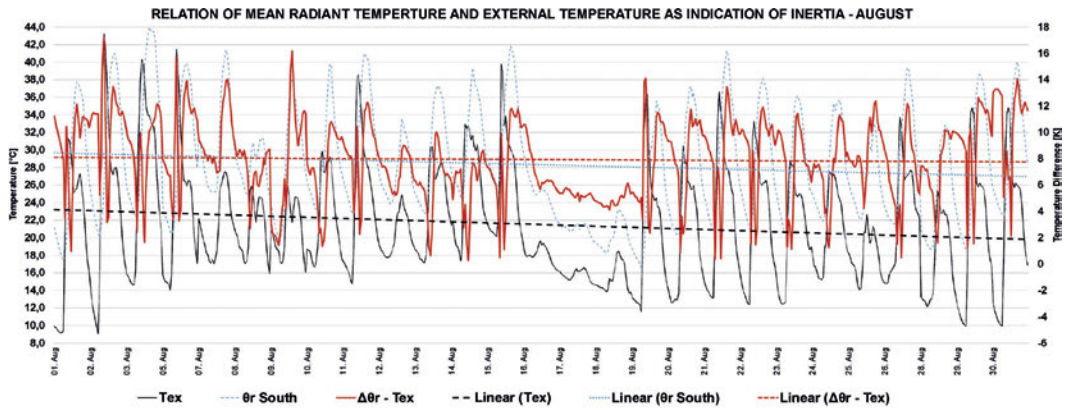


FIGURE APP.B.17

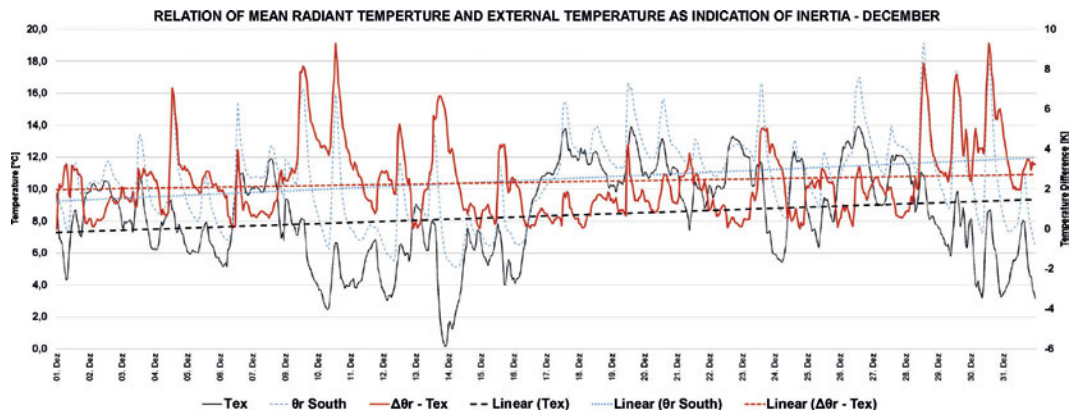


FIGURE APP.B.18

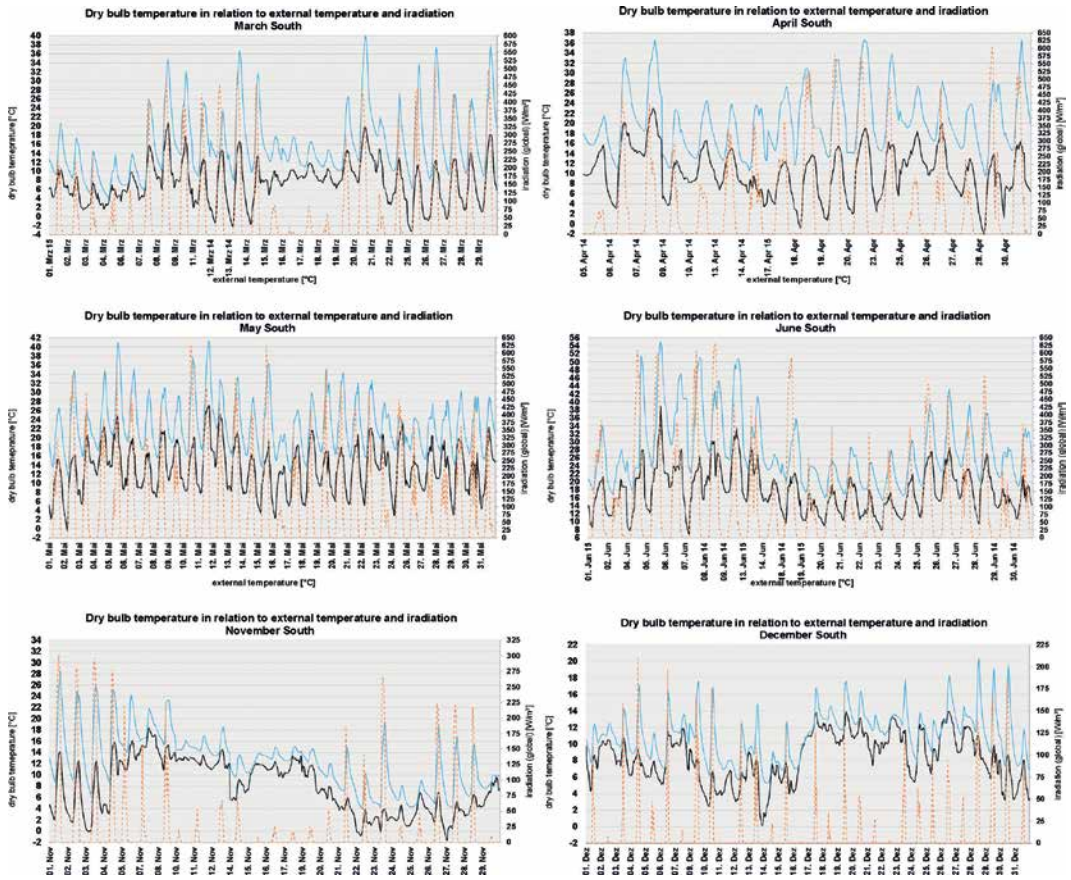


FIGURE APP.B.19

**LOCAL DISCOMFORT - RADIATION ASYMMETRIES**

FEBRUARY							
	624 / 130 hours						
	COLD WALL > 10K	COLD CEILING > 14K	>10K / >14K 5to10PM	PD >5%	>5% in 624h	PD >5% 5to10PM	>5% in 130h
Air Wall-North / Glazing-South	0		0	0	0%	0	0%
Air Wall-North / Glazing-East	624		130	624	100%	130	100%
Air Floor-South / Wall-North	0		0	0	0%	0	0%
Air Wall-North / Glazed-Roof-South		0	0	0	0%	0	0%
Air Floor-South / Glazed-Roof-South		433	82	435	70%	84	69%
Air Floor-South / Glazing-East	624		130	624	100%	130	100%
Air Glazing-South / Glazing-East	621		130	621	100%	130	100%
Air Floor-South / Glazing-South	274		18	172	26%	8	5%
Air Glazing-South / Glazed-Roof-South		0	0	0	0%	0	0%
Air Glazing-East / Glazed-Roof-South		0	0	0	0%	0	0%
Air Wall-East / Glazing-West	0		0	0	0%	0	0%
Air Wall-East / Glazing-North	624		130	624	100%	130	100%
Air Floor-West / Wall-East	0		0	0	0%	0	0%
Air Wall-East / Glazed-Roof-West		0	0	0	0%	0	0%
Air Floor-West / Glazed-Roof-West		502	102	502	80%	102	78%
Air Floor-West / Glazing-North	624		130	624	100%	130	100%
Air Glazing-West / Glazing-North	590		128	572	92%	128	97%
Air Floor-West / Glazing-West	183		8	77	12%	1	1%
Air Glazing-West / Glazed-Roof-West		0	0	0	0%	0	0%
Air Glazing-North / Glazed-Roof-West		0	0	0	0%	0	0%

**LOCAL DISCOMFORT - RADIATION ASYMMETRIES**

MARCH							
	600 / 125 hours						
	COLD WALL > 10K	COLD CEILING > 14K	>10K / >14K 5to10PM	PD >5%	>5% in 600h	PD >5% 5to10PM	>5% in 125h
Air Wall-North / Glazing-South	0		0	0	0%	0	0%
Air Wall-North / Glazing-East	600		125	600	100%	125	101%
Air Floor-South / Wall-North	0		0	0	0%	0	0%
Air Wall-North / Glazed-Roof-South		0	0	0	0%	1	1%
Air Floor-South / Glazed-Roof-South		417	83	419	70%	84	75%
Air Floor-South / Glazing-East	600		125	600	100%	125	101%
Air Glazing-South / Glazing-East	600		125	600	100%	125	101%
Air Floor-South / Glazing-South	317		48	247	41%	35	28%
Air Glazing-South / Glazed-Roof-South		0	0	0	0%	0	0%
Air Glazing-East / Glazed-Roof-South		0	0	0	0%	0	0%
Air Wall-East / Glazing-West	0		0	0	0%	0	0%
Air Wall-East / Glazing-North	600		125	600	100%	125	101%
Air Floor-West / Wall-East	0		0	0	0%	0	0%
Air Wall-East / Glazed-Roof-West		0	0	0	0%	1	1%
Air Floor-West / Glazed-Roof-West		450	87	452	75%	89	79%
Air Floor-West / Glazing-North	600		125	600	100%	125	101%
Air Glazing-West / Glazing-North	600		125	600	100%	125	101%
Air Floor-West / Glazing-West	336		47	251	42%	30	24%
Air Glazing-West / Glazed-Roof-West		0	0	0	0%	0	0%
Air Glazing-North / Glazed-Roof-West		0	0	0	0%	0	0%

**LOCAL DISCOMFORT - RADIATION ASYMMETRIES**

APRIL							
	408 / 85 hours						
	COLD WALL > 10K	COLD CEILING > 14K	>10K / >14K 5to10PM	PD >5%	>5% in 408h	PD >5% 5to10PM	>5% in 85h
Air Wall-North / Glazing-South	0		0	0	0%	0	0%
Air Wall-North / Glazing-East	408		85	408	100%	85	100%
Air Floor-South / Wall-North	0		0	0	0%	0	0%
Air Wall-North / Glazed-Roof-South		0	0	0	0%	0	0%
Air Floor-South / Glazed-Roof-South		258	39	258	63%	39	46%
Air Floor-South / Glazing-East	408		85	408	100%	85	100%
Air Glazing-South / Glazing-East	406		85	405	98%	85	100%
Air Floor-South / Glazing-South	220		19	203	50%	10	12%
Air Glazing-South / Glazed-Roof-South		0	0	0	0%	0	0%
Air Glazing-East / Glazed-Roof-South		0	0	0	0%	0	0%
Air Wall-East / Glazing-West	0		0	0	0%	0	0%
Air Wall-East / Glazing-North	408		85	408	100%	85	100%
Air Floor-West / Wall-East	0		0	0	0%	0	0%
Air Wall-East / Glazed-Roof-West		0	0	0	0%	0	0%
Air Floor-West / Glazed-Roof-West		302	52	302	74%	52	61%
Air Floor-West / Glazing-North	408		85	408	100%	85	100%
Air Glazing-West / Glazing-North	408		85	408	100%	85	100%
Air Floor-West / Glazing-West	235		17	212	52%	9	11%
Air Glazing-West / Glazed-Roof-West		0	0	0	0%	0	0%
Air Glazing-North / Glazed-Roof-West		0	0	0	0%	0	0%

FIGURE APP.B.20

LOCAL DISCOMFORT - RADIATION ASYMMETRIES							
JUNE							
	113 / 111 Hours						
	WARM WALL > 23K	WARM CEILING > 5K	>23K / >5K 5to10PM	PD >5%	>5% in 552h	PD >5% 5to10PM	>5% in 115h
Air Walk-North / Glazing-South	0		0	0	0%	0	0%
Air Walk-North / Glazing-East	4		3	0	0%	0	0%
Air Floor-South / Wall-North	0		0	0	0%	0	0%
Air Walk-North / Glazed-Roof-South		0	0	0	0%	0	0%
Air Floor-South / Glazed-Roof-South		0	0	0	0%	0	0%
Air Floor-South / Glazing-East	231		7	30	5%	0	0%
Air Glazing-South / Glazing-East	0		0	0	0%	0	0%
Air Floor-South / Glazing-South	0		0	0	0%	0	0%
Air Glazing-South / Glazed-Roof-South		0	0	0	0%	0	0%
Air Glazing-East / Glazed-Roof-South		842	115	848	99%	115	100%
Air Walk-East / Glazing-West	0		0	0	0%	0	0%
Air Walk-East / Glazing-North	1		0	0	0%	0	0%
Air Floor-West / Wall-East	0		0	0	0%	0	0%
Air Walk-East / Glazed-Roof-West		0	0	0	0%	0	0%
Air Floor-West / Glazed-Roof-West		0	0	0	0%	0	0%
Air Floor-West / Glazing-North	286		5	35	6%	0	0%
Air Glazing-West / Glazing-North	0		0	0	0%	0	0%
Air Floor-West / Glazing-West	0		0	0	0%	0	0%
Air Glazing-West / Glazed-Roof-West		0	0	0	0%	0	0%
Air Glazing-North / Glazed-Roof-West		550	114	552	100%	115	100%

LOCAL DISCOMFORT - RADIATION ASYMMETRIES							
JULY							
	132 / 90 Hours						
	WARM WALL > 23K	WARM CEILING > 5K	>23K / >5K 5to10PM	PD >5%	>5% in 432h	PD >5% 5to10PM	>5% in 90h
Air Walk-North / Glazing-South	0		0	0	0%	0	0%
Air Walk-North / Glazing-East	2		2	0	0%	0	0%
Air Floor-South / Wall-North	0		0	0	0%	0	0%
Air Walk-North / Glazed-Roof-South		0	0	0	0%	0	0%
Air Floor-South / Glazed-Roof-South		0	0	0	0%	0	0%
Air Floor-South / Glazing-East	189		17	21	5%	0	0%
Air Glazing-South / Glazing-East	0		0	0	0%	0	0%
Air Floor-South / Glazing-South	0		0	0	0%	0	0%
Air Glazing-South / Glazed-Roof-South		0	0	0	0%	0	0%
Air Glazing-East / Glazed-Roof-South		418	90	424	98%	90	100%
Air Walk-East / Glazing-West	0		0	0	0%	0	0%
Air Walk-East / Glazing-North	0		0	0	0%	0	0%
Air Floor-West / Wall-East	0		0	0	0%	0	0%
Air Walk-East / Glazed-Roof-West		0	0	0	0%	0	0%
Air Floor-West / Glazed-Roof-West		0	0	0	0%	0	0%
Air Floor-West / Glazing-North	221		12	17	4%	0	0%
Air Glazing-West / Glazing-North	0		0	0	0%	0	0%
Air Floor-West / Glazing-West	0		0	0	0%	0	0%
Air Glazing-West / Glazed-Roof-West		0	0	0	0%	0	0%
Air Glazing-North / Glazed-Roof-West		432	90	432	100%	90	100%

LOCAL DISCOMFORT - RADIATION ASYMMETRIES							
SEPTEMBER							
	106 / 145 Hours						
	WARM WALL > 23K	WARM CEILING > 5K	>23K / >5K 5to10PM	PD >5%	>5% in 998h	PD >5% 5to10PM	>5% in 145h
Air Walk-North / Glazing-South	0		0	0	0%	0	0%
Air Walk-North / Glazing-East	0		0	0	0%	0	0%
Air Floor-South / Wall-North	0		0	0	0%	0	0%
Air Walk-North / Glazed-Roof-South		0	0	0	0%	0	0%
Air Floor-South / Glazed-Roof-South		0	0	0	0%	0	0%
Air Floor-South / Glazing-East	305		18	0	0%	0	0%
Air Glazing-South / Glazing-East	0		0	0	0%	0	0%
Air Floor-South / Glazing-South	0		0	0	0%	0	0%
Air Glazing-South / Glazed-Roof-South		0	0	0	0%	0	0%
Air Glazing-East / Glazed-Roof-South		698	145	698	100%	145	100%
Air Walk-East / Glazing-West	0		0	0	0%	0	0%
Air Walk-East / Glazing-North	0		0	0	0%	0	0%
Air Floor-West / Wall-East	0		0	0	0%	0	0%
Air Walk-East / Glazed-Roof-West		0	0	0	0%	0	0%
Air Floor-West / Glazed-Roof-West		0	0	0	0%	0	0%
Air Floor-West / Glazing-North	333		21	0	0%	0	0%
Air Glazing-West / Glazing-North	0		0	0	0%	0	0%
Air Floor-West / Glazing-West	0		0	0	0%	0	0%
Air Glazing-West / Glazed-Roof-West		0	0	0	0%	0	0%
Air Glazing-North / Glazed-Roof-West		698	145	698	100%	145	100%

FIGURE APP.B.21

## LOCAL DISCOMFORT - RADIATION ASYMMETRIES

NOVEMBER	600 / 125 Hours						
	COLD WALL > 10K	COLD CEILING > 14K	>10K / >14K 5to10PM	PD > 5%	>5% in 600h	PD > 5% 5to10PM	>5% in 125h
ΔR Wall-North / Glazing-South	0		0	0	0%	0	0%
ΔR Wall-North / Glazing-East	600		125	600	100%	125	100%
ΔR Floor-South / Wall-North	0		0	0	0%	0	0%
ΔR Wall-North / Glazed-Roof-South		0	0	0	0%	0	0%
ΔR Floor-South / Glazed-Roof-South		463	113	463	77%	113	90%
ΔR Floor-South / Glazing-East	600		125	600	100%	125	100%
ΔR Glazing-South / Glazing-East	600		125	600	100%	125	100%
ΔR Floor-South / Glazing-South	268		54	165	26%	26	21%
ΔR Glazing-South / Glazed-Roof-South		0	0	0	0%	0	0%
ΔR Glazing-East / Glazed-Roof-South		0	0	0	0%	0	0%
ΔR Wall-East / Glazing-West	0		0	0	0%	0	0%
ΔR Wall-East / Glazing-North	600		125	600	100%	125	100%
ΔR Floor-West / Wall-East	0		0	0	0%	0	0%
ΔR Wall-East / Glazed-Roof-West		0	0	0	0%	0	0%
ΔR Floor-West / Glazed-Roof-West		535	121	535	89%	121	97%
ΔR Floor-West / Glazing-North	600		125	600	100%	125	100%
ΔR Glazing-West / Glazing-North	600		125	600	100%	125	100%
ΔR Floor-West / Glazing-West	342		84	151	25%	29	23%
ΔR Glazing-West / Glazed-Roof-West		0	0	0	0%	0	0%
ΔR Glazing-North / Glazed-Roof-West		0	0	0	0%	0	0%

## LOCAL DISCOMFORT - RADIATION ASYMMETRIES

DECEMBER	720 / 150 Hours						
	COLD WALL > 10K	COLD CEILING > 14K	>10K / >14K 6to10PM	PD > 5%	>5% in 720h	PD > 5% 6to10PM	>5% in 150h
ΔR Wall-North / Glazing-South	0		0	0	0%	0	0%
ΔR Wall-North / Glazing-East	720		150	720	100%	150	100%
ΔR Floor-South / Wall-North	0		0	0	0%	0	0%
ΔR Wall-North / Glazed-Roof-South		0	0	0	0%	0	0%
ΔR Floor-South / Glazed-Roof-South		542	135	547	76%	137	91%
ΔR Floor-South / Glazing-East	720		150	720	100%	150	100%
ΔR Glazing-South / Glazing-East	720		150	720	100%	150	100%
ΔR Floor-South / Glazing-South	268		40	117	16%	15	10%
ΔR Glazing-South / Glazed-Roof-South		0	0	0	0%	0	0%
ΔR Glazing-East / Glazed-Roof-South		0	0	0	0%	0	0%
ΔR Wall-East / Glazing-West	0		0	0	0%	0	0%
ΔR Wall-East / Glazing-North	720		150	720	100%	150	100%
ΔR Floor-West / Wall-East	0		0	0	0%	0	0%
ΔR Wall-East / Glazed-Roof-West		0	0	0	0%	0	0%
ΔR Floor-West / Glazed-Roof-West		668	150	668	93%	150	100%
ΔR Floor-West / Glazing-North	720		150	720	100%	150	100%
ΔR Glazing-West / Glazing-North	720		150	720	100%	150	100%
ΔR Floor-West / Glazing-West	312		66	109	15%	25	17%
ΔR Glazing-West / Glazed-Roof-West		0	0	0	0%	0	0%
ΔR Glazing-North / Glazed-Roof-West		0	0	0	0%	0	0%

FIGURE APP.B.22

# Appendix C Chapter 03

TECHNOLOGY / SEASON AND GEOGRAPHICAL LOCATION / INCLINATION		evacuated tube collector + sensible storage		evacuated tube collector + seasonal storage		flat plate collector + sensible storage		unglazed flat plate collector + sensible storage		evacuated tube collector + sensible storage		evacuated tube collector + seasonal storage		flat plate collector + sensible storage		unglazed flat plate collector + sensible storage		evacuated tube collector + sensible storage		evacuated tube collector + seasonal storage		flat plate collector + sensible storage		unglazed flat plate collector + sensible storage					
		AUTUMN/SPRING				SUMMER				WINTER																			
		+	++	-	-	+	+	+	-	-	-	-	-	+	+	+	-	-	-	-	-	+	+	+	-	-	-	-	-
NORTHERN GERMANY	roof : 10 to 30° inclined	+	++	-	-	+	+	+	-	-	-	-	-	+	+	+	-	-	-	-	-	+	+	+	-	-	-	-	-
	roof : 30 to 70° inclined	++	+++	+	+	+++	++++	++	+	+-	-	-	-	+	+	+	+	+	+	+	+	+	+	+	+	+	+	+	+
	facade : 90° inclined	+++	++++	++	+	++	+++	+++	+	+	+	+	+	+	+	+	+	+	+	+	+	+	+	+	+	+	+	+	+
MID-GERMANY	roof : 10 to 30° inclined	++	++	-	+	++	++	++	+	+	+	+	+	+	+	+	+	+	+	+	+	+	+	+	+	+	+	+	+
	roof : 30 to 70° inclined	+++	++++	++	++	+++	++++	+++	++	++	++	++	++	++	++	++	++	++	++	++	++	++	++	++	++	++	++	++	++
	facade : 90° inclined	+++	++++	+	+	+++	++++	++	++	+-	-	+-	+-	+	+	+	+	+	+	+	+	+	+	+	+	+	+	+	+
SOUTHERN GERMANY	roof : 10 to 30° inclined	+++	+++	+	+	++	+++	+++	++	+	+	+	+	+	+	+	+	+	+	+	+	+	+	+	+	+	+	+	+
	roof : 30 to 70° inclined	++	+++	++	+	+++	++++	+++	+	+	+	+	+	+	+	+	+	+	+	+	+	+	+	+	+	+	+	+	+
	facade : 90° inclined	++	+++	+-	-	+	++	+	+-	+-	-	+-	+-	+	+	+	+	+	+	+	+	+	+	+	+	+	+	+	+

FIGURE APP.C.1

PARAMETER / POLYMER		BAYER APEC										BAYER
		FEB		PFA	DP9-9343	DP9-9351	DP9-9353	DP9-9373	1897	2097	1803	Makrolon 2405/7
		Perfluorethylenprop	Perfluoralkoxyalkan									
UV resistance	%	X	X	X	X	X	X	X	X	X	X	X
light transmission	%	XXXX	XXXXX	88	88	88	88	89	89	88	88	88
fraction index		0,25	0,21	1,58	1,57	1,57	1,56	1,57	1,56	1,57	1,58	1,58
operation temperature	°C	- 200 bis + 200	- 200 bis + 260	150	162	160	179	150	157	172	159	159
short-time maximum temperature	°C	250 <sup>1</sup>	260 <sup>1</sup>	162	174	172	195	172	172	191	174	174
Vicat softenig temperature	°C	257 - 275	300 - 310	172	185	183	205	182	202	184	145	145
chemical resistance (qual.)		XXXX	XXXXX	-	-	-	-	-	-	-	-	-
water absorption	%	< 0,01	< 0,03	0,2	0,2	0,2	0,2	0,3	0,3	0,3	0,30	0,30
hardness	Shore D	55 - 60	55 - 64	-	-	-	-	-	-	-	-	-
impact resistance DIN 53453	kJ/m²	NO	NO	3,20	1,1	1,1	0,80	8,0	6,0	10,0	65,0	65,0
processing												
<i>deep drawing</i>		-	-	-	-	-	-	-	-	-	-	-
<i>extrusion</i>		X	X	-	-	-	-	-	X	X	-	-
<i>banding</i>		X	X	-	-	-	-	-	-	-	-	-

FIGURE APP.C.2



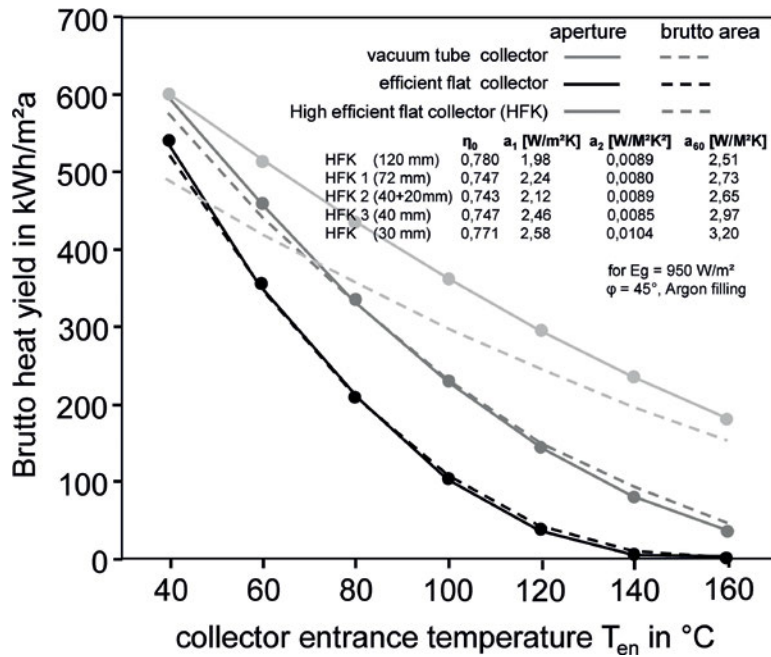


FIGURE APP.C.4

CODE	DIMENSION [mm]	INCLINATION [°]	QUALITIES	$\eta_0$	$a_1$ [W/m <sup>2</sup> K]	$a_2$ [W/m <sup>2</sup> K <sup>2</sup> ]	$a_{40}$ [W/m <sup>2</sup> K]
TIK_L / 45°	64	45	triple-glazing, gilded absorber, air filled cavity	0,785	4,66	0,014	5,22
TIK_Ar / 45°	51	45	triple-glazing, gilded absorber, Argon filled cavity	0,781	3,77	0,0109	4,21
TIK_Ar_2 / 45°	76	45	quadruple-glazing, gilded absorber, Argon filled cavity, double-glazed rear	0,774	3,74	0,0083	4,07
TIK_L / 90°	64	90	triple-glazing, gilded absorber, air filled cavity	0,78	4,09	0,0122	4,58
TIK_Ar / 90°	51	90	triple-glazing, gilded absorber, Argon filled cavity	0,784	3,21	0,0109	3,65
TIK_Ar_6 / 90°	54	90	triple-glazing, ultrasound-welded absorber, Argon filled cavity	0,743	3,41	0,0125	3,91
REFERENCE KBB / 45°	75	45	single-glazed, laser-welded absorber, air filled cavity	0,781	3,83	0,0159	4,46

FIGURE APP.C.5

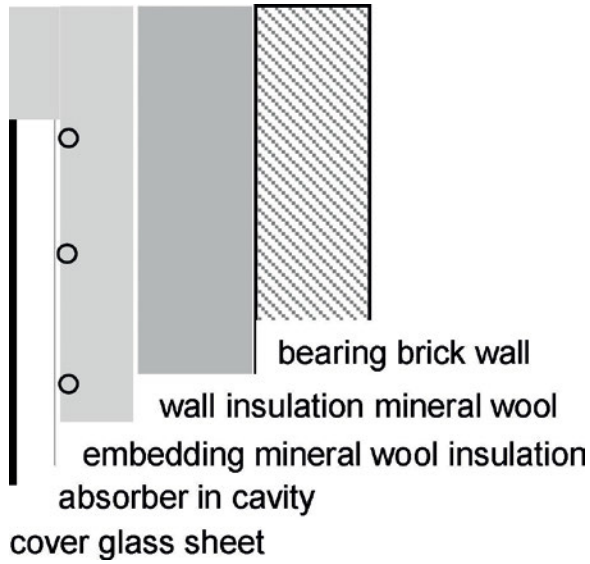


FIGURE APP.C.6

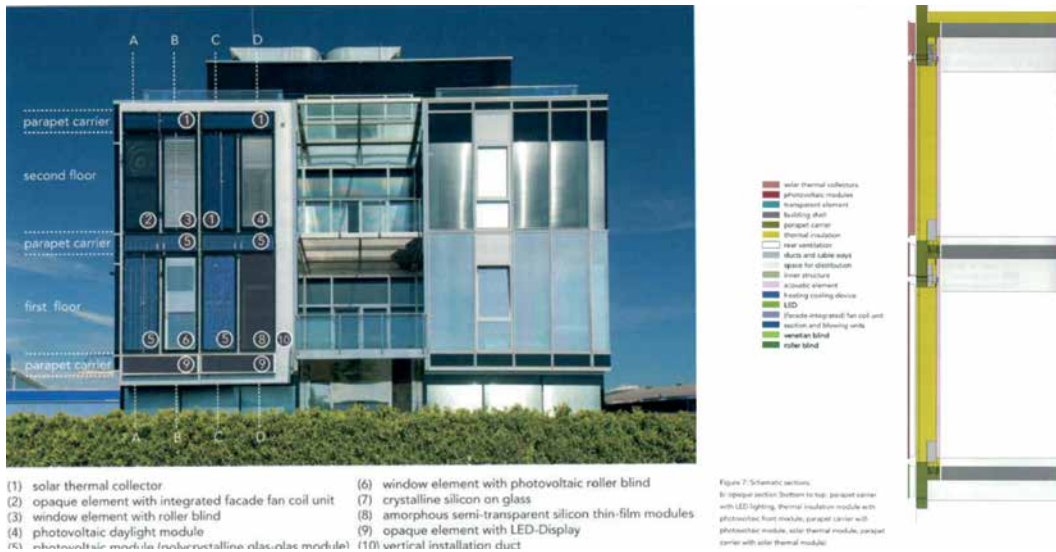


FIGURE APP.C.7

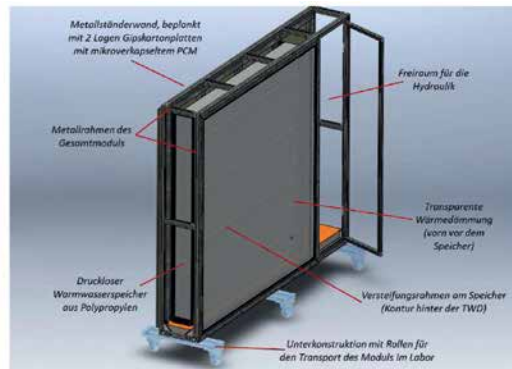
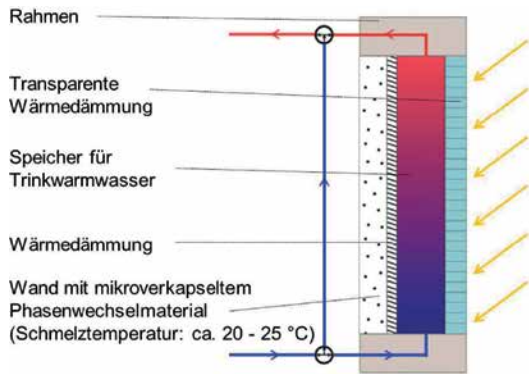


FIGURE APP.C.8



FIGURE APP.C.9

Action related area-wise heat transmission for three different operation scenarios for opaque solid wamm incorporated flat plate collectors

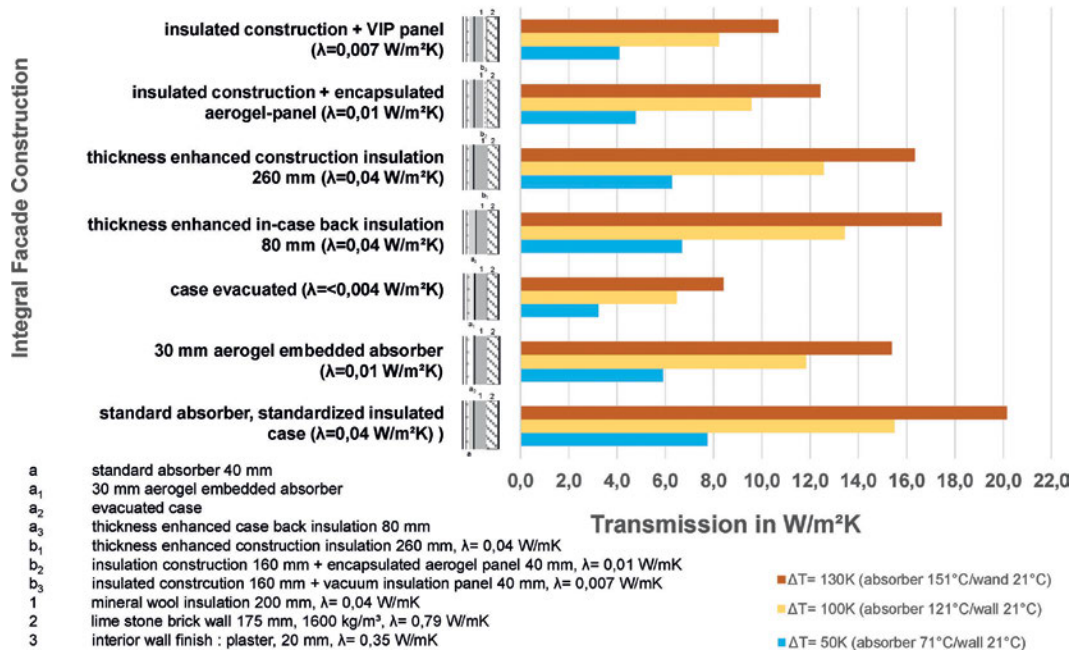


FIGURE APP.C.10



**AUTOMOTIVE HIGH-VOLTAGE ACCUMULATOR TECHNOLOGIES - 2013**

CELL TECHNOLOGY	CELL TYPE	NUMBER OF CELLS	WEIGHT [kg]	VOLTAGE [V]	CAPACITY [Ah]	ENERGY [kWh]	POWER [kW]	TARE WEIGHT [kg]	GRAMMETRIC CAPACITY [Ah/kg]	RANGE [km]	CONSUMPTION [kWh/km]	MODE
LITHIUM-ION	Lithium-Ionen	-	-	-	-	4,4	62	1.400	-	25	-	a.) monovalent, b.) bivalent
	Lithium-Ionen	-	150	400	26,0	11,2	50	1.900	1,47	50	-	a.) monovalent, b.) bivalent
	Lithium-Ionen	-	150	400	30,0	12,0	53	2.130	1,41	55	-	a.) monovalent, b.) bivalent
	Lithium-Ionen	-	-	-	-	-	50,0	-	-	150	-	a.) monovalent
	Lithium-Ionen	-	-	400	107,0	42,8	230	1.665	6,91	250	-	a.) monovalent
	Lithium-Ionen	648	-	388	2910,0	1130,0	240	80.000	3,64	-	-	a.) monovalent
	Lithium-Ionen	-	-	-	-	14,0	125	1.800	-	180	0,12 kWh/km	a.) monovalent
	Lithium-Ionen	-	-	400	67,5	35,0	150	1.460	5,99	160	0,15 kWh/km	a.) monovalent
	Lithium-Ionen	-	420	375	226,7	85,0	225	1.650	13,74	400	0,168 kWh/km	a.) monovalent
	Lithium-Ionen	5831	380	375	146,7	55,0	225	1.335	10,99	340	-	a.) monovalent
LITHIUM-ION	Lithium-Ionen	288	-	-	-	16,0	111	1.650	-	80	0,16 kWh/km	a.) monovalent, b.) bivalent
	Lithium-Ionen	288	-	-	-	16,0	111	1.650	-	80	0,16 kWh/km	a.) monovalent, b.) bivalent
LITHIUM-ION + X	Lithium-Iron-Phosphate	-	-	-	-	92,0	600	1.650	-	600	-	a.) monovalent
	Nanophosphate-Lithium-Ion	-	-	336	59,8	20,1	336	2.404	2,49	80	-	a.) monovalent, b.) bivalent
	Lithium-Polymer	91	-	-	-	-	-	-	-	50	-	a.) monovalent, b.) bivalent
NICKEL + X	Nickel-Metal-Hybride	-	-	202	6,4	1,3	27	1.445	0,46	2	-	a.) monovalent, b.) bivalent
		-	-	-	-	5,2	60	1.460	-	20	-	a.) monovalent, b.) bivalent

FIGURE APP.D.2

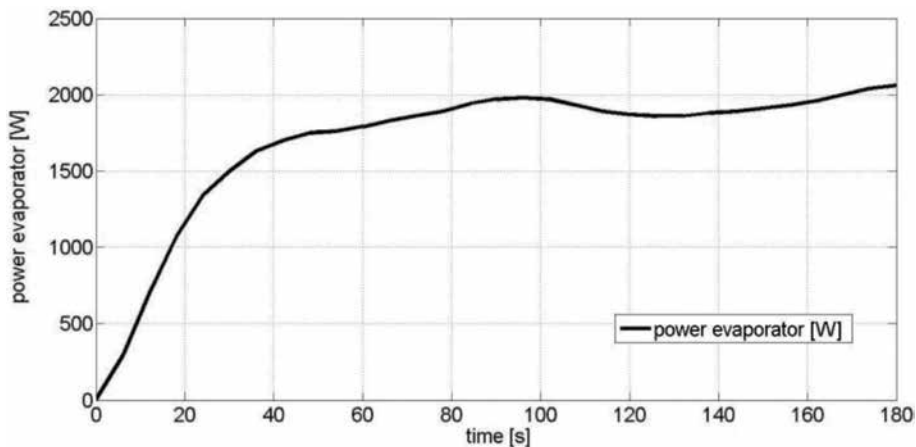


FIGURE APP.D.3

GROUP OF MATERIAL	MATERIAL	observed capacity/output [kWh/m <sup>3</sup> ]	observed capacity/output [kWh/kg]
Zeolite	Zeolith	1.300	
	Zeolith 13x	130	0,185
	NALSX (Na <sub>96</sub> [(AlO <sub>2</sub> ) <sub>96</sub> (SiO <sub>2</sub> ) <sub>96</sub> ])	198	0,291
	NAX (Na <sub>83</sub> [(AlO <sub>2</sub> ) <sub>83</sub> (SiO <sub>2</sub> ) <sub>109</sub> ])	176	0,278
	NAY-1 (Na <sub>96</sub> [(AlO <sub>2</sub> ) <sub>56</sub> (SiO <sub>2</sub> ) <sub>136</sub> ])	169	0,257
	NAY-3 (Na <sub>15</sub> [(AlO <sub>2</sub> ) <sub>15</sub> (SiO <sub>2</sub> ) <sub>177</sub> ])	99	0,207
Silica Gel	Silica Gel	100	–
Metal-hydrate	Fe(OH) <sub>2</sub>	611	–
Zeolite Composite	Zeolite composite attalugite+ poolkohl+ 30%CaCl <sub>2</sub> / water	--	0,2
Salt Hydrate	Magnesia-Chloride MgCl <sub>2</sub> / Water	139	–
	MgCl <sub>2</sub> * 6H <sub>2</sub> O	775	–
	Magnesia-Sulphate MgSO <sub>4</sub> * 7H <sub>2</sub> O	778	–
	MgSO <sub>4</sub> * 6H <sub>2</sub> O	508	–
	MgSO <sub>4</sub> * 6H <sub>2</sub> O	781	–
	Sodium-Sulphate Na <sub>2</sub> S * 5H <sub>2</sub> O	750	–
	Na <sub>2</sub> S * 5H <sub>2</sub> O	739	–
	Na <sub>2</sub> SO * 10H <sub>2</sub> O	711	–
	Clacium-Chloride CaCl <sub>2</sub> * 2H <sub>2</sub> O	306	–
	CaCl <sub>2</sub> * 2H <sub>2</sub> O	783	–
	CaSO <sub>4</sub> *2H <sub>2</sub> O	389	–
	Calcium-Oxide Ca(OH) <sub>2</sub>	323	373
	Bromide-Strontium SBr <sub>2</sub> *6H <sub>2</sub> O / water	430 - 460	–
Metal-organic framework (MOF's)	CuSO <sub>4</sub> * 5H <sub>2</sub> O	514	–

FIGURE APP.D.4

# Appendix E Chapter 08

<b>25m<sup>2</sup> South</b>		<b>BAND WIDTHS OF CUMULATIVE FREQUENCIES</b>												
Passive solar gains		WINTER						SUMMER						
MONTH / DAYTIME		November	December	January	February	March	April	May	June	July	August	September	October	
<b>5PM to 10PM</b>	>18°C	MAX	47	1	0	29	138	150	155	150	155	155	150	151
		MIN	0	0	0	0	44	24	64	86	135	138	115	81
	>20°C	MAX	22	0	0	10	128	122	155	150	155	155	150	151
		MIN	0	0	0	0	29	10	38	47	106	111	70	54
	>26°C	MAX	0	0	0	0	3	6	18	27	35	42	21	14
		MIN	0	0	0	0	0	0	0	0	0	1	0	0
<b>10PM to 5 PM</b>	>18°C	MAX	213	93	67	142	448	466	577	570	589	589	570	583
		MIN	25	0	0	31	174	217	203	335	489	516	410	319
	>20°C	MAX	172	61	46	105	362	332	506	565	589	589	570	513
		MIN	8	0	0	19	169	59	112	184	343	368	330	231
	>26°C	MAX	23	1	1	20	139	48	69	138	188	180	168	134
		MIN	0	0	0	0	22	7	0	4	18	2	49	20

<b>25m<sup>2</sup> East</b>		<b>BAND WIDTHS OF CUMULATIVE FREQUENCIES</b>												
Passive solar gains		WINTER						SUMMER						
MONTH / DAYTIME		November	December	January	February	March	April	May	June	July	August	September	October	
<b>5PM to 10PM</b>	>18°C	MAX	26	0	0	16	134	150	155	150	155	155	150	151
		MIN	0	0	0	0	35	71	42	90	136	134	102	57
	>20°C	MAX	6	0	0	2	116	150	150	150	155	155	150	129
		MIN	0	0	0	0	1	33	19	48	122	110	64	25
	>26°C	MAX	0	0	0	0	1	5	12	28	36	44	16	2
		MIN	0	0	0	0	0	0	0	0	1	0	0	0
<b>10PM to 5 PM</b>	>18°C	MAX	189	48	43	118	413	546	577	570	589	589	570	555
		MIN	14	0	0	24	175	259	234	350	520	528	371	247
	>20°C	MAX	152	24	19	97	277	532	525	558	589	589	570	425
		MIN	4	0	0	18	138	259	149	201	382	386	244	165
	>26°C	MAX	8	0	0	7	126	115	93	157	189	163	141	103
		MIN	0	0	0	0	13	34	4	11	38	26	43	45

<b>25m<sup>2</sup> West</b>		<b>BAND WIDTHS OF CUMULATIVE FREQUENCIES</b>												
Passive solar gains		WINTER						SUMMER						
MONTH / DAYTIME		November	December	January	February	March	April	May	June	July	August	September	October	
<b>5PM to 10PM</b>	>18°C	MAX	28	0	0	7	128	150	155	150	155	155	150	151
		MIN	0	0	0	0	33	37	85	84	123	127	72	53
	>20°C	MAX	6	0	0	2	102	139	155	150	155	155	150	148
		MIN	0	0	0	0	4	19	45	49	82	90	43	25
	>26°C	MAX	0	0	0	0	2	18	16	25	34	37	18	3
		MIN	0	0	0	0	0	0	0	0	0	0	0	0
<b>10PM to 5 PM</b>	>18°C	MAX	161	25	23	99	369	163	586	570	589	589	570	559
		MIN	12	0	0	19	144	503	318	316	437	451	301	227
	>20°C	MAX	118	10	9	60	284	390	550	562	589	589	570	435
		MIN	1	0	0	9	122	108	239	173	293	287	179	164
	>26°C	MAX	5	0	0	4	88	68	154	108	149	131	92	91
		MIN	0	0	0	0	6	9	28	1	9	0	17	6

FIGURE APP.E.1

25m <sup>2</sup> - South - CR 01															
Passive solar gains															
MONTH/ Cumul. Frequency		WINTER							SUMMER						
		November	December	January	February	March	April	SUM	May	June	July	August	September	October	SUM
5PM to 10PM	>16°C	60	0	0	16	121	150	247	155	150	155	155	150	151	916
	>18°C	30	0	0	1	68	150	249	155	150	155	155	150	151	916
	>20°C	0	0	0	0	41	122	163	142	150	155	155	150	125	877
	>26°C	0	0	0	0	0	0	0	1	8	7	14	6	0	36
	>32°C	0	0	0	0	0	0	0	0	0	0	0	0	0	0
10PM to 5 PM	>16°C	271	23	15	115	368	557	1379	589	570	589	589	570	586	3493
	>18°C	158	9	2	88	286	452	995	565	570	589	589	570	541	3424
	>20°C	83	1	0	60	172	294	610	452	580	589	589	570	444	3204
	>26°C	0	0	0	0	19	40	59	14	34	86	89	143	84	450
	>32°C	0	0	0	0	1	2	3	0	0	0	2	32	9	43

25m <sup>2</sup> - East - CR 01															
Passive solar gains															
MONTH/ Cumul. Frequency		WINTER							SUMMER						
		November	December	January	February	March	April	SUM	May	June	July	August	September	October	SUM
5PM to 10PM	>16°C	48	0	0	9	110	150	317	155	150	155	155	150	151	916
	>18°C	15	0	0	0	60	150	225	155	150	155	155	150	151	916
	>20°C	0	0	0	0	30	150	180	132	150	155	155	150	103	845
	>26°C	0	0	0	0	0	2	2	0	8	6	14	5	0	33
	>32°C	0	0	0	0	0	0	0	0	0	0	0	0	0	0
10PM to 5 PM	>16°C	236	11	3	101	378	570	1299	589	570	589	589	570	579	3488
	>18°C	115	1	0	70	255	546	987	572	570	589	589	570	508	3398
	>20°C	63	0	0	34	165	442	704	458	558	589	589	570	412	3176
	>26°C	0	0	0	0	18	115	133	18	48	106	92	129	51	444
	>32°C	0	0	0	0	1	7	8	0	0	0	0	12	5	17

FIGURE APP.E.2

25m <sup>2</sup> - West - CR 15															
Passive solar gains															
MONTH/ Cumul. Frequency		WINTER							SUMMER						
		November	December	January	February	March	April	SUM	May	June	July	August	September	October	SUM
5PM to 10PM	>16°C	58	0	0	8	115	136	317	155	150	155	155	150	151	916
	>18°C	14	0	0	1	95	119	229	155	150	155	155	148	144	907
	>20°C	2	0	0	0	37	77	116	153	136	155	155	140	105	844
	>26°C	0	0	0	0	0	1	1	1	8	6	12	1	0	28
	>32°C	0	0	0	0	0	0	0	0	0	0	0	0	0	0
10PM to 5 PM	>16°C	203	54	30	108	405	483	1283	586	570	589	589	568	559	3461
	>18°C	161	25	14	80	274	354	908	553	555	589	589	550	454	3290
	>20°C	118	8	2	52	227	257	664	472	489	568	543	473	327	2870
	>26°C	5	0	0	0	22	23	50	96	78	119	105	78	63	542
	>32°C	0	0	0	0	0	0	0	13	0	0	0	8	8	29

FIGURE APP.E.3

25m² - West - CR 01															
Passive solar gains															
WINTER															
MONTH / Cumul. Frequency	November	December	January	February	March	April	SUM	SUMMER					SUM		
5PM to 10PM	>16°C	48	0	0	7	90	150	233	155	150	155	155	150	151	916
>18°C	14	0	0	0	0	57	150	221	155	150	155	155	150	151	915
T <sub>sp</sub> [°C]	>20°C	0	0	0	0	29	139	168	155	150	155	155	150	150	863
	>26°C	0	0	0	0	0	5	5	1	9	7	12	4	0	33
	>32°C	0	0	0	0	0	0	0	0	0	0	0	0	0	0
10PM to 5 PM	>16°C	217	5	0	91	347	568	1228	589	570	589	589	570	577	3484
>18°C	102	0	0	56	225	497	880	980	587	570	589	589	570	498	3403
T <sub>sp</sub> [°C]	>20°C	48	0	0	26	145	361	580	534	562	589	589	562	306	3222
	>26°C	0	0	0	0	13	51	64	77	28	62	55	75	35	332
	>32°C	0	0	0	0	0	2	2	6	0	0	0	7	4	17

25m² - South - CR 02															
Passive solar gains															
WINTER															
MONTH / Cumul. Frequency	November	December	January	February	March	April	SUM	SUMMER					SUM		
5PM to 10PM	>16°C	72	0	0	1	120	149	342	155	150	155	155	150	151	916
>18°C	33	0	0	0	100	140	273	238	155	150	155	155	150	151	916
T <sub>sp</sub> [°C]	>20°C	5	0	0	0	79	111	195	129	150	155	155	150	152	871
	>26°C	0	0	0	0	0	0	0	0	11	13	9	21	1	55
	>32°C	0	0	0	0	0	0	0	0	0	0	0	0	0	0
10PM to 5 PM	>16°C	226	5	24	72	416	546	1289	589	570	589	589	570	585	3492
>18°C	141	5	15	57	324	442	984	984	589	570	589	589	570	561	3438
T <sub>sp</sub> [°C]	>20°C	84	3	10	41	245	308	691	423	543	589	589	563	494	3201
	>26°C	3	0	0	1	85	31	120	7	62	101	72	168	120	530
	>32°C	0	0	0	0	2	0	2	0	1	0	0	34	24	69

25m² - East - CR 02															
Passive solar gains															
WINTER															
MONTH / Cumul. Frequency	November	December	January	February	March	April	SUM	SUMMER					SUM		
5PM to 10PM	>16°C	49	0	0	0	110	150	309	155	150	155	155	150	151	916
>18°C	16	0	0	0	77	145	238	238	150	150	155	155	150	149	909
T <sub>sp</sub> [°C]	>20°C	0	0	0	0	41	133	174	120	150	155	155	150	108	838
	>26°C	0	0	0	0	0	1	1	0	11	18	1	18	0	56
	>32°C	0	0	0	0	0	0	0	0	0	0	0	0	0	0
10PM to 5 PM	>16°C	199	4	8	62	354	570	1197	589	570	589	589	570	582	3488
>18°C	101	0	3	45	262	512	923	923	552	570	589	589	570	523	3393
T <sub>sp</sub> [°C]	>20°C	60	0	1	27	212	394	694	424	539	589	589	554	425	3120
	>26°C	0	0	0	0	52	103	155	14	84	133	96	131	88	546
	>32°C	0	0	0	0	0	3	3	1	2	2	0	10	5	20

25m² - West - CR 02															
Passive solar gains															
WINTER															
MONTH / Cumul. Frequency	November	December	January	February	March	April	SUM	SUMMER					SUM		
5PM to 10PM	>16°C	41	0	0	0	112	150	303	155	150	155	155	150	151	916
>18°C	15	0	0	0	81	141	237	237	155	150	155	155	150	147	912
T <sub>sp</sub> [°C]	>20°C	0	0	0	0	57	129	196	148	150	155	155	150	108	868
	>26°C	0	0	0	0	0	3	3	0	11	12	8	18	0	49
	>32°C	0	0	0	0	0	0	0	y	0	0	0	0	0	0
10PM to 5 PM	>16°C	183	1	4	48	353	563	1162	589	570	589	589	570	581	3488
>18°C	96	0	0	28	254	476	854	854	581	570	589	589	569	516	3414
T <sub>sp</sub> [°C]	>20°C	58	0	0	12	192	350	612	500	548	589	589	543	386	3155
	>26°C	0	0	0	0	49	47	96	55	29	52	40	92	67	335
	>32°C	0	0	0	0	0	0	0	3	0	0	0	8	2	13

25m² - South - CR 03															
Passive solar gains															
WINTER															
MONTH / Cumul. Frequency	November	December	January	February	March	April	SUM	SUMMER					SUM		
5PM to 10PM	>16°C	38	0	0	0	97	146	281	155	150	155	155	150	151	916
>18°C	28	0	0	0	68	116	212	212	155	150	155	155	150	151	916
T <sub>sp</sub> [°C]	>20°C	8	0	0	0	40	79	124	150	150	155	155	150	144	854
	>26°C	0	0	0	0	0	8	8	9	7	21	21	4	0	62
	>32°C	0	0	0	0	0	0	0	0	0	0	0	0	0	0
10PM to 5 PM	>16°C	197	32	27	68	333	477	1154	589	570	589	589	570	582	3488
>18°C	133	21	18	31	238	336	777	777	556	568	589	589	565	543	3411
T <sub>sp</sub> [°C]	>20°C	71	16	13	19	189	223	511	473	532	580	574	515	418	3090
	>26°C	3	0	0	0	36	28	67	21	36	107	92	72	72	400
	>32°C	0	0	0	0	4	6	10	0	0	0	0	11	5	16

25m² - East - CR 03															
Passive solar gains															
WINTER															
MONTH / Cumul. Frequency	November	December	January	February	March	April	SUM	SUMMER					SUM		
5PM to 10PM	>16°C	31	0	0	0	83	150	274	155	150	155	155	150	151	916
>18°C	17	0	0	0	50	145	212	212	155	150	155	155	150	150	915
T <sub>sp</sub> [°C]	>20°C	1	0	0	0	27	105	133	148	150	155	155	150	115	873
	>26°C	0	0	0	0	0	4	4	1	7	22	23	9	0	68
	>32°C	0	0	0	0	0	0	0	0	0	0	0	0	0	0
10PM to 5 PM	>16°C	161	18	8	53	302	546	1088	588	570	589	589	570	570	3476
>18°C	98	9	0	24	227	451	809	809	580	568	589	589	560	513	3378
T <sub>sp</sub> [°C]	>20°C	50	0	0	13	196	345	574	479	541	584	576	507	351	3038
	>26°C	1	0	0	0	26	67	94	43	64	128	103	70	37	443
	>32°C	0	0	0	0	1	9	10	0	0	1	9	9	3	22

FIGURE APP.E.4

25m <sup>2</sup> - West - CR 03															
Passive solar gains															
WINTER															
MONTH/ Cumul. Frequency	November	December	January	February	March	April	SUM	SUMMER					SUM		
5PM to 10PM	>18°C	31	0	0	0	93	150	274	155	150	155	155	150	151	916
	>18°C	15	0	0	0	47	131	193	155	150	155	155	150	148	913
	>20°C	1	0	0	0	22	90	113	154	150	155	155	145	106	865
	>26°C	0	0	0	0	0	9	9	7	7	20	19	2	0	95
	>32°C	0	0	0	0	0	0	0	0	0	0	0	0	0	0
10PM to 5 PM	>18°C	159	14	3	43	274	508	1001	589	570	589	589	570	557	3464
	>18°C	88	5	0	19	185	398	695	589	568	589	589	557	482	3354
	>20°C	46	0	0	9	142	275	472	492	530	572	567	466	299	2926
	>26°C	1	0	0	0	13	39	53	81	18	89	82	36	27	313
	>32°C	0	0	0	0	2	6	8	7	0	0	0	3	0	10

25m <sup>2</sup> - South - CR 04															
Passive solar gains															
WINTER															
MONTH/ Cumul. Frequency	November	December	January	February	March	April	SUM	SUMMER					SUM		
5PM to 10PM	>18°C	25	0	2	10	104	150	291	155	150	155	155	150	151	916
	>18°C	5	0	0	7	70	137	219	155	150	155	155	150	151	916
	>20°C	5	0	0	4	54	118	181	152	150	155	155	150	147	909
	>26°C	0	0	0	0	2	3	5	15	13	21	17	5	1	72
	>32°C	0	0	0	0	0	0	0	0	0	1	0	0	0	1
10PM to 5 PM	>18°C	160	22	75	69	362	630	1208	589	570	589	589	570	589	3496
	>18°C	85	14	48	43	281	456	927	577	568	589	589	570	558	3451
	>20°C	53	10	28	27	208	332	658	506	530	589	589	547	449	3210
	>26°C	1	0	1	10	63	48	123	45	132	151	115	136	90	669
	>32°C	0	0	0	4	9	0	13	0	0	8	15	24	11	58

25m <sup>2</sup> - East - CR 04															
Passive solar gains															
WINTER															
MONTH/ Cumul. Frequency	November	December	January	February	March	April	SUM	SUMMER					SUM		
5PM to 10PM	>18°C	9	0	0	7	79	150	245	155	150	155	155	150	151	916
	>18°C	5	0	0	5	56	146	212	155	150	155	155	150	151	916
	>20°C	1	0	0	2	44	131	178	144	150	155	155	150	129	883
	>26°C	0	0	0	0	0	2	2	4	11	20	15	2	1	53
	>32°C	0	0	0	0	0	0	0	0	0	0	0	0	0	1
10PM to 5 PM	>18°C	128	10	33	53	335	553	1112	589	570	589	589	570	577	3493
	>18°C	65	4	20	29	244	509	871	572	568	589	589	569	510	3307
	>20°C	31	0	8	23	183	442	687	511	534	589	589	538	393	3152
	>26°C	0	0	0	7	45	131	183	66	151	189	135	125	56	722
	>32°C	0	0	0	1	3	5	9	0	0	12	12	8	8	40

25m <sup>2</sup> - West - CR 04															
Passive solar gains															
WINTER															
MONTH/ Cumul. Frequency	November	December	January	February	March	April	SUM	SUMMER					SUM		
5PM to 10PM	>18°C	10	0	0	7	76	150	243	155	150	155	155	150	151	916
	>18°C	5	0	0	4	69	141	209	155	150	155	155	150	151	916
	>20°C	0	0	0	2	49	123	174	155	150	155	155	149	123	887
	>26°C	0	0	0	0	1	18	19	5	9	18	15	6	0	54
	>32°C	0	0	0	0	0	0	0	0	0	1	0	0	0	1
10PM to 5 PM	>18°C	119	7	24	44	312	543	1049	589	570	589	589	570	574	3481
	>18°C	52	4	9	26	223	485	799	583	568	589	589	568	451	3378
	>20°C	27	1	5	18	159	390	600	536	523	589	585	505	344	3082
	>26°C	0	0	0	4	41	68	113	129	90	109	82	71	31	512
	>32°C	0	0	0	0	2	12	14	17	0	5	8	6	2	38

25m <sup>2</sup> - South - CR 05															
Passive solar gains															
WINTER															
MONTH/ Cumul. Frequency	November	December	January	February	March	April	SUM	SUMMER					SUM		
5PM to 10PM	>18°C	55	0	0	55	140	149	399	155	150	155	155	150	151	916
	>18°C	10	0	0	7	81	119	217	155	150	155	155	150	146	911
	>20°C	0	0	0	0	33	82	115	149	146	155	155	147	121	872
	>26°C	0	0	0	0	0	1	1	7	6	23	16	7	0	89
	>32°C	0	0	0	0	0	0	0	0	0	0	0	0	0	0
10PM to 5 PM	>18°C	234	20	40	187	423	496	1620	589	570	589	589	570	553	3499
	>18°C	111	9	26	142	294	379	961	568	565	589	589	563	545	3417
	>20°C	66	4	13	106	210	214	812	455	528	584	585	505	438	3143
	>26°C	0	0	0	1	22	23	46	29	60	102	88	125	78	482
	>32°C	0	0	0	0	1	0	1	0	0	0	2	17	4	23

25m <sup>2</sup> - East - CR 05															
Passive solar gains															
WINTER															
MONTH/ Cumul. Frequency	November	December	January	February	March	April	SUM	SUMMER					SUM		
5PM to 10PM	>18°C	47	0	0	19	132	150	348	155	150	155	155	150	151	916
	>18°C	2	0	0	1	66	150	219	155	150	155	155	150	143	908
	>20°C	0	0	0	0	24	123	147	137	146	155	155	145	117	854
	>26°C	0	0	0	0	0	1	1	2	7	22	18	5	0	54
	>32°C	0	0	0	0	0	0	0	0	0	0	0	0	0	0
10PM to 5 PM	>18°C	195	11	28	171	388	561	1324	589	570	589	589	570	578	3485
	>18°C	104	3	15	118	278	499	1017	567	565	589	589	563	532	3405
	>20°C	55	0	5	77	195	387	719	488	536	584	588	543	411	3189
	>26°C	0	0	0	0	23	57	80	39	72	119	82	103	63	487
	>32°C	0	0	0	0	0	0	0	1	0	2	1	6	3	13

FIGURE APP.E.5

25m² - West - CR 05															
Passive solar gains															
WINTER															
MONTH / Cumul. Frequency	November	December	January	February	March	April	SUM	SUMMER					SUM		
5PM to 10PM	>18°C	44	0	0	16	130	150	340	155	150	155	155	150	151	916
	>18°C	2	0	0	1	61	142	206	155	150	155	155	150	141	906
T <sub>sp</sub> [°C]	>20°C	0	0	0	0	24	99	123	155	145	155	155	142	110	862
	>26°C	0	0	0	0	0	3	3	5	7	20	18	4	0	54
	>32°C	0	0	0	0	0	0	0	0	0	0	0	0	0	0
10PM to 5 PM	>18°C	174	9	20	150	371	534	1268	589	570	589	589	570	574	3481
	>18°C	89	3	8	99	264	444	907	586	565	589	589	556	504	3409
T <sub>sp</sub> [°C]	>20°C	36	0	2	60	179	321	598	519	521	584	584	528	382	3118
	>26°C	0	0	0	0	18	32	50	80	46	84	71	56	39	376
	>32°C	0	0	0	0	0	0	0	8	0	0	0	7	2	17

25m² - South - CR 06															
Passive solar gains															
WINTER															
MONTH / Cumul. Frequency	November	December	January	February	March	April	SUM	SUMMER					SUM		
5PM to 10PM	>18°C	29	0	0	32	85	146	292	142	150	155	155	150	151	903
	>18°C	2	0	0	16	44	97	159	130	150	155	155	150	138	878
T <sub>sp</sub> [°C]	>20°C	0	0	0	2	26	57	84	97	139	155	153	148	81	773
	>26°C	0	0	0	0	0	0	0	0	2	2	6	1	0	11
	>32°C	0	0	0	0	0	0	0	0	0	0	0	0	0	0
10PM to 5 PM	>18°C	137	7	29	125	313	427	1008	520	570	589	589	570	567	3395
	>18°C	69	3	12	106	233	297	720	446	563	589	589	567	445	3199
T <sub>sp</sub> [°C]	>20°C	27	0	2	92	171	171	463	296	453	545	533	505	319	2650
	>26°C	0	0	0	2	28	8	38	0	30	85	43	88	26	271
	>32°C	0	0	0	0	0	0	0	0	0	0	0	11	2	13

25m² - East - CR 06															
Passive solar gains															
WINTER															
MONTH / Cumul. Frequency	November	December	January	February	March	April	SUM	SUMMER					SUM		
5PM to 10PM	>18°C	15	0	0	18	60	150	243	141	150	155	155	150	151	902
	>18°C	1	0	0	3	37	144	185	130	150	155	155	150	118	858
T <sub>sp</sub> [°C]	>20°C	0	0	0	0	23	104	127	91	139	155	153	147	68	753
	>26°C	0	0	0	0	0	0	0	0	2	5	6	0	0	13
	>32°C	0	0	0	0	0	0	0	0	0	0	0	0	0	0
10PM to 5 PM	>18°C	110	0	0	109	295	534	1048	542	570	589	589	570	534	3394
	>18°C	50	0	0	95	206	438	789	460	563	589	589	566	428	3195
T <sub>sp</sub> [°C]	>20°C	20	0	0	77	159	323	579	312	455	555	539	498	283	2640
	>26°C	0	0	0	0	25	42	67	4	40	85	53	73	9	264
	>32°C	0	0	0	0	0	1	1	0	0	0	0	3	0	3

25m² - West - CR 06															
Passive solar gains															
WINTER															
MONTH / Cumul. Frequency	November	December	January	February	March	April	SUM	SUMMER					SUM		
5PM to 10PM	>18°C	15	0	0	12	57	150	234	152	150	155	155	150	151	913
	>18°C	1	0	0	2	36	129	168	140	150	155	155	150	101	851
T <sub>sp</sub> [°C]	>20°C	0	0	0	0	20	77	97	120	139	155	152	135	63	764
	>26°C	0	0	0	0	1	0	1	0	2	3	6	0	0	11
	>32°C	0	0	0	0	0	0	0	0	0	0	0	0	0	0
10PM to 5 PM	>18°C	99	0	0	88	272	494	893	572	570	589	589	570	511	3401
	>18°C	44	0	0	75	195	366	630	513	563	589	589	548	399	3201
T <sub>sp</sub> [°C]	>20°C	21	0	0	58	141	258	478	406	463	537	522	438	247	2610
	>26°C	0	0	0	0	14	9	23	37	17	60	33	29	7	183
	>32°C	0	0	0	0	1	0	1	2	0	0	0	1	0	3

25m² - South - CR 07															
Passive solar gains															
WINTER															
MONTH / Cumul. Frequency	November	December	January	February	March	April	SUM	SUMMER					SUM		
5PM to 10PM	>18°C	61	0	0	8	133	150	352	155	150	155	155	150	151	916
	>18°C	14	0	0	5	117	121	257	155	150	155	155	150	145	910
T <sub>sp</sub> [°C]	>20°C	0	0	0	1	102	74	177	134	149	155	155	147	103	843
	>26°C	0	0	0	0	0	0	0	3	8	16	29	4	0	60
	>32°C	0	0	0	0	0	0	0	0	0	0	2	0	0	2
10PM to 5 PM	>18°C	213	12	36	145	483	475	1364	587	570	589	589	570	576	3481
	>18°C	139	4	15	101	406	347	1012	507	564	589	589	567	507	3373
T <sub>sp</sub> [°C]	>20°C	89	3	1	71	307	232	703	438	508	583	587	517	347	2980
	>26°C	0	0	0	0	86	25	111	25	75	125	116	122	38	501
	>32°C	0	0	0	0	0	0	0	0	0	0	17	21	1	39

25m² - East - CR 07															
Passive solar gains															
WINTER															
MONTH / Cumul. Frequency	November	December	January	February	March	April	SUM	SUMMER					SUM		
5PM to 10PM	>18°C	47	0	0	6	124	150	327	155	150	155	155	150	150	915
	>18°C	5	0	0	0	111	150	266	155	150	155	155	150	142	907
T <sub>sp</sub> [°C]	>20°C	0	0	0	0	89	117	206	125	148	155	155	147	87	816
	>26°C	0	0	0	0	0	2	2	0	9	13	28	3	0	53
	>32°C	0	0	0	0	0	0	0	0	0	0	1	0	0	1
10PM to 5 PM	>18°C	181	9	5	124	456	554	1329	587	570	589	589	570	565	3470
	>18°C	120	3	1	78	381	470	1033	507	566	589	589	566	474	3241
T <sub>sp</sub> [°C]	>20°C	65	0	0	46	277	361	749	442	503	584	587	506	325	2947
	>26°C	0	0	0	0	56	67	123	34	92	128	116	96	20	488
	>32°C	0	0	0	0	0	2	2	0	0	0	14	6	0	19

FIGURE APP.E.6

25m <sup>2</sup> - West - CR 07															
Passive solar gains															
WINTER															
MONTH/ Cumul. Frequency	November	December	January	February	March	April	SUM	SUMMER							
5PM to 10PM	>18°C	43	0	0	4	122	150	319	155	150	155	155	150	150	915
	>18°C	3	0	0	0	107	137	247	155	150	155	155	150	136	901
	>20°C	0	0	0	0	86	87	173	154	150	155	155	138	82	834
	>26°C	0	0	0	0	0	1	1	1	8	14	26	2	0	61
	>32°C	0	0	0	0	0	0	0	0	0	0	0	0	0	0
10PM to 5 PM	>18°C	162	4	3	102	441	516	1228	589	570	589	589	570	563	3470
	>18°C	103	3	0	60	335	396	897	585	569	589	589	552	448	3332
	>20°C	53	0	0	34	251	291	629	521	518	581	584	482	297	2983
	>26°C	0	0	0	0	43	31	74	91	65	102	93	56	10	409
	>32°C	0	0	0	0	0	1	1	10	3	0	10	3	0	23

25m <sup>2</sup> - South - CR 08															
Passive solar gains															
WINTER															
MONTH/ Cumul. Frequency	November	December	January	February	March	April	SUM	SUMMER							
5PM to 10PM	>18°C	6	0	0	9	112	90	217	153	150	155	155	150	151	914
	>18°C	0	0	0	0	81	75	156	142	137	155	155	150	114	853
	>20°C	0	0	0	0	29	49	78	91	117	150	134	140	92	724
	>26°C	0	0	0	0	0	0	0	0	0	0	2	0	0	2
	>32°C	0	0	0	0	0	0	0	0	0	0	0	0	0	0
10PM to 5 PM	>18°C	76	3	15	126	349	329	896	555	557	589	589	570	529	3389
	>18°C	25	0	9	102	254	217	607	449	507	589	562	558	439	3104
	>20°C	8	0	3	81	217	140	449	329	405	517	495	459	236	2501
	>26°C	0	0	0	0	26	7	33	5	21	60	36	81	64	267
	>32°C	0	0	0	0	0	0	0	0	0	0	0	9	0	9

25m <sup>2</sup> - East - CR 08															
Passive solar gains															
WINTER															
MONTH/ Cumul. Frequency	November	December	January	February	March	April	SUM	SUMMER							
5PM to 10PM	>18°C	3	0	0	0	100	126	229	151	150	155	155	150	148	909
	>18°C	0	0	0	0	55	94	149	137	137	155	155	149	107	849
	>20°C	0	0	0	0	19	75	94	74	115	152	136	134	65	676
	>26°C	0	0	0	0	0	0	0	0	0	0	2	0	0	2
	>32°C	0	0	0	0	0	0	0	0	0	0	0	0	0	0
10PM to 5 PM	>18°C	61	0	7	107	320	437	922	551	554	589	589	569	497	3349
	>18°C	14	0	4	79	244	363	704	466	507	589	563	546	398	3009
	>20°C	4	0	0	56	209	267	536	370	417	522	500	433	269	2611
	>26°C	0	0	0	0	13	44	57	18	27	66	38	66	33	247
	>32°C	0	0	0	0	0	1	1	0	0	0	0	0	0	0

25m <sup>2</sup> - West - CR 08															
Passive solar gains															
WINTER															
MONTH/ Cumul. Frequency	November	December	January	February	March	April	SUM	SUMMER							
5PM to 10PM	>18°C	1	0	0	0	93	104	198	155	150	155	155	150	142	907
	>18°C	0	0	0	0	52	83	135	151	139	155	155	142	106	848
	>20°C	0	0	0	0	15	63	78	131	115	145	129	105	45	673
	>26°C	0	0	0	0	0	0	0	0	0	0	2	0	0	2
	>32°C	0	0	0	0	0	0	0	0	0	0	0	0	0	0
10PM to 5 PM	>18°C	46	0	7	88	278	384	893	585	568	589	587	569	470	3366
	>18°C	12	0	3	58	220	296	579	539	521	589	558	489	340	3036
	>20°C	1	0	0	40	184	193	418	418	407	503	474	361	241	2404
	>26°C	0	0	0	0	6	14	20	52	7	35	23	18	13	148
	>32°C	0	0	0	0	0	0	0	4	0	0	0	0	0	4

25m <sup>2</sup> - South - CR 09															
Passive solar gains															
WINTER															
MONTH/ Cumul. Frequency	November	December	January	February	March	April	SUM	SUMMER							
5PM to 10PM	>18°C	70	0	1	33	79	113	296	155	150	155	155	150	151	916
	>18°C	45	0	0	11	43	85	184	148	150	155	155	150	151	909
	>20°C	22	0	0	5	7	63	97	122	129	155	155	150	147	858
	>26°C	0	0	0	0	0	0	0	6	7	17	26	12	3	71
	>32°C	0	0	0	0	0	0	0	0	0	0	0	0	0	0
10PM to 5 PM	>18°C	265	67	87	157	293	368	1267	585	568	589	589	570	589	3400
	>18°C	171	50	67	122	174	262	846	502	537	589	589	570	574	3361
	>20°C	113	37	59	94	131	154	618	395	498	579	583	526	474	3016
	>26°C	23	1	1	16	22	18	81	37	76	135	125	133	134	640
	>32°C	0	0	0	0	0	3	4	7	0	0	7	37	31	75

25m <sup>2</sup> - East - CR 09															
Passive solar gains															
WINTER															
MONTH/ Cumul. Frequency	November	December	January	February	March	April	SUM	SUMMER							
5PM to 10PM	>18°C	57	0	0	18	65	140	280	155	150	155	155	150	151	916
	>18°C	26	0	0	3	25	114	168	145	150	155	155	150	151	906
	>20°C	6	0	0	0	1	86	93	102	128	155	155	150	126	818
	>26°C	0	0	0	0	0	2	2	1	8	19	27	3	0	58
	>32°C	0	0	0	0	0	0	0	0	0	0	0	0	0	0
10PM to 5 PM	>18°C	206	33	57	124	251	470	1141	589	568	589	589	570	584	3409
	>18°C	125	11	34	97	163	396	826	510	537	589	589	570	520	3315
	>20°C	84	0	18	75	136	310	693	372	498	585	552	492	404	2933
	>26°C	2	0	0	1	16	73	92	58	90	164	150	121	92	676
	>32°C	0	0	0	0	1	11	12	0	1	3	15	8	22	40

FIGURE APP.E.7

25m <sup>2</sup> - West - CR 09															
Passive solar gains															
WINTER															
MONTH / Cumul. Frequency	November	December	January	February	March	April	SUM	SUMMER							
6PM to 10PM	May	June	July	August	September	October	SUM								
T <sub>req</sub> [°C]	>18°C	57	0	0	13	80	123	263	155	150	155	155	150	151	918
	>18°C	28	0	0	3	24	96	161	153	150	155	155	150	151	914
	>20°C	6	0	0	0	4	77	87	132	130	155	155	143	135	850
	>26°C	0	0	0	0	0	4	4	4	7	16	16	9	0	52
	>32°C	0	0	0	0	0	0	0	0	0	0	0	0	0	0
10PM to 6 PM	>18°C	195	29	38	108	236	435	1341	589	569	589	589	570	564	3499
	>18°C	123	12	17	79	152	331	714	580	538	589	589	560	528	3364
	>20°C	77	3	3	48	122	240	493	472	497	570	572	454	384	2949
	>26°C	4	0	0	0	10	33	47	81	49	100	91	71	90	482
	>32°C	0	0	0	0	0	6	6	0	12	0	0	0	7	13

25m <sup>2</sup> - South - CR 10															
Passive solar gains															
WINTER															
MONTH / Cumul. Frequency	November	December	January	February	March	April	SUM	SUMMER							
6PM to 10PM	May	June	July	August	September	October	SUM								
T <sub>req</sub> [°C]	>18°C	10	0	0	4	117	100	231	155	150	155	155	150	140	965
	>18°C	0	0	0	1	95	93	189	146	150	155	155	150	94	850
	>20°C	0	0	0	0	57	57	114	123	149	155	155	133	41	758
	>26°C	0	0	0	0	0	0	0	0	3	14	15	3	0	35
	>32°C	0	0	0	0	0	0	0	0	0	0	0	0	0	0
10PM to 6 PM	>18°C	124	18	3	64	390	381	960	581	570	589	589	570	528	3405
	>18°C	80	6	0	42	310	248	686	514	501	585	587	554	353	3164
	>20°C	52	1	0	26	248	164	491	372	486	550	555	454	241	2658
	>26°C	0	0	0	0	54	21	75	12	69	98	114	76	20	389
	>32°C	0	0	0	0	0	0	0	0	0	0	0	18	3	21

25m <sup>2</sup> - East - CR 10															
Passive solar gains															
WINTER															
MONTH / Cumul. Frequency	November	December	January	February	March	April	SUM	SUMMER							
6PM to 10PM	May	June	July	August	September	October	SUM								
T <sub>req</sub> [°C]	>18°C	3	0	0	2	110	138	253	155	150	155	155	150	139	964
	>18°C	0	0	0	0	80	101	181	150	150	155	155	150	90	850
	>20°C	0	0	0	0	40	89	129	127	149	155	155	121	31	728
	>26°C	0	0	0	0	0	2	2	0	3	13	18	0	0	34
	>32°C	0	0	0	0	0	0	0	0	0	0	0	0	0	0
10PM to 6 PM	>18°C	105	2	0	49	355	406	917	589	570	589	589	570	502	3899
	>18°C	66	0	0	26	291	387	770	535	505	585	588	549	324	3146
	>20°C	28	0	0	18	235	278	559	415	502	556	557	429	227	2686
	>26°C	0	0	0	0	42	71	113	26	76	115	129	66	17	429
	>32°C	0	0	0	0	0	3	3	0	0	1	5	3	0	9

25m <sup>2</sup> - West - CR 10															
Passive solar gains															
WINTER															
MONTH / Cumul. Frequency	November	December	January	February	March	April	SUM	SUMMER							
6PM to 10PM	May	June	July	August	September	October	SUM								
T <sub>req</sub> [°C]	>18°C	0	0	0	1	105	111	217	155	150	155	155	150	137	902
	>18°C	0	0	0	0	74	98	172	155	150	155	155	145	80	840
	>20°C	0	0	0	0	38	76	112	140	140	154	154	108	24	739
	>26°C	0	0	0	0	0	1	1	0	3	11	12	0	0	26
	>32°C	0	0	0	0	0	0	0	0	0	0	0	0	0	0
10PM to 6 PM	>18°C	87	1	0	39	330	410	967	580	570	589	589	570	480	3588
	>18°C	47	0	0	21	263	305	636	548	558	584	585	515	303	3093
	>20°C	25	0	0	15	206	210	459	473	488	535	540	381	186	2601
	>26°C	0	0	0	0	24	27	51	68	36	67	80	38	6	295
	>32°C	0	0	0	0	0	0	0	4	0	0	0	0	2	6

25m <sup>2</sup> - South - CR 11															
Passive solar gains															
WINTER															
MONTH / Cumul. Frequency	November	December	January	February	March	April	SUM	SUMMER							
6PM to 10PM	May	June	July	August	September	October	SUM								
T <sub>req</sub> [°C]	>18°C	4	0	0	14	90	57	165	101	134	155	155	134	117	798
	>18°C	0	0	0	7	54	24	85	64	86	135	136	115	81	617
	>20°C	0	0	0	1	37	10	48	38	47	108	111	70	54	426
	>26°C	0	0	0	0	2	1	3	0	0	0	1	0	14	18
	>32°C	0	0	0	0	0	0	0	0	0	0	0	0	0	0
10PM to 6 PM	>18°C	43	13	37	92	294	172	851	305	480	563	578	501	409	2808
	>18°C	29	10	23	78	208	94	442	203	335	499	516	410	319	2272
	>20°C	21	5	11	65	181	59	322	112	184	343	368	303	231	1541
	>26°C	7	0	0	20	74	4	105	2	4	18	14	49	69	158
	>32°C	0	0	0	1	21	2	24	0	0	0	3	11	28	42

25m <sup>2</sup> - East - CR 11															
Passive solar gains															
WINTER															
MONTH / Cumul. Frequency	November	December	January	February	March	April	SUM	SUMMER							
6PM to 10PM	May	June	July	August	September	October	SUM								
T <sub>req</sub> [°C]	>18°C	0	0	0	4	58	98	158	94	134	155	155	130	94	782
	>18°C	0	0	0	0	35	71	108	42	80	136	134	102	57	581
	>20°C	0	0	0	0	12	33	45	19	46	112	110	64	25	378
	>26°C	0	0	0	0	0	2	2	0	0	1	0	0	0	1
	>32°C	0	0	0	0	0	0	0	0	0	0	0	0	0	0
10PM to 6 PM	>18°C	30	2	13	76	224	346	691	339	495	573	582	478	342	3809
	>18°C	19	0	2	60	175	259	515	234	350	520	528	371	247	2200
	>20°C	12	0	0	52	148	198	409	149	201	352	356	244	165	1537
	>26°C	0	0	0	7	59	34	97	8	11	38	26	43	45	171
	>32°C	0	0	0	0	15	6	21	1	0	0	0	3	14	18

FIGURE APP.E.8

25m <sup>2</sup> - West - CR 11															
Passive solar gains															
WINTER															
MONTH / Cumul. Frequency	November	December	January	February	March	April	SUM	SUMMER							
5PM to 10PM	>16°C	0	0	0	1	56	77	134	126	134	154	155	116	98	783
	>18°C	0	0	0	0	33	37	70	86	84	123	127	72	53	544
	>20°C	0	0	0	0	13	19	32	46	49	82	90	43	25	334
	>26°C	0	0	0	0	0	1	1	0	0	0	0	0	3	3
	>32°C	0	0	0	0	0	0	0	0	0	0	0	0	0	0
10PM to 5 PM	>16°C	30	1	2	55	189	246	523	438	470	554	567	414	333	2776
	>18°C	20	0	0	45	144	163	372	318	316	437	451	301	227	2050
	>20°C	13	0	0	34	122	108	277	236	173	293	287	179	164	1335
	>26°C	1	0	0	0	35	9	45	28	1	9	0	17	35	90
	>32°C	0	0	0	0	3	3	6	2	0	0	0	2	15	19

25m <sup>2</sup> - South - CR 12															
Passive solar gains															
WINTER															
MONTH / Cumul. Frequency	November	December	January	February	March	April	SUM	SUMMER							
5PM to 10PM	>16°C	90	0	2	58	150	150	450	155	150	155	155	150	151	918
	>18°C	34	0	0	29	138	142	343	153	150	155	155	150	151	914
	>20°C	5	0	0	10	128	120	264	140	150	155	155	150	151	910
	>26°C	0	0	0	0	3	3	6	18	27	35	42	19	4	145
	>32°C	0	0	0	0	0	0	0	0	0	4	1	0	0	5
10PM to 5 PM	>16°C	282	76	81	195	535	652	1721	584	570	589	589	570	589	3491
	>18°C	159	55	64	142	448	468	1304	573	570	589	589	570	583	3474
	>20°C	91	46	42	105	362	320	966	513	565	589	589	570	513	3339
	>26°C	8	0	0	18	139	32	197	69	138	188	180	141	134	850
	>32°C	0	0	0	0	25	3	28	0	5	20	20	41	30	118

25m <sup>2</sup> - East - CR 12															
Passive solar gains															
WINTER															
MONTH / Cumul. Frequency	November	December	January	February	March	April	SUM	SUMMER							
5PM to 10PM	>16°C	51	0	0	44	150	150	395	155	150	155	155	150	151	918
	>18°C	15	0	0	16	134	150	315	154	150	155	155	150	151	915
	>20°C	0	0	0	0	116	132	248	150	150	155	155	150	147	907
	>26°C	0	0	0	0	1	5	6	12	28	36	44	12	1	133
	>32°C	0	0	0	0	0	0	0	0	0	4	1	0	0	5
10PM to 5 PM	>16°C	229	48	67	165	509	570	1588	587	570	589	589	570	589	3494
	>18°C	118	33	43	117	413	532	1266	577	570	589	589	570	555	3450
	>20°C	72	15	19	97	327	419	949	525	561	589	589	570	453	3287
	>26°C	0	0	0	0	126	74	200	90	157	204	205	136	103	895
	>32°C	0	0	0	0	14	6	20	1	7	30	27	21	14	100

25m <sup>2</sup> - West - CR 12															
Passive solar gains															
WINTER															
MONTH / Cumul. Frequency	November	December	January	February	March	April	SUM	SUMMER							
5PM to 10PM	>16°C	56	0	0	37	146	150	389	155	150	155	155	150	151	916
	>18°C	21	0	0	7	128	150	306	155	150	155	155	150	151	918
	>20°C	1	0	0	0	102	129	232	150	150	155	155	150	149	908
	>26°C	0	0	0	0	2	6	8	16	25	34	37	12	1	125
	>32°C	0	0	0	0	0	0	0	0	0	3	1	0	0	4
10PM to 5 PM	>16°C	224	40	44	144	466	568	1688	588	570	589	589	570	589	3495
	>18°C	117	20	20	104	369	503	1133	576	570	589	589	570	559	3453
	>20°C	69	10	9	80	284	372	824	550	566	589	588	554	435	3282
	>26°C	0	0	0	0	88	47	135	141	108	149	131	87	91	707
	>32°C	0	0	0	0	8	5	13	24	1	12	9	10	6	62

25m <sup>2</sup> - South - CR 13															
Passive solar gains															
WINTER															
MONTH / Cumul. Frequency	November	December	January	February	March	April	SUM	SUMMER							
5PM to 10PM	>16°C	61	0	0	5	148	131	345	155	150	155	155	150	151	916
	>18°C	17	0	0	2	78	112	209	153	150	155	155	150	151	914
	>20°C	0	0	0	1	38	72	111	135	146	155	155	150	150	881
	>26°C	0	0	0	0	0	0	0	8	12	28	24	3	1	74
	>32°C	0	0	0	0	0	0	0	0	0	0	1	0	0	1
10PM to 5 PM	>16°C	195	22	100	86	380	446	1229	585	570	589	589	570	579	3492
	>18°C	118	15	63	62	310	324	892	543	561	589	589	568	494	3234
	>20°C	84	7	45	46	242	217	641	434	523	571	586	540	406	3092
	>26°C	2	0	0	5	52	20	79	60	120	166	139	140	106	731
	>32°C	0	0	0	0	2	0	2	0	0	1	14	20	12	47

25m <sup>2</sup> - East - CR 13															
Passive solar gains															
WINTER															
MONTH / Cumul. Frequency	November	December	January	February	March	April	SUM	SUMMER							
5PM to 10PM	>16°C	50	0	0	2	132	149	333	155	150	155	155	150	151	916
	>18°C	8	0	0	1	63	131	203	155	150	155	155	150	150	915
	>20°C	0	0	0	0	33	116	149	142	144	155	155	149	105	850
	>26°C	0	0	0	0	0	0	0	8	12	28	27	1	0	78
	>32°C	0	0	0	0	0	0	0	0	0	0	1	0	0	1
10PM to 5 PM	>16°C	168	7	69	67	363	530	1304	569	570	589	589	570	566	3473
	>18°C	110	0	41	49	301	462	963	563	562	589	589	568	455	3205
	>20°C	72	0	19	30	235	340	696	486	525	577	586	526	383	3048
	>26°C	2	0	0	0	60	56	106	84	137	184	156	141	92	803
	>32°C	0	0	0	0	2	2	4	1	1	4	17	10	10	43

FIGURE APP.E.9

25m <sup>2</sup> - West - CR 13																
Passive solar gains																
MONTH / Cumul. Frequency																
WINTER																
SUMMER																
MONTH / Cumul. Frequency																
WINTER																
SUMMER																
5PM to 10PM	T <sub>sp</sub> [°C]	>18°C	39	0	0	2	111	141	293	156	150	155	155	150	151	916
		>18°C	4	0	0	1	56	125	185	156	150	155	155	150	150	915
		>20°C	0	0	0	0	28	99	127	146	149	155	155	143	98	848
		>26°C	0	0	0	0	0	0	0	12	12	25	21	0	0	70
		>32°C	0	0	0	0	0	0	0	0	0	0	0	0	0	0
10PM to 5 PM	T <sub>sp</sub> [°C]	>18°C	145	1	44	59	330	508	1007	589	570	589	589	570	556	3462
		>18°C	97	0	23	38	272	394	874	576	567	589	589	563	428	3312
		>20°C	55	0	6	20	206	280	567	523	542	569	585	485	334	3038
		>26°C	2	0	0	0	35	32	69	154	107	149	118	82	77	687
		>32°C	0	0	0	0	1	0	1	24	0	1	9	4	5	43

25m <sup>2</sup> - South - CR 14																
Passive solar gains																
MONTH / Cumul. Frequency																
WINTER																
SUMMER																
MONTH / Cumul. Frequency																
WINTER																
SUMMER																
5PM to 10PM	T <sub>sp</sub> [°C]	>18°C	61	0	0	7	89	129	286	142	150	155	155	150	151	903
		>18°C	32	0	0	2	81	87	202	128	147	155	155	150	150	885
		>20°C	9	0	0	0	62	67	138	105	125	154	155	143	120	802
		>26°C	0	0	0	0	0	0	0	2	2	6	4	2	1	17
		>32°C	0	0	0	0	0	0	0	0	0	0	0	0	0	0
10PM to 5 PM	T <sub>sp</sub> [°C]	>18°C	223	30	50	92	370	400	1165	541	570	589	589	570	586	3442
		>18°C	145	15	32	67	291	308	858	464	533	589	589	567	509	3251
		>20°C	80	4	22	43	208	174	531	332	443	548	550	457	398	2728
		>26°C	3	0	0	0	58	20	81	9	58	65	68	80	85	365
		>32°C	0	0	0	0	3	6	9	0	0	0	0	15	10	25

25m <sup>2</sup> - East - CR 14																
Passive solar gains																
MONTH / Cumul. Frequency																
WINTER																
SUMMER																
MONTH / Cumul. Frequency																
WINTER																
SUMMER																
5PM to 10PM	T <sub>sp</sub> [°C]	>18°C	56	0	0	4	86	150	296	148	150	155	155	150	151	909
		>18°C	21	0	0	1	77	136	235	131	145	155	155	150	145	881
		>20°C	3	0	0	0	48	95	146	99	124	154	153	140	94	764
		>26°C	0	0	0	0	0	1	1	1	4	6	6	2	0	19
		>32°C	0	0	0	0	0	0	0	0	0	0	0	0	0	0
10PM to 5 PM	T <sub>sp</sub> [°C]	>18°C	197	3	31	77	355	528	1161	561	570	589	589	570	572	3451
		>18°C	116	1	16	49	289	431	882	496	534	589	589	567	476	3251
		>20°C	67	0	9	26	194	335	631	390	450	554	559	442	369	2724
		>26°C	1	0	0	0	55	55	111	17	81	98	108	79	69	452
		>32°C	0	0	0	0	3	10	13	0	0	1	0	7	8	16

25m <sup>2</sup> - West - CR 14																
Passive solar gains																
MONTH / Cumul. Frequency																
WINTER																
SUMMER																
MONTH / Cumul. Frequency																
WINTER																
SUMMER																
5PM to 10PM	T <sub>sp</sub> [°C]	>18°C	50	0	0	2	85	142	279	156	150	155	155	150	151	916
		>18°C	19	0	0	1	76	110	206	139	150	155	155	148	138	885
		>20°C	1	0	0	0	43	79	123	123	127	154	149	123	84	760
		>26°C	0	0	0	0	0	1	1	1	3	5	5	0	0	14
		>32°C	0	0	0	0	0	0	0	0	0	0	0	0	0	0
10PM to 5 PM	T <sub>sp</sub> [°C]	>18°C	179	5	26	70	329	474	1083	567	570	589	589	570	554	3435
		>18°C	103	1	12	42	242	378	778	542	551	589	589	550	445	3286
		>20°C	57	0	7	22	169	245	500	465	454	546	543	393	328	2729
		>26°C	1	0	0	0	44	29	74	75	41	61	59	48	48	332
		>32°C	0	0	0	0	0	7	7	9	0	0	0	3	2	14

25m <sup>2</sup> - South - CR 15																
Passive solar gains																
MONTH / Cumul. Frequency																
WINTER																
SUMMER																
MONTH / Cumul. Frequency																
WINTER																
SUMMER																
5PM to 10PM	T <sub>sp</sub> [°C]	>18°C	77	5	0	15	131	124	352	156	150	155	155	150	151	916
		>18°C	47	1	0	8	114	100	270	154	150	155	155	150	151	915
		>20°C	10	0	0	1	62	55	158	128	136	155	155	147	129	850
		>26°C	0	0	0	0	0	0	0	1	8	10	11	3	4	57
		>32°C	0	0	0	0	0	0	0	0	0	0	0	0	0	0
10PM to 5 PM	T <sub>sp</sub> [°C]	>18°C	305	120	91	155	467	412	1500	568	570	589	589	570	573	3459
		>18°C	213	93	65	110	329	278	1088	504	553	589	589	557	498	3290
		>20°C	172	61	46	88	260	179	807	395	493	569	553	628	391	2929
		>26°C	20	0	0	5	46	11	82	25	84	131	142	140	90	612
		>32°C	0	0	0	0	0	0	0	0	0	0	4	35	22	61

25m <sup>2</sup> - East - CR 15																
Passive solar gains																
MONTH / Cumul. Frequency																
WINTER																
SUMMER																
MONTH / Cumul. Frequency																
WINTER																
SUMMER																
5PM to 10PM	T <sub>sp</sub> [°C]	>18°C	69	1	0	13	120	147	350	156	150	155	155	150	151	916
		>18°C	24	0	0	3	97	124	248	154	150	155	155	150	146	910
		>20°C	3	0	0	0	48	103	154	124	141	155	155	146	108	829
		>26°C	0	0	0	0	0	1	1	1	7	10	14	2	2	86
		>32°C	0	0	0	0	0	0	0	0	0	0	0	0	0	0
10PM to 5 PM	T <sub>sp</sub> [°C]	>18°C	240	84	52	132	442	503	1453	576	570	589	589	570	563	3457
		>18°C	189	48	30	94	314	420	1085	520	557	589	589	556	477	3285
		>20°C	152	24	12	66	255	311	820	417	501	574	551	518	367	2918
		>26°C	8	0	0	2	33	53	95	35	111	148	163	121	79	657
		>32°C	0	0	0	0	0	3	3	0	0	0	8	13	19	40

FIGURE APP.E.10

# Curriculum Vitae

**Dipl.-Ing (FH) M. Eng. Christian Wiegel**

1977	born in Bocholt, Germany	
1997	final secondary-school examination (A-levels)	
1998-2000	education as architectural draftsman	
2006	Diploma, degree in Architecture, Faculty of Architecture, Münster School of Architecture, Germany	
2007-2010	Project engineer : building physics & facade consulting, Brandt IGH / 1plus Consult GmbH, Germany	
2010	Master degree, International Facade Design and Construction (IFDC), Hochschule Ostwestfalen-Lippe, Germany	
2010-2012	Project engineer : structural and preventive fire protection reports and concepts for Görtzen Ingenieure, Germany	
2012-2017	Project manager of inhouse research & development project SOLARLUX GmbH, Germany	
2013-2017	dissertation thesis at Delft University of Technology, Faculty of Architectural Engineering, Architecture and the Built Environment	
2017 -	Ten Brinke Academy + civil engineer for inhouse consulting of building physics and structural and preventive fire protection, Ten Brinke Group, The Netherlands	



# Imagery credits

## Title page

---

Solarlux GmbH, Germany

## Summary / Samenfattig

---

Solarlux GmbH, Germany

## Chapter 01

---

Boucher, B.. (1994). Palladio–Der Architekt in seiner Zeit, Hirmer Verlag, München  
Lahti, L.. (2004). Alvar Aalto–Paradies für kleine Leute, Taschen GmbH  
Solarlux GmbH, Germany

## Chapter 02

---

Philip Johnson glass house, Carol Highsmith  
Rozenberg Residence, Arthur Brown 1946  
Solarlux GmbH, Germany  
Orangerie – palais de verres, tripadvisor.de  
Orangerie, Parliament Mecklenburg-Vorpommern, guthaeuser.de  
The Eden project Biome, Cornwall, Matt Cardy  
Solarlux GmbH, Germany

## Chapter 03

---

Transsolar GmbH, Germany

## Chapter 05

---

Deutscher Wetterdienst, DWD, Germany  
Solarlux GmbH, Germany

## Chapter 06

---

Solarlux GmbH, Germany

## **Chapter 07**

---

Rijkswaterstaat Utrecht, Joop van Houdt, beeldbank.rws.nl  
Solarlux GmbH, Germany

## **Chapter 08**

---

Solarlux GmbH, Germany

## **Chapter 09**

---

Rijkswaterstaat Utrecht, Joop van Houdt, beeldbank.rws.nl  
Solarlux GmbH, Germany

## **Appendix**

---

Solarlux GmbH, Germany